Draft Final Report

MASH *TL3 EVALUATION OF MASSDOT'S CP-MTL3 BRIDGE RAIL WITH TOP-MOUNTED HANDRAIL USING FINITE ELEMENT ANALYSIS*

Prepared for: **Gill Engineering and the Massachusetts Department of Transportation**

PARS No: **X22LRFDBM1 Q11**

Contract No:

Assignment No:

Report No: **TR23-0630-GEA**

Prepared by: **Chuck A. Plaxico, Ph.D.,** and
Archie M. Ray
ROADSAFE LLC
P.O. BOX 312
CANTON, ME 04221

June 30, 2023

TECHNICAL REPORT DOCUMENTATION PAGE

TABLE OF CONTENTS

TECHNICAL REPORT DOCUMENTATION PAGE ..... **I**

TABLE OF CONTENTS ..... **II**

LIST OF FIGURES ..... **III**

LIST OF TABLES ..... **VI**

LIST OF APPENDICES ..... **VI**

CHAPTER 1 – INTRODUCTION **1**

System Design 1
Background 7
Objectives and Scope 8

CHAPTER 2 – RESEARCH APPROACH AND EVALUATION CRITERIA **9**

CHAPTER 3 – FEA VEHICLE MODELS **12**

CHAPTER 4 – FEA MODEL DEVELOPMENT **15**

Materials 16
Posts 16
Aluminum Railing and Splice Bar 17
Rail-to-Post Mount 18
Anchor Cage 19
Concrete Parapet, sidewalk, and Deck 20
Mitered End of Railing 22
Clamp Bar at Mitered Rail 23
Concrete Clip 24
Concrete Transition and Anchor Connection 25

CHAPTER 5 – MASH TL3 EVALUATION OF THE CP-MTL3 WITH HANDRAIL AT EXPANSION JOINT **26**

Test 3-10 26
Analysis Cases *26*
Summary of Crash Event *27*
Time History Plots and Occupant Risk Measures *29*
Impact Point 1: Impact at 3.6 ft 31
Impact Point 2: Impact at 4.6 ft 31
Damages to the Barrier System *32*
Damages to Vehicle *36*
Occupant Compartment Deformation (OCD) *36*
Exit Box *37*
Results Summary *38*
CIP Recommendation for Test 3-10 for CP-MTL3 at Expansion Joint *38*
Test 3-11 44
Analysis Cases *44*
Summary of Crash Event *44*
Time History Plots and Occupant Risk Measures *46*
Impact Point 1: Impact at 4.26 ft 48
Impact Point 2: Impact at 5.26 ft 48
Damages to the Barrier System *49*
Damages to Vehicle *52*
Occupant Compartment Deformation (OCD) *53*

Exit Box *54*
Results Summary *54*
CIP Recommendation for Test 3-11 for CP-MTL3 at Expansion Joint *55*

CHAPTER 6 – MASH TL3 EVALUATION OF THE CP-MTL3 WITH HANDRAIL AT CONNECTION TO CONCRETE TRANSITION **61**

TEST 3-10 62
Analysis Cases *62*
Summary of Crash Event *63*
Time History Plots and Occupant Risk Measures *65*
Impact Point 1: Impact at 3.6 ft 67
Impact Point 2: Impact at 4.6 ft 67
Damages to the Barrier System *68*
Damages to Vehicle *71*
Occupant Compartment Deformation (OCD) *71*
Exit Box *72*
Results Summary *72*
CIP Recommendation for Test 3-10 for CP-MTL3 at Approach to Transition *73*
TEST 3-11 77
Analysis Cases *77*
Summary of Crash Event *77*
Time History Plots and Occupant Risk Measures *79*
Impact Point 1: Impact at 4.26 ft 81
Impact Point 2: Impact at 5.26 ft 81
Damages to the Barrier System *82*
Damages to Vehicle *85*
Occupant Compartment Deformation (OCD) *86*
Exit Box *86*
Results Summary *87*
CIP Recommendation for Test 3-11 for CP-MTL3 at Approach to Transition *87*

CHAPTER 7 – SUMMARY AND CONCLUSIONS **91**

REFERENCES **94**

LIST OF FIGURES

FIGURE 1. PHOTOGRAPHS OF CP-MTL3 WITH HANDRAIL AT (A) EXPANSION JOINT AND (B) CONCRETE TRANSITION. 1
FIGURE 2. SECTION DRAWING FOR THE CP-MTL3 THROUGH SIDEWALK. 2
FIGURE 3. SECTION DRAWING FOR THE CP-MTL3 WITHOUT SIDEWALK (NOTE: SAFETY CURB OBSOLETE). 3
FIGURE 4. ELEVATION DRAWING FOR ALUMINUM HANDRAIL. 3
FIGURE 5. SECTION DRAWING FOR ALUMINUM HANDRAIL. 4
FIGURE 6. POST AND BASE PLATE DETAIL. 4
FIGURE 7. DRAWINGS FOR CLAMP BARS AT CONCRETE CLIP AND AT POSTS. 5
FIGURE 8. DETAILS FOR THE ANCHOR CAGE. 5
FIGURE 9. SPLICE TUBE DETAILS. 6
FIGURE 10. DRAWING FOR CONCRETE CLIP. 6
FIGURE 11. TESTED DESIGN USED IN FULL-SCALE TESTS 7069-5-6-16. [*BUTH97*] 7
FIGURE 12. MASH EXIT BOX. [*AASHTO16*] 11
FIGURE 13. VEHICLE PROPERTY SHEET FOR THE 1100C VEHICLE MODEL COMPARED WITH THE TEST VEHICLE IN FULL-SCALE TEST 469468-3-1. [*BLIGH19*] 13

FIGURE 14. VEHICLE PROPERTY SHEET FOR THE 2270P VEHICLE MODEL COMPARED WITH THE TEST VEHICLE IN FULL-SCALE TEST 469468-3-2. [*BLIGH19*] 14
FIGURE 15. FEA MODEL OF THE MASSDOT CP-MTL3 BRIDGE RAIL. 15
FIGURE 16. FEA MESH OF ALUMINUM BRIDGE RAIL POST. 17
FIGURE 17. FEA MODEL OF ALUMINUM RAIL AND SPLICE BAR. 18
FIGURE 18. FEA MODEL OF CLAMP BAR. 19
FIGURE 19. FEA MODEL OF RAIL-TO-POST CONNECTION. 19
FIGURE 20. FEA MODEL OF ANCHOR CAGE. 20
FIGURE 21. FEA MESH FOR THE PARAPET, SIDEWALK, AND DECK. 21
FIGURE 22. BOUNDARY CONDITIONS USED TO MODEL CONTINUATION OF DECK 21
FIGURE 23. EXPANSION JOINT GAP FOR THE CP-MTL3. 22
FIGURE 24. SIDEWALK MODEL. 22
FIGURE 25. FEA MODEL OF MITERED END OF RAILING. 23
FIGURE 26. CLAMP BAR AT MITERED END OF RAILING. 24
FIGURE 27. FEA MODEL FOR CONCRETE CLIP AT TRANSITION. 24
FIGURE 28. FEA MODEL FOR THE TRANSITION AND ANCHOR CONNECTION. 25
FIGURE 29. CIP 1 FOR TEST 3-10 FOR MAXIMIZING SNAG ON HANDRAIL POST 27
FIGURE 30. CIP 2 FOR TEST 3-10 FOR MAXIMIZING SNAG AT EXPANSION JOINT. 27
FIGURE 31. 10- AND 50-MILLISECOND RUNNING AVERAGE X-ACCELERATION FROM FEA FOR TEST 3-10. 29
FIGURE 32. 10- AND 50-MILLISECOND RUNNING AVERAGE Y-ACCELERATION FROM FEA OF TEST 3-10. 29
FIGURE 33. 10- AND 50-MILLISECOND RUNNING AVERAGE Z-ACCELERATION FROM FEA OF TEST 3-10. 29
FIGURE 34. YAW RATE AND YAW ANGLE TIME-HISTORY FROM FEA OF TEST 3-10. 30
FIGURE 35. ROLL RATE AND ROLL ANGLE TIME-HISTORY FROM FEA OF TEST 3-10. 30
FIGURE 36. PITCH RATE AND PITCH ANGLE TIME-HISTORY FROM FEA OF TEST 3-10. 30
FIGURE 37. CONTOUR PLOT OF LATERAL DISPLACEMENT FOR TEST 3-10 AT 3.6 FT UPSTREAM OF CRITICAL POST FOR (A) KC MODEL AND (B) RHT MODEL. 33
FIGURE 38. CONTOUR PLOT OF LATERAL DISPLACEMENT FOR TEST 3-10 AT 4.6 FT UPSTREAM OF CRITICAL POST FOR (A) KC MODEL AND (B) RHT MODEL. 33
FIGURE 39. EFFECTIVE PLASTIC STRAIN CONTOURS ON RAIL SPLICE COMPONENTS DURING TEST 3-10 FOR (A) IMPACT AT 3.6 FT AND (B) 4.6 FT UPSTREAM OF CRITICAL POST 34
FIGURE 40. CONTOUR PLOT OF THE DAMAGE VARIABLE ON THE CONCRETE PARAPET AND DECK DURING TEST 3-10 FOR (A) IMPACT AT 3.6 FT AND (B) 4.6 FT UPSTREAM OF CRITICAL POST. 35
FIGURE 41. CONTOUR PLOT OF 1ST PRINCIPAL STRAIN ON THE CONCRETE PARAPET AND DECK DURING TEST 3-10 FOR (A) IMPACT AT 3.6 FT AND (B) 4.6 FT UPSTREAM OF CRITICAL POST. 35
FIGURE 42. DAMAGES TO VEHICLE IN TEST 3-10 FOR (A) IMPACT AT 3.6 FT AND (B) 4.6 FT UPSTREAM OF CRITICAL POST. 36
FIGURE 43. OCCUPANT COMPARTMENT DEFORMATION RESULTING FROM TEST 3-10 FOR (A) IMPACT AT 3.6 FT AND (B) 4.6 FT UPSTREAM OF CRITICAL POST. 37
FIGURE 44. EXIT BOX FOR TEST 3-10 FOR (A) IMPACT AT 3.6 FT AND (B) 4.6 FT UPSTREAM OF CRITICAL POST. 37
FIGURE 45. SUMMARY RESULTS FOR MASH TEST 3-10 WITH IMPACT POINT AT 3.6 FT UPSTREAM OF POST (KC MODEL). 40
FIGURE 46. SUMMARY RESULTS FOR MASH TEST 3-10 WITH IMPACT POINT AT 3.6 FT UPSTREAM OF POST (RHT MODEL). 41
FIGURE 47. SUMMARY RESULTS FOR MASH TEST 3-10 WITH IMPACT POINT AT 4.6 FT UPSTREAM OF POST (KC MODEL). 42
FIGURE 48. SUMMARY RESULTS FOR MASH TEST 3-10 WITH IMPACT POINT AT 4.6 FT UPSTREAM OF POST (RHT MODEL). 43
FIGURE 49. CIP 1 FOR TEST 3-11 FOR MAXIMIZING LOAD ON HANDRAIL POST. 44
FIGURE 50. CIP 2 FOR TEST 3-11 FOR MAXIMIZING LOAD ON EXPANSION JOINT. 44
FIGURE 51. 10- AND 50-MILLISECOND RUNNING AVERAGE X-ACCELERATION FROM FEA FOR TEST 3-11. 46
FIGURE 52. 10- AND 50-MILLISECOND RUNNING AVERAGE Y-ACCELERATION FROM FEA FOR TEST 3-11. 47
FIGURE 53. 10- AND 50-MILLISECOND RUNNING AVERAGE Z-ACCELERATION FROM FEA FOR TEST 3-11. 47
FIGURE 54. YAW RATE AND YAW ANGLE TIME-HISTORY FROM FEA FOR TEST 3-11. 47
FIGURE 55. ROLL RATE AND ROLL ANGLE TIME-HISTORY FROM FEA FOR TEST 3-11. 47
FIGURE 56. PITCH RATE AND PITCH ANGLE TIME-HISTORY FROM FEA FOR TEST 3-11. 48
FIGURE 57. CONTOUR PLOT OF LATERAL DISPLACEMENT FOR TEST 3-11 AT 4.26 FT UPSTREAM OF CRITICAL POST FOR (A) KC MODEL AND (B) RHT MODEL. 50

FIGURE 58. CONTOUR PLOT OF LATERAL DISPLACEMENT FOR TEST 3-11 AT 5.26 FT UPSTREAM OF CRITICAL POST FOR (A) KC MODEL AND (B) RHT MODEL. 50
FIGURE 59. EFFECTIVE PLASTIC STRAIN CONTOURS ON RAIL SPLICE COMPONENTS DURING TEST 3-11 FOR (A) IMPACT AT 4.26 FT AND (B) 5.26 FT UPSTREAM OF CRITICAL POST. 51
FIGURE 60. CONTOUR PLOT OF THE DAMAGE VARIABLE ON THE CONCRETE PARAPET AND DECK DURING TEST 3-11 FOR (A) IMPACT AT 4.26 FT AND (B) 5.26 FT UPSTREAM OF CRITICAL POST. 51
FIGURE 61. CONTOUR PLOT OF 1ST PRINCIPAL STRAIN ON THE CONCRETE PARAPET AND DECK DURING TEST 3-11 FOR (A) IMPACT AT 4.26 FT AND (B) 5.26 FT UPSTREAM OF CRITICAL POST. 52
FIGURE 62. DAMAGES TO VEHICLE IN TEST 3-11 FOR (A) IMPACT AT 4.26 FT AND (B) 5.26 FT UPSTREAM OF CRITICAL POST. 53
FIGURE 63. DAMAGE TO TEST VEHICLE IN TEST 3-11 ON SIMILAR BRIDGE RAIL SYSTEM. [*DOBROVOLNY20*] 53
FIGURE 64. OCCUPANT COMPARTMENT DEFORMATION RESULTING FROM TEST 3-11 FOR (A) IMPACT AT 4.26 FT AND (B) 5.26 FT UPSTREAM OF CRITICAL POST. 54
FIGURE 65. EXIT BOX FOR TEST 3-11 FOR (A) IMPACT AT 4.26 FT AND (B) 5.26 FT UPSTREAM OF CRITICAL POST. 54
FIGURE 66. SUMMARY RESULTS FOR MASH TEST 3-11 WITH IMPACT POINT AT 4.26 FT UPSTREAM OF POST (KC MODEL). 57
FIGURE 67. SUMMARY RESULTS FOR MASH TEST 3-11 WITH IMPACT POINT AT 4.26 FT UPSTREAM OF POST (RHT MODEL). 58
FIGURE 68. SUMMARY RESULTS FOR MASH TEST 3-11 WITH IMPACT POINT AT 5.26 FT UPSTREAM OF POST (KC MODEL). 59
FIGURE 69. SUMMARY RESULTS FOR MASH TEST 3-11 WITH IMPACT POINT AT 5.26 FT UPSTREAM OF POST (RHT MODEL). 60
FIGURE 70. CRITICAL SNAG POINT FOR SYSTEM AT CONNECTION TO TRANSITION 61
FIGURE 71. DRAWINGS FOR THE CP-MTL3 CONNECTION TO TRANSITION. 62
FIGURE 72. ELEVATION VIEW FOR CP-MTL3 MODEL AND TRANSITION. 62
FIGURE 73. TEST 3-10 WITH IMPACT AT 3.6 FT UPSTREAM OF TRANSITION. 63
FIGURE 74. TEST 3-10 WITH IMPACT AT 4.6 FT UPSTREAM OF TRANSITION. 63
FIGURE 75. 10- AND 50-MILLISECOND RUNNING AVERAGE X-ACCELERATION FROM FEA FOR TEST 3-10. 66
FIGURE 76. 10- AND 50-MILLISECOND RUNNING AVERAGE Y-ACCELERATION FROM FEA OF TEST 3-10. 66
FIGURE 77. 10- AND 50-MILLISECOND RUNNING AVERAGE Z-ACCELERATION FROM FEA OF TEST 3-10. 66
FIGURE 78. YAW RATE AND YAW ANGLE TIME-HISTORY FROM FEA OF TEST 3-10. 66
FIGURE 79. ROLL RATE AND ROLL ANGLE TIME-HISTORY FROM FEA OF TEST 3-10. 67
FIGURE 80. PITCH RATE AND PITCH ANGLE TIME-HISTORY FROM FEA OF TEST 3-10. 67
FIGURE 81. CONTOUR PLOT OF LATERAL DISPLACEMENT OF ALUMINUM RAILING FOR TEST 3-10 RESULTING FROM IMPACT AT (A) 3.6 FT AND (B) 4.6 FT UPSTREAM OF TRANSITON. 69
FIGURE 82. CONTOUR PLOT OF LATERAL DISPLACEMENT OF CONCRETE PARAPET FOR TEST 3-10 RESULTING FROM IMPACT AT (A) 3.6 FT AND (B) 4.6 FT UPSTREAM OF TRANSITON. 69
FIGURE 83. EFFECTIVE PLASTIC STRAIN CONTOURS ON RAIL COMPONENTS DURING TEST 3-10 FOR (A) IMPACT AT 3.6 FT AND (B) 4.6 FT UPSTREAM OF THE TRANSITION. 70
FIGURE 84. CONTOUR PLOT OF THE DAMAGE VARIABLE ON THE CONCRETE PARAPET AND DECK DURING TEST 3-10 FOR (A) IMPACT AT 3.6 FT AND (B) 4.6 FT UPSTREAM OF THE TRANSITION 70
FIGURE 85. CONTOUR PLOT OF 1ST PRINCIPAL STRAIN ON THE CONCRETE PARAPET AND DECK DURING TEST 3-10 FOR (A) IMPACT AT 3.6 FT AND (B) 4.6 FT UPSTREAM OF THE TRANSITION. 71
FIGURE 86. DAMAGES TO VEHICLE IN TEST 3-10 FOR (A) IMPACT AT 3.6 FT AND (B) 4.6 FT UPSTREAM OF THE TRANSITION. 71
FIGURE 87. OCCUPANT COMPARTMENT DEFORMATION RESULTING FROM TEST 3-10 FOR (A) IMPACT AT 3.6 FT AND (B) 4.6 FT UPSTREAM OF THE TRANSITION. 72
FIGURE 88. EXIT BOX FOR TEST 3-10 FOR (A) IMPACT AT 3.6 FT AND (B) 4.6 FT UPSTREAM OF THE TRANSITION. 72
FIGURE 89. SUMMARY RESULTS FOR MASH TEST 3-10 WITH IMPACT POINT AT 3.6 FT UPSTREAM OF POST (KC MODEL). 75
FIGURE 90. SUMMARY RESULTS FOR MASH TEST 3-10 WITH IMPACT POINT AT 4.6 FT UPSTREAM OF POST (KC MODEL). 76
FIGURE 91. TEST 3-11 WITH IMPACT AT 4.26 FT UPSTREAM OF TRANSITION. 77
FIGURE 92. TEST 3-11 WITH IMPACT AT 5.26 FT UPSTREAM OF TRANSITION. 77
FIGURE 93. 10- AND 50-MILLISECOND RUNNING AVERAGE X-ACCELERATION FROM FEA FOR TEST 3-11. 80
FIGURE 94. 10- AND 50-MILLISECOND RUNNING AVERAGE Y-ACCELERATION FROM FEA OF TEST 3-11. 80
FIGURE 95. 10- AND 50-MILLISECOND RUNNING AVERAGE Z-ACCELERATION FROM FEA OF TEST 3-11. 80
FIGURE 96. YAW RATE AND YAW ANGLE TIME-HISTORY FROM FEA OF TEST 3-11. 80
FIGURE 97. ROLL RATE AND ROLL ANGLE TIME-HISTORY FROM FEA OF TEST 3-11. 81
FIGURE 98. PITCH RATE AND PITCH ANGLE TIME-HISTORY FROM FEA OF TEST 3-11. 81

FIGURE 99. CONTOUR PLOT OF LATERAL DISPLACEMENT OF ALUMINUM RAILING FOR TEST 3-11 RESULTING FROM IMPACT AT (A) 4.26 FT AND (B) 5.26 FT UPSTREAM OF TRANSITON. 83
FIGURE 100. CONTOUR PLOT OF LATERAL DISPLACEMENT OF CONCRETE PARAPET FOR TEST 3-11 RESULTING FROM IMPACT AT (A) 4.26 FT AND (B) 5.26 FT UPSTREAM OF TRANSITON. 83
FIGURE 101. EFFECTIVE PLASTIC STRAIN CONTOURS ON RAIL COMPONENTS DURING TEST 3-11 FOR (A) IMPACT AT 4.26 FT AND (B) 5.26 FT UPSTREAM OF THE TRANSITION. 84
FIGURE 102. CONTOUR PLOT OF THE DAMAGE VARIABLE ON THE CONCRETE PARAPET AND DECK DURING TEST 3-11 FOR (A) IMPACT AT 4.26 FT AND (B) 5.26 FT UPSTREAM OF THE TRANSITION. 84
FIGURE 103. CONTOUR PLOT OF 1ST PRINCIPAL STRAIN ON THE CONCRETE PARAPET AND DECK DURING TEST 3-11 FOR (A) IMPACT AT 4.26 FT AND (B) 5.26 FT UPSTREAM OF THE TRANSITION. 85
FIGURE 104. CONTOUR PLOT OF 1ST PRINCIPAL STRAIN ON THE CONCRETE PARAPET AND DECK DURING TEST 3-11 FOR IMPACT AT 4.26 FT WITH CONTOUR RANGE CUT OFF AT 0.0267. 85
FIGURE 105. DAMAGES TO VEHICLE IN TEST 3-11 FOR (A) IMPACT AT 4.26 FT AND (B) 5.26 FT UPSTREAM OF THE TRANSITION. 86
FIGURE 106. OCCUPANT COMPARTMENT DEFORMATION RESULTING FROM TEST 3-11 FOR (A) IMPACT AT 4.26 FT AND (B) 5.26 FT UPSTREAM OF THE TRANSITION. 86
FIGURE 107. EXIT BOX FOR TEST 3-11 FOR (A) IMPACT AT 4.26 FT AND (B) 5.26 FT UPSTREAM OF THE TRANSITION. 87
FIGURE 108. SUMMARY RESULTS FOR MASH TEST 3-11 WITH IMPACT POINT AT 4.26 FT UPSTREAM OF POST (KC MODEL). 89
FIGURE 109. SUMMARY RESULTS FOR MASH TEST 3-11 WITH IMPACT POINT AT 5.26 FT UPSTREAM OF POST (KC MODEL). 90

LIST OF TABLES

TABLE 1. SAFETY EVALUATION GUIDELINES FOR STRUCTURAL ADEQUACY AND OCCUPANT RISK. *[AASHTO16]* 9
TABLE 2. EXIT BOX DIMENSIONS FOR MASH TESTS FOR SMALL CAR AND PICKUP 11
TABLE 3. SEQUENCE OF EVENTS FOR TEST 3-10 FOR CIP AT 3.6 FT UPSTREAM OF CRITICAL POST. 28
TABLE 4. SUMMARY OF MASH OCCUPANT RISK METRICS FOR TEST 3-10. 32
TABLE 5. SUMMARY OF MASH TEST 3-10 FOR THE CP-MTL3. 39
TABLE 6. SEQUENCE OF EVENTS FOR TEST 3-11 WITH CIP AT 4.26 FT UPSTREAM OF CRITICAL POST. 45
TABLE 7. SUMMARY OF MASH OCCUPANT RISK METRICS FOR TEST 3-11. 49
TABLE 8. SUMMARY OF MASH TEST 3-11 FOR THE CP-MTL3. 56
TABLE 9. SEQUENCE OF EVENTS FOR TEST 3-10 FOR CIP AT 3.6 FT UPSTREAM OF TRANSITION. 64
TABLE 10. SUMMARY OF MASH OCCUPANT RISK METRICS FOR TEST 3-10. 68
TABLE 11. SUMMARY OF MASH TEST 3-10 FOR THE CP-MTL3 AT TRANSITION. 74
TABLE 12. SEQUENCE OF EVENTS FOR TEST 3-11 FOR CIP AT 4.26 FT UPSTREAM OF TRANSITION. 78
TABLE 13. SUMMARY OF MASH OCCUPANT RISK METRICS FOR TEST 3-11. 82
TABLE 14. SUMMARY OF MASH TEST 3-11 FOR THE CP-MTL3 AT TRANSITION. 88
TABLE 15. SUMMARY OF OCCUPANT RISK METRICS FROM ANALYSIS RESULTS FOR EVALUATIONS AT THE EXPANSION JOINT OF THE BARRIER. 92
TABLE 16. SUMMARY OF OCCUPANT RISK METRICS FROM ANALYSIS RESULTS FOR EVALUATIONS AT THE TRANSITION FOR THE BARRIER. 93

LIST OF APPENDICES

Appendix A: Drawings for the MassDOT CP-MTL3 with Handrail

Appendix B: Sequential Views for Test 3-10 at 3.6 ft upstream of critical post (KC model)

Appendix C: Sequential Views for Test 3-10 at 3.6 ft upstream of critical post (RHT model)

Appendix D: Sequential Views for Test 3-10 at 4.6 ft upstream of critical post (KC model)

Appendix E: Sequential Views for Test 3-10 at 4.6 ft upstream of critical post (RHT model)

Appendix F: Sequential Views for Test 3-11 at 4.3 ft upstream of critical post (KC model)

Appendix G: Sequential Views for Test 3-11 at 4.3 ft upstream of critical post (RHT model)

Appendix H: Sequential Views for Test 3-11 at 5.3 ft upstream of critical post (KC model)

Appendix I: Sequential Views for Test 3-11 at 5.3 ft upstream of critical post (RHT model)

Appendix J: Sequential Views for Test 3-10 at 3.6 ft upstream of transition (KC model)

Appendix K: Sequential Views for Test 3-10 at 4.6 ft upstream of transition (KC model)

Appendix L: Sequential Views for Test 3-11 at 4.26 ft upstream of transition (KC model)

Appendix M: Sequential Views for Test 3-11 at 5.26 ft upstream of transition (KC model)

CHAPTER 1 – INTRODUCTION

The purpose of this project was to evaluate the crash performance of MassDOT's CP-MTL3 bridge rail using finite element analysis (FEA). Two critical regions of the system were evaluated. The first critical region was the expansion joint of the bridge and parapet. Analyses were conducted to assess the critical impact points (CIPs) for maximizing vehicle snag on either the expansion joint or the handrail post located 12 inches downstream of the expansion joint. The second critical region was at the approach to the concrete transition at the downstream end of the system. For this case, analyses were conducted to assess the CIP for maximizing vehicle snag on the upstream edge of the transition at the connection point to the CP-MTL3 system. The evaluations were carried out in accordance with the AASHTO Manual for Assessing Safety Hardware (MASH) for test level 3 (TL3), and the results of those evaluations are presented in the following chapters of this report.

(a) (b)

Figure 1. Photographs of CP-MTL3 with handrail at (a) expansion joint and (b) concrete transition.

System Design

Drawing details for the baseline design are shown in Appendix A. This design includes a 10-inch-tall aluminum post-and-beam railing mounted onto the top of a 32-inch-tall reinforced concrete parapet, as illustrated in Figures 2 through 10. The overall height of the barrier is 42 inches measured from the top of the sidewalk, or from bridge's wearing surface for the non-sidewalk case, to the top of the aluminum rail. The concrete parapet has a vertical face and is 10 inches thick along its stem and approximately 14 inches across the thickened section at the top. The concrete has a minimum unconfined compressive strength of 4,000 psi. The steel reinforcing in the concrete parapet consists of #4 longitudinal bars, #5 vertical steel bars along the stem, and #4 hoop bars in the thickened section, as shown in Figure 3. The vertical steel bars and hoops are spaced 6 inches on centers.

The handrail is an aluminum extrusion that is supported by aluminum posts. The cross-section details for the extruded rail are shown in Figure 5. The posts are fabricated from bent plate and are welded to an aluminum base plate with dimensions 7.5" x 4" x 0.5", as shown in Figures 5 and 6. The posts are spaced along the railing at 6'-6" on centers, and the rail segments are continuous over a minimum of four posts. The railing is fastened to the posts using clamp bars, as shown in Figure 7. The clamp bars include tapped holes for two ½-inch diameter

stainless screws. The base plate is fastened to the top of the parapet using 3.25-inch-long ferrules tapped for 0.75-inch diameter anchor bolts. The ferrules are secured in the concrete parapet with two 3/8-inch diameter steel u-bars embedded 8 inches deep into the parapet. The details for the anchor cage are shown in Figure 8. The rails are spliced together using a 36-inch-long aluminum tube embedded equal distance into each adjoining rail ends, and the splice tube is fastened to the downstream rail using two #10 stainless steel drive screws, as shown in Figure 9. The upstream end of the splice tube slides freely inside the upstream railing. The material for all aluminum components is AISI 6061-T6.

At the connection to the 42-inch-tall vertical-face transition, the end of the rail is mitered at 90 degrees and then extended 9 inches downward toward the parapet, as illustrated at the left end of Figure 4. The mitered section is connected to a concrete clip made from L4x4x3/8 steel using a shortened clamp bar, as illustrated in Figures 7 and 10.

Additional details of the concrete deck and reinforcing are provided in Appendix A.

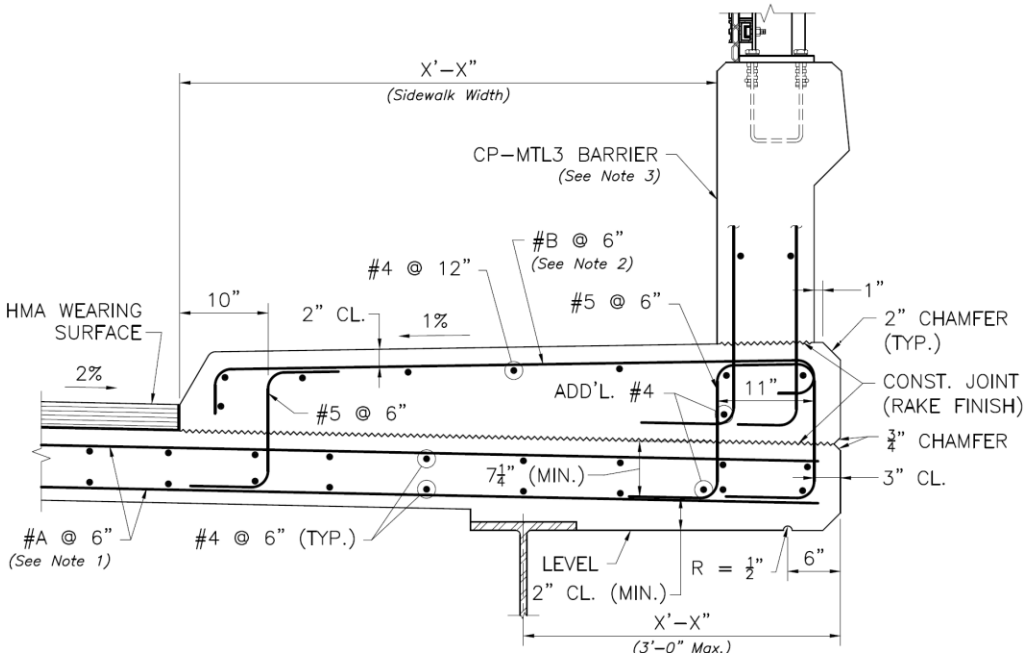

Figure 2. Section drawing for the CP-MTL3 through sidewalk.

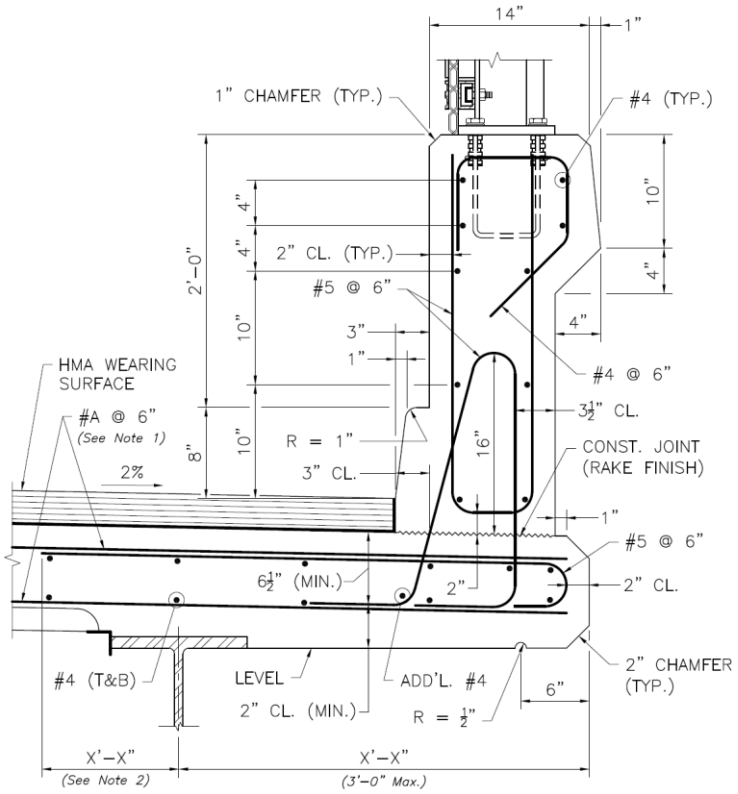

Figure 3. Section drawing for the CP-MTL3 without sidewalk (note: safety curb obsolete).

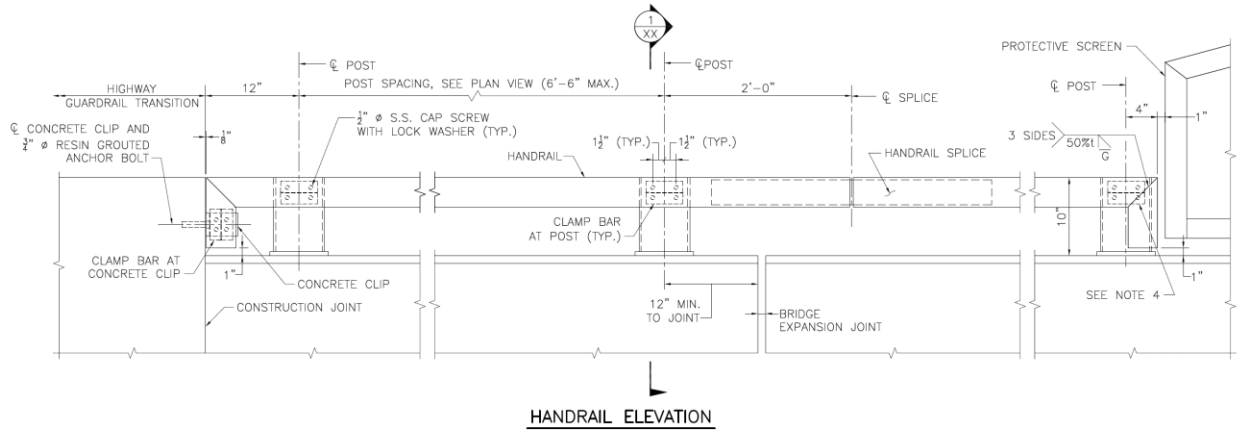

Figure 4. Elevation drawing for aluminum handrail.

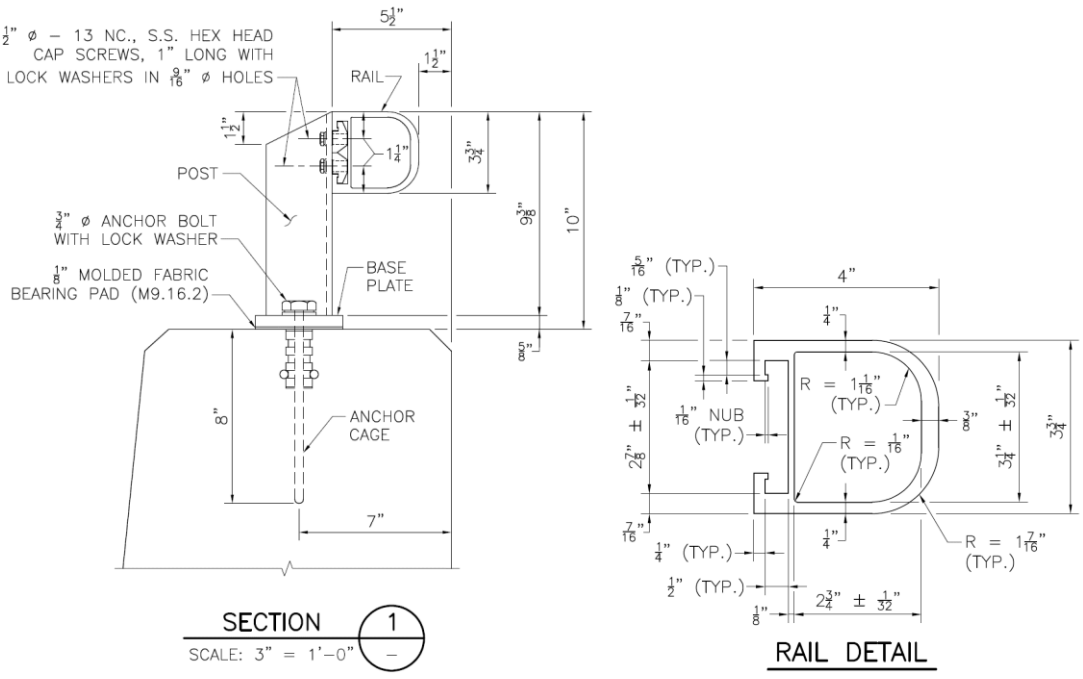

Figure 5. Section drawing for aluminum handrail.

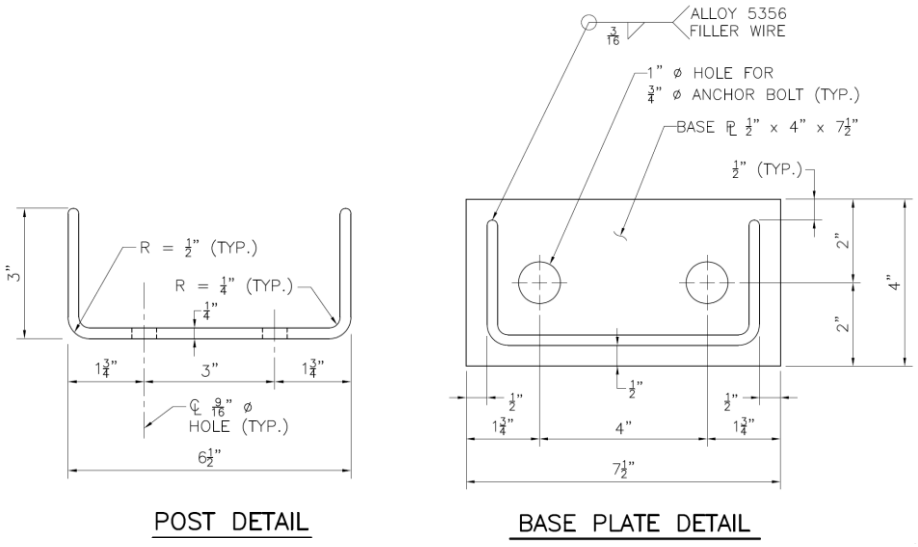

Figure 6. Post and Base plate detail.

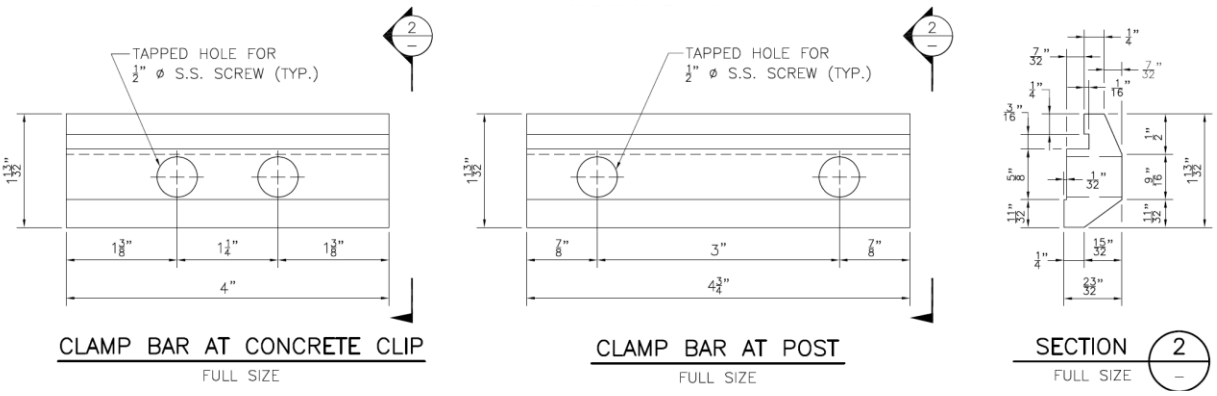

Figure 7. Drawings for clamp bars at concrete clip and at posts.

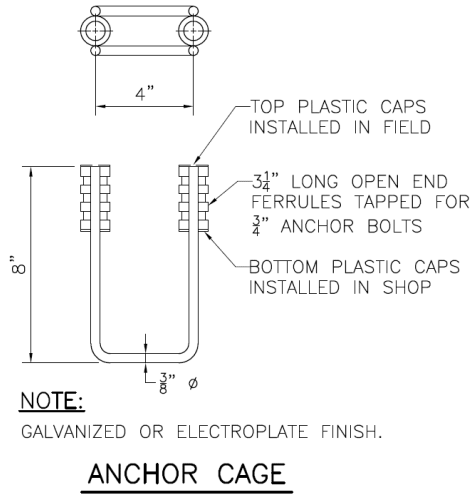

Figure 8. Details for the anchor cage.

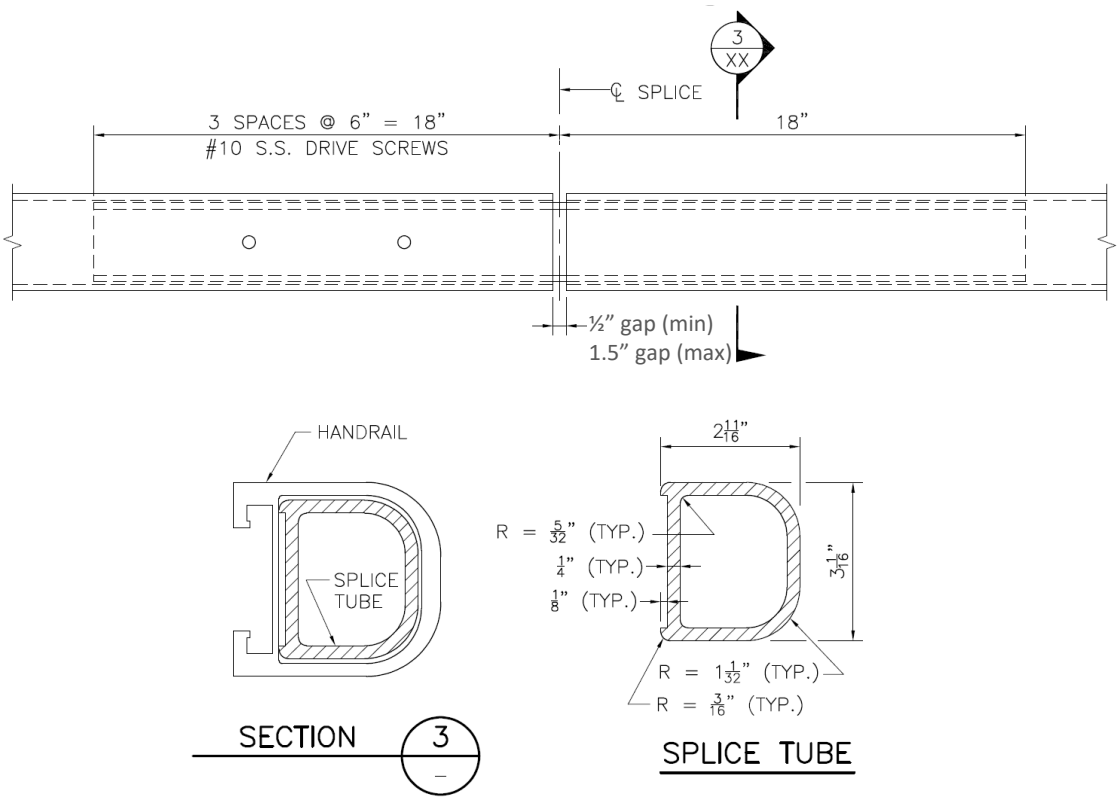

Figure 9. Splice tube details.

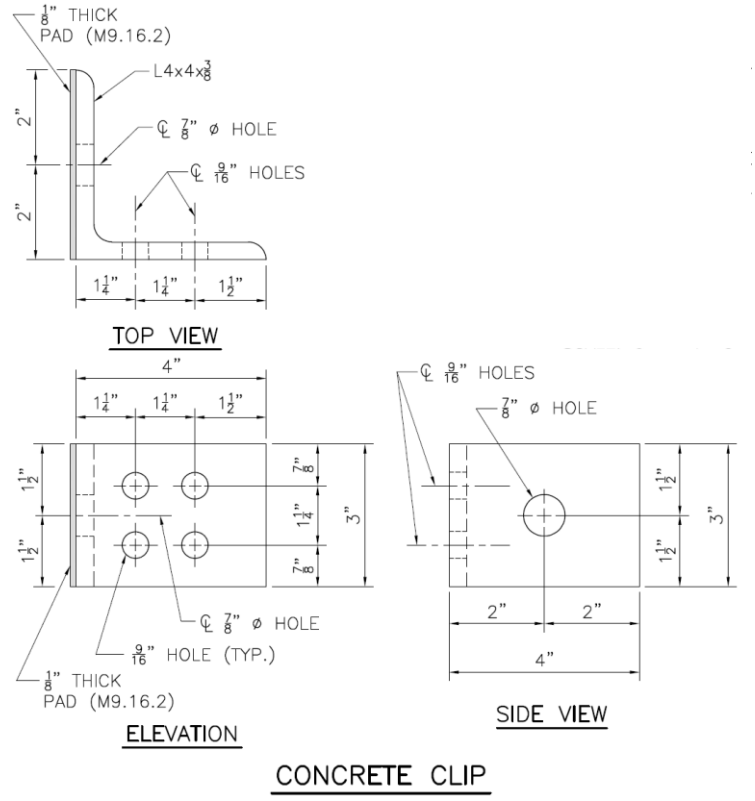

Figure 10. Drawing for concrete clip.

Background

A similar bridge rail design was previously tested by the Texas Transportation Institute (TTI) according to the procedures defined in the 1989 Guide Specifications for Bridge Railings for Performance Level 2 (PL2). [*Buth97*]. Three tests were performed, which included:

- **Test 7069-5**: 1,800-lb passenger car impacting at 60 mph and 20 degrees.
- **Test 7069-6**: 5,400-lb pickup impacting at 60 mph and 20 degrees.
- **Test 7069-16**: 18,000-lb single-unit truck impacting at 50 mph and 15 degrees.

The tested design, shown in Figure 11, was 32 inches tall, included a smaller cross-section than the MassDOT CP-MTL3, and did not include the handrail. The stem of the barrier was 8'inches thick (compared to 10 inches for the CP-MTL3) and the thickened section at the top was 10 inches thick (compared to 14 inches for the CP-MTL3).

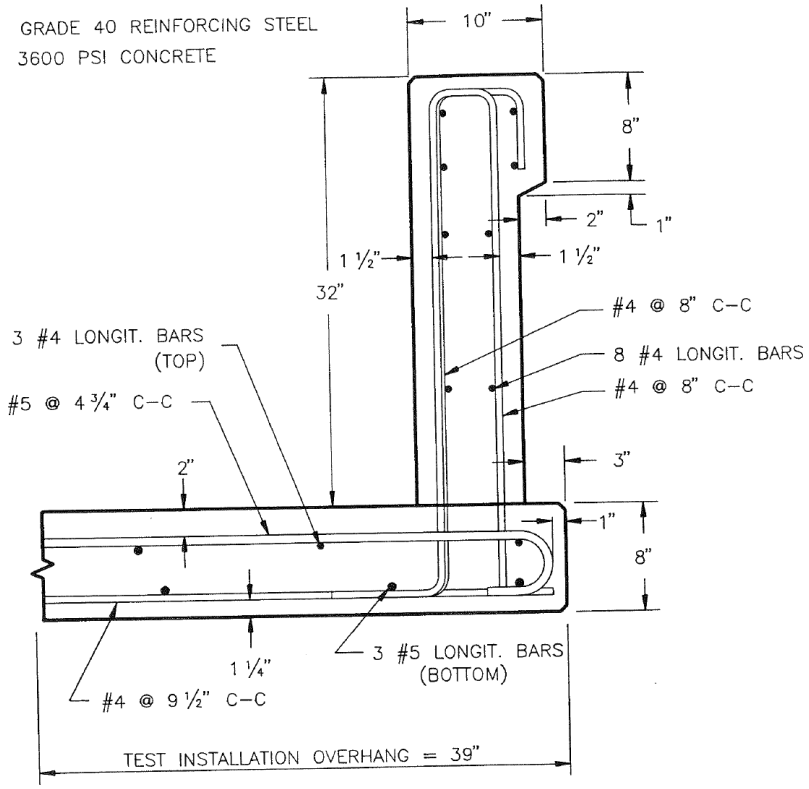

Figure 11. Tested design used in full-scale tests 7069-5-6-16. [*Buth97*]

The steel reinforcing in the tested parapet was also similar to the CP-MTL3 and included eight #4 longitudinal bars, a #4 vertical stirrup that extended from the top of the parapet into the deck, and a #4 hoop at the top thickened section of the parapet. The vertical steel was spaced at 8 inches on centers. In comparison, the CP-MTL3 includes similar longitudinal steel but uses a #5 bar for the vertical stirrup, a #4 hoop bar at the top, with all vertical steel spaced at 6 inches on centers. The deck for the test article was 8 inches thick with a 39-inch overhang. Additional system details can be found in Buth et al. [*Buth97*]

The full-scale tests met all requirements for PL2. The vehicles were smoothly redirected, and there was minimal lateral movement of the barrier during the tests.

Objectives and Scope

The objective of this project was to use finite element analysis (FEA) computer simulation to evaluate the crash performance of the MassDOT CP-MTL3 bridge rail design under the current impact and evaluation criteria of AASHTO *Manual for Assessing Safety Hardware (*MASH*16)* for Test Level 3 (TL3). The crash simulations were performed using the non-linear, dynamic, explicit finite element analysis software LS-DYNA. [*LSDYNA20*]

CHAPTER 2 – RESEARCH APPROACH AND EVALUATION CRITERIA

The basic approach for the study was to develop a finite element model of the CP-MTL3 bridge rail (see Chapter 4) and to use FEA to simulate MASH TL3 crash tests. Two CIPs were evaluated for the system:

1) CIP for maximizing vehicle snag at the expansion joint and/or snag against the handrail-post located 12 inches downstream of the expansion joint (see Chapter 5).
2) CIP for maximizing vehicle snag at the connection to the concrete transition at the downstream end of the CP-MTL3 system (see Chapter 6).

The crash performance of the system was evaluated for structural capacity, occupant risk, vehicle stability and trajectory during impact and redirection in accordance with the recommended procedures and criteria contained in MASH. The required test conditions specified in MASH for test level 3 evaluation of longitudinal barrier are provided below, and Table 1 shows the details for each performance criterion.

- Test 3-10 – the 1100C vehicle (2,225-lb sedan) impacting the barrier at the critical impact point at a nominal speed and angle of 62 mph and 25 degrees, respectively.
- Test 3-11 – the 2270P vehicle (5,000-lb ½-ton quad-cab pickup) impacting the barrier at the critical impact point at a nominal speed and angle of 62 mph and 25 degrees, respectively.

Table 1. Safety evaluation guidelines for structural adequacy and occupant risk. *[AASHTO16*]

Evaluation Factors		Evaluation Criteria
Structural Adequacy	A.	Test article should contain and redirect the vehicle or bring the vehicle to a controlled stop; the vehicle should not penetrate, underride, or override the installation although controlled lateral deflection of the test article is acceptable.
Occupant Risk	D.	Detached elements, fragments or other debris from the test article should not penetrate or show potential for penetrating the occupant compartment, or present an undue hazard to other traffic, pedestrians or personnel in a work zone. Deformations of, or intrusions into, occupant compartment should not exceed limits set forth in Section 5.2.2 and Appendix E.
	F.	The vehicle should remain upright during and after the collision. The maximum roll and pitch angles are not to exceed 75 degrees.
	H.	The longitudinal and lateral occupant impact velocity (OIV) shall not exceed 40 ft/s (12.2 m/s), with a preferred limit of 30 ft/s (9.1 m/s)
	I.	The longitudinal and lateral ridedown acceleration (RA) shall not exceed 20.49 G, with a preferred limit of 15.0 G.

Accelerometers were positioned between the front seat occupants for both the 1100C and 2270P vehicles at the center of gravity for each vehicle model. The acceleration-time histories and angular rate-time histories were collected during the impact event and were used to evaluate

occupant risk metrics according to the procedures outlined in MASH*16*. The acceleration data from the analyses were collected at a frequency of 50,000 Hz and were filtered using the SAE Class 180 filter prior to input into the Test Risk Assessment Program (TRAP). [*TTI22*] The TRAP program calculates standardized occupant risk factors from vehicle crash data in accordance with MASH guidelines and the European Committee for Standardization (EN1317). TRAP computes important evaluation parameters including the occupant impact velocities (OIV), ridedown accelerations (RA), 50 millisecond running average acceleration, and maximum roll, pitch, and yaw. Also computed in TRAP are the EN1317 occupant risk metrics which include the Theoretical Head Impact Velocity (THIV), the Post Impact Head Deceleration (PHD) and the Acceleration Severity Index (ASI). The details of these calculations are provided in MASH. [*AASHTO16*]

With regard to occupant risk, MASH lists certain limitations for passenger compartment deformation and intrusion. Specifically, it states:

"*A clear distinction should be made between: (a) penetration, in which a component of the test article actually penetrates into the occupant compartment; and (b) intrusion or deformation, in which the occupant compartment is deformed and reduced in size, but no actual penetration is observed. No penetration by any element of the test article into the occupant compartment is allowed. As for deformation or intrusion, the extent of deformation varies by area of the vehicle damaged and should be limited as follows:"*

- *"Roof ≤ 4.0 in. (102 mm).*
- *Windshield – no tear of plastic liner and maximum deformation of 3 in. (76 mm).*
- *Window – no shattering of a side window resulting from direct contact with a structural member of the test article, except for special considerations pertaining to tall, continuous barrier elements discussed below (Note: evaluation of this criteria requires the side windows to be in the up position for testing). In cases where side windows are laminated, the guidelines for windshields will apply.*
- *A- and B- pillars – no complete severing of support member and maximum resultant deformation of 5 in. (127 mm). Lateral deformation should be limited to 3 in. (76 mm).*
- *Wheel/foot well and toe pan areas ≤ 9 in. (229 mm).*
- *Side front panel (forward of A-pillar) ≤ 12 in. (305 mm).*
- *Front side door area (above seat) ≤ 9 in. (229 mm).*
- *Front side door area (below seat) ≤ 12 in. (305 mm).*
- *Floor pan and transmission tunnel areas ≤ 12 in. (305 mm)."* [*AASHTO16*]

Post-impact vehicle trajectory, although not required by MASH, was examined for completeness of the evaluations. MASH uses the concept of the "exit box" which was adopted directly from CEN standards. The width of the exit box is the lateral distance "A" in Figure 12, which is defined as 7.2 feet plus the width of the vehicle plus 16 percent of the length of the vehicle. The length of the exit box is the longitudinal distance "B" in Figure 12 which is 32.8 feet. All wheel tracks of the vehicle should remain within the exit box throughout distance "B". [*AASHTO16*] A graphical representation of the exit box is shown in Figure 12.

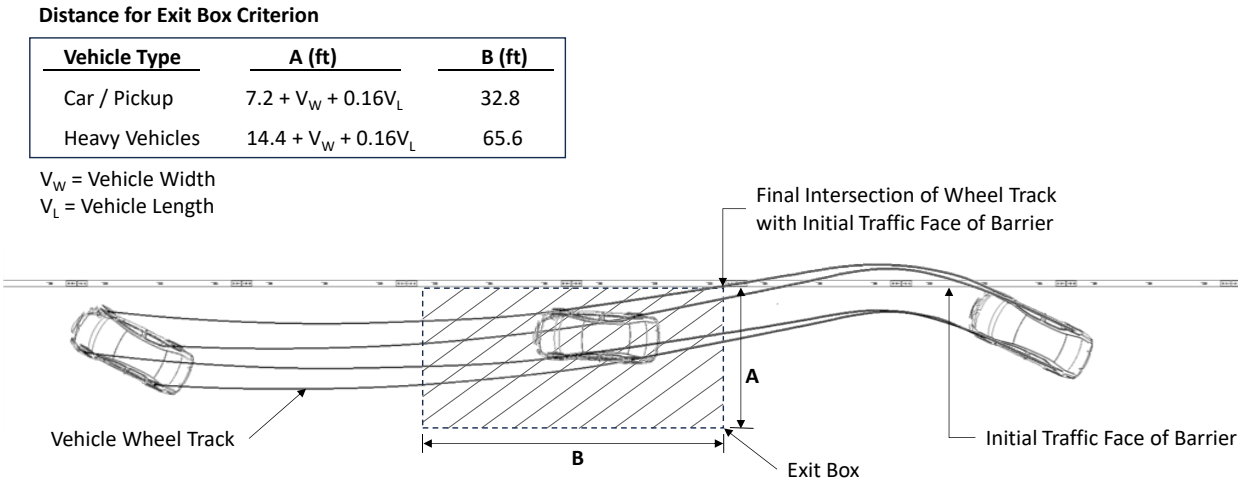

Figure 12. MASH exit box. [*AASHTO16*]

The exit box values were calculated based on the dimensions of the finite element analysis vehicle models that are further described in Chapter 3. Table 3 shows the vehicle widths and lengths and resulting exit box dimensions for the small car and pickup truck.

Table 2. Exit box dimensions for MASH tests for small car and pickup.

Test	V_w (ft)	V_L (ft)	A (ft)	B (ft)
3-10	5.5	14.1	15	32.8
3-11	6.02	16.8	15.86	32.8

CHAPTER 3 – FEA VEHICLE MODELS

The models for the 1100C and 2270P vehicles used for the MASH analysis cases were the YarisC_v1L model (based on a 2010 Toyota Yaris) and the Ram2018_V02u model (based on a 2018 quad-cab Dodge Ram). These vehicles closely represent the two test vehicles specified in MASH. [*AASHTO16*] The vehicle models were developed through the process of reverse engineering by the members of George Mason University (GMU) and were initially validated based on NCAP frontal wall impact tests through comparison with NHTSA test data. The models also include validated suspension and steering subsystems. The Dodge Ram model is relatively new and is continually being improved by GMU as well as the user community. The Yaris model has been used extensively by the research team and has routinely provided good results. [*Plaxico19; Plaxico20*] The validation reports for these vehicles can be accessed from the George Mason University's Center for Collision Safety and Analysis website. [*Marzougui12; CCSA16; CCSA18*] Additional modifications were made to the 1100C and the 2270P models in previous work by the research team, which included development of a new tire model. [*Plaxico21*] The steer response for the 1100C and 2270P models was also corrected in recent projects by the research team. [*Carrigan22; Plaxico22*]

A comparison of the physical and inertial properties of the 1100C and 2270P vehicle models with those of recent full-scale test vehicles (i.e., Test 469468-3-1 and Test 469468-3-2) is provided in Figure 13 and Figure 14, respectively. [*Bligh19*] The most notable difference for the 1100C vehicle was that the center of gravity (c.g.) was set 6.15 inches farther back in the model compared to the test vehicle, which resulted in a 17 percent difference, and the height of the model was approximately 12 percent taller than the test vehicle. For the 2270P vehicle model, except for the *bumper extension* and the *wheel-well clearance*, all other measurements were within 10 percent of those measured on the test vehicle. The longitudinal c.g. and the vertical c.g. of the 2270P model was within 4 percent and 1 percent, respectively, compared to the test vehicle. The accelerometer for both the 1100C and the 2270P models were positioned at the c.g. of the vehicle.

VEHICLE PROPERTIES AND INFORMATION

Date: 5/24/2018 Test No.: 469468-3-1 Vin No.: KNADHA37A6652037
Year: 2010 Make: Kia Model: Rio
Odometer: 217070 Tire Size: 185/65R14 Tire Inflation Pressure: 32 psi

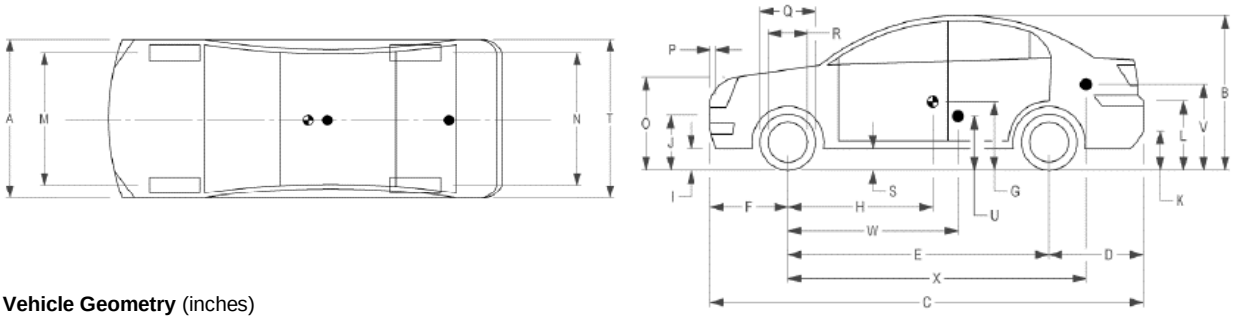

Vehicle Geometry (inches)

		Test	Model	% Error
a	Front Bumper Width:	66.38	65.67	-1.07
b	Overall Height:	51.5	57.68	11.99
c	Overall Length:	165.75	169.17	2.07
d	Rear Overhang:	34	37.09	9.08
e	Wheel Base:	98.75	99.92	1.19
f	Front Overhang:	33	32.13	-2.65
g	C.G. Height:		21.67	
h	C.G. Horz. Dist.	35.9	42.05	17.12
i	Front Bumper Bottom:	7.75	7.91	2.11
j	Front Bumper Top:	21.5	21.42	-0.38
k	Rear Bumper Bottom:	12.25	13.74	12.16
l	Rear Bumper Top:	25.25	25.20	-0.21
m	Front Track Width:	57.75	58.62	1.51
n	Rear Track Width:	57.7	57.64	-0.11
o	Hood Height:	28.25	31.73	12.33

		Test	Model	% Error
p	Bumper Extension:	4.12	3.66	-11.13
q	Front Tire Width:	22.5	22.99	2.19
r	Front Wheel Width:	15.5	15.08	-2.72
s	Bottom Door Height:	8.25	7.87	-4.56
t	Rear Bumper Width:	66.2	65.83	-0.56

Engine Type:	4 cylinder
Engine Size:	1.6 liter

Accelerometer Location (mm) - measured from front axle and ground

	X	Y	Z
Test Vehicle:	35.9	0	15.8
FEA Vehicle:	41.7	0	13.0

Weights (lbs)

	Curb			Gross Static		
	Test	Model	% Error	Test	Model	% Error
$W_{front\ axle}$	1583	-	-	1641	1511.2	-7.91
$W_{rear\ axle}$	907	-	-	971	1097.9	13.07
W_{total}	2518	-	-	2612	2609.1	-0.11

GVWR Ratings (lbs)	Test	Model	% Error
Front	1718	-	-
Rear	1874	-	-

Other Notes:

Figure 13. Vehicle property sheet for the 1100C vehicle model compared with the test vehicle in full-scale test 469468-3-1. [*Bligh19*]

VEHICLE PROPERTIES AND INFORMATION

Date: 5/22/2018 | Test No.: 469468-3-2 | Vin No.: 1C6RR6FPODS500861
Year: 2013 | Make: Dodge | Model: RAM 1500 Quad-Cab
Odometer: 173096 | Tire Size Front: 265/70R17 | Tire Size Rear: 245/70R17

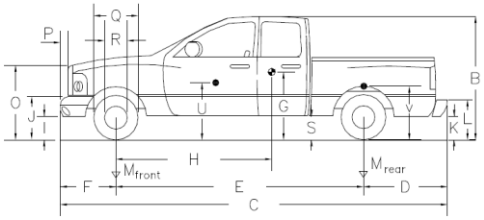

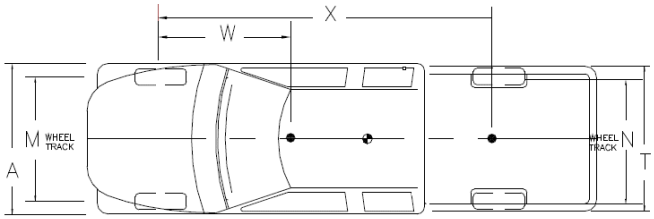

Vehicle Geometry (inches)

		Test	Model	% Error
a	Front Bumper Width:	78.50	76.02	-3.15
b	Overall Height:	74.00	75.51	2.04
c	Overall Length:	227.50	229.33	0.80
d	Rear Overhang:	44.00	48.31	9.79
e	Wheel Base:	140.50	140.20	-0.22
f	Front Overhang:	40.00	40.20	0.49
g	C.G. Height:	28.87	28.98	0.38
h	C.G. Horz. Dist.	62.40	60.11	-3.68
i	Front Bumper Bottom:	11.75	12.56	6.89
j	Front Bumper Top:	27.00	25.94	-3.91
k	Rear Bumper Bottom:	20.00	20.47	2.36
l	Rear frame Top:	30.00	31.14	3.81
m	Front Track Width:	68.50	69.49	1.44
n	Rear Track Width:	68.00	67.24	-1.11
o	Hood Height:	46.00	44.84	-2.52

		Test	Model	% Error
p	Bumper Extension:	3.00	2.6	-12.07
q	Front Tire Width:	30.50	31.8	4.17
r	Front Wheel Width:	18.00	18.4	2.36
s	Bottom of Body Height:	13.00	13.6	4.78
t	Overall Width:	77.00	79.3	2.98
u	Accelerometer Height:	27.75	27.7	-0.21
w	Accelerometer from Axle	62.40	62.4	0.00
	Wheel Center Height Front:	14.75	16.0	8.37
	Wheel Center Height Back:	14.75	16.0	8.37
	Wheel Well Clearance (F):	6.00	NA	
	Wheel Well Clearance (R):	9.25	11.9	28.54
	Frame Height (F):	12.00	12.6	4.66
	Frame Height (R):	25.50	27.0	5.76
	Engine Type:	V-8		
	Engine Size:			

Weights (lbs)

	Curb Test	Curb Model	Curb % Error
$W_{front\ axle}$	2850	-	-
$W_{rear\ axle}$	2106	-	-
W_{total}	4956	-	-

Accelerometer Location (inches) - measured from front axle and ground

	X	Y	Z

	Gross Static Test	Gross Static Model	Gross Static % Error
$W_{front\ axle}$	2870	2960	3.14
$W_{rear\ axle}$	2307	2221	-3.71
W_{total}	5177	5182	0.09

GVWR Ratings (lbs)	Test	Model	% Error
Front	3700	-	-
Rear	3900	-	-

Other Notes:

Figure 14. Vehicle property sheet for the 2270P vehicle model compared with the test vehicle in full-scale test 469468-3-2. [*Bligh19*]

CHAPTER 4 – FEA MODEL DEVELOPMENT

A detailed finite element model of the CP-MTL3 bridge rail design was developed, as shown in Figure 15. This model is based on the system drawings provided by MassDOT, which are included in Appendix A. The overall FEA model included a 52-ft length of the CP-MTL3 bridge rail and a 3-ft width of the bridge deck and sidewalk. The extension of the 5.5-ft sidewalk to curb at the edge of the roadway was modeled as a rigid surface. The basic components of the bridge rail model include:

- Eight (8) posts spaced at 6'-6" on center,
- Thirty-two (32) stainless steel screws (i.e., four at each post) with washers ,
- Eight (8) base plates (i.e., one at each post),
- Eight (8) anchor cages (i.e., one at each post connecting the base plate to the concrete parapet) including two anchor bars, two ferrules, and two anchor bolts with hardware,
- Two (2) tube rails that are 25.875 feet long (each),
- Sixteen (16) clamp bars (two at each post),
- One (1) splice tube, and
- Concrete parapet, sidewalk, and bridge deck with steel reinforcement.

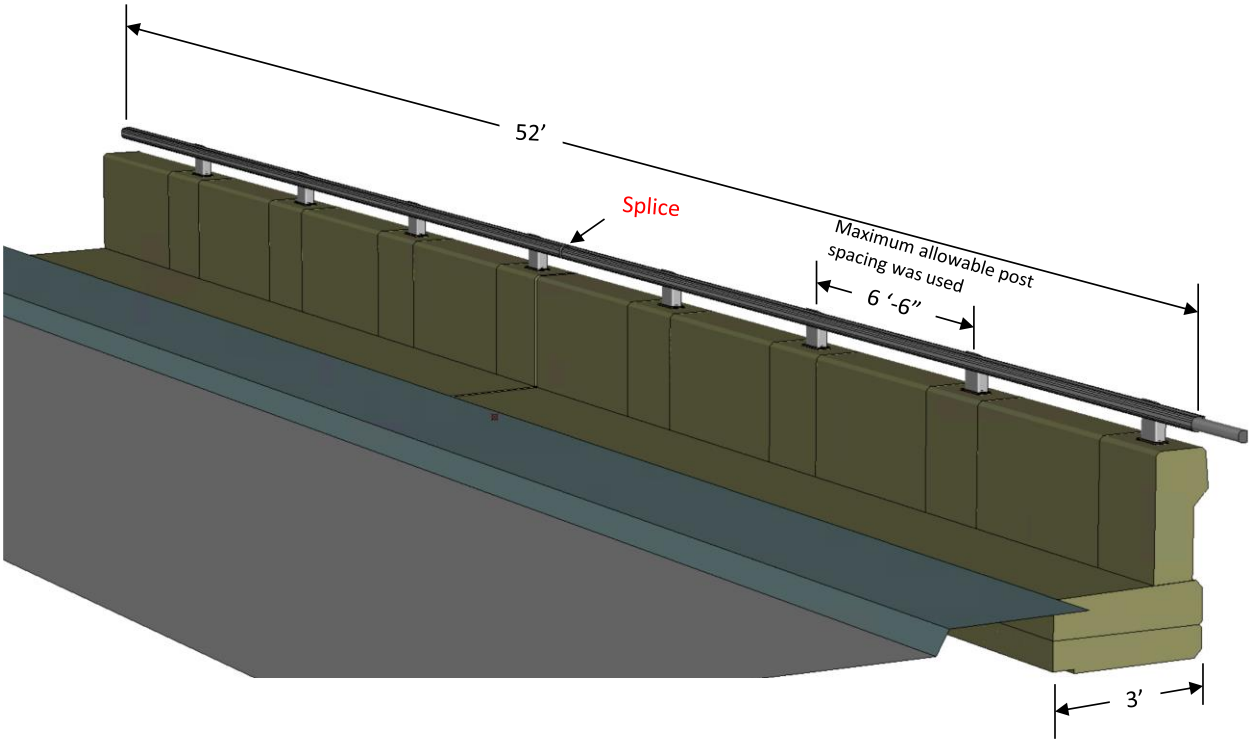

Figure 15. FEA model of the MassDOT CP-MTL3 bridge rail.

Materials

All steel and aluminum materials were modeled in LS-DYNA using material model Mat-Piecewise-Linear-Plasticity. For steel, the Young's modulus was set to 29,000 ksi and the Poisson's ratio was set to 0.33. For aluminum, the Young's modulus was set to 10,005 ksi and the Poisson's ratio was set to 0.33.

The aluminum material for posts, rails, and base plates were modeled as AISI 6061-T6. The calibration of the material properties was based on a nominal stress-nominal strain curve obtained from the literature and converted to true stress versus true strain for input into LS-DYNA. The stress strain data was digitized from the Atlas of Stress-Strain Curves 2nd Edition (2002) (Plate WA.181), which included a yield strength and tensile strength of 38.8 ksi and 50 ksi, respectively, and a percent elongation of approximately 14 percent. The minimum mechanical property values for 6061-T6 are 34.8 ksi and 42 ksi for yield strength and tensile strength, respectively, and 10 percent elongation. [*ASTM B209*]

The material for the stainless-steel fasteners is ASTM A193 Grade B8 Type 304. The stress strain data was digitized from the Atlas of Stress-Strain Curves 2nd Edition (2002) (Plate SS.041), which included a yield strength and tensile strength of 35.8 ksi and 84 ksi, respectively. [*ASM02*] The mechanical specifications for ASTM A193[1] include:

- Minimum Yield Strength = 30 ksi
- Minimum Tensile Strength = 75 ksi
- Minimum elongation = 30 percent

The 3/4" diameter anchor bolts were modeled as ASTM F3125 Grade A325 Type 1 with material properties based on engineering stress-strain properties measured by Kulak and converted to true-stress vs. true-plastic-strain for inclusion in the model. [*Kulak 2005*] The nominal yield strength was modeled as 91 ksi and the nominal tensile strength was modeled as 116 ksi.

The concrete material was modeled in LS-DYNA using material model MAT-RHT and MAT-CONCRETE-DAMAGE-REL3 with properties corresponding to unconstrained compressive strength of 4,000 psi. The material properties for the reinforcing steel conformed to ASTM A615 Grade 60 steel. [*TFHRC15*]

Posts

The geometry of the posts was modeled according to the detailed drawings in Appendix A. The FEA model of the post is shown in Figure 16. The post was modeled as ¼-inch-thick formed aluminum with a ½-inch-thick mounting plate, and a 1/8-inch-thick bearing pad. The post was modeled using thin-shell Belytschko-Tsay elements (Type 2 in LS-DYNA) with five integration points through the thickness. The part was meshed with a nominal element size of 0.5 x 0.37 inches, and the minimum element side length was 0.22 inches.

[1] https://www.portlandbolt.com/technical/specifications/astm-a193/

The mounting plate was modeled with thin-shell Type 2 elements with five integration points through the thickness. This part was meshed with a nominal element size of 0.33 x 0.34 inches, and the minimum element side length was 0.26 inches.

The bearing pad was modeled with thin-shell Type 2 elements with five integration points through the thickness. This part was meshed with a nominal element size of 0.30 x 0.36 inches, and the minimum element side length was 0.26 inches.

The material for all post parts was modeled as AISI 6061-T6. The weld connecting the post to the mounting plate was simulated using the tied-shell-edge-to-surface option in LS-DYNA.

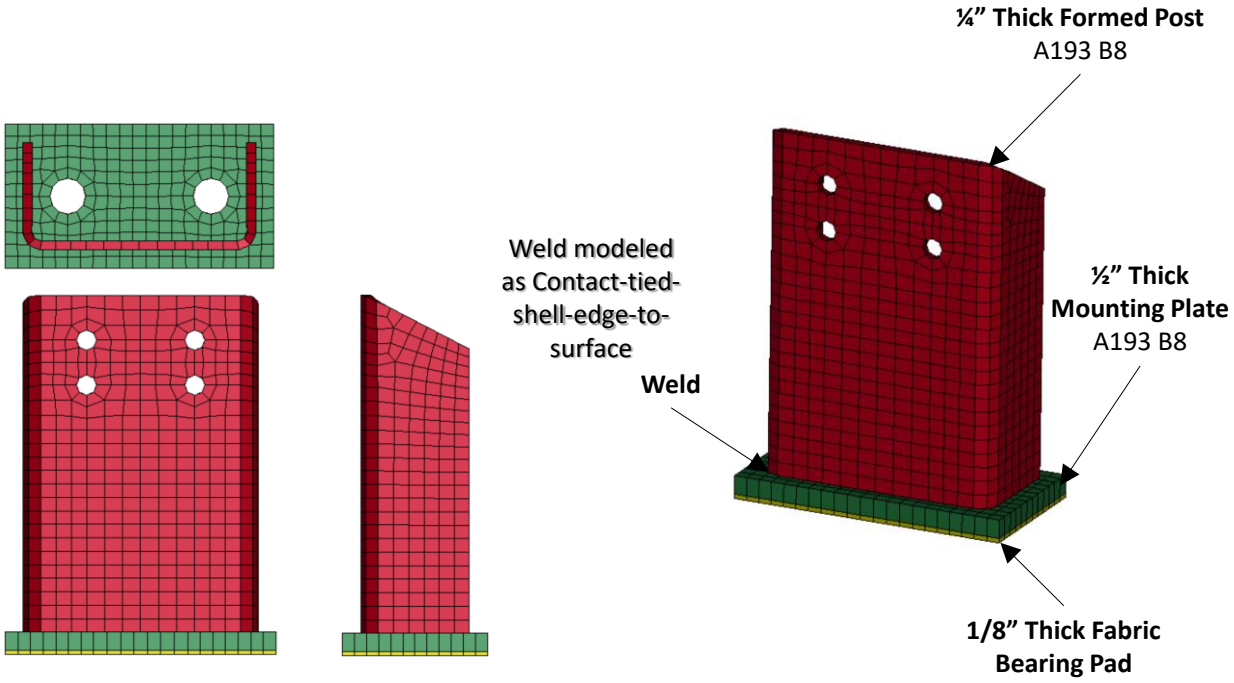

Figure 16. FEA mesh of aluminum bridge rail post.

Aluminum Railing and Splice Bar

A representative portion of the rail model is shown in Figure 17. The material for the railing conformed to AISI 6061-T6. The extruded rail was modeled using fully integrated thin shell elements modified for higher accuracy (Type -16 in LS-DYNA) including warping stiffness and five integration points through the thickness. The dimensions of the rail model and thickness for each section corresponded as closely as possible to the drawing details, as illustrated in Figure 17. The part was meshed with a nominal element size of 0.43 x 0.75 inches, and the minimum side length was 0.125 inches at the short side of the flange/tab, as indicated in Figure 17. This resulted in a total of 6.15 lb being added to the tab component over a 26 ft length of rail (3.6% increase).

The splice connection at the adjoining tube rails included a 36-inch-long open section bar inserted equal distance into each end of the adjoining rails. The material for the splice bar conformed to AISI 6061-T6, and the dimensions were modeled according to the drawing in Appendix A. The part was modeled with Type -16 shell elements in LS-DYNA with a thickness

of ¼ inch and with five integration points through the thickness. The splice bar was meshed with a nominal element size of 0.35 x 0.35 inches. One end of the splice bar was fastened to the main rail using constrained-spotwelds in LS-DYNA to simulate the two #10 screws, as illustrated in Figure 17. The other end of the splice bar was inserted into the adjoining main rail section and was free to slide inside the rail (see Appendix A for additional dimension details).

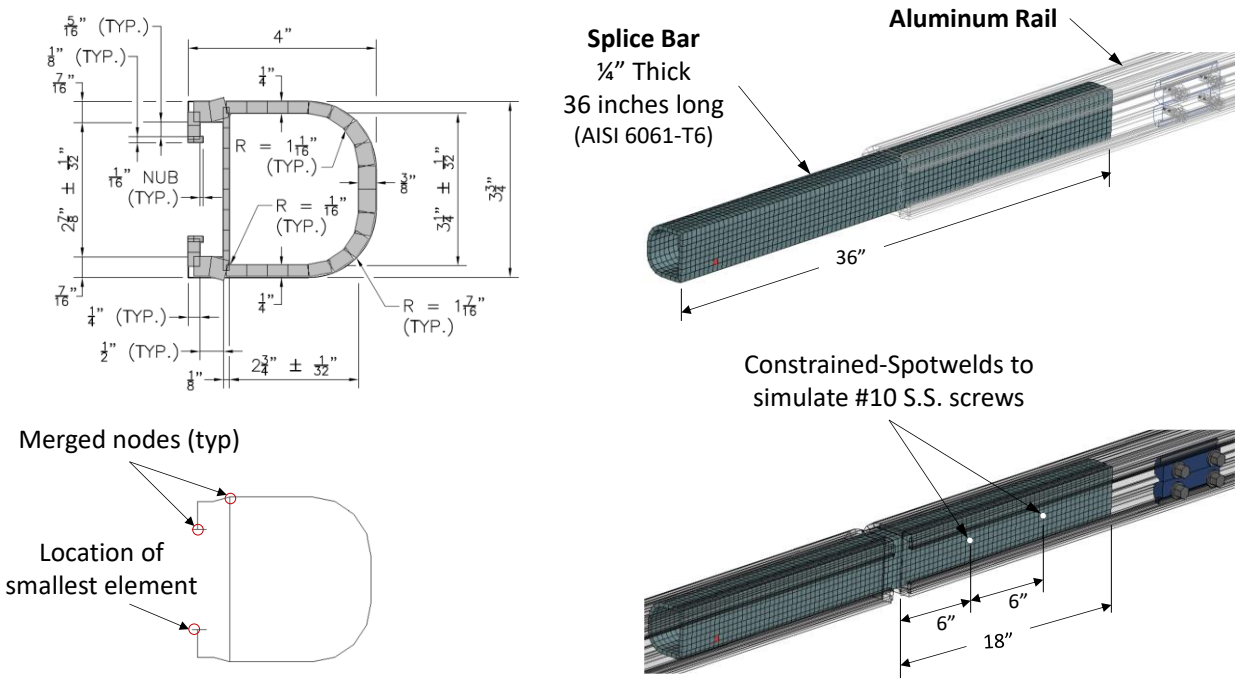

Figure 17. FEA model of aluminum rail and splice bar.

Rail-to-Post Mount

Two clamp bars are used at each post location to connect the rail to the post. Two ½-inch diameter holes are tapped into each clamp bar, and the rail is fastened to the post by passing two stainless steel screws through the holes. A flat washer was used under the head of each screw. The screws were embedded into the clamp bar and the threaded connection was modeled using constrained-nodal-rigid-bodies in LS-DYNA. Figure 18 shows the FEA model of the clamp bar overlaid with the drawing dimensions, and Figure 19 shows the model of the clamp bar used in the rail-to-post connection.

The clamp bar was modeled with fully integrated quadratic 8 node element with nodal rotations (Type 3 in LS-DYNA). The dimensions corresponded as closely as possible to the drawing details, as illustrated by the overlay of the FEA model and drawing in Figure 18. The part was meshed with a nominal element side length of 0.28 x 0.36 x .44 inches, and the minimum element side length was 0.267 inches. The tab on the clamp bar was modeled with Type -16 shell elements in LS-DYNA with warping stiffness. The material for the clamp bars corresponded to AISI 6061-T6.

The two ½-inch diameter stainless steel screws were modeled with Hughes-Liu beam elements (Type 1) with the *Piecewise-Linear-Plasticity* material model (Type 24) in LS-DYNA with properties corresponding to ASTM A 193 Grade B8 Type 304. The screws were modeled

with a nominal element length of 0.36 inches. The yield strength and tensile strength were 35.8 ksi and 84 ksi, respectively.

The bolts were preloaded to 4,060 lb at the start of the analysis using the *Initial-Axial-Force-Beam* option in LS-DYNA. The initial pre-load was applied to a single element on the bolt, which was modeled with element type Spot-Weld-Beam in LS-DYNA, and with material characterized using the Mat-Spotweld option. A rigid head and deformable washer was included to fasten the screws against the back surface of the post.

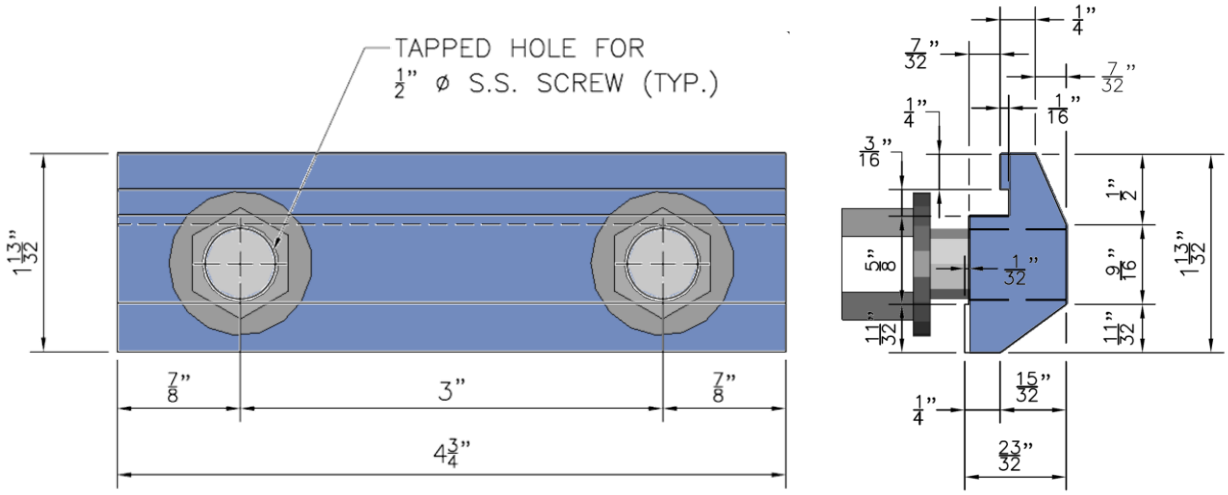

Figure 18. FEA model of clamp bar.

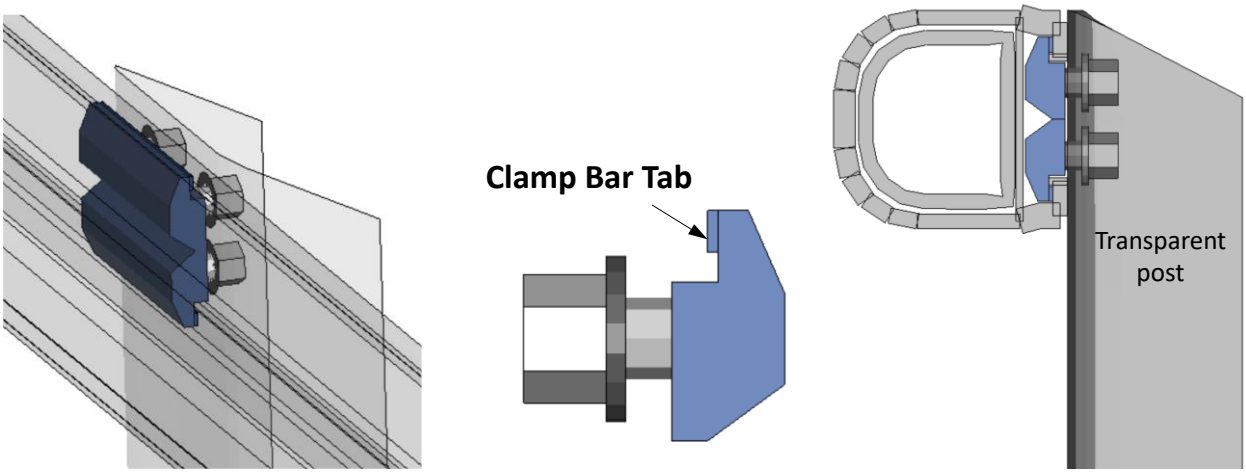

Figure 19. FEA Model of rail-to-post connection.

Anchor Cage

The FEA model of the anchor cage is shown in Figure 20. The ferrules were modeled with Type 2 thin shell elements in LS-DYNA with 5-integration points through the thickness. The material for the ferrules corresponded to ASTM A36. The anchor cage bars were modeled with Hughes-Liu beam elements (Type 1) with piecewise linear plasticity material (Type 24) in LS-DYNA with material properties corresponding to ASTM A615 Gr 60. The welded connection of the anchor-cage-bars to the ferrules was modeled using Type 9 elements in LS-

DYNA (spot weld beams) and *Mat-Spotweld. The anchor Bolts were modeled with Hughes-Liu beam elements (Type 1) with piecewise linear plasticity material (Type 24) in LS-DYNA with material properties corresponding the ASTM F3125 Gr A325. The nominal element length for the anchor bolts was 0.57 inches. The anchor bolts were fully embedded into the ferrules, and the threaded connection was modeled using constrained-nodal-rigid-bodies at 6 locations along the ferrule, as illustrated in Figure 20. A rigid nut and deformable washer were included to fasten the anchor rods against the top surface of the bearing plate.

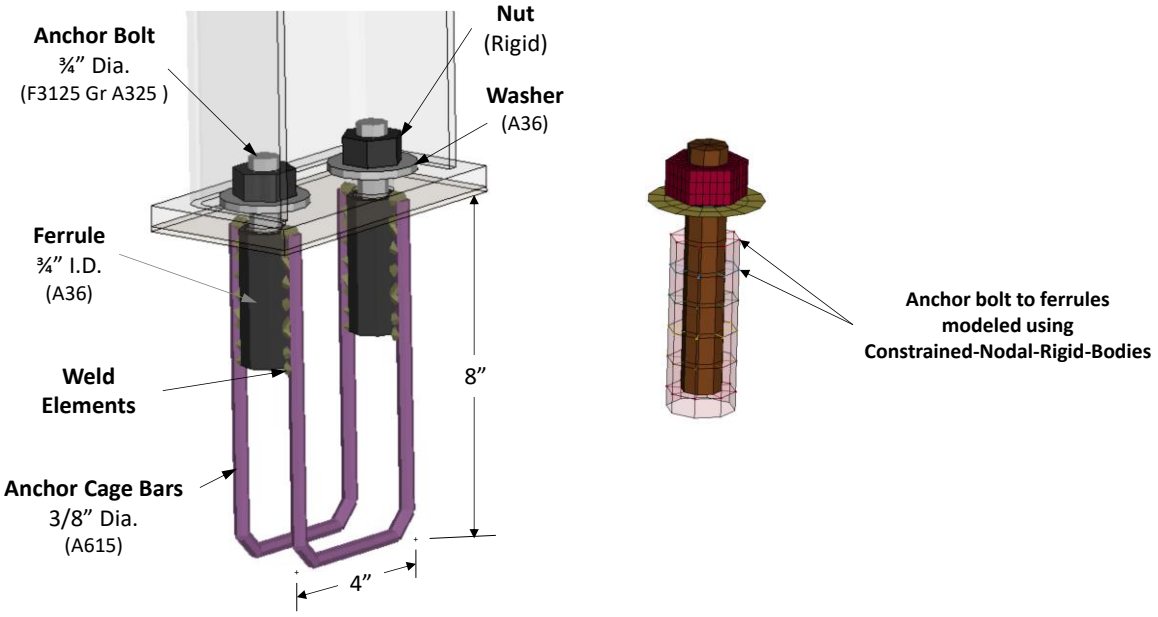

Figure 20. FEA model of anchor cage.

Concrete Parapet, sidewalk, and Deck

The concrete for the parapet and deck was modeled with Type 1 hexahedral elements in LS-DYNA with nominal element size of 1" x 1" x 1" in the regions where the posts are mounted and with nominal element size of 1" x 1" x 1.5" elsewhere, as illustrated in Figure 21. All reinforcing bars were modeled with Type 1 beam elements with a nominal element length of ½ inch. The material properties for the reinforcing steel conformed to ASTM A615 Grade 60 steel. [*TFHRC15*]

The concrete material for the parapet, sidewalk, and deck was modeled using two different concrete constitutive models in LS-DYNA (i.e., *Mat-RHT* and *MAT-Concrete-Damage-REL3)*. The material properties for the concrete in each case were based on an unconfined compressive strength of 4,000 psi (27.5 MPa) which corresponds to MassDOT's current minimum strength specification. Bonding of the reinforcing steel within the concrete was modeled using the *Constrained-Beam-in-Solid* option in LS-DYNA. Fixed constraints were imposed on the boundary ends of the rebar in the deck and on the boundary face of the concrete, as indicated in Figure 22 by "x" symbols. A 1.5" gap was included at the splice connection and in the concrete parapet to represent the expansion joint, as illustrated in Figure 23.

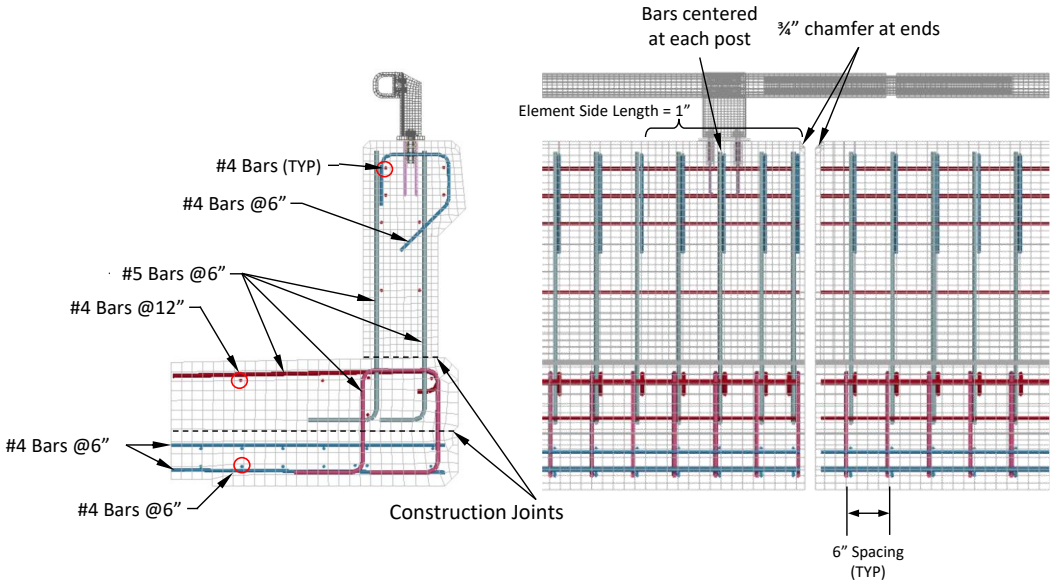

Figure 21. FEA mesh for the parapet, sidewalk, and deck.

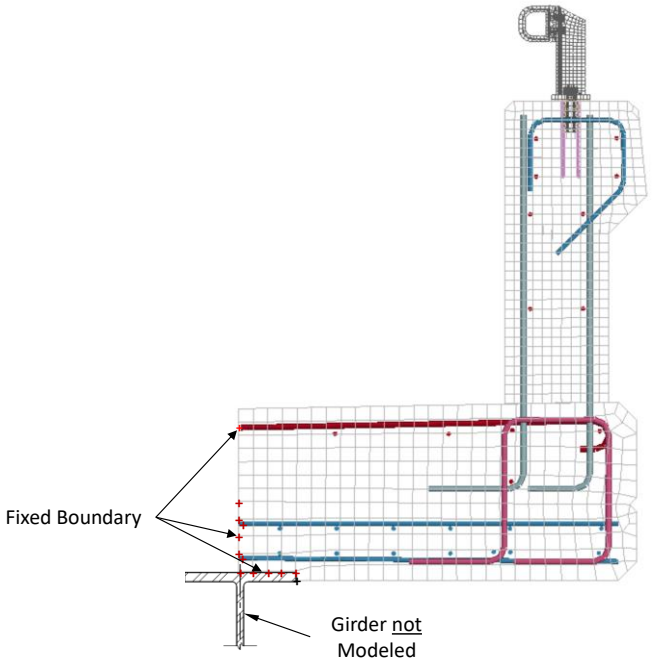

Figure 22. Boundary conditions used to model continuation of deck.

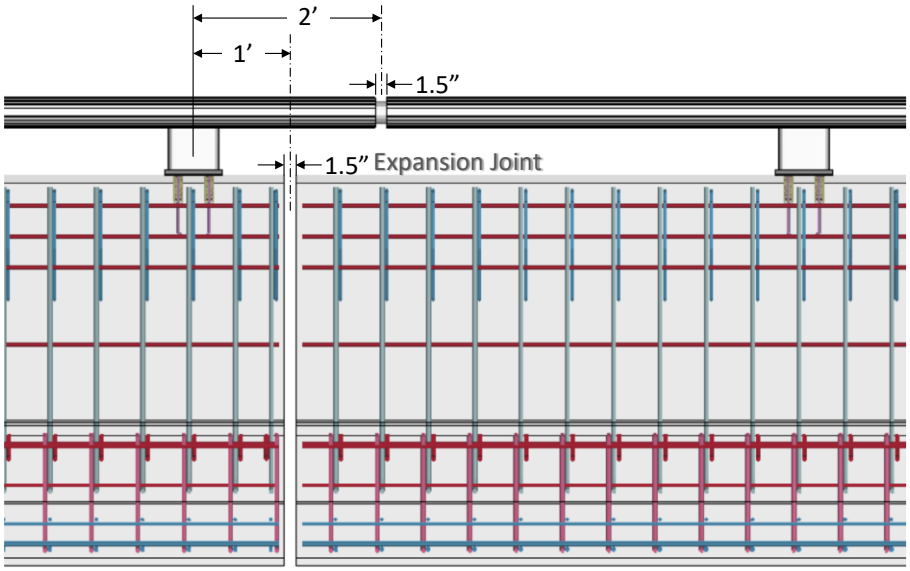

Figure 23. Expansion joint gap for the CP-MTL3.

The total width of the sidewalk is 5’-6” measured from the face of the parapet to the base of the curb. A 28-inch section of the sidewalk nearest to the parapet was modeled as deformable (see Figures 21 and 22). A rigid surface was then used to extend the sidewalk from the end of the deformable section out to the face of the curb using the rigidwall-planar-finite option in LS-DYNA. The curb on the face of the sidewalk is 6 inches tall and is sloped back 3.5 inches from the base of the curb to the top surface of the sidewalk.

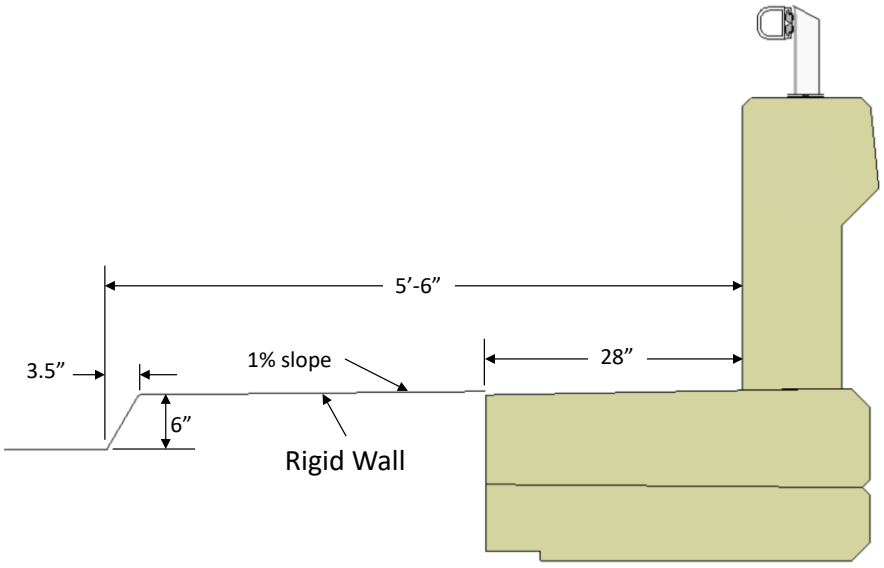

Figure 24. Sidewalk model.

Mitered End of Railing

The mitered end of the aluminum railing was modeled using fully integrated thin shell elements modified for higher accuracy (Type -16 in LS-DYNA) with warping stiffness and with five integration points through the thickness. The dimensions of the rail and thickness of the

cross-section corresponded as closely as possible to the drawing details, as illustrated by the overlay of the FEA model and the drawing in Figure 25. The joints were connected using merged nodes. The material was modeled as AISI 6061-T6. The part was meshed with a nominal element size of 0.43 x 0.75 inches, and the minimum side length was 0.125 inches at the short side of the flange/tab, as indicated in Figure 25.

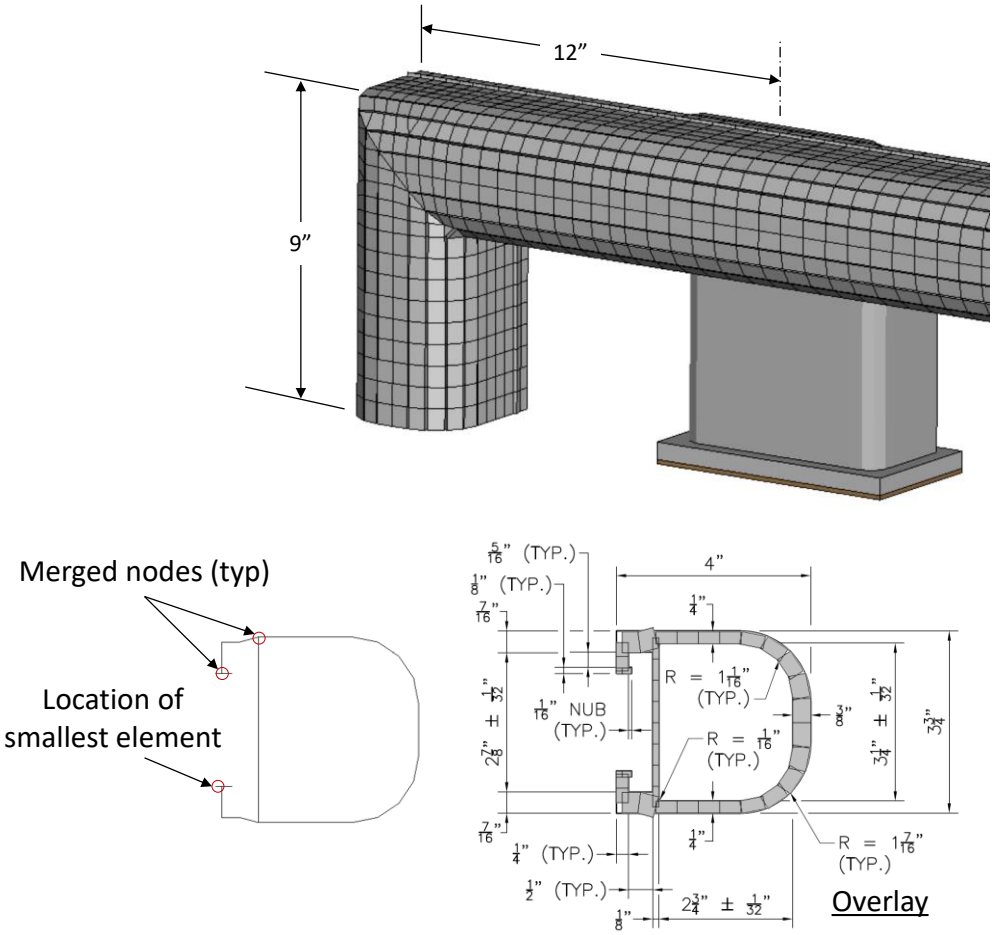

Figure 25. FEA model of mitered end of railing.

Clamp Bar at Mitered Rail

Two clamp bars are used at the mitered end to connect the rail to the concrete clip, as shown in Figure 26. Two ½-inch diameter holes are tapped into each clamp bar, and stainless-steel screws and washers are used to fasten to the post. The clamp bar was modeled with fully integrated quadratic 8 node element with nodal rotations (Type 3 in LS-DYNA). The part was modeled as AISI 6061-T6A. The two ½-inch diameter stainless-steel screws were modeled using Hughes-Liu beam elements (Type 1) with piecewise linear plasticity material (Type 24) in LS-DYNA with properties corresponding to ASTM A 193 Grade B8 Type 304. The screws were embedded into the clamp bar and the connection with the tapped hole was modeled using constrained-nodal-rigid-bodies in LS-DYNA.

The screws were preloaded to 4,060 lb at the start of the analysis using the *Initial-Axial-Force-Beam* option in LS-DYNA. The initial pre-load was applied to a single element on the

bolt, which was modeled with element type Spot-Weld-Beam in LS-DYNA, and with material characterized using the Mat-Spotweld option. A rigid head and deformable washer were included to fasten the screws against the back surface of the clip.

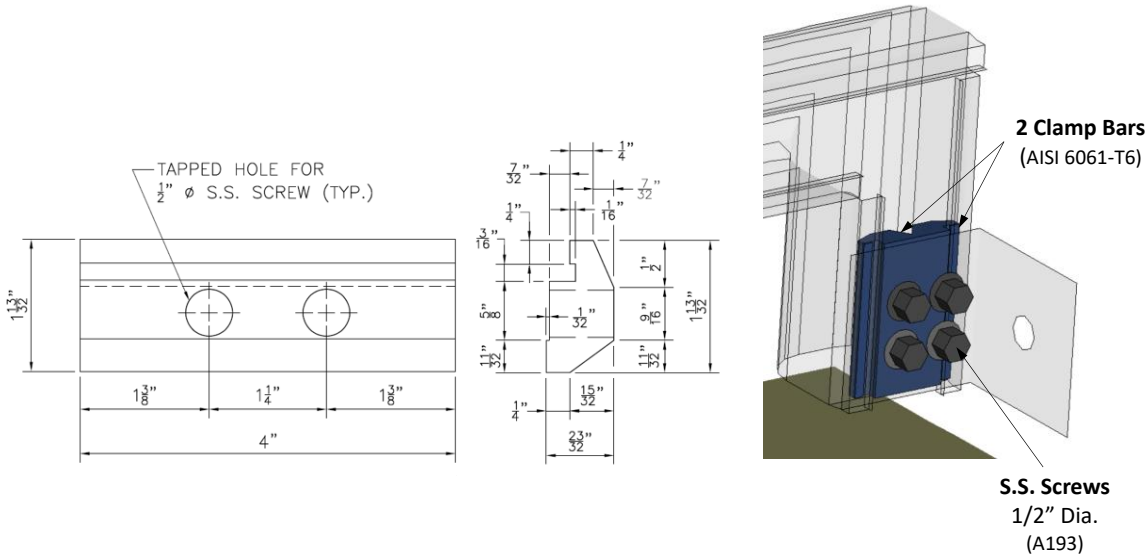

Figure 26. Clamp bar at mitered end of railing.

Concrete Clip

The L4x4x3/8 concrete clip was modeled with Type 16 shell elements in LS-DYNA with five integration points through the thickness. The dimensions of the clip model corresponded to the drawing details shown in Figure 27. The material was modeled as AISI 6061-T6. The part was meshed with a nominal element size of 0.35 x 0.35 inches.

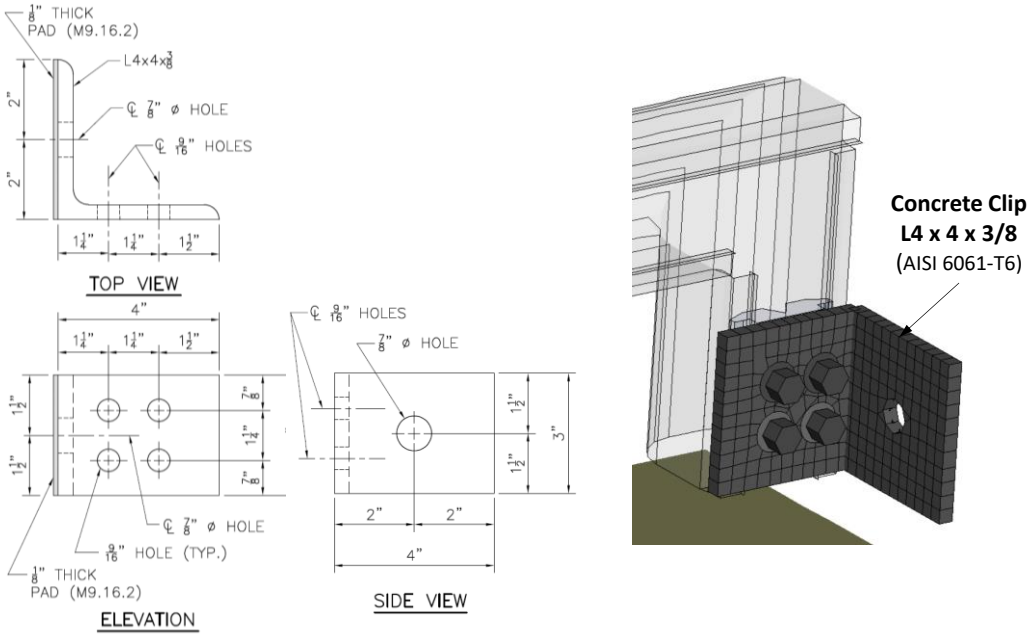

Figure 27. FEA model for concrete clip at transition.

Concrete Transition and Anchor Connection

The transition was modeled as a 42-inch-tall vertical parapet with ¾" chamfers at the edges. A 15.65-ft section of the transition was modeled. The face of the transition was flush with the face of the CP-MTL3 concrete parapet, and the top of the transition was flush with the top of the aluminum handrail. The transition was modeled with rigid material properties in order to simulate a worse-case scenario for vehicle snag. The surface of the transition was modeled with thin shell elements and was meshed with nominal element side length of 0.79 x 0.79 inches. The ¾-inch diameter anchor bolt connecting the clip to the concrete transition was modeled as a rigid SPC constraint in LS-DYNA.

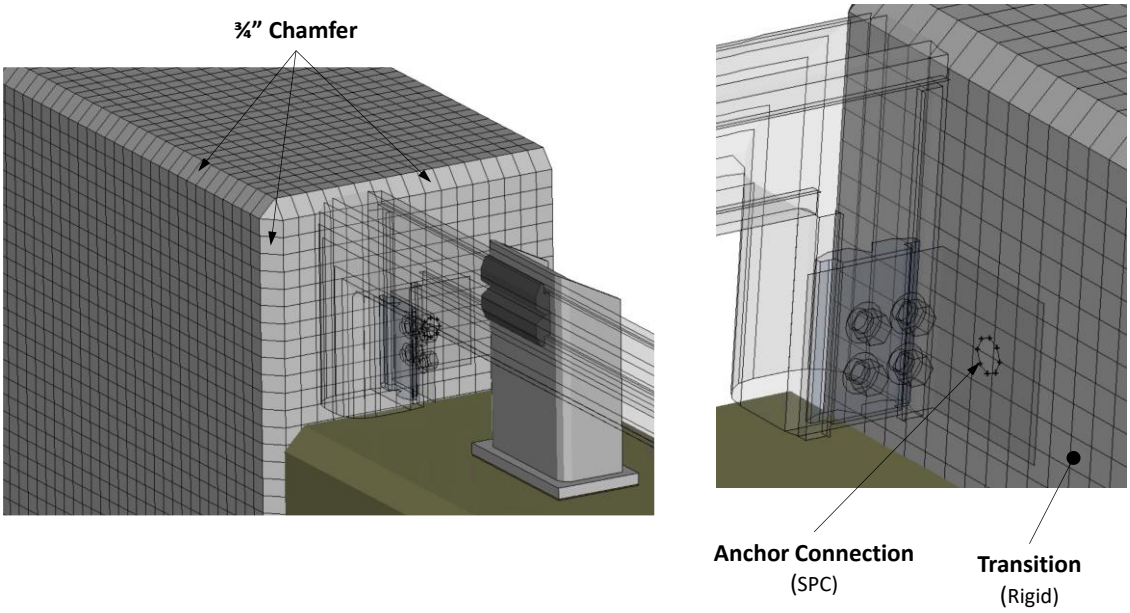

Figure 28. FEA model for the transition and anchor connection.

CHAPTER 5 – MASH TL3 EVALUATION OF THE CP-MTL3 WITH HANDRAIL AT EXPANSION JOINT

FEA was used to evaluate the crash performance of the CP-MTL3 with top-mounted handrail. The evaluations were based on structural adequacy, vehicle stability during and after redirection, and occupant risk factors using criteria specified in MASH for Test Level 3. The analyses were performed using LS-DYNA version mpp_s_R13 revision number R13.1.0-3-g4cd30680f9 with a time-step of 1.0 microsecond. The critical impact point was determined using FEA. The evaluations included:

- **Simulation of Test 3-10** with the 1100C Yaris model ballasted to a gross static weight of 2,609 lb (1183 kg) impacting the barrier at 62 mph and 25 degrees.
- **Simulation of Test 3-11** with the 2270P Chevrolet Silverado model ballasted to a gross static weight of 5,182 lb (2,351 kg) impacting the railing at 63 mph and 25 degrees.

Test 3-10

Analysis Cases

MASH considers the critical impact point (CIP) for longitudinal barrier to be the one most likely to result in a significant snag on the barrier system and which results in the highest occupant risk. For rigid longitudinal barriers, this is generally associated with a snag on post, rail splice, or an expansion joint. MASH Table 2-7 provides estimated CIP for passenger vehicle tests with rigid barriers. These estimates were based on full-scale testing under previous test procedures and may not be precise for MASH test vehicles; however, these values are considered to represent minimum distances for the CIP relative to the critical reference points for the test article.

In this case, two impact points were evaluated under Test 3-10 conditions. The first impact point was 3.6 ft upstream of the critical post, as illustrated in Figure 29, and was selected to maximize loading and potential snag at the critical post. For this analysis case, the initial impact point with the face of the sidewalk curb was 15.39 ft upstream of the critical post. The second target impact point was 4.6 ft upstream of the critical post, as illustrated in Figure 30, and was selected to maximize loading and potential snag at the expansion joint on the concrete parapet. For this analysis case, the initial impact point with the face of the sidewalk curb was 16.39 ft upstream of the critical post.

Each impact point was evaluated using two different concrete material models in LS-DYNA, which included *Mat-Concrete-Damage-Rel3 (a.k.a, KC) and *Mat-RHT, as described in Chapter 4. This resulted in a total of four analysis cases for Test 3-10.

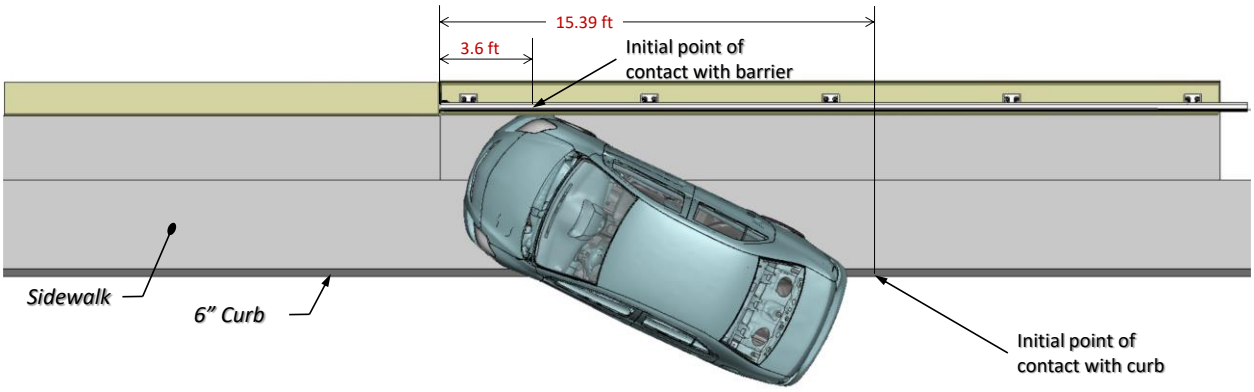

Figure 29. CIP 1 for Test 3-10 for maximizing snag on handrail post.

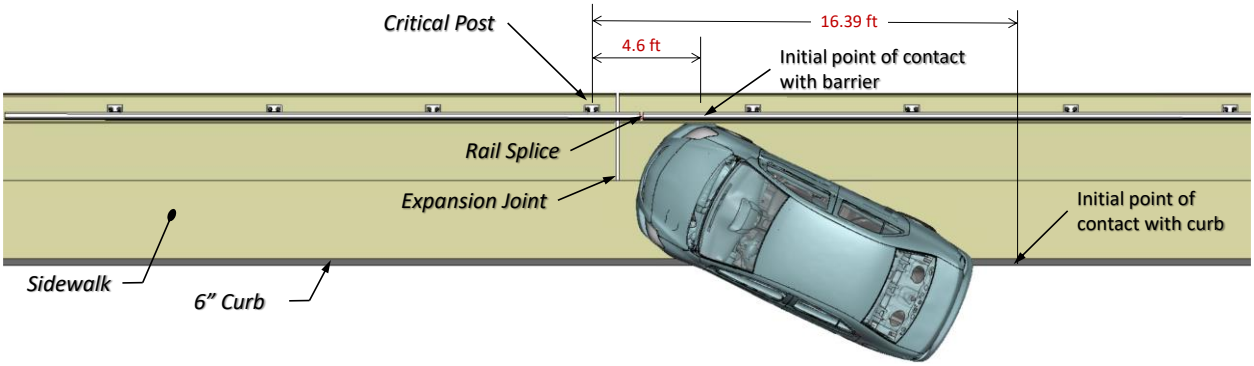

Figure 30. CIP 2 for Test 3-10 for maximizing snag at expansion joint.

Summary of Crash Event

The 2,609-lb Yaris model struck the curb-face of the sidewalk at a speed of 62 mph and at an impact angle of 25 degrees, as illustrated in Figures 29 and 30. The sequential views for impact at 3.6 ft upstream of the critical post are shown in Appendix B and Appendix C for the KC and RHT model cases, respectively. The sequential views of the impact event for impact at 4.6 ft upstream of the critical post are shown in Appendix D and Appendix E for the KC and RHT model cases, respectively. Additional details regarding the sequence of key events for the CIP case at 3.6 ft upstream of the critical post are provided in Table 3. The following sections provide time-history data evaluation, occupant risk assessments, and damages sustained by the barrier and vehicle.

Table 3. Sequence of events for Test 3-10 for CIP at 3.6 ft upstream of critical post.

Event		KC	RHT
1	Initial contact with curb - Front right tire contacts curb	0.000 sec Impact speed = 62.0 mph Impact angle = 25 deg	0.000 sec Impact speed = 62.0 mph Impact angle = 25 deg
2	Rear right tire crosses curb	0.100 sec	0.100 sec
3	Front left tire crosses curb	0.125 sec	0.125 sec
4	Rear right tire leaves the ground	0.125 sec	0.125 sec
5	Vehicle contacts barrier with bumper and fender	0.145 sec Impact speed = 60.2 mph Impact angle = 24.7 deg	0.145 sec Impact speed = 60.2 mph Impact angle = 24.7 deg
6	Front right tire compresses against barrierand begins to climb	0.150 sec	0.155 sec
7	Bumper passes rail splice	0.160 sec	0.160 sec
8	Bumper passes expansion joint	0.170 sec	0.170 sec
9	Peak 10-ms average x-acceleration	-21.10 G @ 0.170 sec	-20.80 G @ 0.168 sec
10	Peak 10-ms average y-acceleration	-36.14 G @ 0.172 sec	-35.80 G @ 0.171 sec
11	Rear right tire returns to ground	0.175 sec	0.170 sec
12	Bumper passes critical post	0.180 sec	0.180 sec
13	Front right tire returns to the ground	0.180 sec	0.185 sec
14	Maximum concrete parapet deflection	0.14-inches @ 0.185 sec	0.08-inches @ 0.185 sec
15	1st peak pitch angle (front pitched upward)	pitch = 3.6 deg at 0.190 sec	pitch = 3.6 deg at 0.190 sec
16	Front right wheel rim snags expansion joint	0.190 sec	0.190 sec
17	Rear left tire leaves the ground	0.190 sec	0.180 sec
18	Maximum occupant compartment deformation (OCD).	0.195 sec Maximum permenant OCD of 2.32 inches at the right-front toe pan at the wheel well	0.195 sec Maximum permenant OCD of 2.27 inches at the right-front toe pan at the wheel well
19	Front left tire leaves the ground	0.200 sec	0.210 sec
20	Maximum rail deflection at splice	0.37-inches @ 0.200 sec	0.20-inches @ 0.355 sec
21	Occupant impact with vehicle interior	0.2124 sec OIV_x = 25.3 ft/s OIV_y = 26.9 ft/s	0.2120 sec OIV_x = 24.3 ft/s OIV_y = 26.9 ft/s
22	Maximum ORA_x	-2.7 G @ 0.2268 - 0.2368 sec	-2.8 G @ 0.2266 - 0.2366 sec
23	Rear of vehicle contacts barrier (tail slap)	0.330 sec	0.325 sec
24	Maximum ORA_y	-12.5 G @ 0.3348 - 0.3448 sec	-12.0 G @ 0.3320 - 0.3420 sec
25	Vehicle loses contact with barrier	0.425 sec Exit speed = 42.8 mph Exit angle = 6.6 deg	0.450 sec Exit speed = 42.7 mph Exit angle = 7.1 deg
26	Maximum yaw (counter clockwise) begins to yaw clockwise	-32.1 deg @ 0.482 sec	-32.4 deg @ 0.515 sec
27	Vehicle front bumper passes end of barrier	0.515 sec	0.515 sec
28	Rear right tire leaves the ground	0.555 sec	0.55 sec
29	Front left tire returns to ground	0.730 sec	0.750 sec
30	Maximum pitch occurs (front pitched downward)	-5.9 deg @ 0.744 sec	-6.0 deg @ 0.747 sec
31	Rear left tire returns to ground	0.825 sec	0.850 sec
32	Maximum roll angle (roll away from barrier)	Max Roll = -14.9 deg @ 0.855 sec	Max Roll = -14.8 deg @ 0.868 sec
33	Rear right tire returns to ground	0.920 sec	0.95 sec
34	End of analysis	1.000 sec Speed = 37.8 mph Yaw angle = 26.9 deg	1.000 sec Speed = 38.3 mph Yaw angle = 27.5 deg

Time History Plots and Occupant Risk Measures

Figures 31 through 33 show the longitudinal, transverse, and vertical acceleration-time histories, respectively, computed from the center of gravity of the vehicle; Figures 34 through 36 show a comparison of angular rates and angular displacements (i.e., yaw, roll, and pitch) at the center of gravity of the vehicle. Table 4 shows the results for the occupant risk calculations.

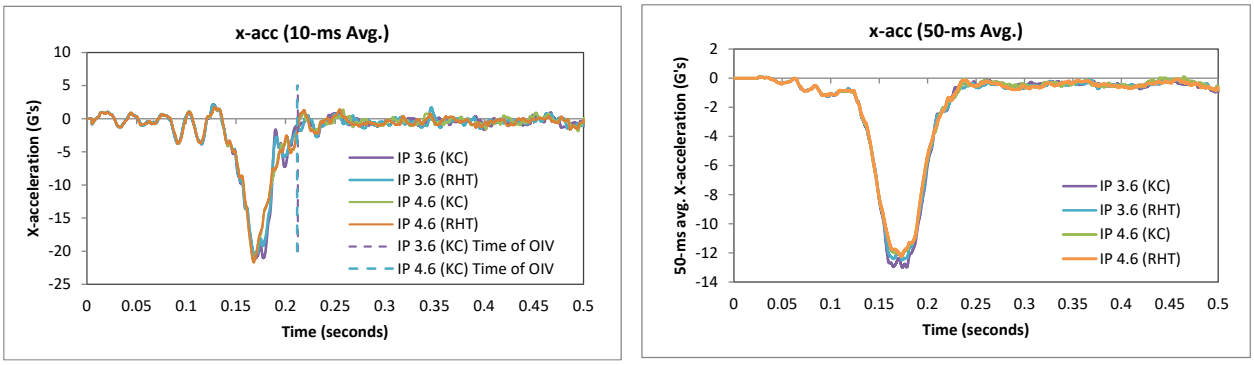

Figure 31. 10- and 50-millisecond running average X-acceleration from FEA for Test 3-10.

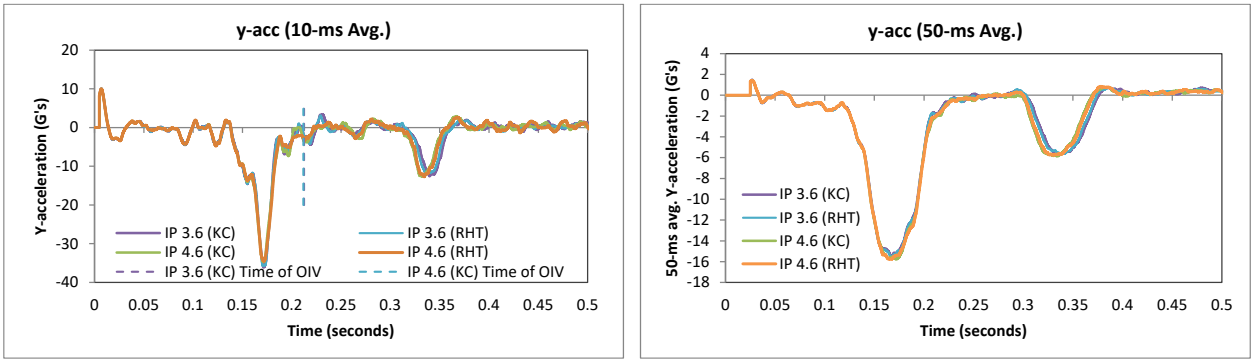

Figure 32. 10- and 50-millisecond running average Y-acceleration from FEA of Test 3-10.

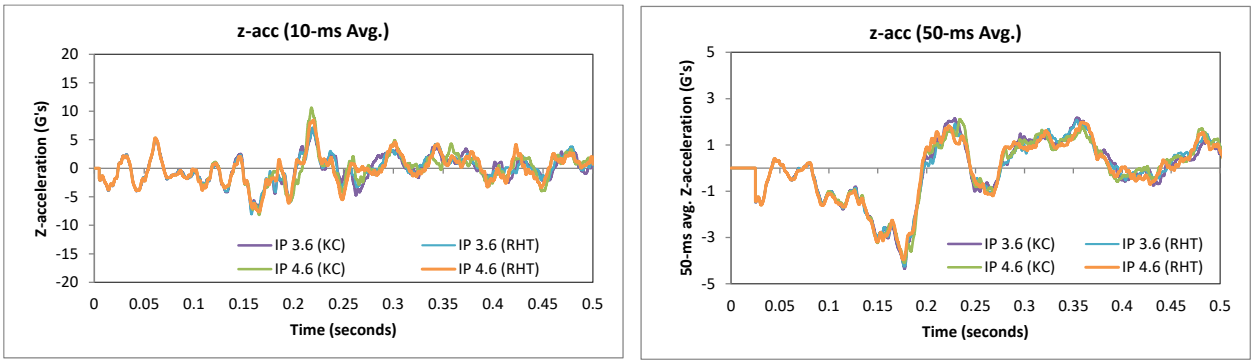

Figure 33. 10- and 50-millisecond running average Z-acceleration from FEA of Test 3-10.

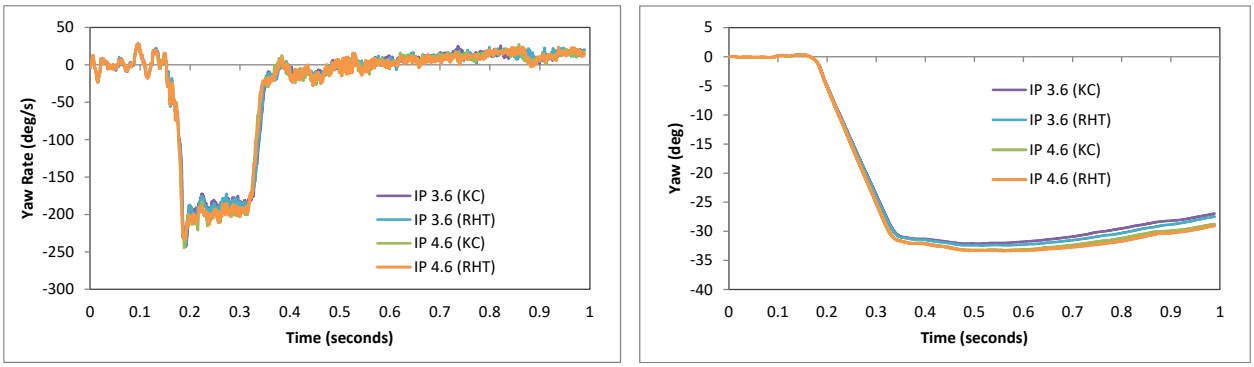

Figure 34. Yaw rate and yaw angle time-history from FEA of Test 3-10.

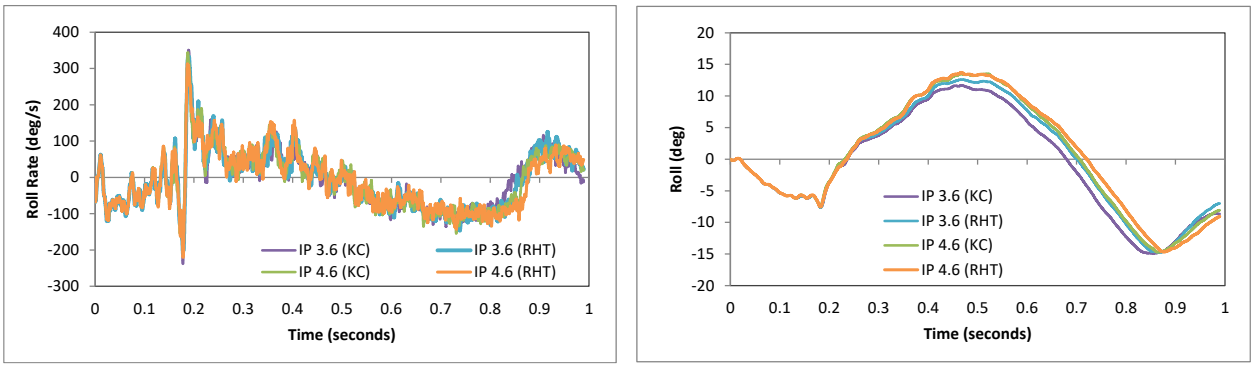

Figure 35. Roll rate and roll angle time-history from FEA of Test 3-10.

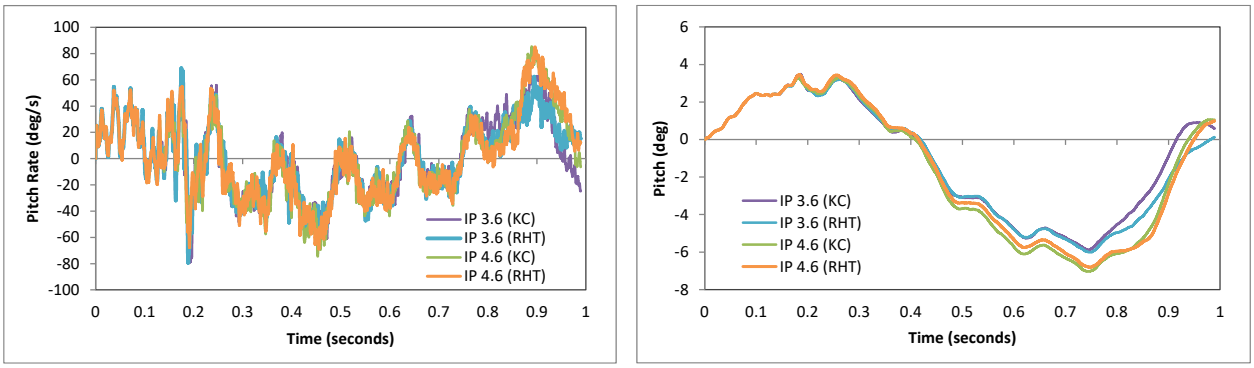

Figure 36. Pitch rate and pitch angle time-history from FEA of Test 3-10.

Impact Point 1: Impact at 3.6 ft

For the impact case at 3.6 ft upstream of the critical post, the peak 10-ms running average accelerations in the longitudinal direction were -21.1 G and -20.8 G for the KC and RHT cases, respectively, as shown in Figure 31. The peak 10-ms running average accelerations in the lateral direction were -36.1 G and –36.0 G for the KC and RHT cases, respectively, as shown in Figure 32. The occupant impact velocity (OIV) in the longitudinal direction ranged from 24.3 ft/s to 25.3 ft/s for the analysis cases. The OIV in the lateral direction was 26.9 ft/s. The highest ridedown acceleration (RA) in the longitudinal direction ranged from -2.7 to -2.8 G, and the highest RA in the lateral direction ranged from -12.0 to -12.5 G. All OIV and RA values were within the preferred limits recommended in MASH.

The first peak roll angle occurred during impact with the barrier at approximately 0.47 seconds of the impact with values ranging from 11.7 to 12.6 degrees (roll toward barrier), as shown in Figure 35. The maximum roll angle occurred during redirection and ranged from -14.8 to -14.9 degrees at approximately 0.86 seconds. The maximum pitch angle ranged from -5.9 to -6.0 degrees (rear pitching upward). All roll and pitch values were well within critical limits specified in MASH.

Impact Point 2: Impact at 4.6 ft

For the impact case at 4.6 ft upstream of the critical post, the peak 10-ms running average acceleration in the longitudinal direction was -21.3 G and -21.7 G for the KC and RHT cases, respectively, as shown in Figure 31. The peak 10-ms running average acceleration in the lateral direction was -34.8 G and -34.5 G for the KC and RHT cases, respectively, as shown in Figure 32. The occupant impact velocity (OIV) in the longitudinal direction ranged from 24.0 ft/s to 24.3 ft/s, and the OIV in the lateral direction ranged from 27.6 ft/s to 27.9 ft/s. The highest ridedown acceleration (RA) in the longitudinal direction ranged from -2.2 to -2.3 G, and the highest RA in the lateral direction was -12.7 G. All OIV and RA values were within the preferred limits recommended in MASH.

The first peak roll angle occurred during impact with the barrier at approximately 0.5 seconds of the impact with values ranging from 13.5 to 13.7 degrees (roll toward barrier), as shown in Figure 35. The maximum roll angle occurred during redirection and was -14.7 degrees at approximately 0.87 seconds. The maximum pitch angle ranged from -6.8 to -7.0 degrees (rear pitching upward). All roll and pitch values were well within critical limits specified in MASH.

Table 4. Summary of MASH occupant risk metrics for Test 3-10.

Occupant Risk Factors		MASH Test 3-10			
		IP 3.6 (KC)	IP 3.6 (RHT)	IP 4.6 (KC)	IP 4.6 (RHT)
Occupant Impact Velocity (ft/s)	x-direction	25.3	24.3	24.3	24.0
	y-direction	26.9	26.9	27.6	27.9
	at time	at 0.2124 seconds on right side of interior	at 0.2120 seconds on right side of interior	at 0.2117 seconds on right side of interior	at 0.2117 seconds on right side of interior
THIV (ft/s)		37.1 at 0.2083 seconds on right side of interior	37.1 at 0.2081 seconds on right side of interior	36.7 at 0.2078 seconds on right side of interior	36.7 at 0.2079 seconds on right side of interior
Ridedown Acceleration (g's)	x-direction	-2.7 (0.2268 - 0.2368 seconds)	-2.8 (0.2266 - 0.2366 seconds)	-2.2 (0.5241 - 0.5341 seconds)	-2.3 (0.2272 - 0.2372 seconds)
	y-direction	-12.5 (0.3348 - 0.3448 seconds)	-12 (0.3320 - 0.3420 seconds)	-12.7 (0.3276 - 0.3376 seconds)	-12.7 (0.3292 - 0.3392 seconds)
PHD (g's)		12.6 (0.3348 - 0.3448 seconds)	12.1 (0.3320 - 0.3420 seconds)	12.7 (0.3276 - 0.3376 seconds)	12.7 (0.3292 - 0.3392 seconds)
ASI		2.39 (0.1700 - 0.2200 seconds)	2.38 (0.1699 - 0.2199 seconds)	2.39 (0.1698 - 0.2198 seconds)	2.39 (0.1699 - 0.2199 seconds)
Max 50-ms moving avg. acc. (g's)	x-direction	-13 (0.1490 - 0.1990 seconds)	-12.5 (0.1487 - 0.1987 seconds)	-12.2 (0.1486 - 0.1986 seconds)	-12.2 (0.1478 - 0.1978 seconds)
	y-direction	-15.4 (0.1426 - 0.1926 seconds)	-15.6 (0.1427 - 0.1927 seconds)	-15.8 (0.1470 - 0.1970 seconds)	-15.8 (0.1417 - 0.1917 seconds)
	z-direction	-4.3 (0.1525 - 0.2025 seconds)	-4.3 (0.1522 - 0.2022 seconds)	-4.1 (0.1521 - 0.2021 seconds)	-4 (0.1510 - 0.2010 seconds)
Maximum Angular Disp. (deg)	Roll	-14.9 (0.8553 seconds)	-14.8 (0.8680 seconds)	-14.7 (0.8657 seconds)	-14.7 (0.8769 seconds)
	Pitch	-5.9 (0.7437 seconds)	-6 (0.7474 seconds)	-7 (0.7457 seconds)	-6.8 (0.7471 seconds)
	Yaw	-32.1 (0.4822 seconds)	-32.4 (0.5154 seconds)	-33.3 (0.5634 seconds)	-33.4 (0.5616 seconds)

Damages to the Barrier System

Figures 37 and 38 show images of maximum deflection of the barrier for impact at 3.6 ft and 4.6 ft upstream of the critical post, respectively. Deflection-time history plots at the point of maximum deflection are also shown in the figures. In all cases the rail deflection was relatively minimal and tended to coincide with impact of the rear of the vehicle against the barrier at approximately 0.35 seconds, and occurred near the midspan between posts 5 and 6, as illustrated in Figures 37 and 38. The maximum deflection in those cases was only 0.2 inches. Only one analysis case resulted in the highest deflection of the rail occurring during initial stages of the impact with the barrier at approximately 0.2 seconds. That case involved impact at 3.6 ft upstream of the critical post using the KC model, and the maximum deflection was 0.37 inches and occurred at the splice.

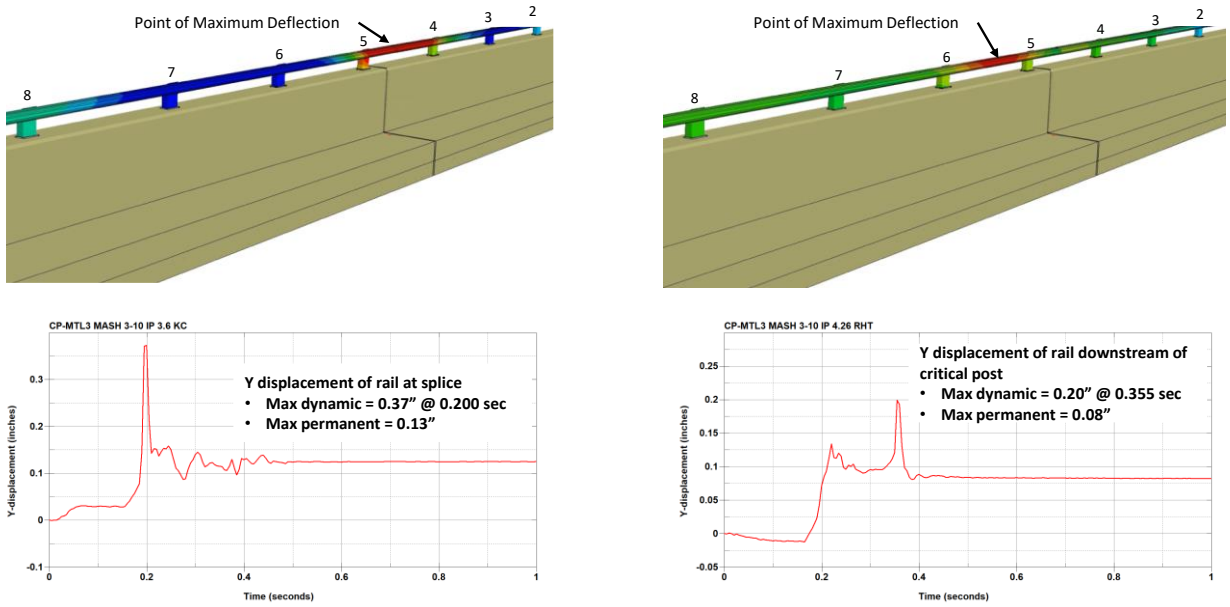

(a) 3.6 feet upstream of critical post – (KC)

(b) 3.6 feet upstream of critical post – (RHT)

Figure 37. Contour plot of lateral displacement for Test 3-10 at 3.6 ft upstream of critical post for (a) KC model and (b) RHT model.

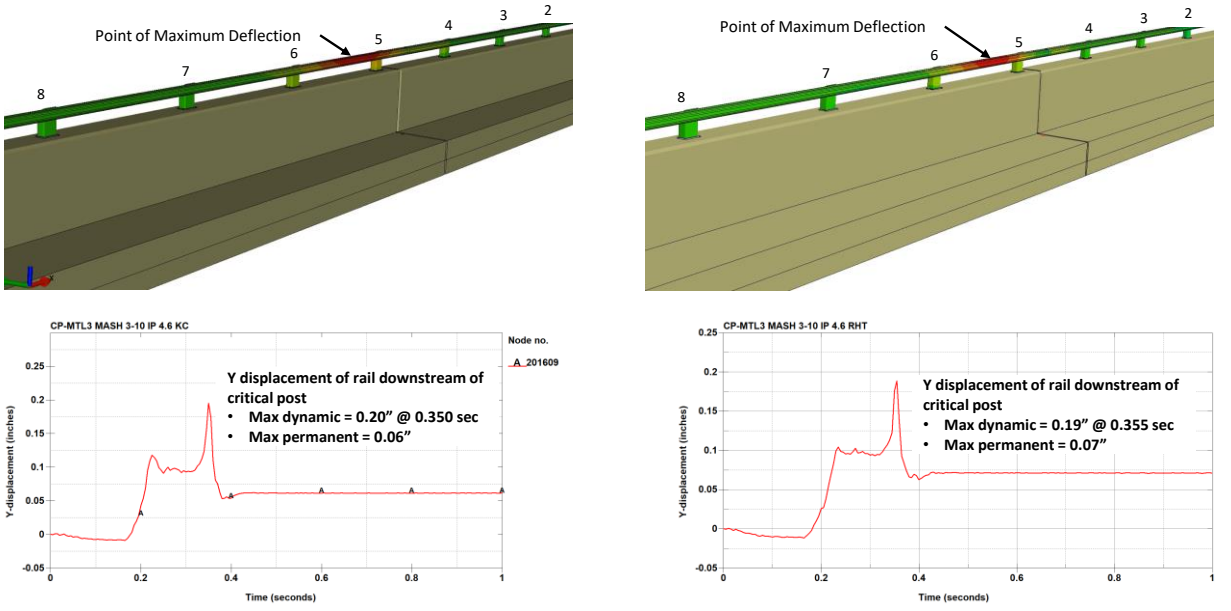

(a) 4.6 feet upstream of critical post – (KC)

(b) 4.6 feet upstream of critical post – (RHT)

Figure 38. Contour plot of lateral displacement for Test 3-10 at 4.6 ft upstream of critical post for (a) KC model and (b) RHT model.

Figure 39 shows a contour plot of effective plastic strain on the splice components. Due to the height of the barrier with respect to the small car, there was minimal contact between the car and the handrail during impact. As a result, there was no plastic strain in the splice components for any of the analysis cases.

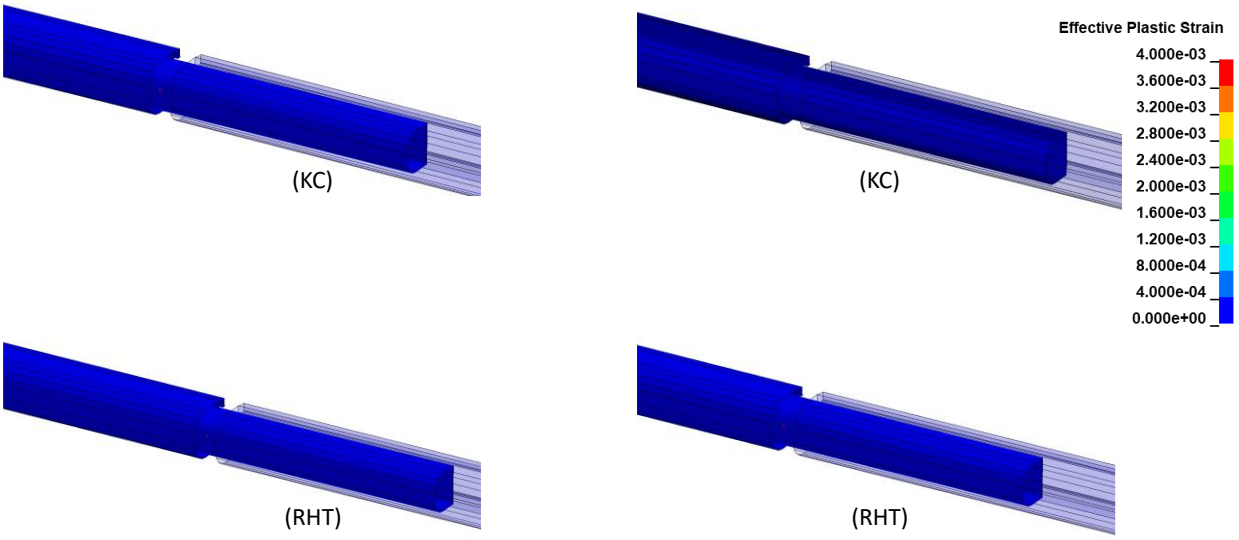

(a) Impact at 3.6 feet upstream of critical post **(b)** Impact at 4.6 feet upstream of critical post

Figure 39. Effective plastic strain contours on rail splice components during Test 3-10 for (a) impact at 3.6 ft and (b) 4.6 ft upstream of critical post.

Figure 40 shows contour plots of the damage parameter for each concrete model case, and Figure 41 shows contours of 1st principal strain. The results indicate potential for concrete spalling on the front face of barrier, as evident from the damage parameter contours, but little to no potential for any major damage or cracks in the concrete, as interpreted from the 1st principal strain contours. In an earlier project conducted by the research team, the RHT concrete material model was validated against full-scale tests involving a rigid pendulum impacting into fixed-fixed steel reinforced concrete columns. [*Ray18a; Ray18b*] The results of that study indicated that values of 1st Principal strain of 0.05 to 0.065 (yellow contours) indicated initial moderate crack openings in the concrete, when correlated to the column impact tests, and that strains values of 0.065 to 0.08 (orange/red contours) corresponded to significant crack openings.

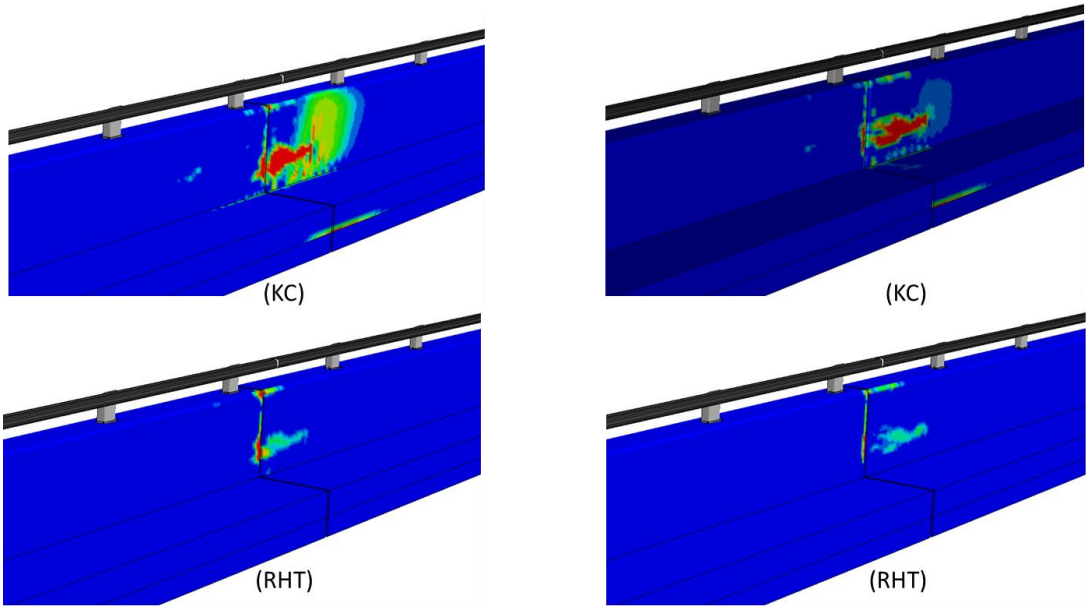

(a) Impact at 3.6 ft upstream of critical post **(b)** Impact at 4.6 ft upstream of critical post

Figure 40. Contour plot of the damage variable on the concrete parapet and deck during Test 3-10 for (a) impact at 3.6 ft and (b) 4.6 ft upstream of critical post.

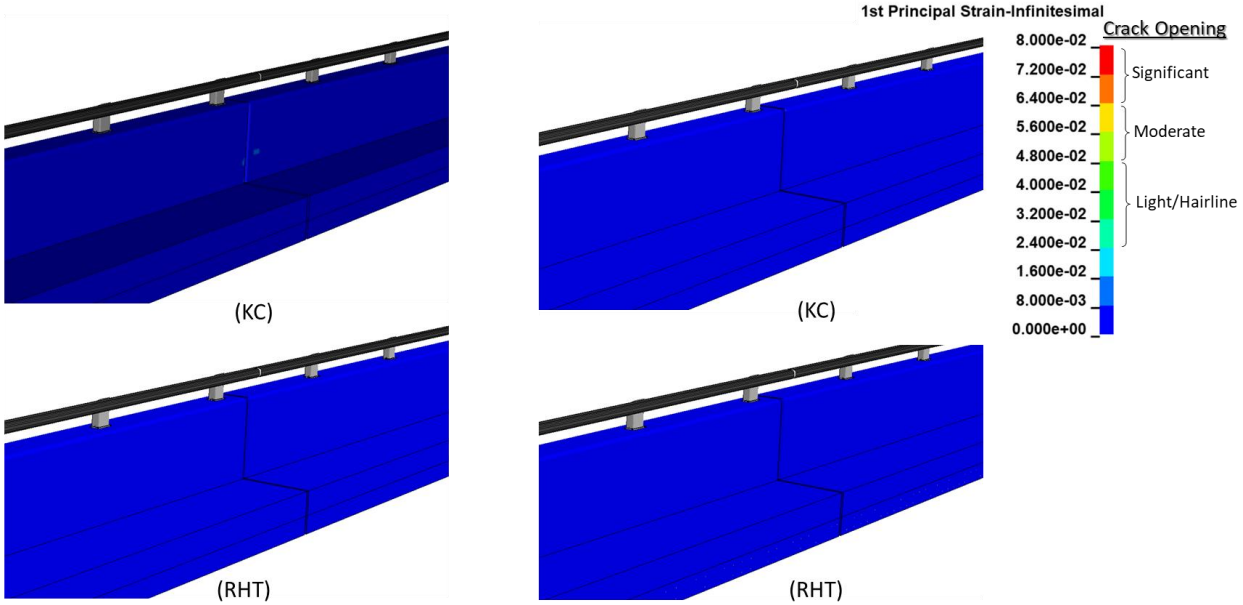

(a) Impact at 3.6 ft upstream of critical post **(b)** Impact at 4.6 ft upstream of critical post

Figure 41. Contour plot of 1st principal strain on the concrete parapet and deck during Test 3-10 for (a) impact at 3.6 ft and (b) 4.6 ft upstream of critical post.

Damages to Vehicle

Figure 42 shows contour plots of effective plastic strain for the vehicle during Test 3-10 for each analysis case. The damage to the vehicle was limited to the impact side front bumper, fender, front wheel assembly, front edge of door, rear side panel, and the rear wheel.

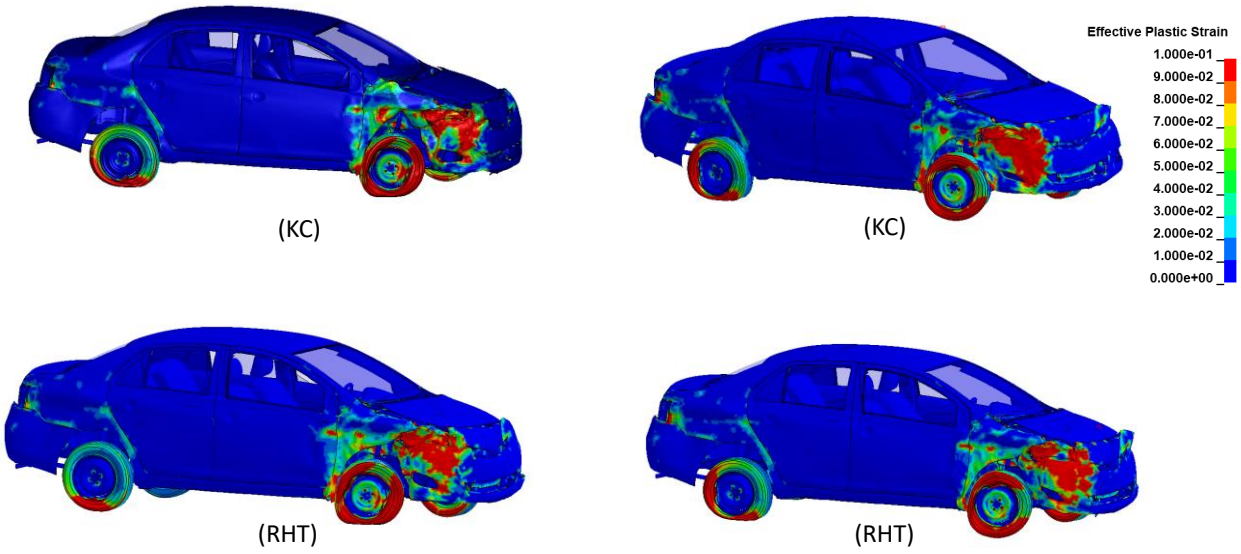

(a) Impact at 3.6 feet upstream of critical post **(b)** Impact at 4.6 feet upstream of critical post

Figure 42. Damages to vehicle in Test 3-10 for (a) impact at 3.6 ft and (b) 4.6 ft upstream of critical post.

Occupant Compartment Deformation (OCD)

The maximum deformation of the occupant compartment ranged from 2.20 – 2.32 inches and occurred at the right, front toe-pan at the wheel well for all analysis cases. Figure 43 shows a post-impact view of the vehicle floor pan with all other components removed to facilitate viewing. The maximum deformation was less than the critical limit of 9 inches specified in MASH for this area of the occupant compartment.

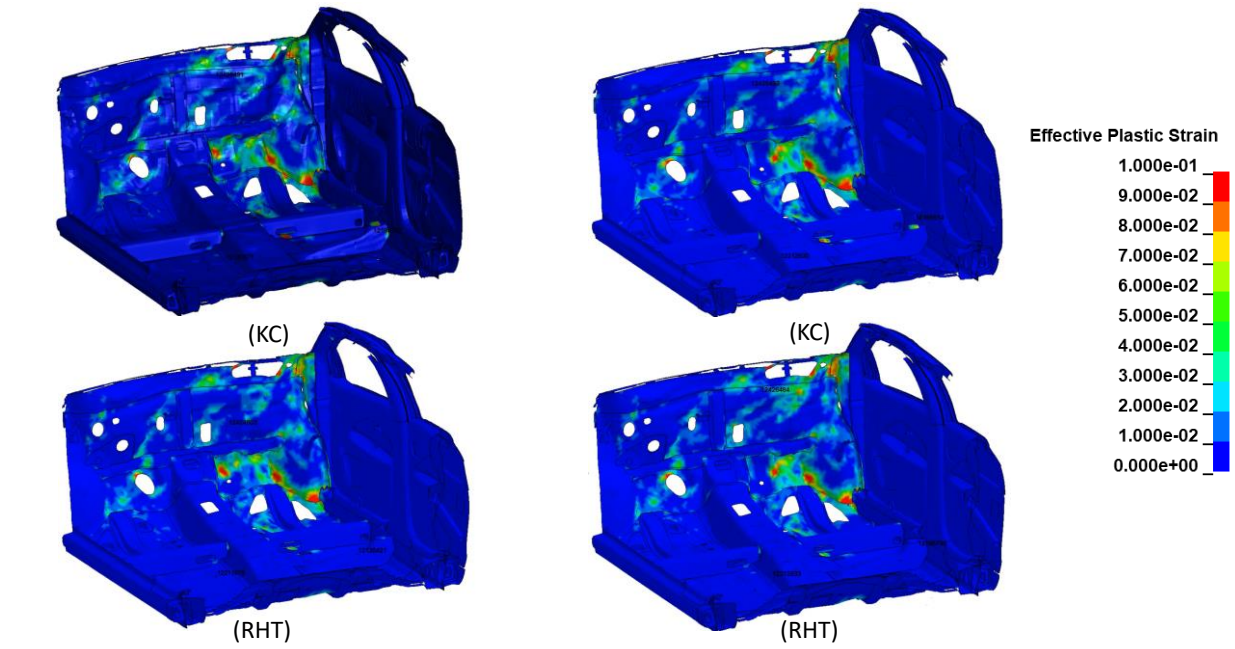

(a) Impact at 3.6 ft upstream of critical post **(b)** Impact at 4.6 ft upstream of critical post

Figure 43. Occupant compartment deformation resulting from Test 3-10 for (a) impact at 3.6 ft and (b) 4.6 ft upstream of critical post.

Exit Box

Figure 44 shows the exit box for Test 3-10. Although the exit box analysis is not required in MASH, it was included here for completeness. The post trajectory response was similar for all cases, and the vehicle was redirected with its path well within the exit box criteria of MASH.

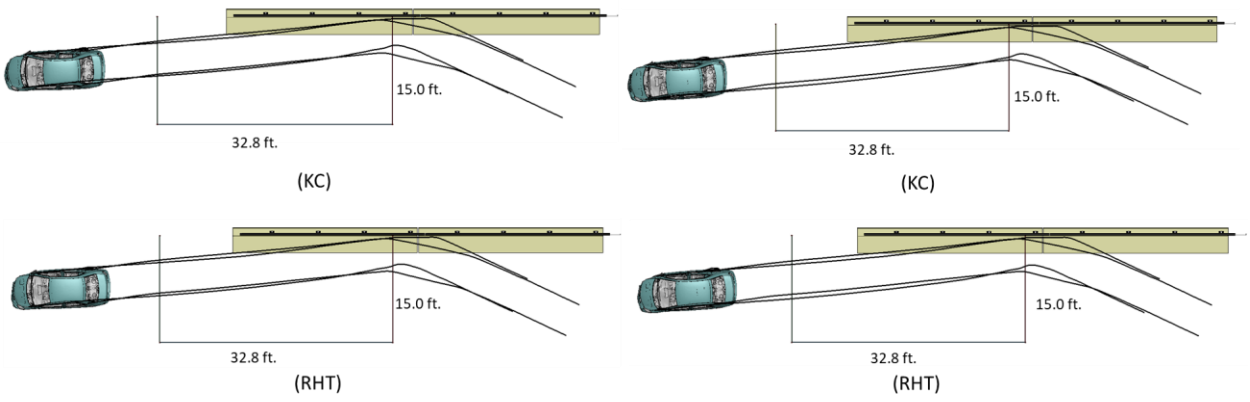

(a) Impact at 3.6 ft upstream of critical post **(b)** Impact at 4.6 ft upstream of critical post

Figure 44. Exit box for Test 3-10 for (a) impact at 3.6 ft and (b) 4.6 ft upstream of critical post.

Results Summary

A summary of MASH Test 3-10 results is shown in Table 5 and in Figures 45 through 48. The bridge rail successfully contained and redirected the small car with minimal damage to the concrete parapet and aluminum handrailing. There were no detached elements from the barrier that showed potential for penetrating into the occupant compartment or presenting undue hazard to other traffic. The maximum occupant compartment deformation was well within critical limits specified in MASH. The windshield showed no sign of cracking or failure. The vehicle remained upright and did not experience excessive roll or pitch angle displacements. The vehicle also remained within the exit-box criteria of MASH. The OIV and maximum RA values were within preferred limits specified in MASH. Based on the results of this analysis, the barrier is expected to meet all structural and occupant risk criteria in MASH for Test 3-10 impact conditions.

CIP Recommendation for Test 3-10 for CP-MTL3 at Expansion Joint

The recommended CIP for Test 3-10 for this section of the bridge rail is 3.6 ft upstream of the critical post positioned 12 inches downstream of the expansion joint in the concrete parapet. As mentioned previously, the OIV's and the RAs were within preferred limits for all cases; however, the values in the longitudinal direction were slightly higher for the impact point at 3.6 ft, and the values in the lateral direction were slightly higher for the impact at 4.6 ft upstream of the critical post. The OCDs were essentially the same for all cases. There was negligible contact between the vehicle and the handrail in all cases, and, consequently, the deflections of the handrail were also negligible. The deflections of the concrete parapet were negligible for all cases as well, and the maximum deflections were less than 3/16 inch. It is the researcher team's opinion that both cases (i.e., 3.6 ft or 4.6 ft) provide equivalent potential for being the more critical, so it was decided to remain consistent with the recommendation provided in MASH for Test 3-10 on rigid barriers.

Table 5. Summary of MASH Test 3-10 for the CP-MTL3.

Evaluation Factors		Evaluation Criteria	Impact at 3.6 ft		Impact at 4.6 ft	
			KC	RHT	KC	RHT
Structural Adequacy	A	Test article should contain and redirect the vehicle or bring the vehicle to a controlled stop; the vehicle should not penetrate, underride, or override the installation although controlled lateral deflection of the test article is acceptable.	Pass	Pass	Pass	Pass
Occupant Risk	D	Detached elements, fragments, or other debris from the test article should not penetrate or show potential for penetrating the occupant compartment, or present undue hazard to other traffic, pedestrians, or personnel in a work zone. Deformations of, or intrusions into, to occupant compartment should not exceed limits set forth in Section 5.2.2 and Appendix E.	Pass	Pass	Pass	Pass
	F	The vehicle should remain upright during and after collision. The maximum roll and pitch angles are not to exceed 75 degrees.	Pass	Pass	Pass	Pass
	H	The longitudinal and lateral occupant impact velocity (OIV) shall not exceed 40 ft/s, with a preferred limit of 30 ft/s.	Pass	Pass	Pass	Pass
	I	The longitudinal and lateral ridedown acceleration (RA) shall not exceed 20.49 G, with a preferred limit of 15.0 G	Pass	Pass	Pass	Pass

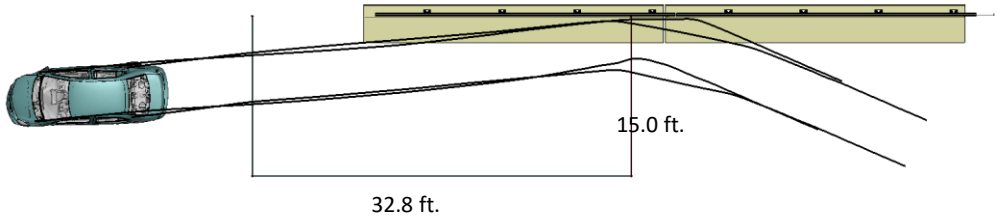

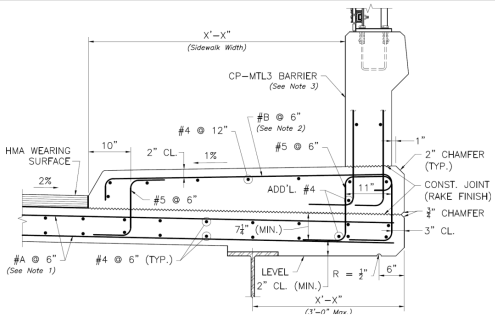

General Information

Analysis Agency	Roadsafe LLC
Test Standard Test No.	MASH Test 3-10
Analysis No.	CP-MTL3_Test3-10-IP3p6ft_KC
Analysis Date	5/28/2023

Test Article

Type	Bridge Rail
Name	CP-MTL3
Installation Length	52.0 feet
Material or Key Elements	Continuous concrete with top mounted aluminum post-and-beam rail
Soil Type and Condition	NA

Analysis Vehicle

Type / Designation	1100C
FEA Model name	YarisC_V1I_R200522.k w/ RS tire
Mass	2,595 lb

Impact Conditions

Speed	62.0 mph
Angle	25 degrees
Location	3.6 ft upstream of post
Impact Severity	55.7 kip-ft

Exit Conditions

Speed	42.8 mph
Angle	6.6 degrees
Time	0.425 seconds

Occupant Risk Values

Longitudinal OIV	25.3 ft/s
Lateral OIV	26.9 ft/s
Longitudinal ORA	-2.7 g
Lateral ORA	-12.5 g
THIV	37.1 ft/s
PHD	12.6 g
ASI	2.39

Max50-millisecond Avg. (G)

Longitudinal	-13.0 g
Lateral	-15.4 g
Vertical	-4.3 g

Test Article Deflections (in)

Dynamic	0.37 inches
Permanent	0.13 inches
Working Width	15.14 inches
Max. OCD	2.32 inches

Vehicle Stability

Roll	-14.9 degees
Pitch	-5.9 degrees
Yaw	-32.1 degrees

Figure 45. Summary results for MASH Test 3-10 with impact point at 3.6 ft upstream of post (KC model).

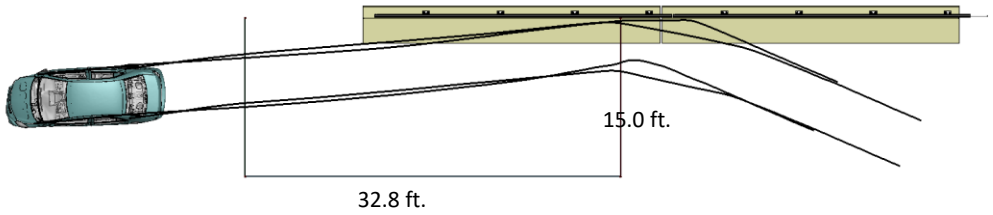

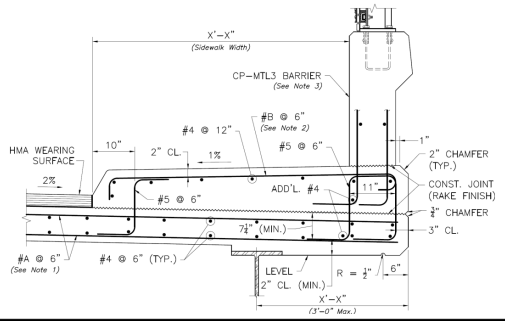

General Information

Analysis Agency	Roadsafe LLC
Test Standard Test No.	MASH Test 3-10
Analysis No.	CP-MTL3_Test3-10-IP3p6ft_RHT
Analysis Date	5/29/2023

Test Article

Type	Bridge Rail
Name	CP-MTL3
Installation Length	52.0 feet
Material or Key Elements	Continuous concrete with top mounted aluminum post-and-beam rail
Soil Type and Condition	NA

Analysis Vehicle

Type / Designation	1100C
FEA Model name	YarisC_V1I_R200522.k w/ RS tire
Mass	2,595 lb

Impact Conditions

Speed	62.0 mph
Angle	25 degrees
Location	3.6 ft upstream of post
Impact Severity	55.7 kip-ft

Exit Conditions

Speed	42.7 mph
Angle	7.1 degrees
Time	0.450 seconds

Occupant Risk Values

Longitudinal OIV	24.3 ft/s
Lateral OIV	26.9 ft/s
Longitudinal ORA	-2.8 g
Lateral ORA	-12.0 g
THIV	37.1 ft/s
PHD	12.1 g
ASI	2.38

Max50-millisecond Avg. (G)

Longitudinal	-12.5 g
Lateral	-15.6 g
Vertical	-4.3 g

Test Article Deflections (in)

Dynamic	0.20 inches
Permanent	0.08 inches
Working Width	15.08 inches
Max. OCD	2.27 inches

Vehicle Stability

Roll	-14.8 degees
Pitch	-6.0 degrees
Yaw	-32.4 degrees

Figure 46. Summary results for MASH Test 3-10 with impact point at 3.6 ft upstream of post (RHT model).

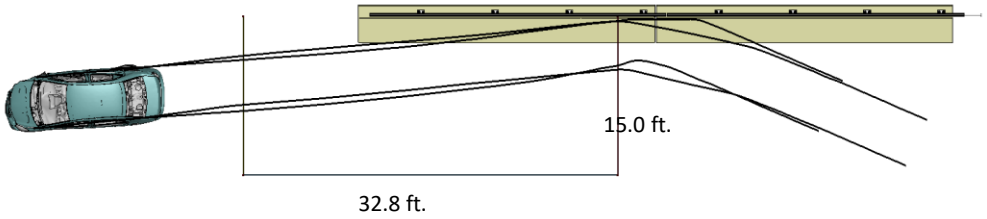

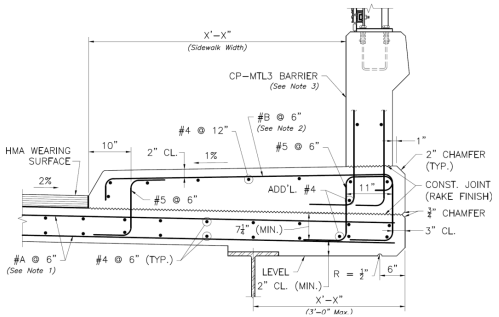

General Information

Analysis Agency	Roadsafe LLC
Test Standard Test No.	MASH Test 3-10
Analysis No.	CP-MTL3_Test3-10-IP4p6ft_KC
Analysis Date	5/29/2023

Test Article

Type	Bridge Rail
Name	CP-MTL3
Installation Length	52.0 feet
Material or Key Elements	Continuous concrete with top mounted aluminum post-and-beam rail
Soil Type and Condition	NA

Analysis Vehicle

Type / Designation	1100C
FEA Model name	YarisC_V1I_R200522.k w/ RS tire
Mass	2,595 lb

Impact Conditions

Speed	62.0 mph
Angle	25 degrees
Location	4.6 ft upstream of post
Impact Severity	55.7 kip-ft

Exit Conditions

Speed	43.3 mph
Angle	7.8 degrees
Time	0.450 seconds

Occupant Risk Values

Longitudinal OIV	24.3 ft/s
Lateral OIV	27.6 ft/s
Longitudinal ORA	-2.2 g
Lateral ORA	-12.7 g
THIV	36.7 ft/s
PHD	12.7 g
ASI	2.39

Max50-millisecond Avg. (G)

Longitudinal	-12.2 g
Lateral	-15.8 g
Vertical	-4.1 g

Test Article Deflections (in)

Dynamic	0.20 inches
Permanent	0.06 inches
Working Width	15.12 inches
Max. OCD	2.20 inches

Vehicle Stability

Roll	-14.7 degees
Pitch	-7.0 degrees
Yaw	-33.3 degrees

Figure 47. Summary results for MASH Test 3-10 with impact point at 4.6 ft upstream of post (KC model).

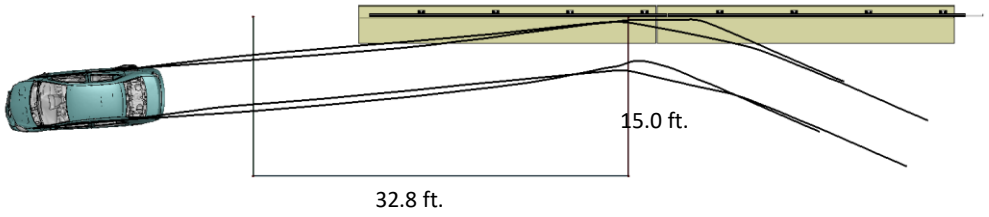

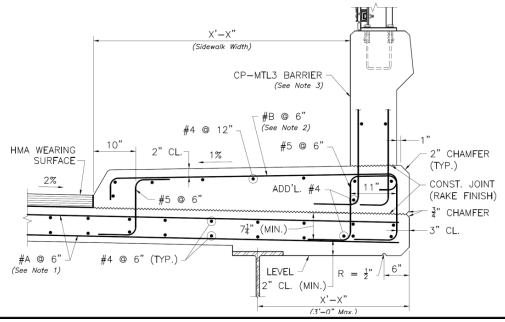

General Information

Analysis Agency	Roadsafe LLC
Test Standard Test No.	MASH Test 3-10
Analysis No.	CP-MTL3_Test3-10-IP4p6ft_RHT
Analysis Date	5/30/2023

Test Article

Type	Bridge Rail
Name	CP-MTL3
Installation Length	52.0 feet
Material or Key Elements	Continuous concrete with top mounted aluminum post-and-beam rail
Soil Type and Condition	NA

Analysis Vehicle

Type / Designation	1100C
FEA Model name	YarisC_V1I_R200522.k w/ RS tire
Mass	2,595 lb

Impact Conditions

Speed	62.0 mph
Angle	25 degrees
Location	4.6 ft upstream of post
Impact Severity	55.7 kip-ft

Exit Conditions

Speed	43.3 mph
Angle	7.9 degrees
Time	0.450 seconds

Occupant Risk Values

Longitudinal OIV	24.0 ft/s
Lateral OIV	27.9 ft/s
Longitudinal ORA	-2.3 g
Lateral ORA	-12.7 g
THIV	36.7 ft/s
PHD	12.7 g
ASI	2.39

Max50-millisecond Avg. (G)

Longitudinal	-12.2 g
Lateral	-15.8 g
Vertical	-4.0 g

Test Article Deflections (in)

Dynamic	0.19 inches
Permanent	0.07 inches
Working Width	15.08 inches
Max. OCD	2.23 inches

Vehicle Stability

Roll	-14.7 degees
Pitch	-6.8 degrees
Yaw	-33.4 degrees

Figure 48. Summary results for MASH Test 3-10 with impact point at 4.6 ft upstream of post (RHT model).

Test 3-11

Analysis Cases

This region of the barrier has a lower strength due to the presence of the 1.5-inch-wide expansion joint in the concrete parapet and bridge deck, as well as the rail splice. A hand-rail post is located 12 inches downstream of the expansion joint, which further magnifies the loading on the concrete at this critical region of the parapet.

Two target impact points were evaluated to assess the crash performance of the CP-MTL3 for the critical section of the bridge rail at the expansion joint under Test 3-11 conditions. The first target impact point was 4.26 ft upstream of the critical post, as illustrated in Figure 49, and was selected to maximize loading and potential snag at the critical post. For the first analysis case, the initial impact point with the face of the sidewalk curb was 16.05 ft upstream of the critical post. The second target impact point was 5.26 ft upstream of the critical post, as illustrated in Figure 50, and was selected to maximize loading and potential snag at the expansion joint on the concrete parapet. For the second analysis case, the initial impact point with the face of the sidewalk curb was 17.05 ft upstream of the critical post.

Each impact point was evaluated using two different concrete material models in LS-DYNA, which included *Mat-Concrete-Damage-Rel3 (KC) and *Mat-RHT, as described in Chapter 4. This resulted in a total of four analysis cases being performed.

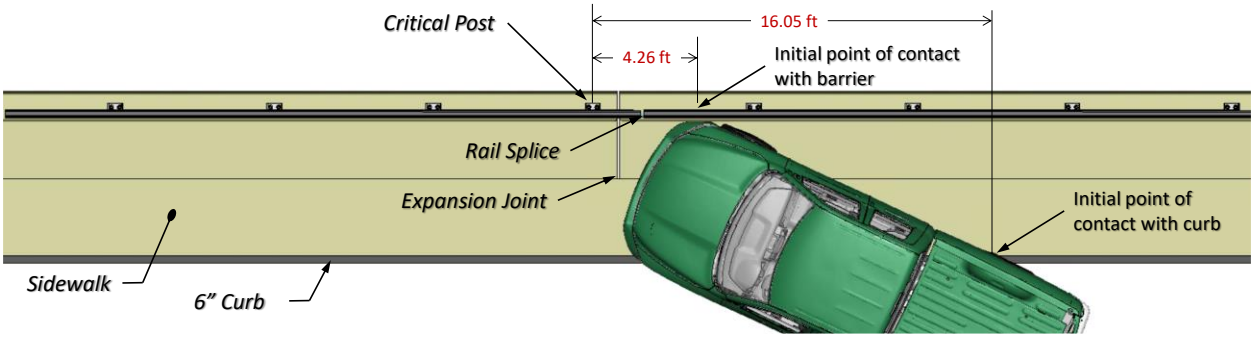

Figure 49. CIP 1 for Test 3-11 for maximizing load on handrail post.

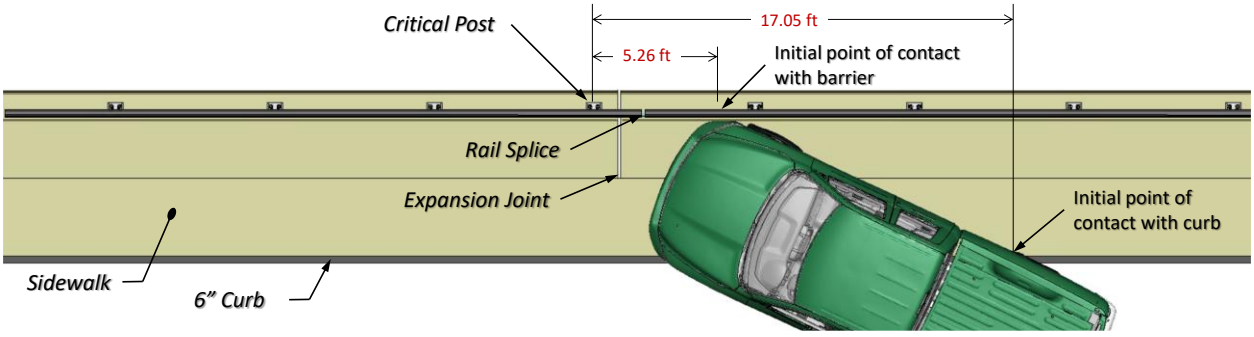

Figure 50. CIP 2 for Test 3-11 for maximizing load on expansion joint.

Summary of Crash Event

The 5,182-lb pickup model struck the face of the sidewalk curb at barrier at a speed of 63 mph and at an angle of 25 degrees, as illustrated in Figures 49 and 50. The sequential views for impact at 4.26 ft upstream of the critical post are shown in Appendix F and Appendix G for the KC and RHT model cases, respectively. The sequential views for impact at 5.26 ft upstream of the critical post are shown in Appendix H and Appendix I for the KC and RHT model cases, respectively. Additional details regarding the sequence of key events are provided in Table 6, for the critical impact point case which was impact at 4.26 ft upstream of the critical post. The following sections provide time-history data evaluation, occupant risk assessments, and damages sustained by the barrier and vehicle.

Table 6. Sequence of events for Test 3-11 with CIP at 4.26 ft upstream of critical post.

Event		KC	RHT
1	Initial contact with curb - Front right tire contacts curb	0.000 sec Impact speed = 62.0 mph Impact angle = 25 deg	0.000 sec Impact speed = 62.0 mph Impact angle = 25 deg
2	Vehicle contacts barrier with bumper and fender	0.135 sec Impact speed = 61.0 mph Impact angle = 24.8 deg	0.135 sec Impact speed = 61.0 mph Impact angle = 24.8 deg
3	Front right tire deflates	0.148 sec	Not recorded
4	Front right tire compresses against barrierand begins to climb	0.150 sec	0.150 sec
5	Front left tire crosses curb	0.150 sec	0.150 sec
6	Rear right tire crosses curb	0.150 sec	0.150 sec
7	Bumper passes rail splice	0.160 sec	0.160 sec
8	Bumper passes expansion joint	0.170 sec	0.170 sec
9	Peak 10-ms average x-acceleration	-14.71 G @ 0.176 sec	-15.66 G @ 0.175 sec
10	Peak 10-ms average y-acceleration	-20.69 G @ 0.178 sec	-21.24 G @ 0.191 sec
11	Bumper passes critical post	0.180 sec	0.180 sec
12	1st peak pitch angle (front pitched upward)	pitch = 1.77 deg at 0.185 sec	pitch = 1.71 deg at 0.295 sec
13	Front right wheel rim snags expansion joint	0.195 sec	0.195 sec
14	Maximum concrete parapet deflection	0.33-inches @ 0.195 sec	0.22-inches @ 0.195 sec
15	Maximum occupant compartment deformation (OCD).	0.205 sec Maximum permenant OCD of 4.72 inches at the right-front toe pan at the wheel well	0.205 sec Maximum permenant OCD of 4.57 inches at the right-front toe pan at the wheel well
16	Occupant impact with vehicle interior	0.2163 sec OIV_x = 21.7 ft/s OIV_y = 26.9 ft/s	0.2169 sec OIV_x = 21.0 ft/s OIV_y = 26.9 ft/s
17	Rear left tire leaves the ground	0.235 sec	0.230 sec
18	Rear right tire leaves the ground	0.245 sec	0.245
19	Front left tire leaves the ground	0.270 sec	0.270 sec
20	Maximum rail deflection at splice	2.14-inches @ 0.355 sec	2.14-inches @ 0.355 sec

Table 6 [CONTINUED] Sequence of events for Test 3-11 with CIP at 4.26 ft upstream of critical post.

21	Rear of vehicle contacts barrier (tail slap)	0.335 sec	0.335 sec
22	Maximum ORA_y	-14.8 G @ 0.3393 - 0.3493 sec	-14.2 G @ 0.3379 - 0.3479 sec
23	Rear right tire deflates	0.341 sec	Not recorded
24	Front right tire returns to the ground	0.400 sec	0.400 sec
25	Vehicle loses contact with barrier	0.495 sec Exit speed = 44.6 mph Exit angle = 6.7 deg	0.525 sec Exit speed = 43.9 mph Exit angle = 7.2 deg
26	Vehicle front bumper passes end of barrier	0.505 sec	0.505 sec
27	Maximum pitch occurs (front pitched downward)	-6.0 deg @ 0.545 sec	-6.3 deg @ 0.542 sec
28	Maximum roll angle (roll away from barrier)	Max Roll = -9.6 deg @ 0.558 sec	Max Roll = -9.3 deg @ 0.587 sec
29	Front left tire returns to ground	0.750 sec	0.765 sec
30	Front right tire leaves the ground	0.775 sec	0.775 sec
31	Rear left tire returns to ground	0.790 sec	0.800 sec
32	Rear right tire returns to ground	0.825 sec	0.81
33	Front right tire returns to the ground	0.945 sec	0.950 sec
34	Maximum ORA_x	-6.3 G @ 0.9611 - 0.9711 sec	-6.2 G @ 0.9663 - 0.9763 sec
35	End of analysis	1.000 sec Speed = 37.0 mph Yaw angle (continues to slightly increase) = 36.7 deg	1.000 sec Speed = 36.9 mph Yaw angle (continues to slightly increase) = 36.9 deg

Time History Plots and Occupant Risk Measures

Figures 51 through 53 show the longitudinal, transverse, and vertical acceleration-time histories, respectively, computed from the center of gravity of the vehicle; Figure 54 through 56 show the comparison of the angular rates and angular displacements (i.e., yaw, roll, and pitch) at the center of gravity of the vehicle. Table 7 shows the results for the occupant risk calculations for all cases.

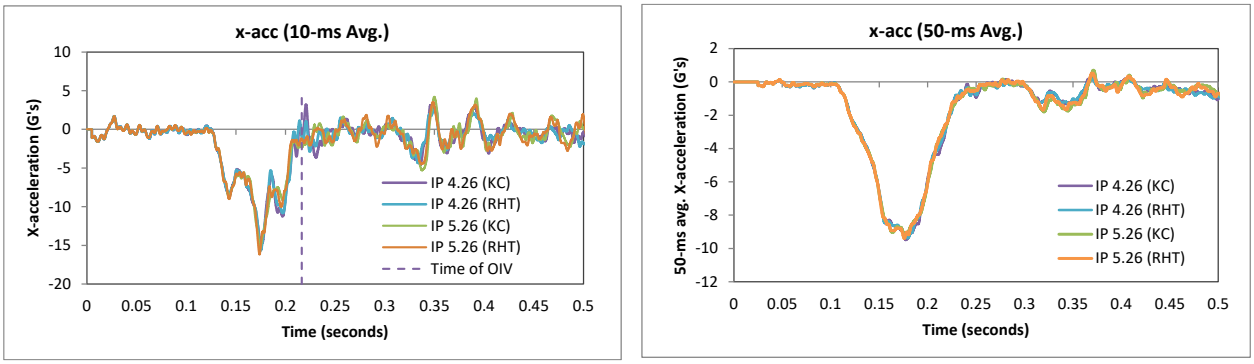

Figure 51. 10- and 50-millisecond running average X-acceleration from FEA for Test 3-11.

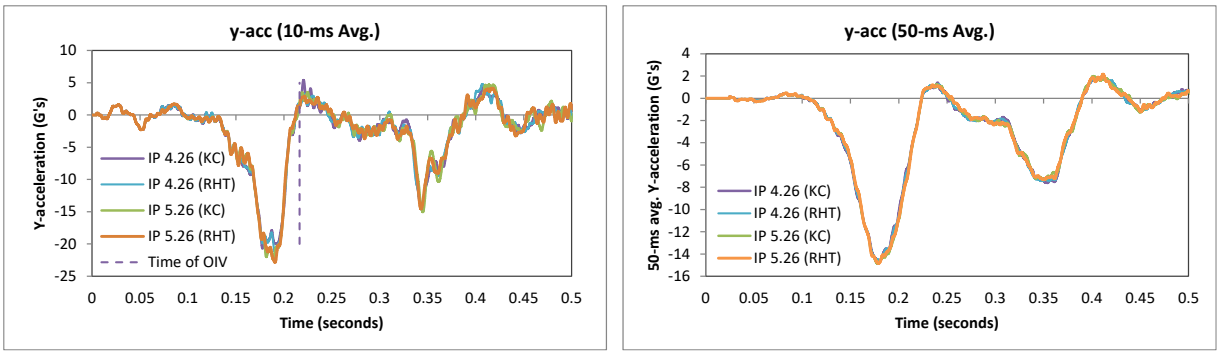

Figure 52. 10- and 50-millisecond running average Y-acceleration from FEA for Test 3-11.

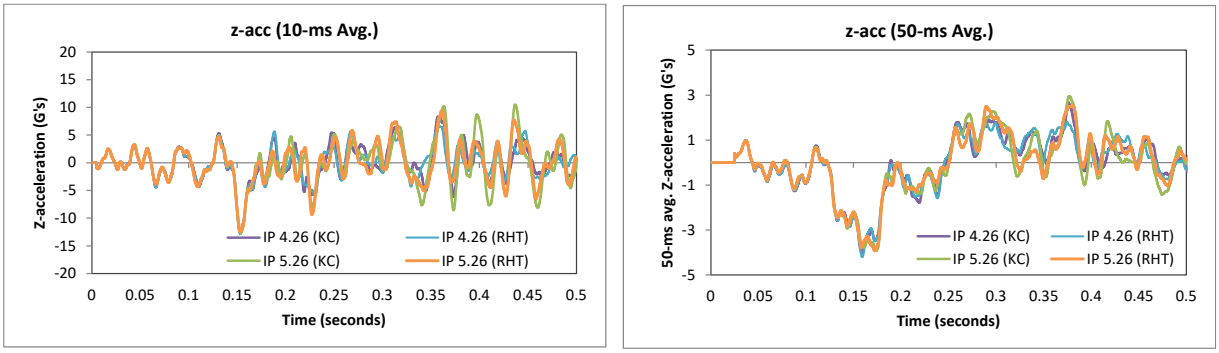

Figure 53. 10- and 50-millisecond running average Z-acceleration from FEA for Test 3-11.

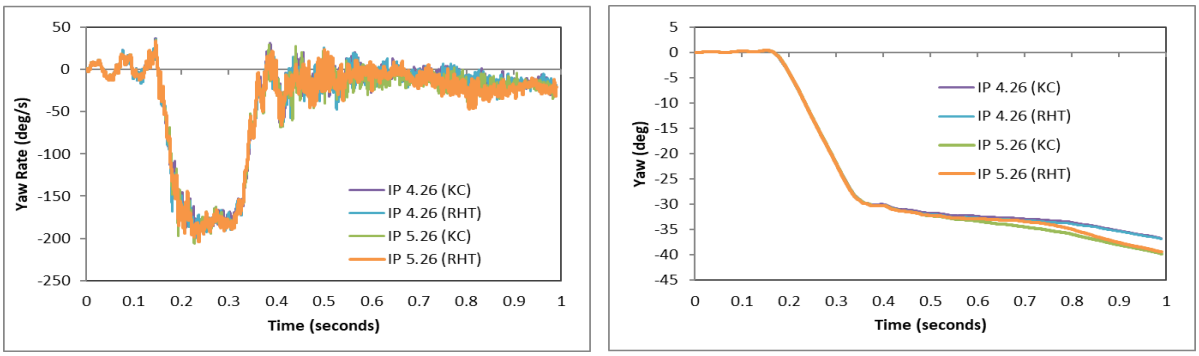

Figure 54. Yaw rate and yaw angle time-history from FEA for Test 3-11.

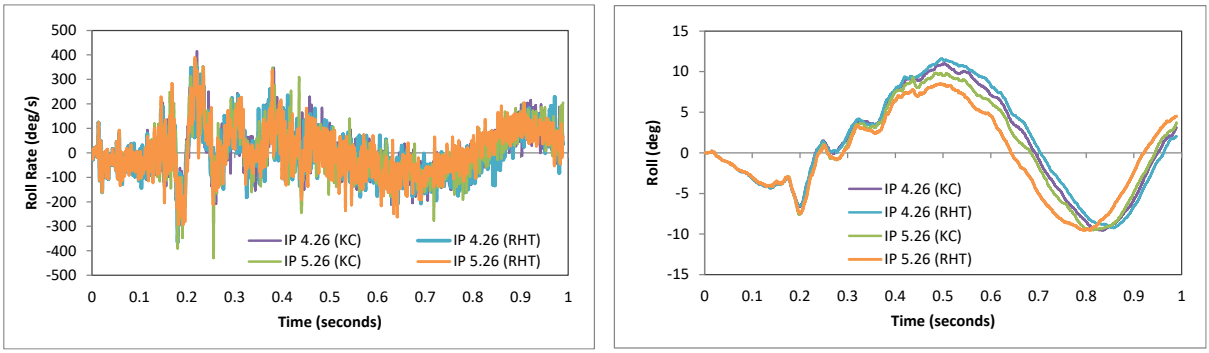

Figure 55. Roll rate and roll angle time-history from FEA for Test 3-11.

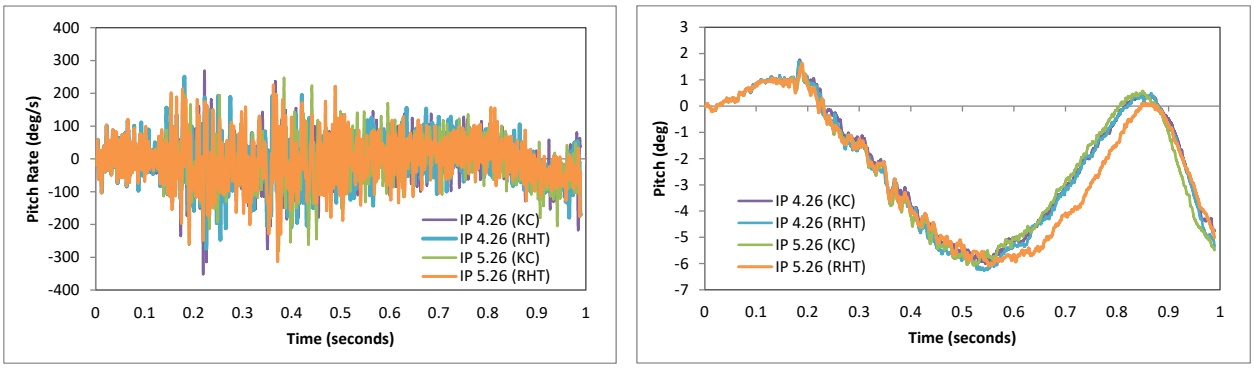

Figure 56. Pitch rate and pitch angle time-history from FEA for Test 3-11.

Impact Point 1: Impact at 4.26 ft

For the impact case at 4.26 ft upstream of the critical post, the peak 10-ms running average accelerations in the longitudinal direction were -14.7 G and -15.7 G for the KC and RHT cases, respectively, as shown in Figure 51. The peak 10-ms running average accelerations in the lateral direction were -20.7 G and –22.4 G for the KC and RHT cases, respectively, as shown in Figure 52. The occupant impact velocity (OIV) in the longitudinal direction ranged from 21.0 ft/s to 21.7 ft/s for the analysis cases. The OIV in the lateral direction was 26.9 ft/s. The highest ridedown acceleration (RA) in the longitudinal direction ranged from -6.2 to -6.3 G, and the highest RA in the lateral direction ranged from -14.2 to -14.8 G. All OIV and RA values were within the preferred limits recommended in MASH.

The maximum roll angle ranged from 11 to 11.6 degrees (roll toward barrier) and occurred at approximately 0.5 seconds into the impact event. A second peak roll occurred after redirection at approximately 0.84 seconds with value ranging from -9.3 to -9.6 degrees (roll away from barrier). The maximum pitch angle ranged from -6 to -6.3 degrees (rear pitching upward), which were all well within critical limits specified in MASH.

Impact Point 2: Impact at 5.26 ft

For the impact case at 5.26 ft upstream of the critical post, the peak 10-ms running average accelerations in the longitudinal direction were -15.4 G and -16.8 G for the KC and RHT cases, respectively, as shown in Figure 51. The peak 10-ms running average accelerations in the lateral direction were -22.4 G and –22.9 G for the KC and RHT cases, respectively, as shown in Figure 52. The occupant impact velocity (OIV) in the longitudinal direction ranged was 21.0 ft/s for both analysis cases, and the OIV in the lateral direction was 26.9 ft/s. The highest ridedown acceleration (RA) in the longitudinal direction ranged from -4.5 to -5.3 G, and the highest RA in the lateral direction ranged from -14.6 to -15.1 G. The OIV values were within the preferred limits recommended in MASH, while the RA was just over the preferred limit for the KC analysis case. All RA values were within critical limits specified in MASH.

The first peak roll angle occurred during impact with the barrier at approximately 0.5 seconds into the impact with value ranging from 8.5 to 9.8 degrees (roll toward barrier), as shown in Figure 55. The maximum roll angle occurred during redirection and was -9.5 degrees at approximately 0.8 seconds for both cases. The maximum pitch angle was -6.1 degrees (rear pitching upward). All roll and pitch values were well within critical limits specified in MASH.

Table 7. Summary of MASH occupant risk metrics for Test 3-11.

Occupant Risk Factors		MASH Test 3-11			
		IP 4.26 (KC)	IP 4.26 (RHT)	IP 5.26 (KC)	IP 5.26 (RHT)
Occupant Impact Velocity (ft/s)	x-direction	21.7	21.0	21.0	21.0
	y-direction	26.9	26.9	26.9	26.9
	at time	at 0.2163 seconds on right side of interior	at 0.2169 seconds on right side of interior	at 0.2164 seconds on right side of interior	at 0.2166 seconds on right side of interior
THIV (ft/s)		35.1 at 0.2128 seconds on right side of interior	34.4 at 0.2132 seconds on right side of interior	35.1 at 0.2129 seconds on right side of interior	34.8 at 0.2131 seconds on right side of interior
Ridedown Acceleration (g's)	x-direction	-6.3 (0.9611 - 0.9711 seconds)	-6.2 (0.9663 - 0.9763 seconds)	-5.3 (0.3323 - 0.3423 seconds)	-4.5 (0.3319 - 0.3419 seconds)
	y-direction	-14.8 (0.3393 - 0.3493 seconds)	-14.2 (0.3379 - 0.3479 seconds)	-15.1 (0.3399 - 0.3499 seconds)	-14.6 (0.3379 - 0.3479 seconds)
PHD (g's)		14.9 (0.3394 - 0.3494 seconds)	14.2 (0.3380 - 0.3480 seconds)	15.1 (0.3399 - 0.3499 seconds)	14.6 (0.3378 - 0.3478 seconds)
ASI		1.94 (0.1816 - 0.2316 seconds)	1.95 (0.1818 - 0.2318 seconds)	2 (0.1825 - 0.2325 seconds)	1.99 (0.1825 - 0.2325 seconds)
Max 50-ms moving avg. acc. (g's)	x-direction	-9.5 (0.1524 - 0.2024 seconds)	-9.4 (0.1546 - 0.2046 seconds)	-9.2 (0.1514 - 0.2014 seconds)	-9.4 (0.1509 - 0.2009 seconds)
	y-direction	-14.6 (0.1542 - 0.2042 seconds)	-14.7 (0.1554 - 0.2054 seconds)	-14.9 (0.1532 - 0.2032 seconds)	-14.8 (0.1542 - 0.2042 seconds)
	z-direction	-4.1 (0.1339 - 0.1839 seconds)	-4.2 (0.1342 - 0.1842 seconds)	-3.9 (0.1490 - 0.1990 seconds)	-3.9 (0.1474 - 0.1974 seconds)
Maximum Angular Disp. (deg)	Roll	11 (0.5005 seconds)	11.6 (0.4967 seconds)	9.8 (0.4842 seconds)	-9.5 (0.8083 seconds)
	Pitch	-6 (0.5448 seconds)	-6.3 (0.5423 seconds)	-6.1 (0.5233 seconds)	-6.1 (0.5519 seconds)
	Yaw	-36.7 (0.9893 seconds)	-36.8 (0.9893 seconds)	-39.8 (0.9893 seconds)	-39.4 (0.9893 seconds)

Damages to the Barrier System

Figures 57 and 58 show images of maximum deflection of the barrier for impact at 4.26 ft and 5.26 ft upstream of the critical post, respectively. Deflection-time history plots at the point of maximum deflection are also shown in the figures. In all cases, the maximum deflection occurred at the splice connection on the railing and coincides with impact of the rear of the vehicle against the barrier at approximately 0.36 seconds. For the impact case at 4.26 ft upstream of the critical post, the maximum deflection was 2.14 inches for both the KC model and the RHT model. For the impact case at 5.26 ft upstream of the critical post, the maximum deflection was 1.95 inches for the KC model and was 1.97 inches for the RHT model.

The first peak displacement at the rail splice resulted when the front of the vehicle was in contact with the rail at approximately 0.18 seconds. For the impact case at 4.26 ft upstream of the critical post, the initial peak displacement was 1.25 inches for the KC model case and was 1.49 inches for the RHT model case; the maximum permanent deflection was 0.53 inches for the KC model and was 0.54 inches for the RHT model. For the impact case at 5.26 ft upstream of the critical post the initial peak displacement was 1.5 inches for both the KC model and the RHT model; the maximum permanent deflection was 0.46 inches for the KC model and was 0.50 inches for the RHT model.

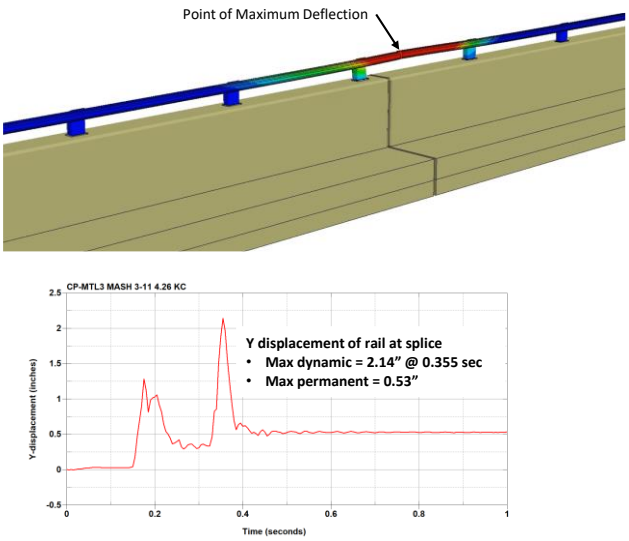

(a) 4.26 feet upstream of critical post – (KC)

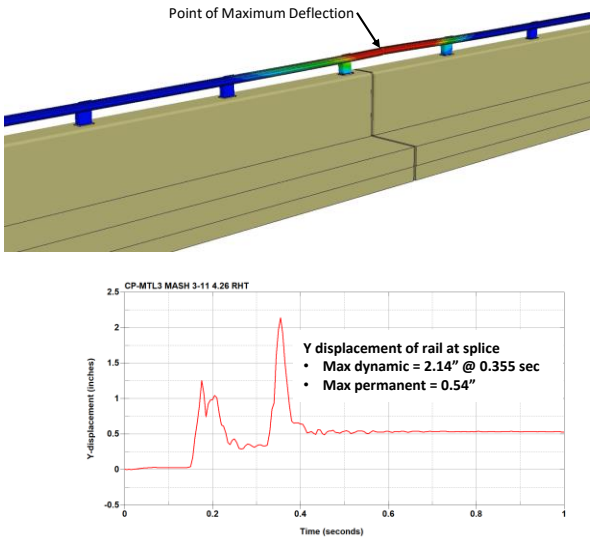

(b) 4.26 feet upstream of critical post – (RHT)

Figure 57. Contour plot of lateral displacement for Test 3-11 at 4.26 ft upstream of critical post for (a) KC model and (b) RHT model.

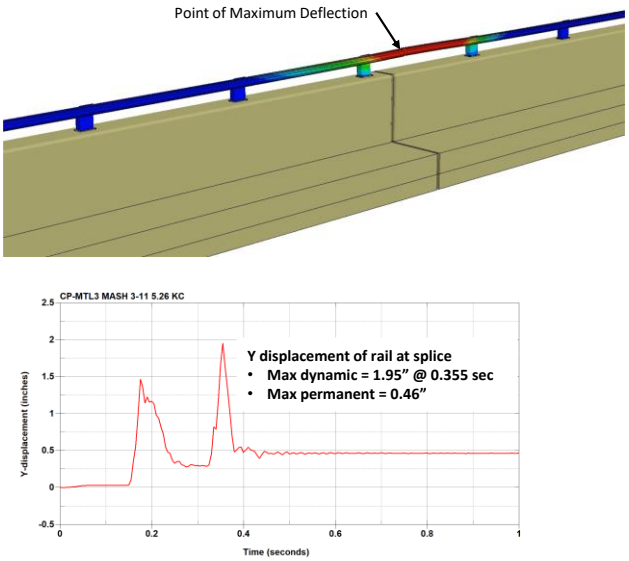

(a) 5.26 feet upstream of critical post – (KC)

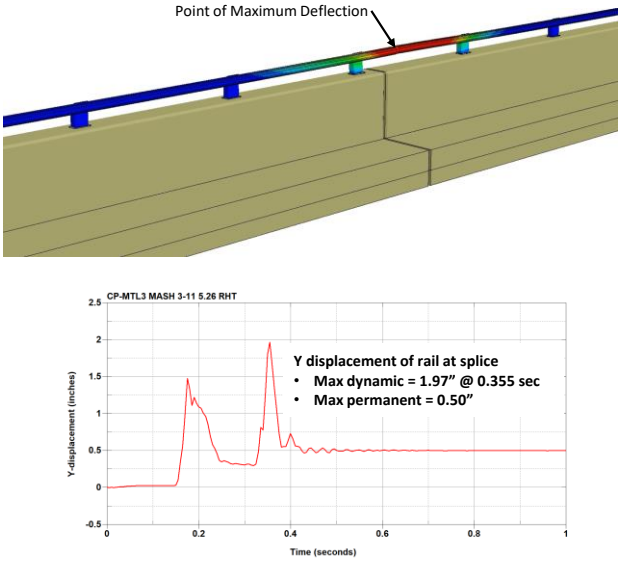

(b) 5.26 feet upstream of critical post – (RHT)

Figure 58. Contour plot of lateral displacement for Test 3-11 at 5.26 ft upstream of critical post for (a) KC model and (b) RHT model.

Figure 59 shows a contour plot of effective plastic strain on the splice components. The highest effective plastic strain occurred on the splice tube and resulted from the edge of the main rail pressing against the front surface of the splice tube. The peak magnitudes were slightly higher for impact at 4.26 ft upstream of the critical post but were less than 0.02 for all analysis cases and were considered negligible for the material.

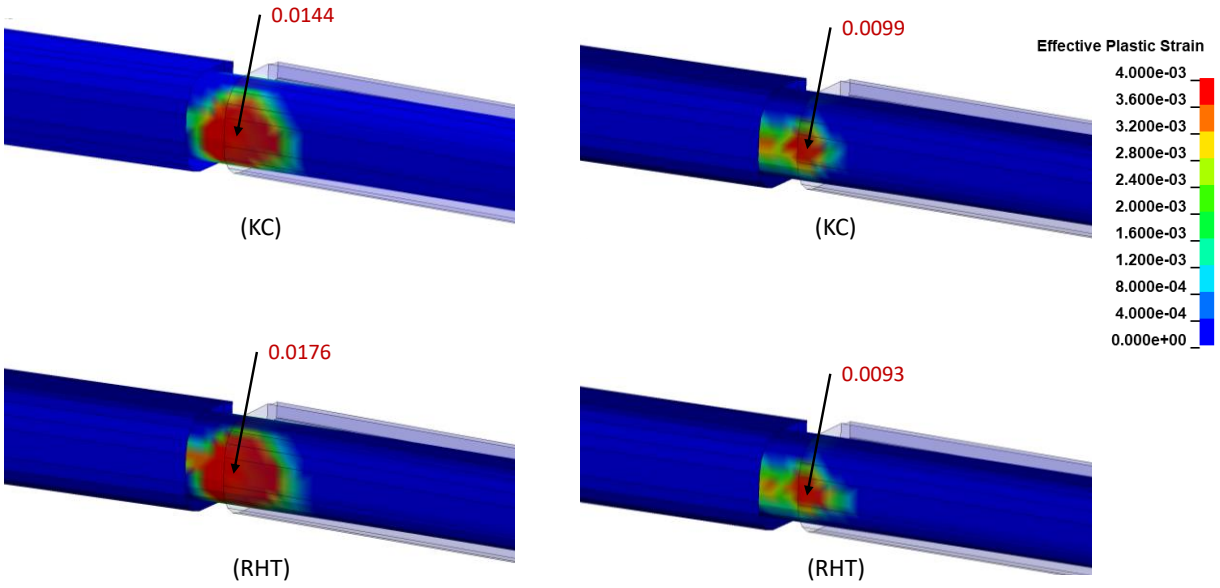

(a) Impact at 4.26 feet upstream of critical post **(b)** Impact at 5.26 feet upstream of critical post

Figure 59. Effective plastic strain contours on rail splice components during Test 3-11 for (a) impact at 4.26 ft and (b) 5.26 ft upstream of critical post.

Figure 60 shows contour plots of the damage parameter on the concrete parapet for both impact cases, and Figure 61 shows contours of 1st principal strain. There was slightly higher damage for the impact case at 4.26-ft upstream of the critical post and the KC model indicated more damage than the RHT model. However, the damage was primarily limited to the surface of the barrier in the form of spalling. The location on the barrier with the greatest amount of spalling, as indicated by the contours of 1st principal strain for the KC model, was at the expansion joint at the end of the upstream parapet on the front upper edge.

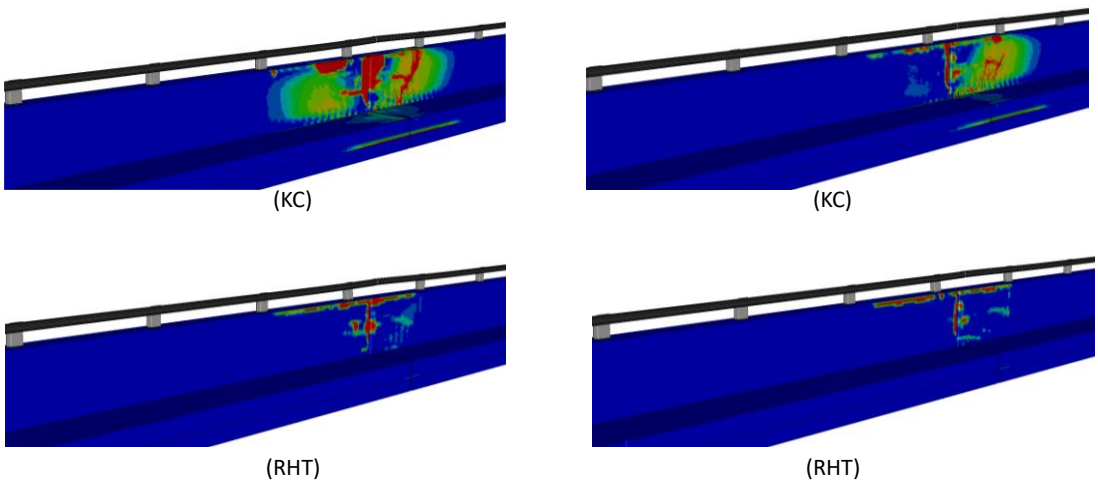

(a) Impact at 4.26 feet upstream of critical post **(b)** Impact at 5.26 feet upstream of critical post

Figure 60. Contour plot of the damage variable on the concrete parapet and deck during Test 3-11 for (a) impact at 4.26 ft and (b) 5.26 ft upstream of critical post.

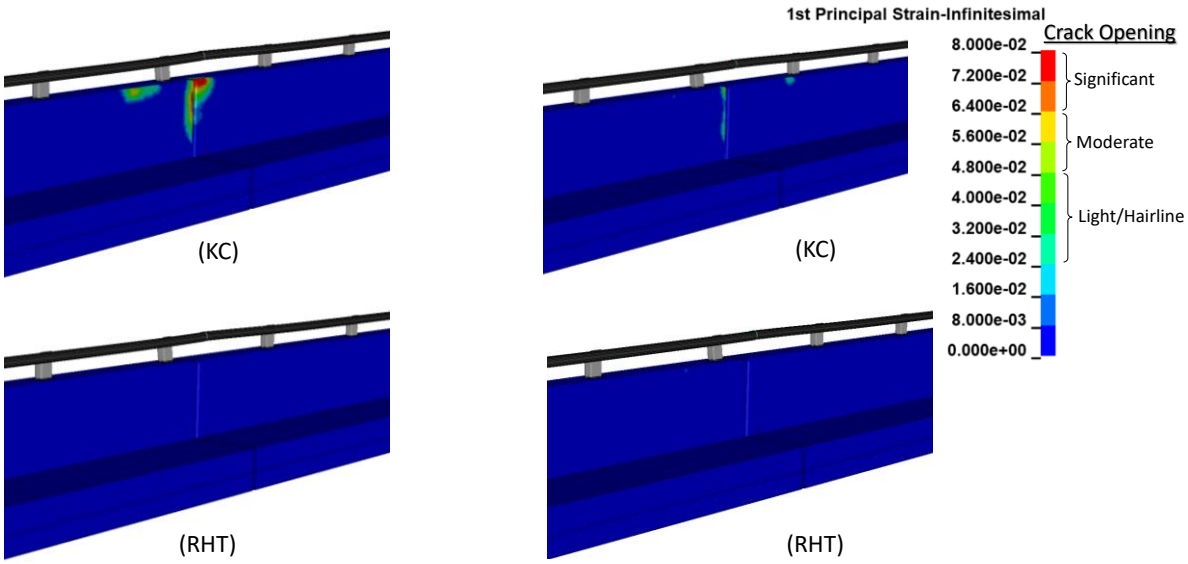

(a) Impact at 4.26 feet upstream of critical post **(b)** Impact at 5.26 feet upstream of critical post

Figure 61. Contour plot of 1st principal strain on the concrete parapet and deck during Test 3-11 for (a) impact at 4.26 ft and (b) 5.26 ft upstream of critical post.

Damages to Vehicle

Figure 62 shows contour plots of effective plastic strain for the vehicle. The damage to the vehicle was similar for all analysis cases and was limited to the impact side of the vehicle. The most significant damages included the front cap, the front wheel assembly, edge of front door, edge of the rear door, front edge of the truck bed, rear wheel, rear bumper, and lower, rear section of the truck bed. The windshield also cracked around all four edges but did not separate from the vehicle. The damage to the windshield was not caused by direct contact with any part of the barrier. It is also expected that the model likely overestimated this damage; however, the damage to the windshield around the a-pillar is common for Test 3-11 on rigid barriers. For example, Figure 63 shows vehicle damages from test 3-11 on a similar concrete barrier with aluminum handrail. [*Dobrovolny20*]

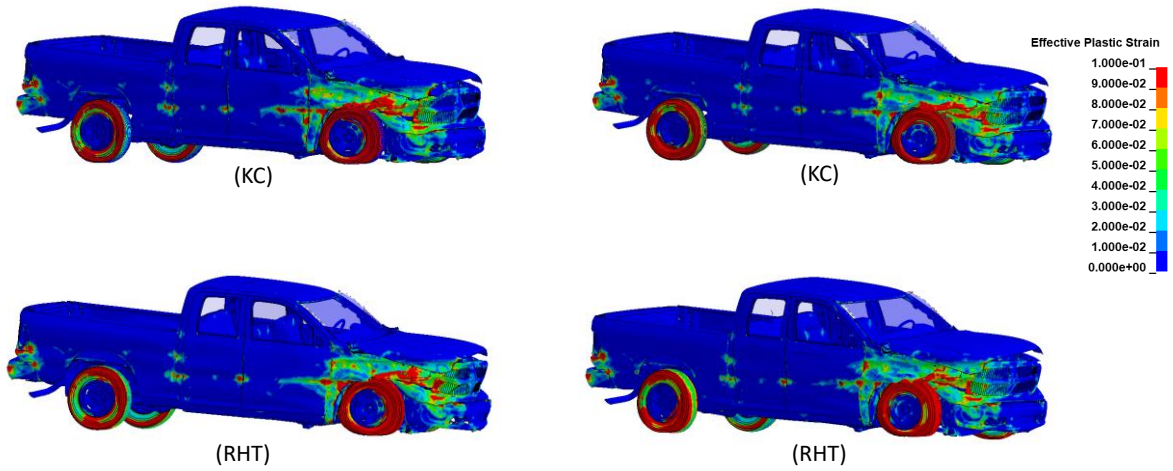

(a) Impact at 4.26 feet upstream of critical post **(b)** Impact at 5.26 feet upstream of critical post

Figure 62. Damages to vehicle in Test 3-11 for (a) impact at 4.26 ft and (b) 5.26 ft upstream of critical post.

Figure 63. Damage to test vehicle in Test 3-11 on similar bridge rail system. [*Dobrovolny20*]

Occupant Compartment Deformation (OCD)

The maximum deformation of the occupant compartment for Test 3-11 ranged from 4.31 – 4.72 inches and occurred at the right-front toe pan at the wheel well. Figure 64 shows a contour plot of effective plastic strain on the floor pan of the vehicle with a with all other components removed to facilitate viewing. The maximum deformation was less than the critical limit of 9 inches specified in MASH for this area of the occupant compartment.

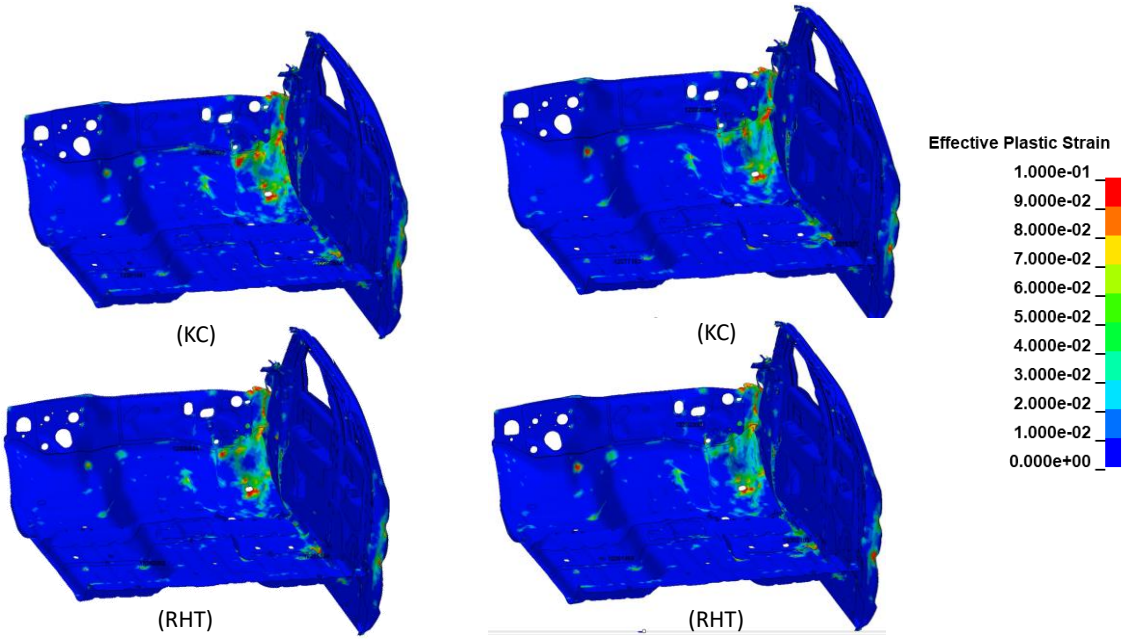

(a) Impact at 4.26 feet upstream of critical post **(b)** Impact at 5.26 feet upstream of critical post

Figure 64. Occupant compartment deformation resulting from Test 3-11 for (a) impact at 4.26 ft and (b) 5.26 ft upstream of critical post.

Exit Box

Figure 65 shows the exit box for Test 3-11 for each analysis case. Although the exit box analysis is not required in MASH, it was included here for completeness. The post trajectory response was similar for all cases, and the vehicle was redirected with its path well within the exit box criteria of MASH.

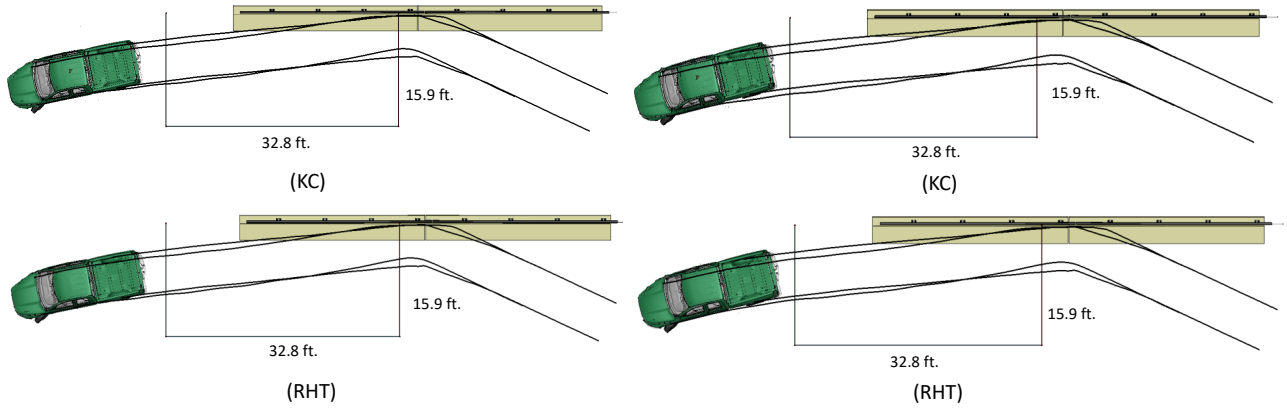

(a) Impact at 4.26 feet upstream of critical post **(b)** Impact at 5.26 feet upstream of critical post

Figure 65. Exit box for Test 3-11 for (a) impact at 4.26 ft and (b) 5.26 ft upstream of critical post.

Results Summary

A summary of the MASH Test 3-11 results for the CP-MTL3 is shown in Table 8 and in Figures 66 through 69. The bridge rail successfully contained and redirected the pickup with minor spalling on the concrete parapet and moderate damage to the aluminum handrail components for all analysis cases. There were no detached elements from the barrier that showed potential for penetrating into the occupant compartment or presenting undue hazard to other traffic. The OIV and maximum RA values were within critical limits specified in MASH. The maximum occupant compartment deformation was well within critical limits specified in MASH. The windshield was cracked around the edges, but the damage was not caused by direct contact with any part of the barrier. The vehicle remained upright and did not experience excessive roll or pitch angle displacements. The vehicle also remained within the exit-box criteria of MASH. Based on the results of this analysis, the barrier is expected to meet all structural and occupant risk criteria in MASH for Test 3-11 impact conditions.

CIP Recommendation for Test 3-11 for CP-MTL3 at Expansion Joint

The recommended CIP for Test 3-11 for this section of the bridge rail is at 4.26 ft upstream of the critical post positioned 12 inches downstream of the expansion joint in the concrete parapet. As previously mentioned, the longitudinal and lateral OIV's were within preferred limits in all cases, and the longitudinal RAs were also within preferred limits in all cases. The lateral RAs were essentially the same for all cases with values just above or below the preferred limit of 15 G. The OCDs were similar for all cases; however, the highest values occurred for the 4.26-ft impact case. The highest deflections for the handrail occurred for the impact at 5.26 ft upstream of the critical post; however, these deformations were relatively low and occurred during the tail-slap of the vehicle. The greatest deflection of the concrete parapet occurred at the upstream section of the parapet at the expansion joint for impact at 4.26 ft upstream of the critical post. This case also resulted in the highest loading on the concrete anchors at the critical post. It is the research team's opinion that the greatest potential for a serious vehicle snag on the system is at the expansion joint on the parapet, and this impact point maximizes the deflection of the upstream section of the parapet at the expansion joint and also maximizes the occupant compartment deformation.

Table 8. Summary of MASH Test 3-11 for the CP-MTL3.

Evaluation Factors		Evaluation Criteria	Impact at 4.26 ft		Impact at 5.26 ft	
			KC	RHT	KC	RHT
Structural Adequacy	A	Test article should contain and redirect the vehicle or bring the vehicle to a controlled stop; the vehicle should not penetrate, underride, or override the installation although controlled lateral deflection of the test article is acceptable.	Pass	Pass	Pass	Pass
Occupant Risk	D	Detached elements, fragments, or other debris from the test article should not penetrate or show potential for penetrating the occupant compartment, or present undue hazard to other traffic, pedestrians, or personnel in a work zone. Deformations of, or intrusions into, to occupant compartment should not exceed limits set forth in Section 5.2.2 and Appendix E.	Pass	Pass	Pass	Pass
	F	The vehicle should remain upright during and after collision. The maximum roll and pitch angles are not to exceed 75 degrees.	Pass	Pass	Pass	Pass
	H	The longitudinal and lateral occupant impact velocity (OIV) shall not exceed 40 ft/s, with a preferred limit of 30 ft/s.	Pass	Pass	Pass	Pass
	I	The longitudinal and lateral ridedown acceleration (RA) shall not exceed 20.49 G, with a preferred limit of 15.0 G	Pass	Pass	Pass	Pass

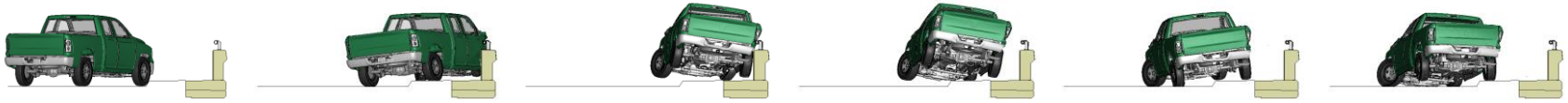

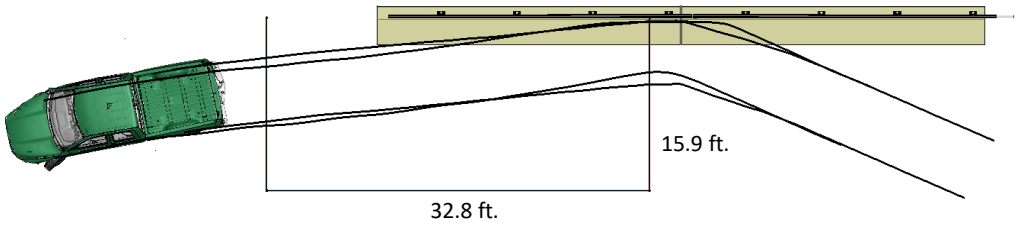

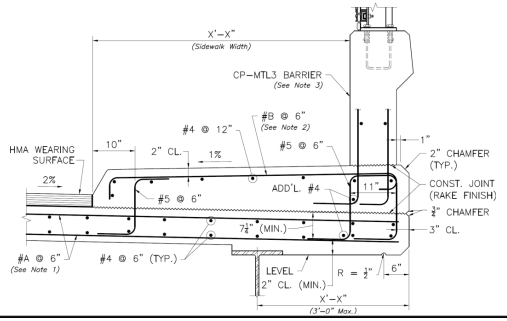

General Information

Analysis Agency	Roadsafe LLC
Test Standard Test No.	MASH Test 3-11
Analysis No.	CP-MTL3_Test3-11_IP4.26ft_KC
Analysis Date	5/25/2023

Test Article

Type	Bridge Rail
Name	CP-MTL3
Installation Length	52.0 feet
Material or Key Elements	Continuous concrete with top mounted aluminum post-and-beam rail
Soil Type and Condition	NA

Analysis Vehicle

Type / Designation	2270P
FEA Model name	Ram2018C_V2u.k w/ RS tire
Mass	5,001 lb

Impact Conditions

Speed	62.0 mph
Angle	25 degrees
Location	4.26 ft upstream of post

Impact Severity 114.7 kip-ft

Exit Conditions

Speed	44.6 mph
Angle	6.7 degrees
Time	0.495 seconds

Occupant Risk Values

Longitudinal OIV	21.7 ft/s
Lateral OIV	26.9 ft/s
Longitudinal ORA	-6.3 g
Lateral ORA	-14.8 g
THIV	35.1 ft/s
PHD	14.9 g
ASI	1.94

Max50-millisecond Avg. (G)

Longitudinal	-9.5 g
Lateral	-14.6 g
Vertical	-4.1 g

Test Article Deflections (in)

Dynamic	2.14 inches
Permanent	0.53 inches
Working Width	15.33
Max. OCD	4.72 inches

Vehicle Stability

Roll	11.0 degees
Pitch	-6.0 degrees
Yaw	-36.7 degrees

Figure 66. Summary results for MASH Test 3-11 with impact point at 4.26 ft upstream of post (KC model).

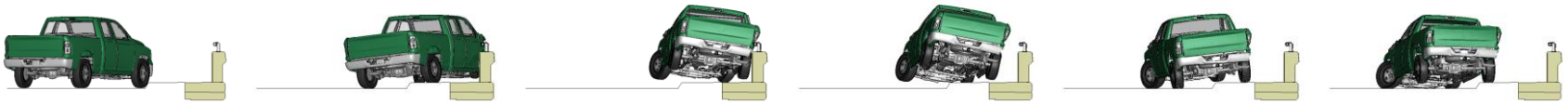

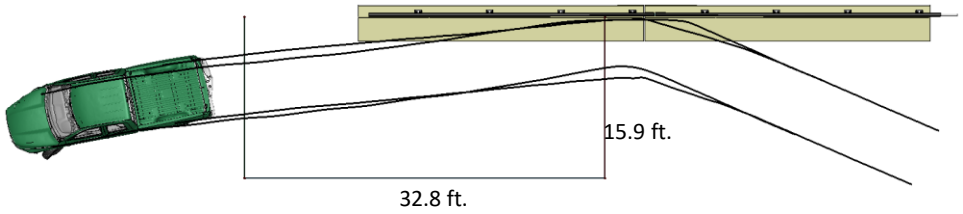

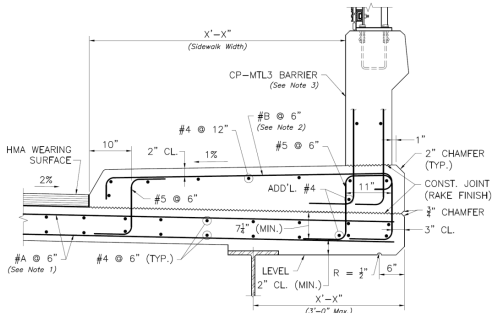

General Information

Analysis Agency	Roadsafe LLC
Test Standard Test No.	MASH Test 3-11
Analysis No.	CP-MTL3_Test3-11_IP4.26ft_RHT
Analysis Date	5/26/2023

Test Article

Type	Bridge Rail
Name	CP-MTL3
Installation Length	52.0 feet
Material or Key Elements	Continuous concrete with top mounted aluminum post-and-beam rail
Soil Type and Condition	NA

Analysis Vehicle

Type / Designation	2270P
FEA Model name	Ram2018C_V2u.k w/ RS tire
Mass	5,001 lb

Impact Conditions

Speed	62.0 mph
Angle	25 degrees
Location	4.26 ft upstream of post
Impact Severity	114.7 kip-ft

Exit Conditions

Speed	43.9 mph
Angle	7.2 degrees
Time	0.525 seconds

Occupant Risk Values

Longitudinal OIV	21.0 ft/s
Lateral OIV	26.9 ft/s
Longitudinal ORA	-6.2 g
Lateral ORA	-14.2 g
THIV	34.4 ft/s
PHD	14.2 g
ASI	1.95

Max50-millisecond Avg. (G)

Longitudinal	-9.4 g
Lateral	-14.7 g
Vertical	-4.2 g

Test Article Deflections (in)

Dynamic	2.14 inches
Permanent	0.54 inches
Working Width	15.22
Max. OCD	4.57 inches

Vehicle Stability

Roll	11.6 degees
Pitch	-6.3 degrees
Yaw	-36.8 degrees

Figure 67. Summary results for MASH Test 3-11 with impact point at 4.26 ft upstream of post (RHT model).

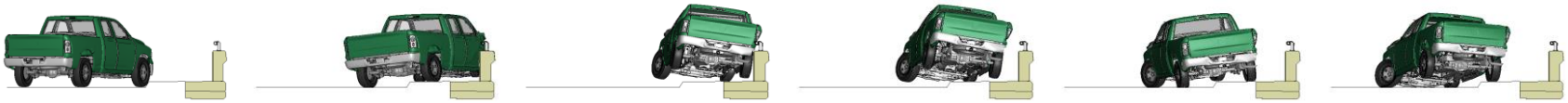

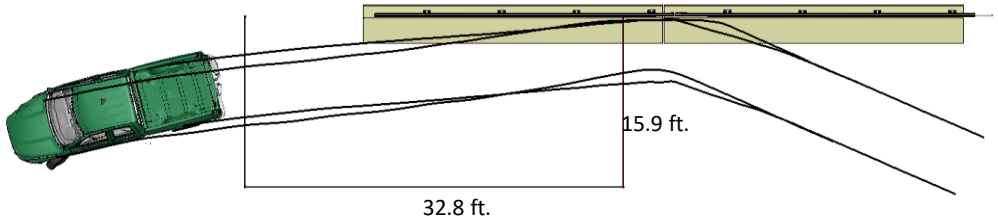

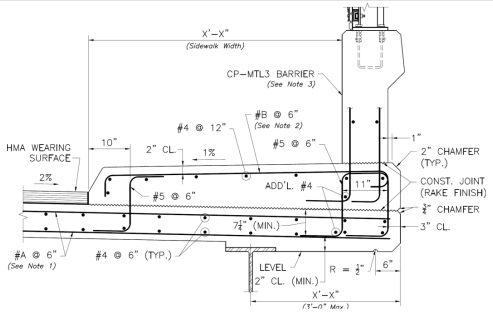

General Information

Analysis Agency	Roadsafe LLC
Test Standard Test No.	MASH Test 3-11
Analysis No.	CP-MTL3_Test3-11_IP5.26ft_KC
Analysis Date	5/27/2023

Test Article

Type	Bridge Rail
Name	CP-MTL3
Installation Length	52.0 feet
Material or Key Elements	Continuous concrete with top mounted aluminum post-and-beam rail
Soil Type and Condition	NA

Analysis Vehicle

Type / Designation	2270P
FEA Model name	Ram2018C_V2u.k w/ RS tire
Mass	5,001 lb

Impact Conditions

Speed	62.0 mph
Angle	25 degrees
Location	5.26 ft upstream of post
Impact Severity	114.7 kip-ft

Exit Conditions

Speed	44.0 mph
Angle	7.5 degrees
Time	0.525 seconds

Occupant Risk Values

Longitudinal OIV	21.0 ft/s
Lateral OIV	26.9 ft/s
Longitudinal ORA	-5.3 g
Lateral ORA	-115.1 g
THIV	35.1 ft/s
PHD	15.1 g
ASI	2

Max50-millisecond Avg. (G)

Longitudinal	-9.2 g
Lateral	-14.9 g
Vertical	-3.9 g

Test Article Deflections (in)

Dynamic	1.95 inches
Permanent	0.46 inches
Working Width	15.22
Max. OCD	4.37 inches

Vehicle Stability

Roll	9.8 degees
Pitch	-6.1 degrees
Yaw	-39.8 degrees

Figure 68. Summary results for MASH Test 3-11 with impact point at 5.26 ft upstream of post (KC model).

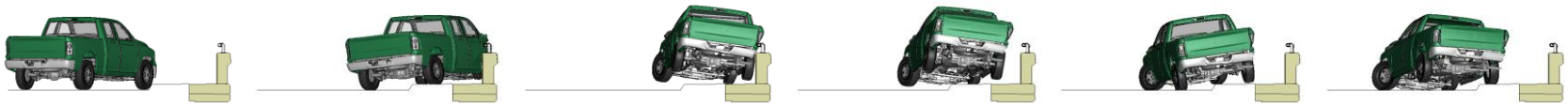

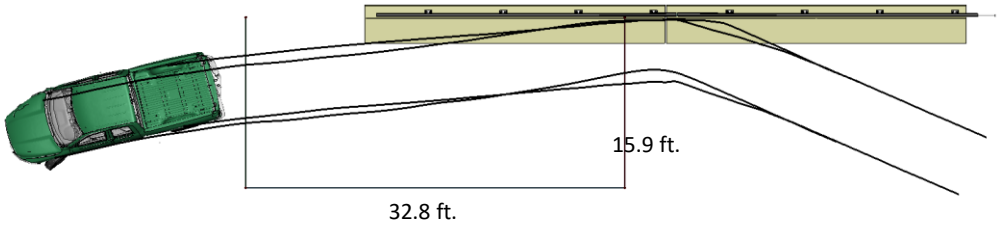

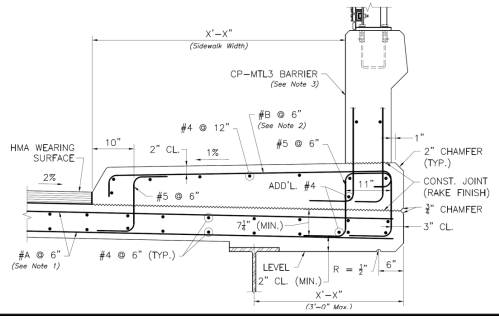

General Information

Analysis Agency	Roadsafe LLC
Test Standard Test No.	MASH Test 3-11
Analysis No.	CP-MTL3_Test3-11_IP5.26ft_RHT
Analysis Date	5/27/2023

Test Article

Type	Bridge Rail
Name	CP-MTL3
Installation Length	52.0 feet
Material or Key Elements	Continuous concrete with top mounted aluminum post-and-beam rail
Soil Type and Condition	NA

Analysis Vehicle

Type / Designation	2270P
FEA Model name	Ram2018C_V2u.k w/ RS tire
Mass	5,001 lb

Impact Conditions

Speed	62.0 mph
Angle	25 degrees
Location	5.26 ft upstream of post
Impact Severity	114.7 kip-ft

Exit Conditions

Speed	44.2 mph
Angle	7.7 degrees
Time	0.545 seconds

Occupant Risk Values

Longitudinal OIV	21.0 ft/s
Lateral OIV	26.9 ft/s
Longitudinal ORA	-4.5 g
Lateral ORA	-14.6 g
THIV	34.8 ft/s
PHD	14.6 g
ASI	1.99

Max50-millisecond Avg. (G)

Longitudinal	-9.4 g
Lateral	-14.8 g
Vertical	-3.9 g

Test Article Deflections (in)

Dynamic	1.97 inches
Permanent	0.50 inches
Working Width	15.17
Max. OCD	4.31 inches

Vehicle Stability

Roll	-9.5 degees
Pitch	-6.1 degrees
Yaw	-39.4 degrees

Figure 69. Summary results for MASH Test 3-11 with impact point at 5.26 ft upstream of post (RHT model).

CHAPTER 6 – MASH TL3 EVALUATION OF THE CP-MTL3 WITH HANDRAIL AT CONNECTION TO CONCRETE TRANSITION

FEA was again used to evaluate the crash performance of the CP-MTL3 with top-mounted handrail at a second critical region of the bridge rail, which was at the connection point to the downstream transition, as illustrated in Figure 70. Figure 71 shows the drawing details for this section of the bridge rail system. A portion of the CP-MTL3 model used in the previous analysis case (see Chapter 4) was updated to include the concrete clip. A portion of the transition was also included in the model, as described in Chapter 4. The total length of the system was 44.65 feet which included 29 feet of the CP-MTL3 with handrail and 15.65 feet of the 42-inch-tall transition, as shown in the elevation view in Figure 72. The transition was modeled as rigid to represent a worse case for the analysis (i.e., maximize potential for snag on the end of the transition).

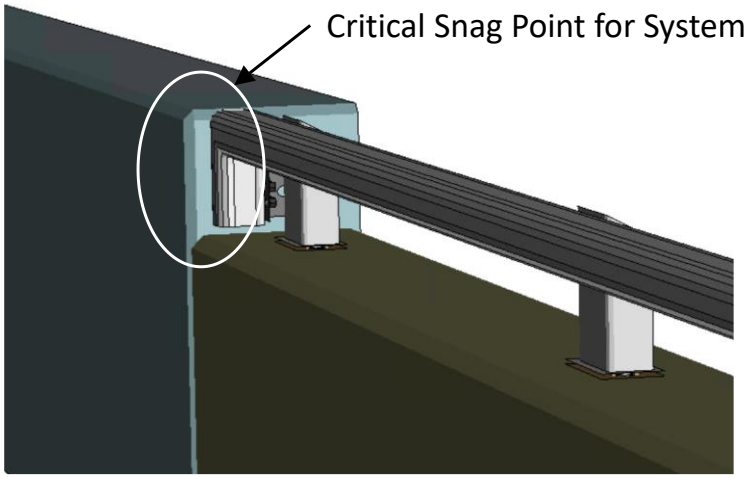

Figure 70. Critical snag point for system at connection to transition.

The evaluations were based on structural adequacy, vehicle stability during and after redirection, and occupant risk factors using criteria specified in MASH for Test Level 3. The analyses were performed using LS-DYNA version mpp_s_R13 revision number R13.1.0-3-g4cd30680f9 with a time-step of 1.0 microsecond. The critical impact point was determined using FEA. The evaluations included:

- **Simulation of Test 3-10** with the 1100C Yaris model ballasted to a gross static weight of 2,609 lb (1183 kg) impacting the barrier at 62 mph and 25 degrees.
- **Simulation of Test 3-11** with the 2270P Chevrolet Silverado model ballasted to a gross static weight of 5,182 lb (2,351 kg) impacting the railing at 63 mph and 25 degrees.

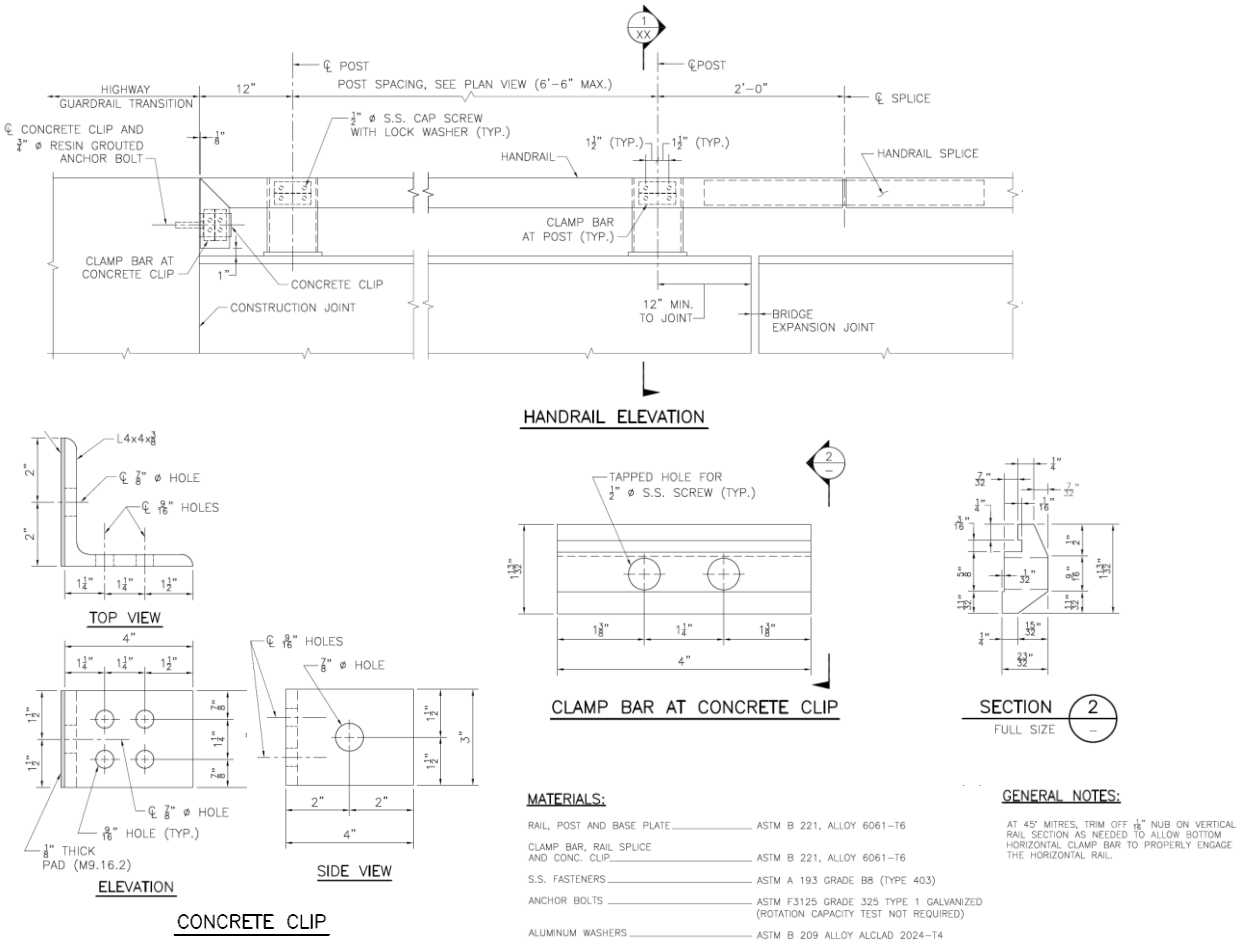

Figure 71. Drawings for the CP-MTL3 connection to transition.

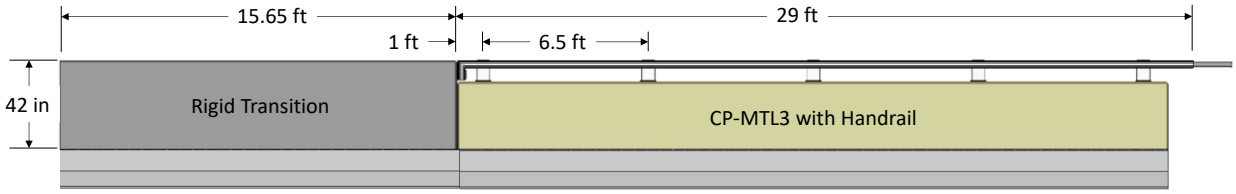

Figure 72. Elevation view for CP-MTL3 model and transition.

Test 3-10

Analysis Cases

Two impact points were evaluated under Test 3-10 conditions: (1) impact at 3.6 ft upstream of the transition and (2) impact at 4.6 ft upstream of the transition, as illustrated in Figures 73 and 74, respectively. For these analysis cases, the initial impact points at the face of the sidewalk-curb were 15.39 ft and 16.39 ft, respectively, measured from the end of the transition. The concrete parapet was modeled using *Mat-Concrete-Damage-Rel3 (KC), as described in Chapter 4.

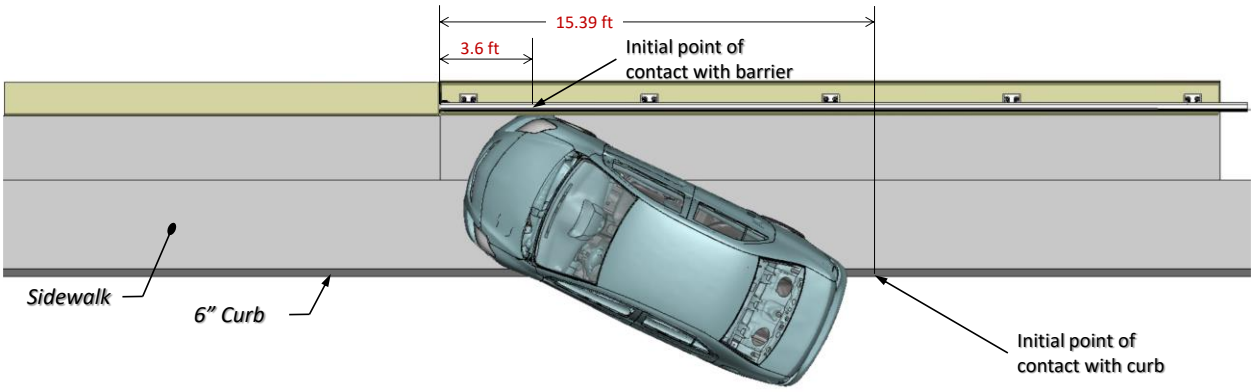

Figure 73. Test 3-10 with impact at 3.6 ft upstream of transition.

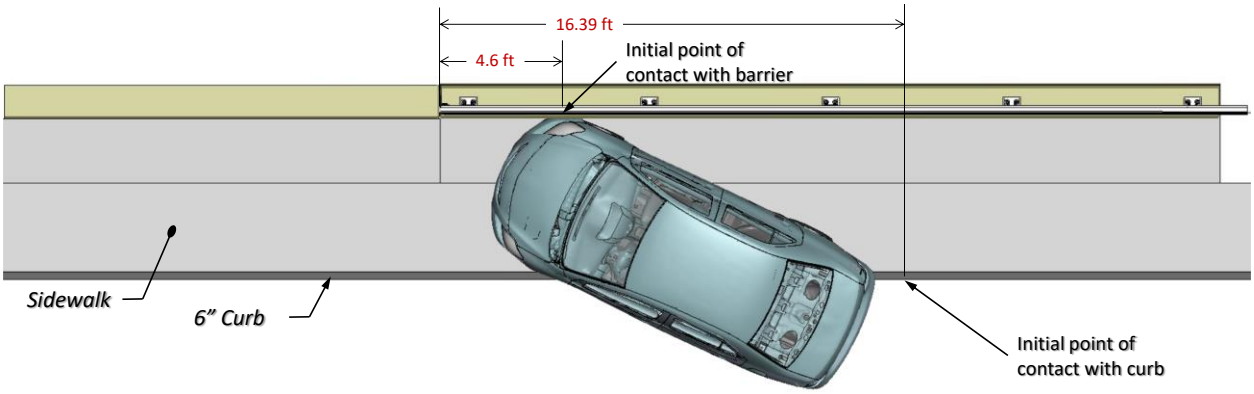

Figure 74. Test 3-10 with impact at 4.6 ft upstream of transition.

Summary of Crash Event

The 2,609-lb Yaris model struck the curb-face of the sidewalk at a speed of 62 mph and at an impact angle of 25 degrees, as illustrated in Figures 73 and 74. The sequential views for impact at 3.6 ft and 4.6 ft upstream of the transition are shown in Appendix J and Appendix K, respectively. Additional details regarding the sequence of key events for the CIP case at 3.6 ft upstream of the transition are provided in Table 9. The following sections provide time-history data evaluation, occupant risk assessments, and damages sustained by the barrier and vehicle.

Table 9. Sequence of events for Test 3-10 for CIP at 3.6 ft upstream of transition.

Event		KC
1	Initial contact with curb - Front right tire contacts curb	0.000 sec Impact speed = 62.0 mph Impact angle = 25 deg
2	Rear right tire crosses curb	0.100 sec
3	Front left tire crosses curb	0.125 sec
4	Rear right tire leaves the ground	0.125 sec
5	Vehicle contacts barrier with bumper and fender	0.145 sec Impact speed = 60.0 mph Impact angle = 24.6 deg
6	Front right tire compresses against barrierand begins to climb	0.150 sec
7	Peak 10-ms average x-acceleration	-20.58 G @ 0.167 sec
8	Bumper passes critical post	0.170 sec
9	Peak 10-ms average y-acceleration	-35.18 G @ 0.171 sec
10	Rear right tire returns to ground	0.175 sec
11	Front right tire returns to the ground	0.175 sec
12	Bumper passes transition	0.185 sec
13	Maximum concrete parapet deflection	0.11-inches @ 0.185 sec
14	Rear left tire leaves the ground	0.185 sec
15	Front left tire leaves the ground	0.195 sec
16	Maximum rail deflection	0.15-inches @ 0.200 sec
17	Front right wheel rim snags expansion joint	0.205 sec
18	Maximum occupant compartment deformation (OCD).	0.205 sec Maximum permenant OCD of 3.07 inches at the right, side front panel forward of the A-pillar
19	Occupant impact with vehicle interior	0.2113 sec OIV_x = 28.2 ft/s OIV_y = 27.9 ft/s
20	1st peak pitch angle (front pitched upward)	pitch = 3.9 deg at 0.277 sec

Table 9 [CONTINUED] Sequence of events for Test 3-10 for CIP at 3.6 ft upstream of transition.

21	Front right tire leaves the ground	0.325 sec
22	Maximum ORA_y	-10.3 G @ 0.3484 - 0.3584 sec
23	Rear of vehicle contacts barrier (tail slap)	0.350 sec
24	Vehicle front bumper passes end of barrier	0.380 sec
25	Front right tire returns to the ground	0.445 sec
26	Vehicle loses contact with barrier	0.445 sec Exit speed = 41.3 mph Exit angle = 9.4 deg
27	Maximum ORA_x	-2.1 G @ 0.4966 - 0.5066 sec
28	Maximum yaw (counter clockwise) begins to yaw clockwise	-35.2 deg @ 0.561 sec
29	Rear right tire leaves the ground	0.570 sec
30	Front left tire returns to ground	0.695 sec
31	Maximum pitch occurs (front pitched downward)	-6.7 deg @ 0.744 sec
32	Maximum roll angle (roll away from barrier)	Max Roll = -14.0 deg @ 0.813 sec
33	Rear left tire returns to ground	0.820 sec
34	Front right tire leaves the ground	0.970 sec
35	End of analysis	1.000 sec Speed = 37.1 mph Yaw angle = 32.5 deg

Time History Plots and Occupant Risk Measures

Figures 75 through 77 show the longitudinal, transverse, and vertical acceleration-time histories, respectively, computed from the center of gravity of the vehicle; Figures 78 through 80 show a comparison of angular rates and angular displacements (i.e., yaw, roll, and pitch) at the center of gravity of the vehicle. Table 10 shows the results for the occupant risk calculations. The results were very similar for both cases.

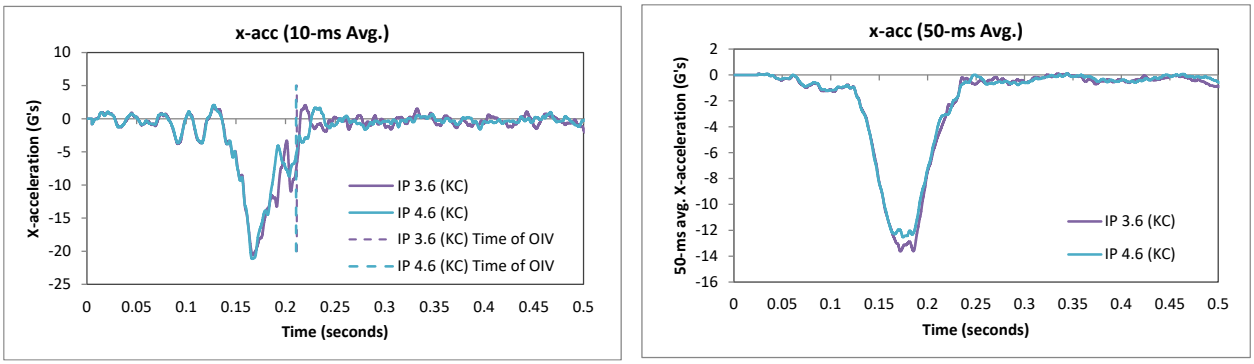

Figure 75. 10- and 50-millisecond running average X-acceleration from FEA for Test 3-10.

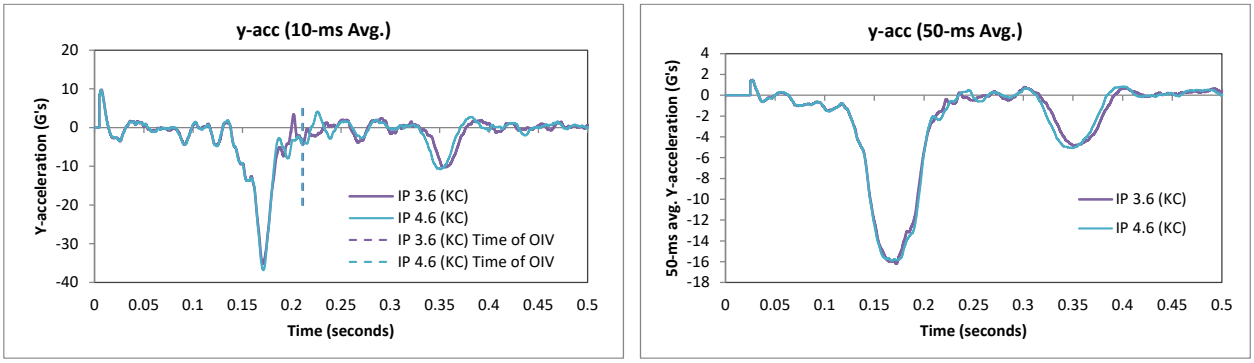

Figure 76. 10- and 50-millisecond running average Y-acceleration from FEA of Test 3-10.

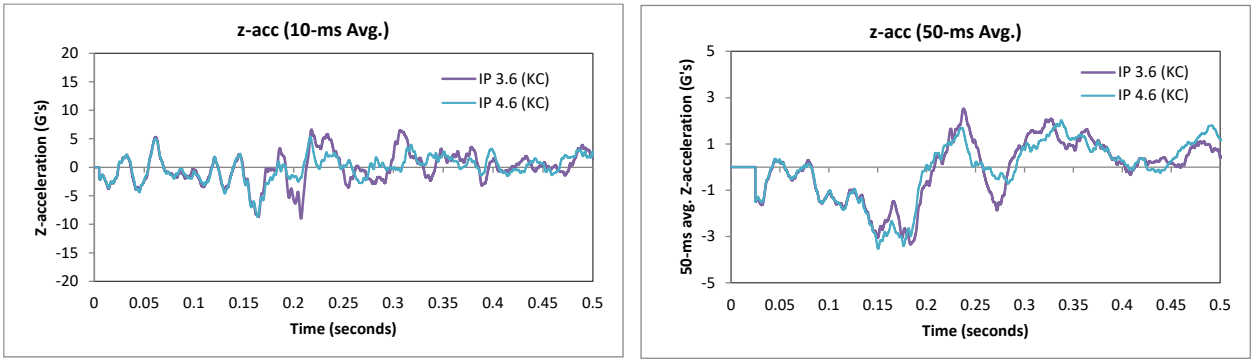

Figure 77. 10- and 50-millisecond running average Z-acceleration from FEA of Test 3-10.

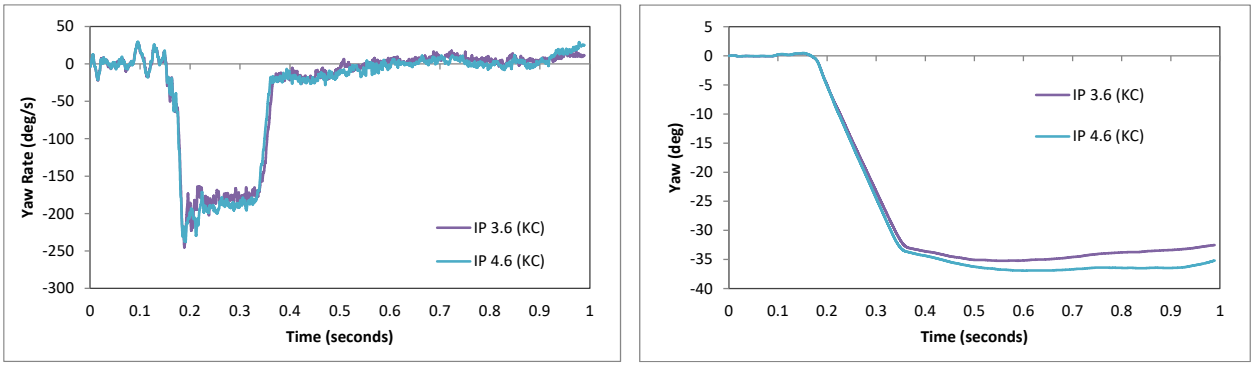

Figure 78. Yaw rate and yaw angle time-history from FEA of Test 3-10.

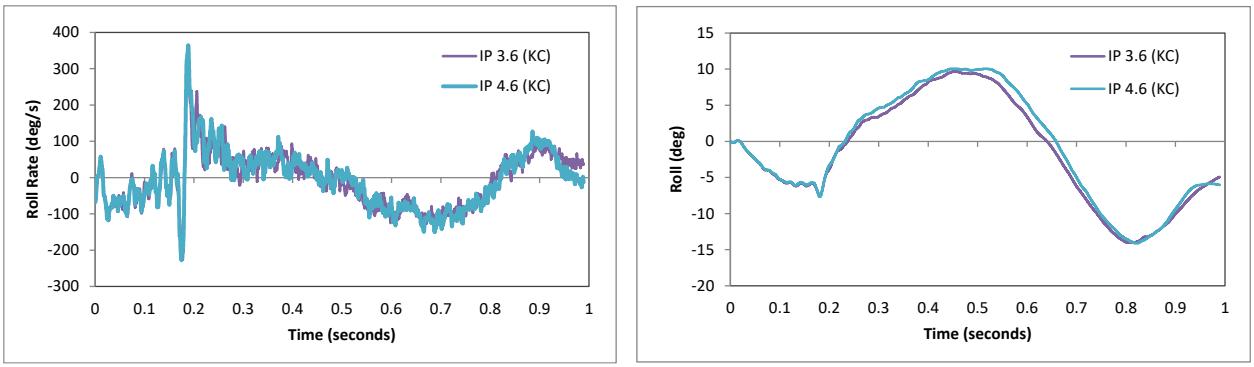

Figure 79. Roll rate and roll angle time-history from FEA of Test 3-10.

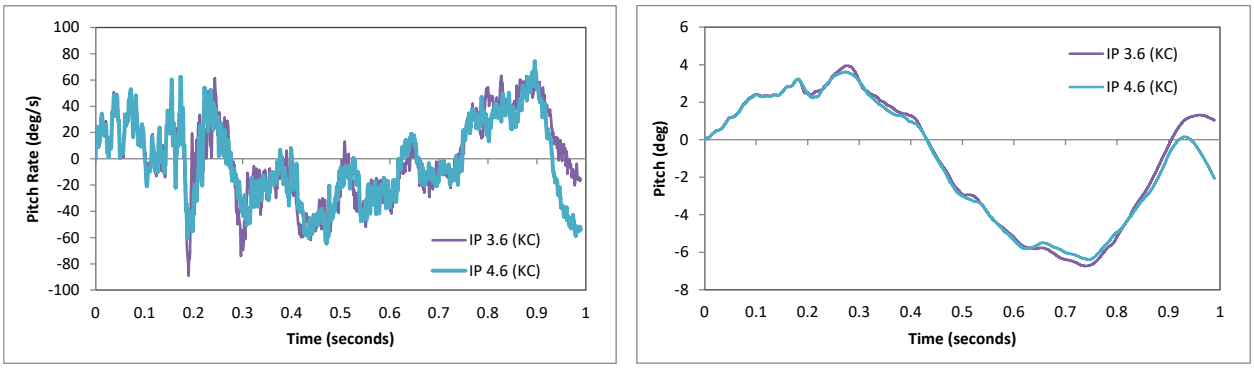

Figure 80. Pitch rate and pitch angle time-history from FEA of Test 3-10.

Impact Point 1: Impact at 3.6 ft

For the impact case at 3.6 ft upstream of the transition, the peak 10-ms running average accelerations in the longitudinal and lateral directions were -20.6 G and -35.2, respectively, as shown in Figure 75 and Figure 76. The occupant impact velocity (OIV) in the longitudinal direction was 28.2 ft/s and was 27.9 ft/s in the lateral direction. The highest ridedown accelerations (RA) were -2.1 G in the longitudinal direction and -10.3 in the lateral direction. All OIV and RA values were within the preferred limits recommended in MASH.

The first peak roll angle for the vehicle was 9.7 degrees (roll toward barrier) and occurred during impact with the barrier at approximately 0.45 seconds into the impact, as shown in Figure 79. The maximum roll angle was -14.0 degrees (roll away from barrier) and occurred during redirection at approximately 0.81 seconds. The maximum pitch angle was -6.7 degrees (rear pitching upward), as shown in Figure 80. All roll and pitch values were well within critical limits specified in MASH.

Impact Point 2: Impact at 4.6 ft

For the impact case at 4.6 ft upstream of the transition, the peak 10-ms running average accelerations in the longitudinal and lateral directions were -21.2 G and -36.9, respectively, as shown in Figure 75 and Figure 76. The occupant impact velocity (OIV) in the longitudinal direction was 25.9 ft/s and was 28.9 ft/s in the lateral direction. The highest ridedown accelerations (RA) were -3.6 G in the longitudinal direction and -10.8 in the lateral direction. All OIV and RA values were within the preferred limits recommended in MASH.

The first peak roll angle for the vehicle was 10.1 degrees (roll toward barrier) and occurred during impact with the barrier at approximately 0.45 seconds into the impact, as shown in Figure 79. The maximum roll angle was -14.1 degrees (roll away from barrier) and occurred during redirection at approximately 0.82 seconds. The maximum pitch angle was -6.4 degrees (rear pitching upward), as shown in Figure 80. All roll and pitch values were well within critical limits specified in MASH.

Table 10. Summary of MASH occupant risk metrics for Test 3-10.

Occupant Risk Factors		MASH Test 3-10	
		IP 3.6 (KC)	IP 4.6 (KC)
Occupant Impact Velocity (ft/s)	x-direction	28.2	25.9
	y-direction	27.9	28.9
	at time	at 0.2113 seconds on right side of interior	at 0.2106 seconds on right side of interior
THIV (ft/s)		38.1 at 0.2074 seconds on right side of interior	38.4 at 0.2069 seconds on right side of interior
Ridedown Acceleration (g's)	x-direction	-2.1 (0.4966 - 0.5066 seconds)	-3.6 (0.2122 - 0.2222 seconds)
	y-direction	-10.3 (0.3484 - 0.3584 seconds)	-10.8 (0.3457 - 0.3557 seconds)
PHD (g's)		10.3 (0.3483 - 0.3583 seconds)	10.8 (0.3457 - 0.3557 seconds)
ASI		2.43 (0.1702 - 0.2202 seconds)	2.44 (0.1698 - 0.2198 seconds)
Max 50-ms moving avg. acc. (g's)	x-direction	-13.6 (0.1469 - 0.1969 seconds)	-12.5 (0.1499 - 0.1999 seconds)
	y-direction	-16.2 (0.1470 - 0.1970 seconds)	-15.9 (0.1428 - 0.1928 seconds)
	z-direction	-3.3 (0.1586 - 0.2086 seconds)	-3.5 (0.1255 - 0.1755 seconds)
Maximum Angular Disp. (deg)	Roll	-14 (0.8131 seconds)	-14.1 (0.8197 seconds)
	Pitch	-6.7 (0.7374 seconds)	-6.4 (0.7479 seconds)
	Yaw	-35.2 (0.5619 seconds)	-36.9 (0.6023 seconds)

MASH Criteria

< 30 ft/s (preferred) ✓
< 40 ft/s (limit)

< 15 G (preferred) ✓
< 20.49 G (limit)

< 75 deg ✓

Damages to the Barrier System

Figures 81 and 82 show images of maximum deflection of the barrier for impact at 3.6 ft and 4.6 ft upstream of the transition. Deflection-time history plots at the point of maximum deflection are also shown in the figures. The maximum lateral deflection occurred for the impact case at 4.6 ft upstream of transition. The maximum dynamic deflection of the aluminum railing was 0.21 inches at 0.195 seconds into the impact event. The maximum lateral deflection of the concrete parapet was 0.13 inches at 0.185 seconds.

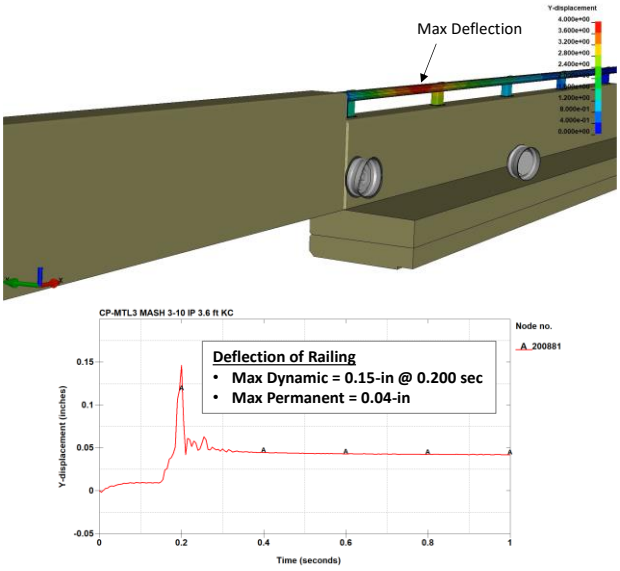

(a) Impact at 3.6 feet upstream of transition

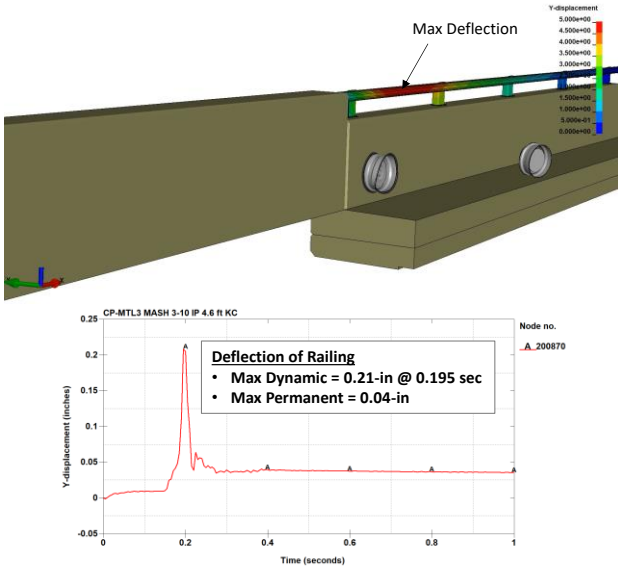

(b) Impact at 4.6 feet upstream of transition

Figure 81. Contour plot of lateral displacement of aluminum railing for Test 3-10 resulting from impact at (a) 3.6 ft and (b) 4.6 ft upstream of transiton.

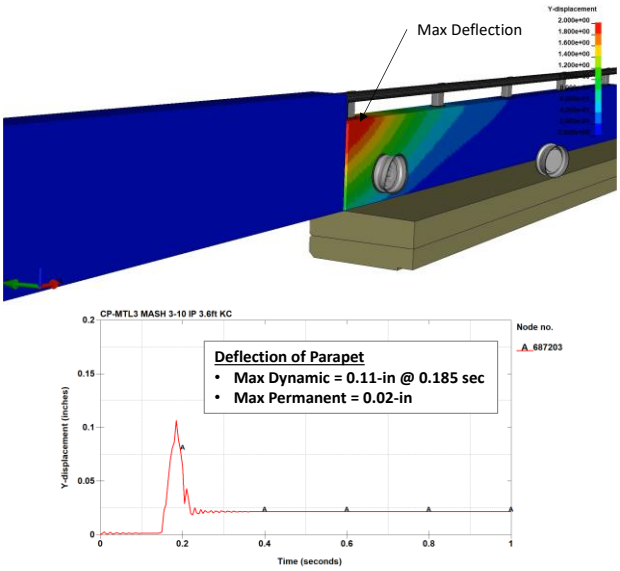

(a) Impact at 3.6 feet upstream of transition

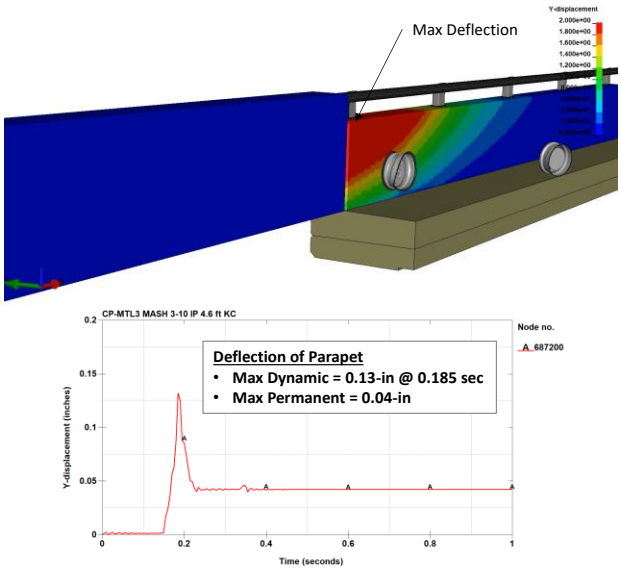

(b) Impact at 4.6 feet upstream of transition

Figure 82. Contour plot of lateral displacement of concrete parapet for Test 3-10 resulting from impact at (a) 3.6 ft and (b) 4.6 ft upstream of transiton.

Figure 83 shows a contour plot of effective plastic strain on the aluminum railing components. Due to the height of the barrier with respect to the small car, there was minimal contact between the car and the handrail during impact. As a result, the plastic strain in the railing was negligible for both analysis cases.

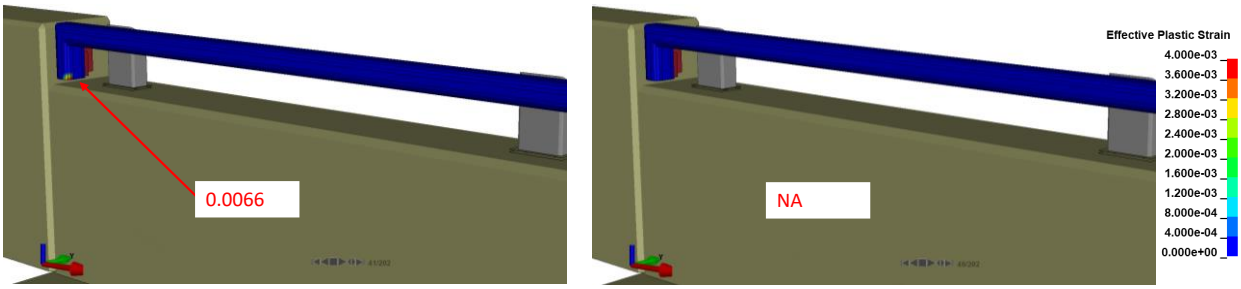

(a) Impact at 3.6 feet upstream of transition

(b) Impact at 4.6 feet upstream of transition

Figure 83. Effective plastic strain contours on rail components during Test 3-10 for (a) impact at 3.6 ft and (b) 4.6 ft upstream of the transition.

Figure 84 shows contour plots of the damage parameter for the two analysis cases, and Figure 85 shows contours of 1st principal strain. The results indicate a low potential for concrete spalling on the front face of the barrier, as evident from the damage parameter contours, but no potential for any major damage or cracks in the concrete, as interpreted from the 1st principal strain contours.

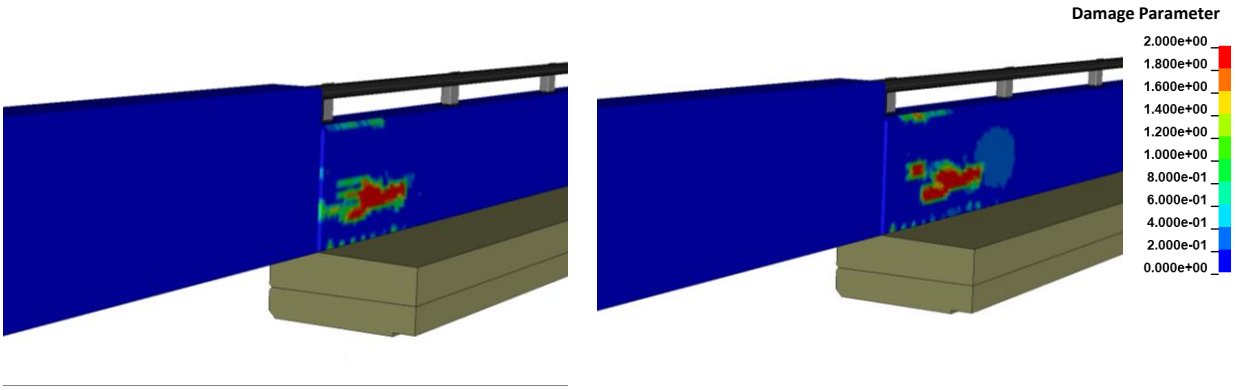

(a) Impact at 3.6 feet upstream of transition

(b) Impact at 4.6 feet upstream of transition

Figure 84. Contour plot of the damage variable on the concrete parapet and deck during Test 3-10 for (a) impact at 3.6 ft and (b) 4.6 ft upstream of the transition.

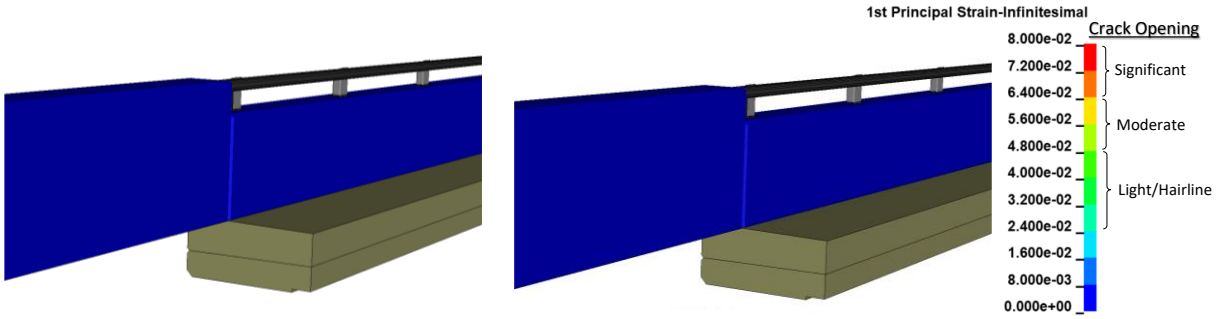

(a) Impact at 3.6 feet upstream of transition **(b)** Impact at 4.6 feet upstream of transition

Figure 85. Contour plot of 1st principal strain on the concrete parapet and deck during Test 3-10 for (a) impact at 3.6 ft and (b) 4.6 ft upstream of the transition.

Damages to Vehicle

Figure 86 shows contour plots of effective plastic strain for the vehicle during Test 3-10 for each analysis case. The damage to the vehicle was limited to the impact side front bumper, fender, front wheel assembly, front door, lower portion of the A-pillar, rear side panel, rear bumper, and the rear wheel.

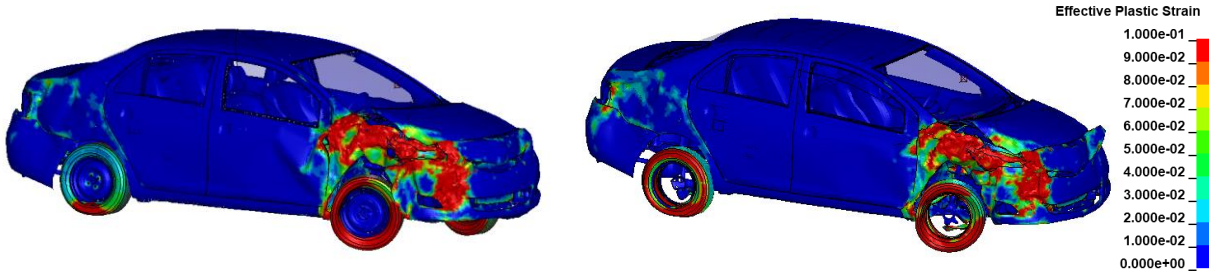

(a) Impact at 3.6 ft upstream of critical post **(b)** Impact at 4.6 ft upstream of critical post

Figure 86. Damages to vehicle in Test 3-10 for (a) impact at 3.6 ft and (b) 4.6 ft upstream of the transition.

Occupant Compartment Deformation (OCD)

The maximum deformation of the occupant compartment was 3.07 inches for impact at 3.6 ft upstream of the transition and was 2.62 inches for impact at 4.6 ft upstream of the transition and occurred at the right, side front panel forward of the A-pillar for both analysis cases. Figure 87 shows a post-impact view of the vehicle floor pan with all other components removed to facilitate viewing. The maximum deformation was well within the critical limit of 12 inches specified in MASH for this area of the occupant compartment.

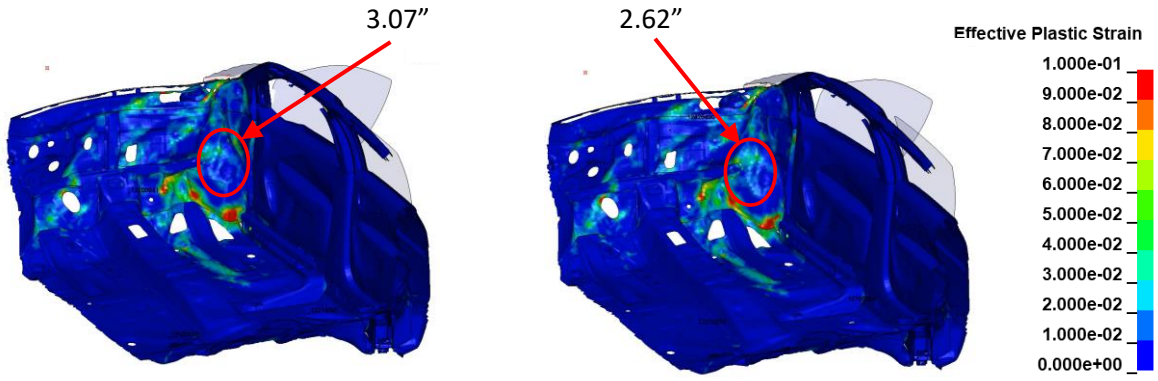

(a) Impact at 3.6 ft upstream of critical post

(b) Impact at 4.6 ft upstream of critical post

Figure 87. Occupant compartment deformation resulting from Test 3-10 for (a) impact at 3.6 ft and (b) 4.6 ft upstream of the transition.

Exit Box

Figure 88 shows the exit box for Test 3-10. The post trajectory response was similar for both cases, and the vehicle was redirected with its path well within the exit box criteria of MASH.

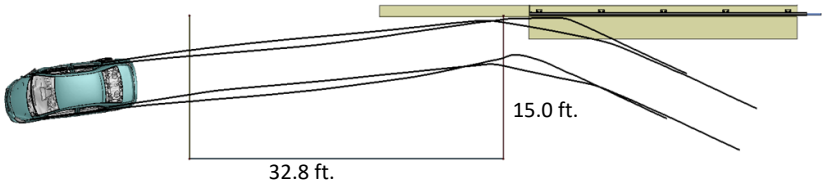

(a) Impact at 3.6 ft upstream of critical post

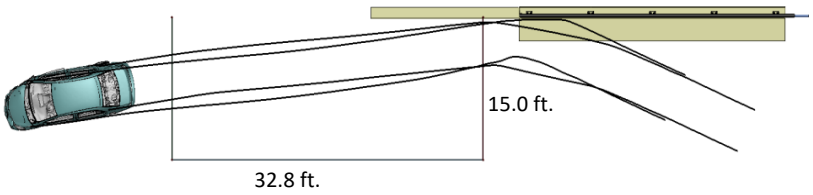

(b) Impact at 4.6 ft upstream of critical post

Figure 88. Exit box for Test 3-10 for (a) impact at 3.6 ft and (b) 4.6 ft upstream of the transition.

Results Summary

A summary of MASH Test 3-10 results is shown in Table 11 and in Figures 89 and 90. The bridge rail successfully contained and redirected the small car with minimal damage to the concrete parapet and aluminum handrailing. There were no detached elements from the barrier that showed potential for penetrating into the occupant compartment or presenting undue hazard to other traffic. The maximum occupant compartment deformation was well within critical

limits specified in MASH. The windshield showed no sign of cracking or failure. The vehicle remained upright and did not experience excessive roll or pitch angle displacements. The vehicle also remained within the exit-box criteria of MASH. The OIV and maximum RA values were within preferred limits specified in MASH. Based on the results of this analysis, the barrier is expected to meet all structural and occupant risk criteria in MASH for Test 3-10 impact conditions.

CIP Recommendation for Test 3-10 for CP-MTL3 at Approach to Transition

The recommended CIP for Test 3-10 for this section of the bridge rail is 3.6 ft upstream of the transition. As mentioned previously, the OIV's and the RAs were within preferred limits in all cases. However, the longitudinal OIV was slightly higher for the 3.6-ft impact case, and the lateral OIV and RA were slightly higher for the 4.6-ft impact case. The OCD was slightly higher for the 3.6-ft impact case. There was negligible contact between the vehicle and the handrail in all cases. As a result, the deflections of the handrail were also negligible in all cases. The deflections of the concrete parapet were negligible in all cases as well, and the maximum deflections were less than 1/8 inch. It is the research team's opinion that either of the analysis cases (i.e., 3.6 ft or 4.6 ft) provides equivalent potential for being the more critical, so it was decided to remain consistent with the recommendation provided in MASH for Test 3-10 on rigid barriers.

Table 11. Summary of MASH Test 3-10 for the CP-MTL3 at transition.

Evaluation Factors		Evaluation Criteria	IP 3.6ft	IP 4.6 ft
Structural Adequacy	A	Test article should contain and redirect the vehicle or bring the vehicle to a controlled stop; the vehicle should not penetrate, underride, or override the installation although controlled lateral deflection of the test article is acceptable.	Pass	Pass
Occupant Risk	D	Detached elements, fragments, or other debris from the test article should not penetrate or show potential for penetrating the occupant compartment, or present undue hazard to other traffic, pedestrians, or personnel in a work zone. Deformations of, or intrusions into, to occupant compartment should not exceed limits set forth in Section 5.2.2 and Appendix E.	Pass	Pass
	F	The vehicle should remain upright during and after collision. The maximum roll and pitch angles are not to exceed 75 degrees.	Pass	Pass
	H	The longitudinal and lateral occupant impact velocity (OIV) shall not exceed 40 ft/s, with a preferred limit of 30 ft/s.	Pass	Pass
	I	The longitudinal and lateral ridedown acceleration (RA) shall not exceed 20.49 G, with a preferred limit of 15.0 G	Pass	Pass

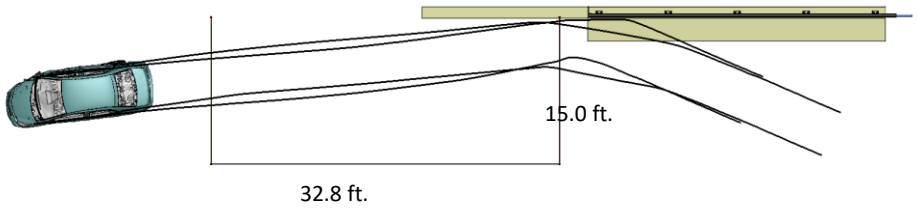

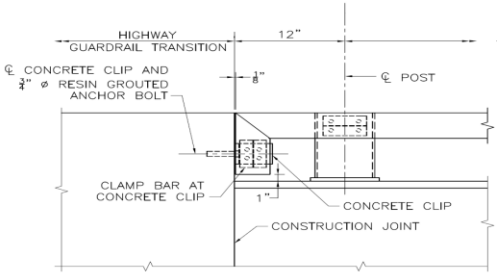

General Information		**Impact Conditions**		**Max50-millisecond Avg. (G)**	
Analysis Agency	Roadsafe LLC	Speed	62.0 mph	Longitudinal	-13.6 g
Test Standard Test No.	MASH Test 3-10	Angle	25 degrees	Lateral	-16.2 g
Analysis No.	CP-MTL3_Test3-10-IP3p6ft_KC	Location	3.6 ft upstream of transition	Vertical	-3.3 g
Analysis Date	6/14/2023				
Test Article		**Impact Severity**	55.7 kip-ft	**Test Article Deflections (in)**	
Type	Bridge Rail at Transition	**Exit Conditions**		Dynamic	0.15 inches
Name	CP-MTL3	Speed	41.3 mph	Permanent	0.04 inches
Installation Length	44.65 feet	Angle	9.4 degrees	Working Width	15.11 inches
Material or Key Elements	Continuous concrete with top mounted aluminum post-and-beam rail	Time	0.445 seconds	**Max. OCD**	3.07 inches
Soil Type and Condition	NA	**Occupant Risk Values**		**Vehicle Stability**	
Analysis Vehicle		Longitudinal OIV	28.2 ft/s	Roll	-14.0 degees
Type / Designation	1100C	Lateral OIV	27.9 ft/s	Pitch	-6.7 degrees
FEA Model name	YarisC_V1I_R200522.k w/ RS tire	Longitudinal ORA	-2.1 g	Yaw	-35.2 degrees
Mass	2,595 lb	Lateral ORA	-10.3 g		
		THIV	38.1 ft/s		
		PHD	10.3 g		
		ASI	2.43		

Figure 89. Summary results for MASH Test 3-10 with impact point at 3.6 ft upstream of post (KC model).

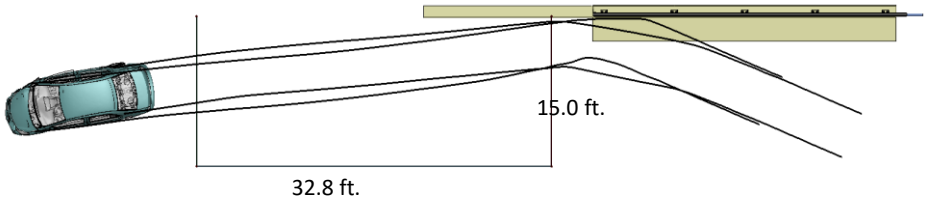

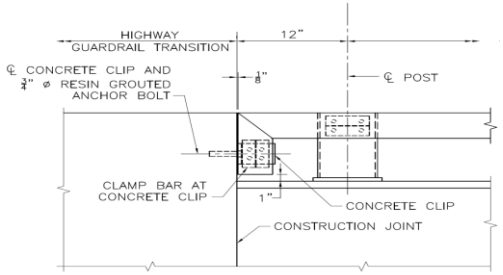

General Information		**Impact Conditions**		**Max50-millisecond Avg. (G)**	
Analysis Agency	Roadsafe LLC	Speed	62.0 mph	Longitudinal	-12.5 g
Test Standard Test No.	MASH Test 3-10	Angle	25 degrees	Lateral	-15.9 g
Analysis No.	CP-MTL3_Test3-10-IP4p6ft_KC	Location	4.6 ft upstream of transition	Vertical	-3.5 g
Analysis Date	6/15/2023				
Test Article		**Impact Severity**	55.7 kip-ft	**Test Article Deflections (in)**	
Type	Bridge Rail at Transition	**Exit Conditions**		Dynamic	0.21 inches
Name	CP-MTL3	Speed	42.0 mph	Permanent	0.04 inches
Installation Length	44.65 feet	Angle	10.3 degrees	Working Width	15.13 inches
Material or Key Elements	Continuous concrete with top mounted aluminum post-and-beam rail	Time	0.445 seconds	**Max. OCD**	2.62 inches
Soil Type and Condition	NA	**Occupant Risk Values**		**Vehicle Stability**	
Analysis Vehicle		Longitudinal OIV	25.9 ft/s	Roll	-14.1 degees
Type / Designation	1100C	Lateral OIV	28.9 ft/s	Pitch	-6.4 degrees
FEA Model name	YarisC_V1I_R200522.k w/ RS tire	Longitudinal ORA	-3.6 g	Yaw	-36.9 degrees
Mass	2,595 lb	Lateral ORA	-10.8 g		
		THIV	38.4 ft/s		
		PHD	10.8 g		
		ASI	2.44		

Figure 90. Summary results for MASH Test 3-10 with impact point at 4.6 ft upstream of post (KC model).

Test 3-11

Analysis Cases

Two impact points were evaluated under Test 3-11 conditions: (1) impact at 4.26 ft upstream of the transition and (2) impact at 5.26 ft upstream of the transition, as illustrated in Figures 91 and 92, respectively. For these analysis cases, the initial impact points at the face of the sidewalk-curb were 16.05 ft and 17.05 ft, respectively, measured from the upstream end of the transition. The concrete parapet was modeled using *Mat-Concrete-Damage-Rel3 (KC), as described in Chapter 4.

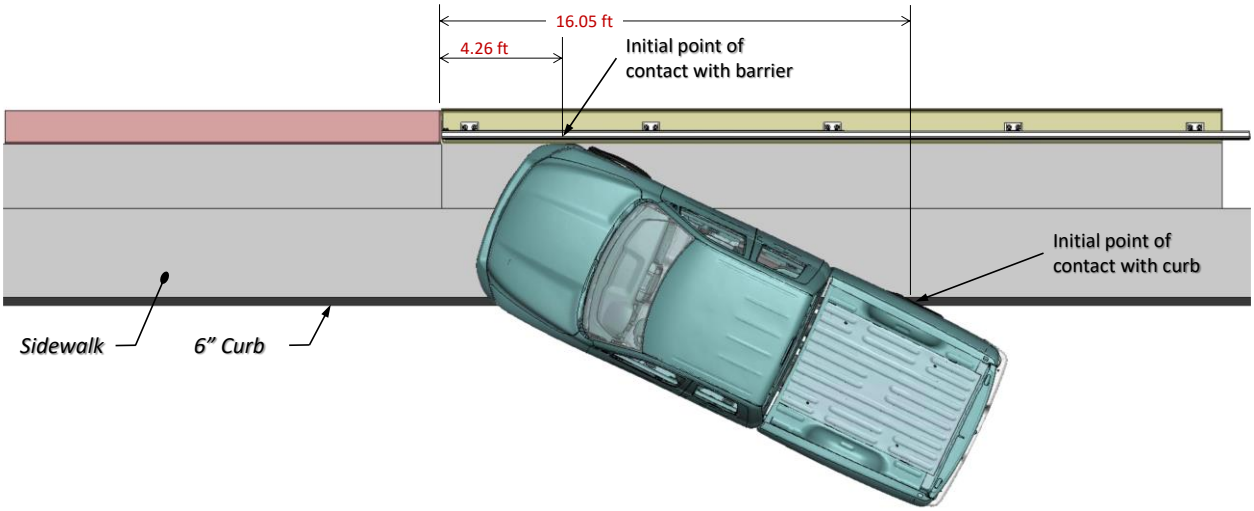

Figure 91. Test 3-11 with impact at 4.26 ft upstream of transition.

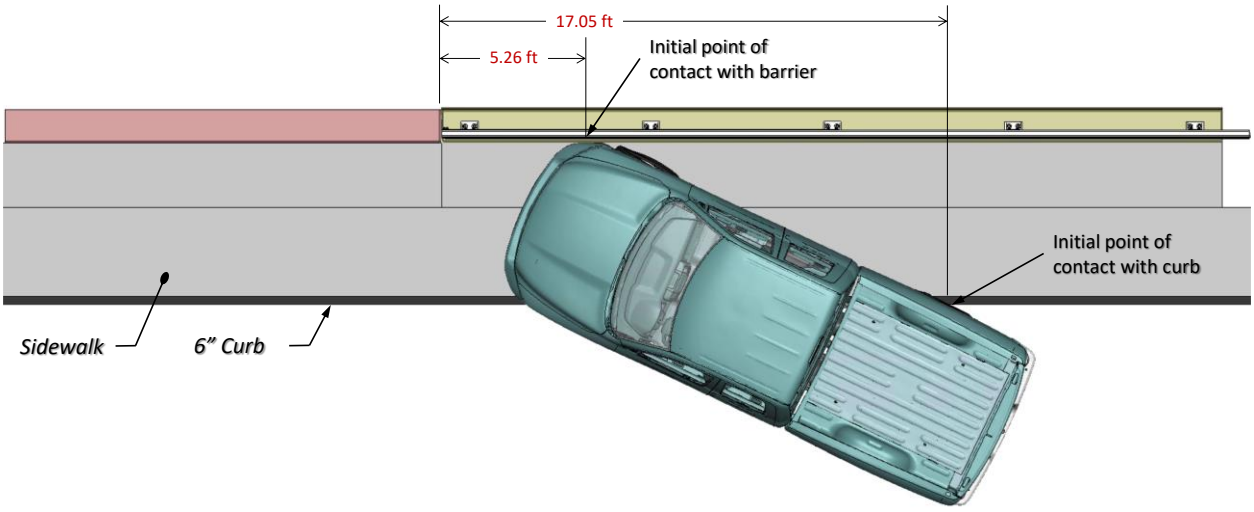

Figure 92. Test 3-11 with impact at 5.26 ft upstream of transition.

Summary of Crash Event

The 5,182-lb pickup model struck the curb-face of the sidewalk at a speed of 63 mph and at an impact angle of 25 degrees, as illustrated in Figures 91 and 92. The sequential views for

impact at 4.26 ft and 5.26 ft upstream of the transition are shown in Appendix L and Appendix M, respectively. Additional details regarding the sequence of key events for the CIP case at 4.26 ft upstream of the transition are provided in Table 12. The following sections provide time-history data evaluation, occupant risk assessments, and damages sustained by the barrier and vehicle.

Table 12. Sequence of events for Test 3-11 for CIP at 4.26 ft upstream of transition.

Event		KC
1	Initial contact with curb - Front right tire contacts curb	0.000 sec Impact speed = 62.0 mph Impact angle = 25 deg
2	Vehicle contacts barrier with bumper and fender	0.135 sec Impact speed = 61.0 mph Impact angle = 24.8 deg
3	Rear right tire crosses curb	0.150 sec
4	Front left tire crosses curb	0.150 sec
5	Front right tire compresses against barrierand begins to climb	0.150 sec
6	Bumper passes critical post	0.165 sec
7	Peak 10-ms average x-acceleration	-14.3 G @ 0.175 sec
8	Bumper passes transition	0.175 sec
9	1st peak pitch angle (front pitched	pitch = 1.4 deg at 0.189 sec
10	Peak 10-ms average y-acceleration	-23.63 G @ 0.191 sec
11	Maximum concrete parapet deflection	0.24-inches @ 0.200 sec
12	Front right wheel rim snags expansion	0.210 sec
13	Occupant impact with vehicle interior	0.2169 sec OIV_x = 23.0 ft/s OIV_y = 27.2 ft/s
14	Maximum ORA_x	-8.7 G @ 0.2200 - 0.2300 sec
15	Maximum occupant compartment deformation (OCD).	0.225 sec Maximum permenant OCD of 5.59 inches at the right, side front panel forward of the A-pillar
16	Rear left tire leaves the ground	0.235 sec
17	Rear right tire leaves the ground	0.250 sec
18	Front left tire leaves the ground	0.265 sec
19	Rear right tire returns to ground	0.275 sec
20	Front right tire returns to the ground	0.275 sec

Table 12 [CONTINUED] Sequence of events for Test 3-11 for CIP at 4.26 ft upstream of transition.

21	Front right tire leaves the ground	0.345 sec
22	Rear right tire leaves the ground	0.345 sec
23	Rear of vehicle contacts barrier (tail slap)	0.355 sec
24	Maximum ORA_y	-12.1 G @ 0.3613 - 0.3713 sec
25	Maximum rail deflection	1.23-inches @ 0.365 sec
26	Vehicle front bumper passes end of	0.370 sec
27	Front right tire returns to the ground	0.380 sec
28	Vehicle loses contact with barrier	0.470 sec Exit speed = 42.7 mph Exit angle = 5.9 deg
29	Front left tire returns to ground	0.680 sec
30	Rear left tire returns to ground	0.755 sec
31	Rear right tire returns to ground	0.780 sec
32	Maximum roll angle (roll away from barrier)	Max Roll = -10.3 deg @ 0.791 sec
33	Front right tire leaves ground while crossing curb	0.855 sec
34	Front right tire returns to the ground	0.930 sec
35	Rear left tire leaves the ground	0.930 sec
36	Maximum pitch occurs (front pitched downward)	-5.2 deg @ 0.989 sec
37	End of analysis	1.000 sec Speed = 36.2 mph Yaw angle = 34.8 deg

Time History Plots and Occupant Risk Measures

Figures 93 through 95 show the longitudinal, transverse, and vertical acceleration-time histories, respectively, computed from the center of gravity of the vehicle; Figures 96 through 98 show a comparison of angular rates and angular displacements (i.e., yaw, roll, and pitch) at the center of gravity of the vehicle. Table 13 shows the results for the occupant risk calculations. The results were very similar for both cases.

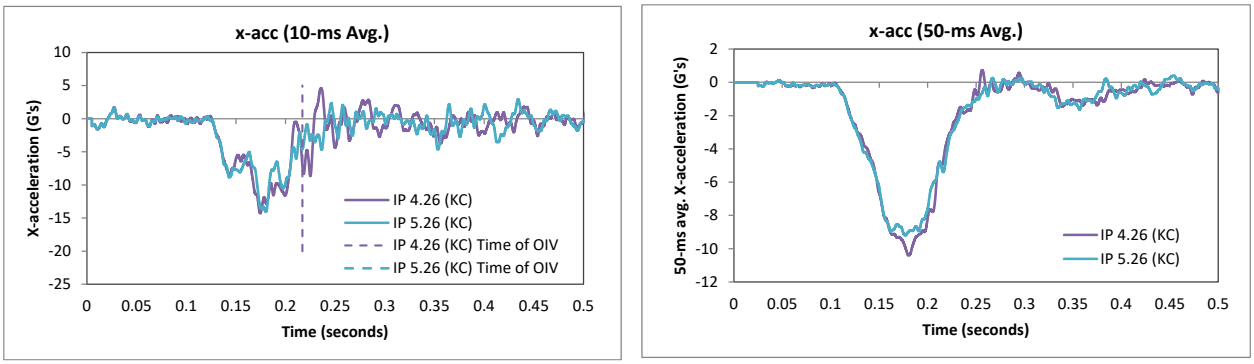

Figure 93. 10- and 50-millisecond running average X-acceleration from FEA for Test 3-11.

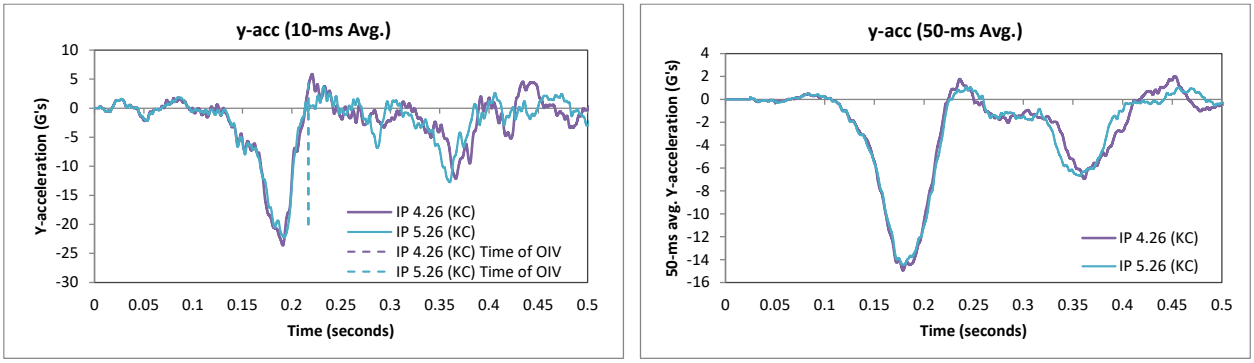

Figure 94. 10- and 50-millisecond running average Y-acceleration from FEA of Test 3-11.

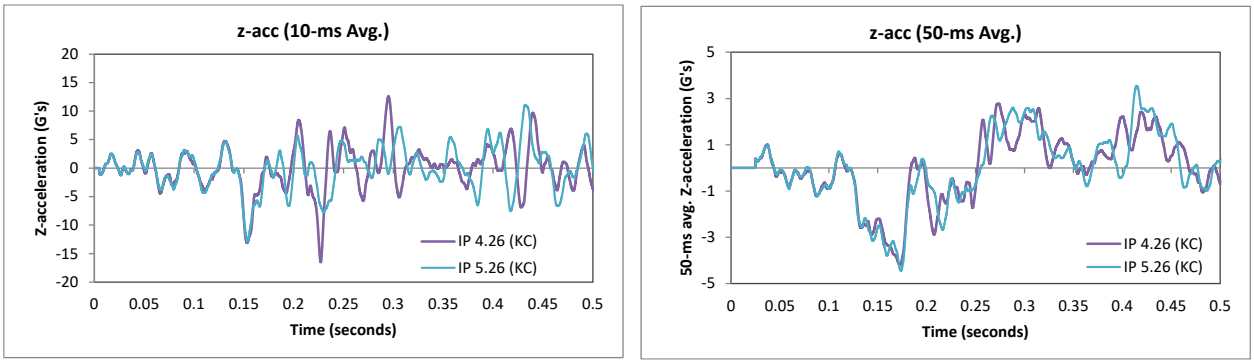

Figure 95. 10- and 50-millisecond running average Z-acceleration from FEA of Test 3-11.

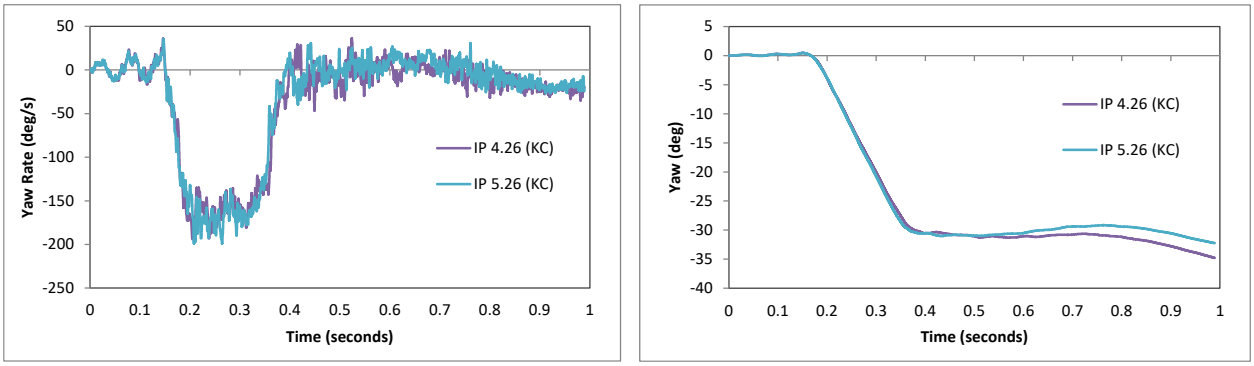

Figure 96. Yaw rate and yaw angle time-history from FEA of Test 3-11.

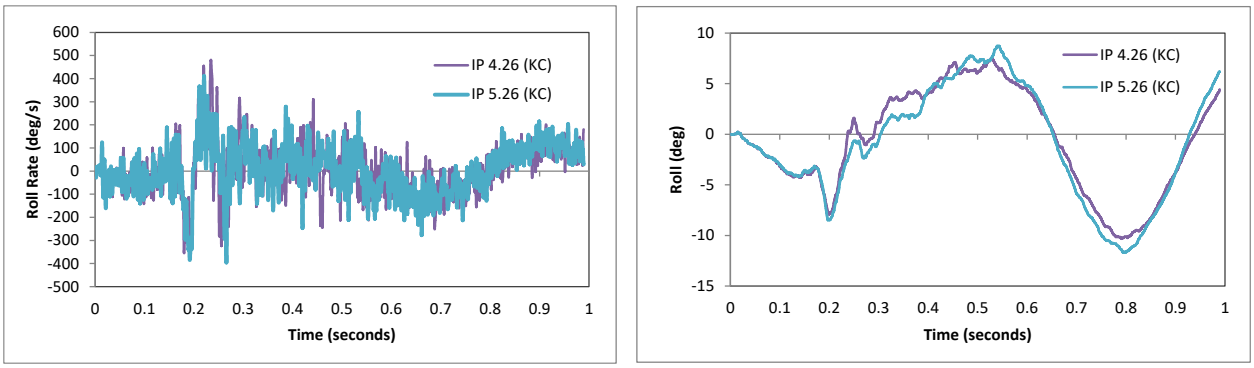

Figure 97. Roll rate and roll angle time-history from FEA of Test 3-11.

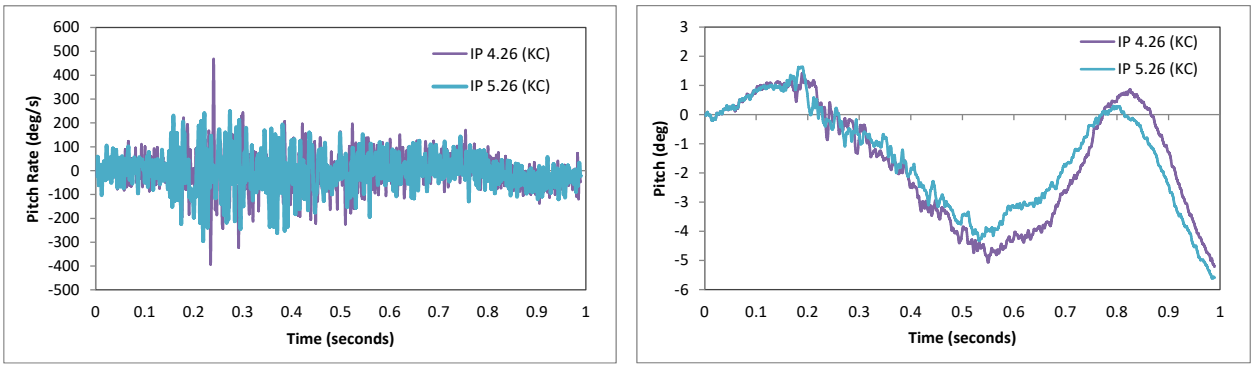

Figure 98. Pitch rate and pitch angle time-history from FEA of Test 3-11.

Impact Point 1: Impact at 4.26 ft

For the impact case at 4.26 ft upstream of the transition, the peak 10-ms running average accelerations in the longitudinal and lateral directions were -14.3 G and -23.6, respectively, as shown in Figure 93 and Figure 94. The occupant impact velocity (OIV) in the longitudinal direction was 23.0 ft/s and was 27.2 ft/s in the lateral direction. The highest ridedown accelerations (RA) were -8.1 G in the longitudinal direction and -12.1 in the lateral direction. All OIV and RA values were within the preferred limits recommended in MASH.

The first peak roll angle for the vehicle was 7.4 degrees (roll toward barrier) and occurred during impact with the barrier at approximately 0.53 seconds of the impact, as shown in Figure 97. The maximum roll angle was -10.3 degrees (roll away from barrier) and occurred during redirection at approximately 0.79 seconds. The maximum pitch angle was -5.2 degrees (rear pitching upward), as shown in Figure 98. All roll and pitch values were well within critical limits specified in MASH.

Impact Point 2: Impact at 5.26 ft

For the impact case at 5.26 ft upstream of the transition the peak 10-ms running average accelerations in the longitudinal and lateral directions were -14.0 G and -22.3, respectively, as shown in Figure 93 and Figure 94. The occupant impact velocity (OIV) in the longitudinal direction was 22.6 ft/s and was 26.6 ft/s in the lateral direction. The highest ridedown accelerations (RA) were -4.7 G in the longitudinal direction and -12.8 in the lateral direction. All OIV and RA values were within the preferred limits recommended in MASH.

The first peak roll angle for the vehicle was 8.7 degrees (roll toward barrier) and occurred during impact with the barrier at approximately 0.54 seconds of the impact, as shown in Figure 97. The maximum roll angle was -11.7 degrees (roll away from barrier) and occurred during redirection at approximately 0.80 seconds. The maximum pitch angle was -5.6 degrees (rear pitching upward), as shown in Figure 98. All roll and pitch values were well within critical limits specified in MASH.

Table 13. Summary of MASH occupant risk metrics for Test 3-11.

Occupant Risk Factors		MASH Test 3-11	
		IP 4.26 (KC)	IP 5.26 (KC)
Occupant Impact Velocity (ft/s)	x-direction	23.0	22.6
	y-direction	27.2	26.6
	at time	at 0.2169 seconds on right side of interior	at 0.2174 seconds on right side of interior
THIV (ft/s)		36.4 at 0.2134 seconds on right side of interior	35.4 at 0.2137 seconds on right side of interior
Ridedown Acceleration (g's)	x-direction	-8.7 (0.2200 - 0.2300 seconds)	-4.7 (0.2313 - 0.2413 seconds)
	y-direction	-12.1 (0.3613 - 0.3713 seconds)	-12.8 (0.3552 - 0.3652 seconds)
PHD (g's)		12.1 (0.3613 - 0.3713 seconds)	12.9 (0.3551 - 0.3651 seconds)
ASI		2.04 (0.1832 - 0.2332 seconds)	1.95 (0.1838 - 0.2338 seconds)
Max 50-ms moving avg. acc. (g's)	x-direction	-10.4 (0.1554 - 0.2054 seconds)	-9.2 (0.1518 - 0.2018 seconds)
	y-direction	-14.9 (0.1538 - 0.2038 seconds)	-14.4 (0.1553 - 0.2053 seconds)
	z-direction	-4.2 (0.1478 - 0.1978 seconds)	-4.5 (0.1486 - 0.1986 seconds)
Maximum Angular Disp. (deg)	Roll	-10.3 (0.7913 seconds)	-11.7 (0.7984 seconds)
	Pitch	-5.2 (0.9893 seconds)	-5.6 (0.9852 seconds)
	Yaw	-34.8 (0.9893 seconds)	-32.2 (0.9893 seconds)

MASH Criteria

< 30 ft/s (preferred) ✓
< 40 ft/s (limit)

< 15 G (preferred) ✓
< 20.49 G (limit)

< 75 deg ✓

Damages to the Barrier System

Figures 99 and 100 show images of maximum deflection of the barrier for impact at 4.26 ft and 5.26 ft upstream of the transition. Deflection-time history plots at the point of maximum deflection are also shown in the figures. The maximum lateral deflection of the aluminum railing occurred near the midspan between the two end posts. For impact at 4.26 ft upstream of the transition, the maximum dynamic deflection of the aluminum railing was 1.23 inches at 0.37 seconds and occurred near the mid-span between the two end posts. For impact at 5.26 ft upstream of the transition, the maximum dynamic deflection of the aluminum railing was 1.45 inches at 0.36 seconds at the midspan between the two end posts.

The maximum lateral dynamic deflection of the concrete parapet was 0.24 inches for the impact case at 4.26 ft upstream of the transition and was 0.17 inches for the impact case at 5.26 ft upstream of the transition. In both cases the maximum deflection of the parapet occurred at the upper downstream edge of the parapet where is abuts to the transition.

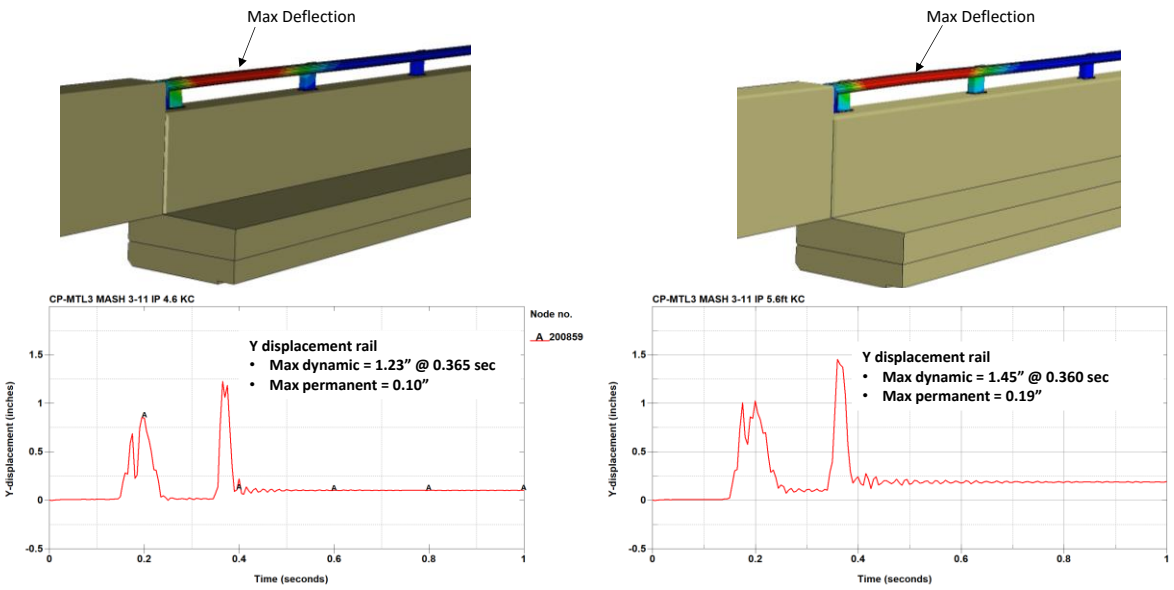

(a) Impact at 4.26 ft upstream of transition

(b) Impact at 5.26 feet upstream of transition

Figure 99. Contour plot of lateral displacement of aluminum railing for Test 3-11 resulting from impact at (a) 4.26 ft and (b) 5.26 ft upstream of transiton.

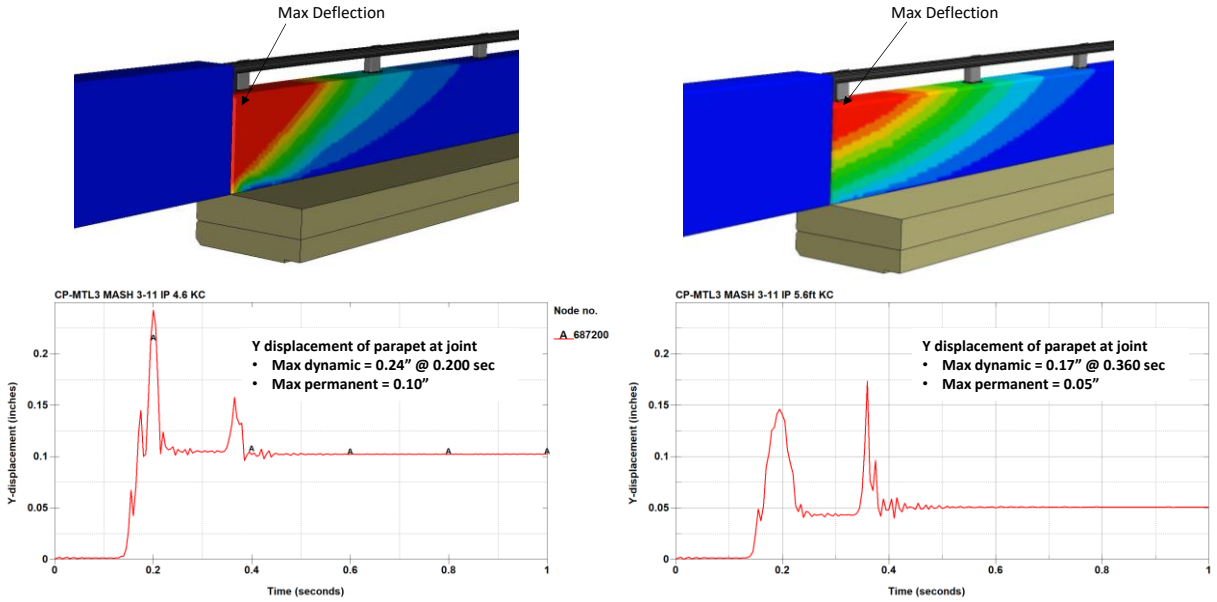

(a) Impact at 4.26 ft upstream of transition

(b) Impact at 5.26 feet upstream of transition

Figure 100. Contour plot of lateral displacement of concrete parapet for Test 3-11 resulting from impact at (a) 4.26 ft and (b) 5.26 ft upstream of transiton.

Figure 101 shows a contour plot of effective plastic strain on the aluminum railing components. The highest effective plastic strain values were similar for both cases with magnitudes of 0.063 and 0.061 for the impact cases at 4.26 ft and 5.26 upstream of the transition, respectively, and occurred at the lower back edge of the post near the transition. These strains

are less than the minimum failure strain of 10 percent for the material and they occur on a compression area of the post.

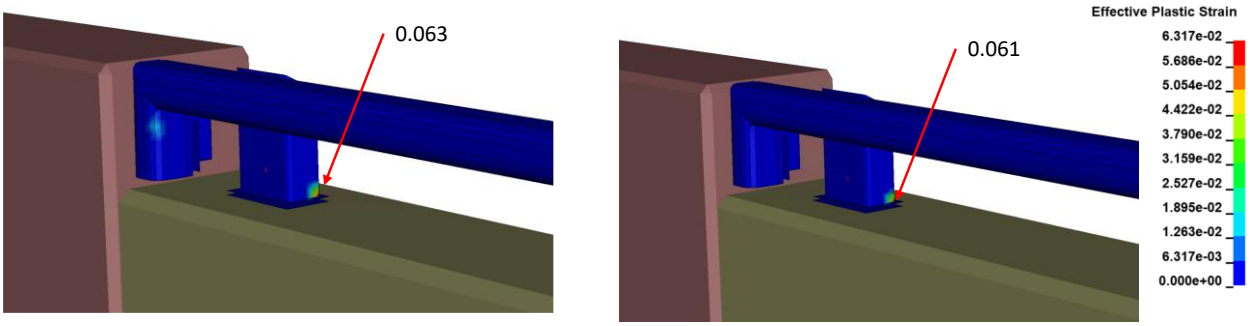

(a) Impact at 4.26 feet upstream of transition

(b) Impact at 5.26 feet upstream of transition

Figure 101. Effective plastic strain contours on rail components during Test 3-11 for (a) impact at 4.26 ft and (b) 5.26 ft upstream of the transition.

Figure 102 shows contour plots of the damage parameter for the two analysis cases, and Figure 103 shows contours of 1st principal strain. The damage parameter plot indicates a high potential for spalling on the face of the concrete parapet for both cases and a possible hairline crack running at approximately 45 degrees across the face of the barrier starting at 5.54 ft from the downstream end of the parapet. The results of the 1st principal strain assessment, shown in Figure 103, indicate that there is very low potential for any notable cracks. However, cutting the contour range off at 0.0267 for the 1st principal strain as shown in Figure 104, results in a similar damage pattern as that shown on the damage parameter contour plot. Since the crack did not extend through to the backside of the barrier and given that the maximum deformation of the parapet was less than ¼-inch, then the crack should have minimal to negligible effect on the barrier's crash performance.

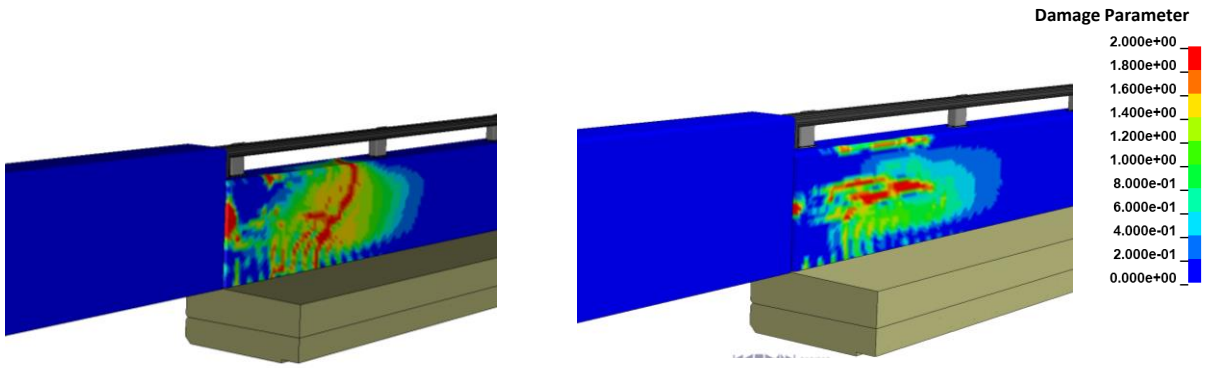

(a) Impact at 4.26 feet upstream of transition

(b) Impact at 5.26 feet upstream of transition

Figure 102. Contour plot of the damage variable on the concrete parapet and deck during Test 3-11 for (a) impact at 4.26 ft and (b) 5.26 ft upstream of the transition.

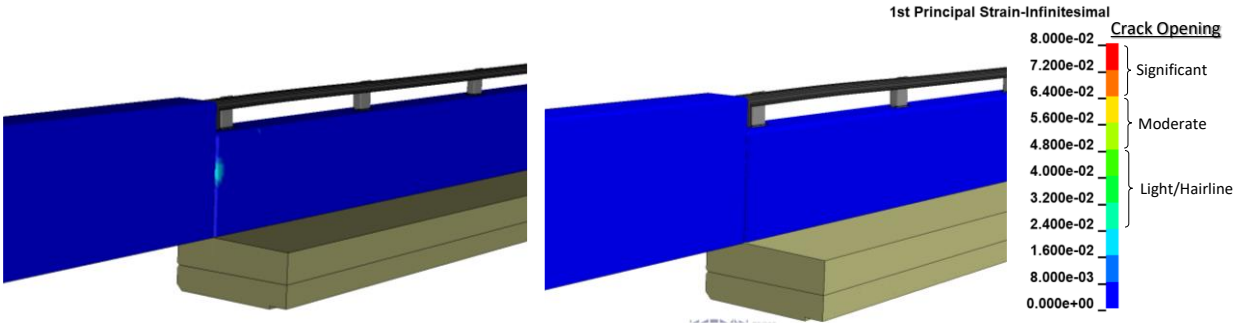

(a) Impact at 4.26 feet upstream of transition **(b)** Impact at 5.26 feet upstream of transition

Figure 103. Contour plot of 1st principal strain on the concrete parapet and deck during Test 3-11 for (a) impact at 4.26 ft and (b) 5.26 ft upstream of the transition.

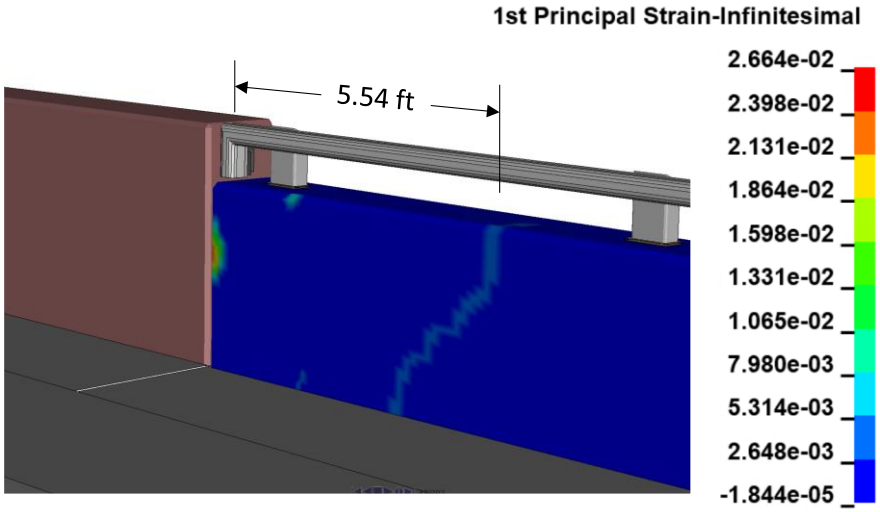

Figure 104. Contour plot of 1st principal strain on the concrete parapet and deck during Test 3-11 for impact at 4.26 ft with contour range cut off at 0.0267.

Damages to Vehicle

Figure 105 shows contour plots of effective plastic strain for the vehicle during Test 3-11 for each analysis case. The damage to the vehicle was similar for both cases and was limited to the impact side of the vehicle. The most significant damages included the front cap, the front wheel assembly, front door, edge of the rear door, front edge and side of the truck bed, rear wheel, rear bumper, and lower, rear section of the truck bed. The windshield also cracked around all four edges but did not separate from the vehicle. The damage to the windshield was not caused by direct contact with any part of the barrier.

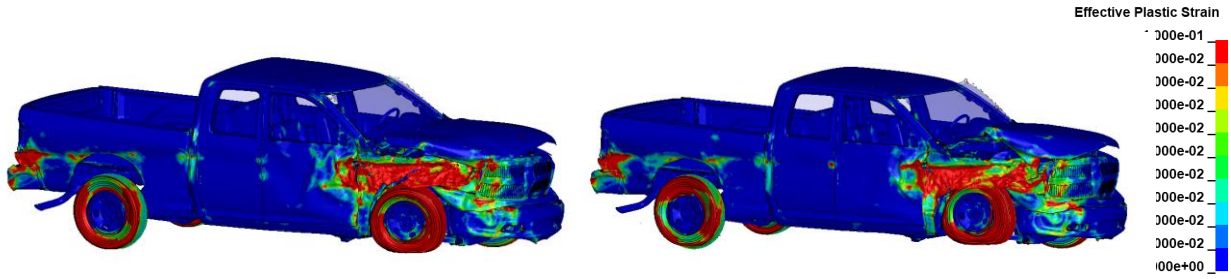

(a) Impact at 4.26 ft upstream of critical post **(b)** Impact at 5.26 ft upstream of critical post

Figure 105. Damages to vehicle in Test 3-11 for (a) impact at 4.26 ft and (b) 5.26 ft upstream of the transition.

Occupant Compartment Deformation (OCD)

The maximum deformation of the occupant compartment was 5.59 inches for impact at 4.26 ft upstream of transition and was 5.53 inches for impact at 5.26 ft upstream of transition and occurred at the right-front toe-pan at the wheel well for both analysis cases. Figure 106 shows a post-impact view of the vehicle floor pan with all other components removed to facilitate viewing. The maximum deformation was well within the critical limit of 9 inches specified in MASH for this area of the occupant compartment.

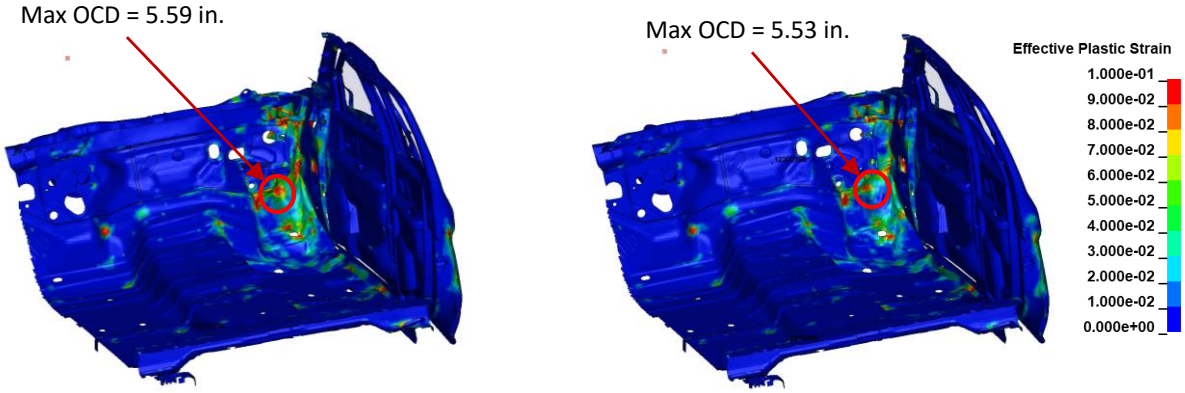

(a) Impact at 4.26 feet upstream of transition **(b)** Impact at 5.26 feet upstream of transition

Figure 106. Occupant compartment deformation resulting from Test 3-11 for (a) impact at 4.26 ft and (b) 5.26 ft upstream of the transition.

Exit Box

Figure 107 shows the exit box for Test 3-11. The post trajectory response was similar for both cases, and the vehicle was redirected with its path well within the exit box criteria of MASH.

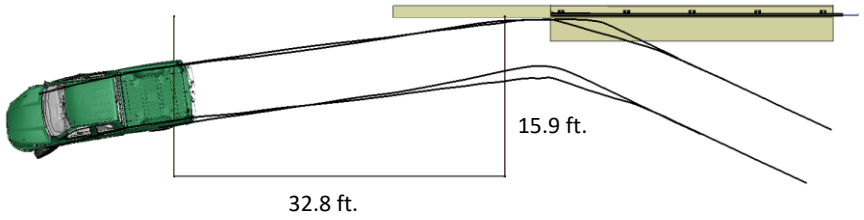

(a) Impact at 4.26 feet upstream of transition

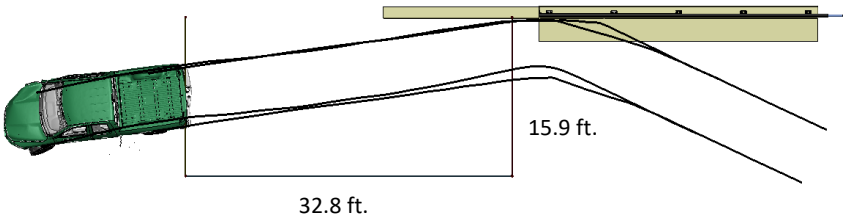

(b) Impact at 5.26 feet upstream of transition

Figure 107. Exit box for Test 3-11 for (a) impact at 4.26 ft and (b) 5.26 ft upstream of the transition.

Results Summary

A summary of MASH Test 3-11 results is shown in Table 14 and in Figures 108 109. The bridge rail successfully contained and redirected the pickup with minimal to moderate damage to the concrete parapet and aluminum handrailing. There were no detached elements from the barrier that showed potential for penetrating into the occupant compartment or presenting undue hazard to other traffic. The OIV and maximum RA values were within preferred limits specified in MASH. The maximum occupant compartment deformation was well within critical limits specified in MASH. The windshield was cracked around the edges but was not caused by direct contact with any part of the barrier. The vehicle remained upright and did not experience excessive roll or pitch angle displacements. The vehicle also remained within the exit-box criteria of MASH. Based on the results of this analysis, the barrier is expected to meet all structural and occupant risk criteria in MASH for Test 3-11 impact conditions.

CIP Recommendation for Test 3-11 for CP-MTL3 at Approach to Transition

The recommended CIP for Test 3-11 for this section of the bridge rail is 4.26 ft upstream of the transition. Although both impact points resulted in very similar performance of the barrier and were well within MASH criteria for all metrics, the impact case at 4.26 ft upstream of the transition resulted in slightly higher damages to the barrier that could lead to greater potential for snag on the end of the transition. This is also consistent with the recommendation provided in MASH for Test 3-11 on rigid barriers.

Table 14. Summary of MASH Test 3-11 for the CP-MTL3 at transition.

Evaluation Factors	Evaluation Criteria		IP 4.26 ft	IP 5.26 ft
Structural Adequacy	A	Test article should contain and redirect the vehicle or bring the vehicle to a controlled stop; the vehicle should not penetrate, underride, or override the installation although controlled lateral deflection of the test article is acceptable.	Pass	Pass
Occupant Risk	D	Detached elements, fragments, or other debris from the test article should not penetrate or show potential for penetrating the occupant compartment, or present undue hazard to other traffic, pedestrians, or personnel in a work zone. Deformations of, or intrusions into, to occupant compartment should not exceed limits set forth in Section 5.2.2 and Appendix E.	Pass	Pass
	F	The vehicle should remain upright during and after collision. The maximum roll and pitch angles are not to exceed 75 degrees.	Pass	Pass
	H	The longitudinal and lateral occupant impact velocity (OIV) shall not exceed 40 ft/s, with a preferred limit of 30 ft/s.	Pass	Pass
	I	The longitudinal and lateral ridedown acceleration (RA) shall not exceed 20.49 G, with a preferred limit of 15.0 G	Pass	Pass

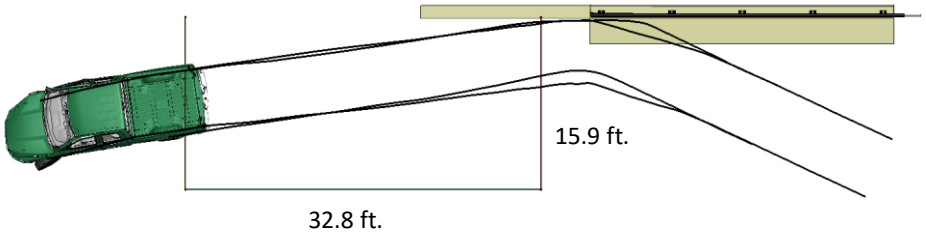

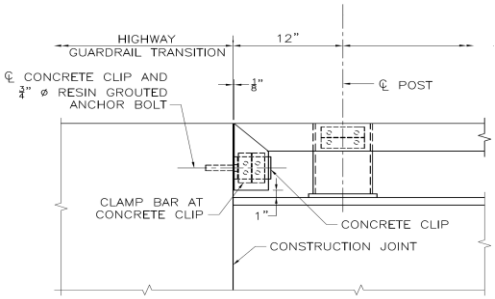

General Information

Analysis Agency	Roadsafe LLC
Test Standard Test No.	MASH Test 3-11
Analysis No.	CP-MTL3_Test3-11_IP4.26ft_KC
Analysis Date	6/13/2023

Test Article

Type	Bridge Rail at Transition
Name	CP-MTL3
Installation Length	44.65 feet
Material or Key Elements	Continuous concrete with top mounted aluminum post-and-beam
Soil Type and Condition	NA

Analysis Vehicle

Type / Designation	2270P
FEA Model name	Ram2018C_V2u.k w/ RS tire
Mass	5,001 lb

Impact Conditions

Speed	62.0 mph
Angle	25 degrees
Location	4.26 ft upstream of transition
Impact Severity	114.7 kip-ft

Exit Conditions

Speed	42.7 mph
Angle	5.9 degrees
Time	0.470 seconds

Occupant Risk Values

Longitudinal OIV	23.0 ft/s
Lateral OIV	27.2 ft/s
Longitudinal ORA	-8.7 g
Lateral ORA	-12.1 g
THIV	36.4 ft/s
PHD	12.1 g
ASI	2.04

Max50-millisecond Avg. (G)

Longitudinal	-10.4 g
Lateral	-14.9 g
Vertical	-4.2 g

Test Article Deflections (in)

Dynamic	1.23 inches
Permanent	0.10 inches
Working Width	15.24
Max. OCD	5.59 inches

Vehicle Stability

Roll	-10.3 degees
Pitch	-5.2 degrees
Yaw	-34.8 degrees

Figure 108. Summary results for MASH Test 3-11 with impact point at 4.26 ft upstream of post (KC model).

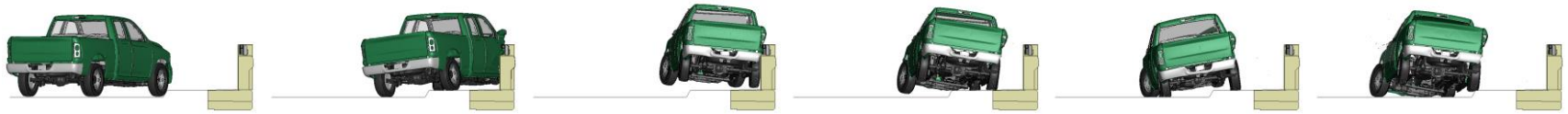

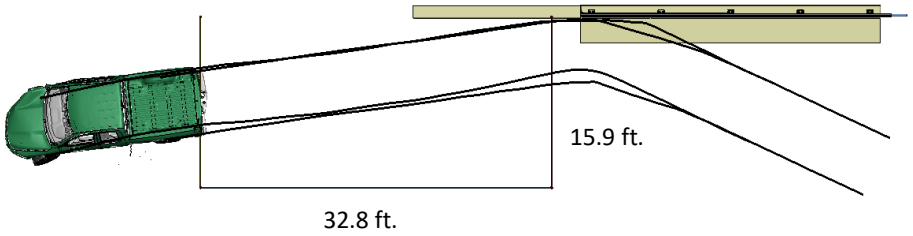

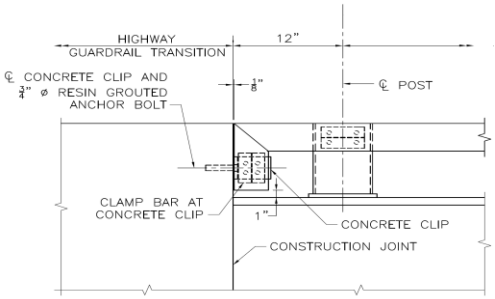

General Information

Analysis Agency	Roadsafe LLC
Test Standard Test No.	MASH Test 3-11
Analysis No.	CP-MTL3_Test3-11_IP5.26ft_KC
Analysis Date	6/14/2023

Test Article

Type	Bridge Rail at Transition
Name	CP-MTL3
Installation Length	44.65 feet
Material or Key Elements	Continuous concrete with top mounted aluminum post-and-beam
Soil Type and Condition	NA

Analysis Vehicle

Type / Designation	2270P
FEA Model name	Ram2018C_V2u.k w/ RS tire
Mass	5,001 lb

Impact Conditions

Speed	62.0 mph
Angle	25 degrees
Location	5.26 ft upstream of transition
Impact Severity	114.7 kip-ft

Exit Conditions

Speed	42.9 mph
Angle	5.9 degrees
Time	0.500 seconds

Occupant Risk Values

Longitudinal OIV	22.6 ft/s
Lateral OIV	26.6 ft/s
Longitudinal ORA	-4.7 g
Lateral ORA	-12.8 g
THIV	35.4 ft/s
PHD	12.9 g
ASI	1.95

Max50-millisecond Avg. (G)

Longitudinal	-9.2 g
Lateral	-14.4 g
Vertical	-4.5 g

Test Article Deflections (in)

Dynamic	1.45 inches
Permanent	0.19 inches
Working Width	15.17
Max. OCD	5.53 inches

Vehicle Stability

Roll	-11.7 degees
Pitch	-5.6 degrees
Yaw	-32.2 degrees

Figure 109. Summary results for MASH Test 3-11 with impact point at 5.26 ft upstream of post (KC model).

CHAPTER 7 – SUMMARY AND CONCLUSIONS

The objective of this project was to evaluate the crash performance of MassDOT's CP-MTL3 bridge rail using finite element analysis (FEA) in accordance with MASH TL3 impact conditions and evaluation criteria. Two critical regions of the system were evaluated. The first critical region was the expansion joint of the bridge and parapet. Analyses were conducted to assess the critical impact points (CIPs) for maximizing vehicle snag on either the expansion joint or the handrail post located 12 inches downstream of the expansion joint. The second critical region was at the approach to the concrete transition at the downstream end of the system. For that case, analyses were conducted to assess the CIP for maximizing vehicle snag on the upstream edge of the transition at the connection point to the CP-MTL3 system.

The results of the finite element analyses indicated that the CP-MTL3 bridge rail met MASH crash performance criteria for test level 3. The bridge rail successfully contained and redirected the 1100C and 2270P vehicles under TL3 impact conditions at the critical impact points for both critical regions of the barrier system. A summary of the analysis results, including occupant risk metrics, angular displacements, maximum occupant compartment deformations, and maximum 10-ms-running-average accelerations are provided in Tables 15 and 16 for the analysis cases at the expansion joint and at the downstream transition, respectively.

Table 15. Summary of occupant risk metrics from analysis results for evaluations at the expansion joint of the barrier.

MASH Test	Analysis Case		OIV_x (ft/s)	OIV (ft/s)	RA_x (G)	RA_y (G)	Roll (deg)	Pitch (deg)	Yaw (deg)	OCD (in)	Max 10-ms X (g's)	Max 10-ms Y (g's)
	Impact Point	Concrete Model										
3-10	3.6 ft (CIP)	KC	25.3	26.9	-2.7	-12.5	-14.9	-5.9	-32.1	2.32	-21.1	-36.1
		RHT	24.3	26.9	-2.8	-12.0	-14.8	-6.0	-32.4	2.27	-20.8	-35.8
	4.6 ft	KC	24.3	27.6	-2.2	-12.7	-14.7	-7.0	-33.3	2.20	-21.3	-34.8
		RHT	24.0	27.9	-2.3	-12.7	-14.7	-6.8	-33.4	2.23	-21.7	-34.5
3-11	4.26 ft (CIP)	KC	21.7	26.9	-6.3	-14.8	11.0	-6.0	-36.7	4.72	-14.7	-20.7
		RHT	21.0	26.9	-6.2	-14.2	11.6	-6.3	-36.8	4.57	-15.7	-21.2
	5.26	KC	21.0	26.9	-5.3	-15.1	9.8	-6.1	-39.8	4.37	-15.4	-22.4
		RHT	21.0	26.9	-4.5	-14.6	-9.5	-6.1	-39.4	4.31	-16.2	-22.9
MASH Preferred Criteria			≤ 30 ft/s		≤ 15 G		N.A.			N.A.	N.A.	N.A.
MASH Allowable Limits			≤ 40 ft/s		≤ 20.49 G		≤ 75 deg			≤ 9 in	N.A.	N.A.

Table 16. Summary of occupant risk metrics from analysis results for evaluations at the transition for the barrier.

MASH Test	Analysis Case		OIV_x (ft/s)	OIV (ft/s)	RA_x (G)	RA_y (G)	Roll (deg)	Pitch (deg)	Yaw (deg)	OCD (in)	Max 10-ms X (g's)	Max 10-ms Y (g's)
	Impact Point	Concrete Model										
3-10	3.6 ft (CIP)	KC	28.2	27.9	-2.1	-10.3	-14.0	-6.7	-35.2	3.07	-20.6	-35.2
	4.6 ft	KC	25.9	28.9	-3.6	-10.8	-14.1	-6.4	-36.9	2.62	-21.2	-36.9
3-11	4.26 ft (CIP)	KC	23.0	27.2	-8.7	-12.1	-10.3	-5.2	-34.8	5.59	-14.3	-23.6
	5.26 ft	KC	22.6	26.6	-4.7	-12.8	-11.7	-5.6	-32.2	5.53	-14.0	-22.3
MASH Preferred Criteria			≤ 30 ft/s		≤ 15 G		N.A.			N.A.	N.A.	N.A.
MASH Allowable Limits			≤ 40 ft/s		≤ 20.49 G		≤ 75 deg			≤ 9 in	N.A.	N.A.

REFERENCES

AASHTO16 Technical Committee for Roadside Safety, Manual for Assessing Safety Hardware, American Association of State Highway and Transportation Officials, Washington, D.C. (2016).

ASM02 Atlas of Stress-Strain Curves, 2nd Edition, ASM International, ISBN-13: 978-0-87170-739-0, Materials Park, OH (2002).

ASTM B209 *ASTM B209_B209M ,* "Standard Specification for Aluminum and Aluminum-Alloy Sheet and Plate, , ASTM International, West Conshohocken, PA (2023).

Buth97 Buth, C., T.J. Hirsch, and W.L. Menges, "Testing of New Bridge Rail and Transition Designs Volume V: Appendix D," Report No. FHWA-RD-93-062, Texas Transportation Institute, College Station, TX (1997).

Carrigan22 Carrigan, C.E. and Chuck A. Plaxico, "Guide for Bridge Curb/Rail and Approach Treatment for Extremely Low Volume Road," 2022 Expected.

CCSA16 George Mason University Center for Collision Safety and Analysis, "2010 Toyota Yaris Finite Element Model Validation Detailed Mesh." https://doi.org/10.13021/G8CC7G. Accessed 7/30/2021.

CCSA18 George Mason University Center for Collision Safety and Analysis, "2018 Dodge Ram Model Development." https://www.ccsa.gmu.edu/models/ Accessed 7/30/2021.

Dobrovolny20 Dobrovolny, C.S., J.C. Kovar, W.L. Menges, and D.L. Kuhn, MASH Test 3-11 Evaluation of Combination Traffic-Pedestrian-Bicycle Bridge Railing, "Test Report No. 611971-02-1, Texas A&€ Transportation Institute Proving Ground, College Station, TX (2020).

Bligh19 Bligh, R.P, W.L. Menges, B.L. Griffith, G.E. Schroeder, and D.L. Kuhn, "MASH Evaluation of TXDOT Roadside Safety Features – Phase II," Report No. FHWA-TX-18/0-6946-R2, Texas Transportation Institute, College Station, TX (2019).

Kulak05 Kulak, G.L., "High Strength Bolting for Canadian Engineers," Canadian Institute of Steel Construction 1st Edition, ISBN 0-88811-109-6, Willowdale, Ontario (2005).

LSDYNA20 "LSDYNA User's Manual" Volumes I, II and III, Livermore Software Technology Corporation (LSTC), Livermore, CA (2020).

Marzougui12 Marzougui, D., R.R. Samaha, C. Cui, and C.D. Kan, "Extended Validation of the Finite Element Model for the 2010 Toyota Yaris Passenger Sedan." https://www.ccsa.gmu.edu/models/2010-toyota-yaris/ https://media.ccsa.gmu.edu/cache/NCAC-2012-W-005.pdf. Accessed 7/30/2021.

Plaxico19 Plaxico, C.A., "MASH TL4 Evaluation of MassDOT's Curb-Mounted and Sidewalk-Mounted S3-TL4 Steel Bridge Railing Using Finite Element

Analysis," Technical Report No. TR 19-0429-GEA, Performed for Gill Engineering Associates, Performed by Roadsafe LLC, Canton, ME (April 2019).

Plaxico20 Plaxico, C.A. and E.M. Ray, "Development of MASH Computer Simulated Steel Bridge Rail and Transition Details," Technical Report No. TR-200323-NETC115, Performed for New England Transportation Consortium, Performed by Roadsafe LLC, Canton, ME (April 2020).

Plaxico21 Plaxico, C.A., "MASH TL3 Evaluation of MassDOT's Curb-Mounted and Sidewalk-Mounted CT-TL3 Bridge Rail Using Finite Element Analysis," Technical Report No. TR 21-0121-GEA, Performed for Gill Engineering Associates, Performed by Roadsafe LLC, Canton, ME (April 2021).

Plaxico22 Plaxico, C.A., "Modifications to the Steer Mechanism for the 1100C Vehicle Model," Unpublished work, Roadsafe, LLC, Canton, Maine, 2022.

Ray18a Ray, M.H., C.E. Carrigan, and C.A. Plaxico, "Guidelines for Shielding Bridge Piers," Final Report, Project 12-90 (Appendix D), National Cooperative Highway Research Program, National Academy of Science (April 2018).

Ray18b Ray, M.H., C.E. Carrigan, and C.A. Plaxico, "Guidelines for Shielding Bridge Piers," NCHRP Research Report 892, National Cooperative Highway Research Program, National Academy of Science (April 2018).

TFHRC15 "Stress vs strain for ASTM A615 Grade 69 steel", Provided by Z.B. Haber, Bridge engineer for Professional Service Industries and consultant for Turner-Fairbanks Highway Research Center, McLean, VA, (2015).

TTI22 TTI, "Test Risk Assessment Program (TRAP) Version 1.01: User's Manual," Texas Transportation Institute, College Station, TX (2022).

Appendix A

Drawings for the MassDOT CP-MTL3 with Handrail

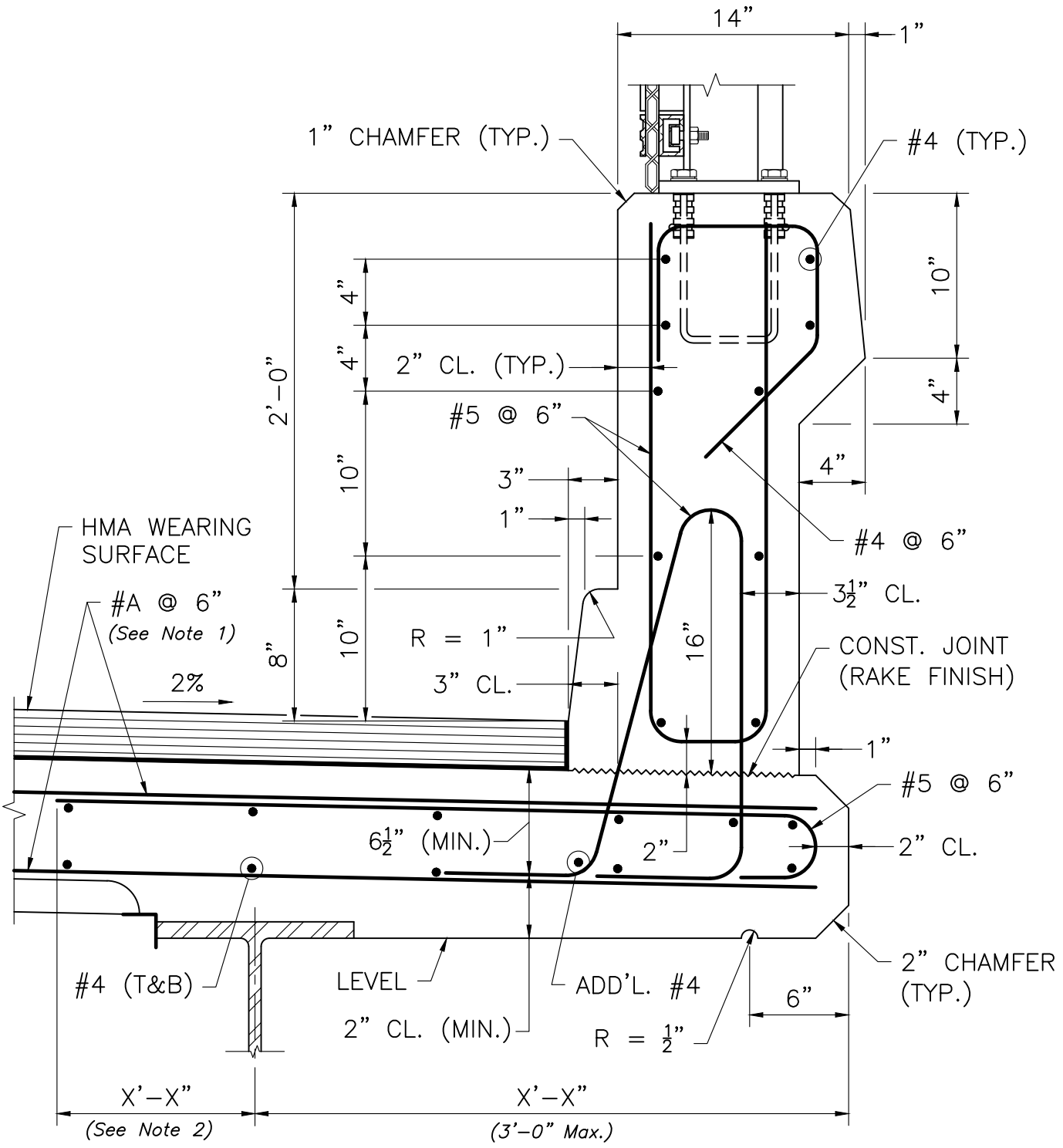

SECTION THRU SAFETY CURB

SCALE: $1\frac{1}{2}$" = 1'-0"

NOTES:

1. *#A = Size of the primary deck slab reinforcement as per Design Tables of Chapter 7.*
2. *Additional Overhang Reinforcement extension (Lext.) as per Design Tables of Chapter 7.*

MassDOT Highway Division BRIDGE MANUAL PART II	SECTION THRU SAFETY CURB STRINGERS CP-MTL3 BARRIER	DATE OF ISSUE XXXX 2020 DRAWING NUMBER **12.4.1**

1/20/2023 6:33:15 AM

SECTION THRU SIDEWALK STRINGERS

CP-MTL3 BARRIER

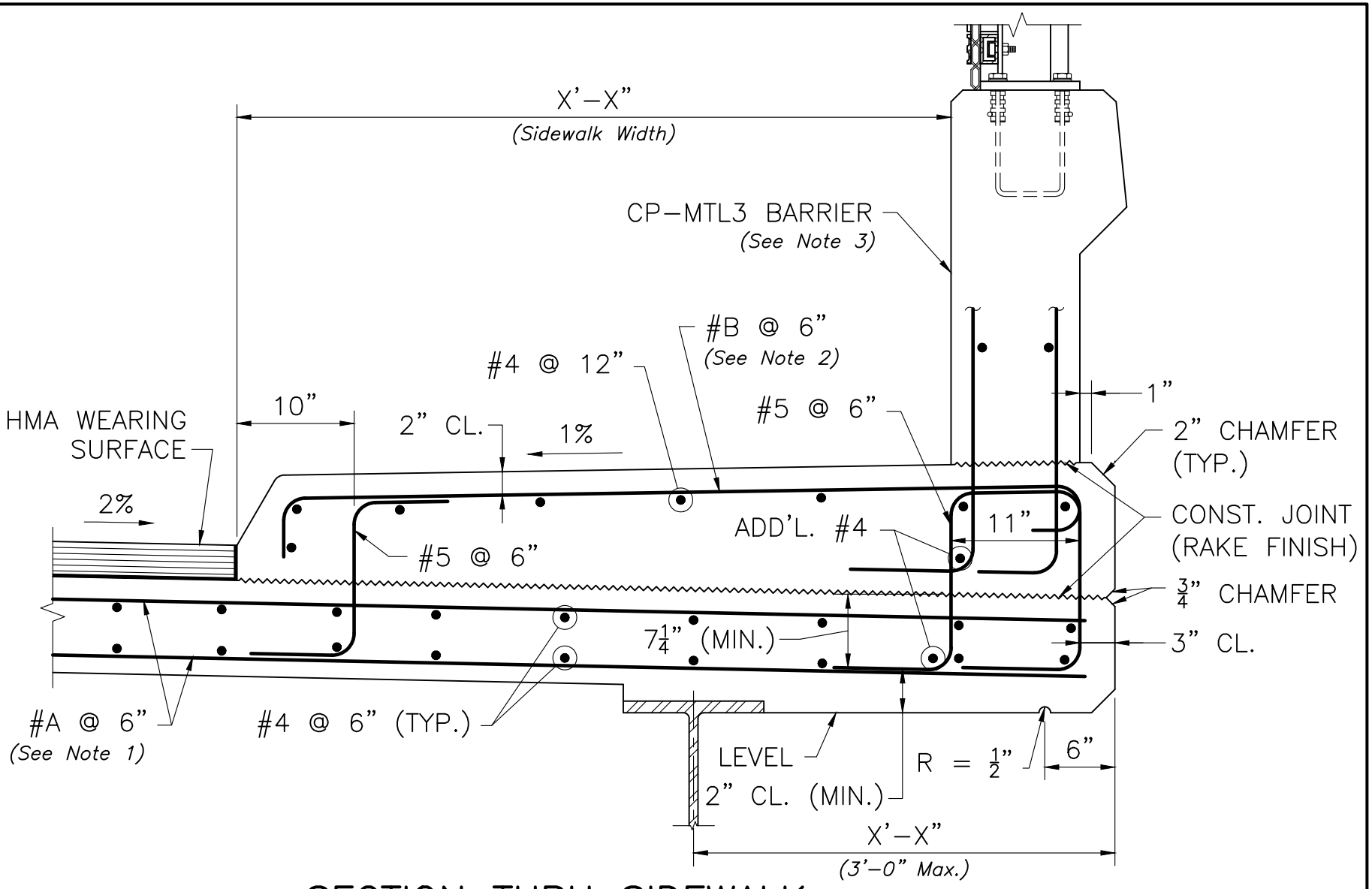

SECTION THRU SIDEWALK

SCALE: 1" = 1'–0"

NOTES:

1. *#A = Size of the primary deck slab reinforcement as per Design Tables of Chapter 7.*
2. *#B = The sidewalk top reinforcement shall be one size larger than the primary deck reinforcement.*
3. *Provide all required barrier geometry and reinforcement information as per Dwg. No. 12.4.11.*

DATE OF ISSUE
XXXX 2020

DRAWING NUMBER
12.4.6

MUNICIPALITY
STREET NAME/ROUTE #

STATE	FED. AID PROJ. NO.	SHEET NO.	TOTAL SHEETS
MA	######	####	X
	PROJECT FILE NO.	######	

HANDRAIL FOR CP-MTL3 BARRIER

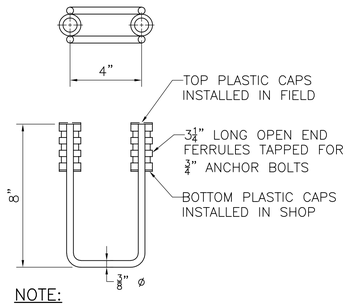

NOTE:
GALVANIZED OR ELECTROPLATE FINISH.

ANCHOR CAGE
SCALE: 3" = 1'–0"

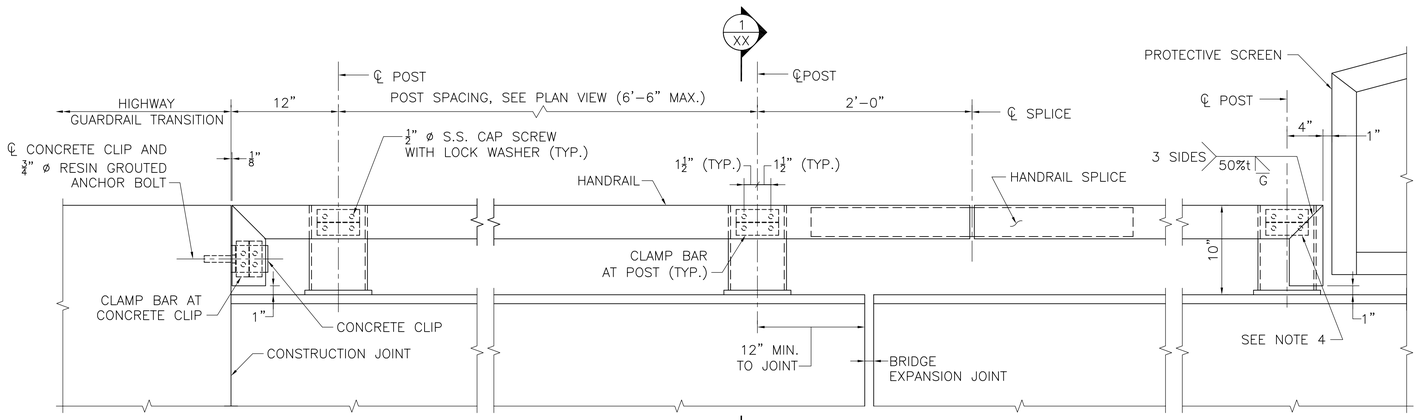

HANDRAIL ELEVATION
SCALE: 1½" = 1'–0"

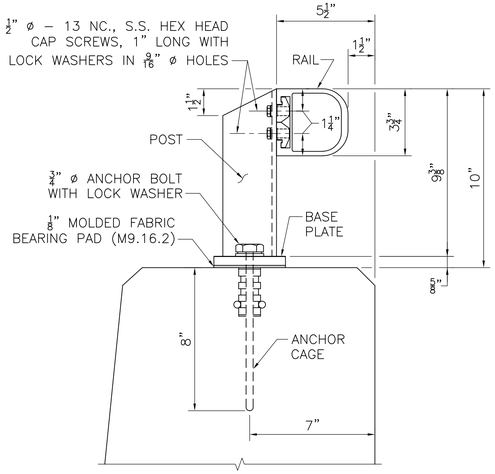

SECTION 1
SCALE: 3" = 1'–0"

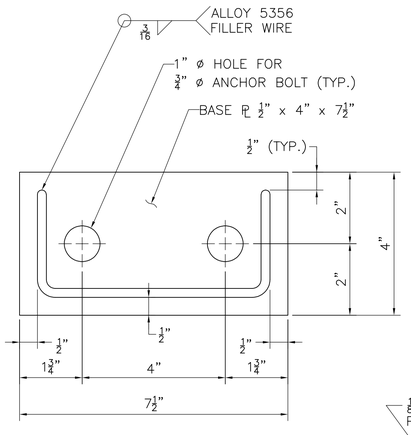

BASE PLATE DETAIL
SCALE: 6" = 1'–0"

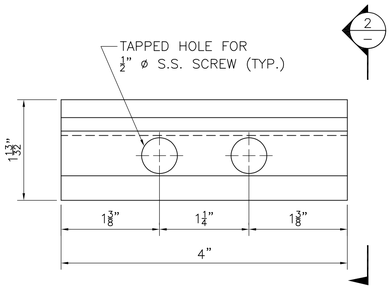

CLAMP BAR AT CONCRETE CLIP
FULL SIZE

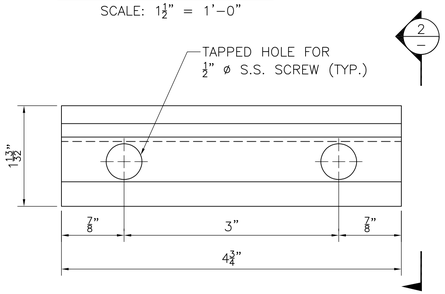

CLAMP BAR AT POST
FULL SIZE

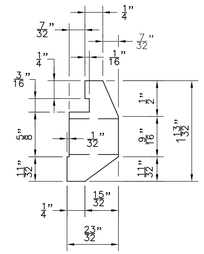

SECTION 2
FULL SIZE

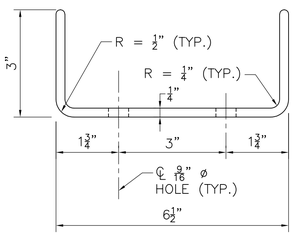

POST DETAIL
SCALE: 6" = 1'–0"

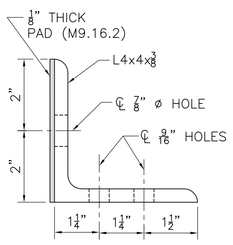

TOP VIEW

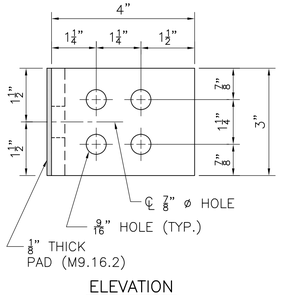

ELEVATION

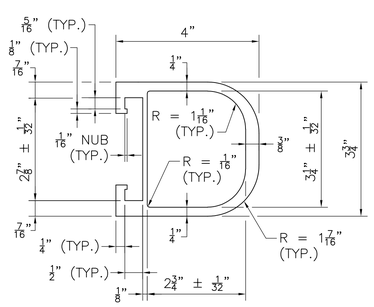

RAIL DETAIL
SCALE: 6" = 1'–0"

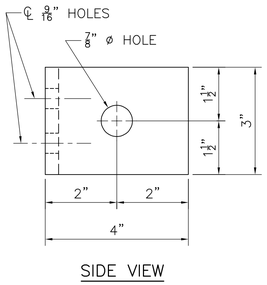

SIDE VIEW

CONCRETE CLIP
SCALE: 6" = 1'–0"

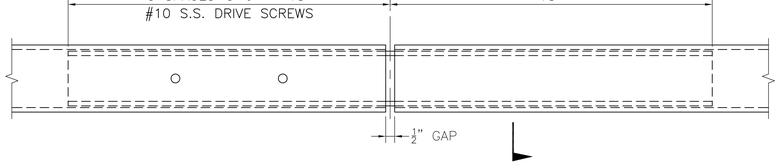

HANDRAIL SPLICE
SCALE: 3" = 1'–0"

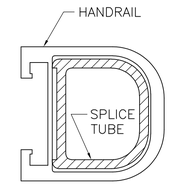

SECTION 3
SCALE: 6" = 1'–0"

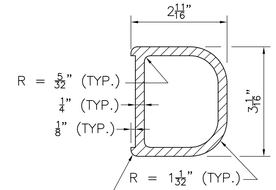

SPLICE TUBE
SCALE: 6" = 1'–0"

FINISH:

POSTS, RAILS, BASE PLATES, CONCRETE CLIP AND SPLICE TUBE SHALL RECEIVE A DARK BRONZE ANODIZED FINISH.

MATERIALS:

RAIL, POST AND BASE PLATE	ASTM B 221, ALLOY 6061–T6
CLAMP BAR, RAIL SPLICE AND CONC. CLIP	ASTM B 221, ALLOY 6061–T6
S.S. FASTENERS	ASTM A 193 GRADE B8 (TYPE 403)
ANCHOR BOLTS	ASTM F3125 GRADE 325 TYPE 1 GALVANIZED (ROTATION CAPACITY TEST NOT REQUIRED)
ALUMINUM WASHERS	ASTM B 209 ALLOY ALCLAD 2024–T4

GENERAL NOTES:

1. RAILS SHALL BE CONTINUOUS OVER A MINIMUM OF FOUR POST, IF POSSIBLE.
2. RAILS SHALL HAVE A HANDRAIL SPLICE, WITH A ½" GAP, BETWEEN CONTINUOUS LENGTHS OF RAIL AND IN THE PANEL OVER A BRIDGE EXPANSION JOINT. ½" GAP SHALL BE INCREASE AS REQUIRED.
3. OTHER CONFIGURATIONS OF THE INTERNAL WALLS OF THE RAIL EXTRUSION MAY BE SUBMITTED FOR APPROVAL.
4. AT 45° MITRES, TRIM OFF 1/16" NUB ON VERTICAL RAIL SECTION AS NEEDED TO ALLOW BOTTOM HORIZONTAL CLAMP BAR TO PROPERLY ENGAGE THE HORIZONTAL RAIL.

MMMM DD, YYYY	ISSUED FOR CONSTRUCTION
DATE	DESCRIPTION

THIS SHEET IS APPROVED FOR CONSTRUCTION BY MASSDOT _____
AUTHORIZED SIGNATORY: STATE BRIDGE ENGINEER
USE ONLY PRINTS OF LATEST DATE

Date: MONTH 20XX

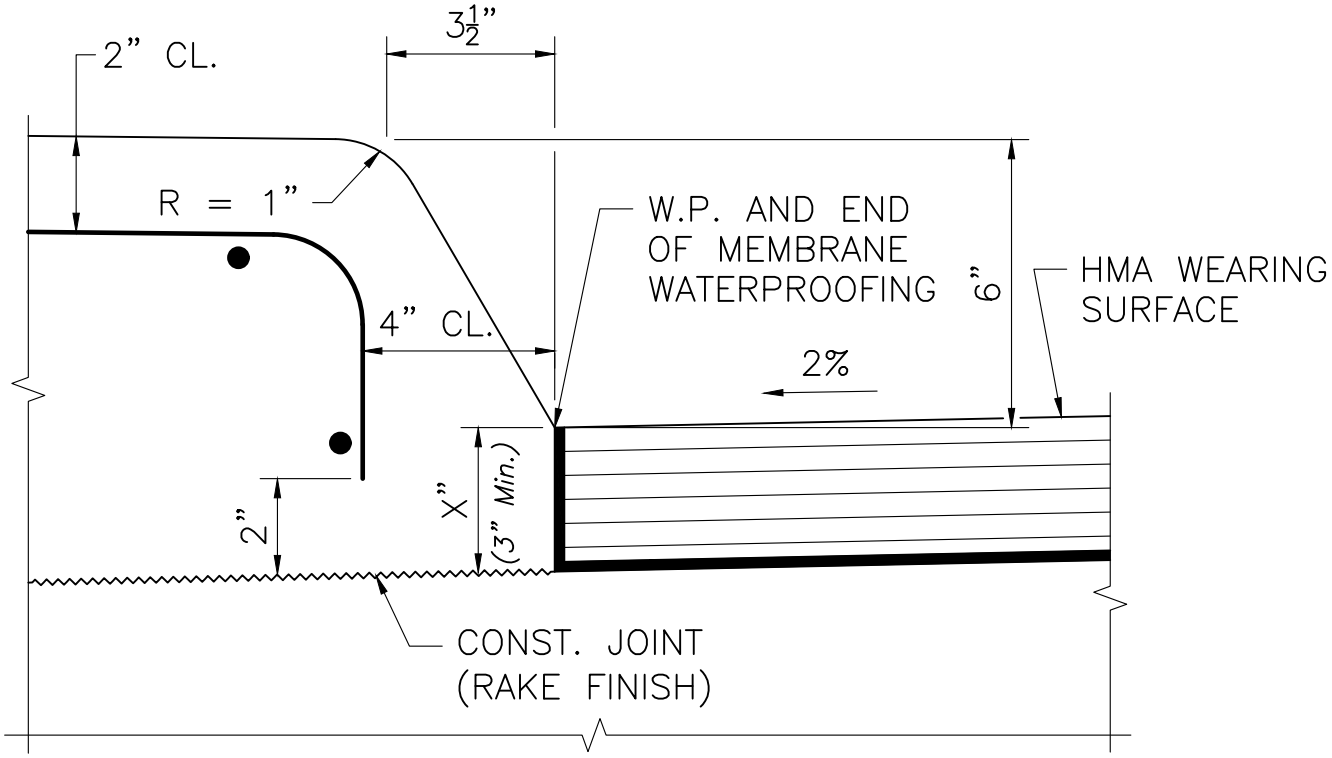

FACE OF SIDEWALK CURB DETAILS

SCALE: 3" = 1'–0"

MassDOT Massachusetts Department of Transportation Highway Division BRIDGE MANUAL PART II	SIDEWALK CURB FOR BRIDGES WITH HMA W.S. FACE OF CURB DETAILS	DATE OF ISSUE XXXX 2020 DRAWING NUMBER **12.7.1**

3/15/2023 6:58:23 AM

Appendix B

Sequential Views for Test 3-10 at 3.6 ft Upstream of Critical Post (KC Model)

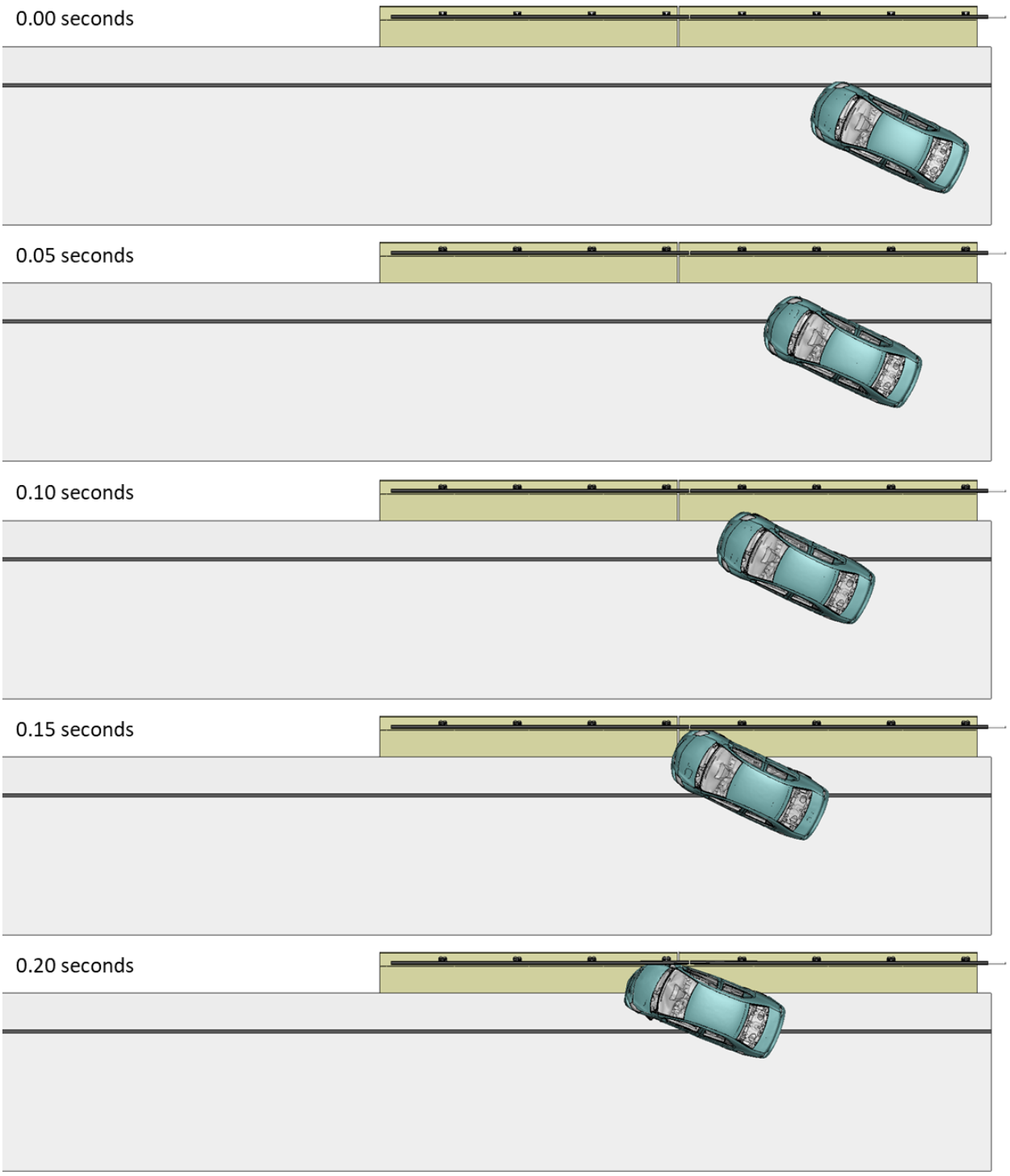

Figure 1. Sequential views from analysis of MASH Test 3-10 at 3.6 ft upstream of critical post from an overhead viewpoint (KC Model).

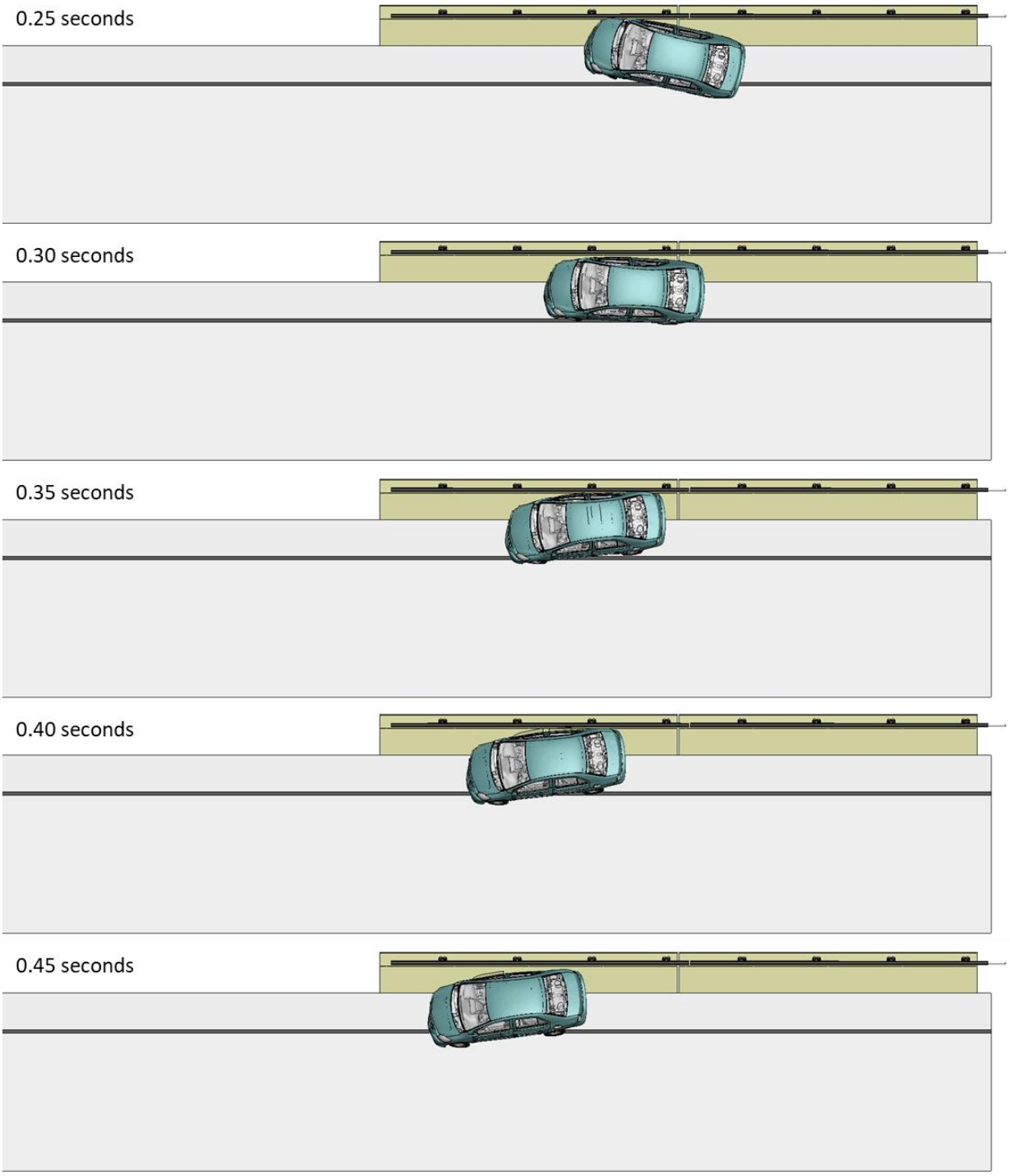

Figure 1 [CONTINUED] Sequential views from analysis of MASH Test 3-10 at 3.6 ft upstream of critical post from an overhead viewpoint (KC Model).

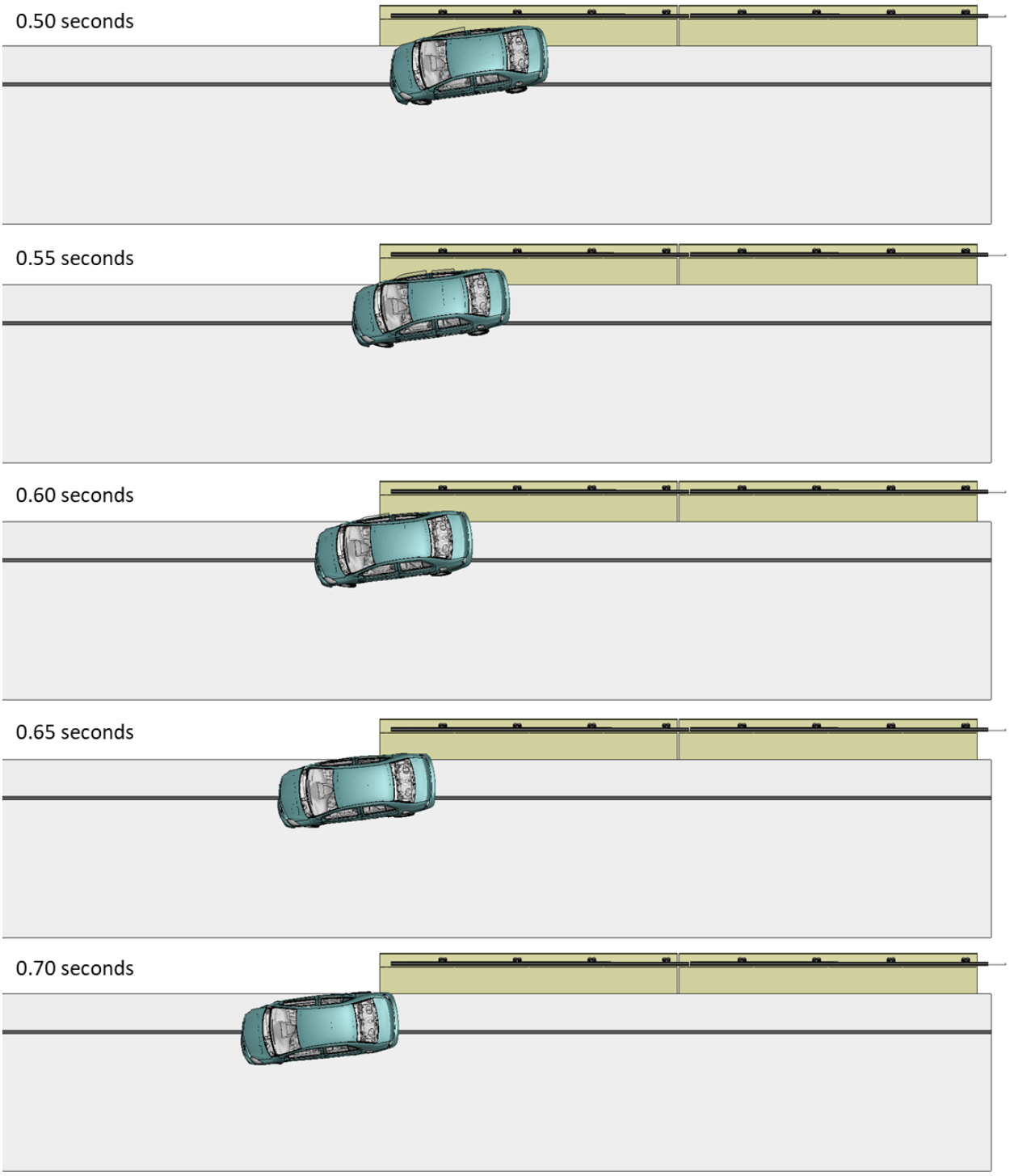

Figure 1 [CONTINUED] Sequential views from analysis of MASH Test 3-10 at 3.6 ft upstream of critical post from an overhead viewpoint (KC Model).

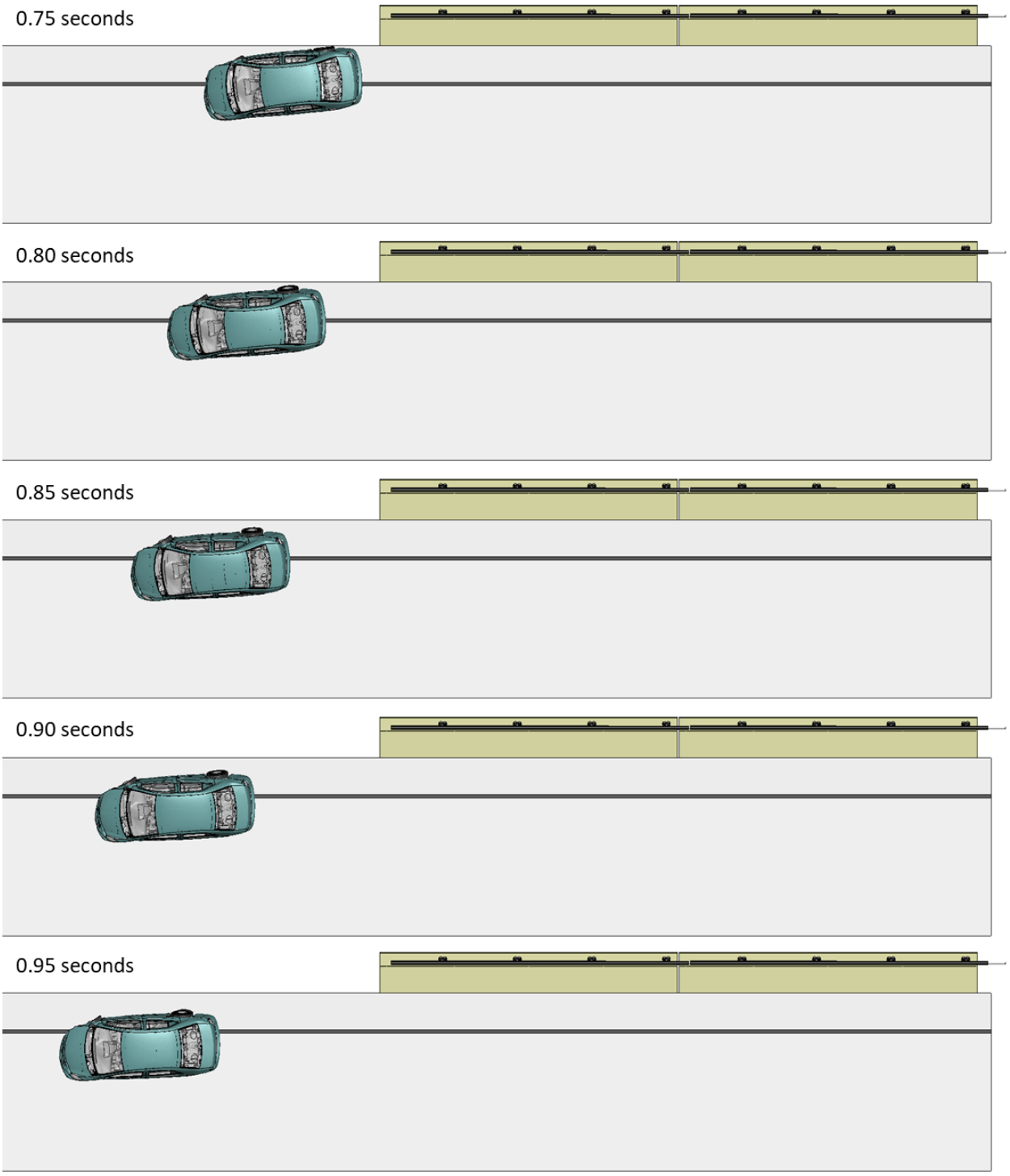

Figure 1 [CONTINUED] Sequential views from analysis of MASH Test 3-10 at 3.6 ft upstream of critical post from an overhead viewpoint (KC Model).

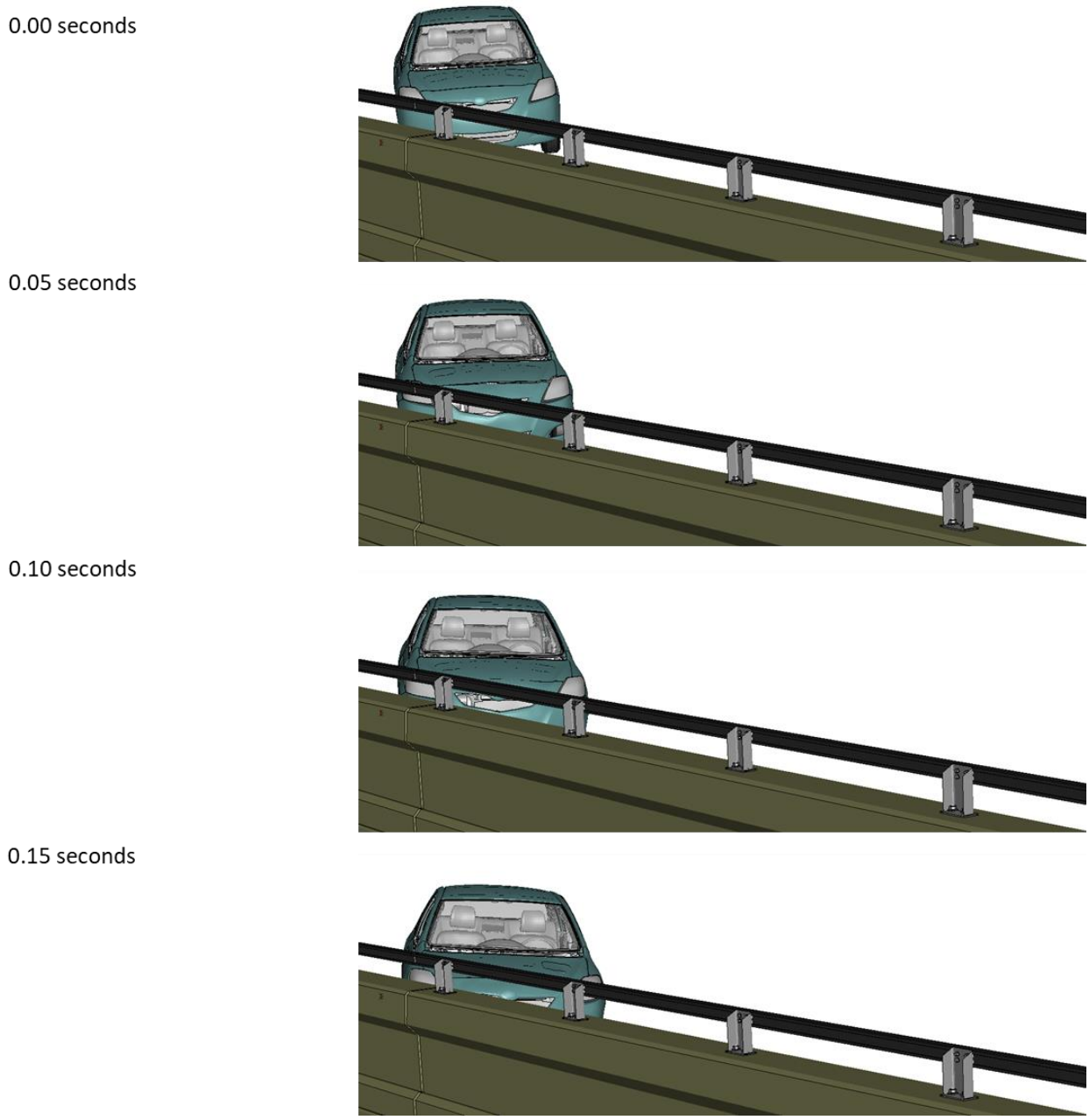

Figure 2. Sequential views from analysis of MASH Test 3-10 at 3.6 ft upstream of critical post from an isometric viewpoint (KC Model).

0.20 seconds

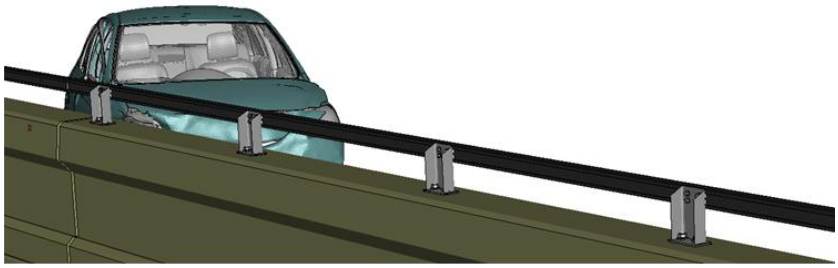

0.25 seconds

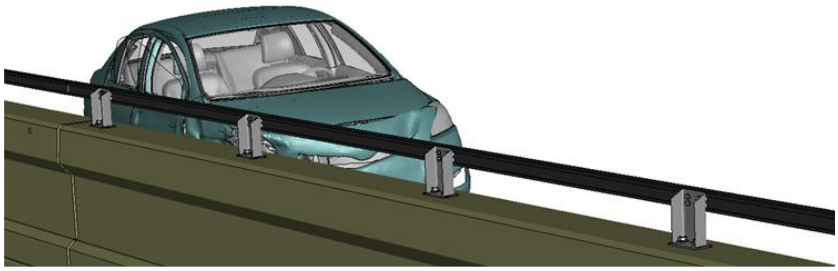

0.30 seconds

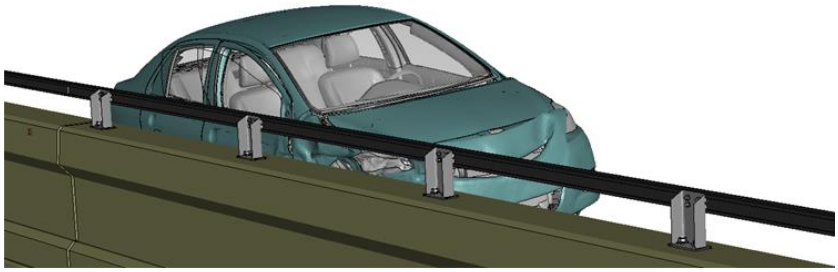

0.35 seconds

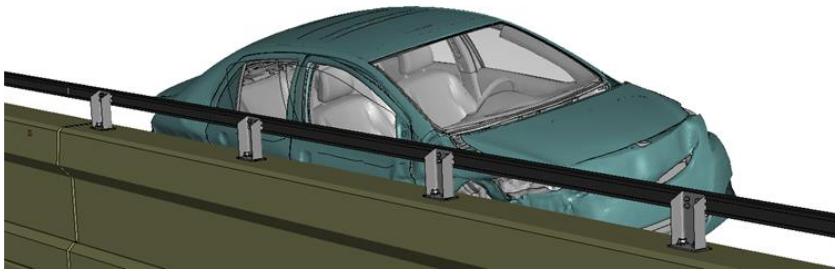

Figure 2 [CONTINUED] Sequential views from analysis of MASH Test 3-10 at 3.6 ft upstream of critical post from an isometric viewpoint (KC Model).

0.40 seconds

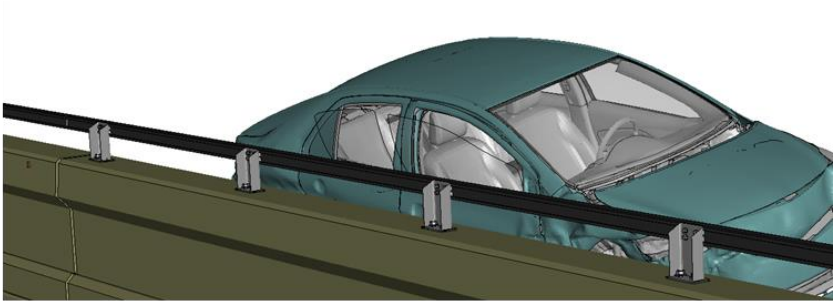

0.45 seconds

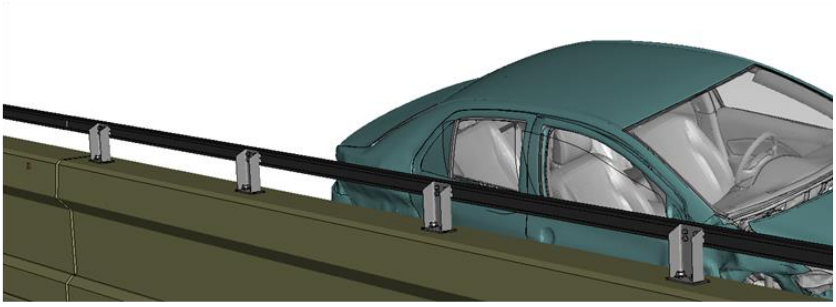

0.50 seconds

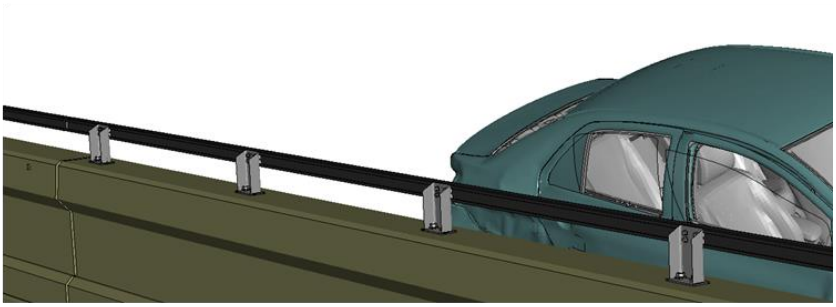

0.55 seconds

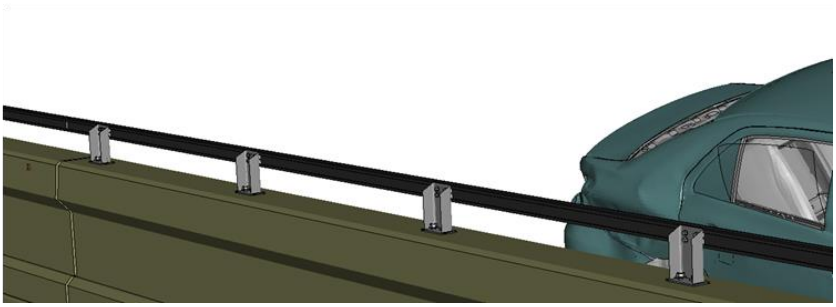

Figure 2 [CONTINUED] Sequential views from analysis of MASH Test 3-10 at 3.6 ft upstream of critical post from an isometric viewpoint (KC Model).

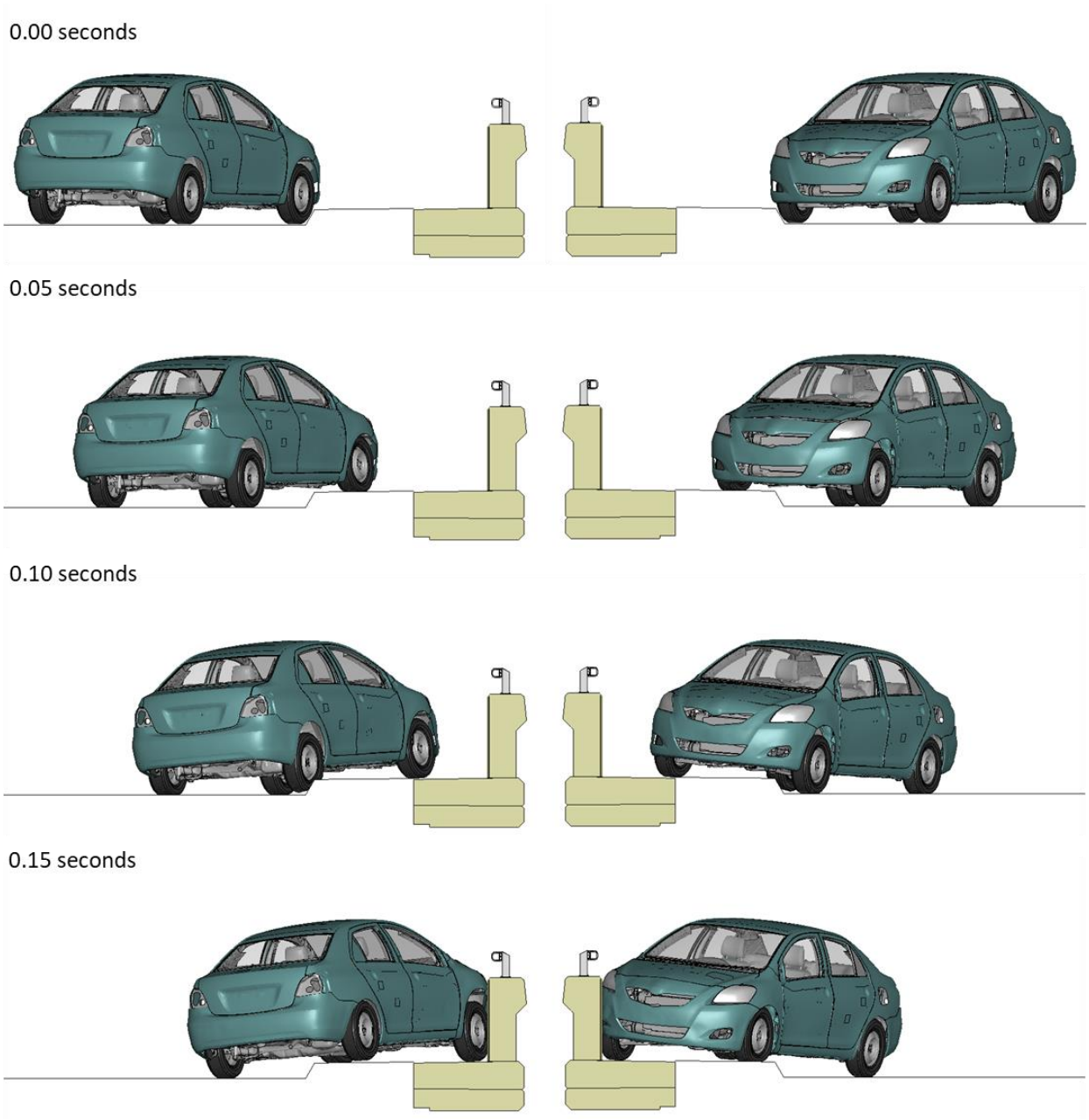

Figure 3. Sequential views from analysis of MASH Test 3-10 at 3.6 ft upstream of critical post from a front and back viewpoint (KC Model).

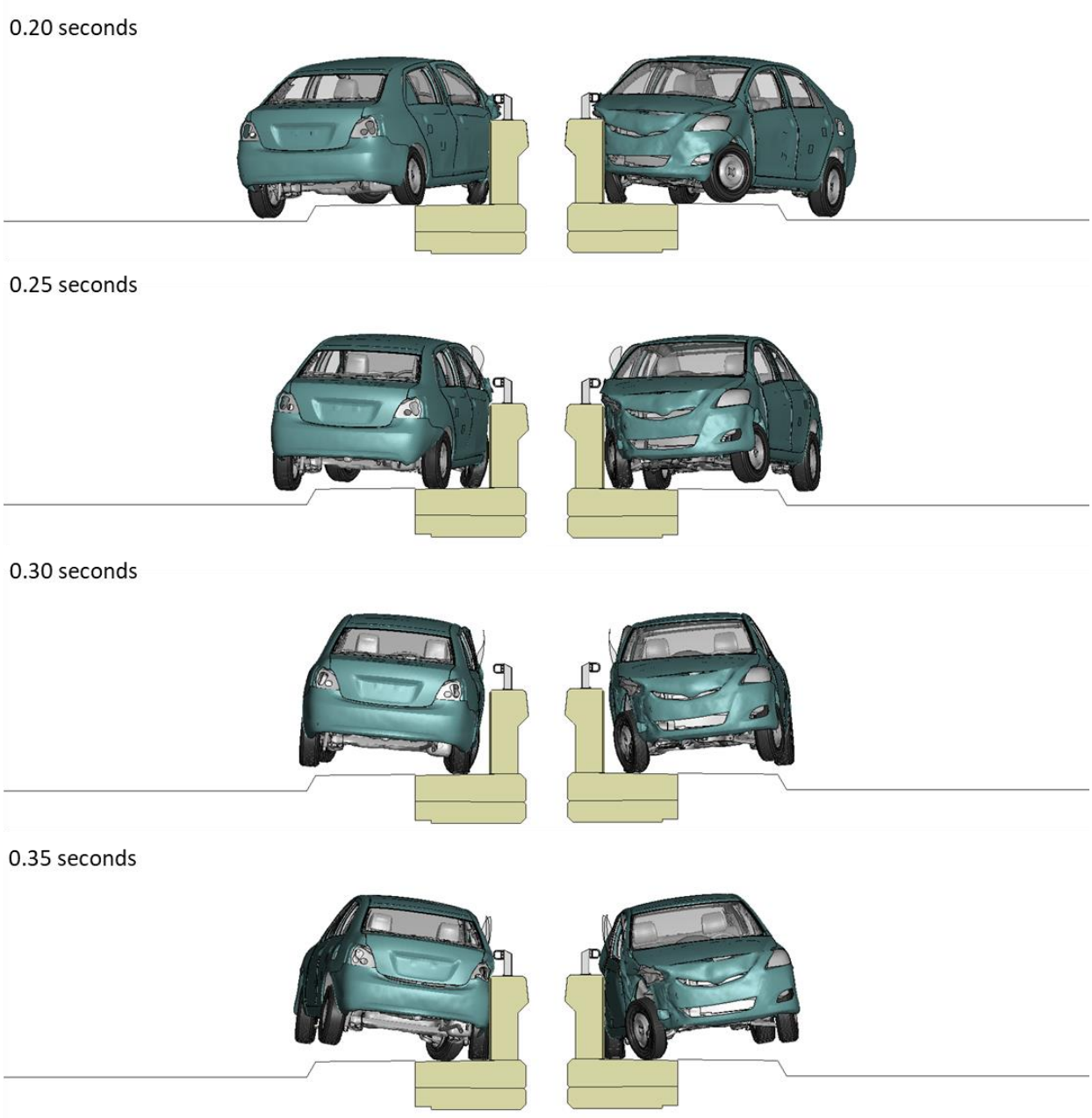

Figure 3 [CONTINUED] Sequential views from analysis of MASH Test 3-10 at 3.6 ft upstream of critical post from a front and back viewpoint (KC Model).

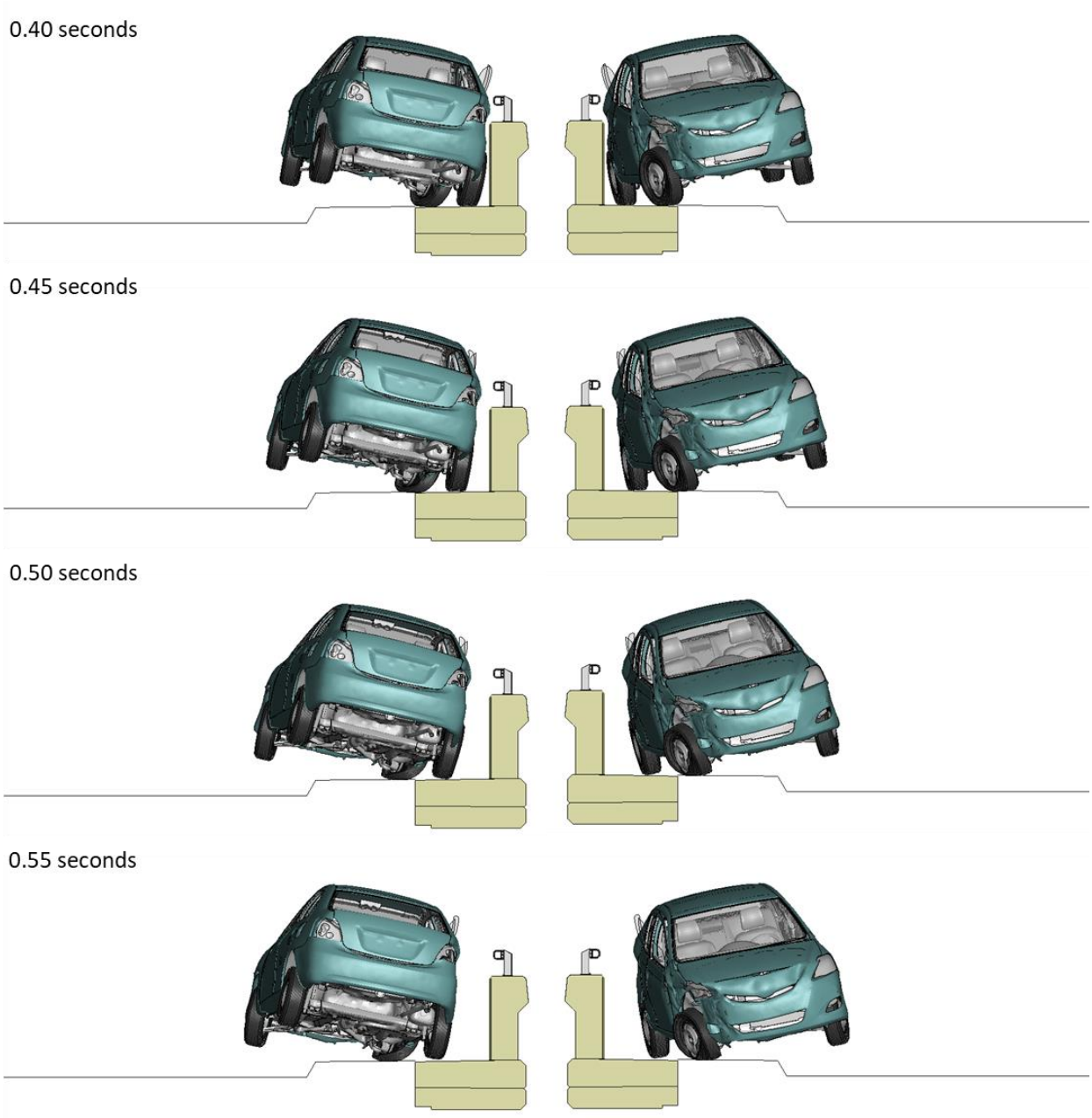

Figure 3 [CONTINUED] Sequential views from analysis of MASH Test 3-10 at 3.6 ft upstream of critical post from a front and back viewpoint (KC Model).

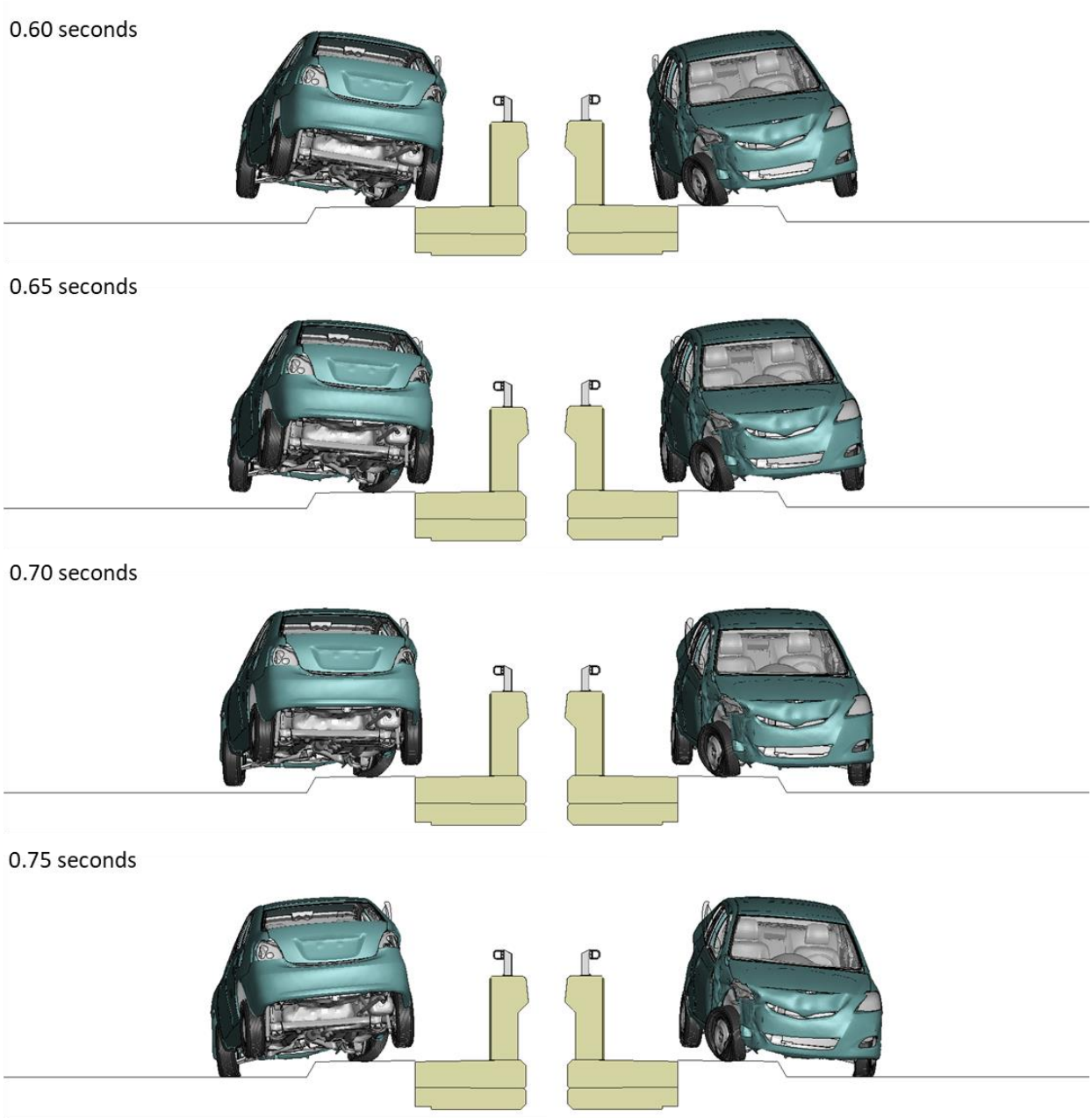

Figure 3 [CONTINUED] Sequential views from analysis of MASH Test 3-10 at 3.6 ft upstream of critical post from a front and back viewpoint (KC Model).

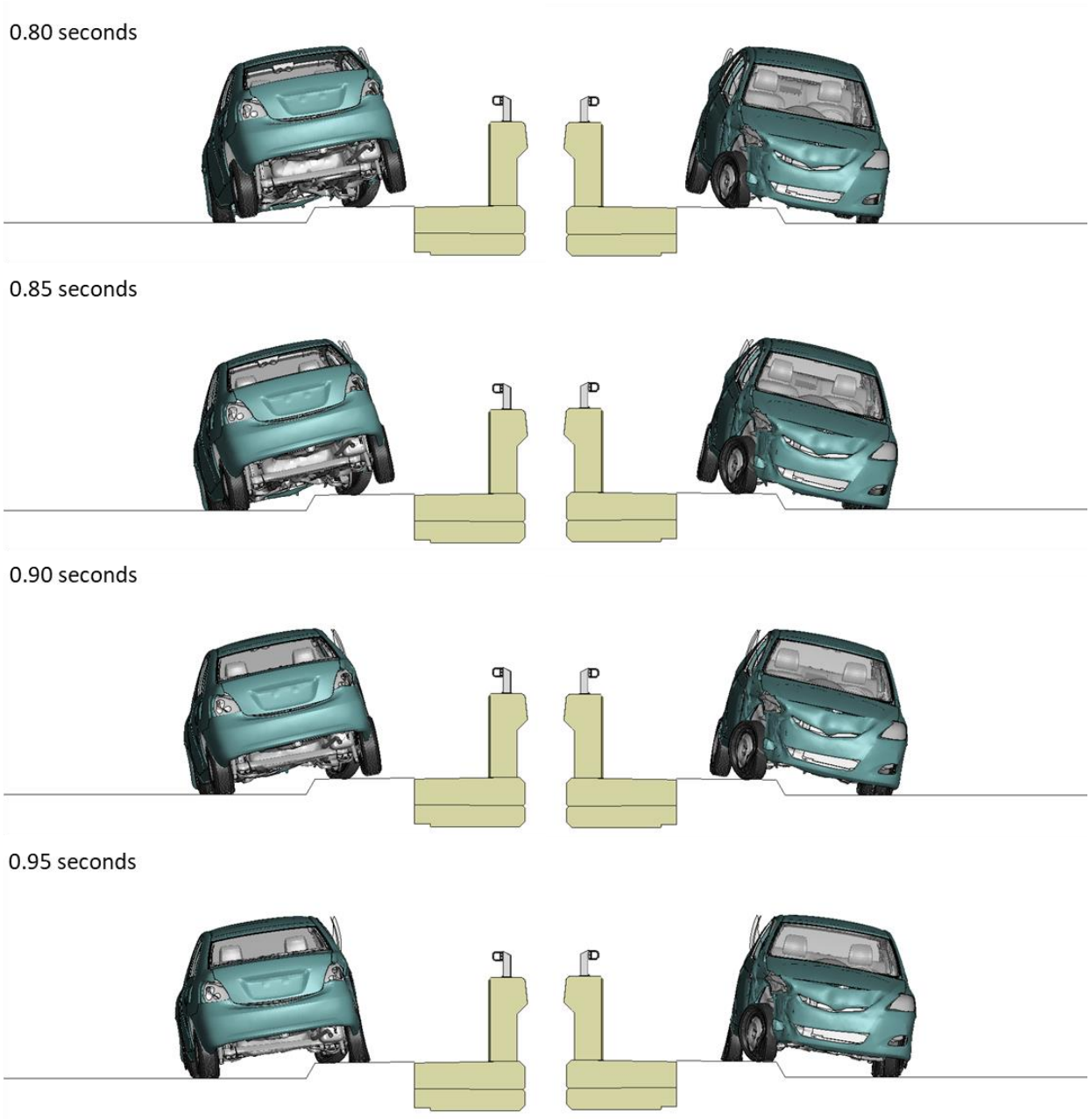

Figure 3 [CONTINUED] Sequential views from analysis of MASH Test 3-10 at 3.6 ft upstream of critical post from a front and back viewpoint (KC Model).

Appendix C

Sequential Views for Test 3-10 at 3.6 ft Upstream of Critical Post (RHT Model)

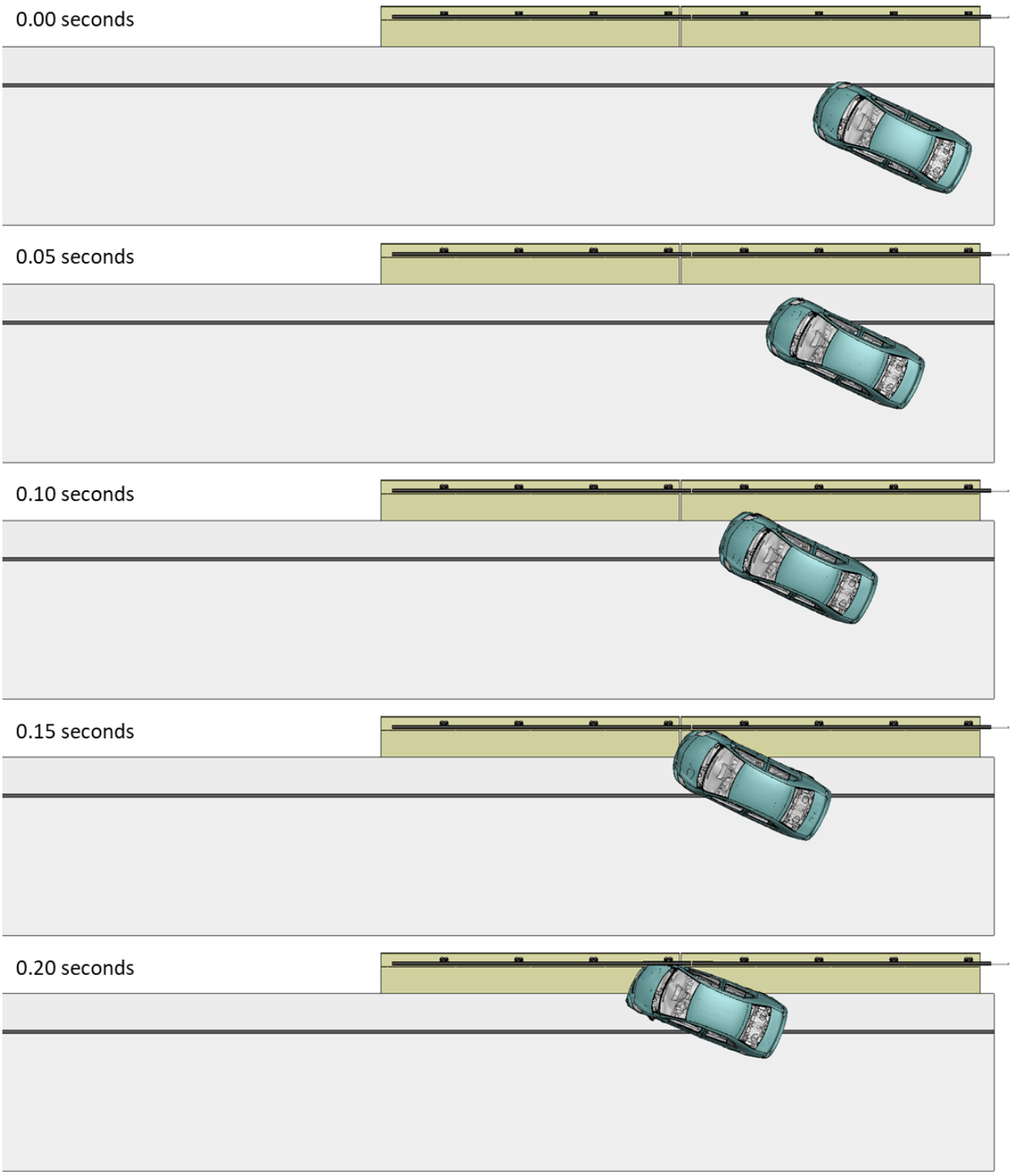

Figure 1. Sequential views from analysis of MASH Test 3-10 at 3.6 ft upstream of critical post from an overhead viewpoint (RHT Model).

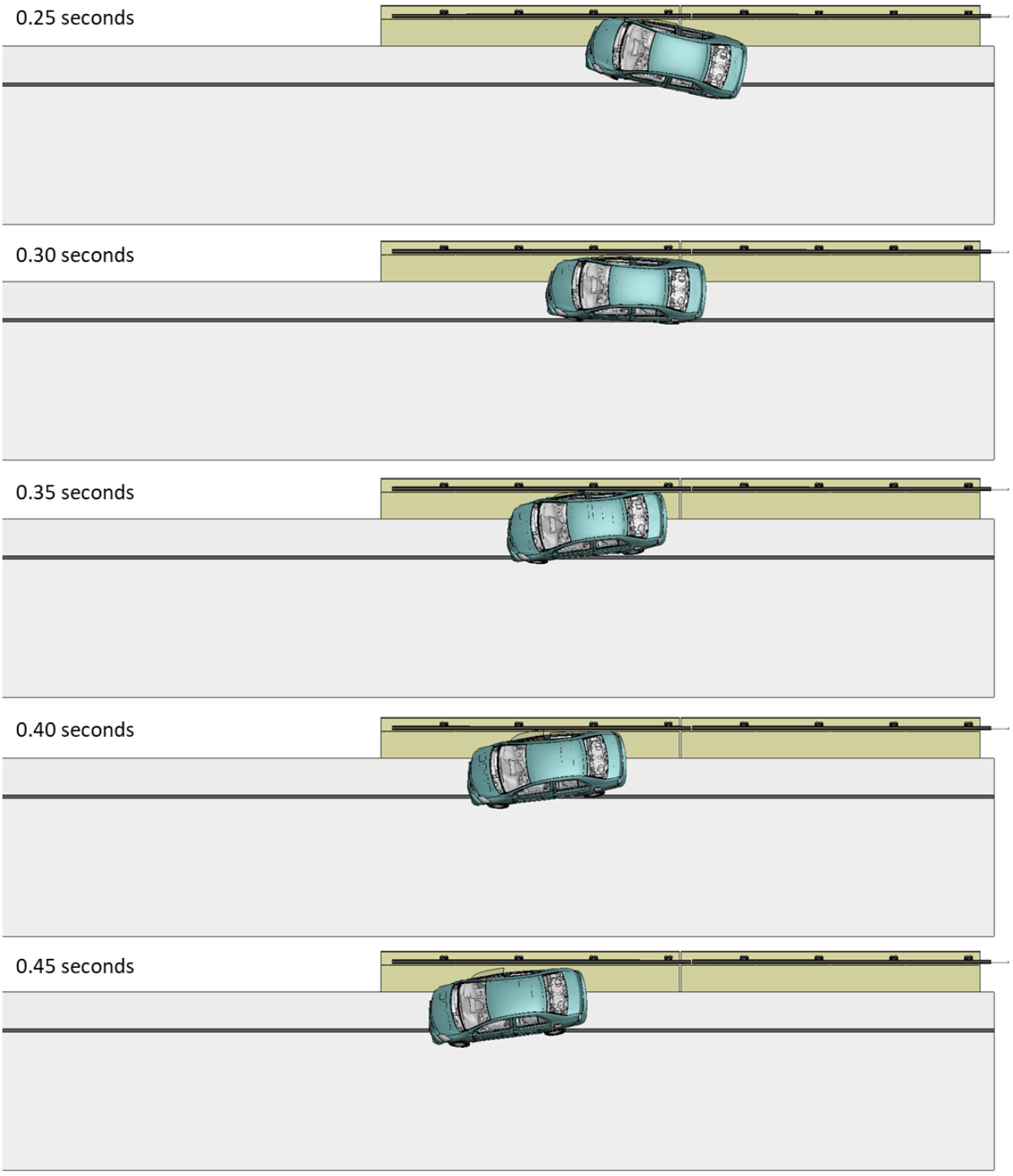

Figure 1 [CONTINUED] Sequential views from analysis of MASH Test 3-10 at 3.6 ft upstream of critical post from an overhead viewpoint (RHT Model).

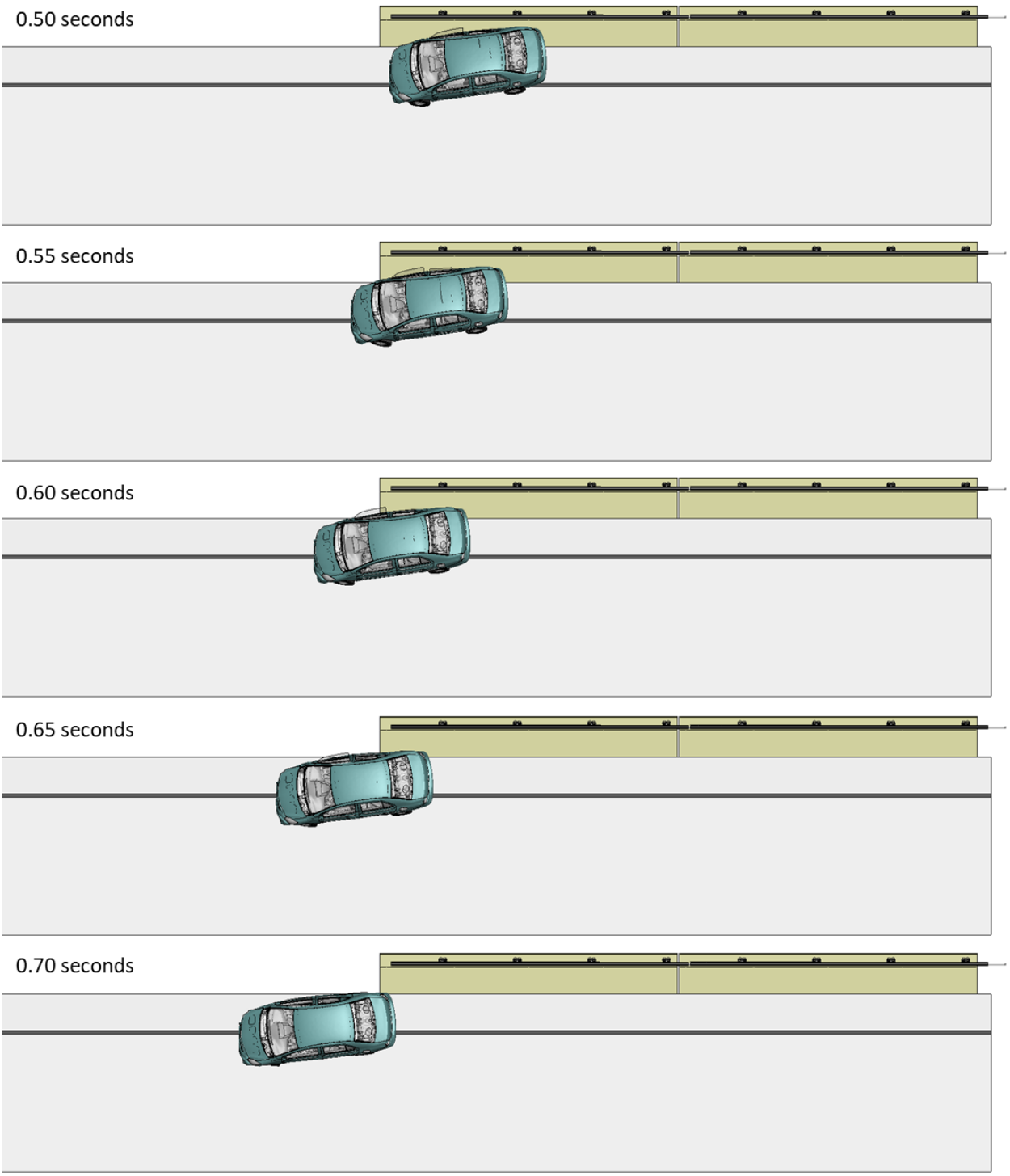

Figure 1 [CONTINUED] Sequential views from analysis of MASH Test 3-10 at 3.6 ft upstream of critical post from an overhead viewpoint (RHT Model).

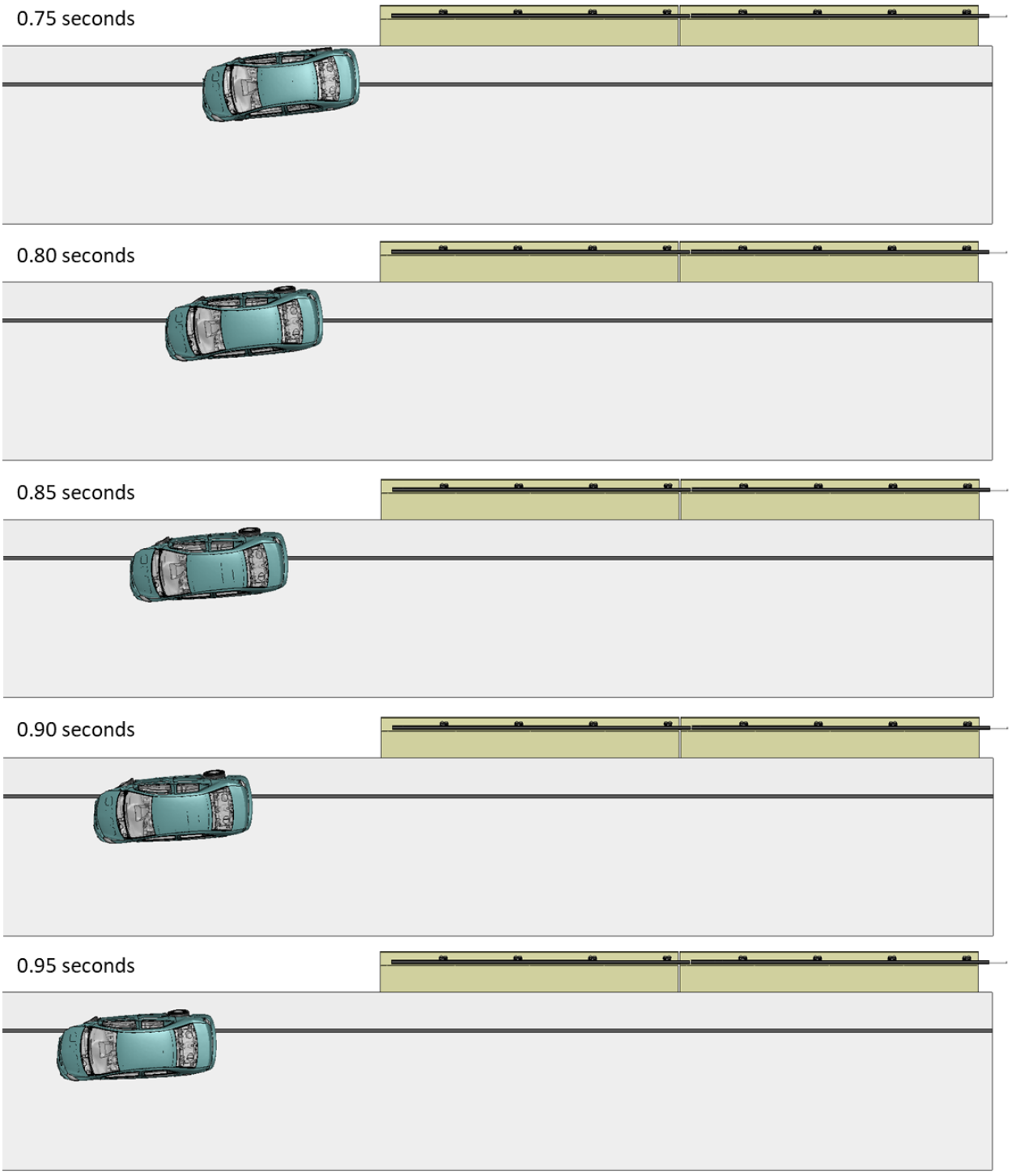

Figure 1 [CONTINUED] Sequential views from analysis of MASH Test 3-10 at 3.6 ft upstream of critical post from an overhead viewpoint (RHT Model).

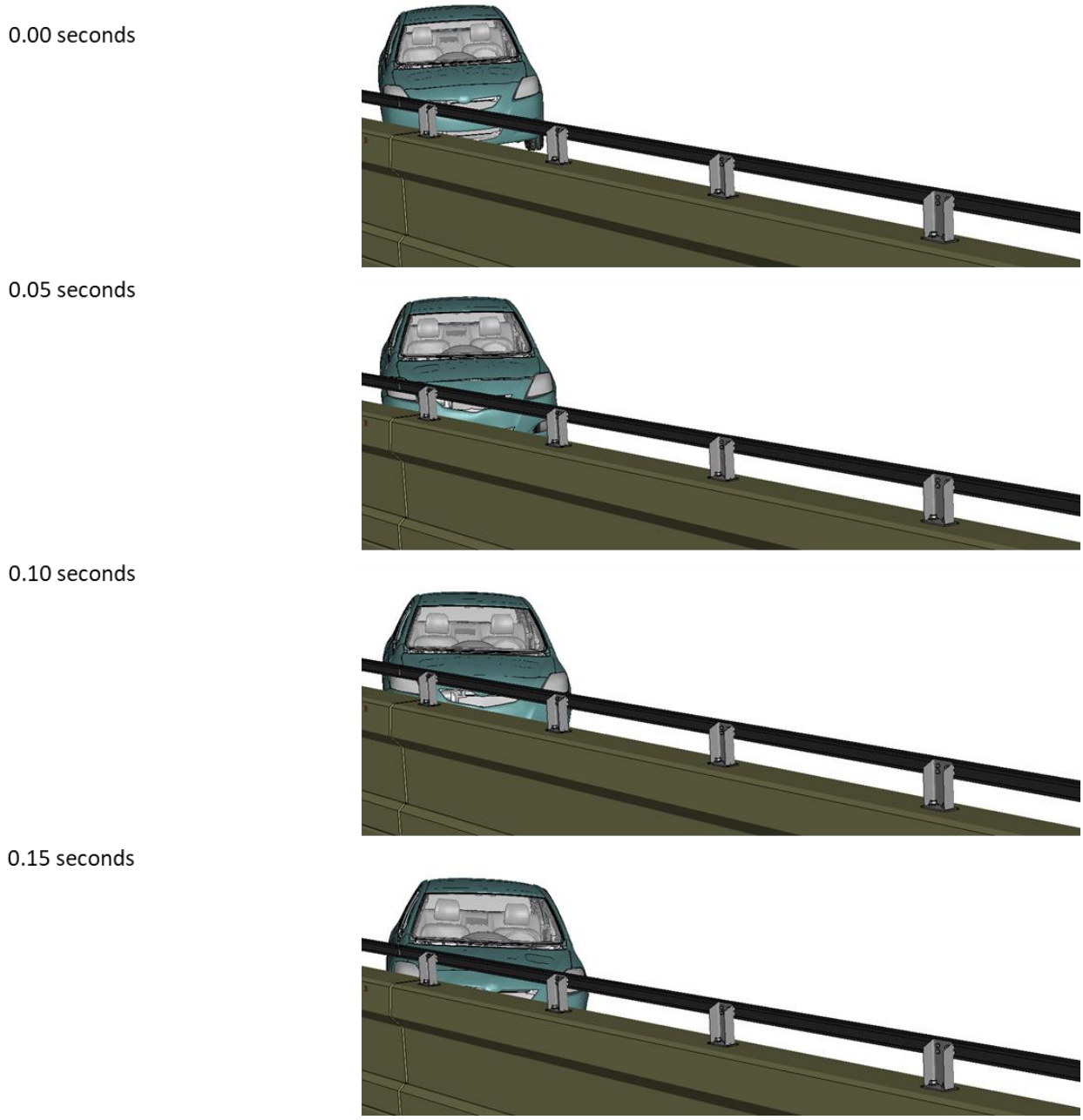

Figure 2. Sequential views from analysis of MASH Test 3-10 at 3.6 ft upstream of critical post from an isometric viewpoint (RHT Model).

0.20 seconds

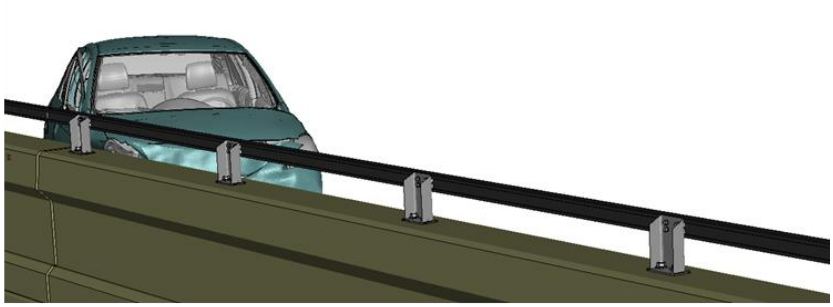

0.25 seconds

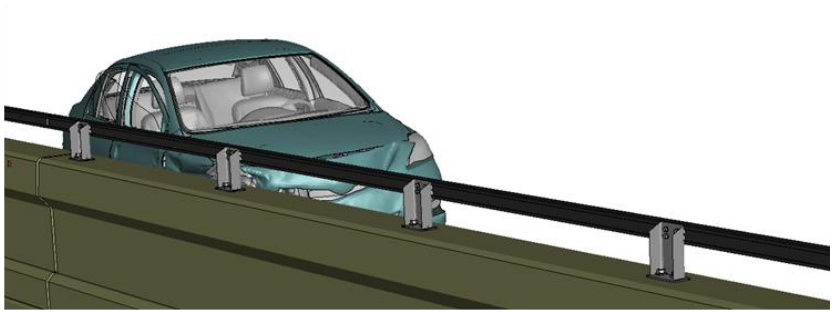

0.30 seconds

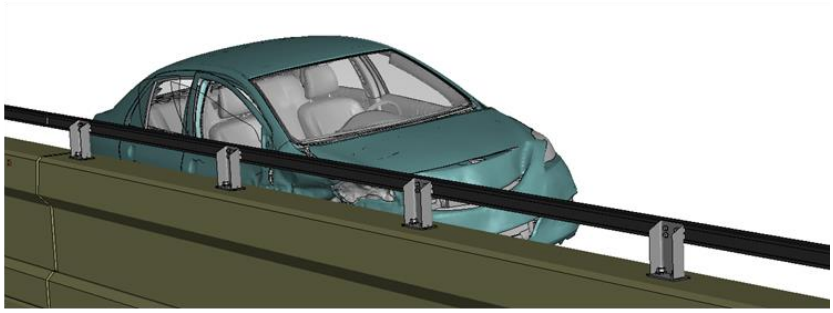

0.35 seconds

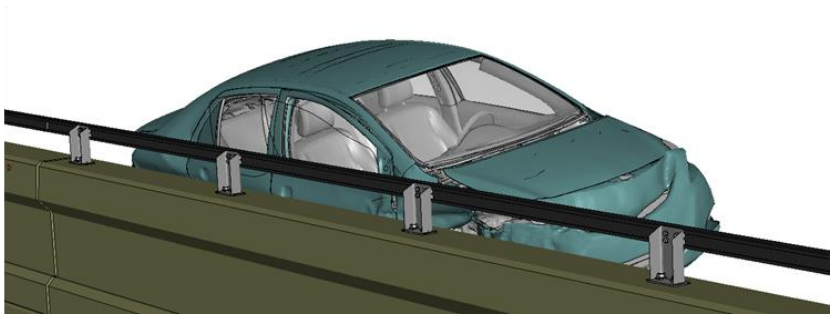

Figure 2 [CONTINUED] Sequential views from analysis of MASH Test 3-10 at 3.6 ft upstream of critical post from an isometric viewpoint (RHT Model).

0.40 seconds

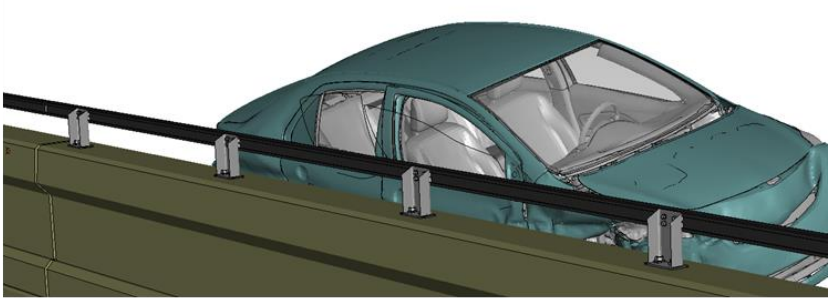

0.45 seconds

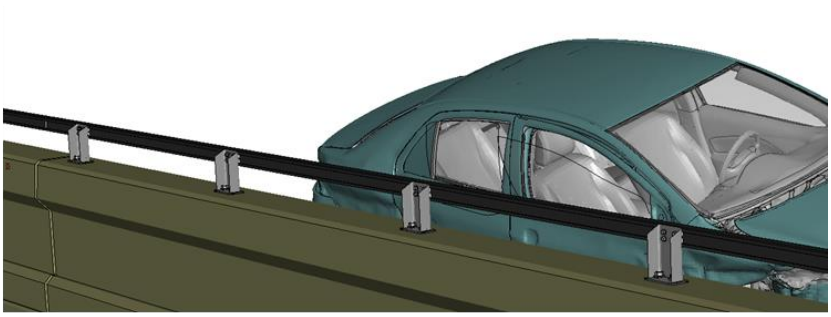

0.50 seconds

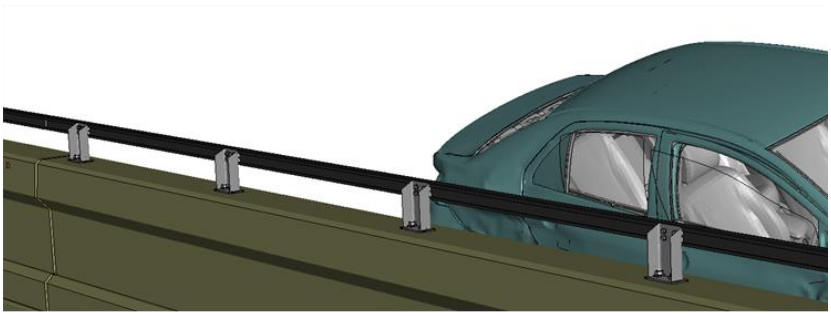

0.55 seconds

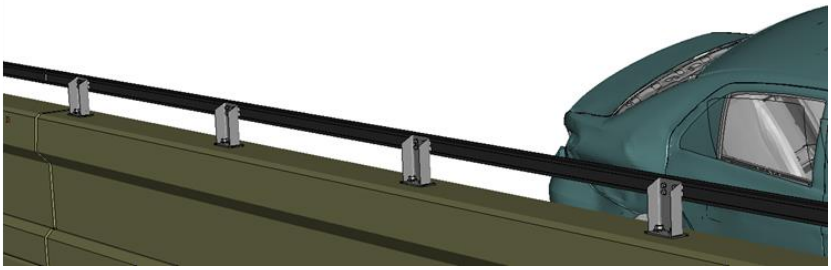

Figure 2 [CONTINUED] Sequential views from analysis of MASH Test 3-10 at 3.6 ft upstream of critical post from an isometric viewpoint (RHT Model).

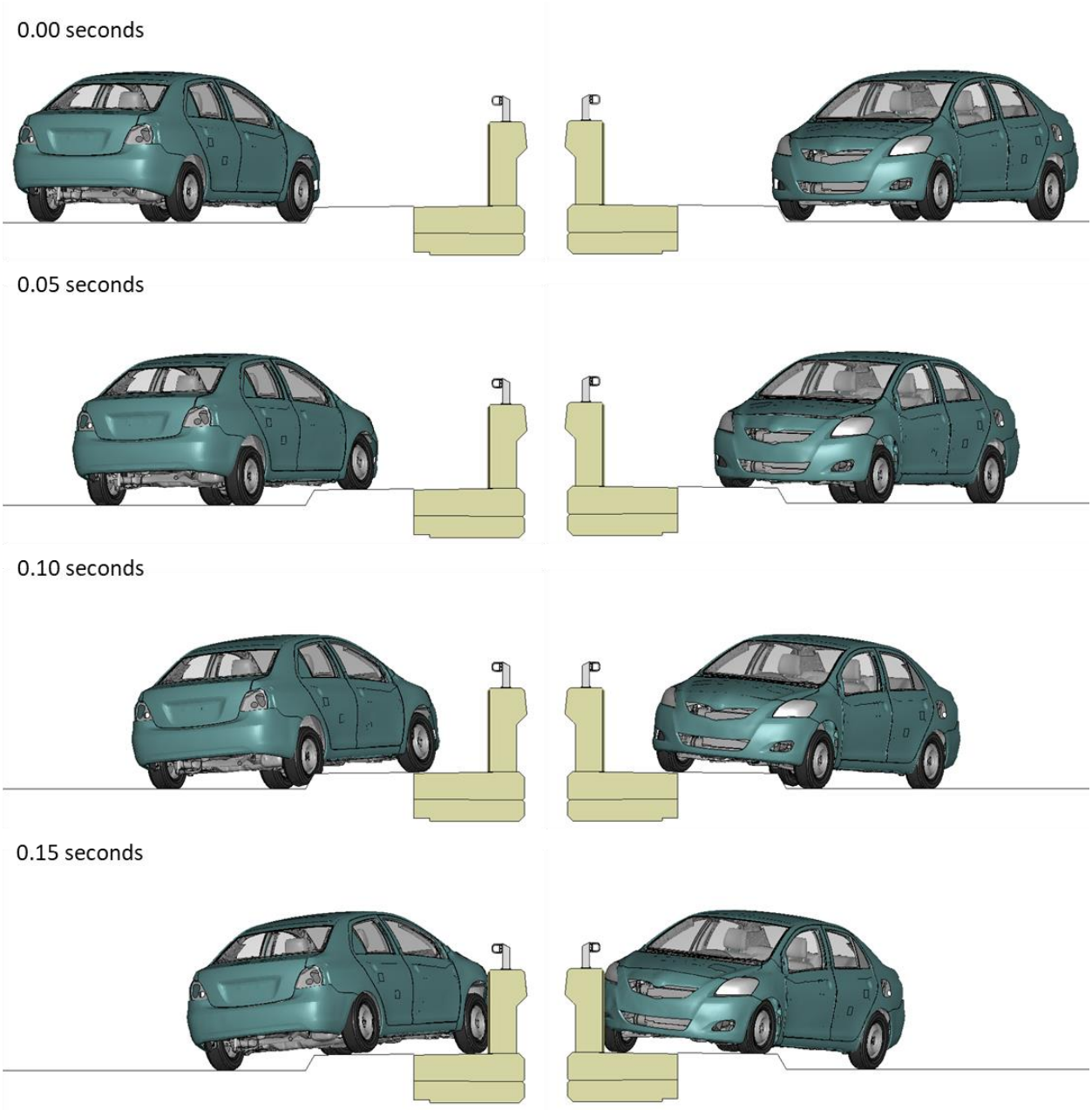

Figure 3. Sequential views from analysis of MASH Test 3-10 at 3.6 ft upstream of critical post from a front and back viewpoint (RHT Model).

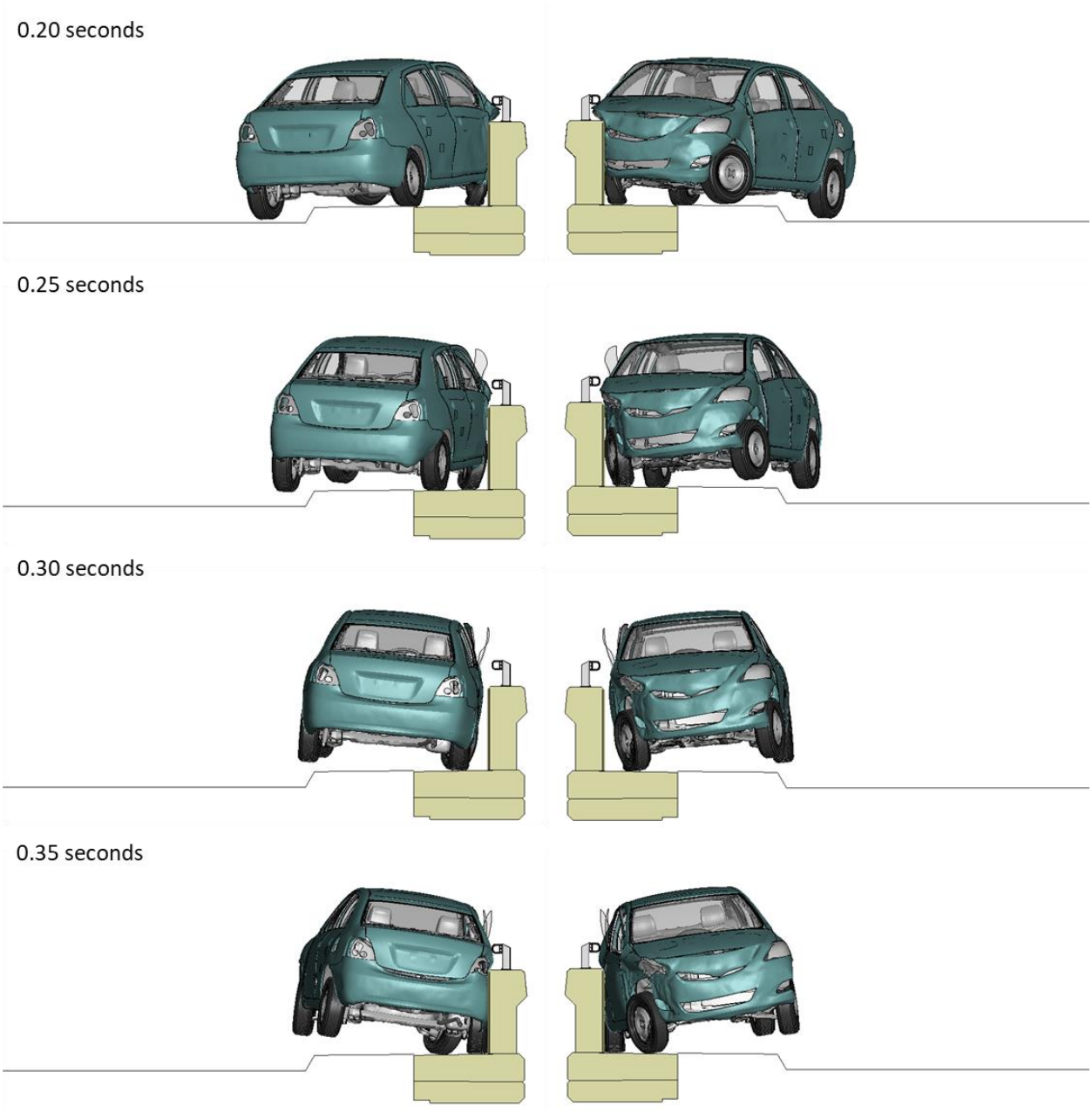

Figure 3 [CONTINUED] Sequential views from analysis of MASH Test 3-10 at 3.6 ft upstream of critical post from a front and back viewpoint (RHT Model).

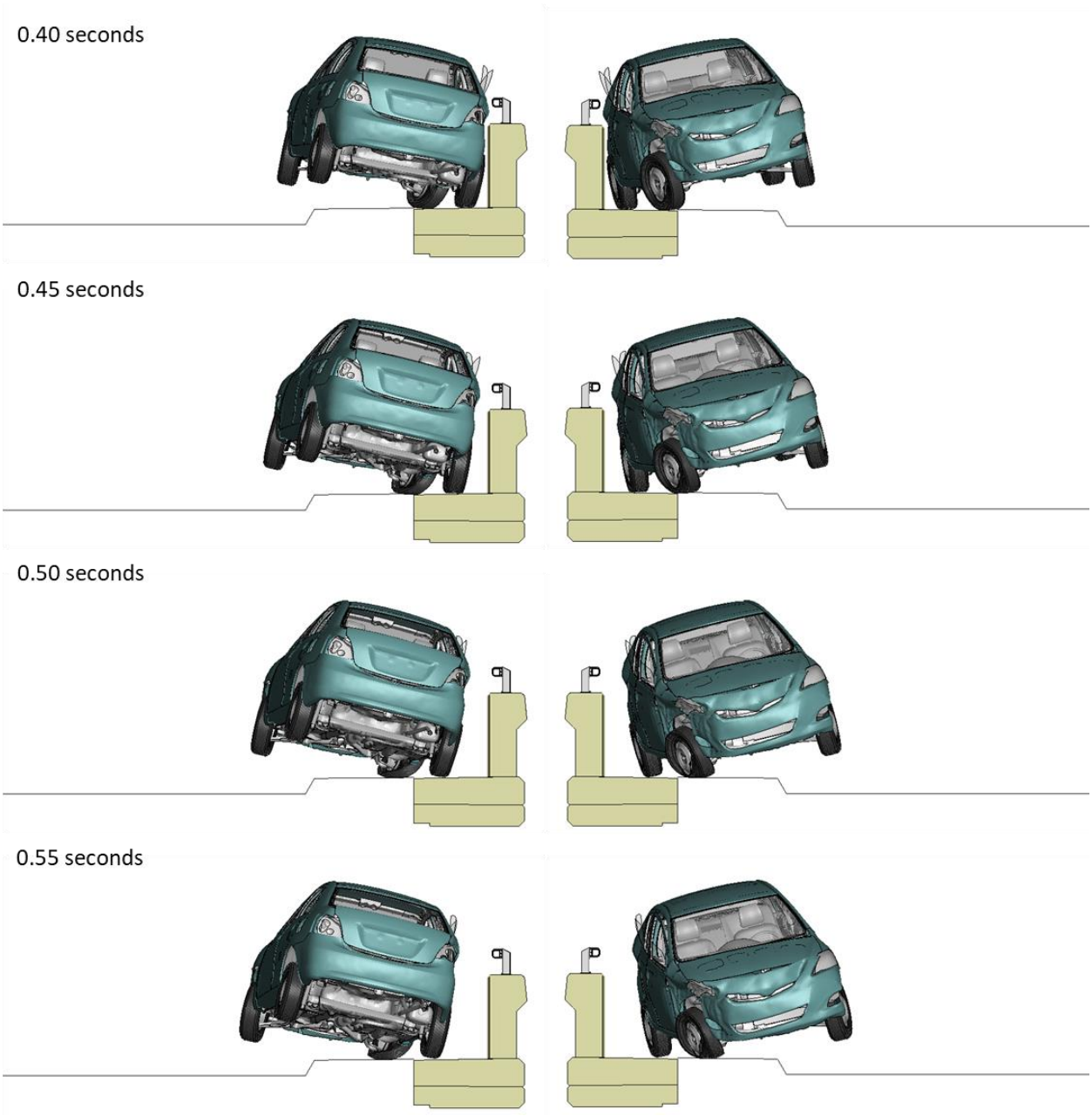

Figure 3 [CONTINUED] Sequential views from analysis of MASH Test 3-10 at 3.6 ft upstream of critical post from a front and back viewpoint (RHT Model).

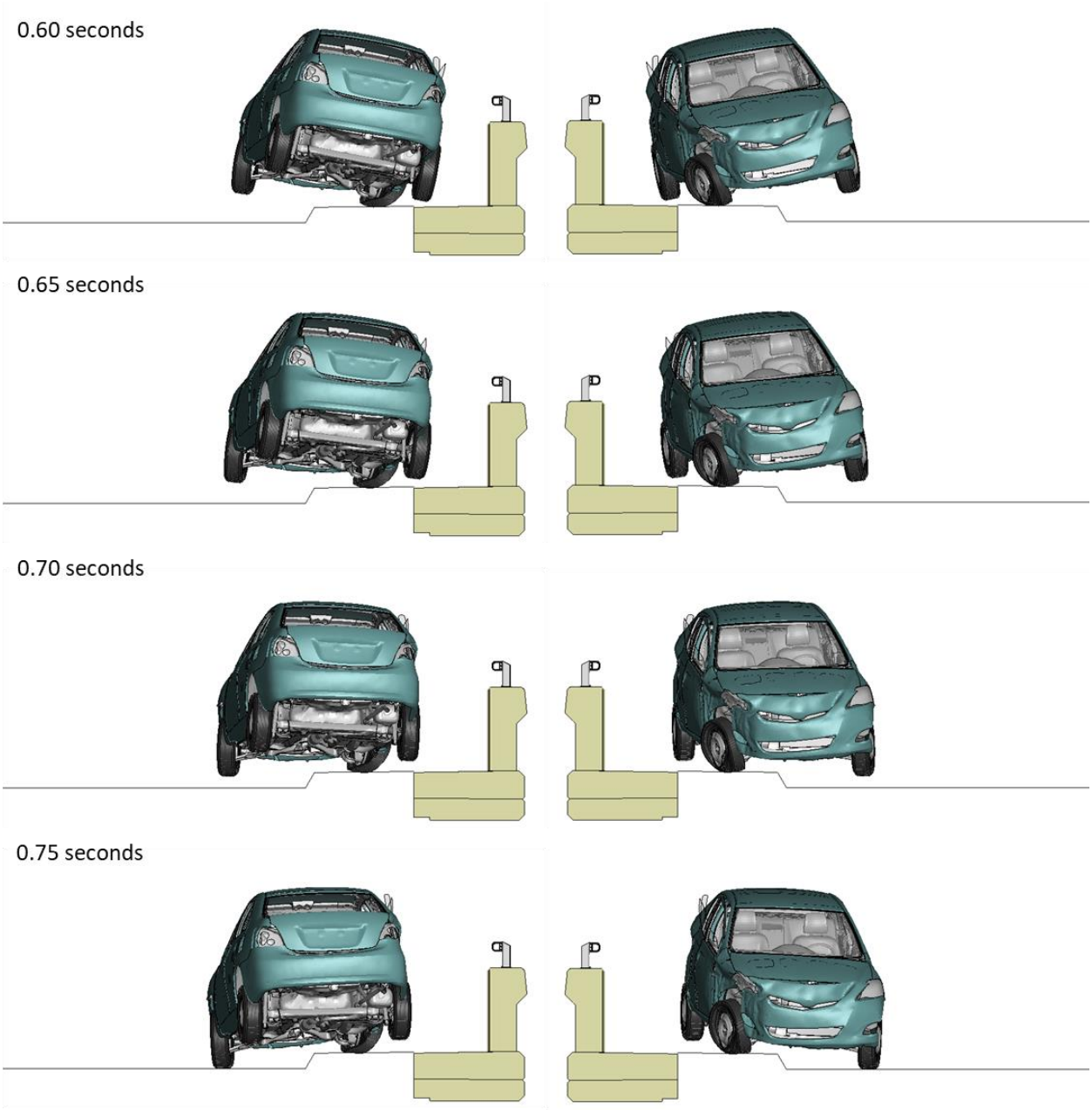

Figure 3 [CONTINUED] Sequential views from analysis of MASH Test 3-10 at 3.6 ft upstream of critical post from a front and back viewpoint (RHT Model).

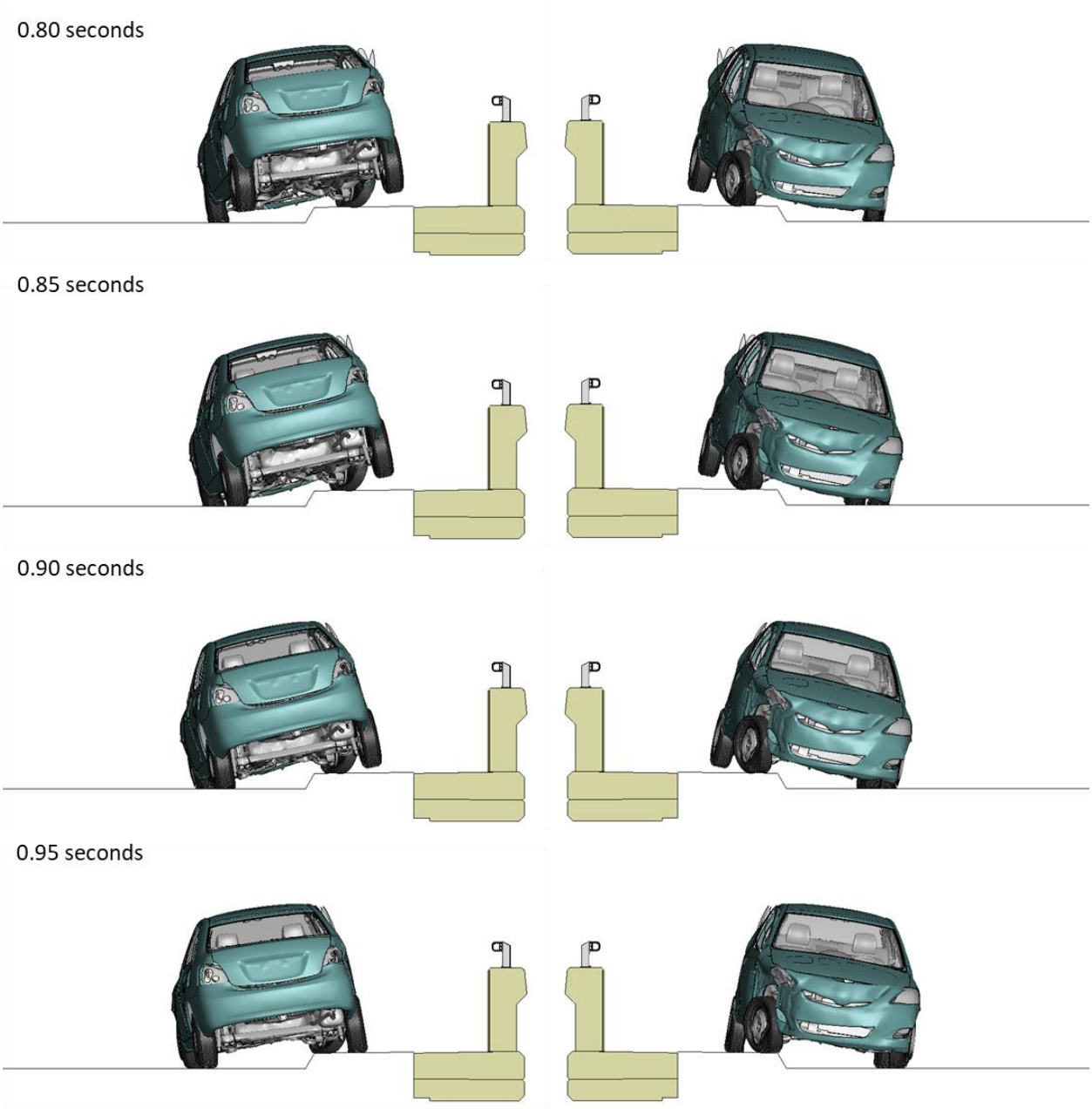

Figure 3 [CONTINUED] Sequential views from analysis of MASH Test 3-10 at 3.6 ft upstream of critical post from a front and back viewpoint (RHT Model).

Appendix D

Sequential Views for Test 3-10 at 4.6 ft Upstream of Critical Post (KC Model)

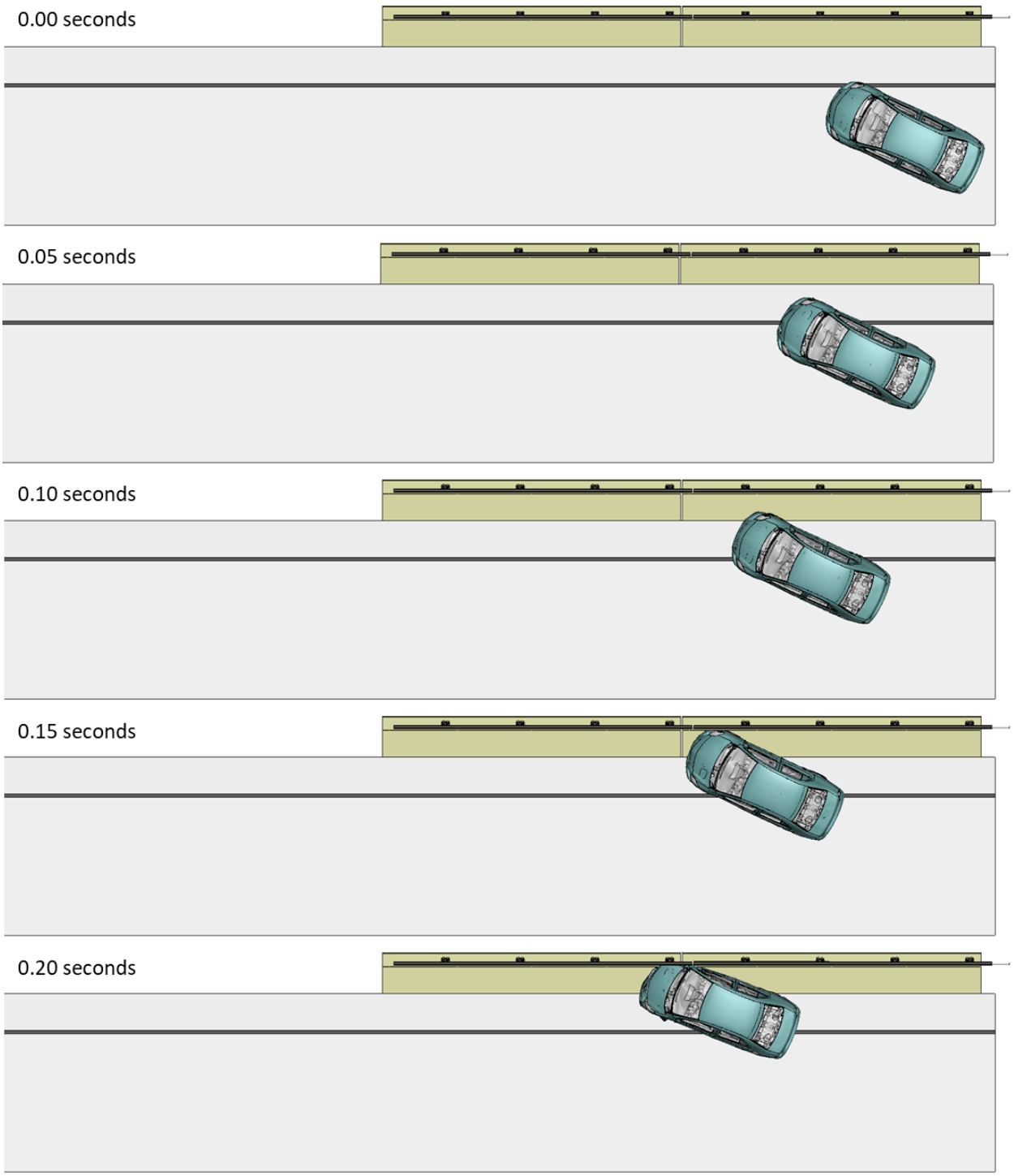

Figure 1. Sequential views from analysis of MASH Test 3-10 at 4.6 ft upstream of critical post from an overhead viewpoint (KC Model).

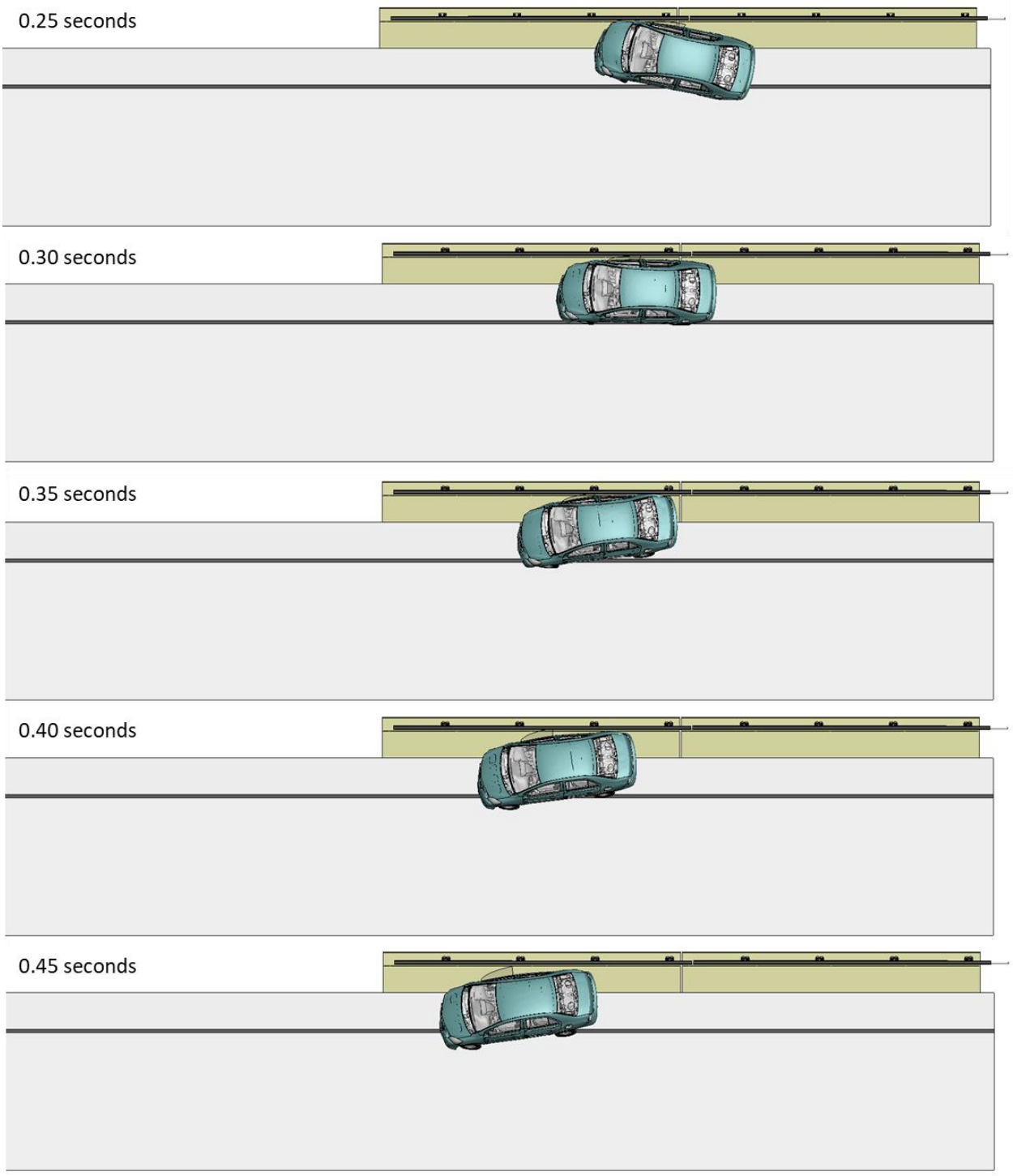

Figure 1 [CONTINUED] Sequential views from analysis of MASH Test 3-10 at 4.6 ft upstream of critical post from an overhead viewpoint (KC Model).

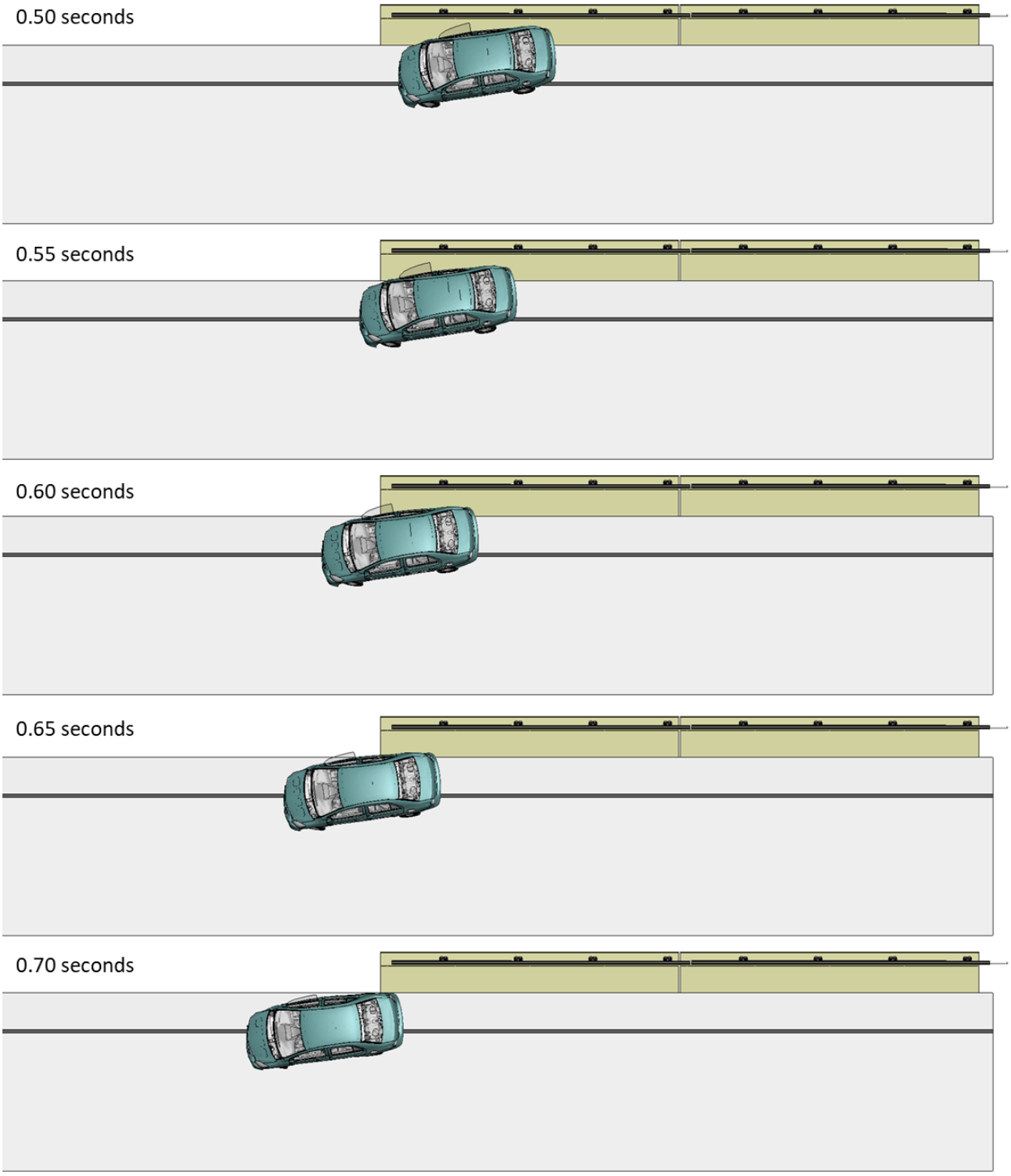

Figure 1 [CONTINUED] Sequential views from analysis of MASH Test 3-10 at 4.6 ft upstream of critical post from an overhead viewpoint (KC Model).

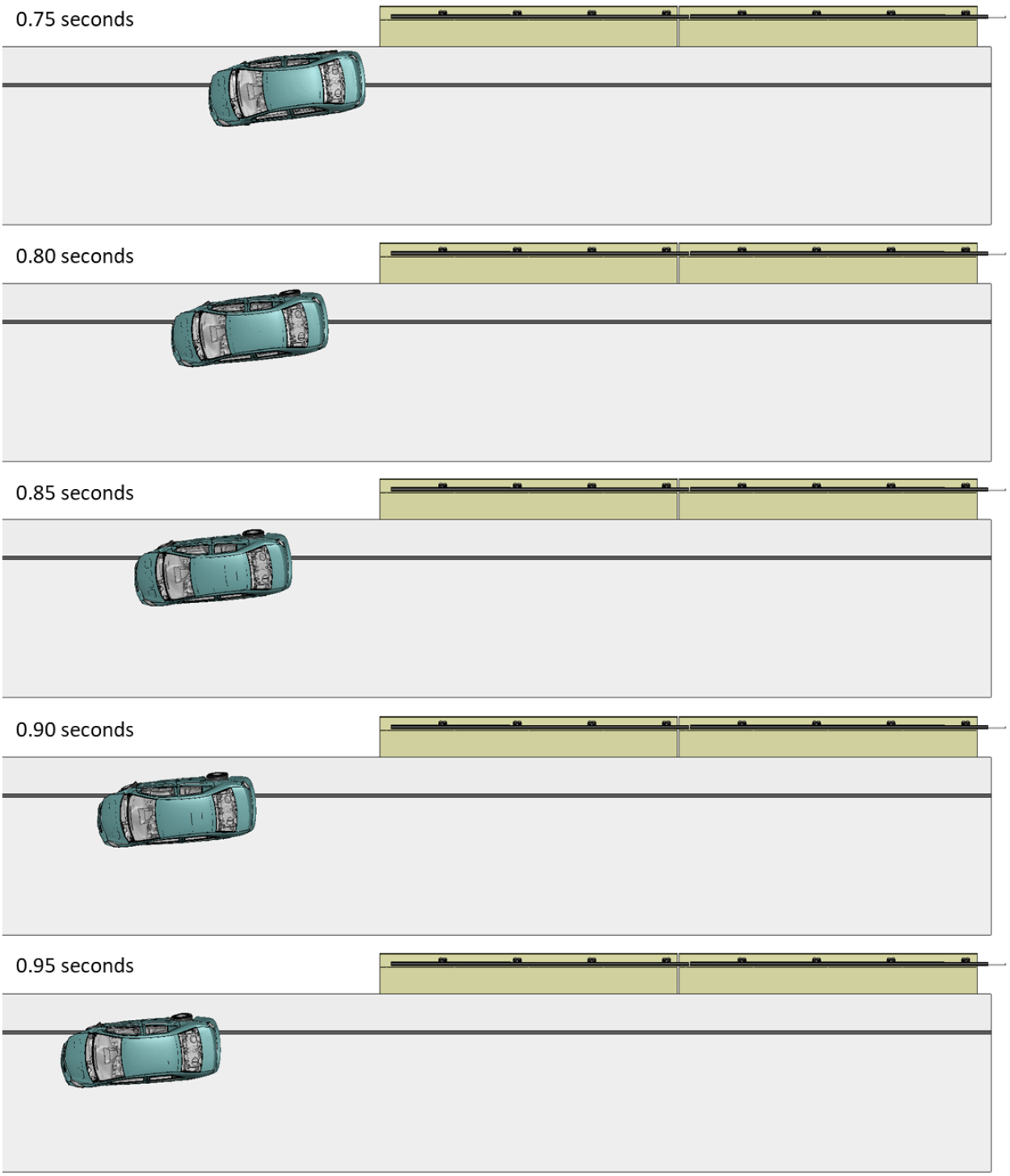

Figure 1 [CONTINUED] Sequential views from analysis of MASH Test 3-10 at 4.6 ft upstream of critical post from an overhead viewpoint (KC Model).

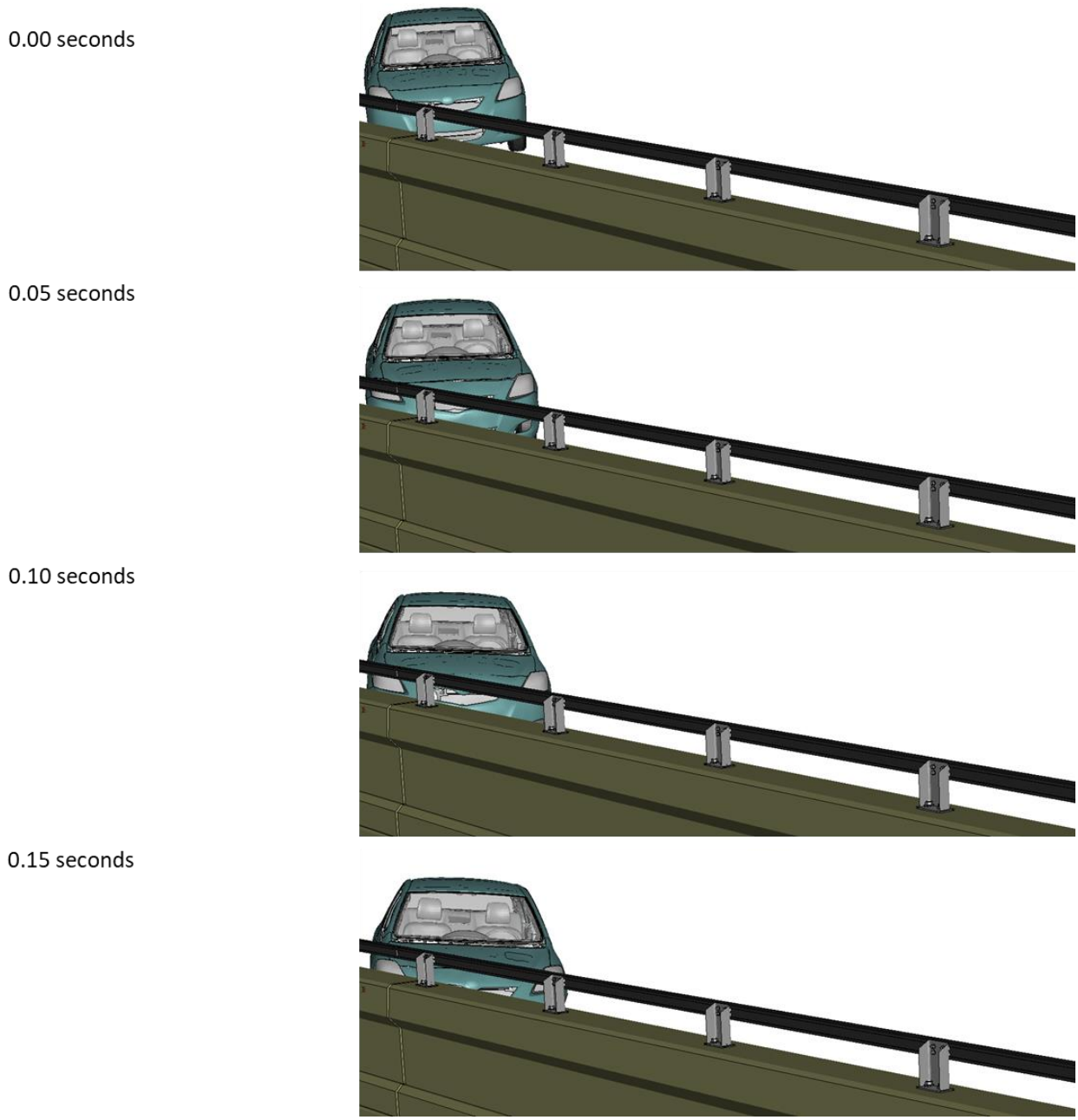

Figure 2. Sequential views from analysis of MASH Test 3-10 at 4.6 ft upstream of critical post from an isometric viewpoint (KC Model).

0.20 seconds

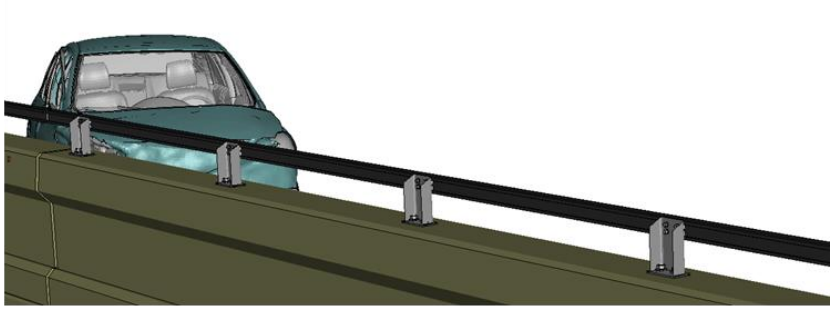

0.25 seconds

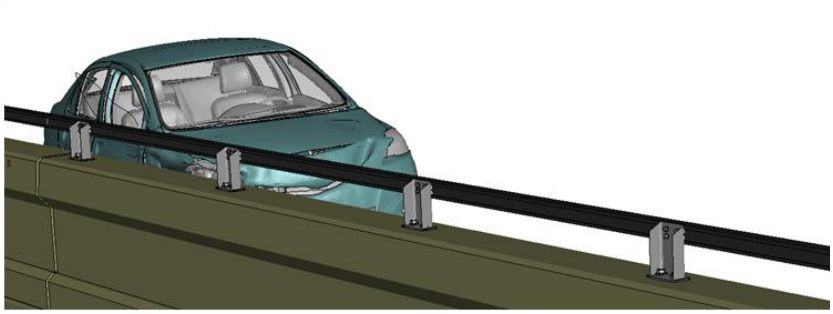

0.30 seconds

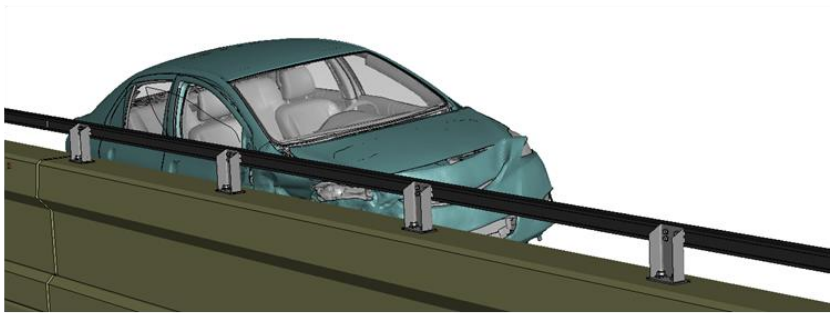

0.35 seconds

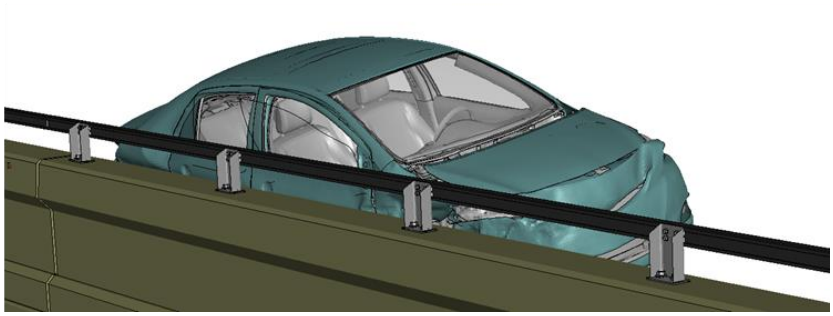

Figure 2 [CONTINUED] Sequential views from analysis of MASH Test 3-10 at 4.6 ft upstream of critical post from an isometric viewpoint (KC Model).

0.40 seconds

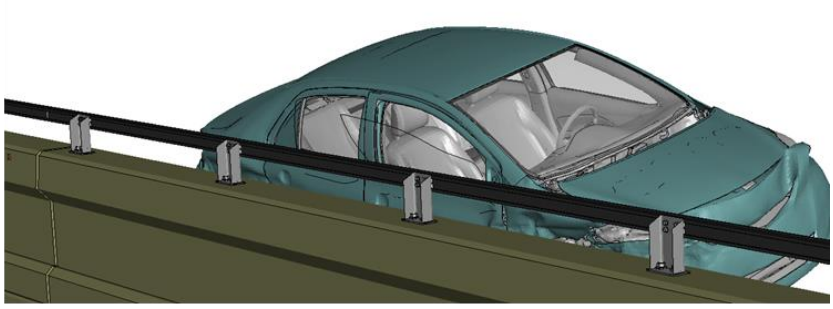

0.45 seconds

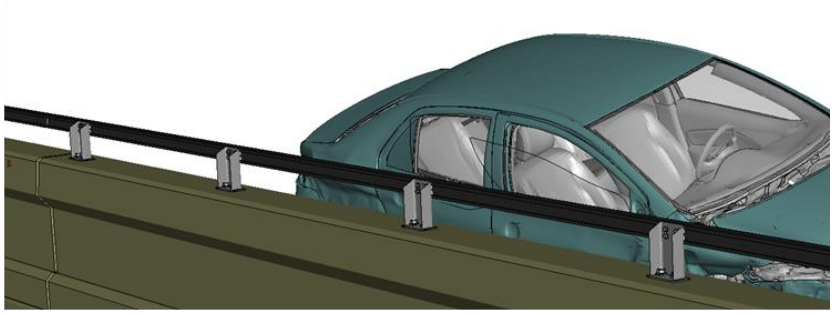

0.50 seconds

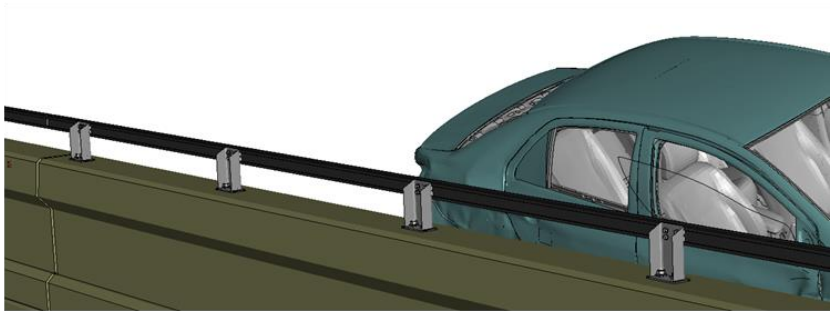

0.55 seconds

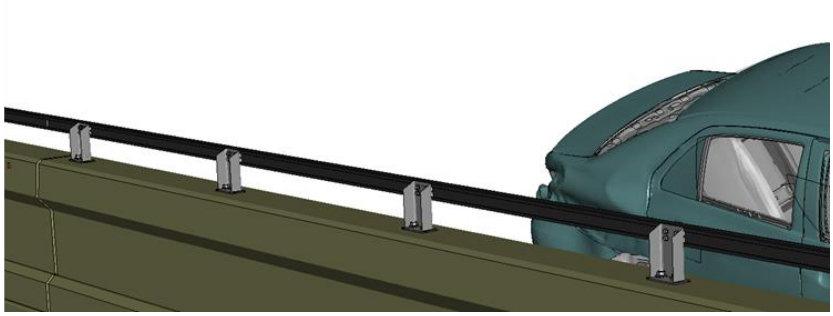

Figure 2 [CONTINUED] Sequential views from analysis of MASH Test 3-10 at 4.6 ft upstream of critical post from an isometric viewpoint (KC Model).

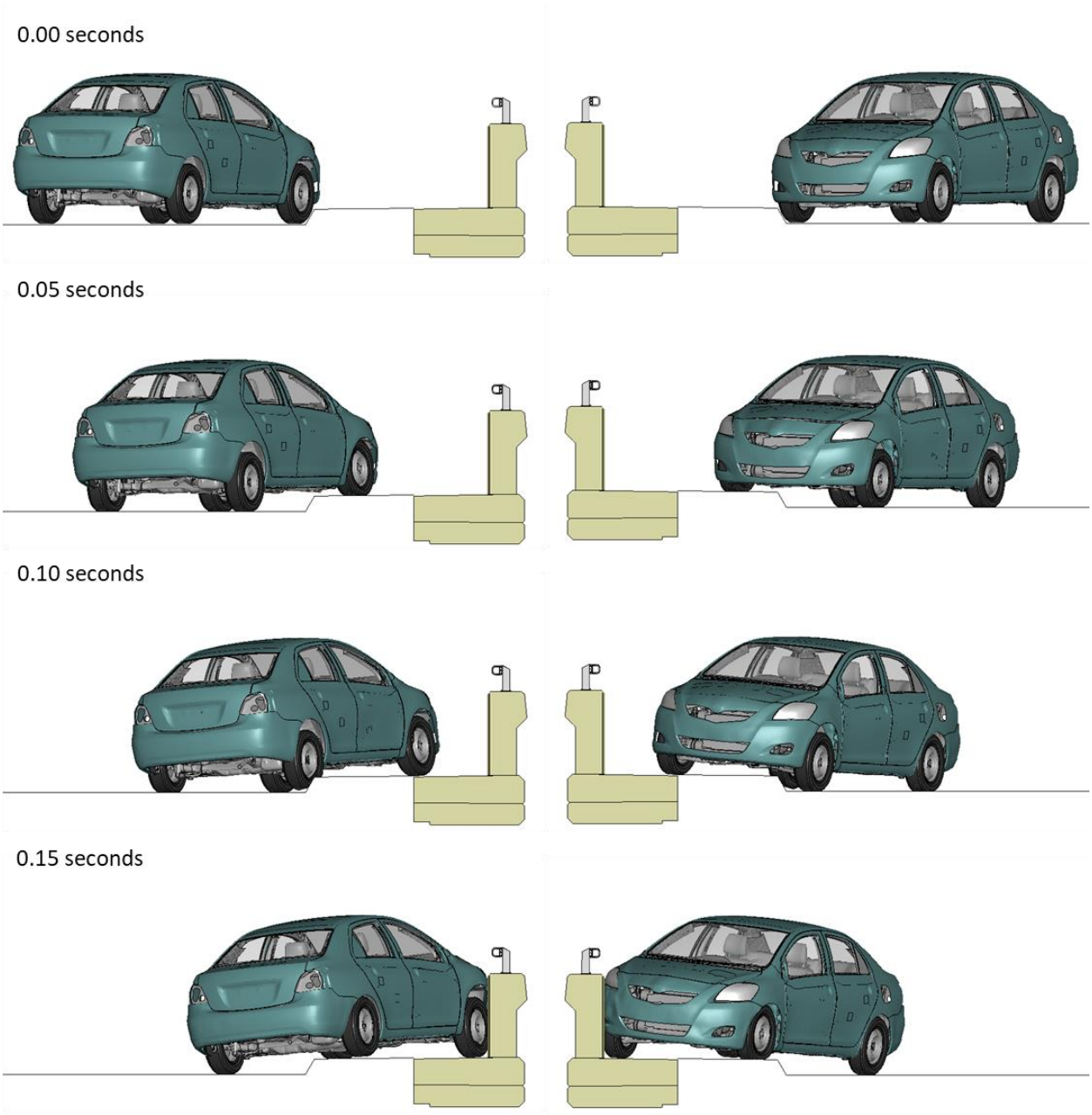

Figure 3. Sequential views from analysis of MASH Test 3-10 at 4.6 ft upstream of critical post from a front and back viewpoint (KC Model).

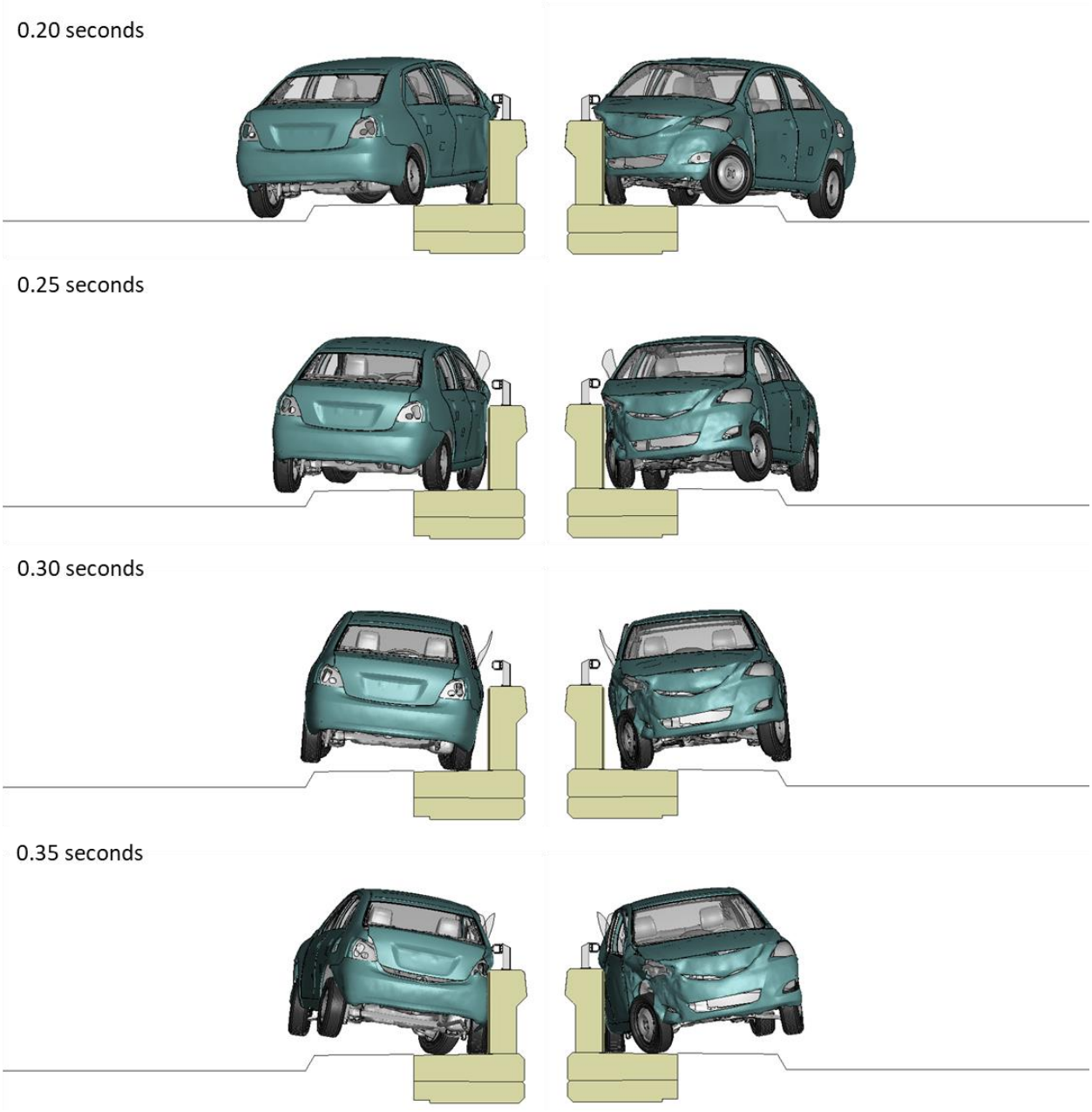

Figure 3 [CONTINUED] Sequential views from analysis of MASH Test 3-10 at 4.6 ft upstream of critical post from a front and back viewpoint (KC Model).

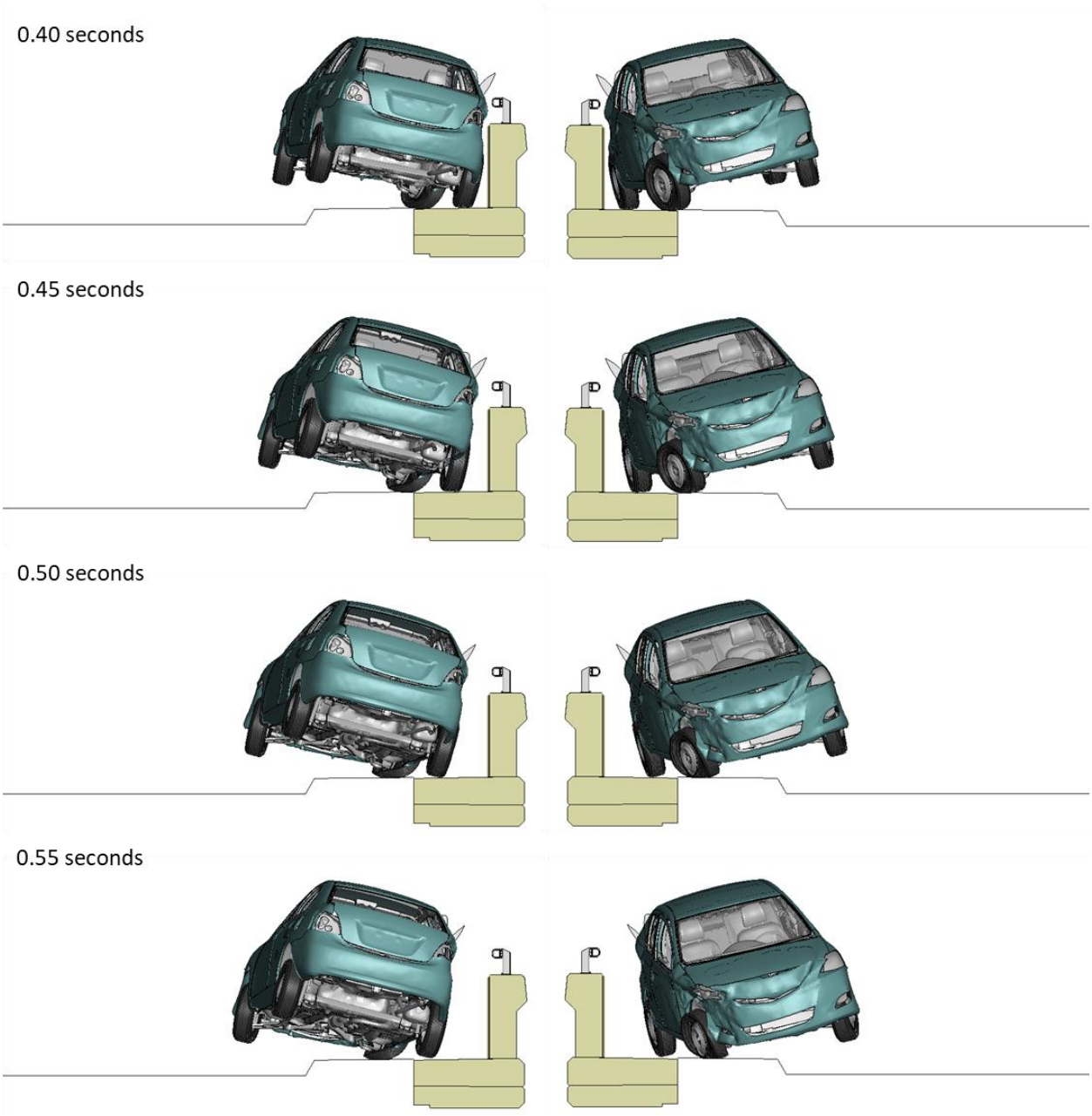

Figure 3 [CONTINUED] Sequential views from analysis of MASH Test 3-10 at 4.6 ft upstream of critical post from a front and back viewpoint (KC Model).

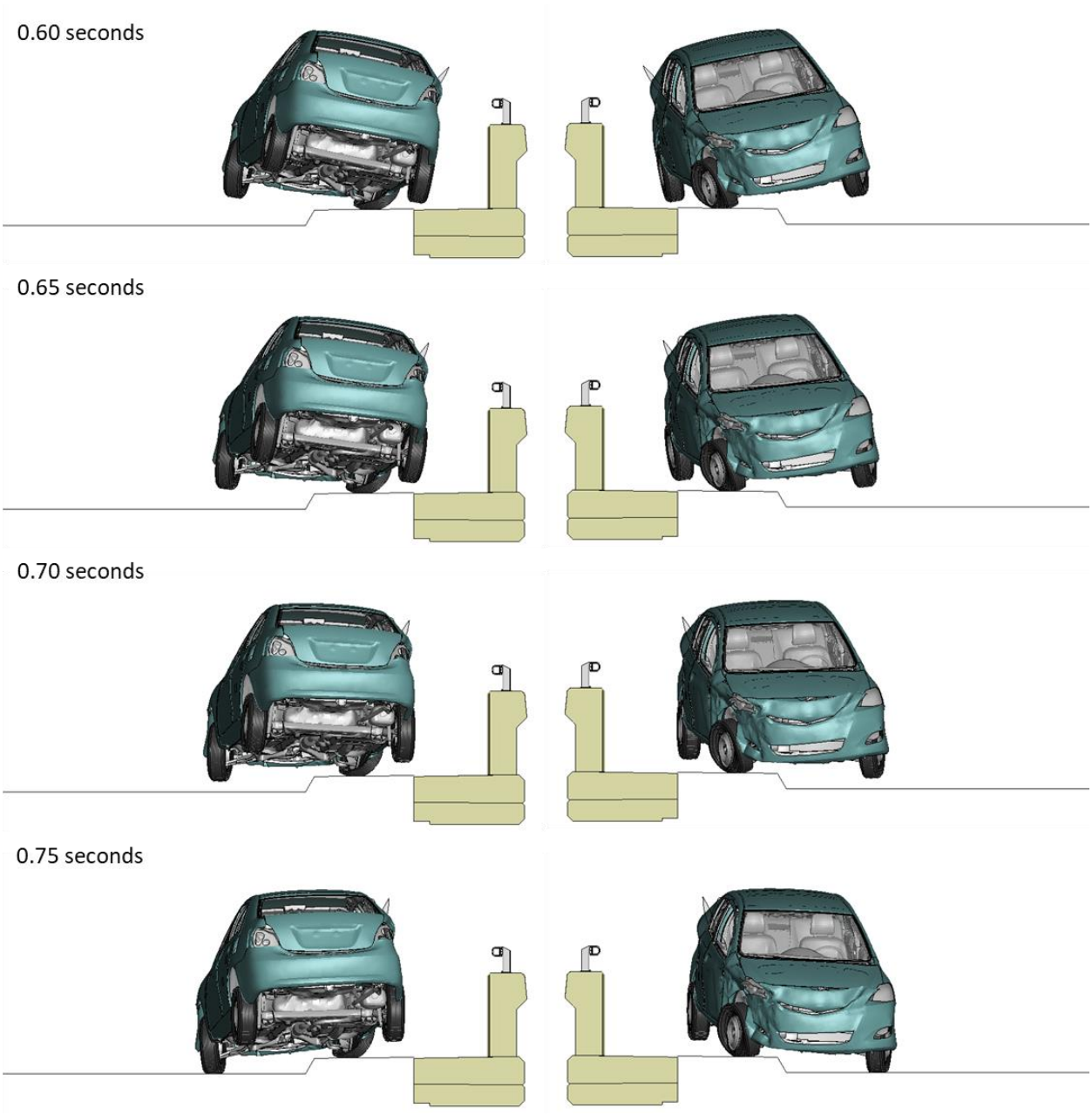

Figure 3 [CONTINUED] Sequential views from analysis of MASH Test 3-10 at 4.6 ft upstream of critical post from a front and back viewpoint (KC Model).

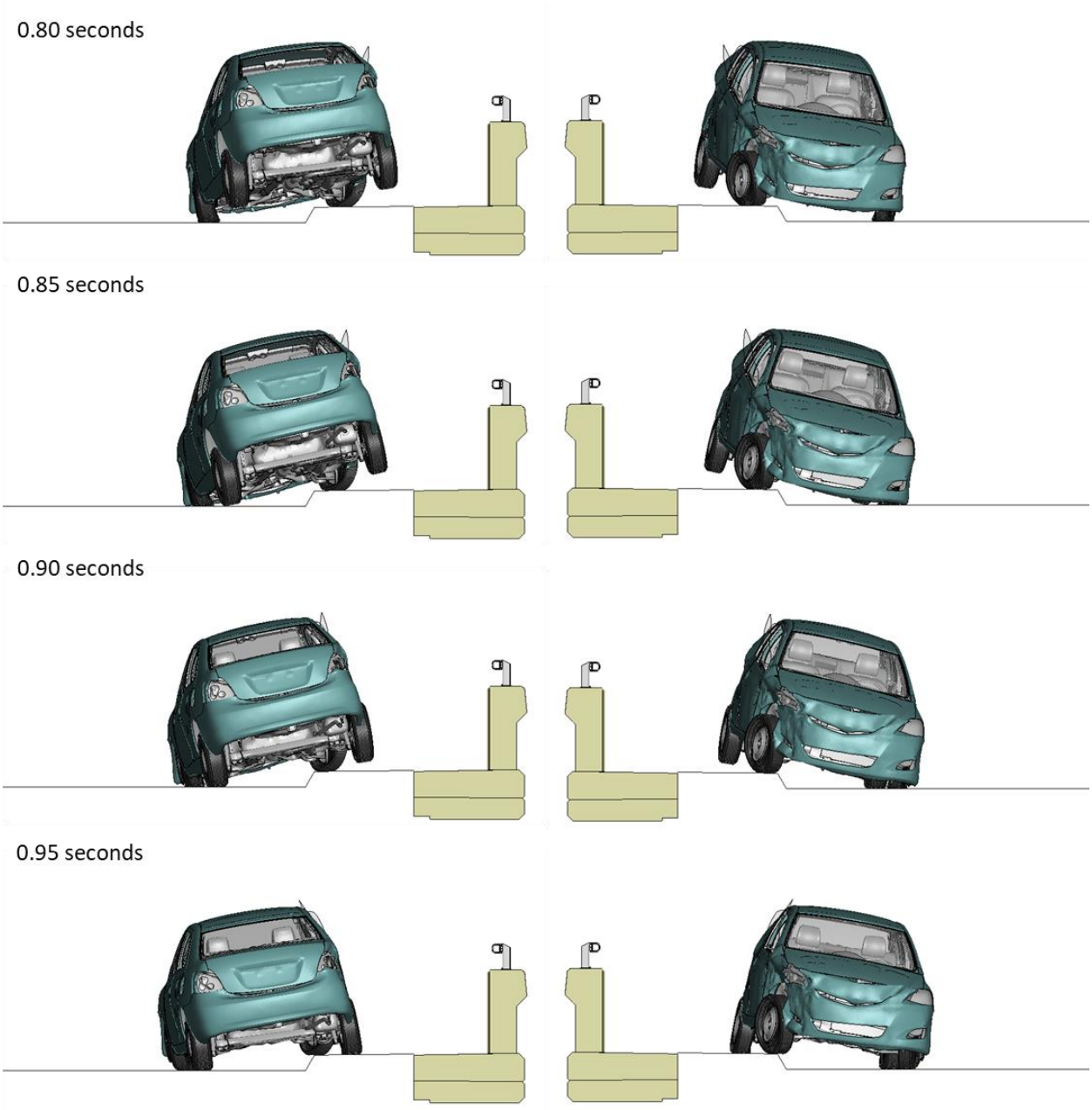

Figure 3 [CONTINUED] Sequential views from analysis of MASH Test 3-10 at 4.6 ft upstream of critical post from a front and back viewpoint (KC Model).

Appendix E

Sequential Views for Test 3-10 at 4.6 ft Upstream of Critical Post (RHT Model)

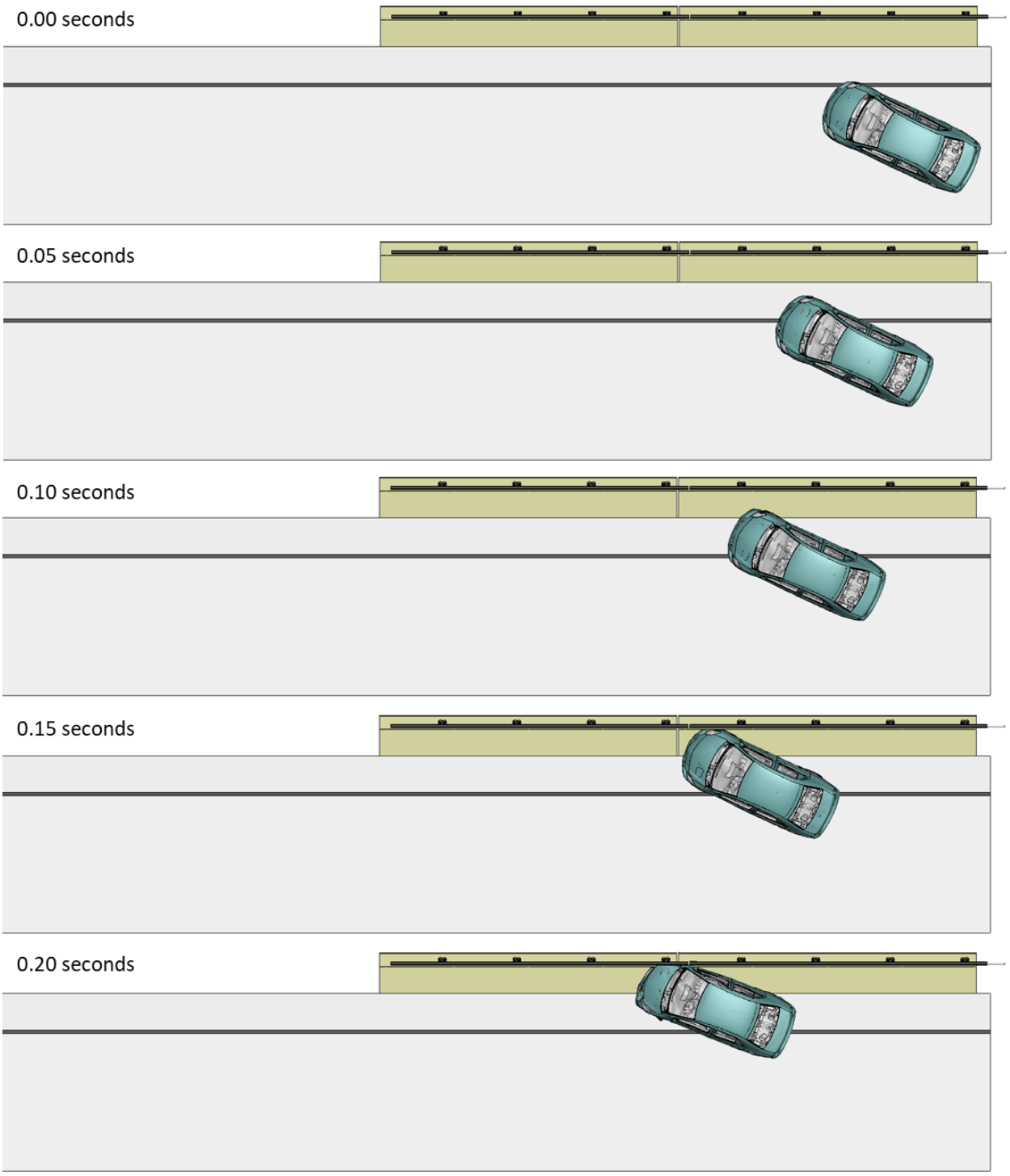

Figure 1. Sequential views from analysis of MASH Test 3-10 at 4.6 ft upstream of critical post from an overhead viewpoint (RHT Model).

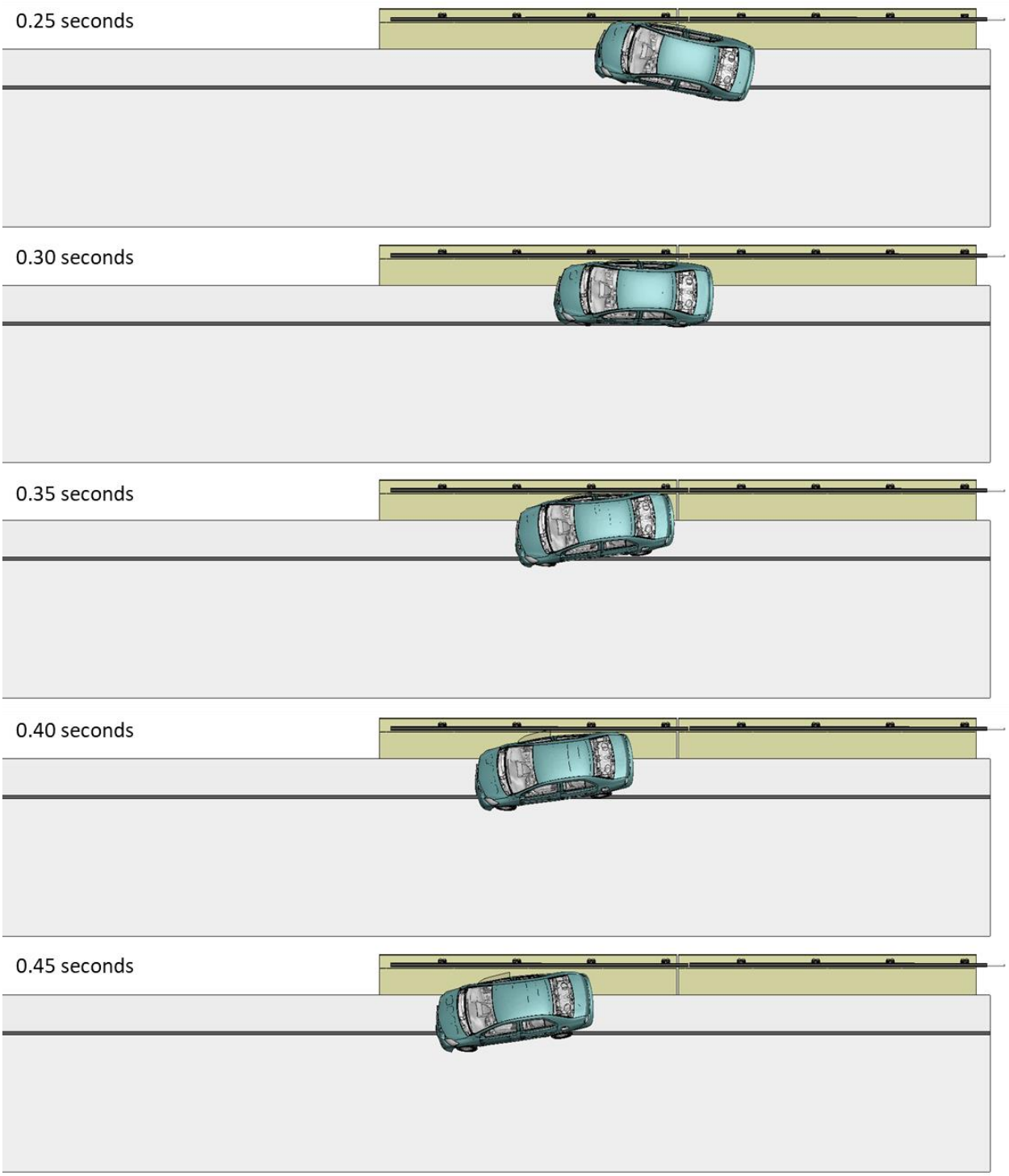

Figure 1 [CONTINUED] Sequential views from analysis of MASH Test 3-10 at 4.6 ft upstream of critical post from an overhead viewpoint (RHT Model).

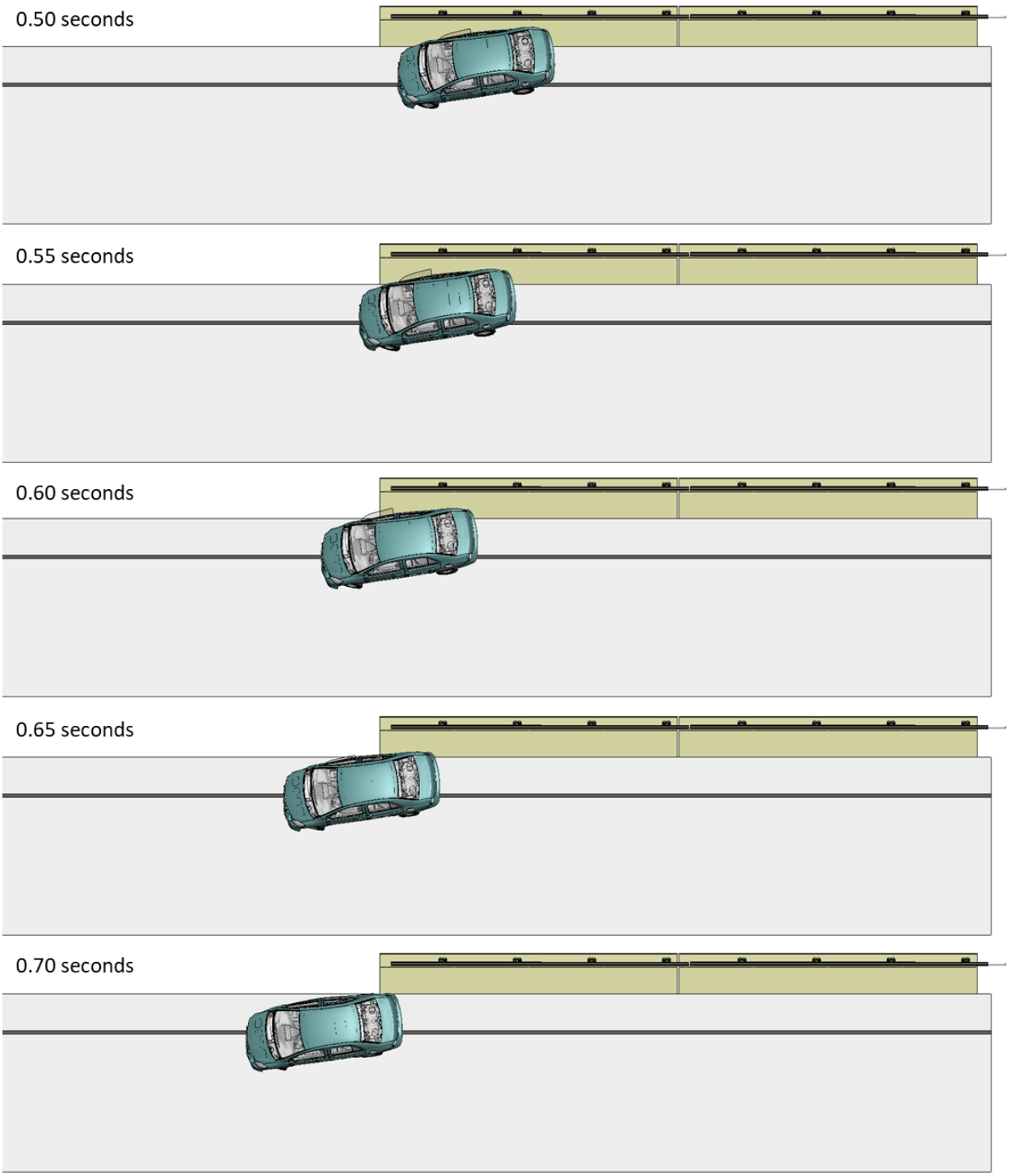

Figure 1 [CONTINUED] Sequential views from analysis of MASH Test 3-10 at 4.6 ft upstream of critical post from an overhead viewpoint (RHT Model).

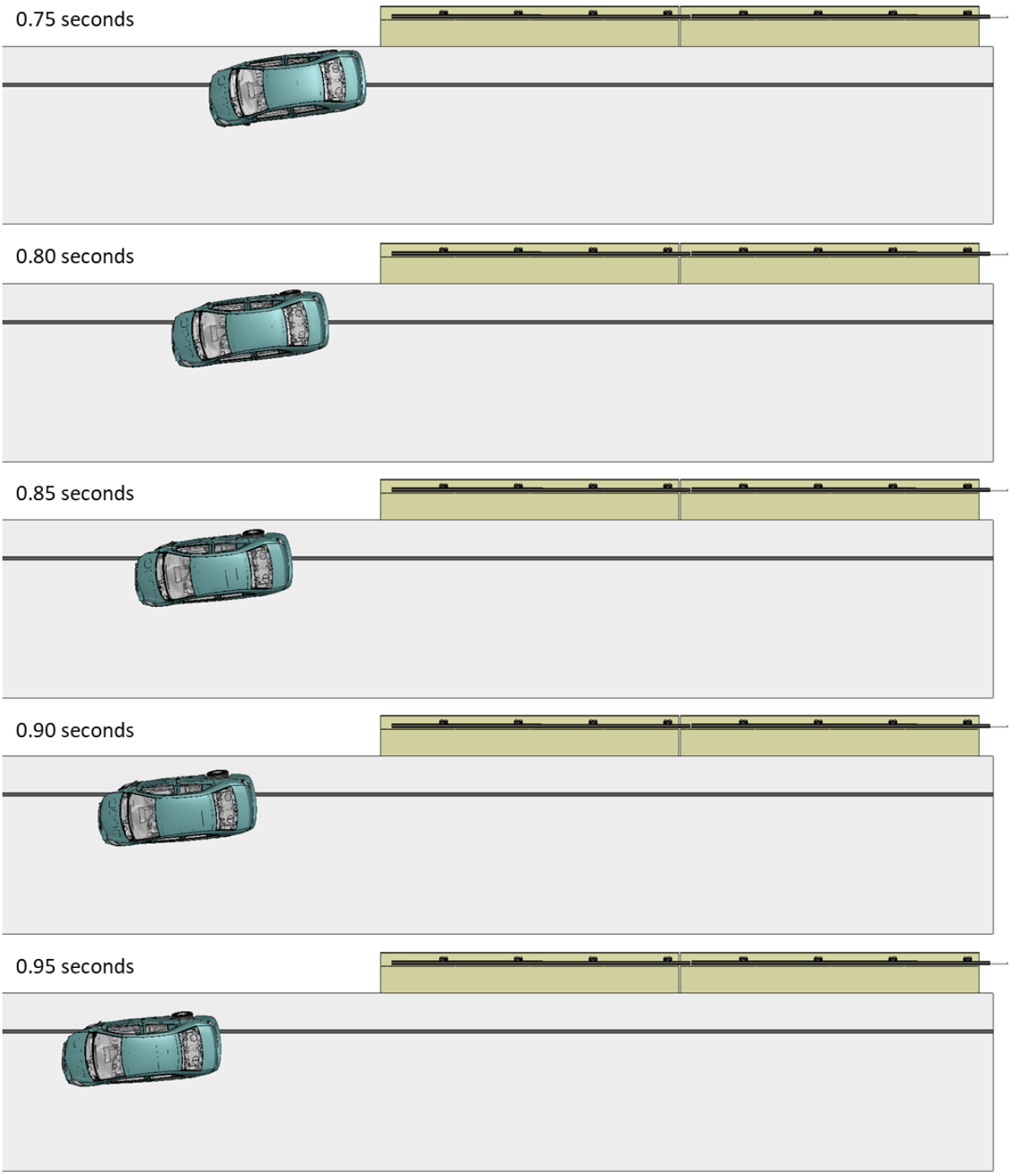

Figure 1 [CONTINUED] Sequential views from analysis of MASH Test 3-10 at 4.6 ft upstream of critical post from an overhead viewpoint (RHT Model).

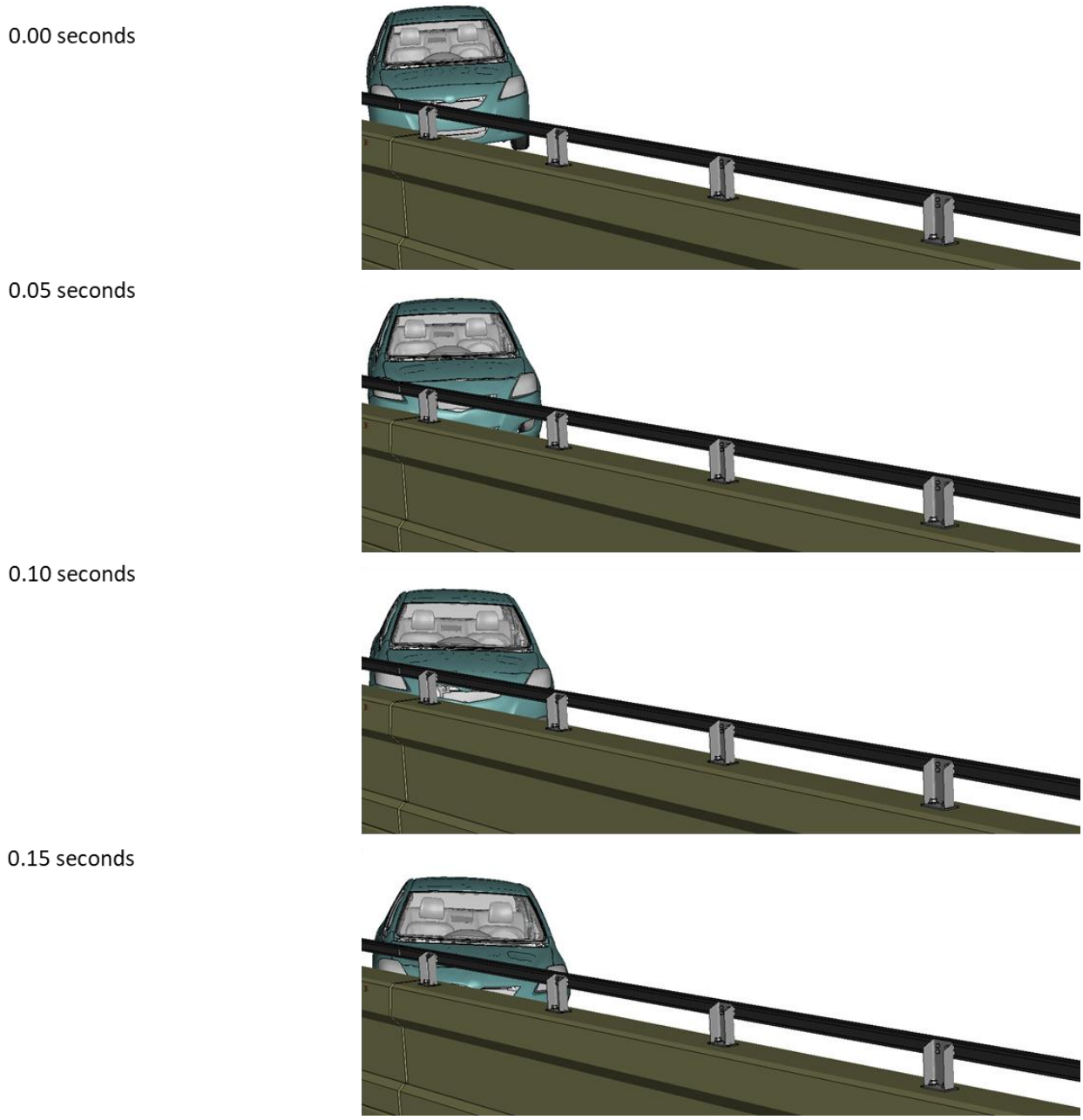

Figure 2. Sequential views from analysis of MASH Test 3-10 at 4.6 ft upstream of critical post from an isometric viewpoint (RHT Model).

0.20 seconds

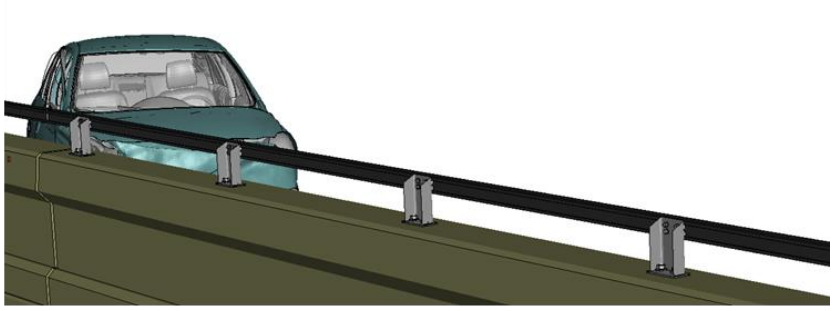

0.25 seconds

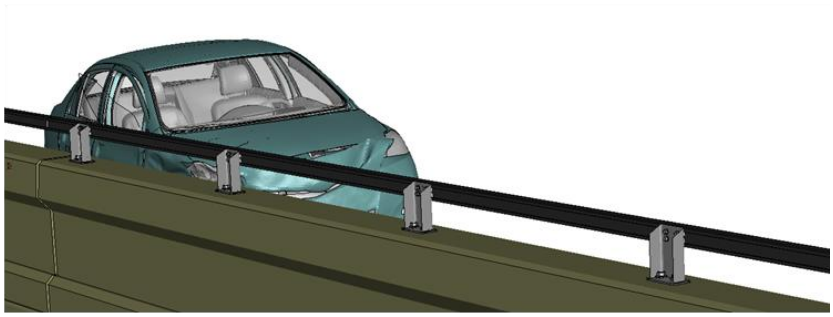

0.30 seconds

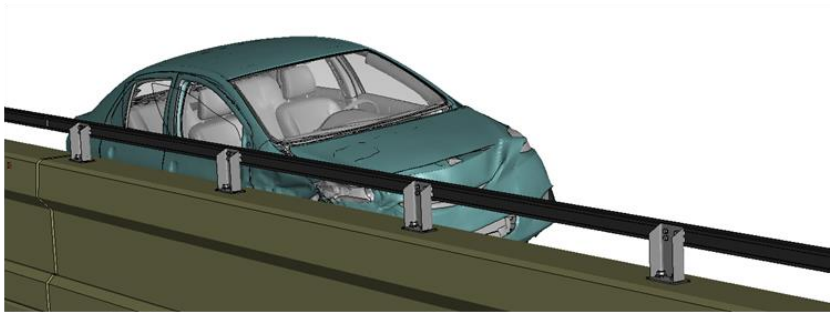

0.35 seconds

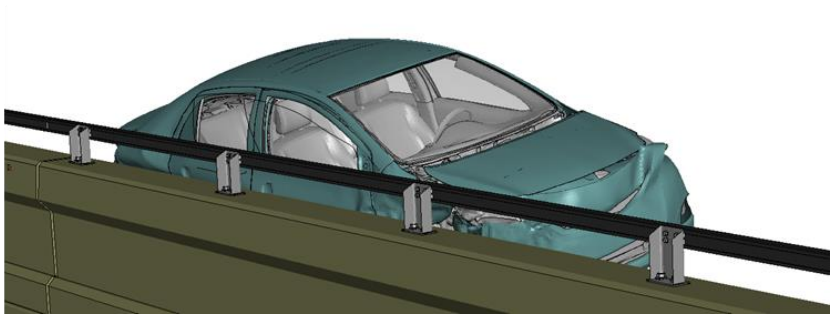

Figure 2 [CONTINUED] Sequential views from analysis of MASH Test 3-10 at 4.6 ft upstream of critical post from an isometric viewpoint (RHT Model).

0.40 seconds

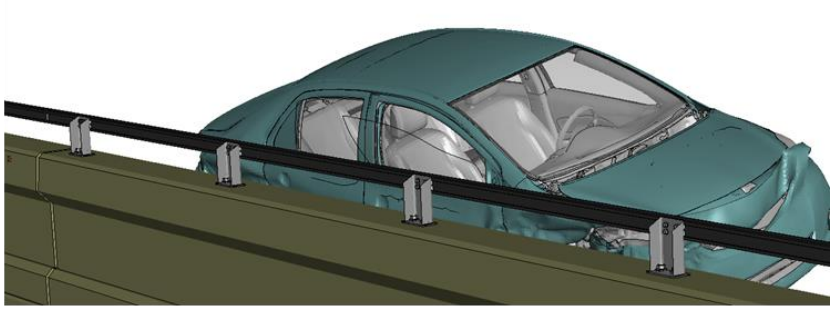

0.45 seconds

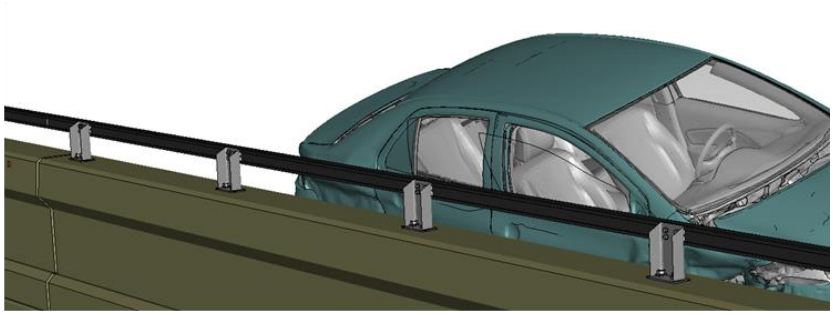

0.50 seconds

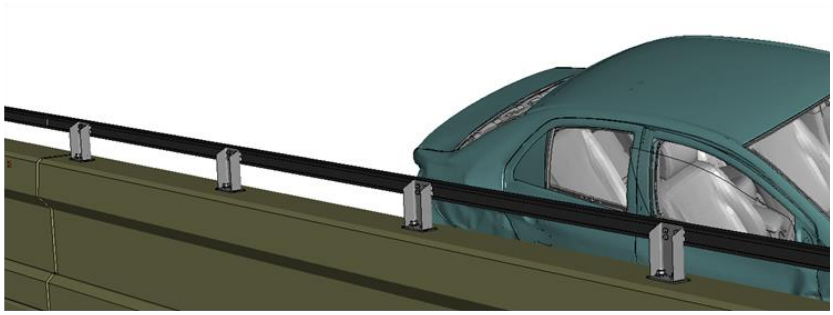

0.55 seconds

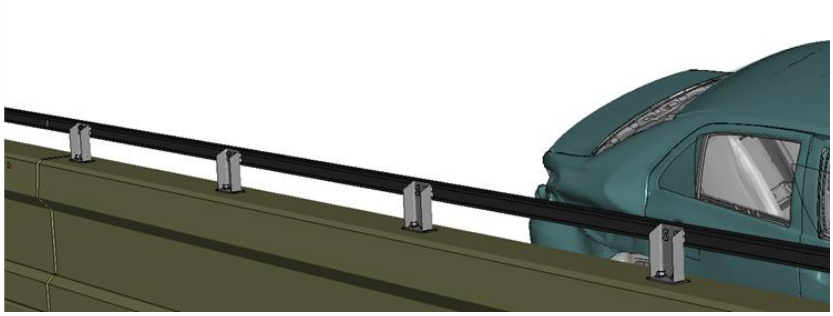

Figure 2 [CONTINUED] Sequential views from analysis of MASH Test 3-10 at 4.6 ft upstream of critical post from an isometric viewpoint (RHT Model).

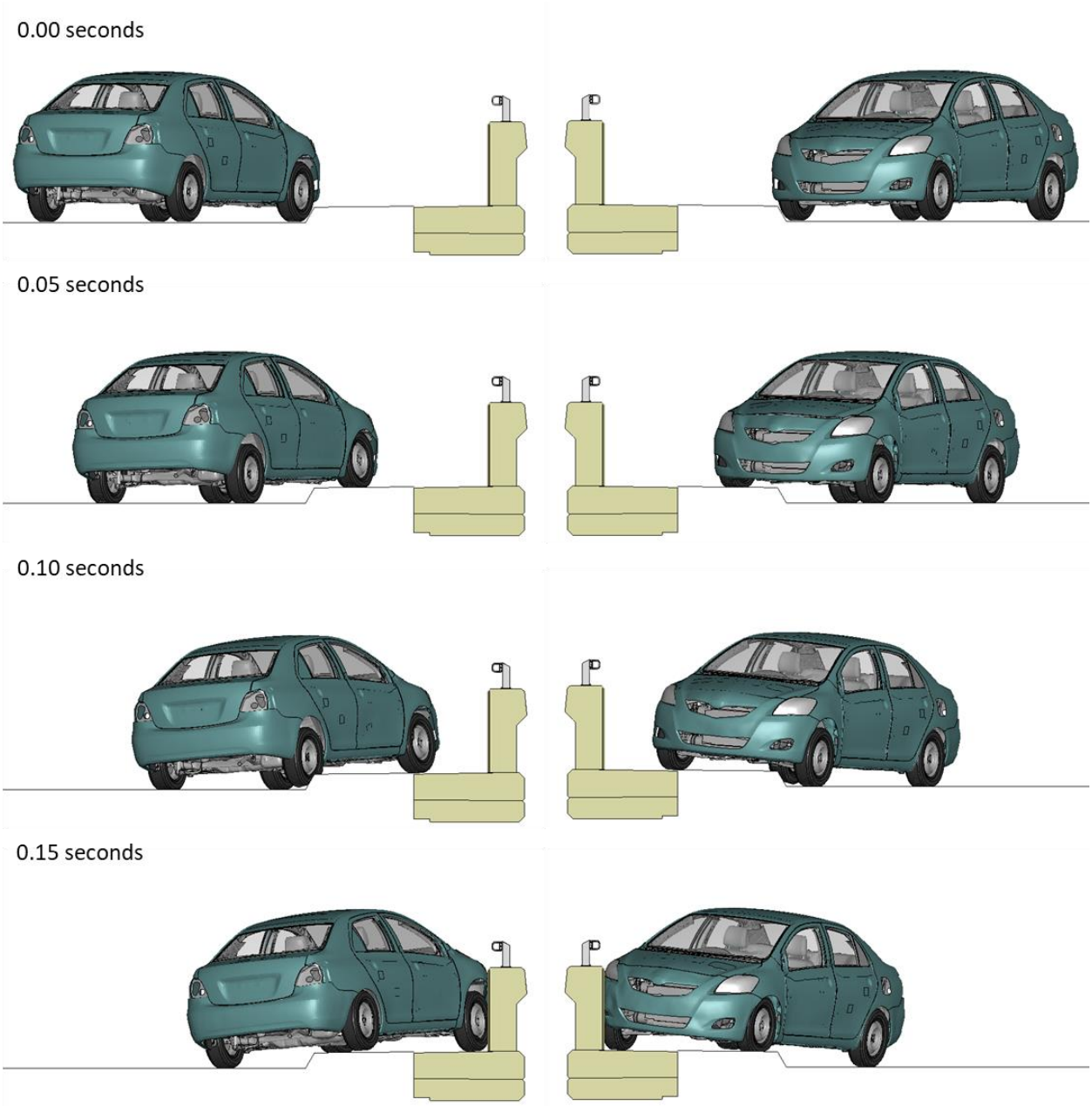

Figure 3. Sequential views from analysis of MASH Test 3-10 at 4.6 ft upstream of critical post from a front and back viewpoint (RHT Model).

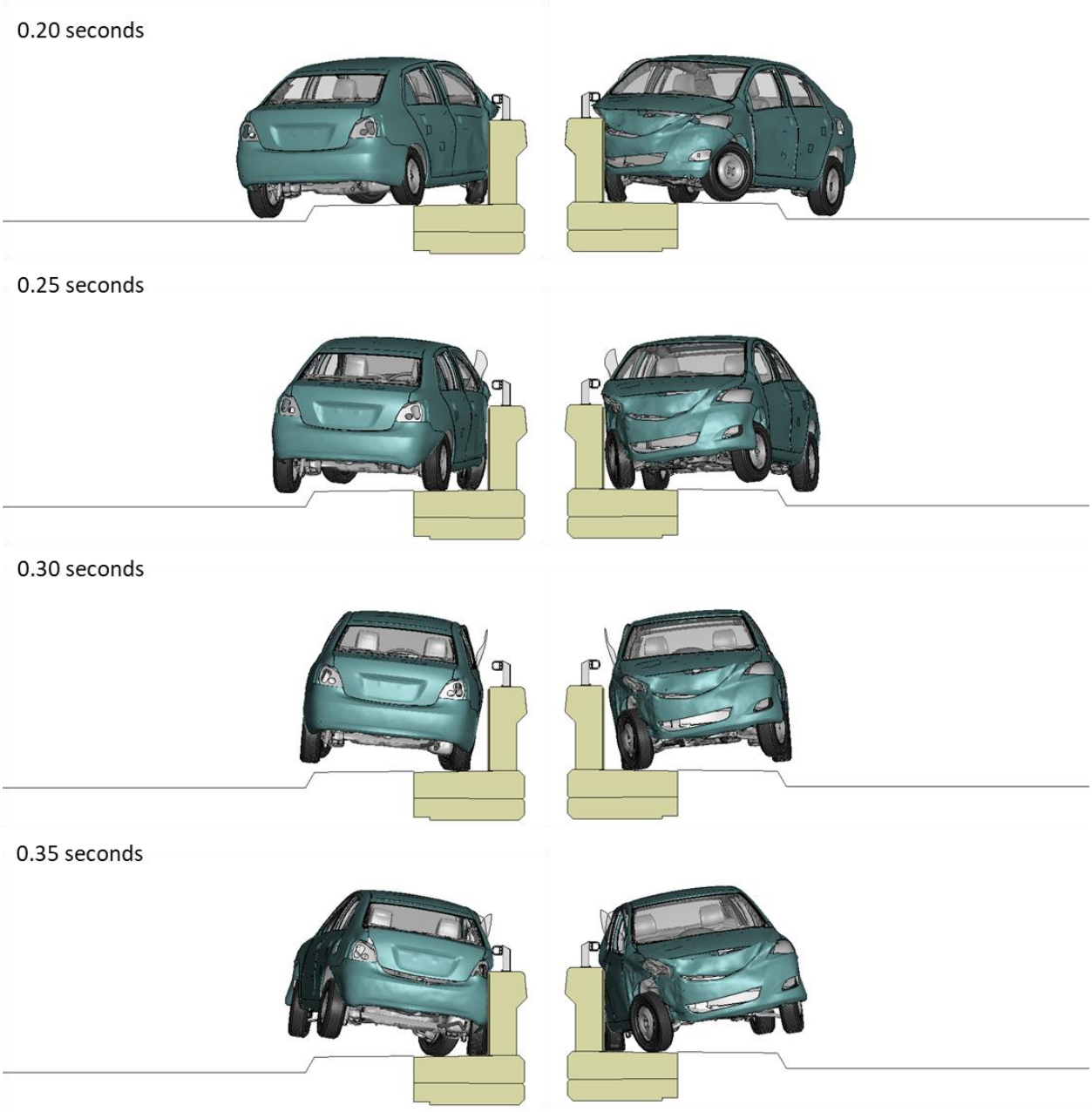

Figure 3 [CONTINUED] Sequential views from analysis of MASH Test 3-10 at 4.6 ft upstream of critical post from a front and back viewpoint (RHT Model).

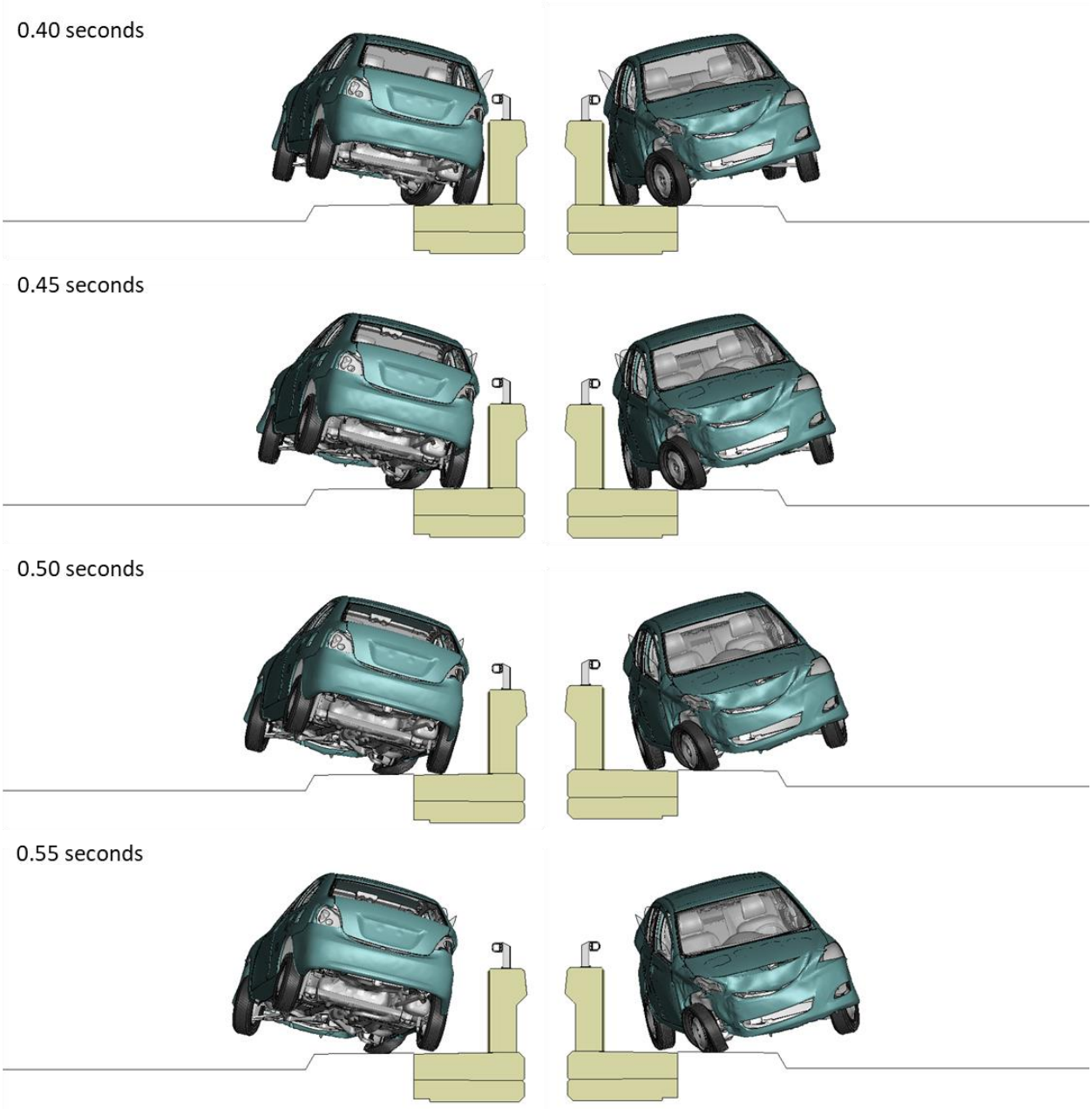

Figure 3 [CONTINUED] Sequential views from analysis of MASH Test 3-10 at 4.6 ft upstream of critical post from a front and back viewpoint (RHT Model).

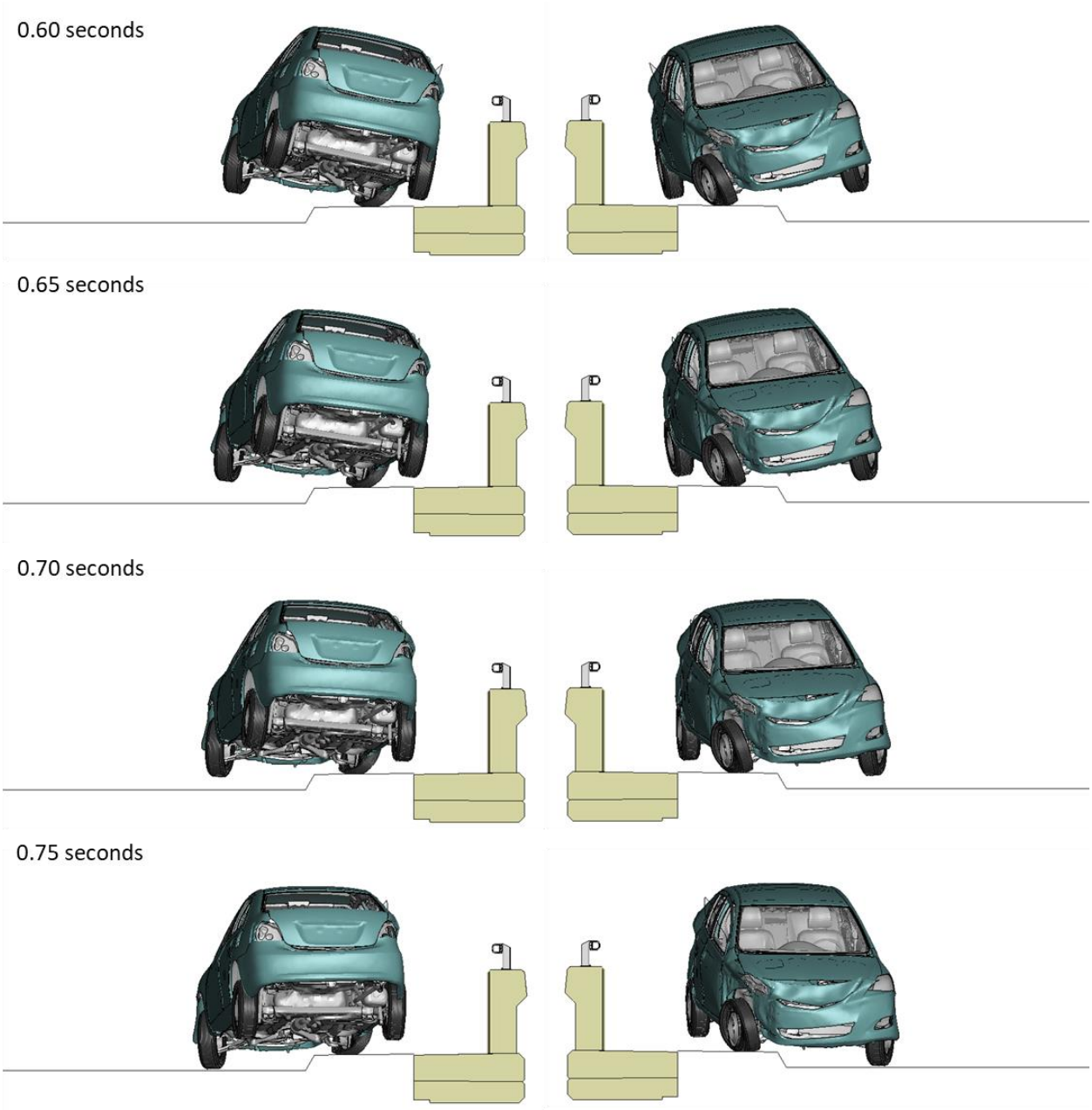

Figure 3 [CONTINUED] Sequential views from analysis of MASH Test 3-10 at 4.6 ft upstream of critical post from a front and back viewpoint (RHT Model).

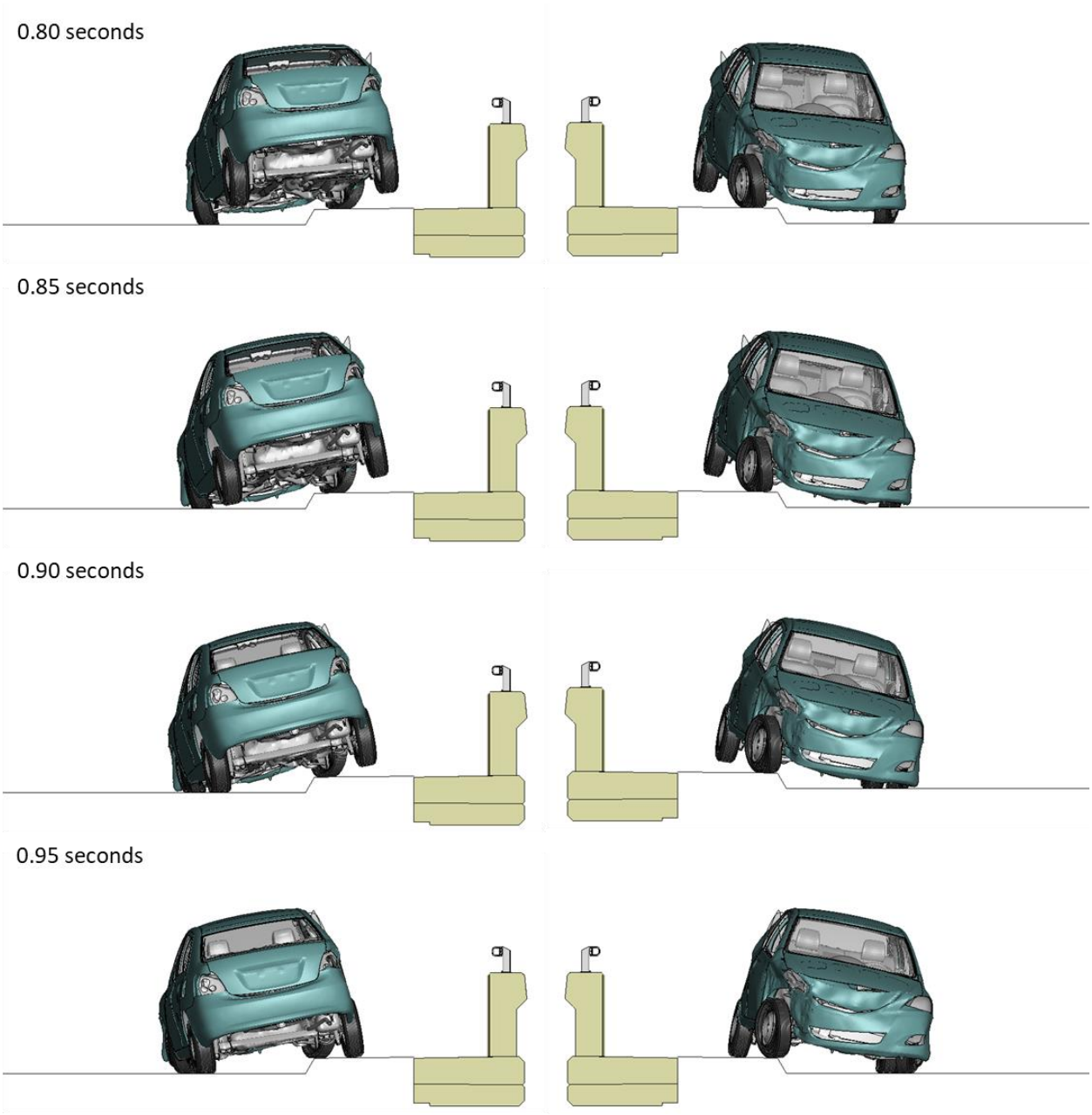

Figure 3 [CONTINUED] Sequential views from analysis of MASH Test 3-10 at 4.6 ft upstream of critical post from a front and back viewpoint (RHT Model).

Appendix F

Sequential Views for Test 3-11 at 4.3 ft Upstream of Critical Post (KC Model)

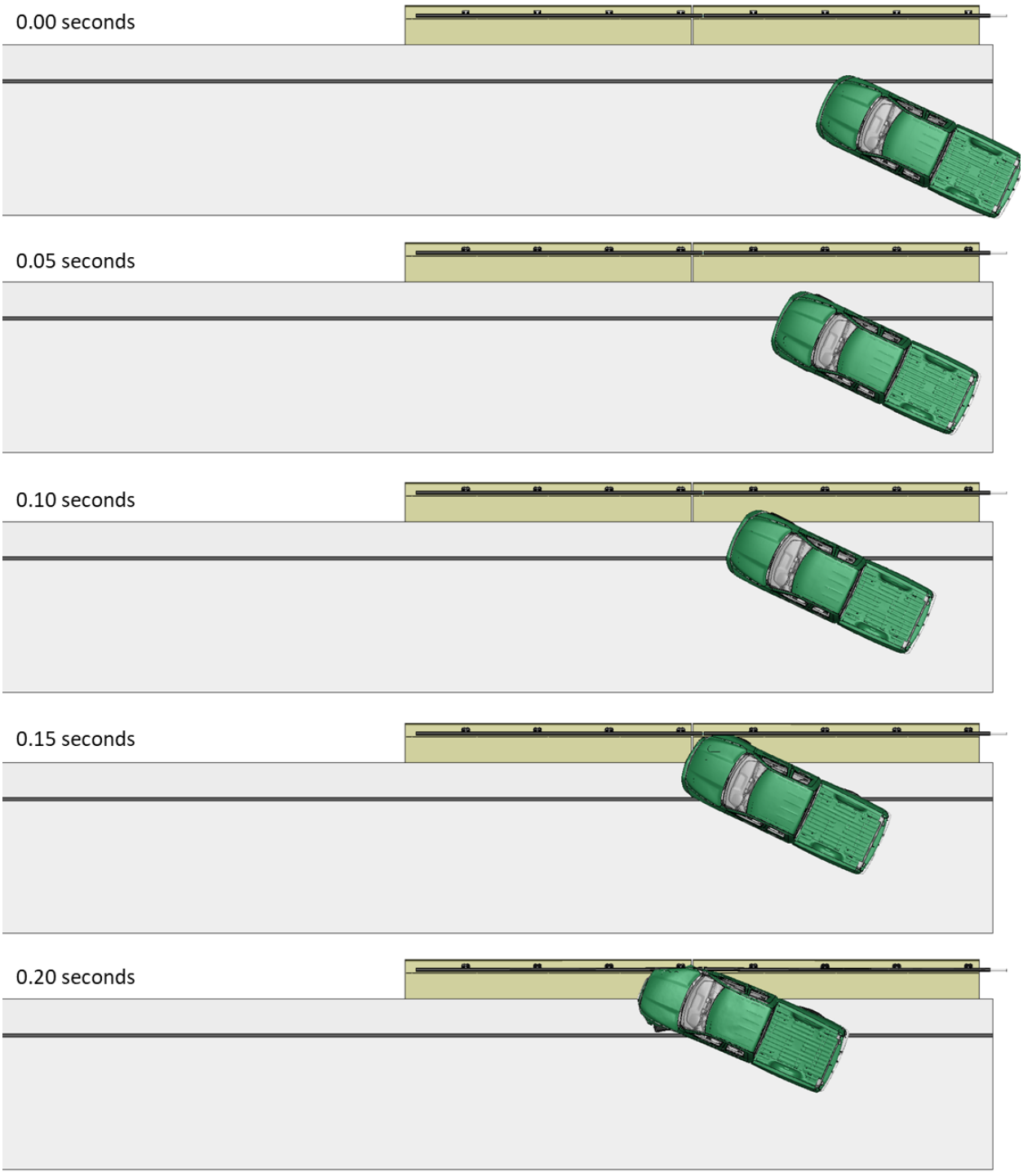

Figure 1. Sequential views from analysis of MASH Test 3-11 at 4.3 ft upstream of critical post from an overhead viewpoint (KC Model).

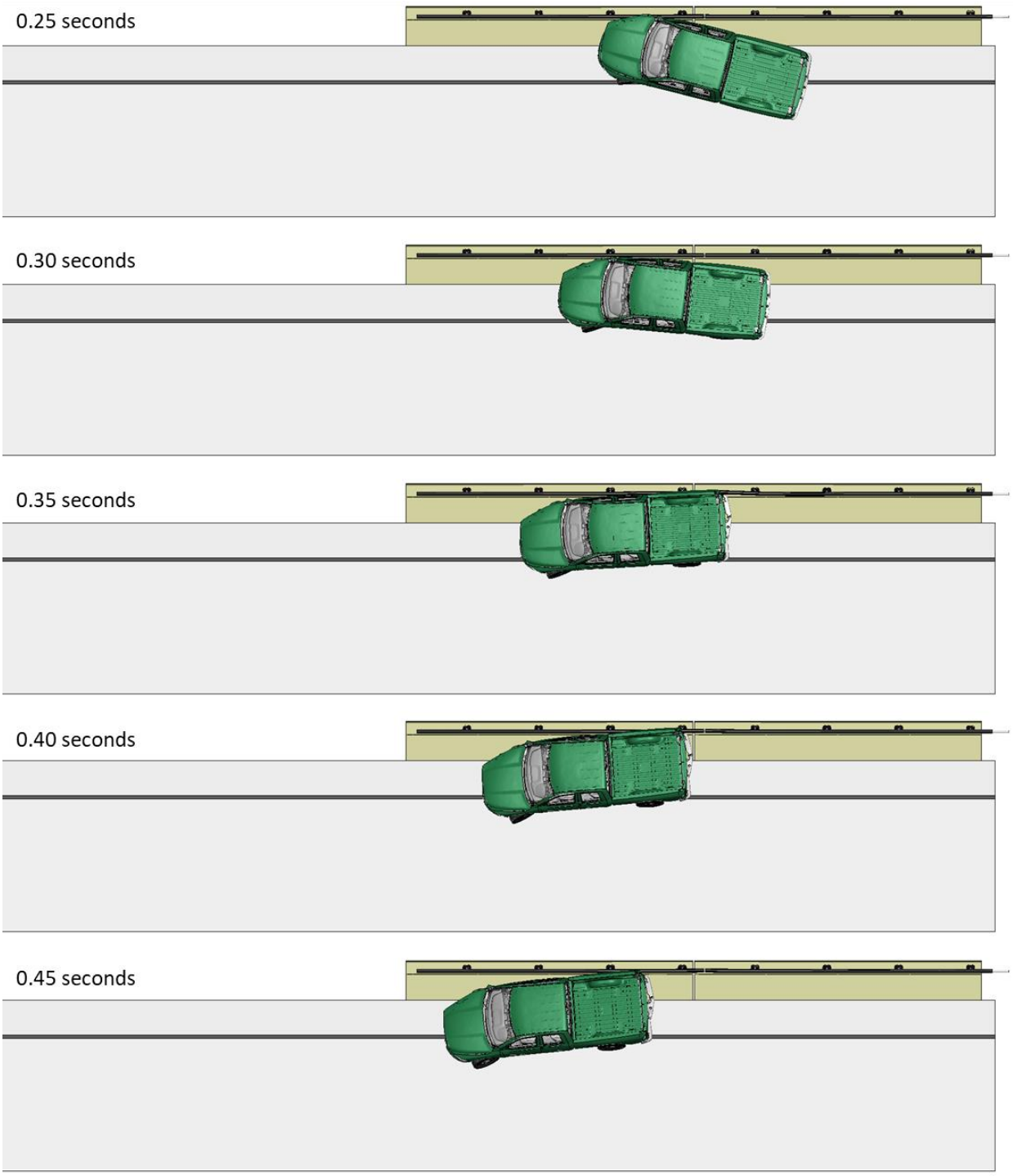

Figure 1 [CONTINUED] Sequential views from analysis of MASH Test 3-11 at 4.3 ft upstream of critical post from an overhead viewpoint (KC Model).

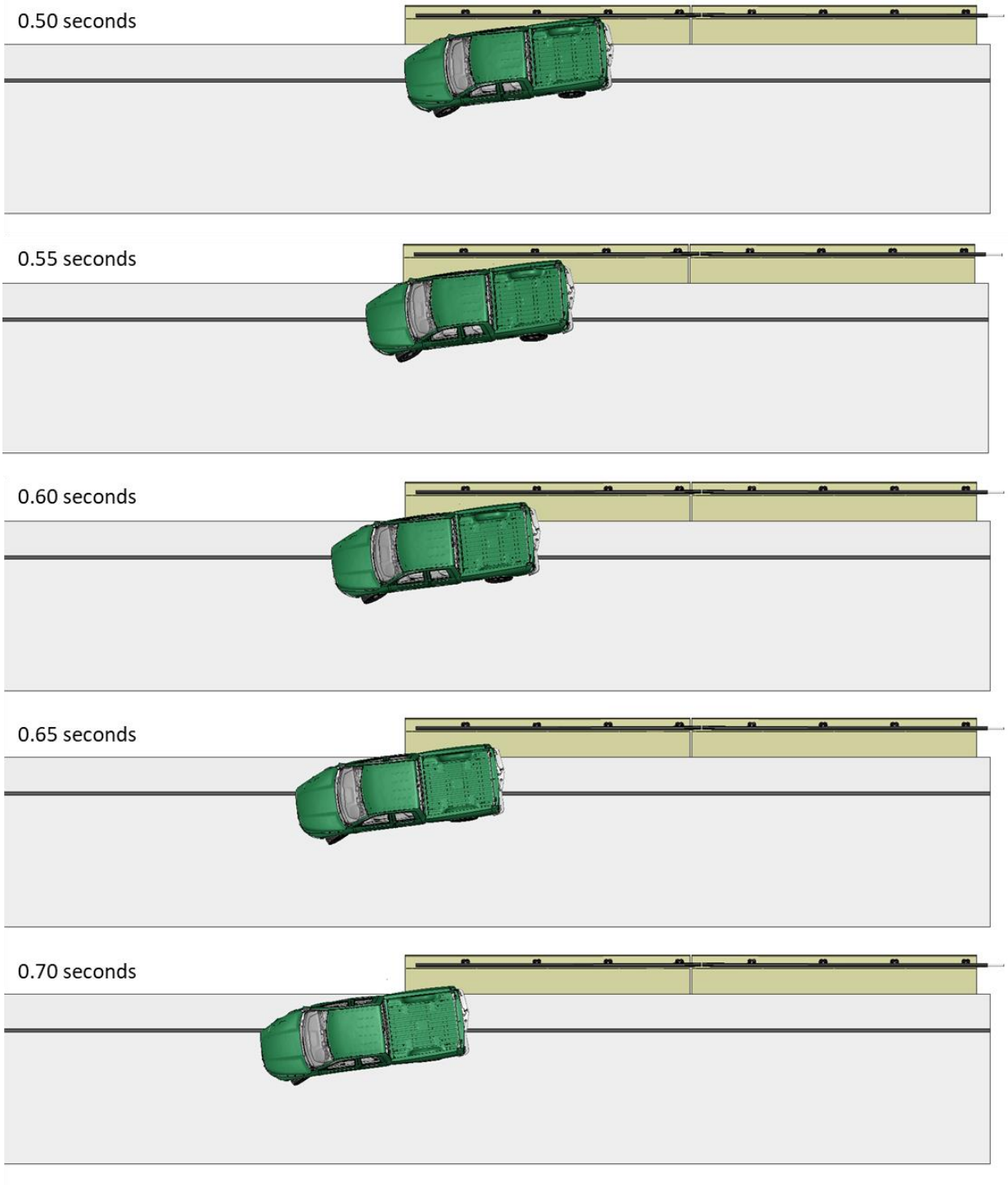

Figure 1 [CONTINUED] Sequential views from analysis of MASH Test 3-11 at 4.3 ft upstream of critical post from an overhead viewpoint (KC Model).

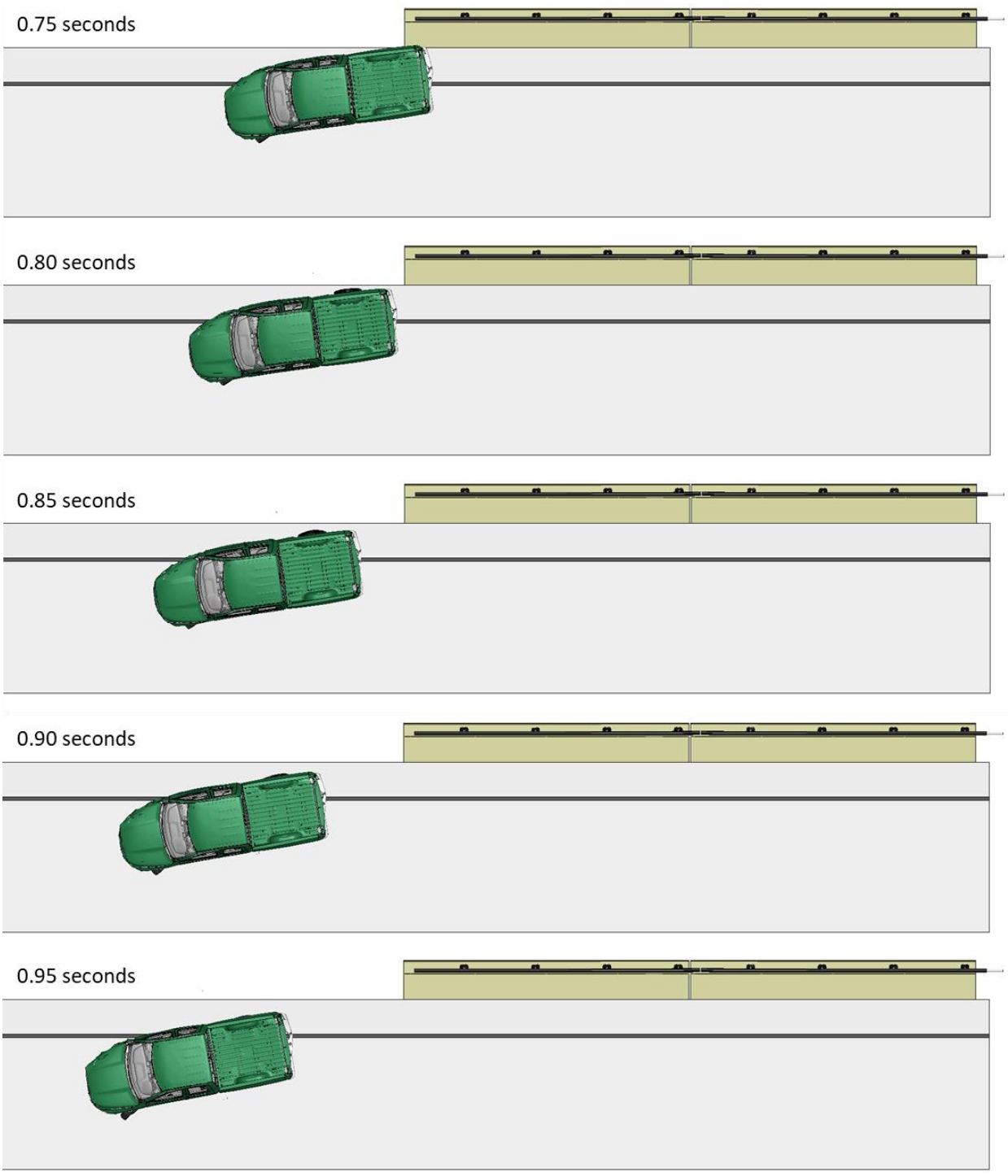

Figure 1 [CONTINUED] Sequential views from analysis of MASH Test 3-11 at 4.3 ft upstream of critical post from an overhead viewpoint (KC Model).

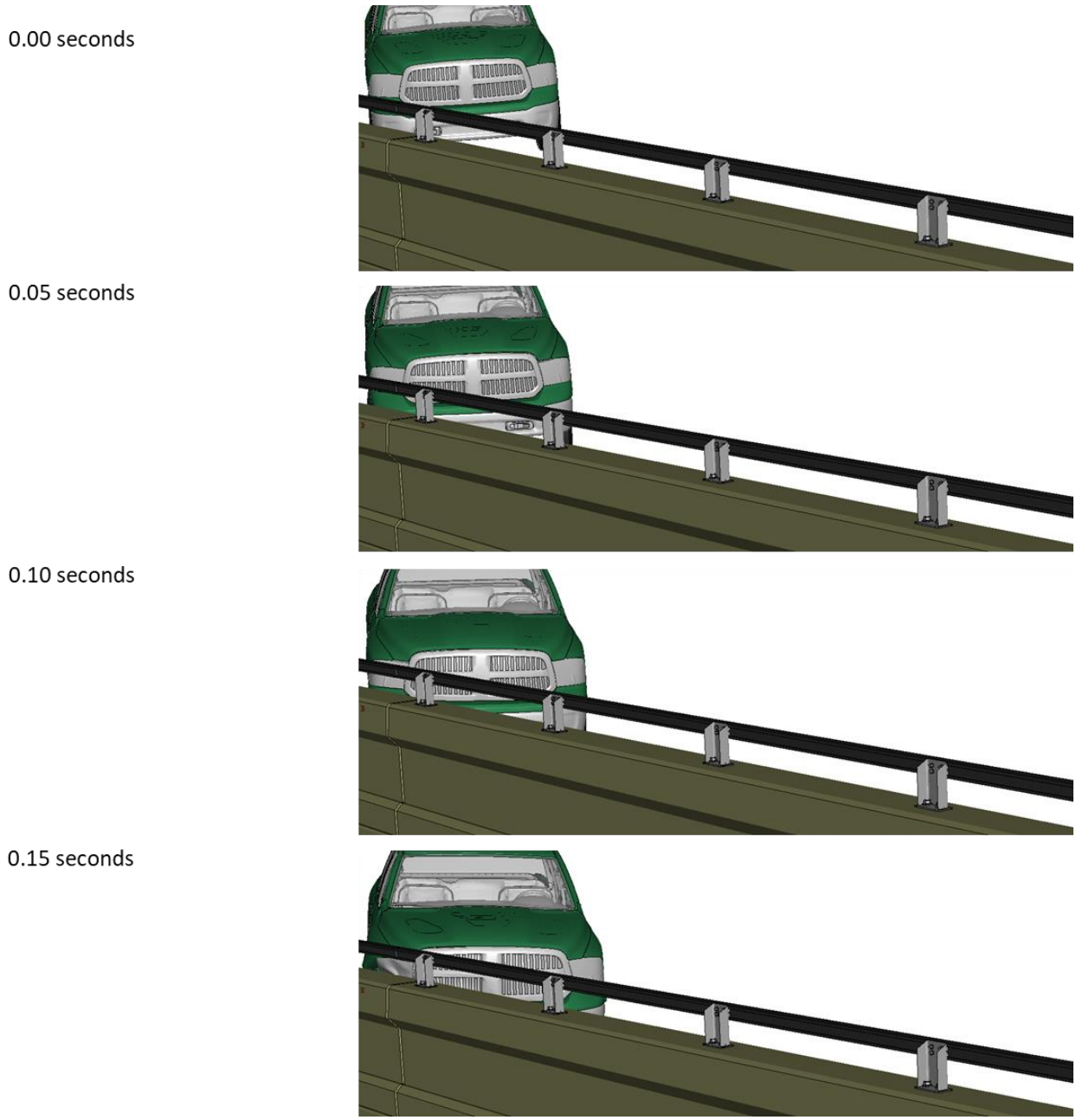

Figure 2. Sequential views from analysis of MASH Test 3-11 at 4.3 ft upstream of critical post from an isometric viewpoint (KC Model).

0.20 seconds

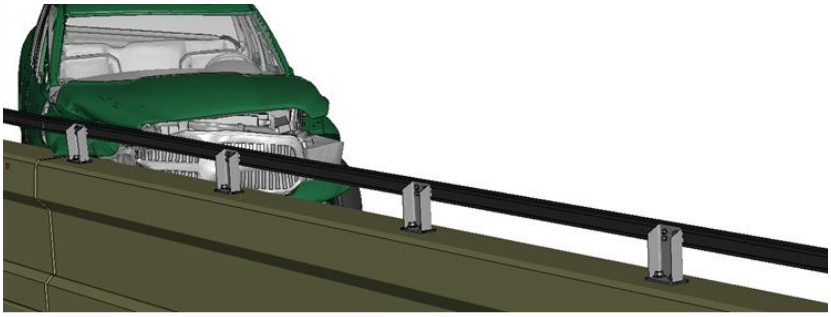

0.25 seconds

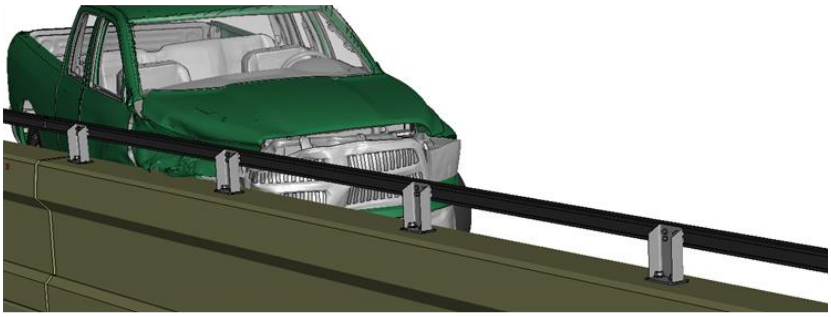

0.30 seconds

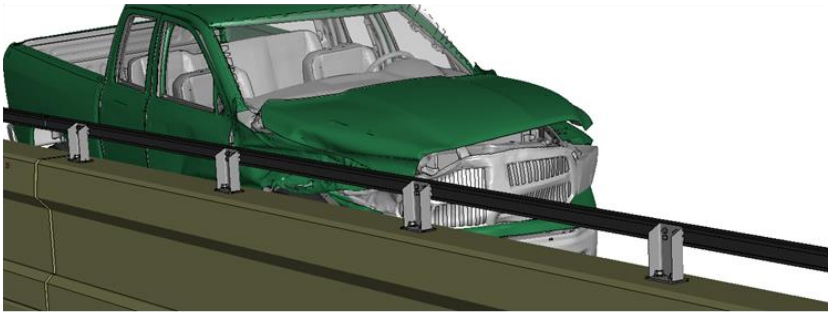

0.35 seconds

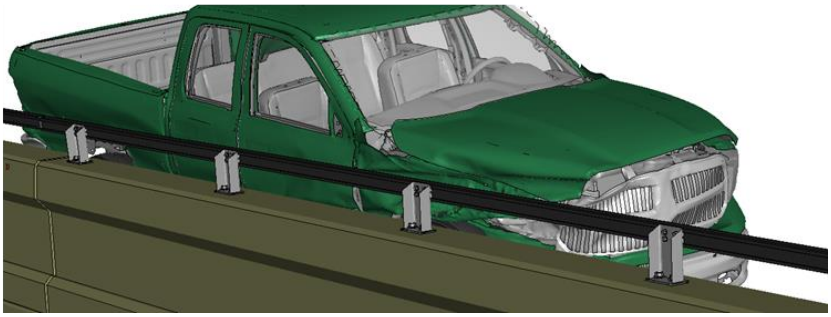

Figure 2 [CONTINUED] Sequential views from analysis of MASH Test 3-11 at 4.3 ft upstream of critical post from an isometric viewpoint (KC Model).

0.40 seconds

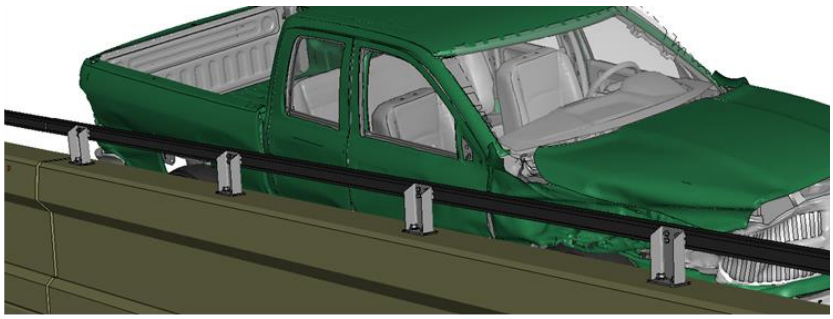

0.45 seconds

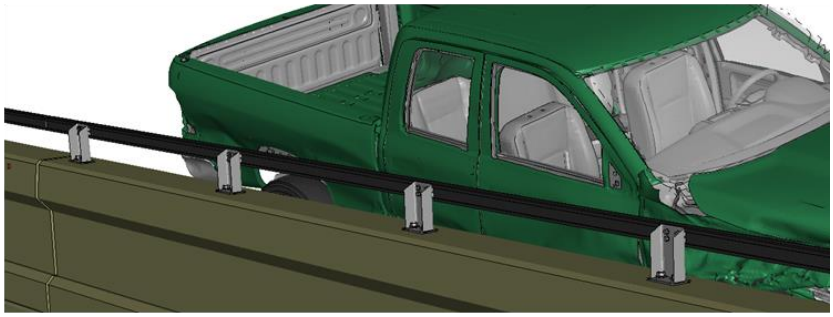

0.50 seconds

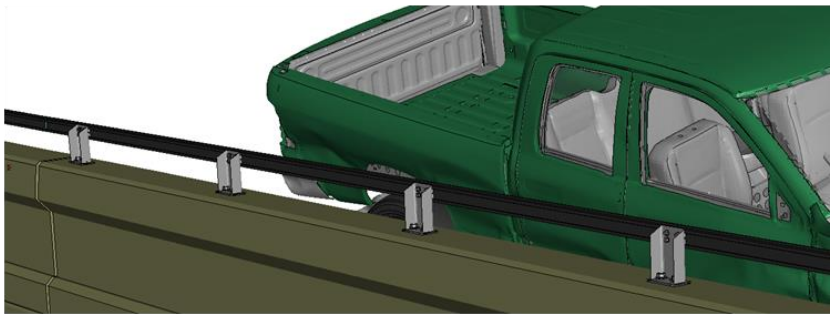

0.55 seconds

Figure 2 [CONTINUED] Sequential views from analysis of MASH Test 3-11 at 4.3 ft upstream of critical post from an isometric viewpoint (KC Model).

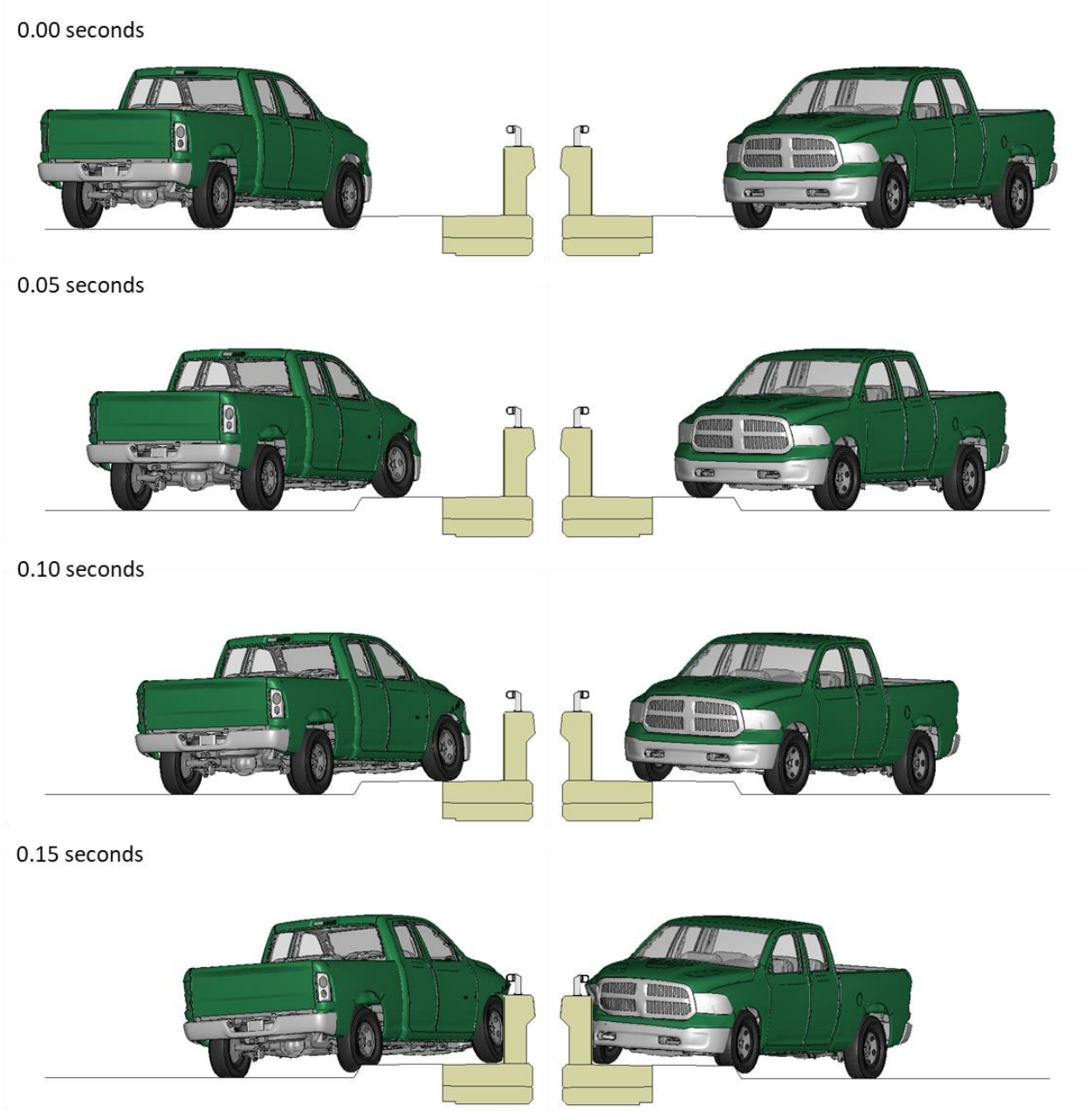

Figure 3. Sequential views from analysis of MASH Test 3-11 at 4.3 ft upstream of critical post from a front and back (KC Model).

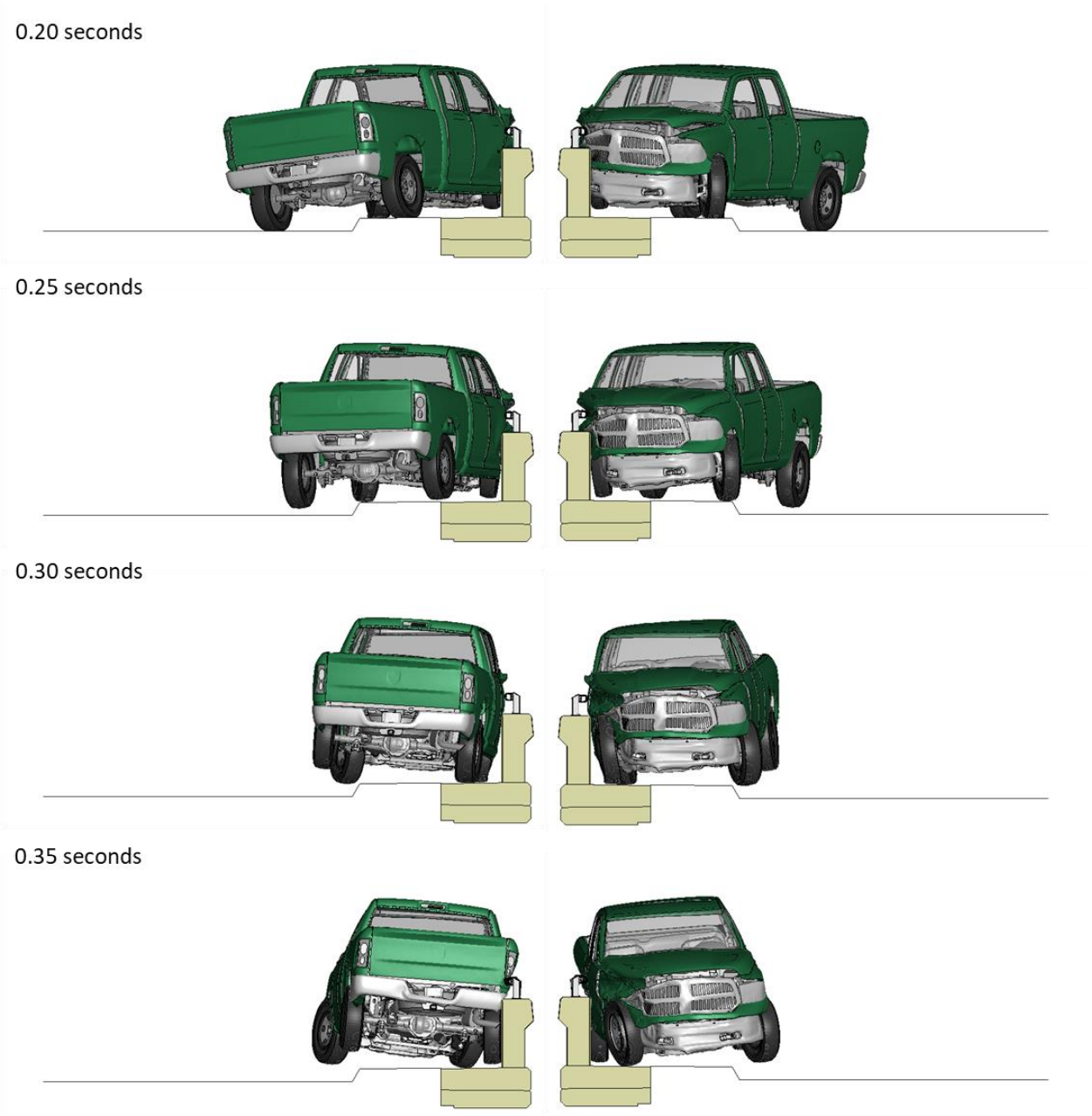

Figure 3 [CONTINUED] Sequential views from analysis of MASH Test 3-11 at 4.3 ft upstream of critical post from a front and back (KC Model).

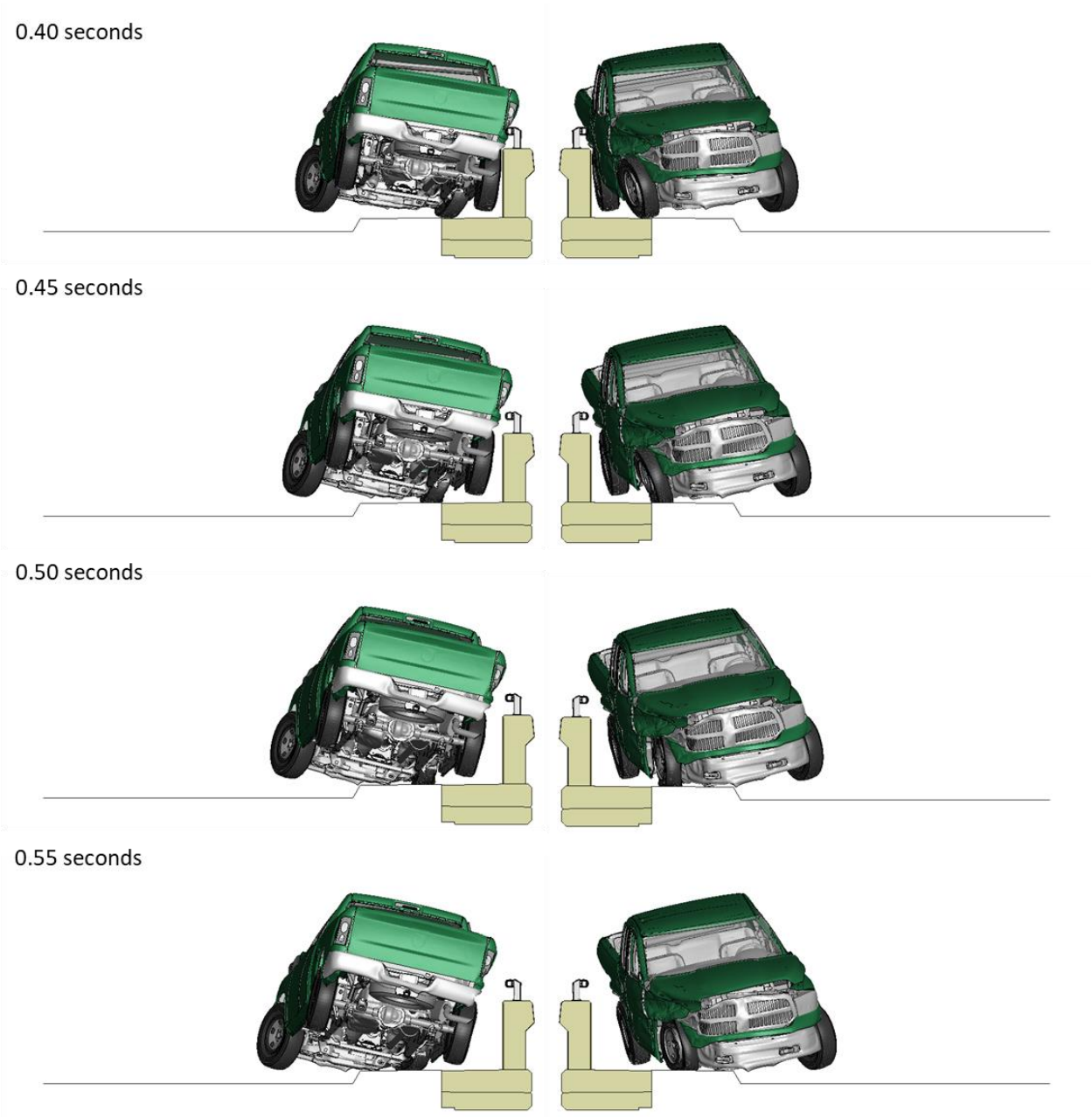

Figure 3 [CONTINUED] Sequential views from analysis of MASH Test 3-11 at 4.3 ft upstream of critical post from a front and back (KC Model).

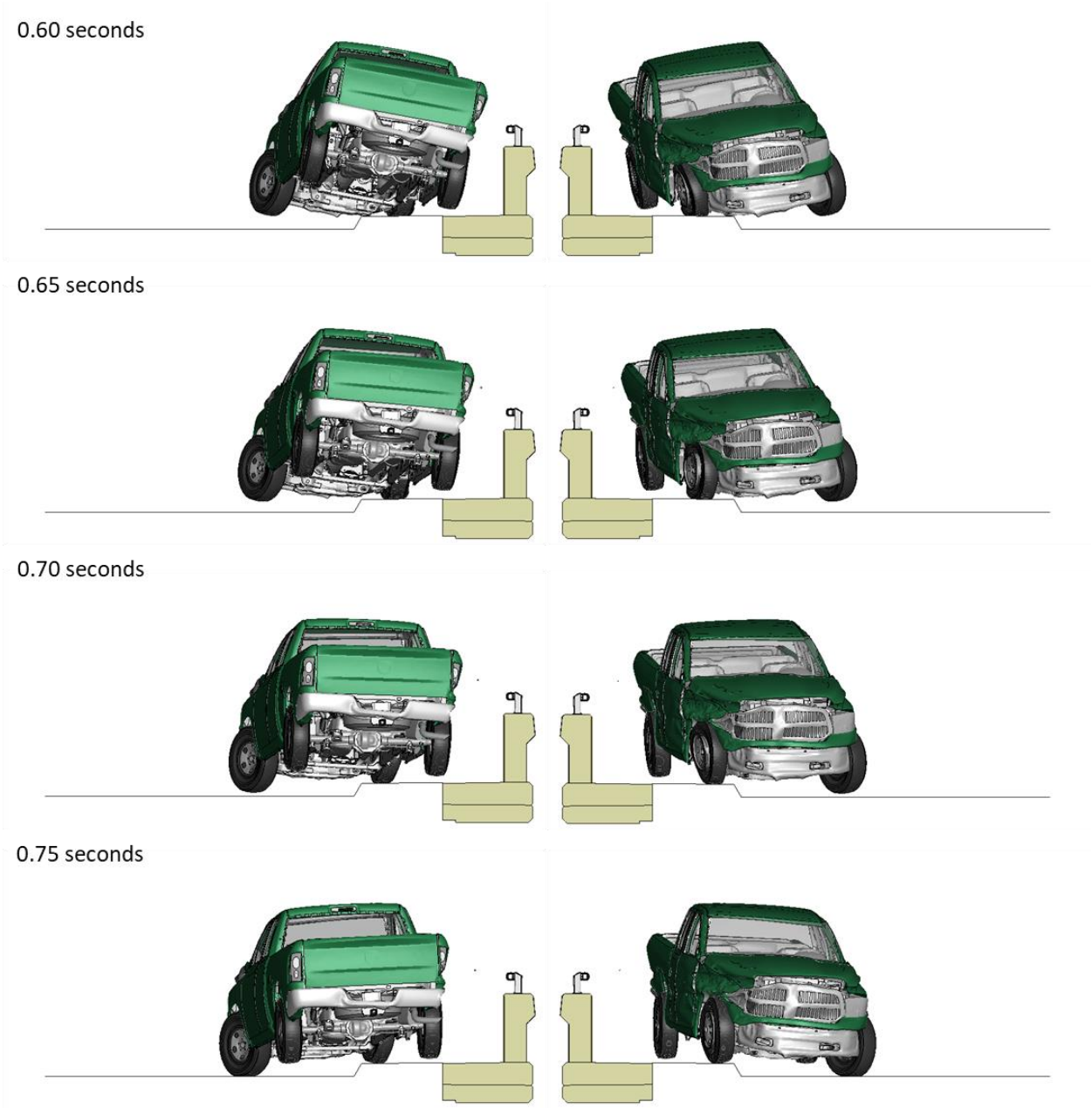

Figure 3 [CONTINUED] Sequential views from analysis of MASH Test 3-11 at 4.3 ft upstream of critical post from a front and back (KC Model).

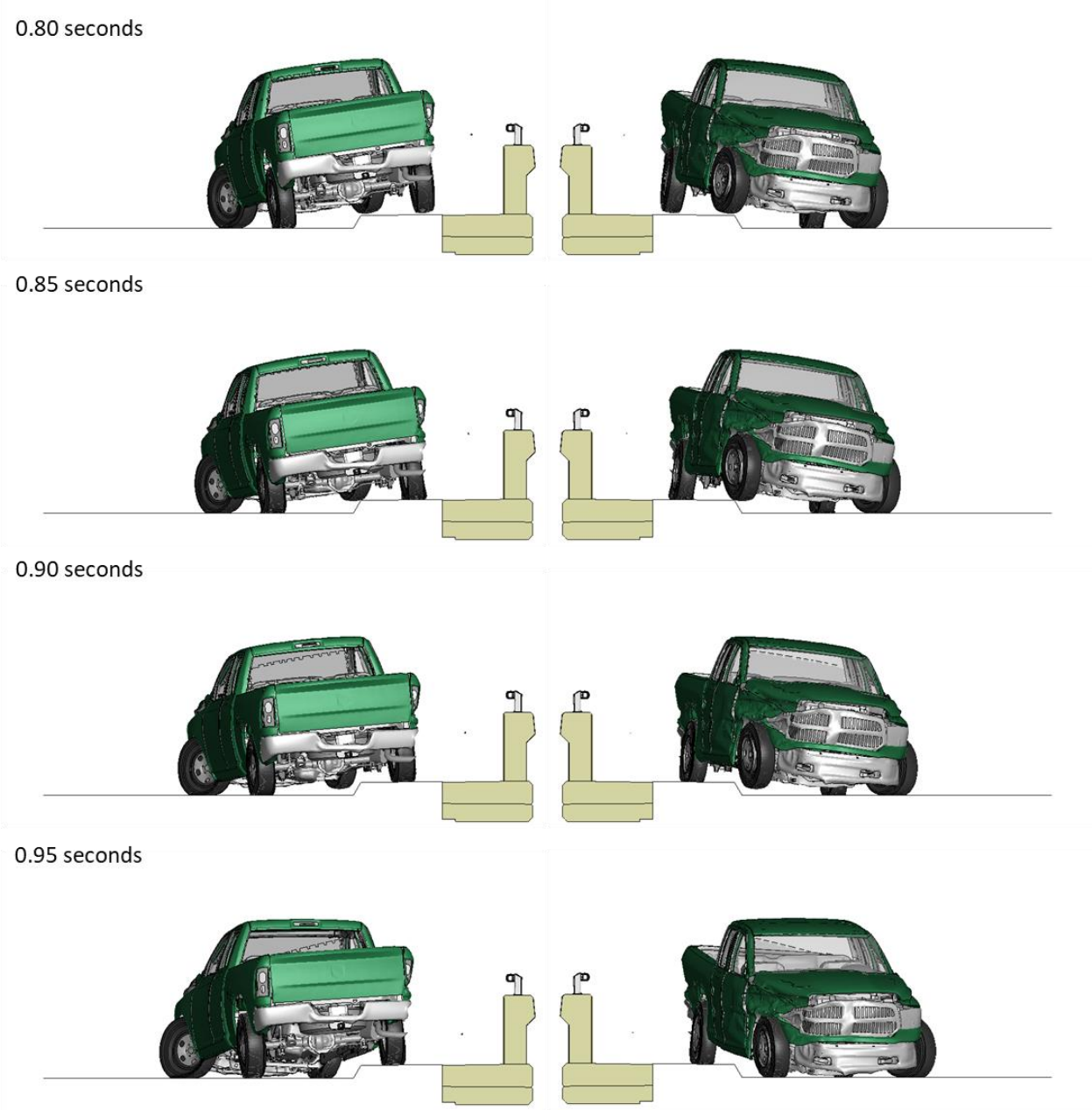

Figure 3 [CONTINUED] Sequential views from analysis of MASH Test 3-11 at 4.3 ft upstream of critical post from a front and back (KC Model).

Appendix G

Sequential Views for Test 3-11 at 4.3 ft Upstream of Critical Post (RHT Model)

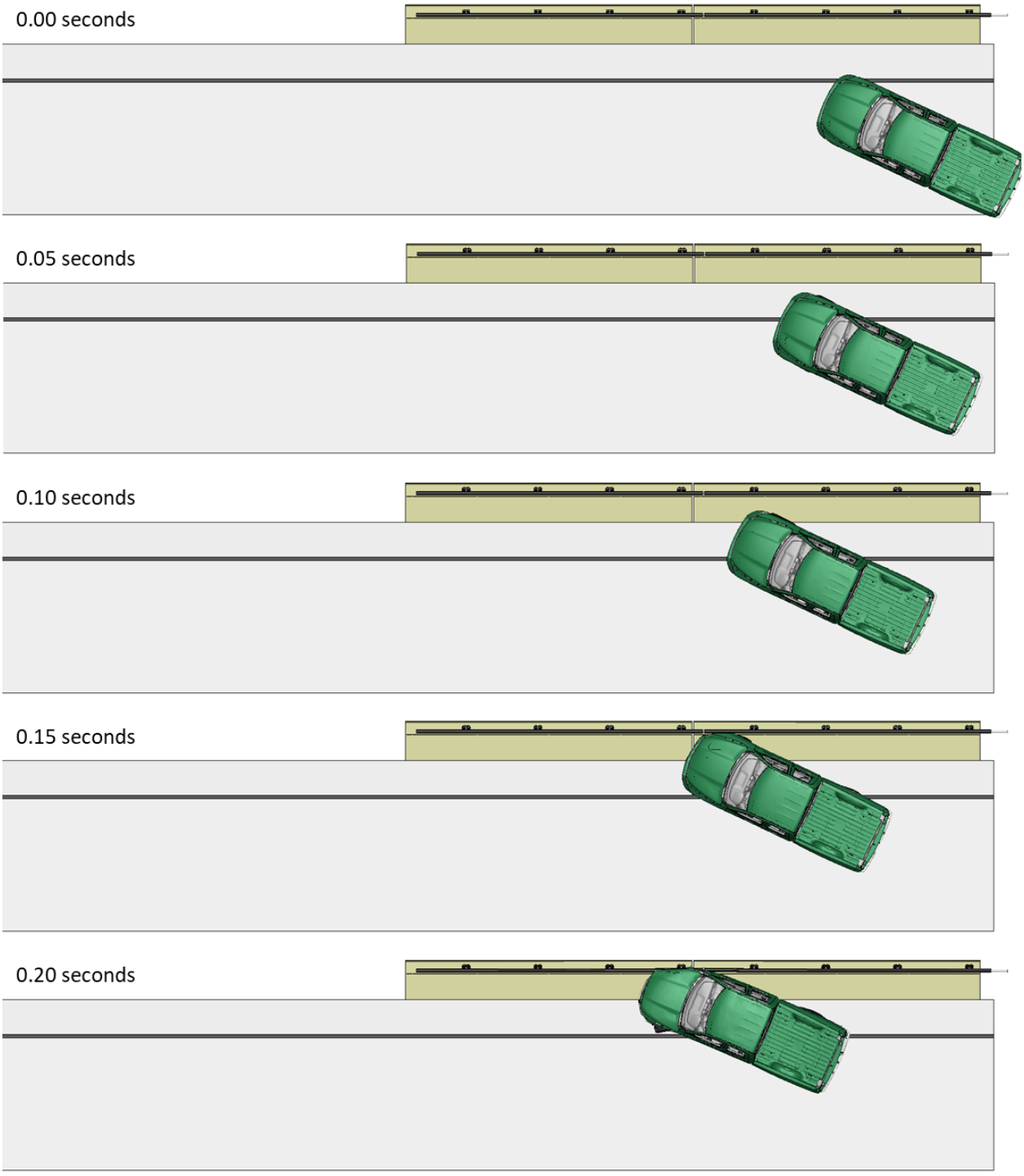

Figure 1. Sequential views from analysis of MASH Test 3-11 at 4.3 ft upstream of critical post from an overhead viewpoint (RHT Model).

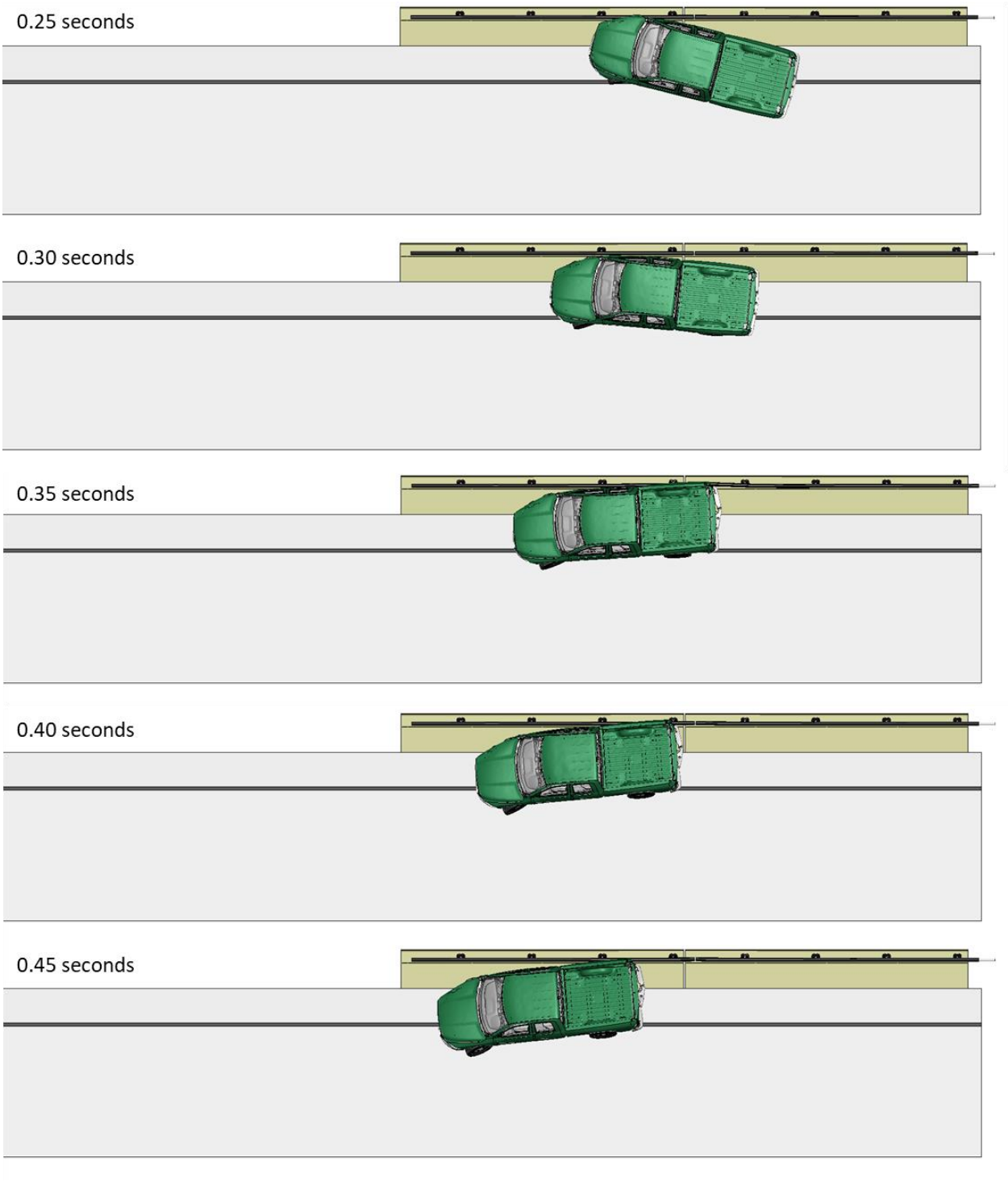

Figure 1 [CONTINUED] Sequential views from analysis of MASH Test 3-11 at 4.3 ft upstream of critical post from an overhead viewpoint (RHT Model).

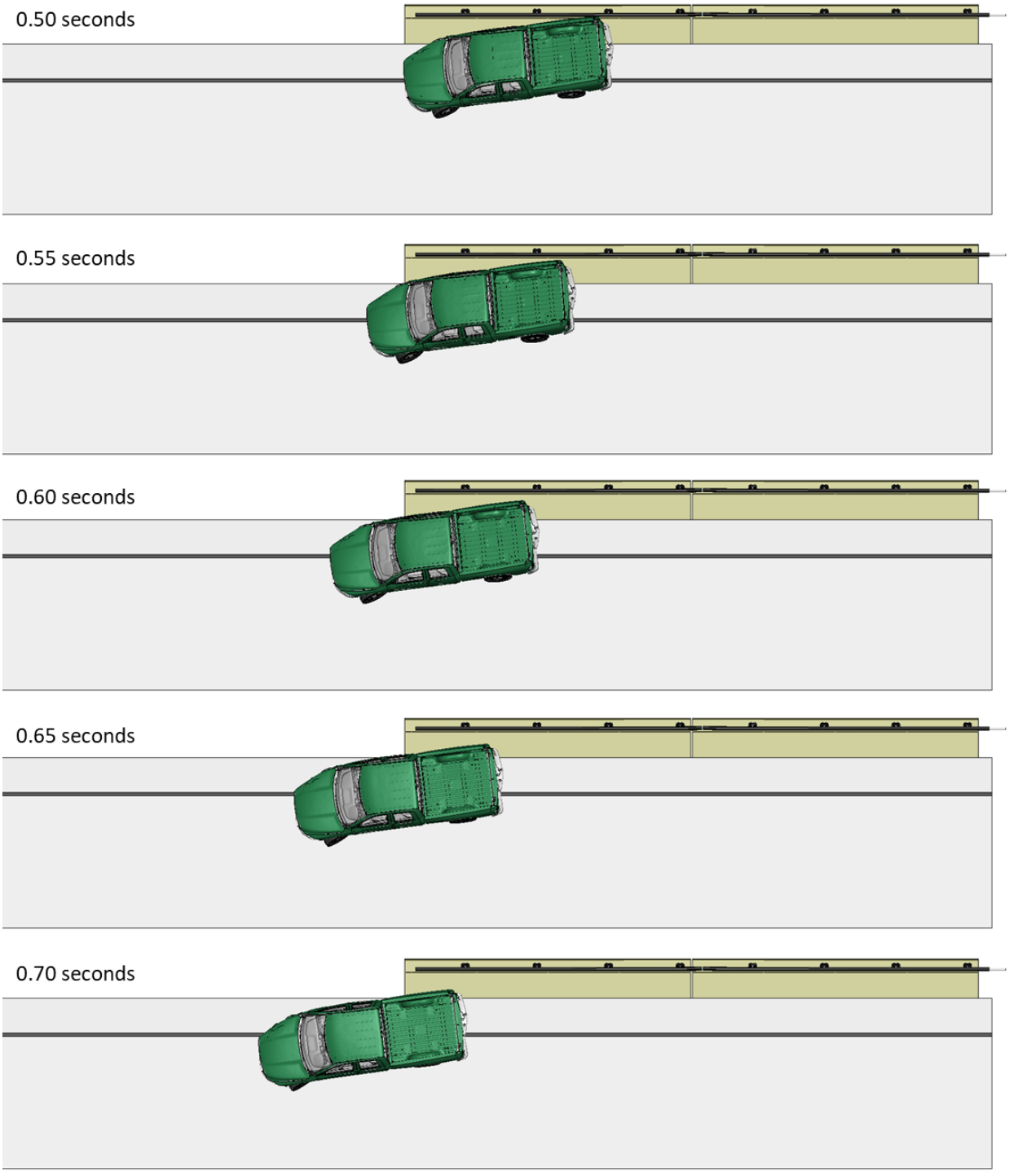

Figure 1 [CONTINUED] Sequential views from analysis of MASH Test 3-11 at 4.3 ft upstream of critical post from an overhead viewpoint (RHT Model).

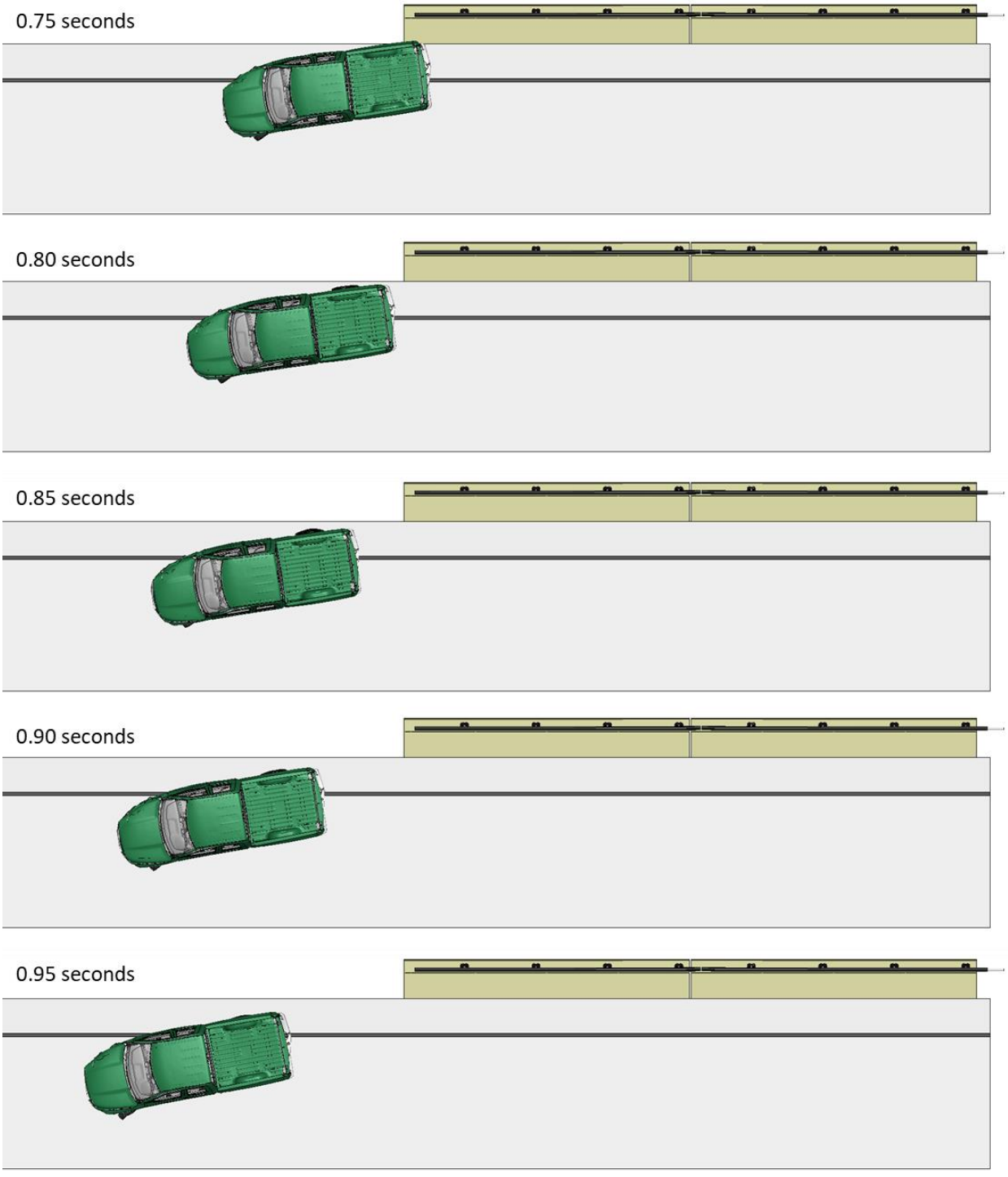

Figure 1 [CONTINUED] Sequential views from analysis of MASH Test 3-11 at 4.3 ft upstream of critical post from an overhead viewpoint (RHT Model).

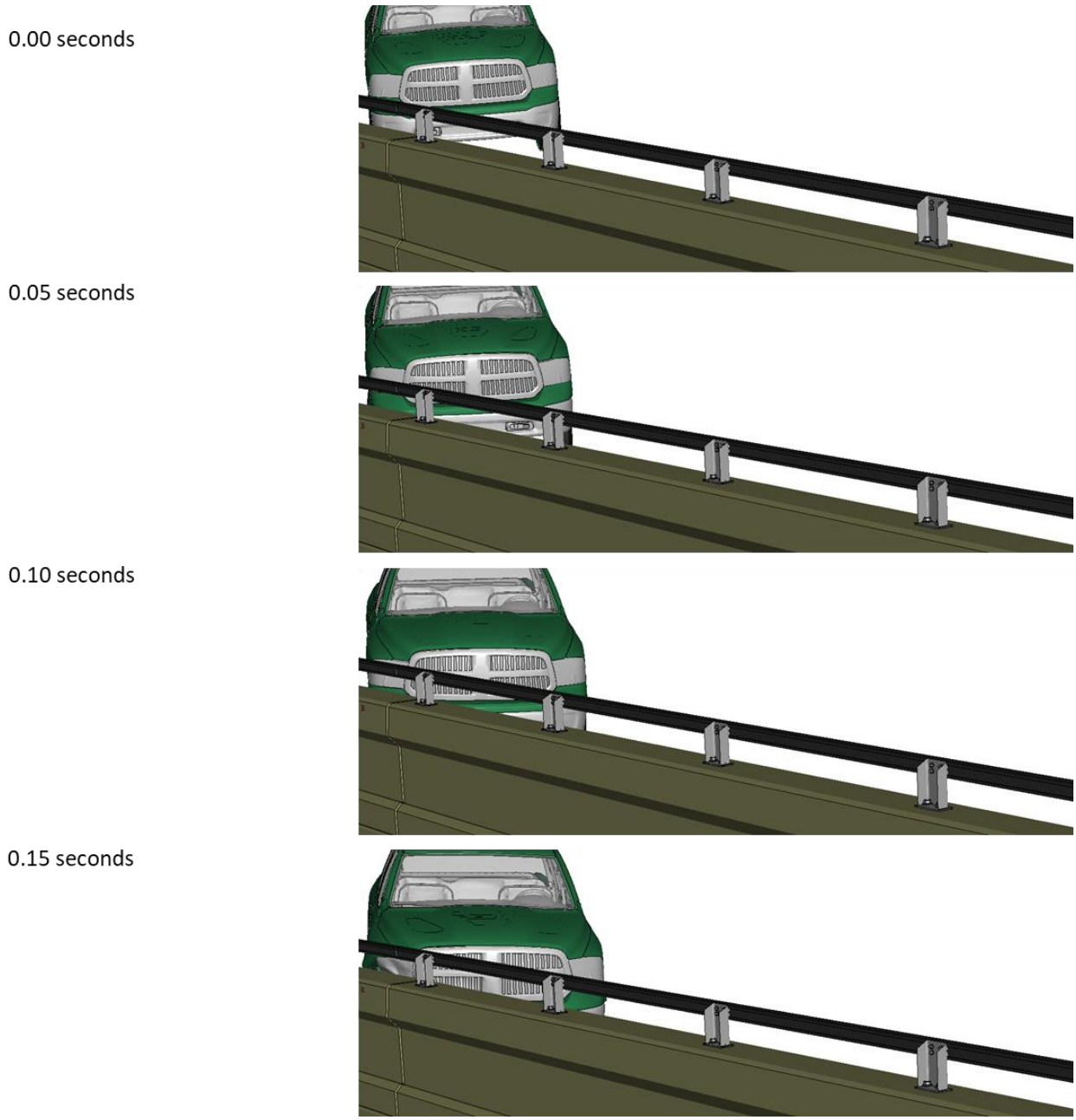

Figure 2. Sequential views from analysis of MASH Test 3-11 at 4.3 ft upstream of critical post from an isometric viewpoint (RHT Model).

0.20 seconds

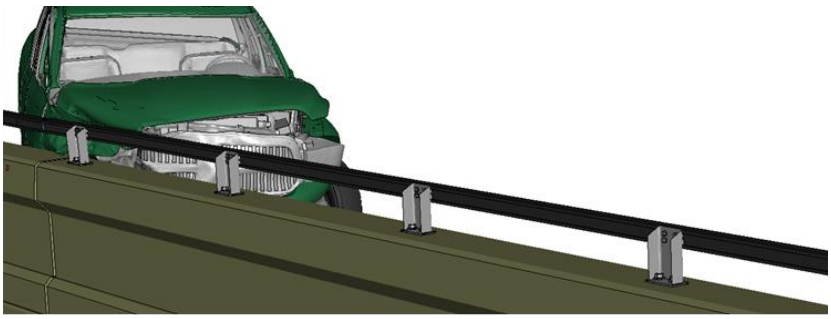

0.25 seconds

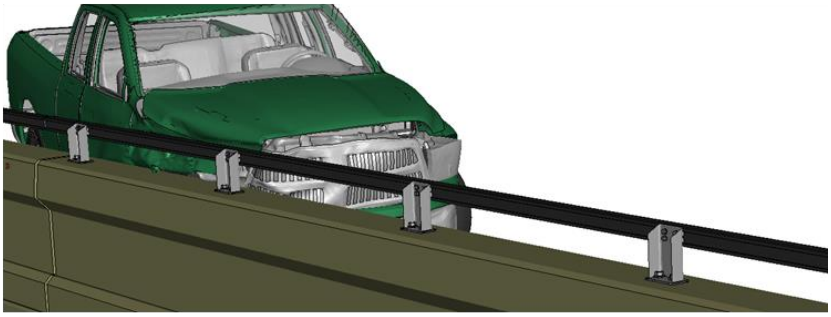

0.30 seconds

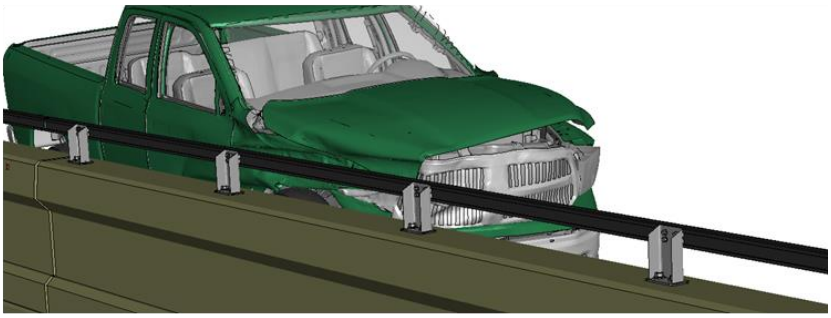

0.35 seconds

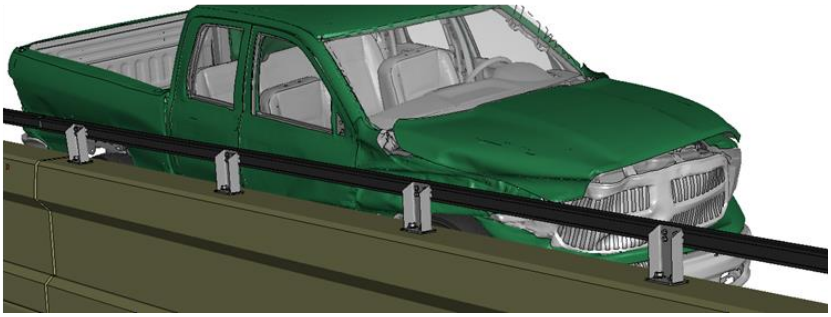

Figure 2 [CONTINUED] Sequential views from analysis of MASH Test 3-11 at 4.3 ft upstream of critical post from an isometric viewpoint (RHT Model).

0.40 seconds

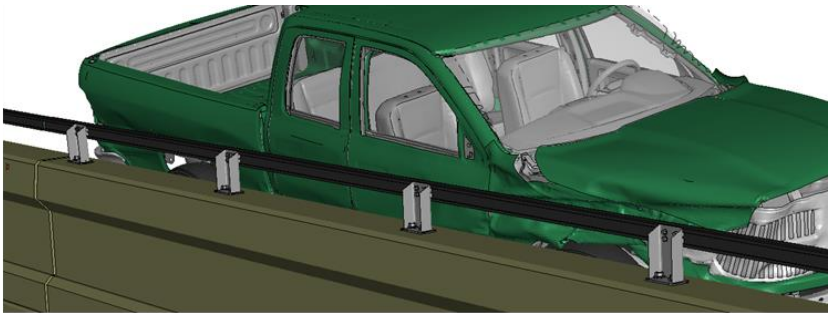

0.45 seconds

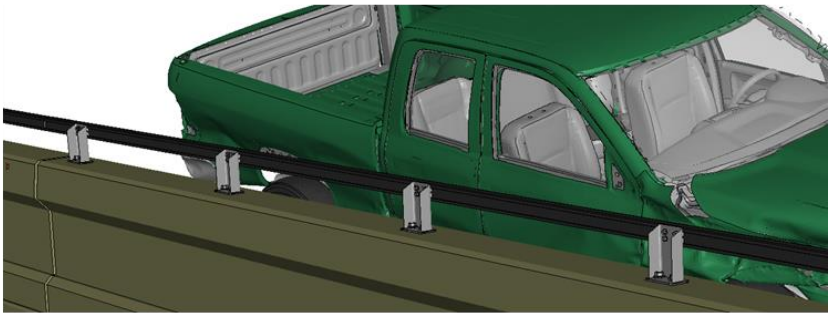

0.50 seconds

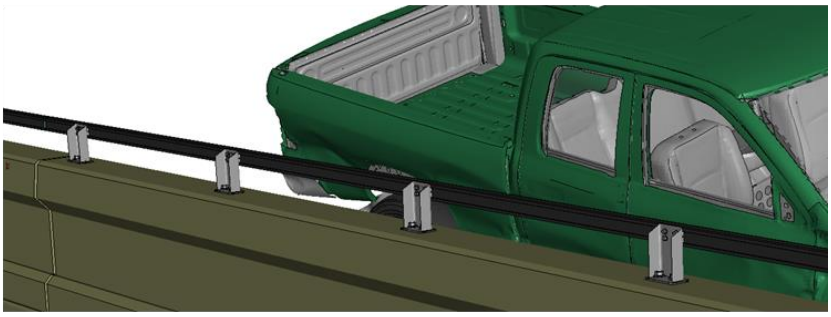

0.55 seconds

Figure 2 [CONTINUED] Sequential views from analysis of MASH Test 3-11 at 4.3 ft upstream of critical post from an isometric viewpoint (RHT Model).

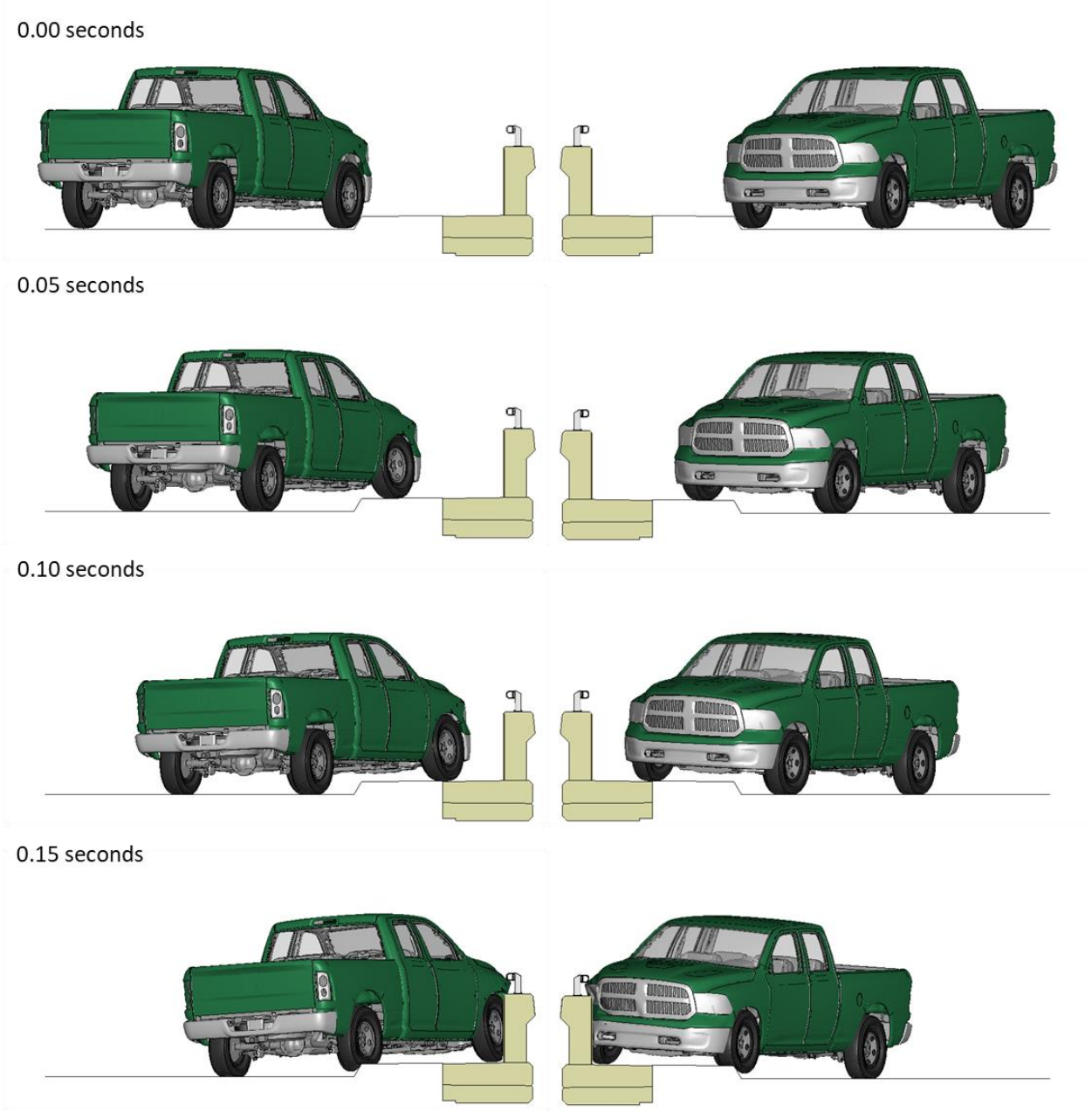

Figure 3. Sequential views from analysis of MASH Test 3-11 at 4.3 ft upstream of critical post from a front and back viewpoint (RHT Model).

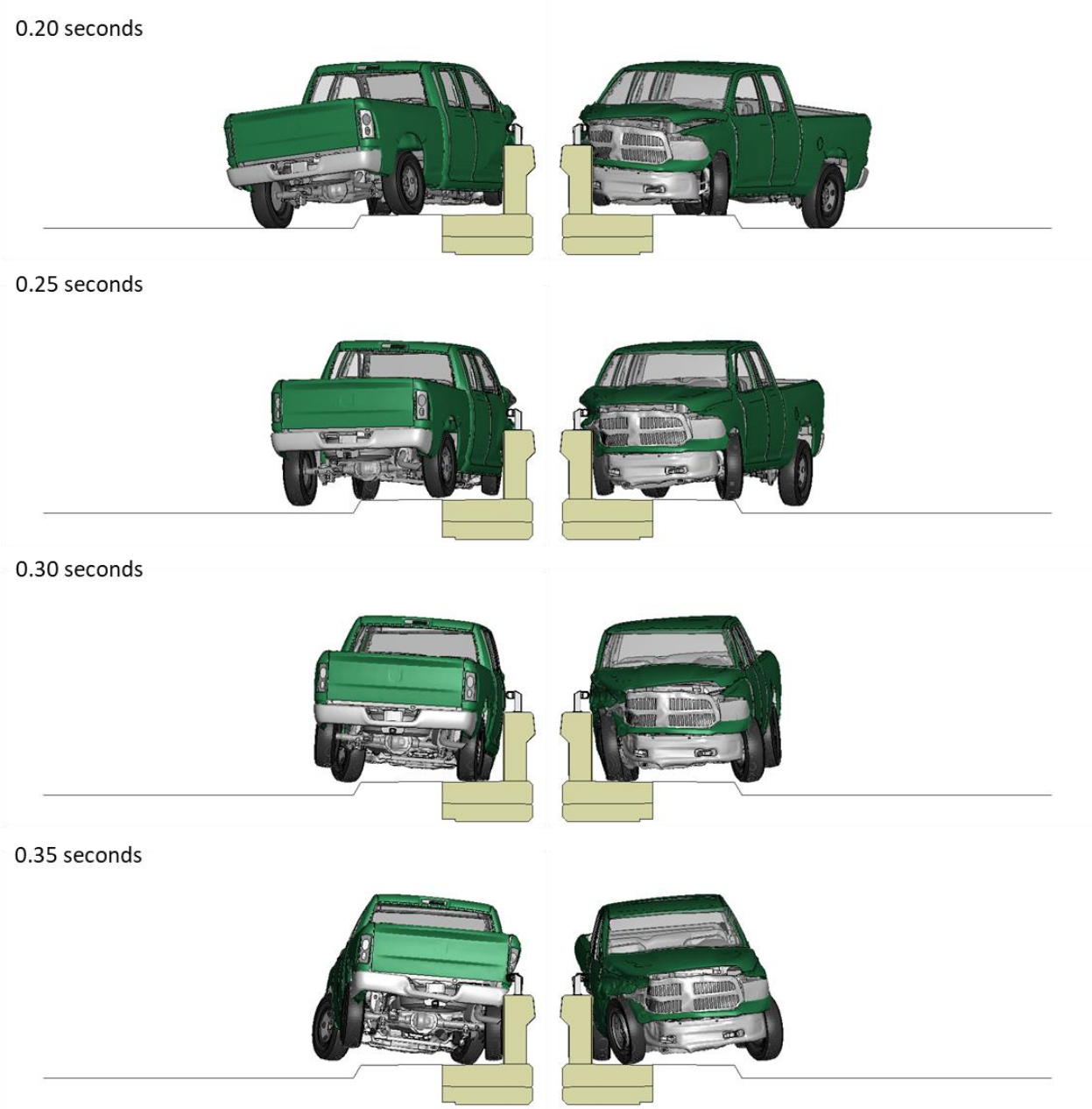

Figure 3 [CONTINUED] Sequential views from analysis of MASH Test 3-11 at 4.3 ft upstream of critical post from a front and back viewpoint (RHT Model).

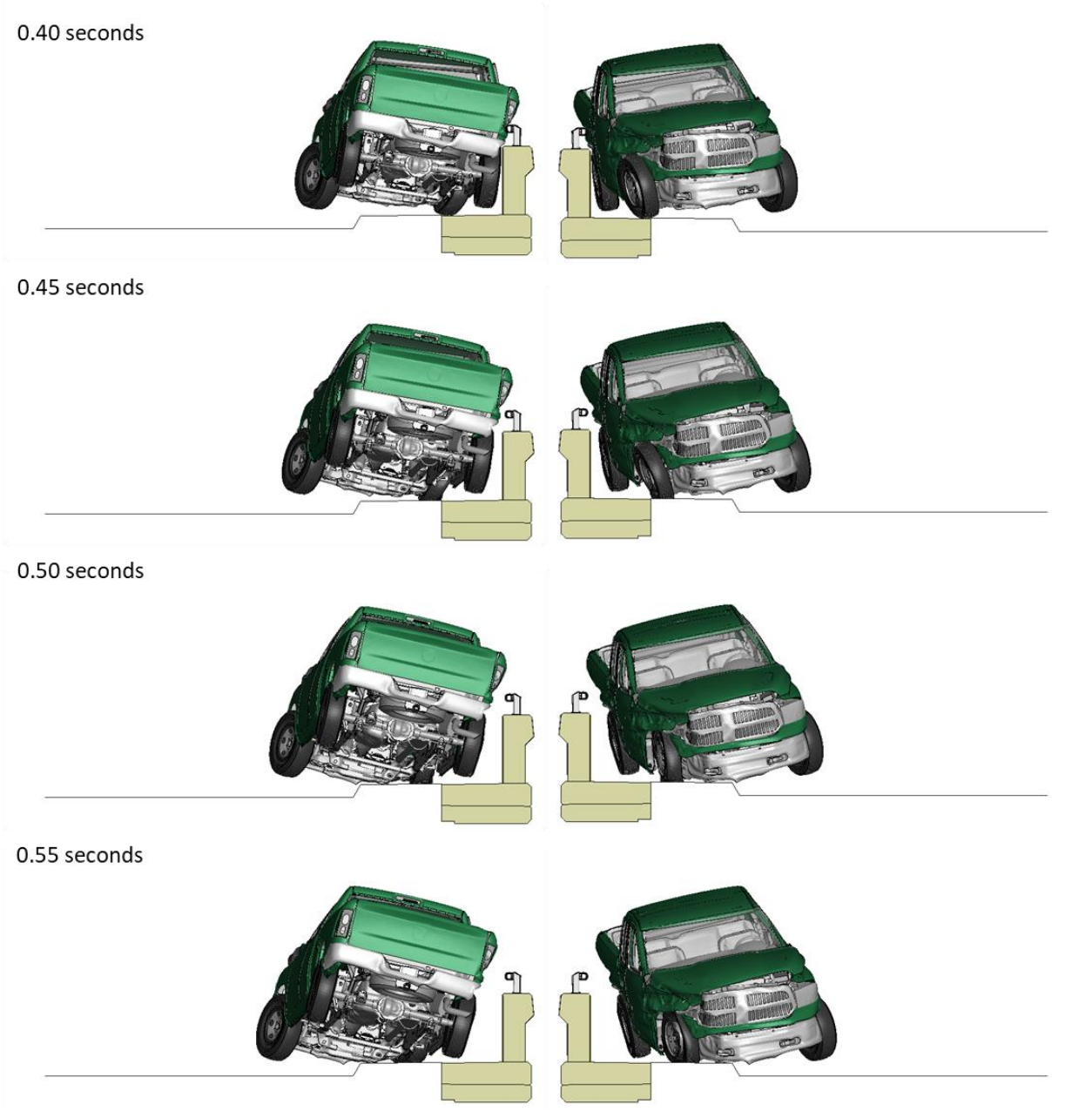

Figure 3 [CONTINUED] Sequential views from analysis of MASH Test 3-11 at 4.3 ft upstream of critical post from a front and back viewpoint (RHT Model).

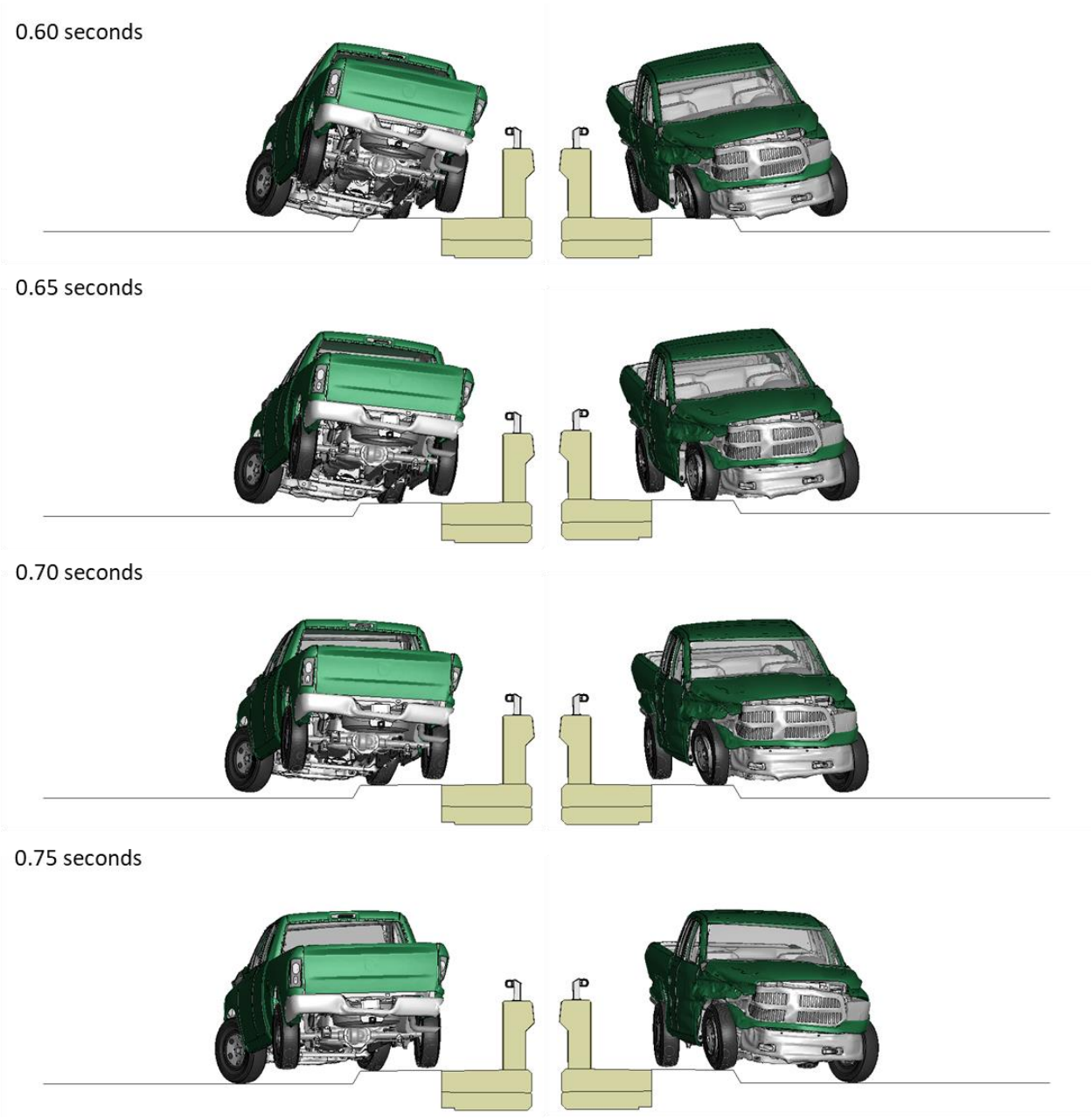

Figure 3 [CONTINUED] Sequential views from analysis of MASH Test 3-11 at 4.3 ft upstream of critical post from a front and back viewpoint (RHT Model).

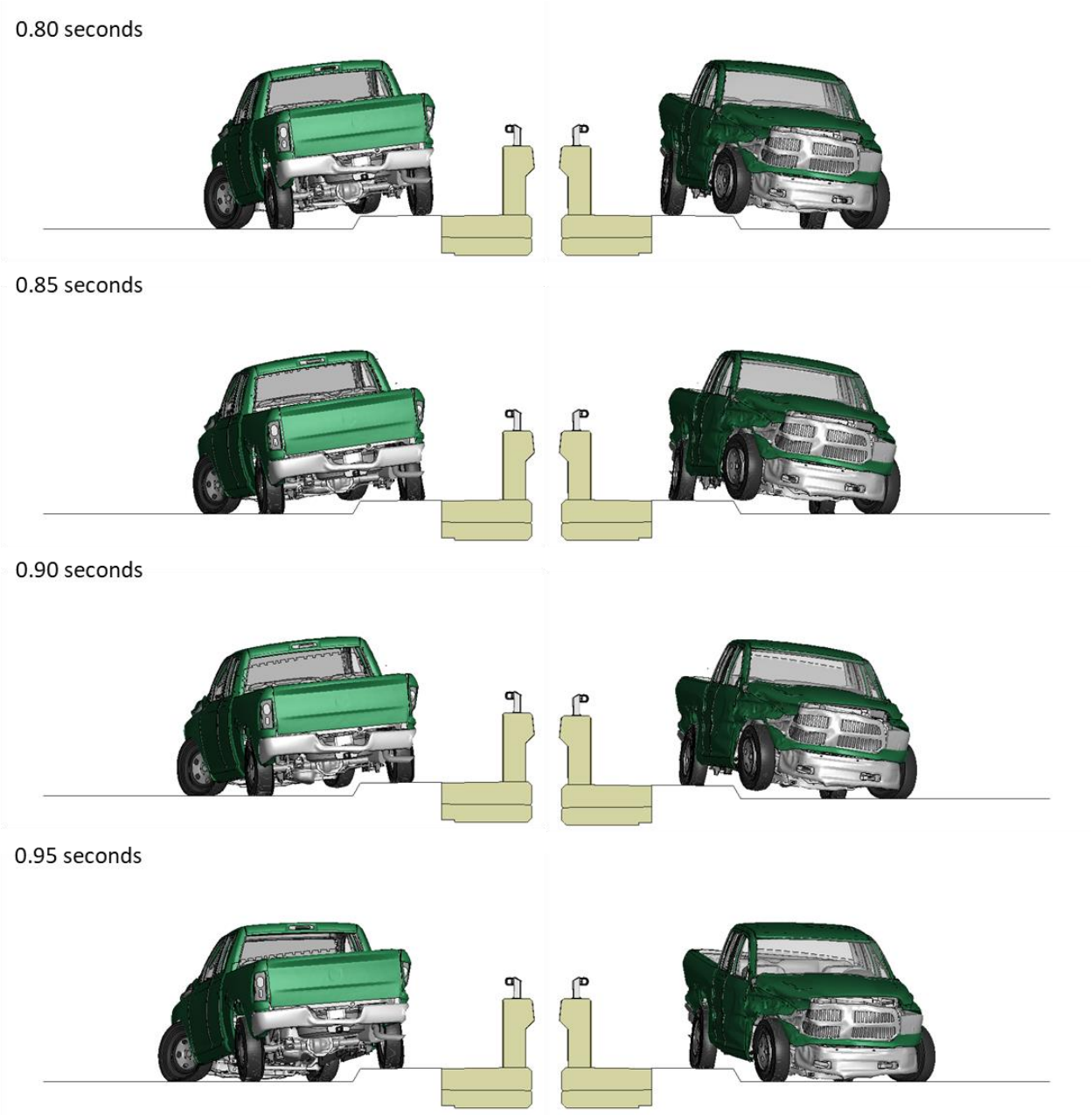

Figure 3 [CONTINUED] Sequential views from analysis of MASH Test 3-11 at 4.3 ft upstream of critical post from a front and back viewpoint (RHT Model).

Appendix H

Sequential Views for Test 3-11 at 5.3 ft Upstream of Critical Post (KC Model)

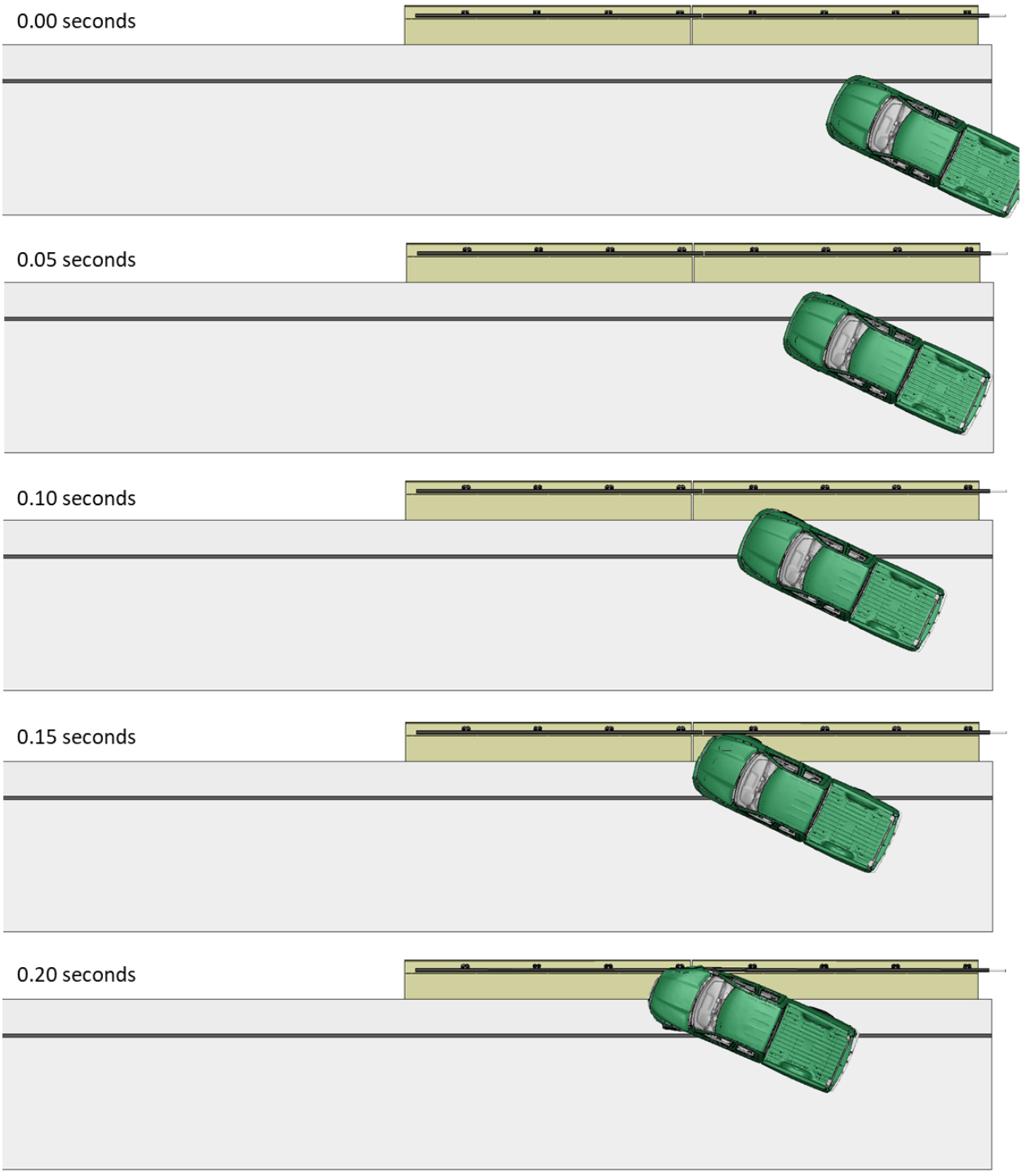

Figure 1. Sequential views from analysis of MASH Test 3-11 at 5.3 ft upstream of critical post from an overhead viewpoint (KC Model).

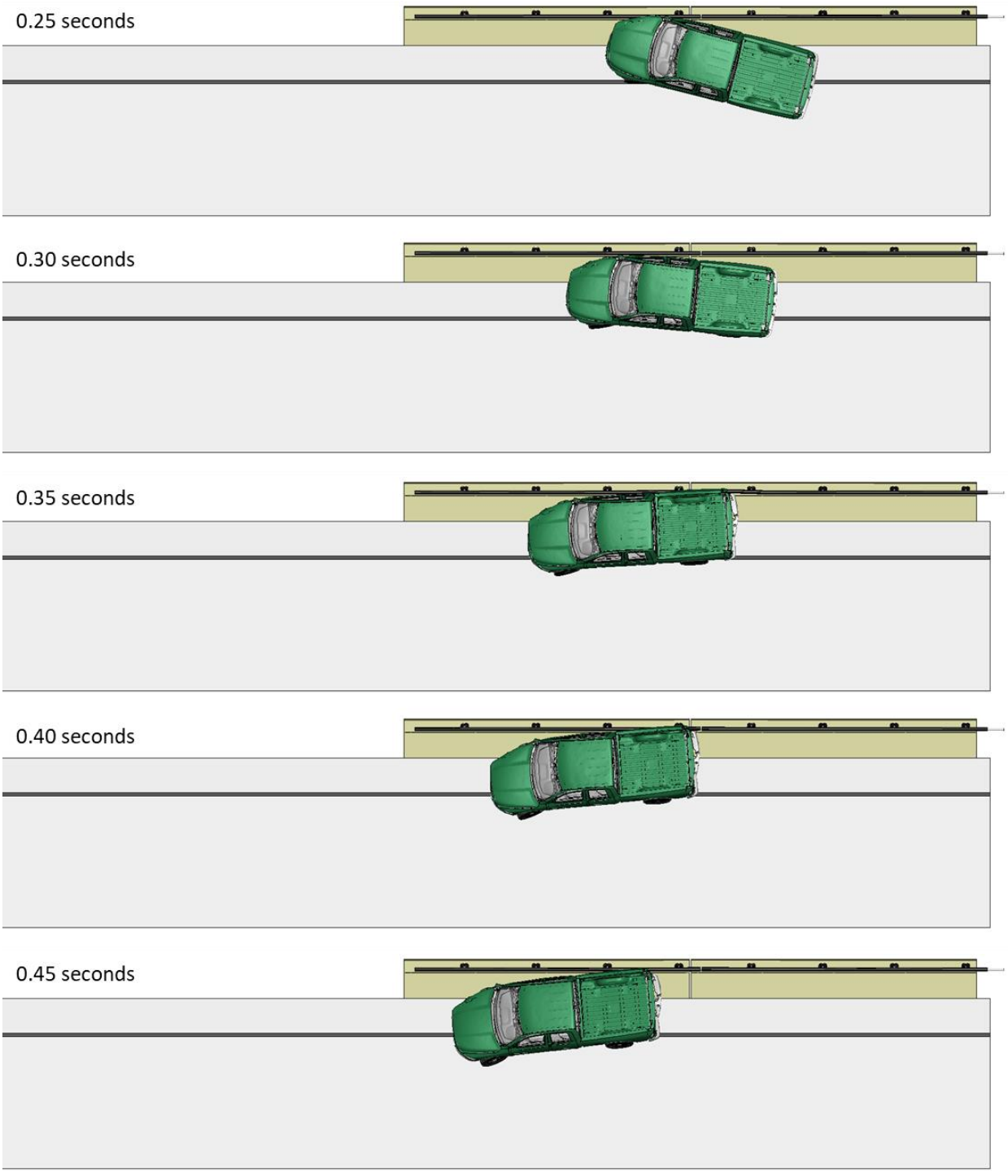

Figure 1 [CONTINUED] Sequential views from analysis of MASH Test 3-11 at 5.3 ft upstream of critical post from an overhead viewpoint (KC Model).

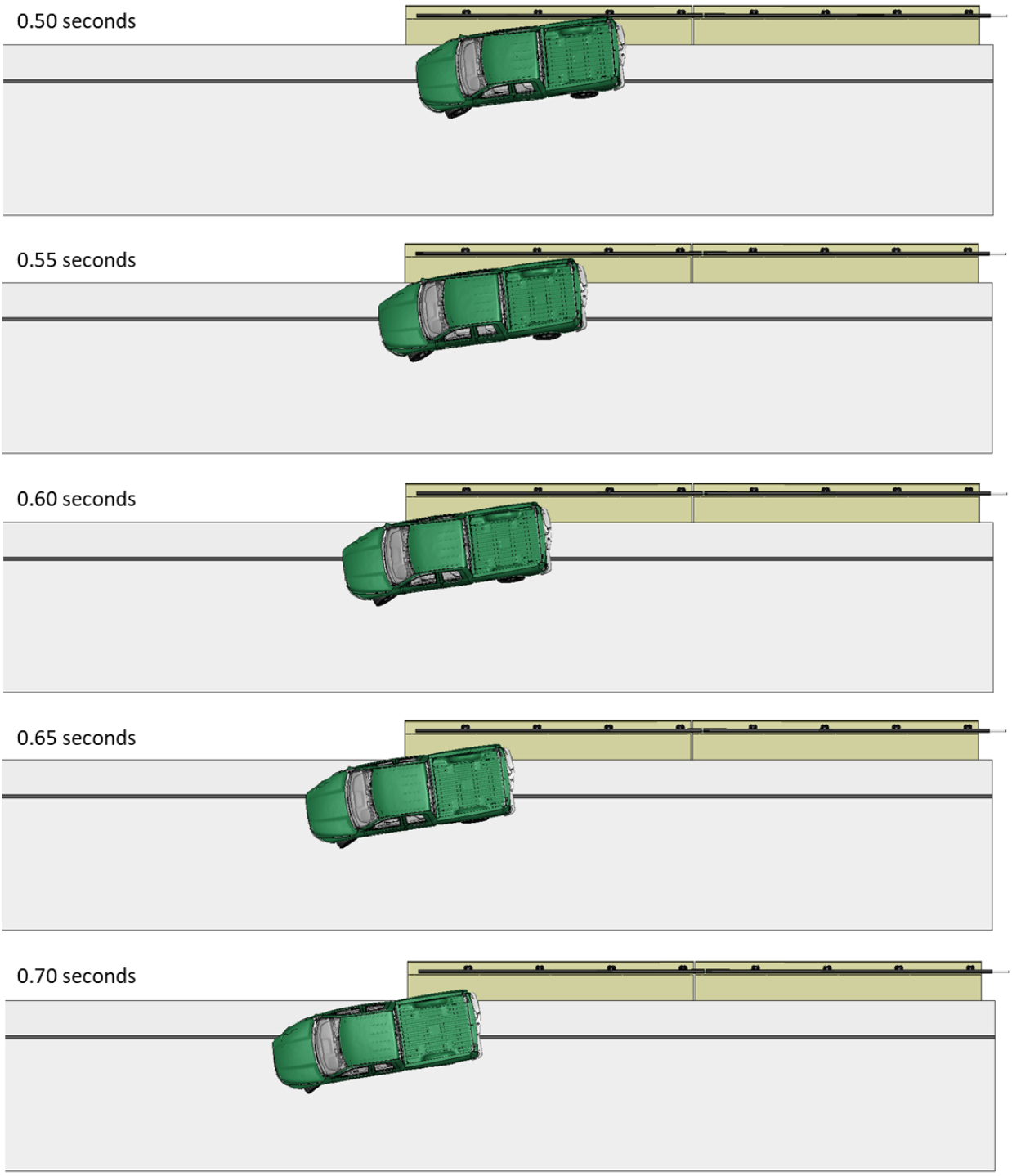

Figure 1 [CONTINUED] Sequential views from analysis of MASH Test 3-11 at 5.3 ft upstream of critical post from an overhead viewpoint (KC Model).

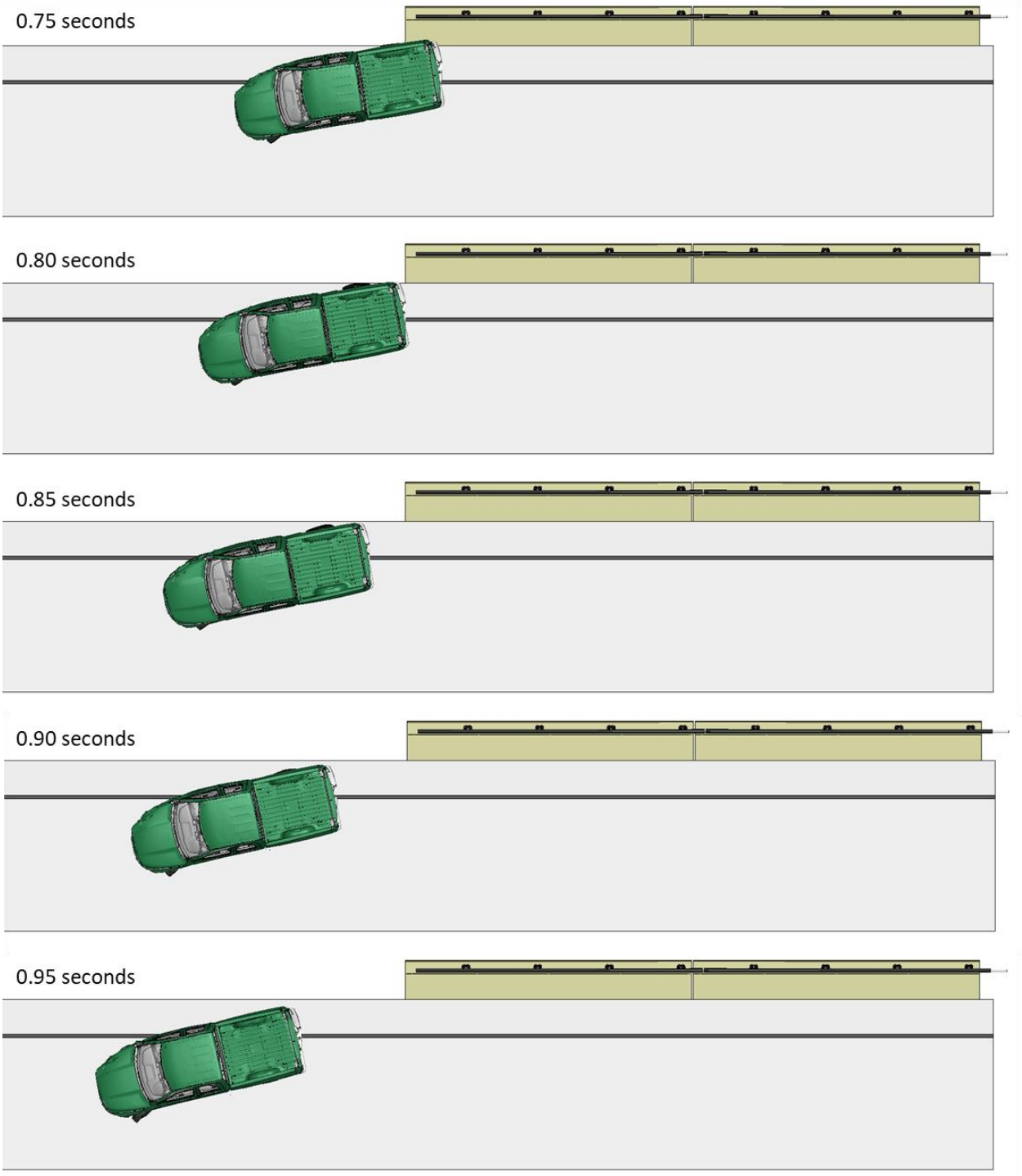

Figure 1 [CONTINUED] Sequential views from analysis of MASH Test 3-11 at 5.3 ft upstream of critical post from an overhead viewpoint (KC Model).

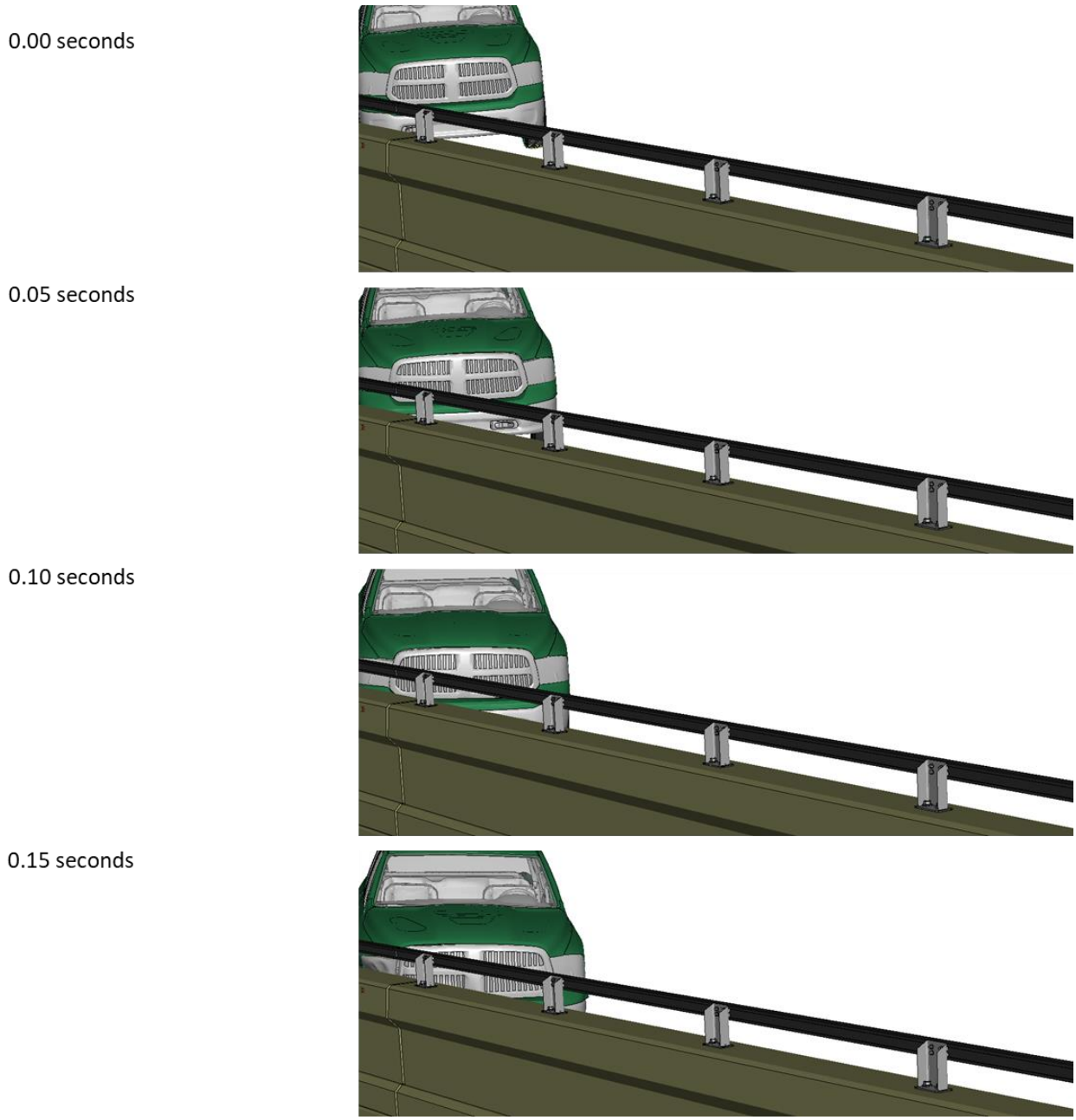

Figure 2. Sequential views from analysis of MASH Test 3-11 at 5.3 ft upstream of critical post from an isometric viewpoint (KC Model).

0.20 seconds

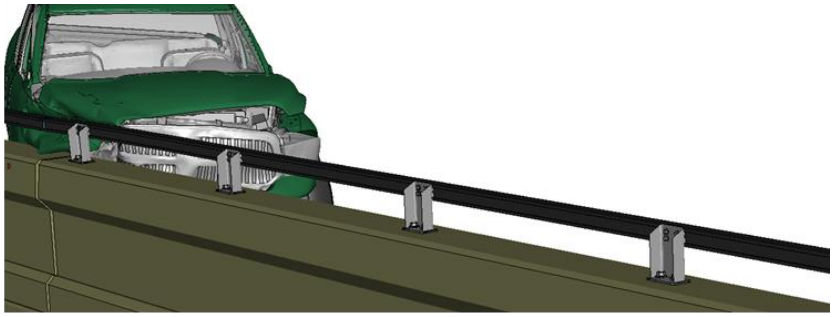

0.25 seconds

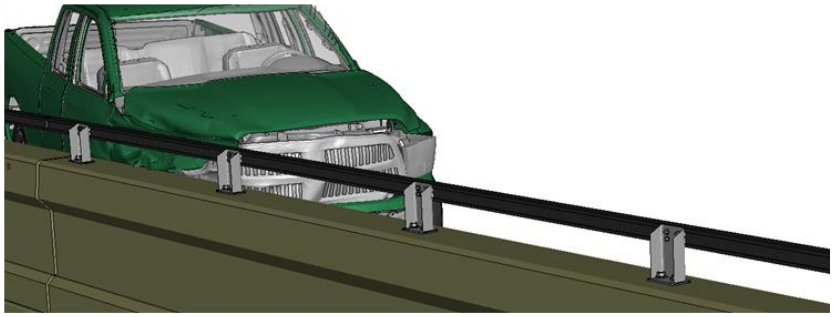

0.30 seconds

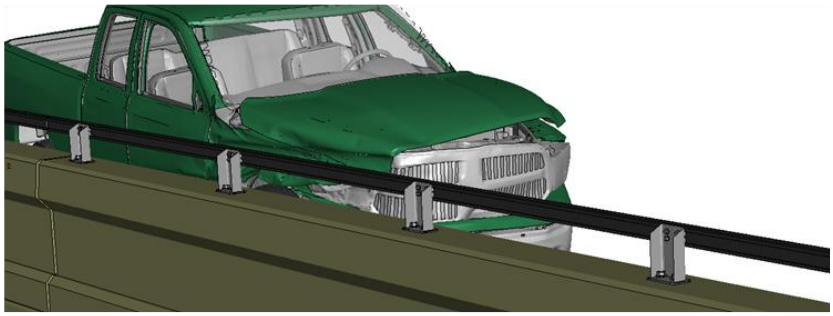

0.35 seconds

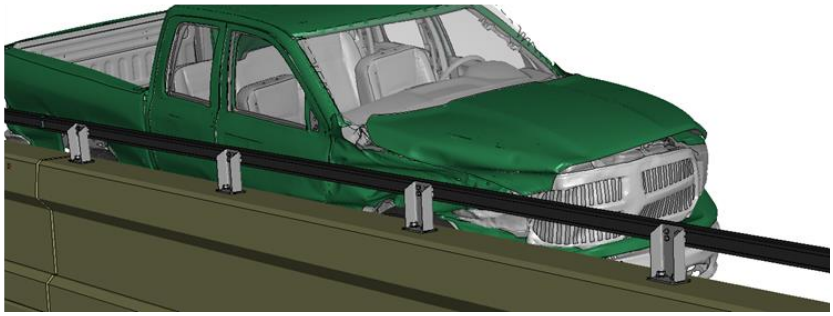

Figure 2 [CONTINUED] Sequential views from analysis of MASH Test 3-11 at 5.3 ft upstream of critical post from an isometric viewpoint (KC Model).

0.40 seconds

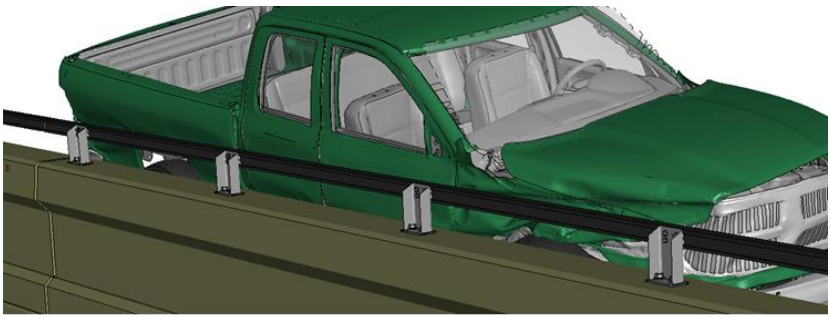

0.45 seconds

0.50 seconds

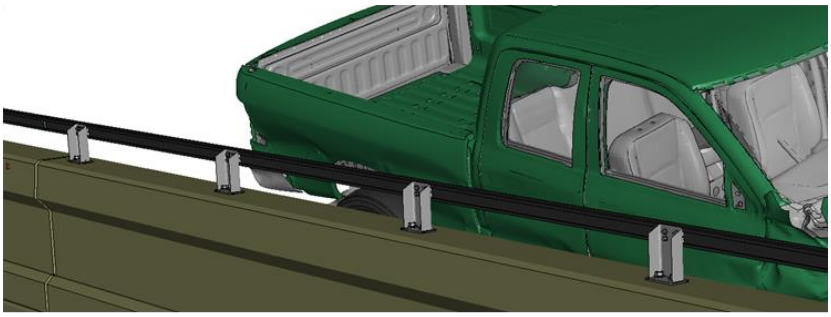

0.55 seconds

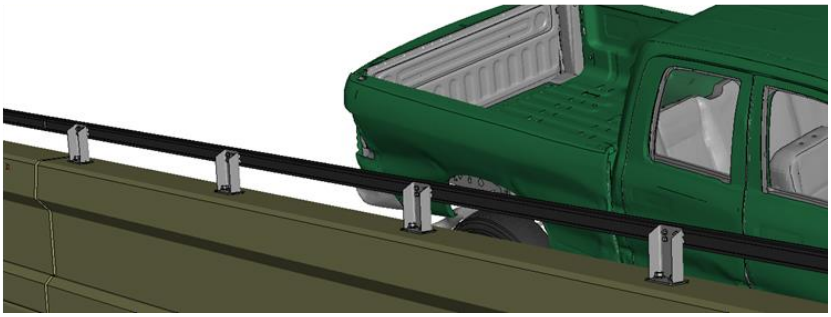

Figure 2 [CONTINUED] Sequential views from analysis of MASH Test 3-11 at 5.3 ft upstream of critical post from an isometric viewpoint (KC Model).

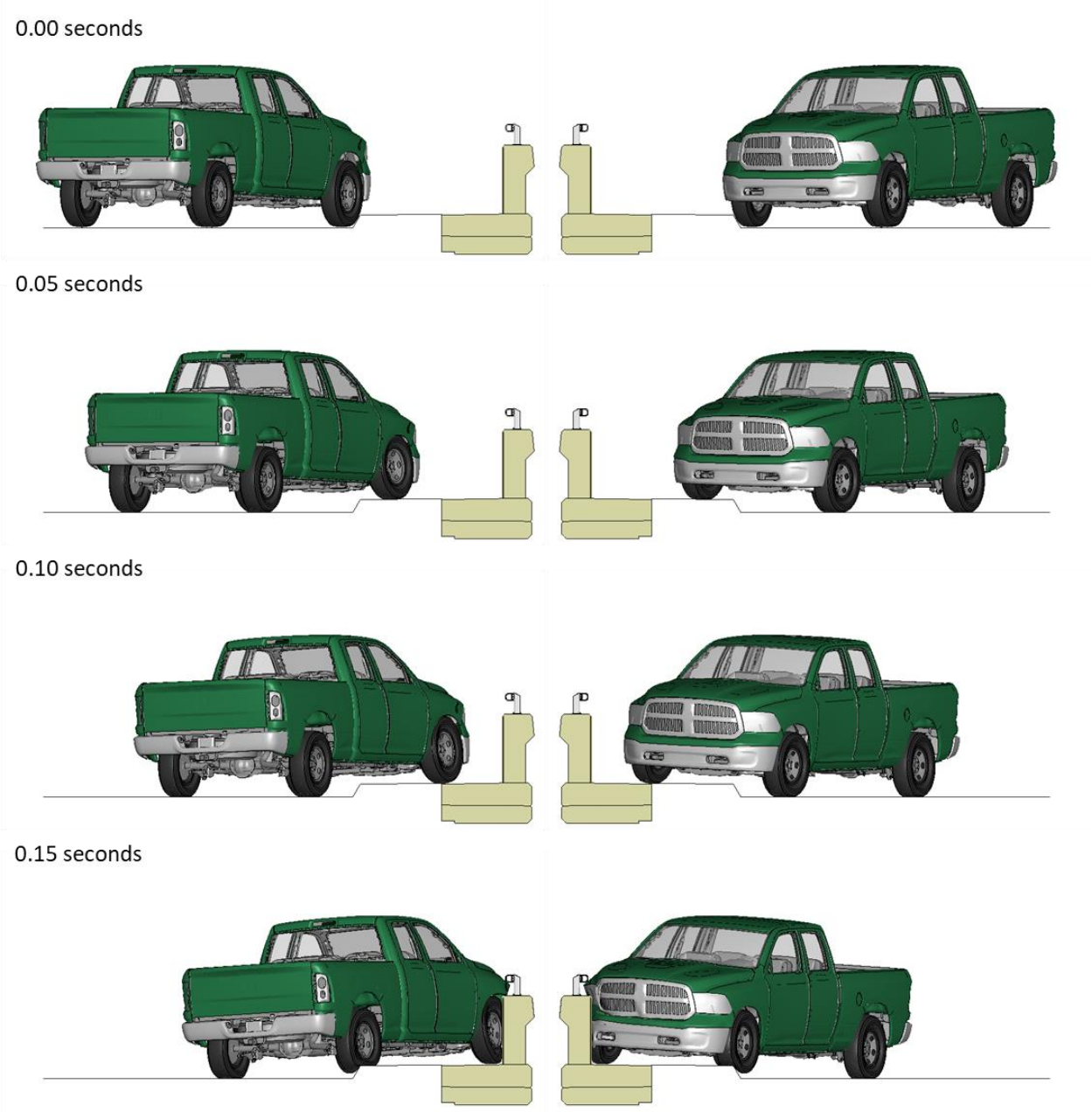

Figure 3. Sequential views from analysis of MASH Test 3-11 at 5.3 ft upstream of critical post from a front and back viewpoint (KC Model).

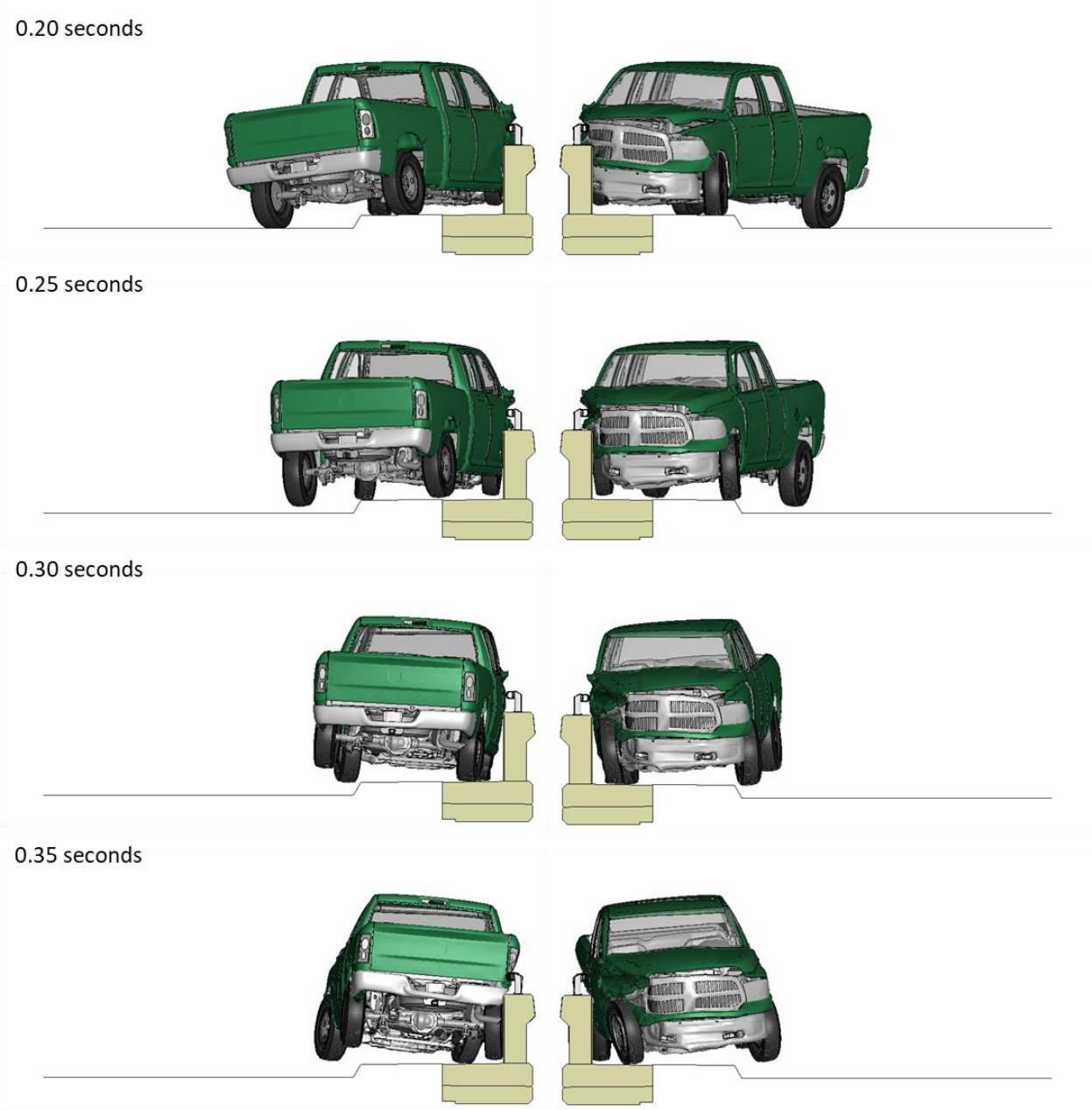

Figure 3 [CONTINUED] Sequential views from analysis of MASH Test 3-11 at 5.3 ft upstream of critical post from a front and back viewpoint (KC Model).

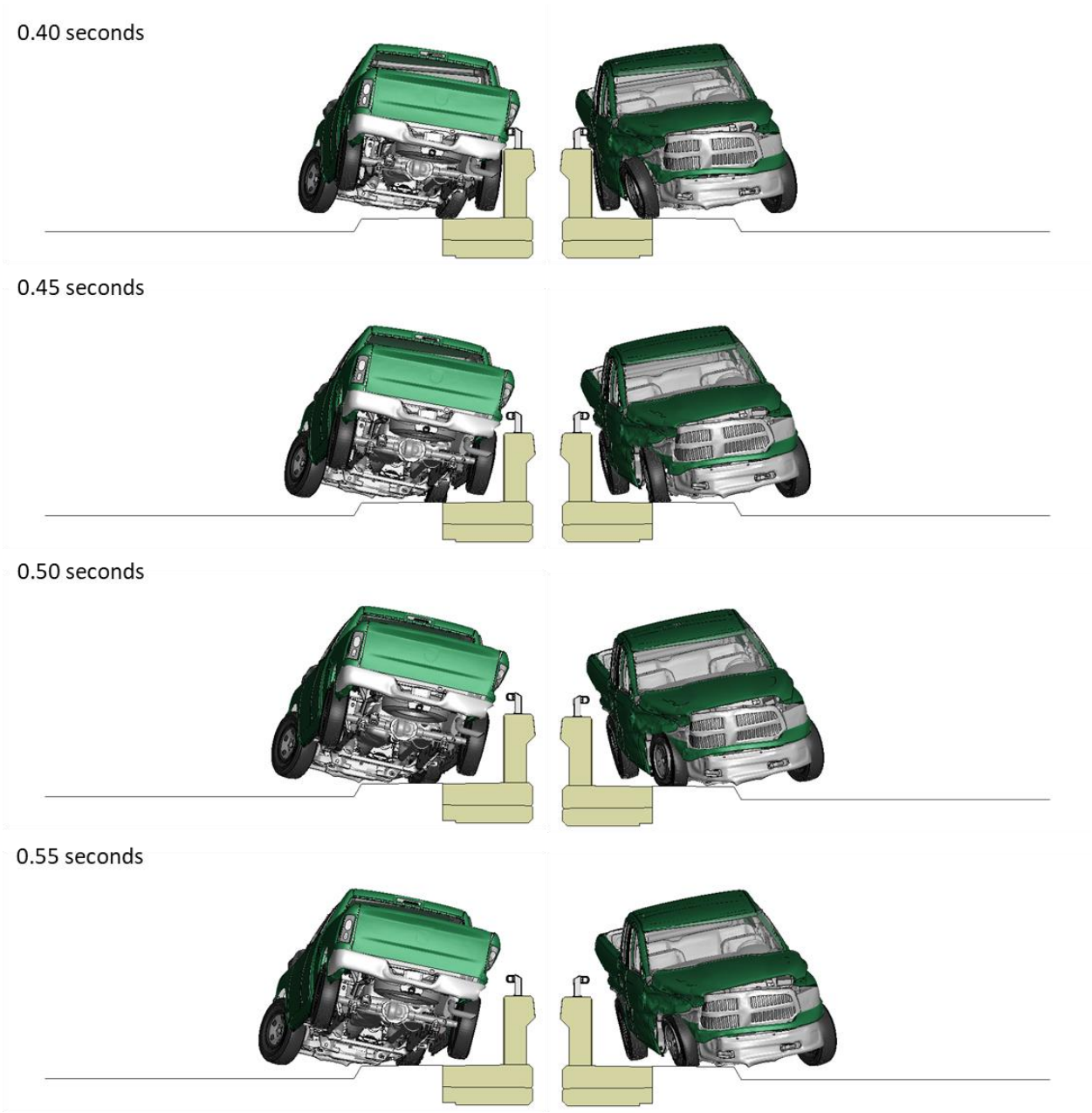

Figure 3 [CONTINUED] Sequential views from analysis of MASH Test 3-11 at 5.3 ft upstream of critical post from a front and back viewpoint (KC Model).

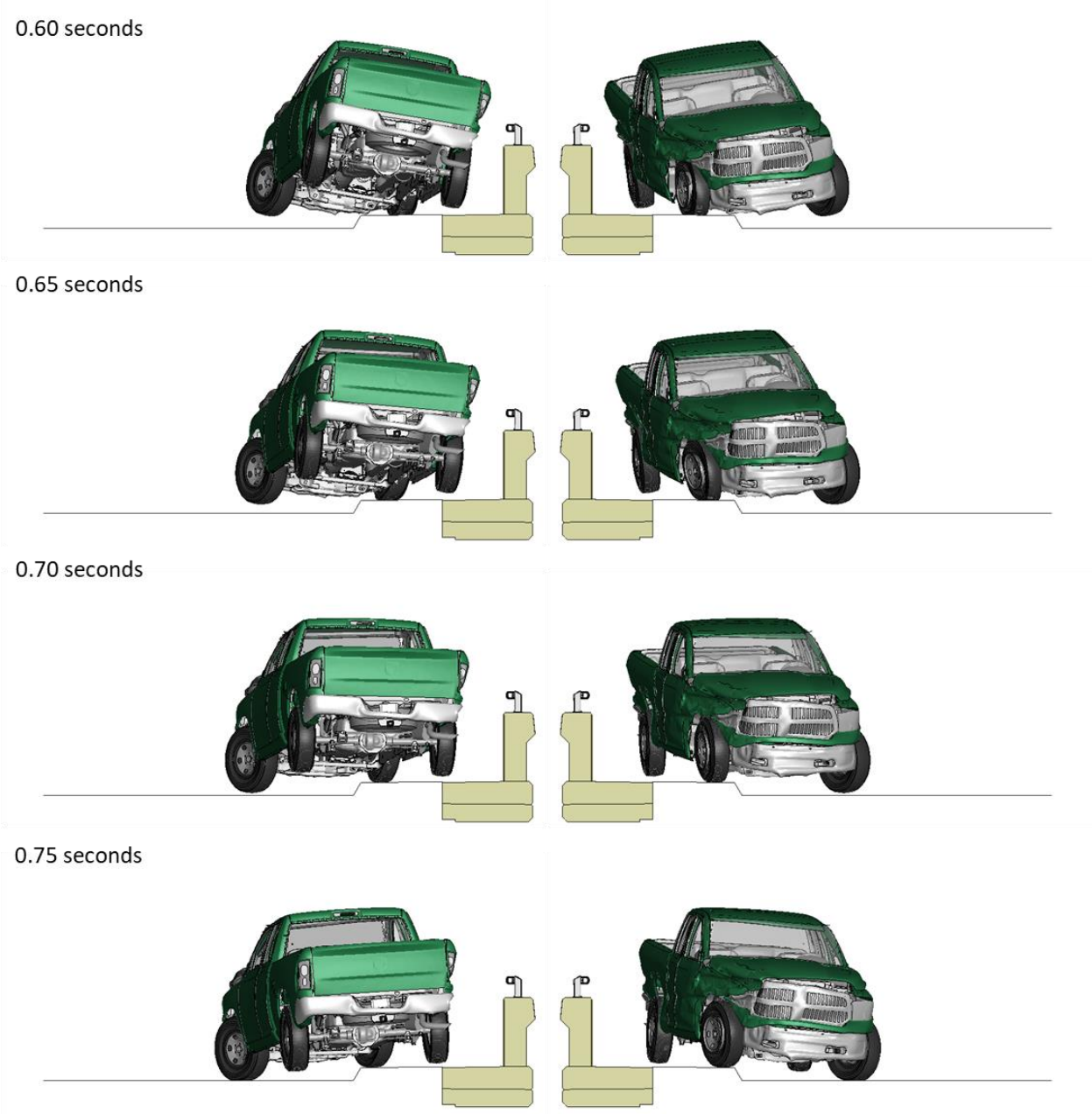

Figure 3 [CONTINUED] Sequential views from analysis of MASH Test 3-11 at 5.3 ft upstream of critical post from a front and back viewpoint (KC Model).

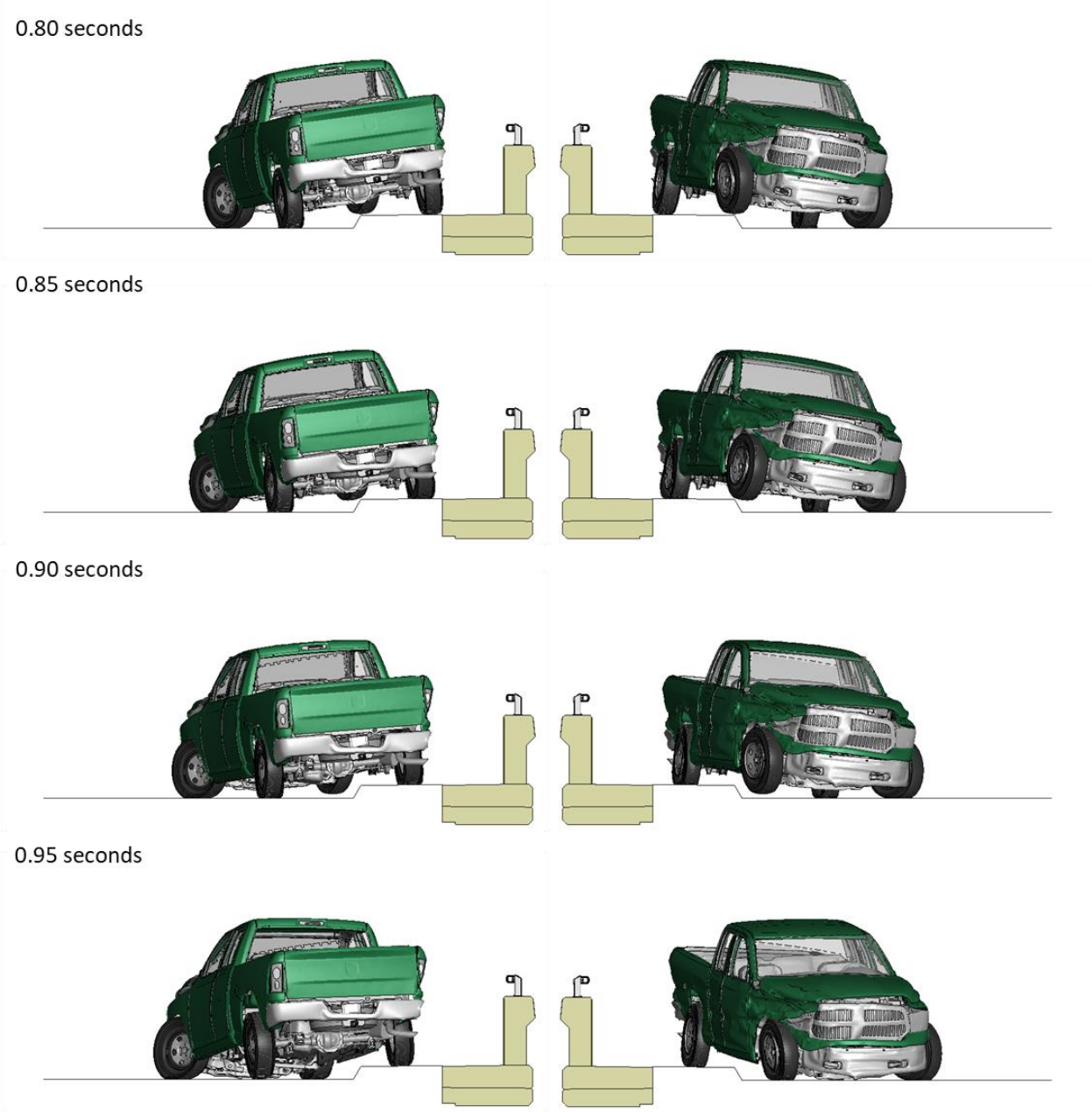

Figure 3 [CONTINUED] Sequential views from analysis of MASH Test 3-11 at 5.3 ft upstream of critical post from a front and back viewpoint (KC Model).

Appendix I

Sequential Views for Test 3-11 at 5.3 ft Upstream of Critical Post (RHT Model)

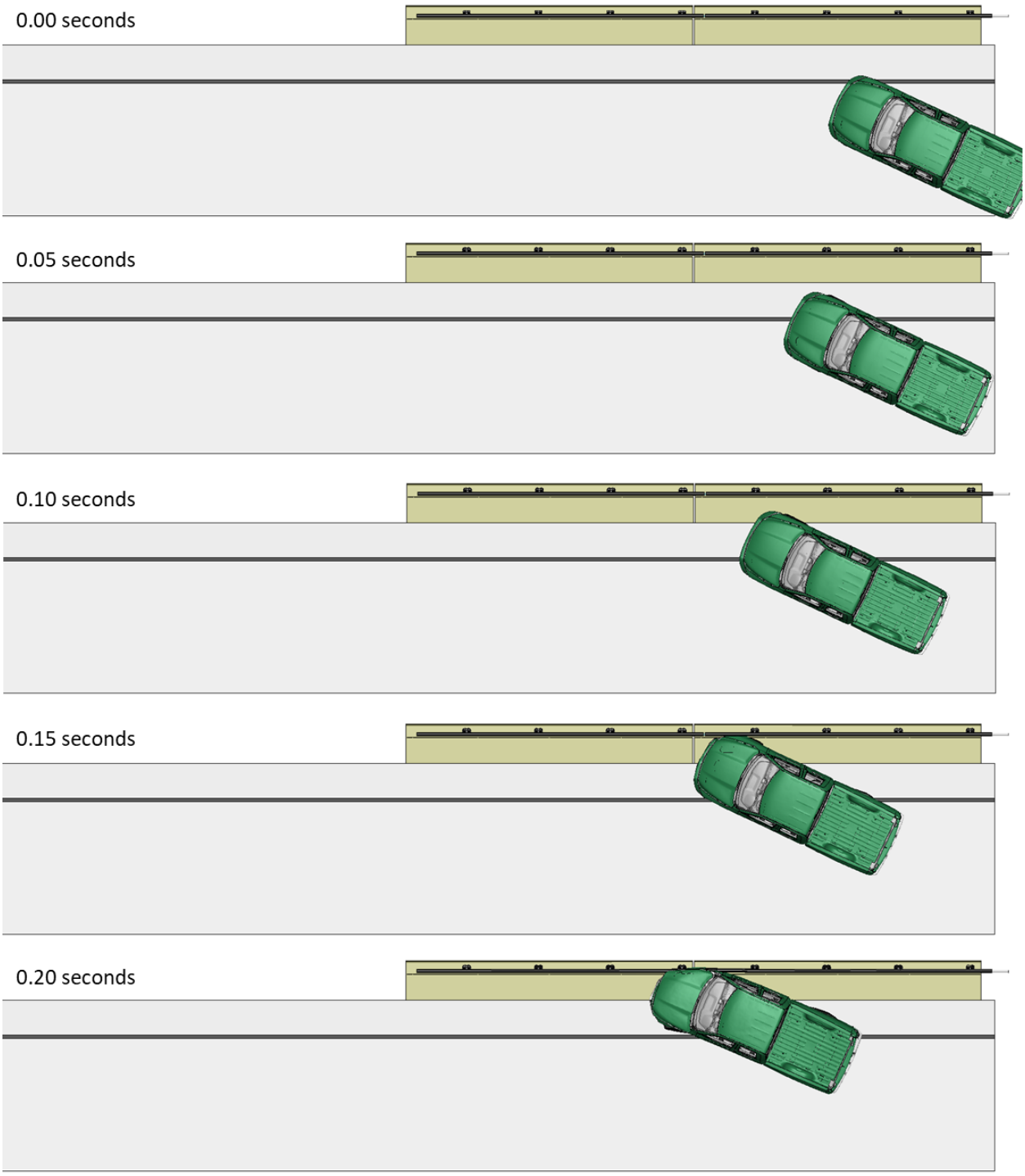

Figure 1. Sequential views from analysis of MASH Test 3-11 at 5.3 ft upstream of critical post from an overhead viewpoint (RHT Model).

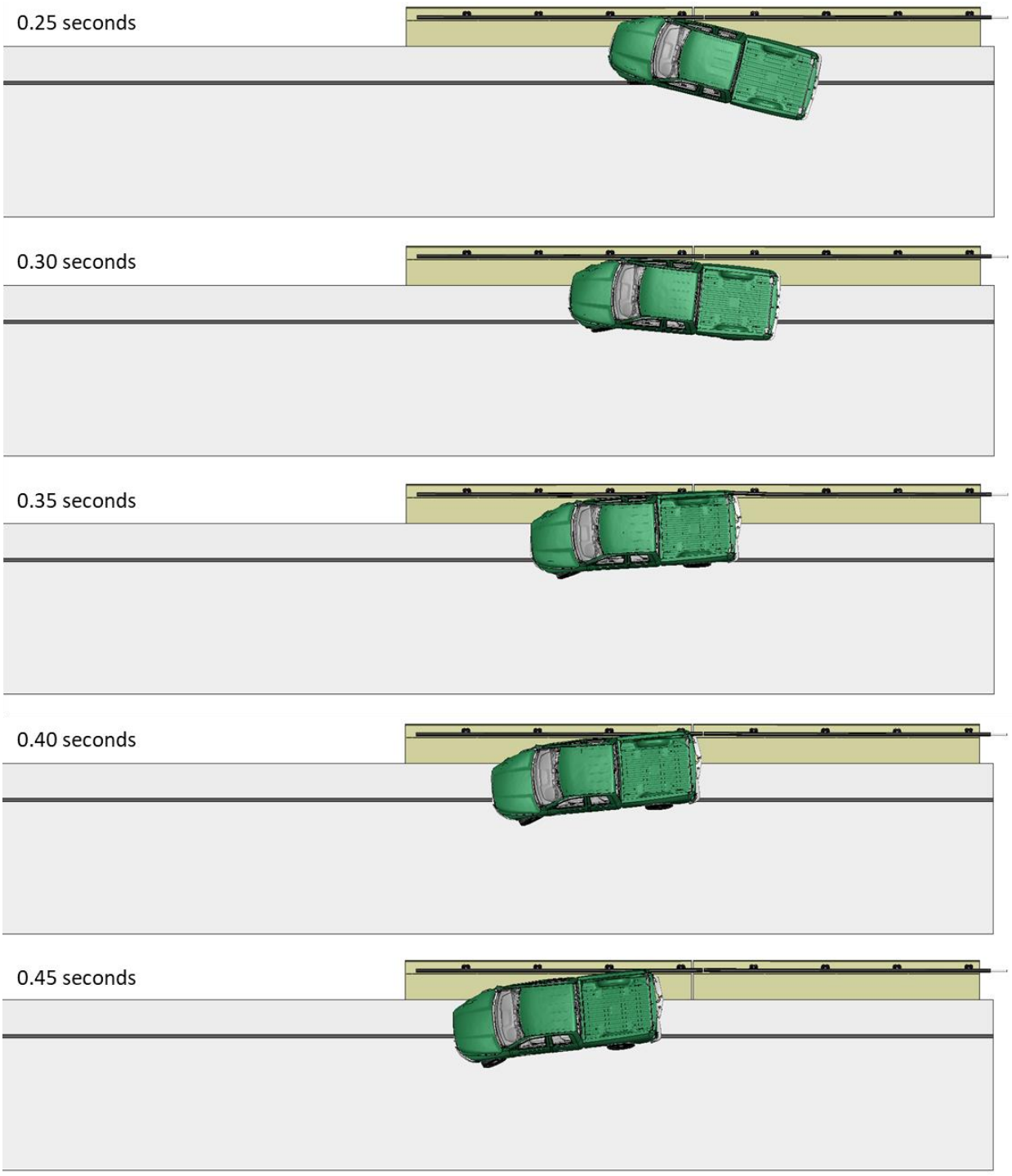

Figure 1 [CONTINUED] Sequential views from analysis of MASH Test 3-11 at 5.3 ft upstream of critical post from an overhead viewpoint (RHT Model).

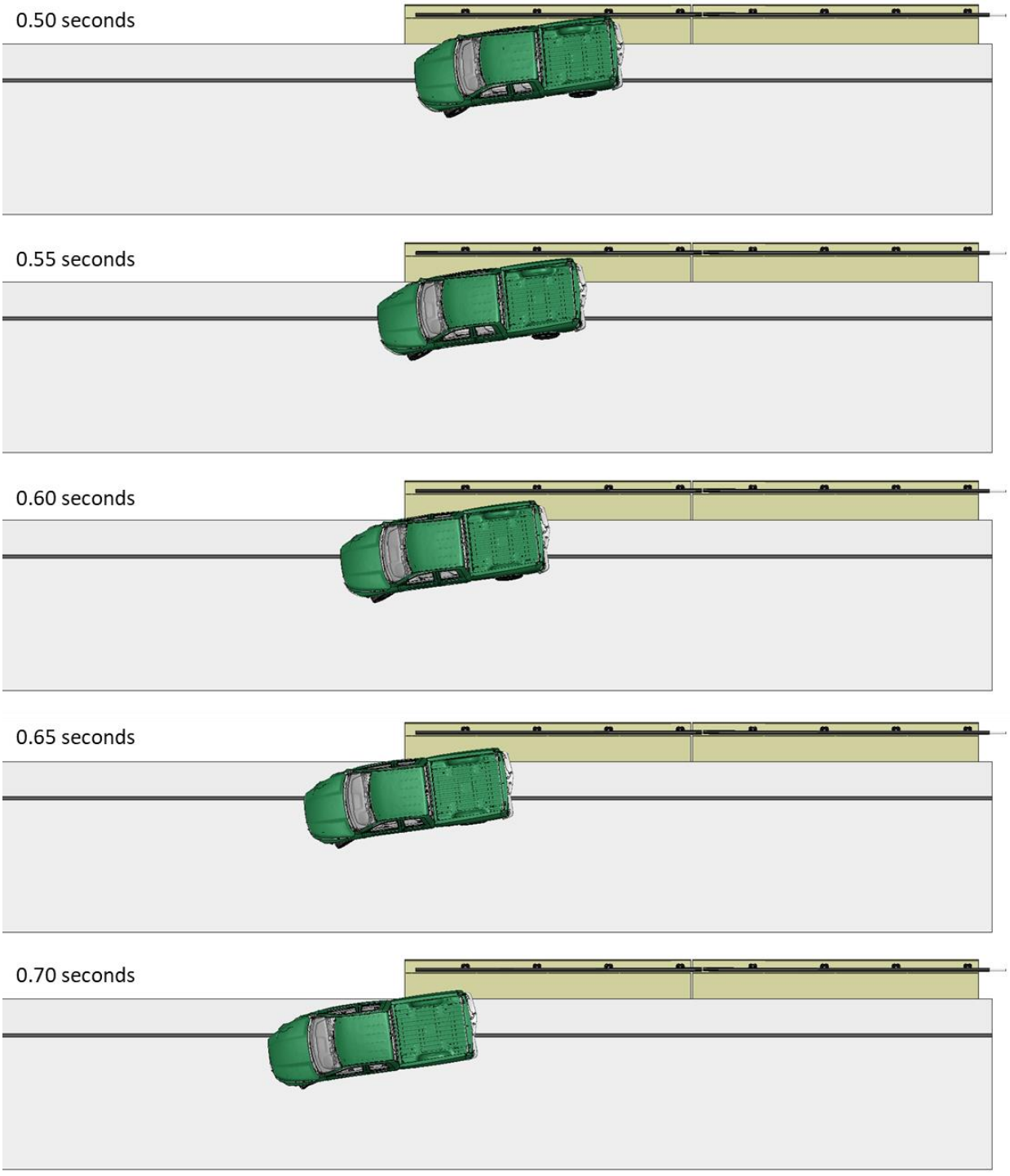

Figure 1 [CONTINUED] Sequential views from analysis of MASH Test 3-11 at 5.3 ft upstream of critical post from an overhead viewpoint (RHT Model).

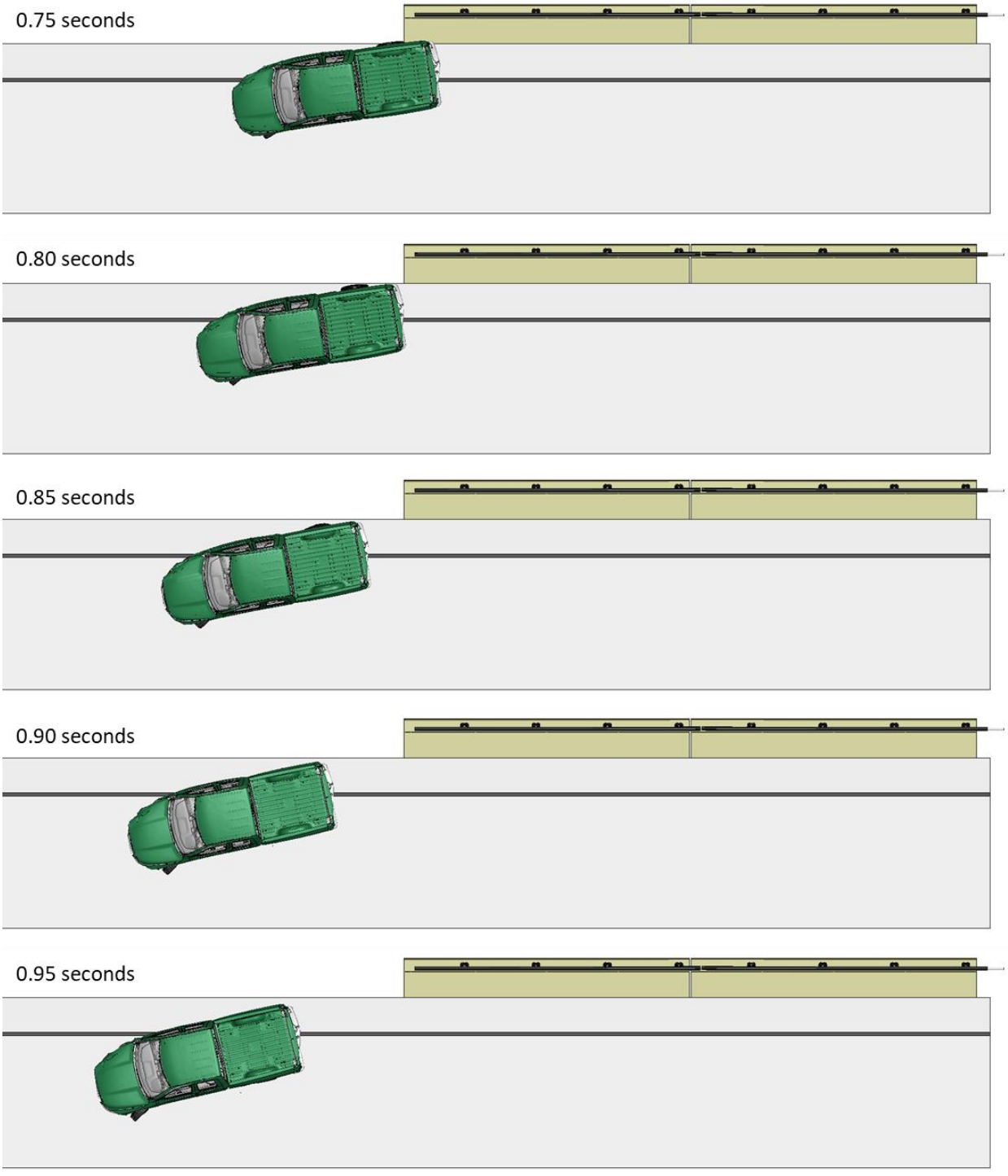

Figure 1 [CONTINUED] Sequential views from analysis of MASH Test 3-11 at 5.3 ft upstream of critical post from an overhead viewpoint (RHT Model).

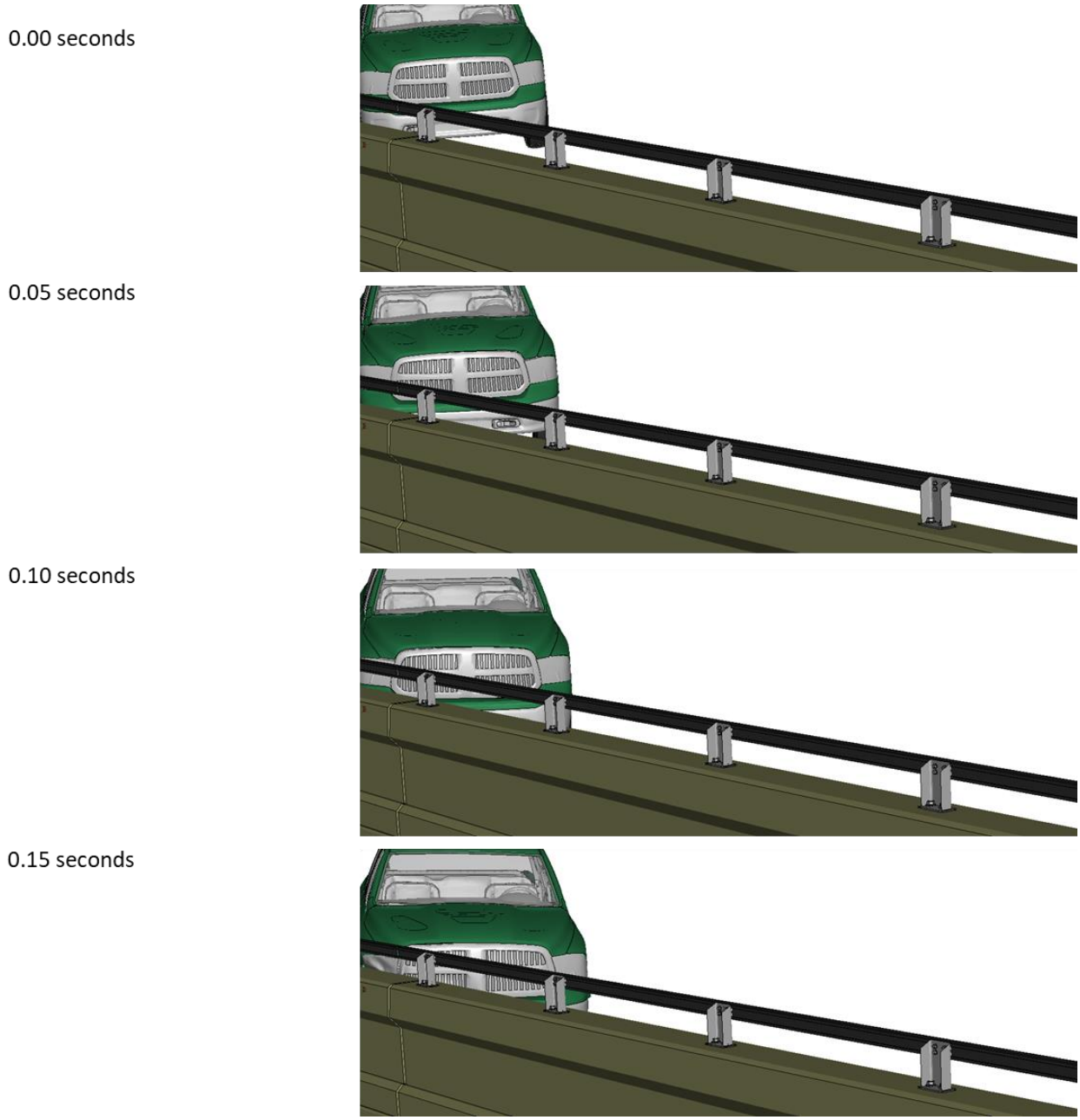

Figure 2. Sequential views from analysis of MASH Test 3-11 at 5.3 ft upstream of critical post from an isometric viewpoint (RHT Model).

0.20 seconds

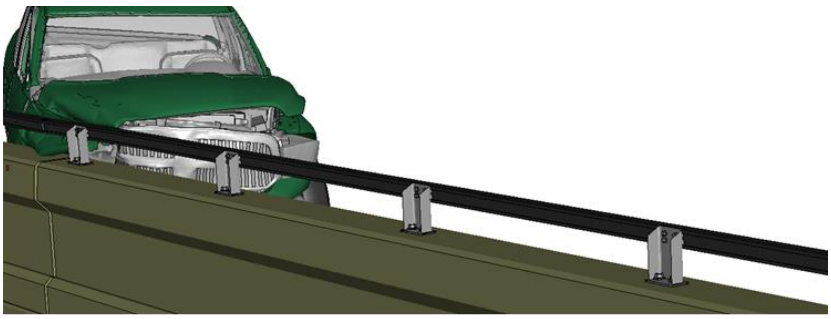

0.25 seconds

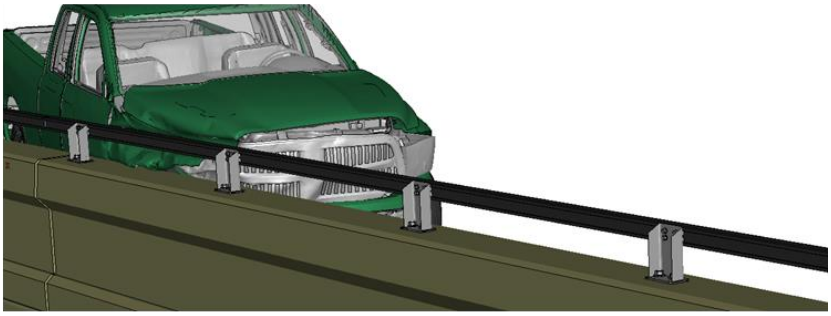

0.30 seconds

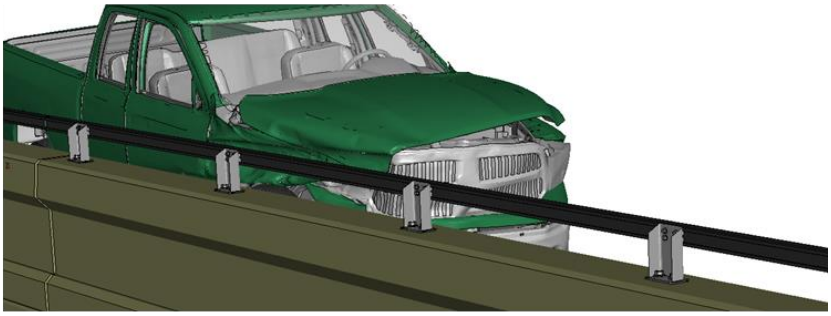

0.35 seconds

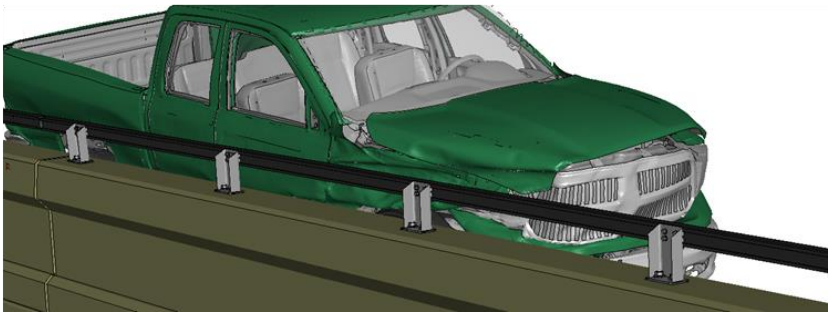

Figure 2 [CONTINUED] Sequential views from analysis of MASH Test 3-11 at 5.3 ft upstream of critical post from an isometric viewpoint (RHT Model).

0.40 seconds

0.45 seconds

0.50 seconds

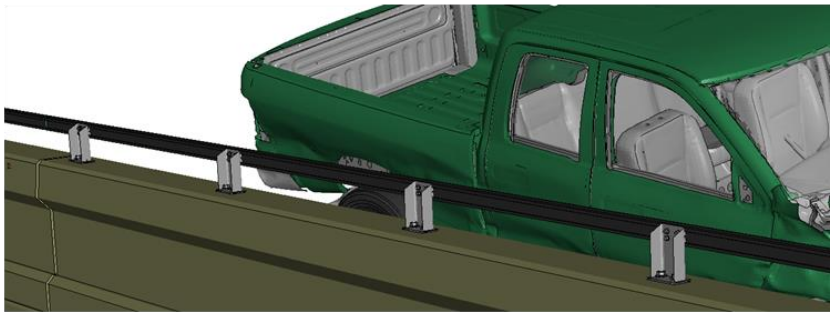

0.55 seconds

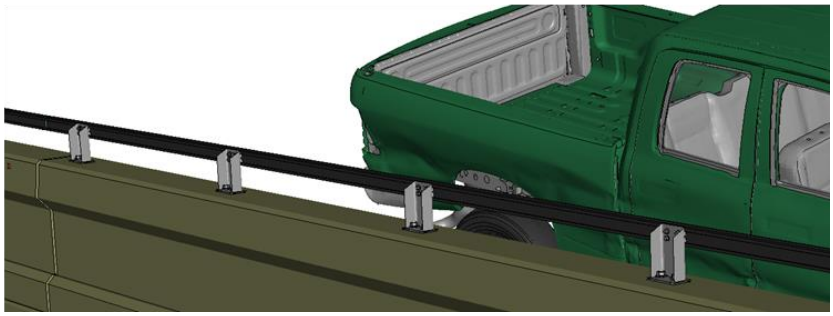

Figure 2 [CONTINUED] Sequential views from analysis of MASH Test 3-11 at 5.3 ft upstream of critical post from an isometric viewpoint (RHT Model).

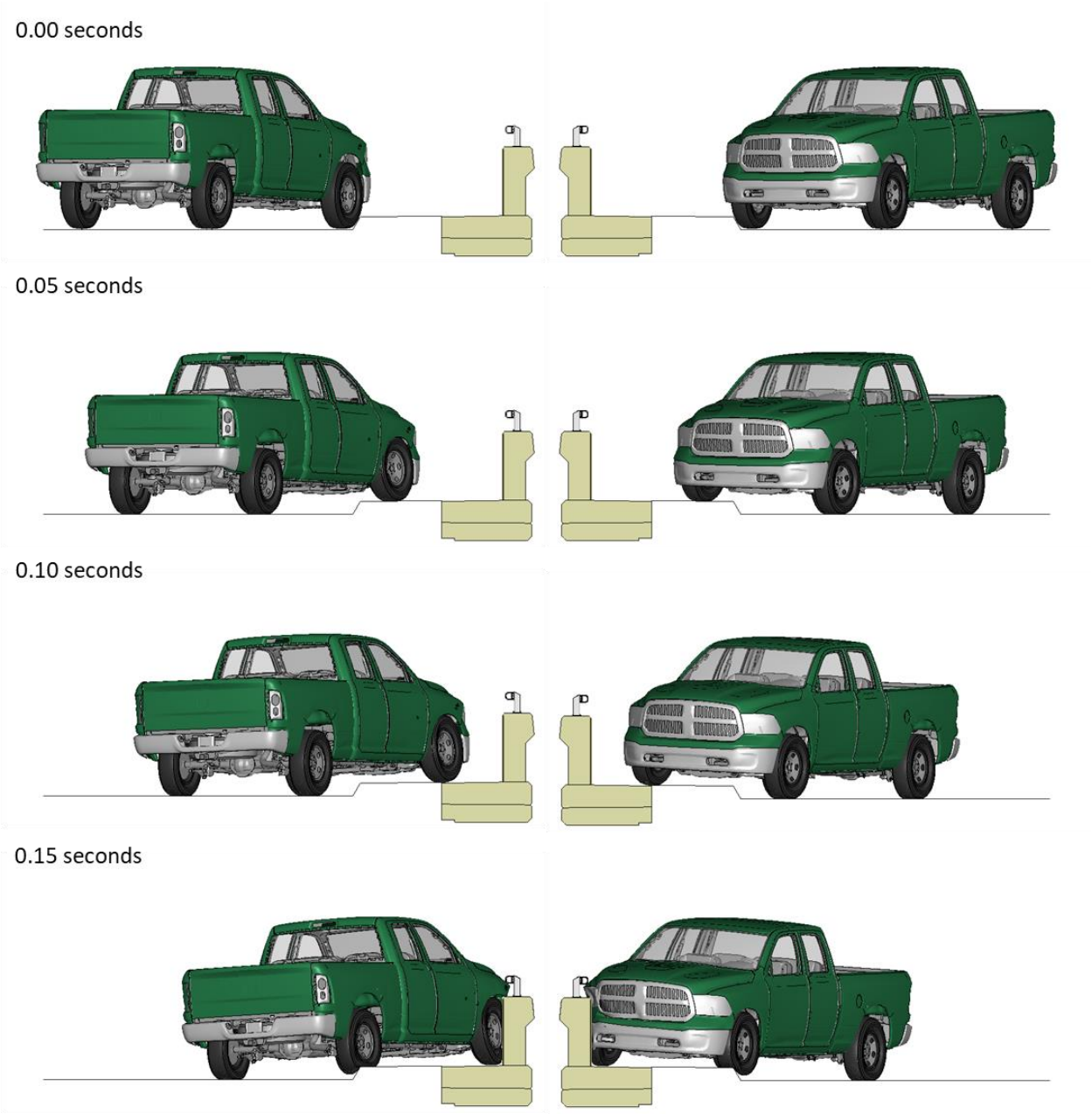

Figure 3. Sequential views from analysis of MASH Test 3-11 at 5.3 ft upstream of critical post from a front and back viewpoint (RHT Model).

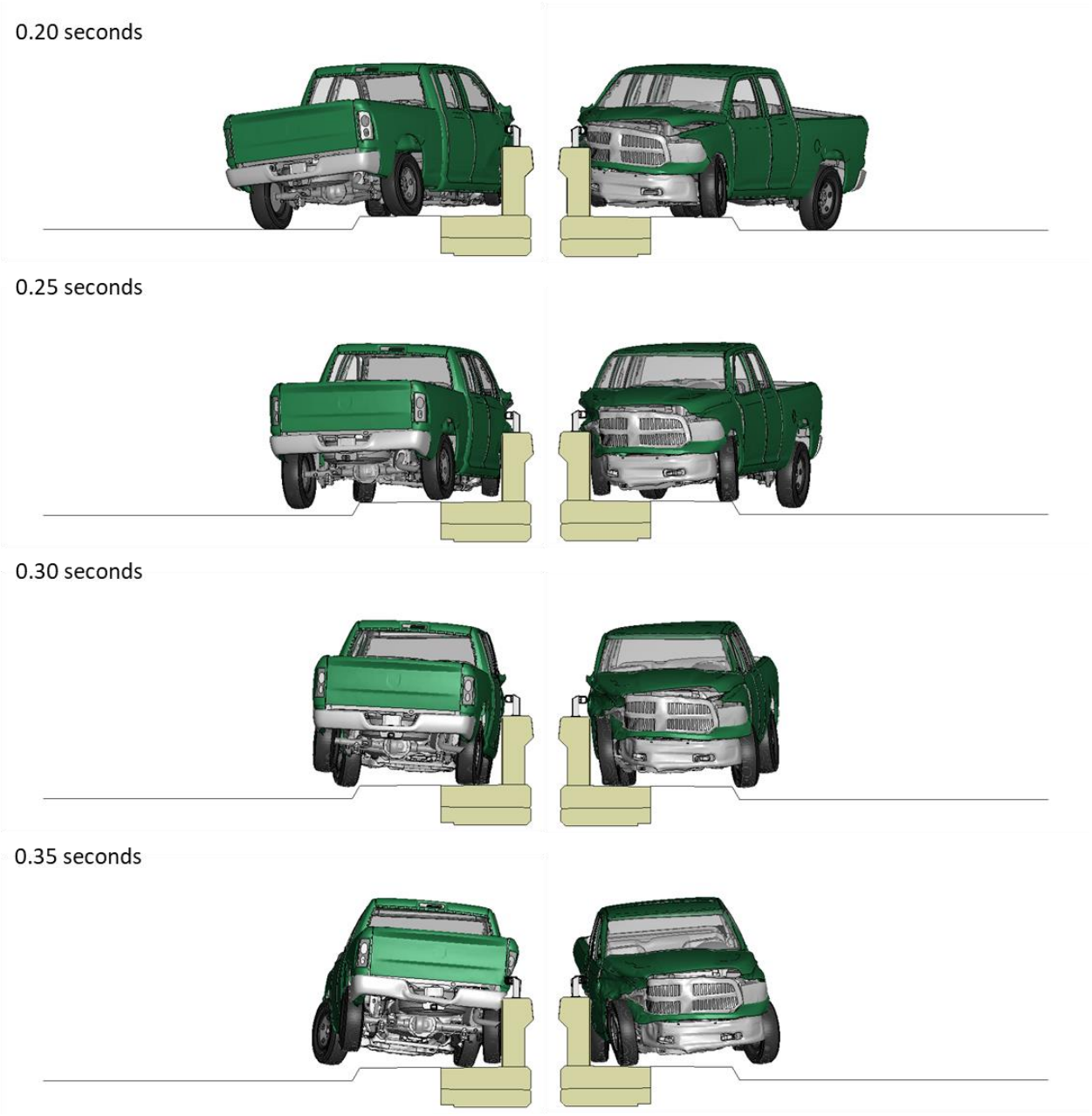

Figure 3 [CONTINUED] Sequential views from analysis of MASH Test 3-11 at 5.3 ft upstream of critical post from a front and back viewpoint (RHT Model).

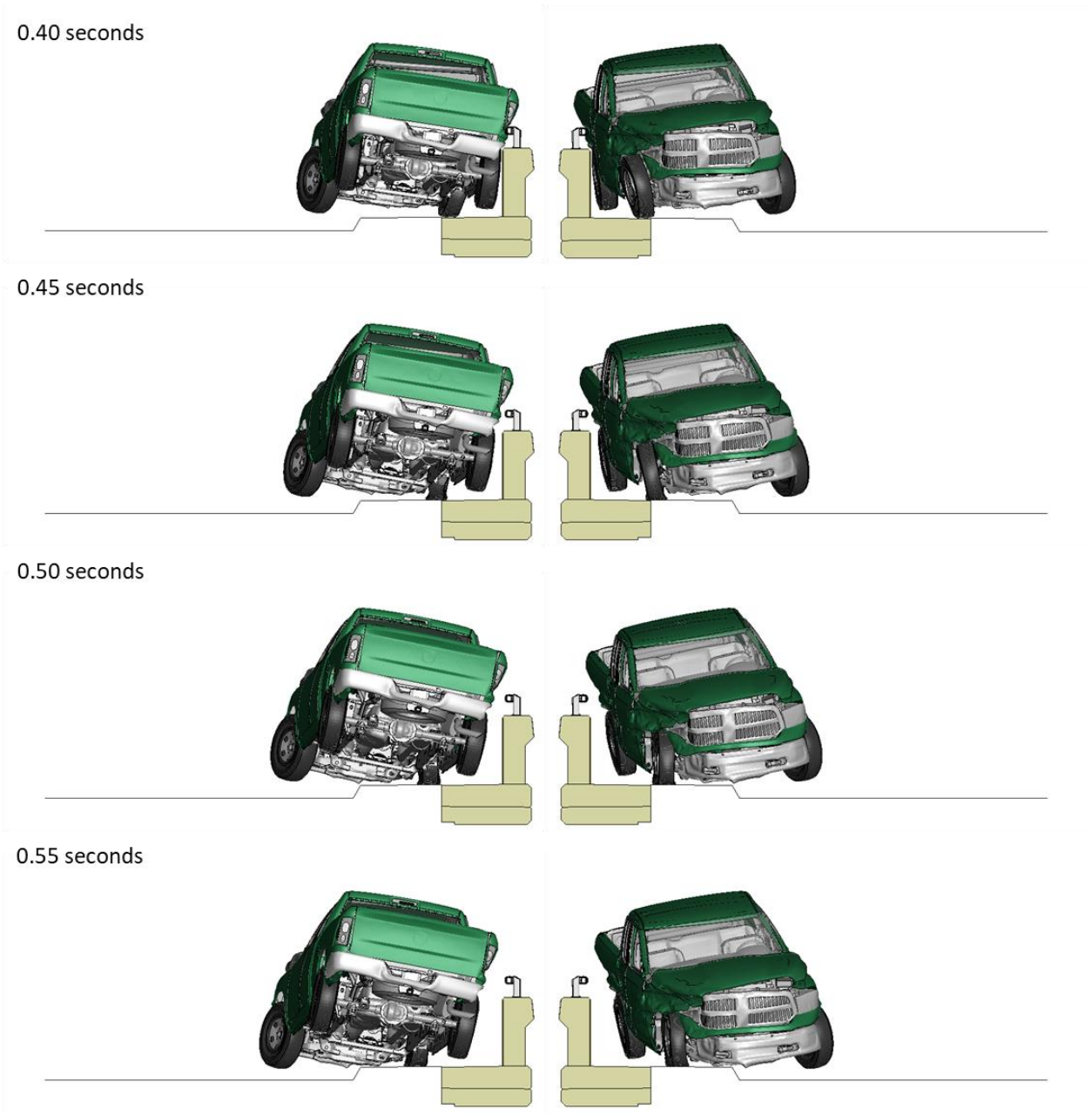

Figure 3 [CONTINUED] Sequential views from analysis of MASH Test 3-11 at 5.3 ft upstream of critical post from a front and back viewpoint (RHT Model).

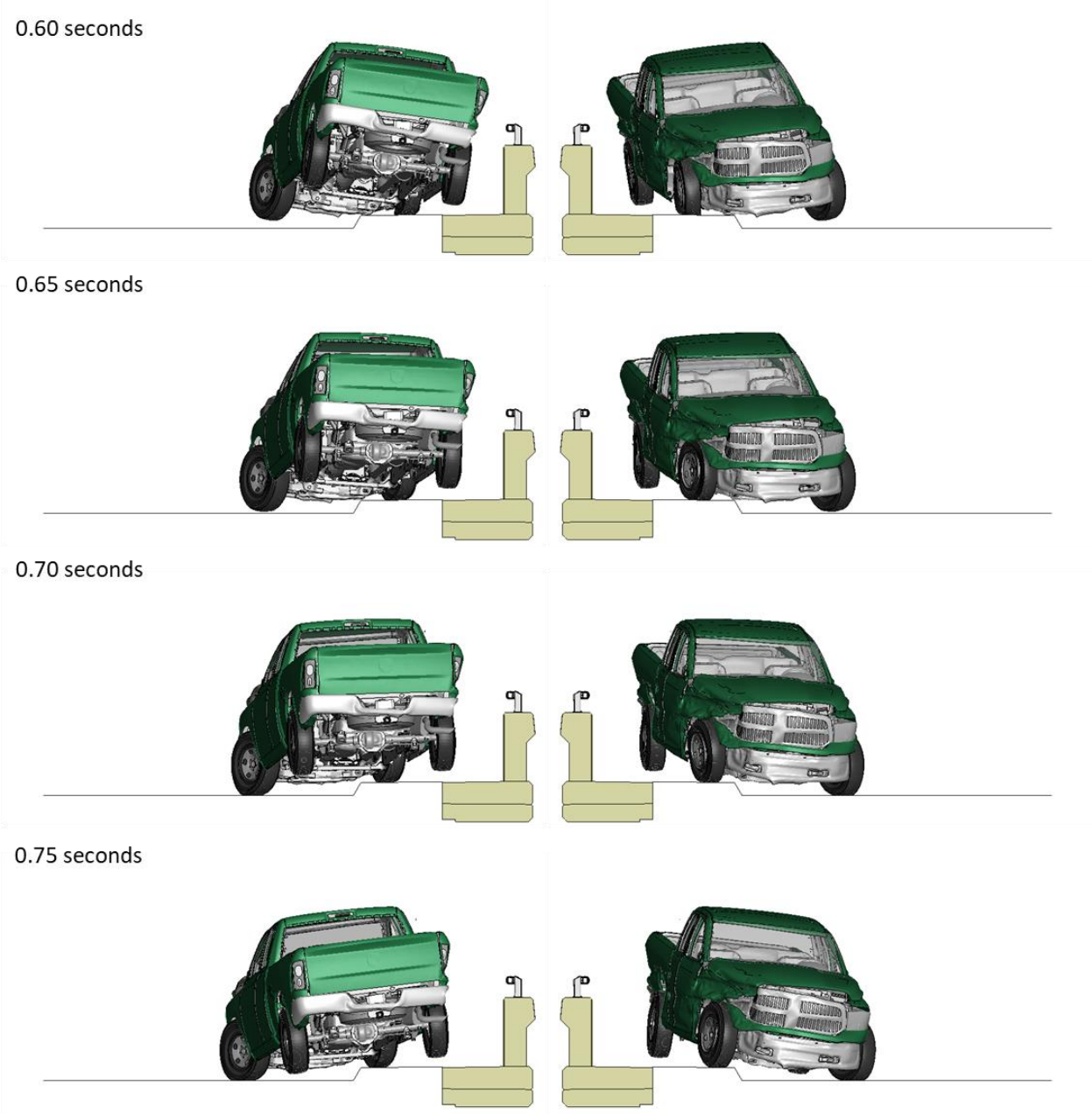

Figure 3 [CONTINUED] Sequential views from analysis of MASH Test 3-11 at 5.3 ft upstream of critical post from a front and back viewpoint (RHT Model).

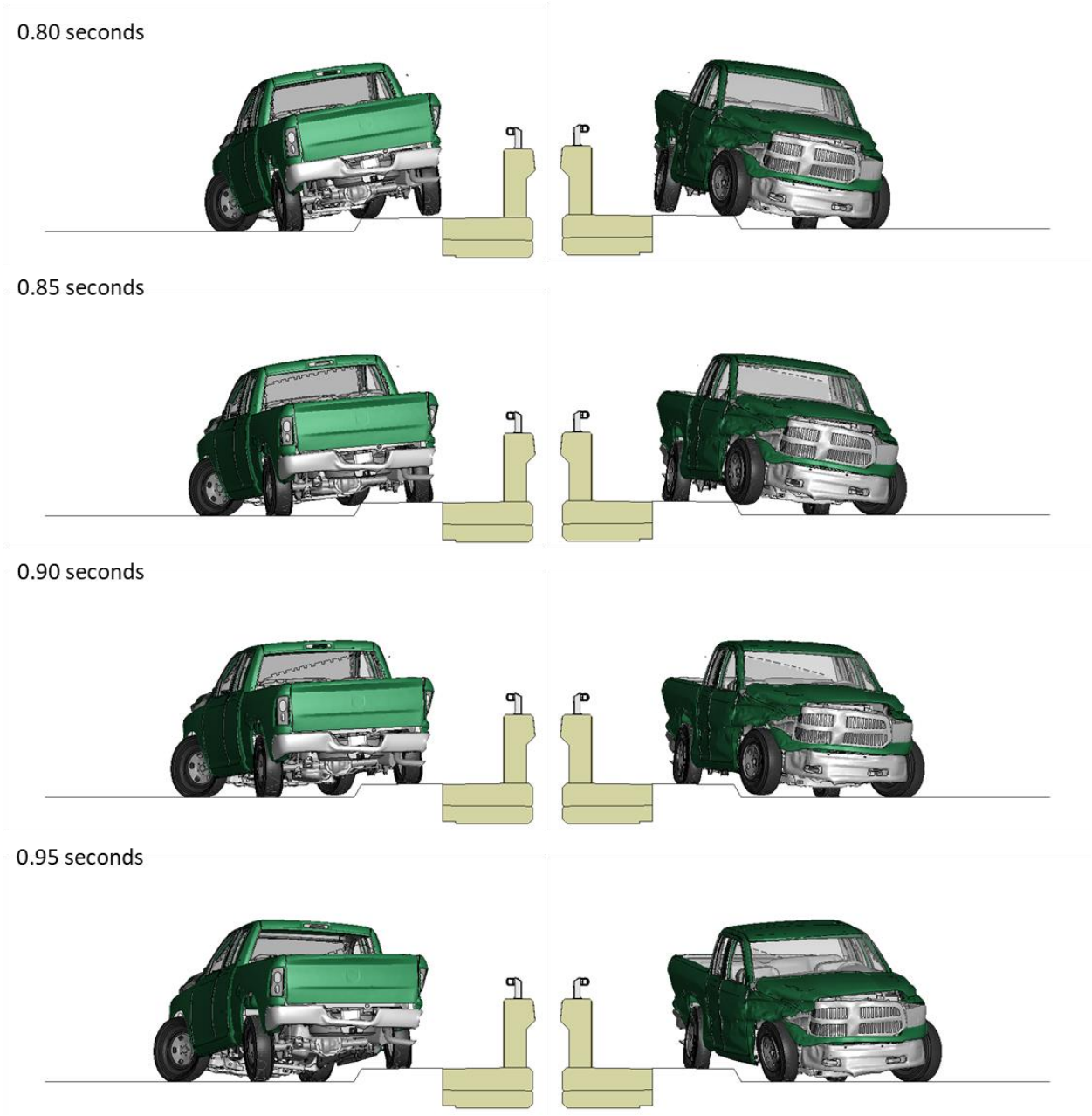

Figure 3 [CONTINUED] Sequential views from analysis of MASH Test 3-11 at 5.3 ft upstream of critical post from a front and back viewpoint (RHT Model).

Appendix J

Sequential Views for Test 3-10 at 3.6 ft Upstream of Transition (KC Model)

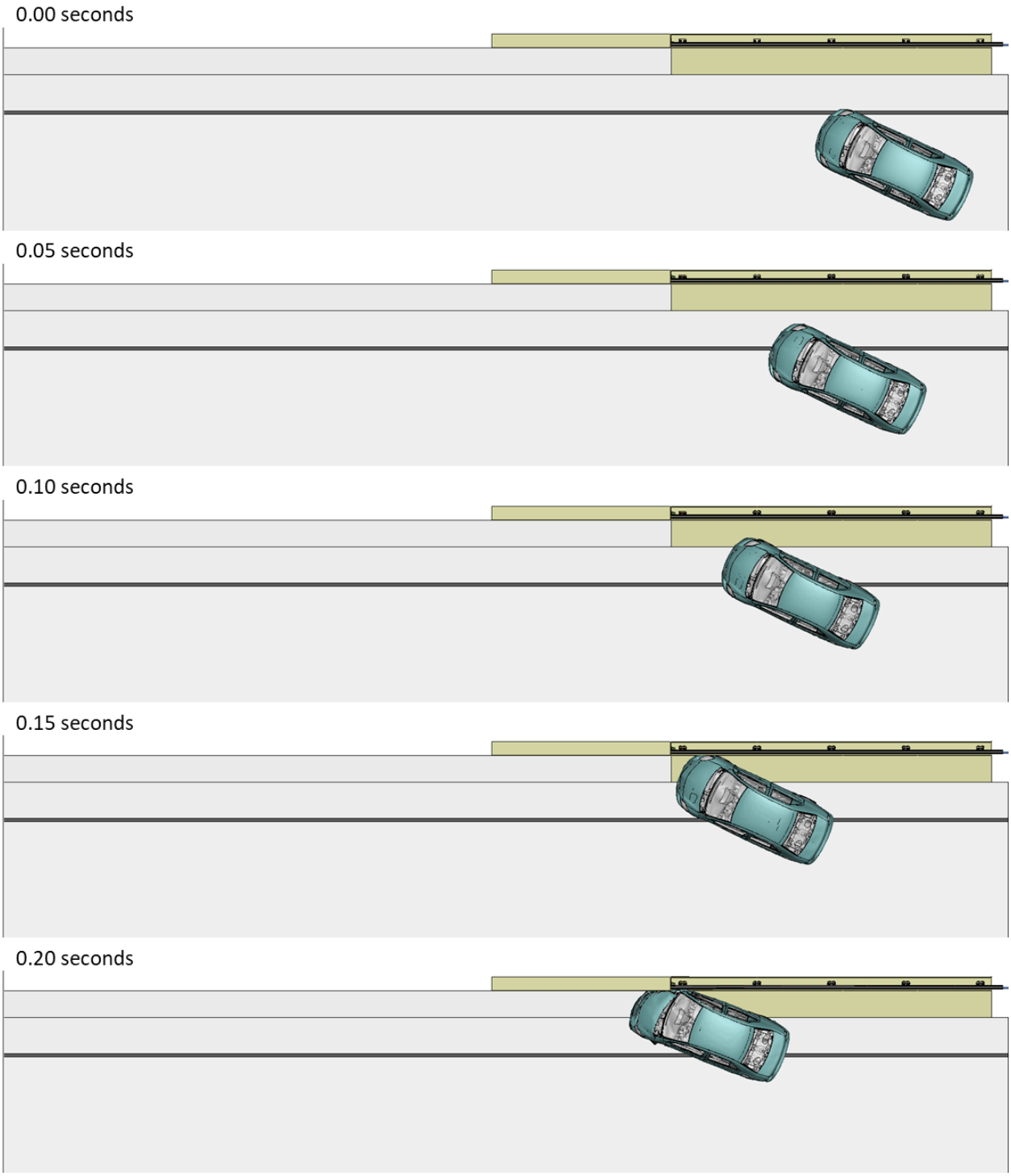

Figure 1. Sequential views from analysis of MASH Test 3-10 at 3.6 ft upstream of transition from an overhead viewpoint (KC Model).

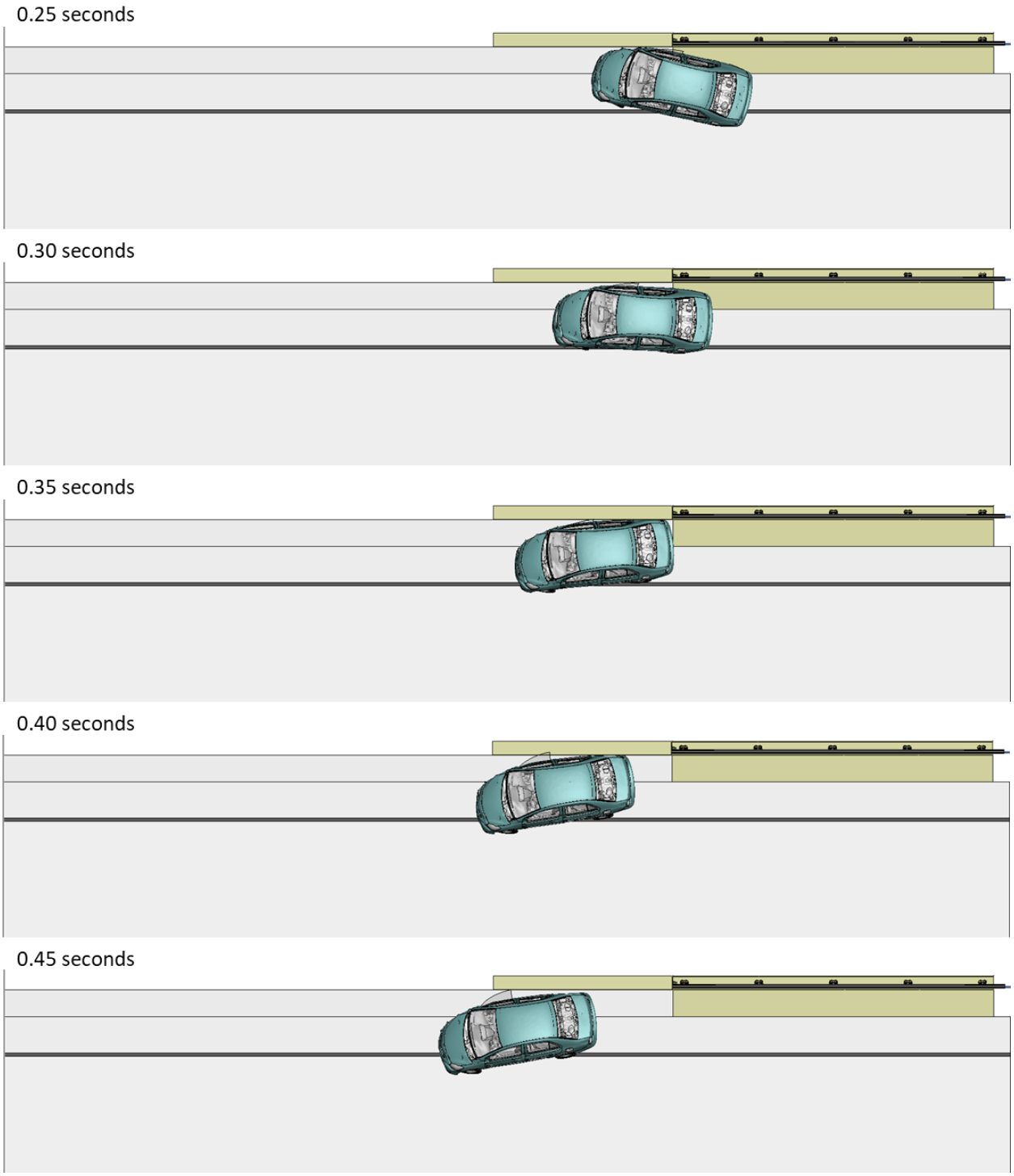

Figure 1 [CONTINUED] Sequential views from analysis of MASH Test 3-10 at 3.6 ft upstream of transition from an overhead viewpoint (KC Model).

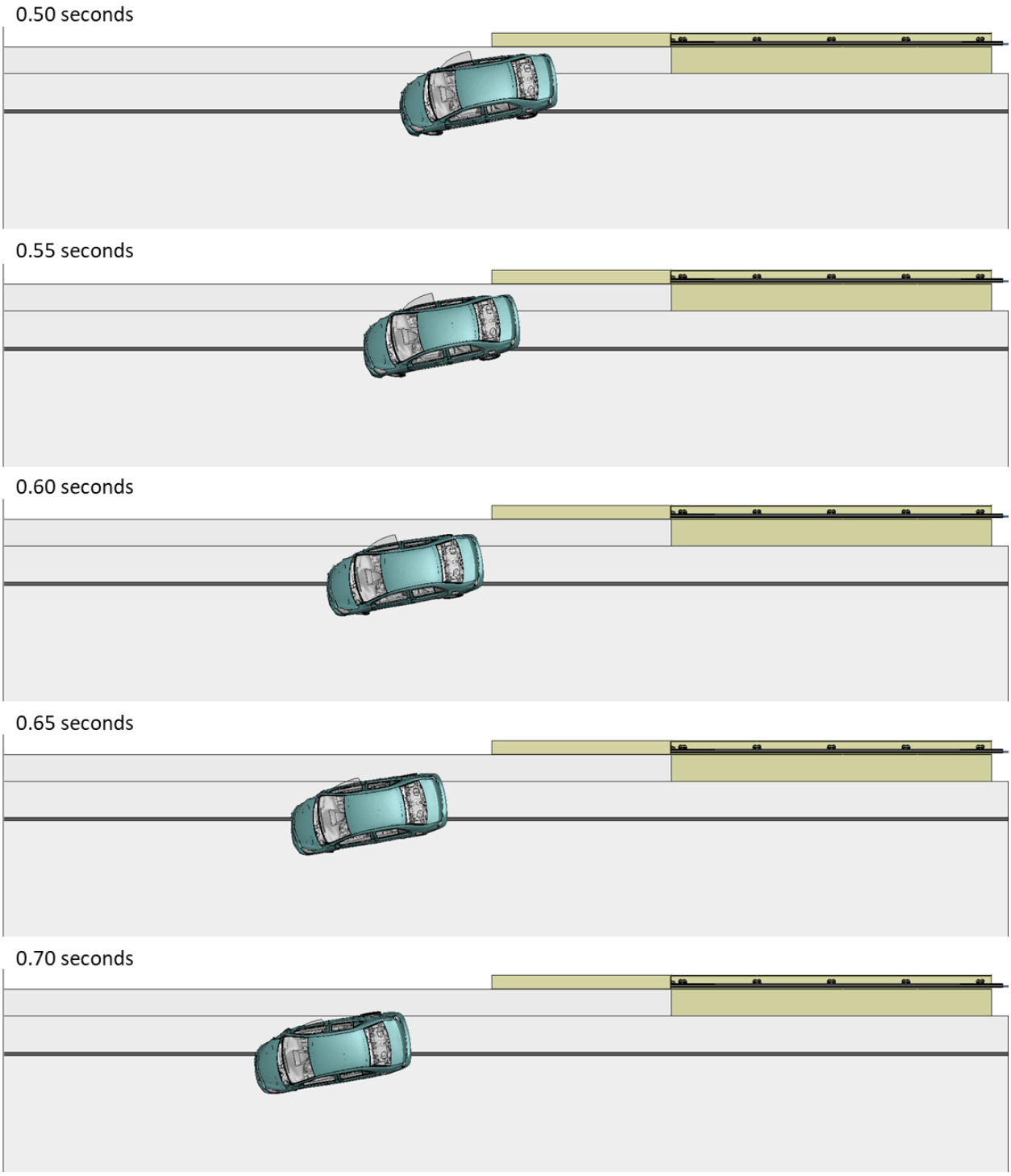

Figure 1 [CONTINUED] Sequential views from analysis of MASH Test 3-10 at 3.6 ft upstream of transition from an overhead viewpoint (KC Model).

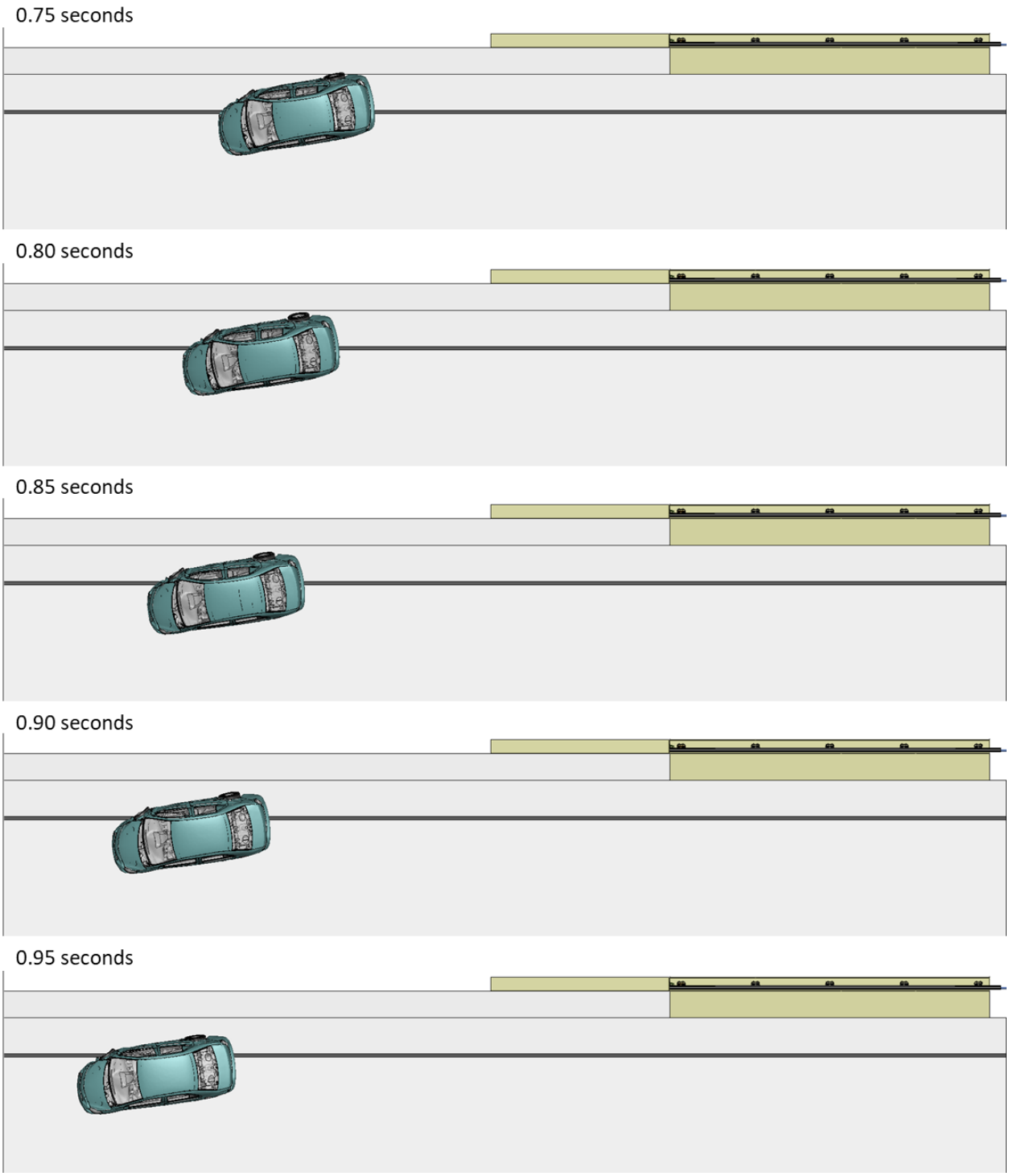

Figure 1 [CONTINUED] Sequential views from analysis of MASH Test 3-10 at 3.6 ft upstream of transition from an overhead viewpoint (KC Model).

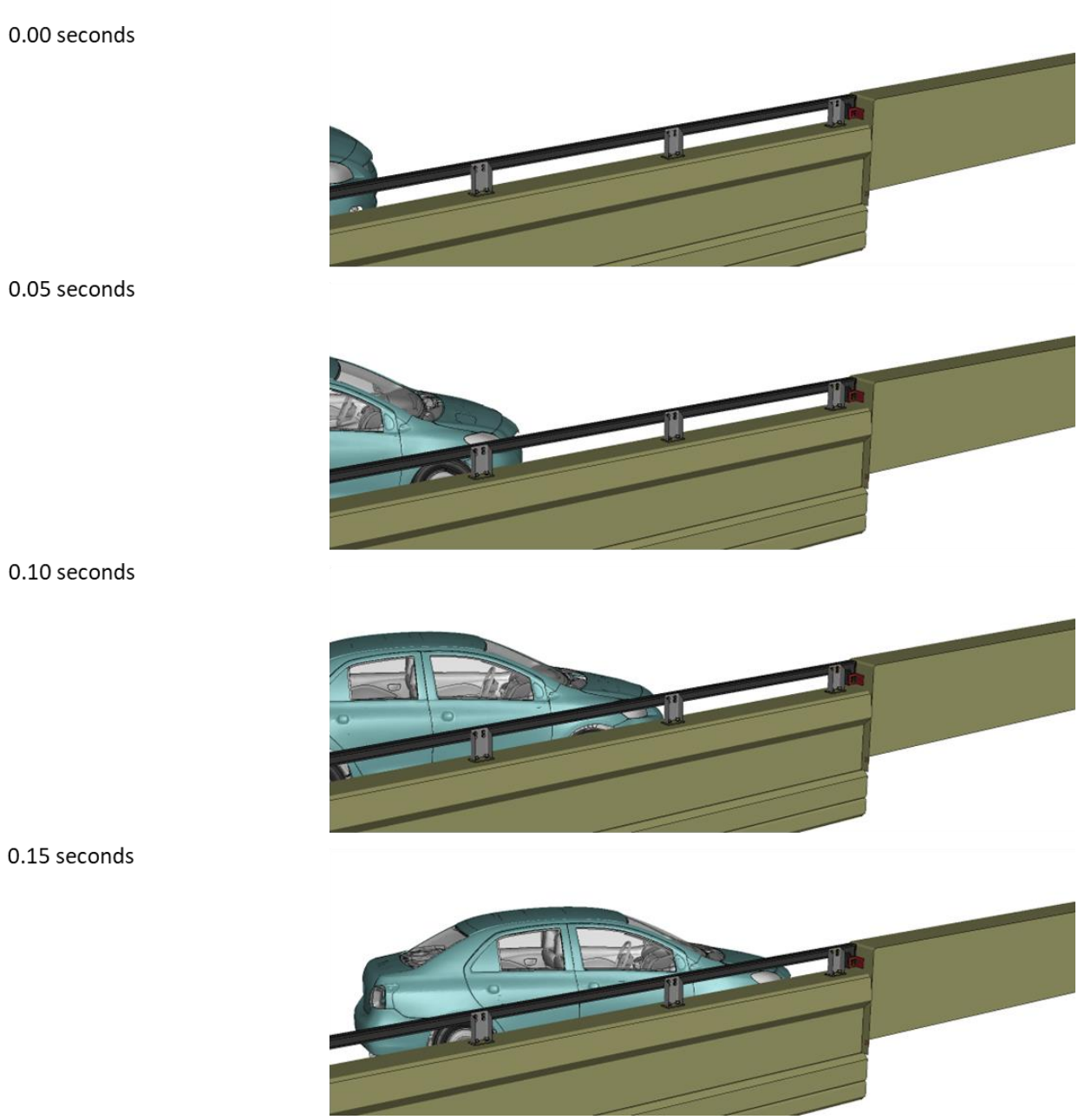

Figure 2. Sequential views from analysis of MASH Test 3-10 at 3.6 ft upstream of transition from an isometric viewpoint (KC Model).

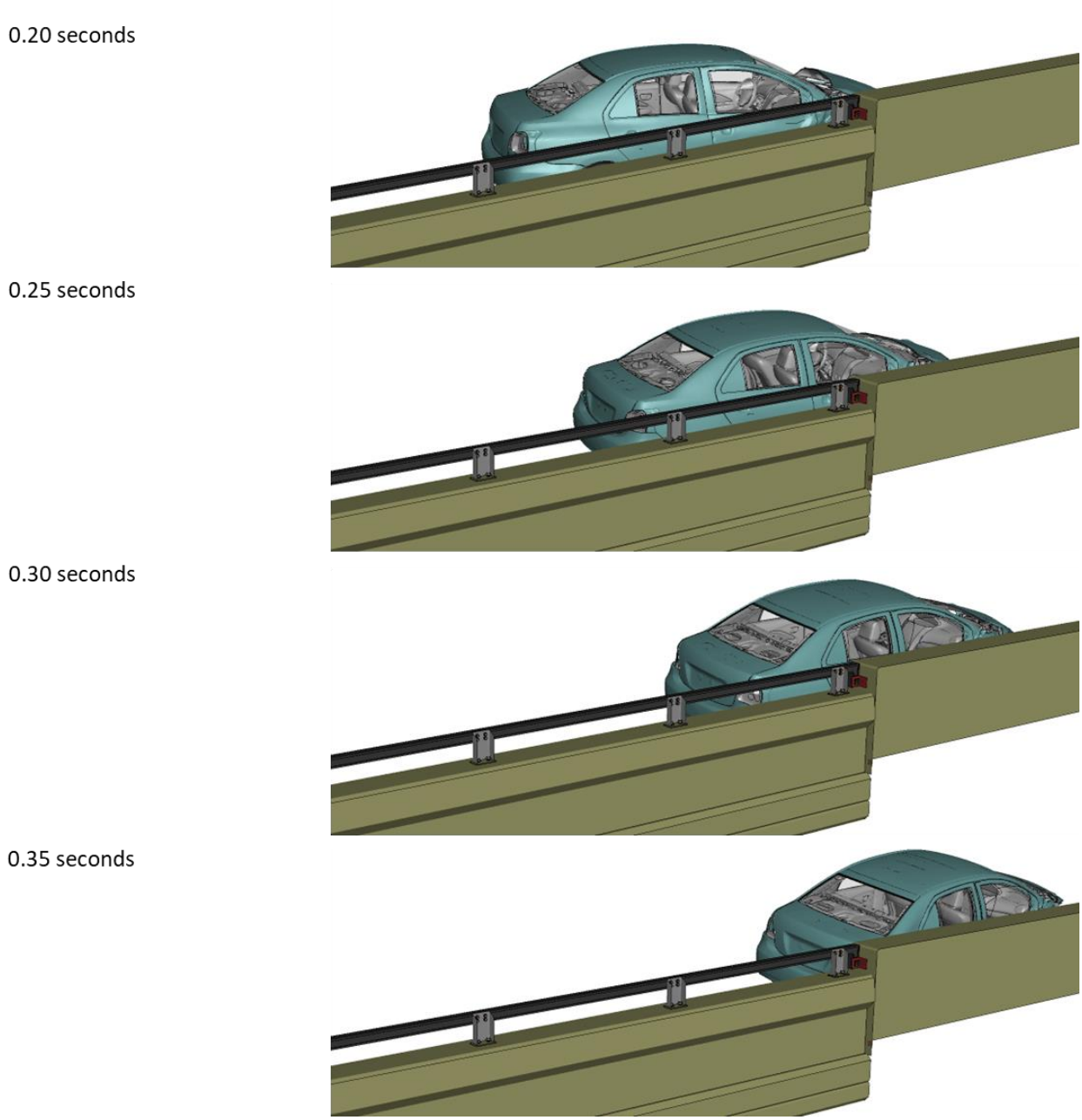

Figure 2 [CONTINUED] Sequential views from analysis of MASH Test 3-10 at 3.6 ft upstream of transition from an isometric viewpoint (KC Model).

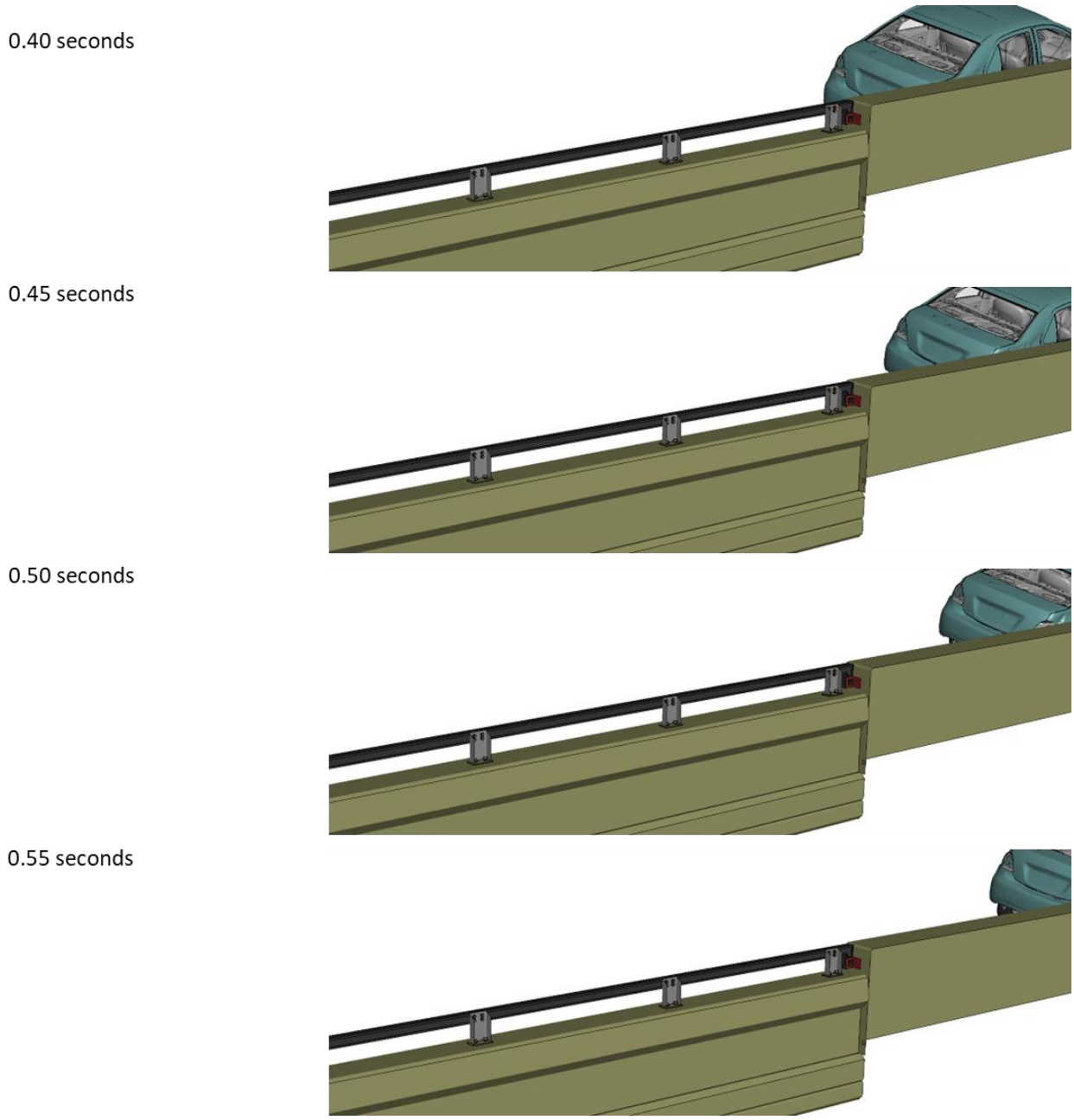

Figure 2 [CONTINUED] Sequential views from analysis of MASH Test 3-10 at 3.6 ft upstream of transition from an isometric viewpoint (KC Model).

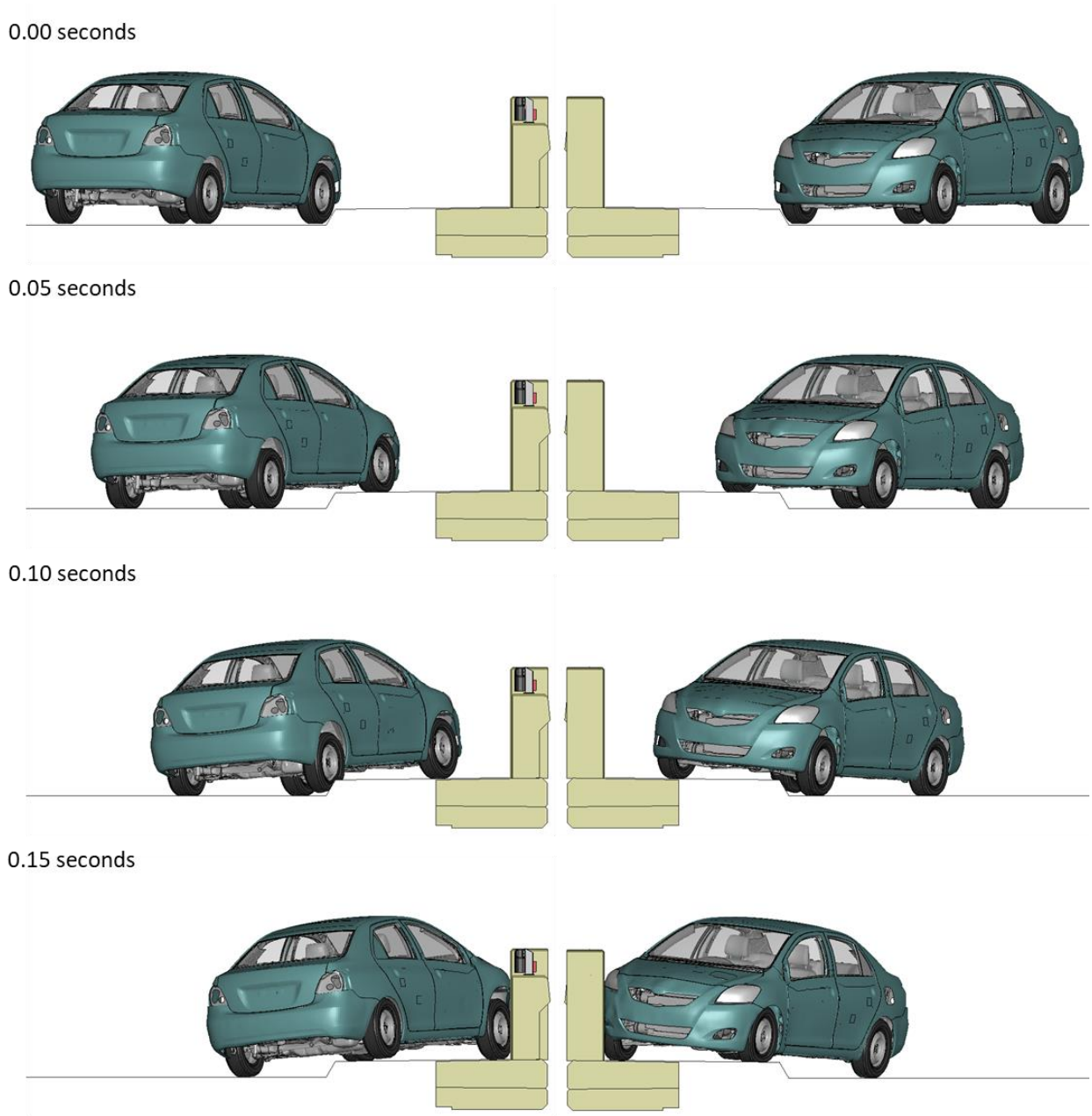

Figure 3. Sequential views from analysis of MASH Test 3-10 at 3.6 ft upstream of transition from a front and back viewpoint (KC Model).

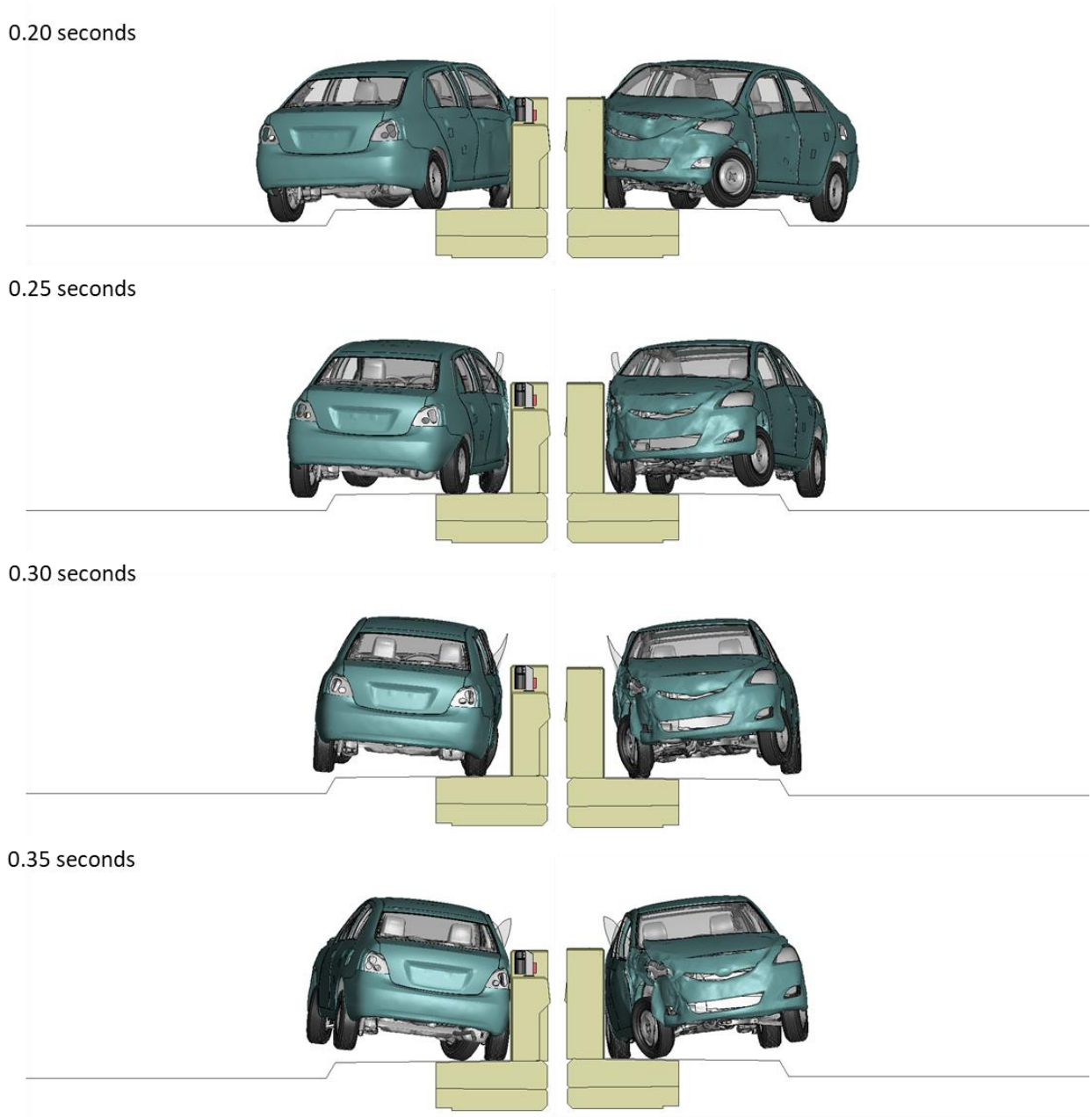

Figure 3 [CONTINUED] Sequential views from analysis of MASH Test 3-10 at 3.6 ft upstream of transition from a front and back viewpoint (KC Model).

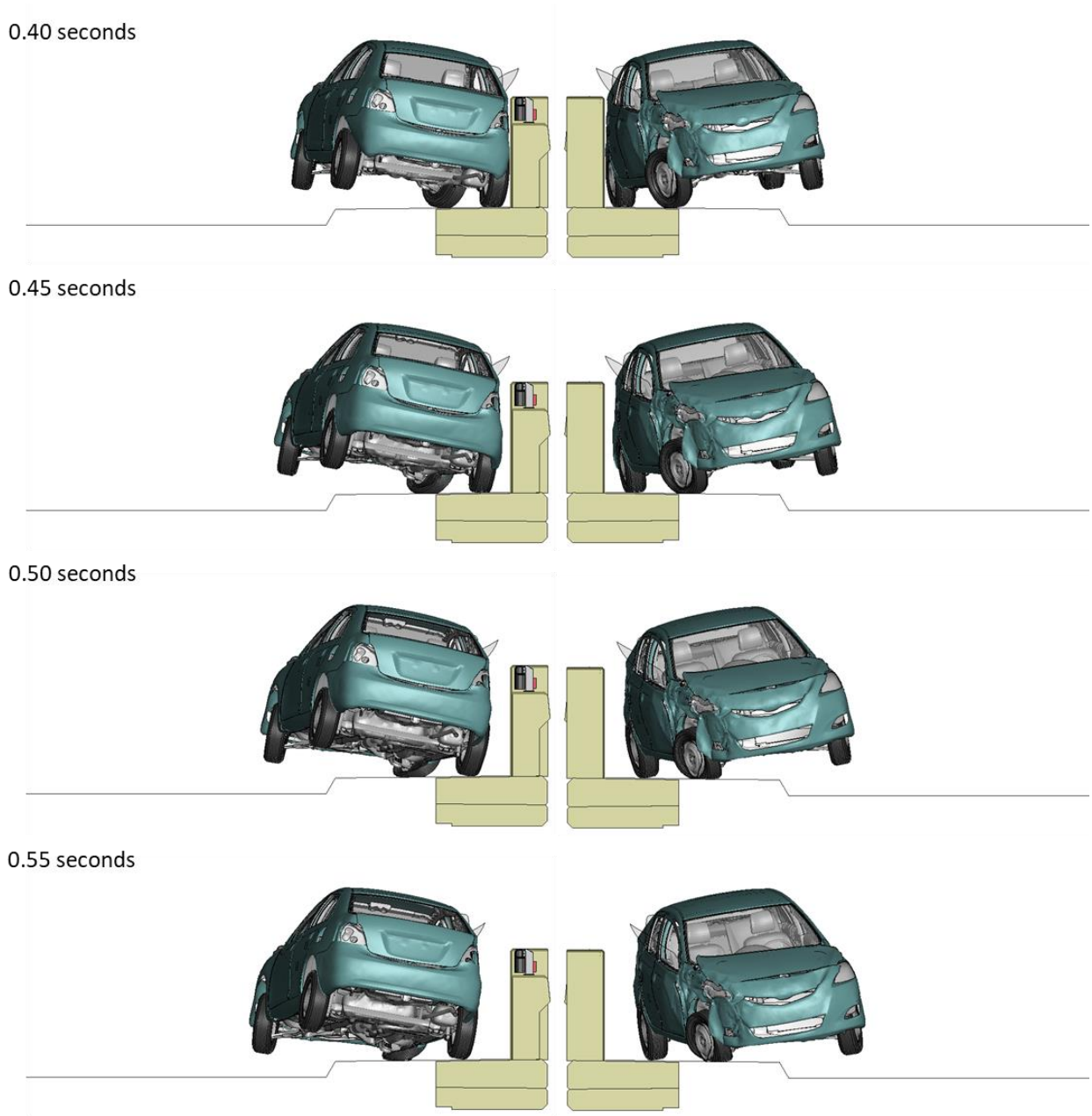

Figure 3 [CONTINUED] Sequential views from analysis of MASH Test 3-10 at 3.6 ft upstream of transition from a front and back viewpoint (KC Model).

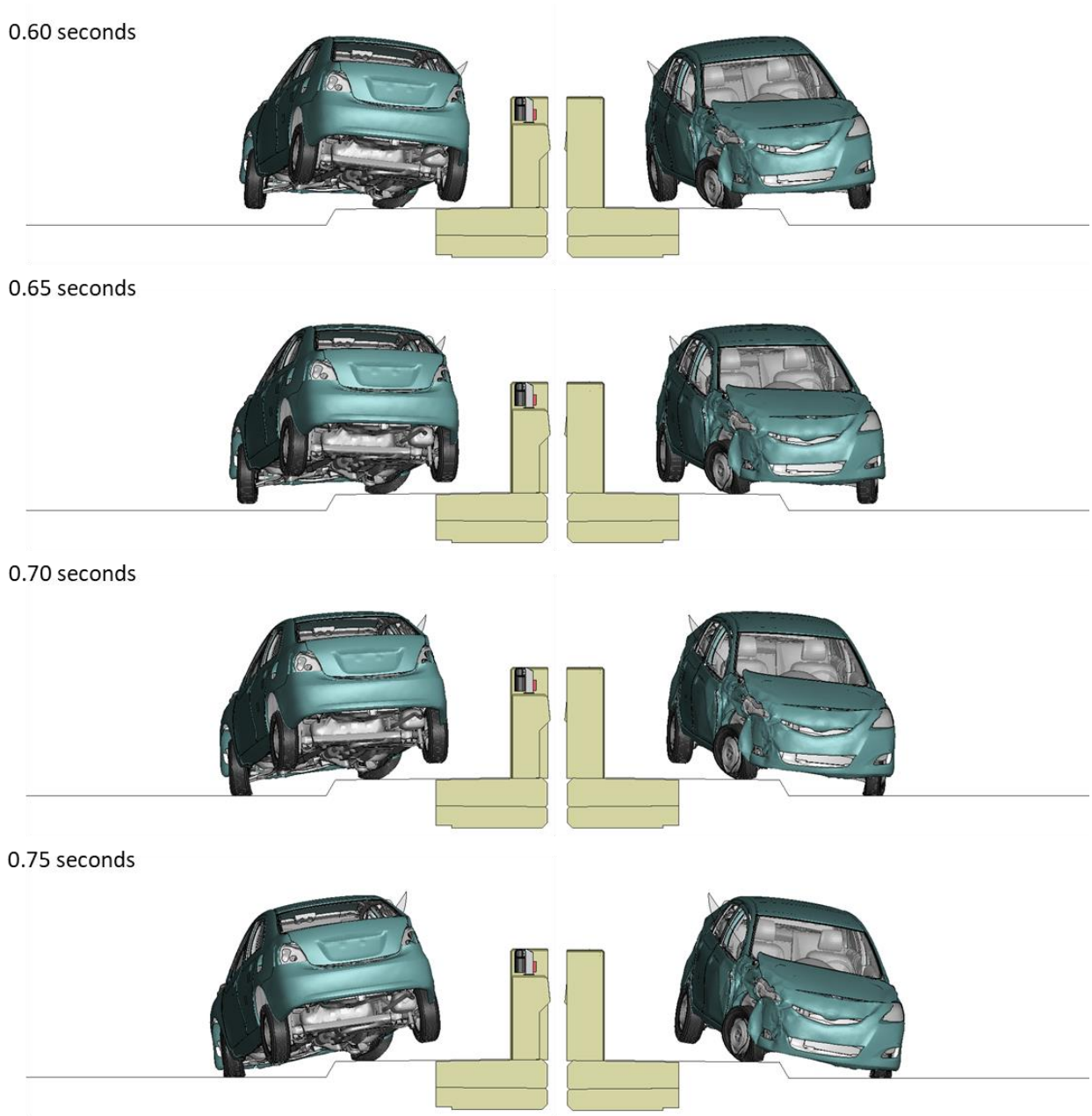

Figure 3 [CONTINUED] Sequential views from analysis of MASH Test 3-10 at 3.6 ft upstream of transition from a front and back viewpoint (KC Model).

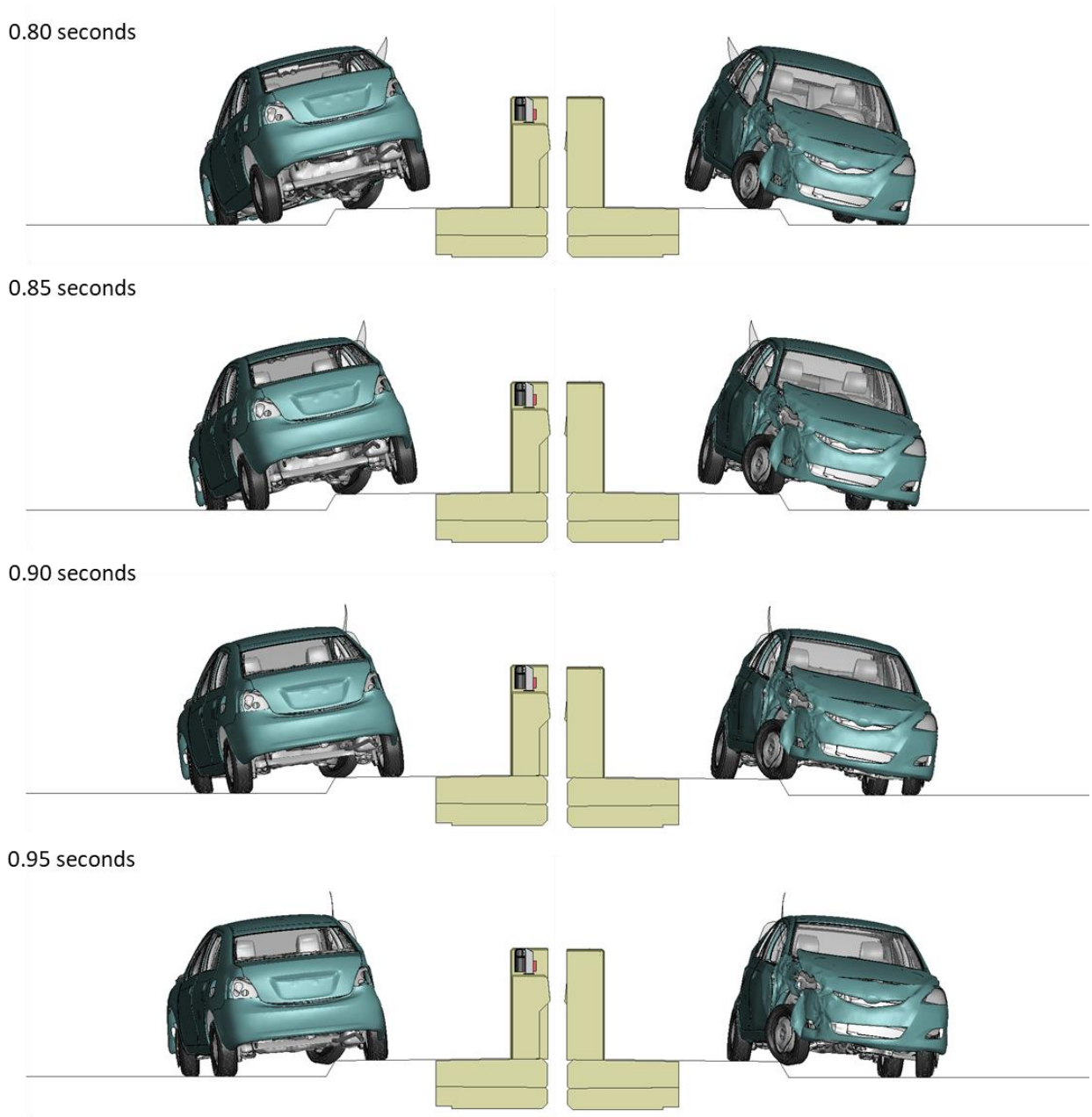

Figure 3 [CONTINUED] Sequential views from analysis of MASH Test 3-10 at 3.6 ft upstream of transition from a front and back viewpoint (KC Model).

Appendix K

Sequential Views for Test 3-10 at 4.6 ft Upstream of Transition (KC Model)

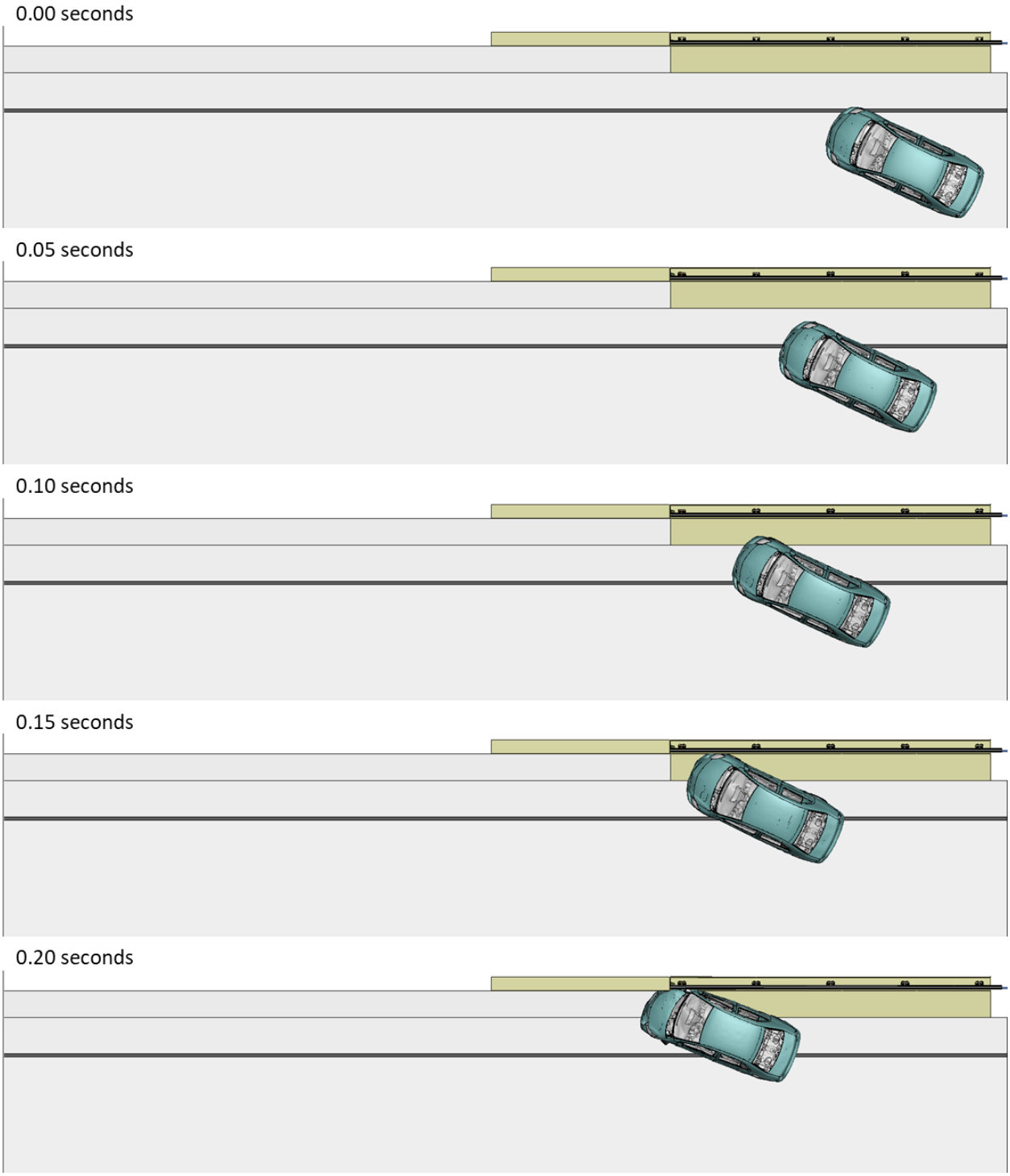

Figure 1. Sequential views from analysis of MASH Test 3-10 at 4.6 ft upstream of transition from an overhead viewpoint (KC Model).

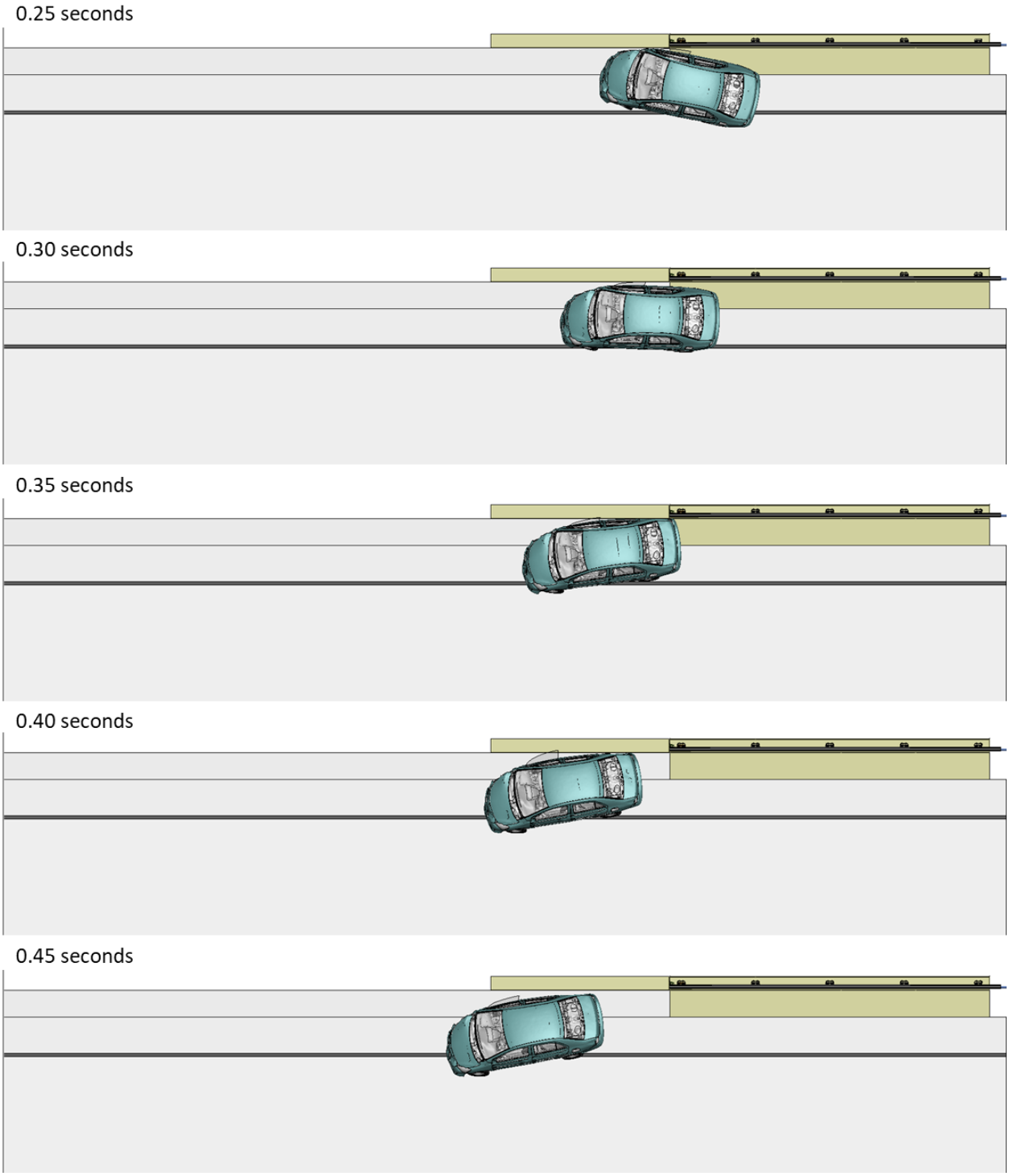

Figure 1 [CONTINUED] Sequential views from analysis of MASH Test 3-10 at 4.6 ft upstream of transition from an overhead viewpoint (KC Model).

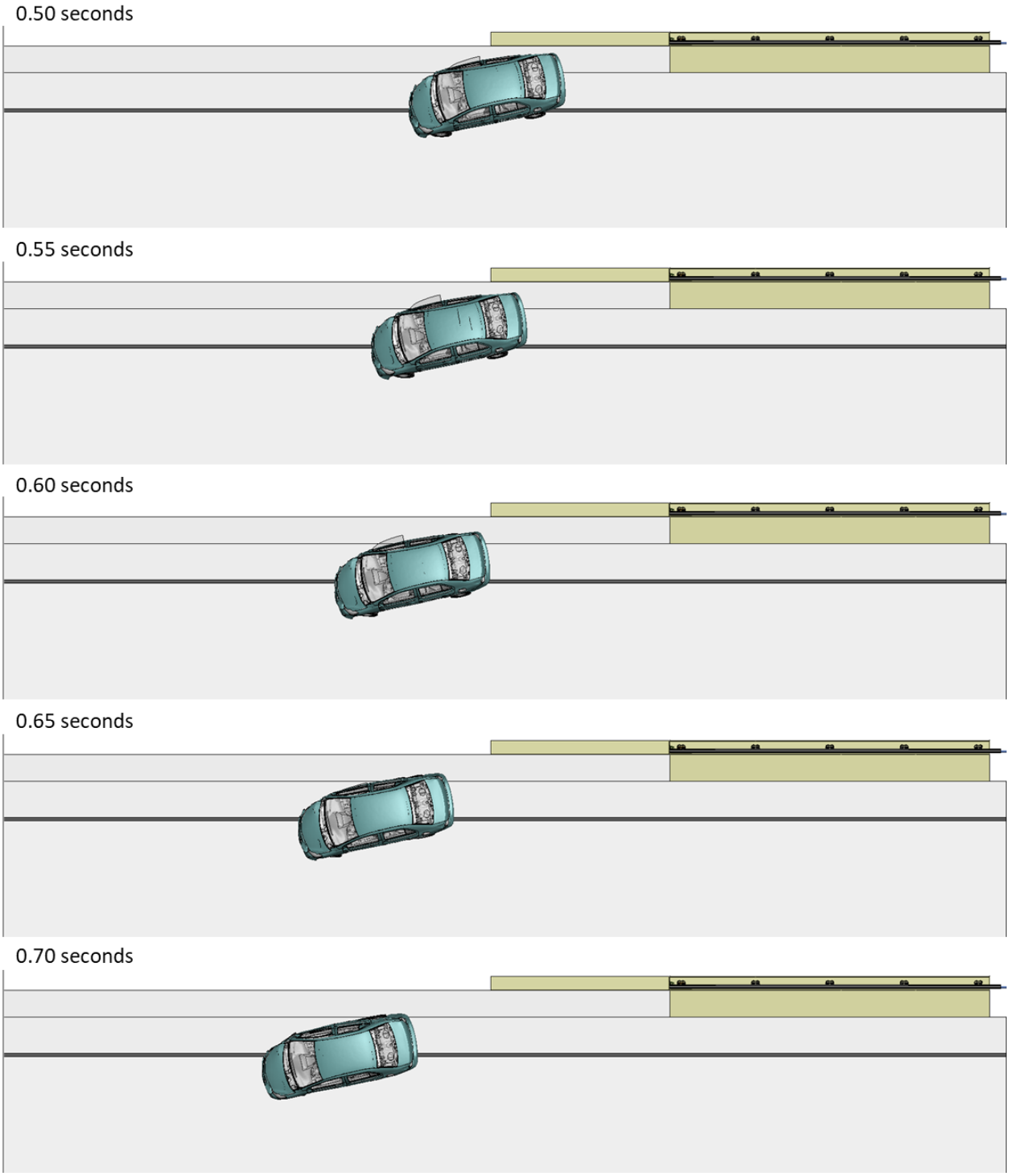

Figure 1 [CONTINUED] Sequential views from analysis of MASH Test 3-10 at 4.6 ft upstream of transition from an overhead viewpoint (KC Model).

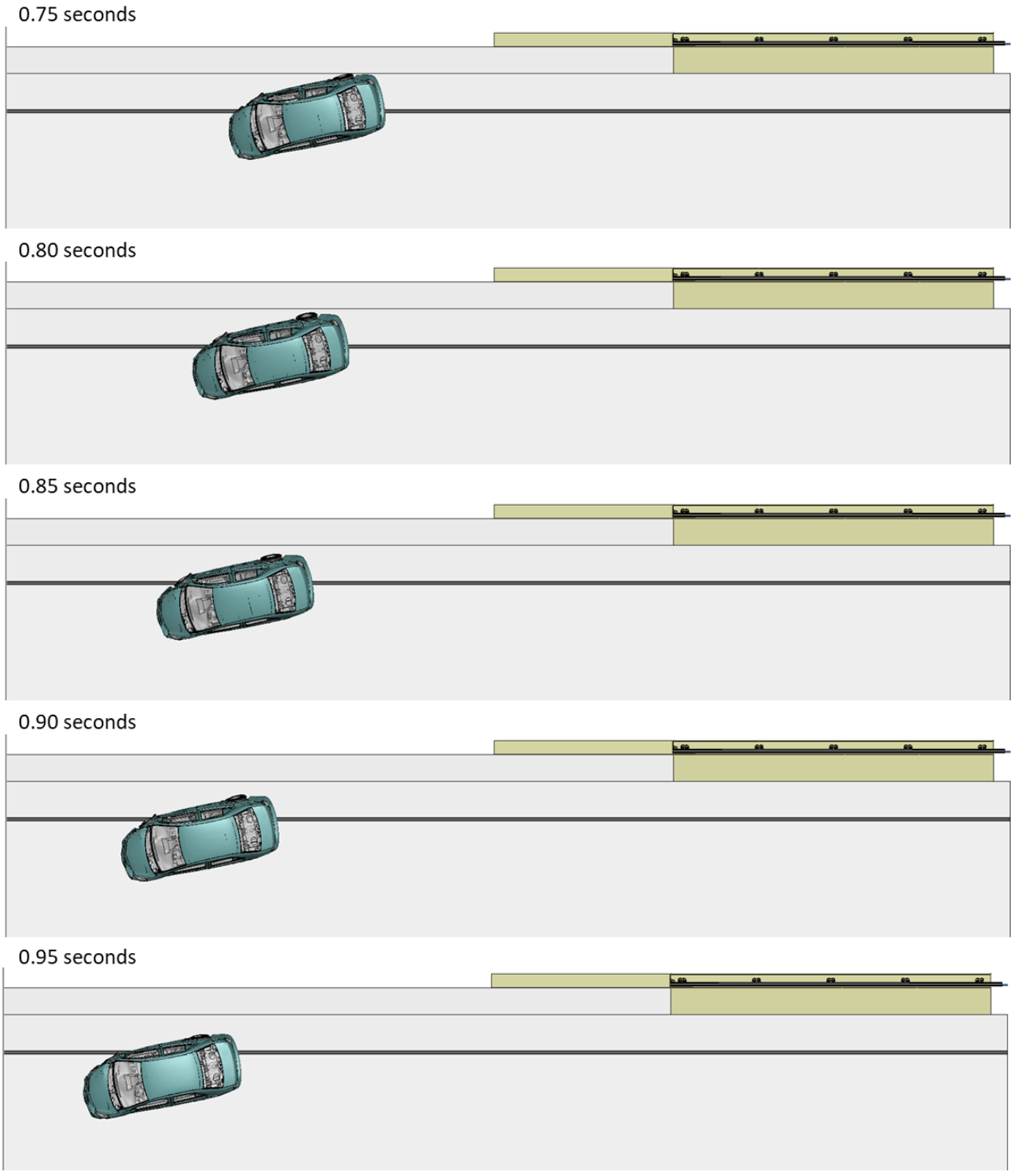

Figure 1 [CONTINUED] Sequential views from analysis of MASH Test 3-10 at 4.6 ft upstream of transition from an overhead viewpoint (KC Model).

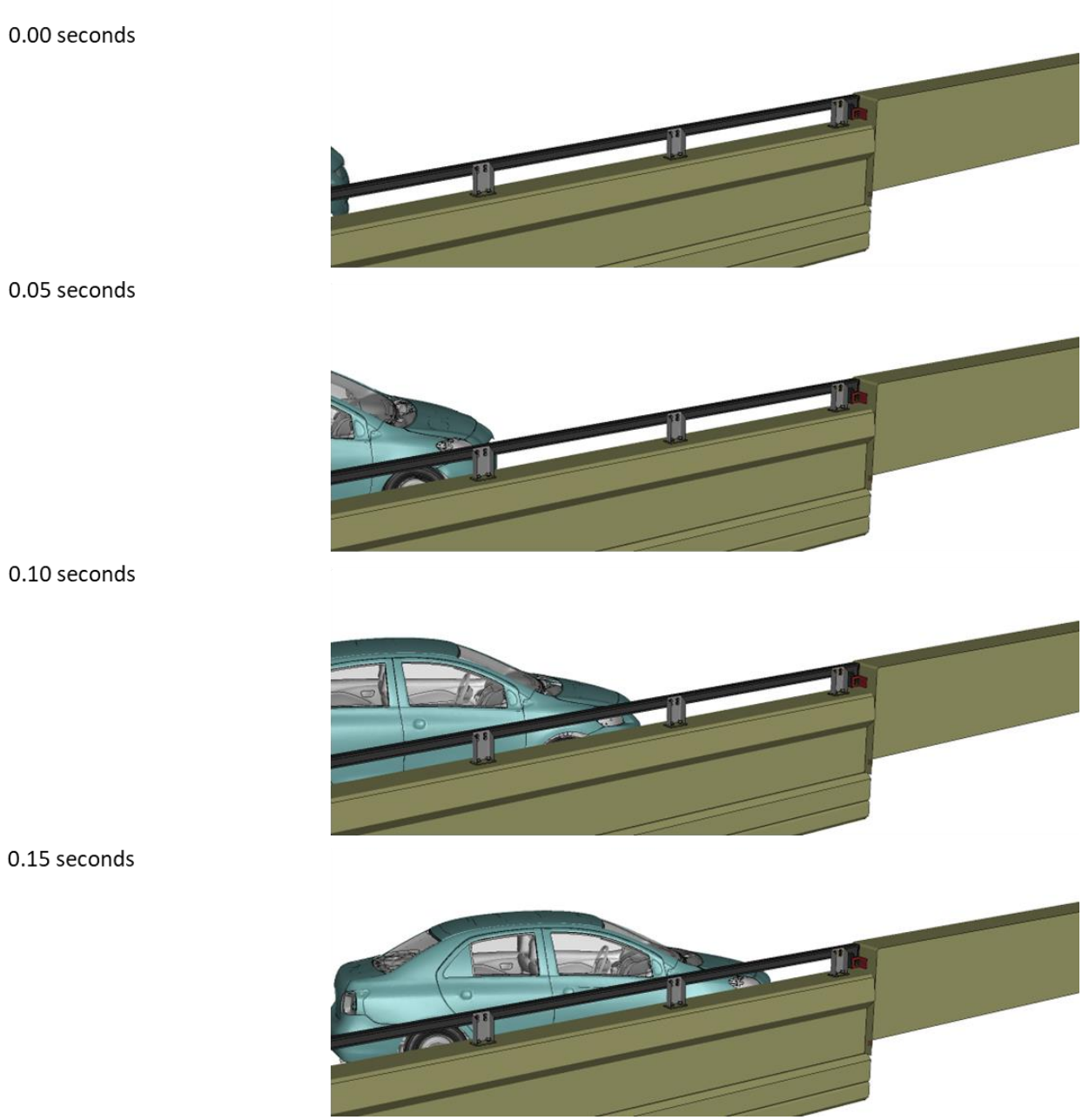

Figure 2. Sequential views from analysis of MASH Test 3-10 at 4.6 ft upstream of transition from an isometric viewpoint (KC Model).

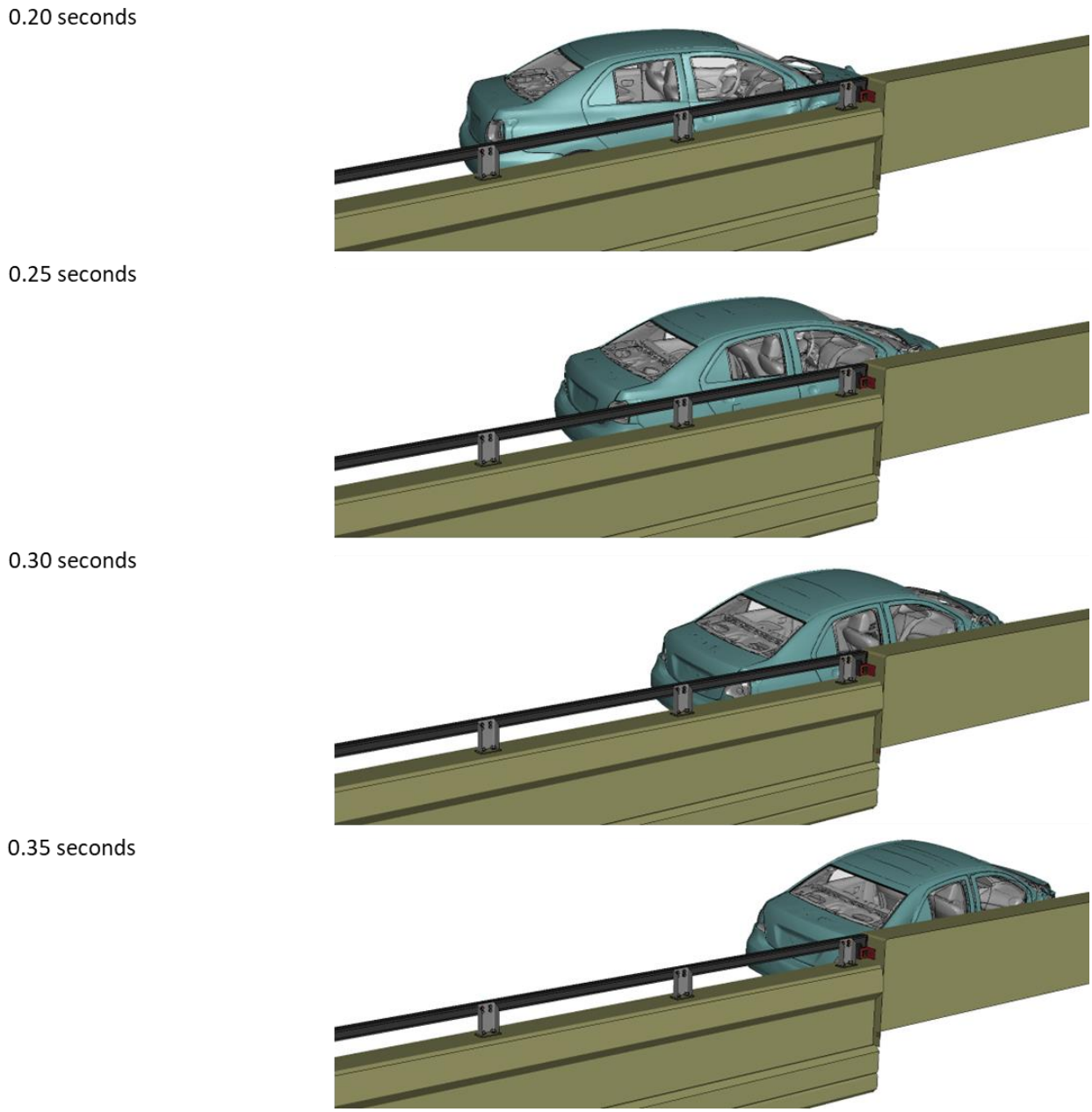

Figure 2 [CONTINUED] Sequential views from analysis of MASH Test 3-10 at 4.6 ft upstream of transition from an isometric viewpoint (KC Model).

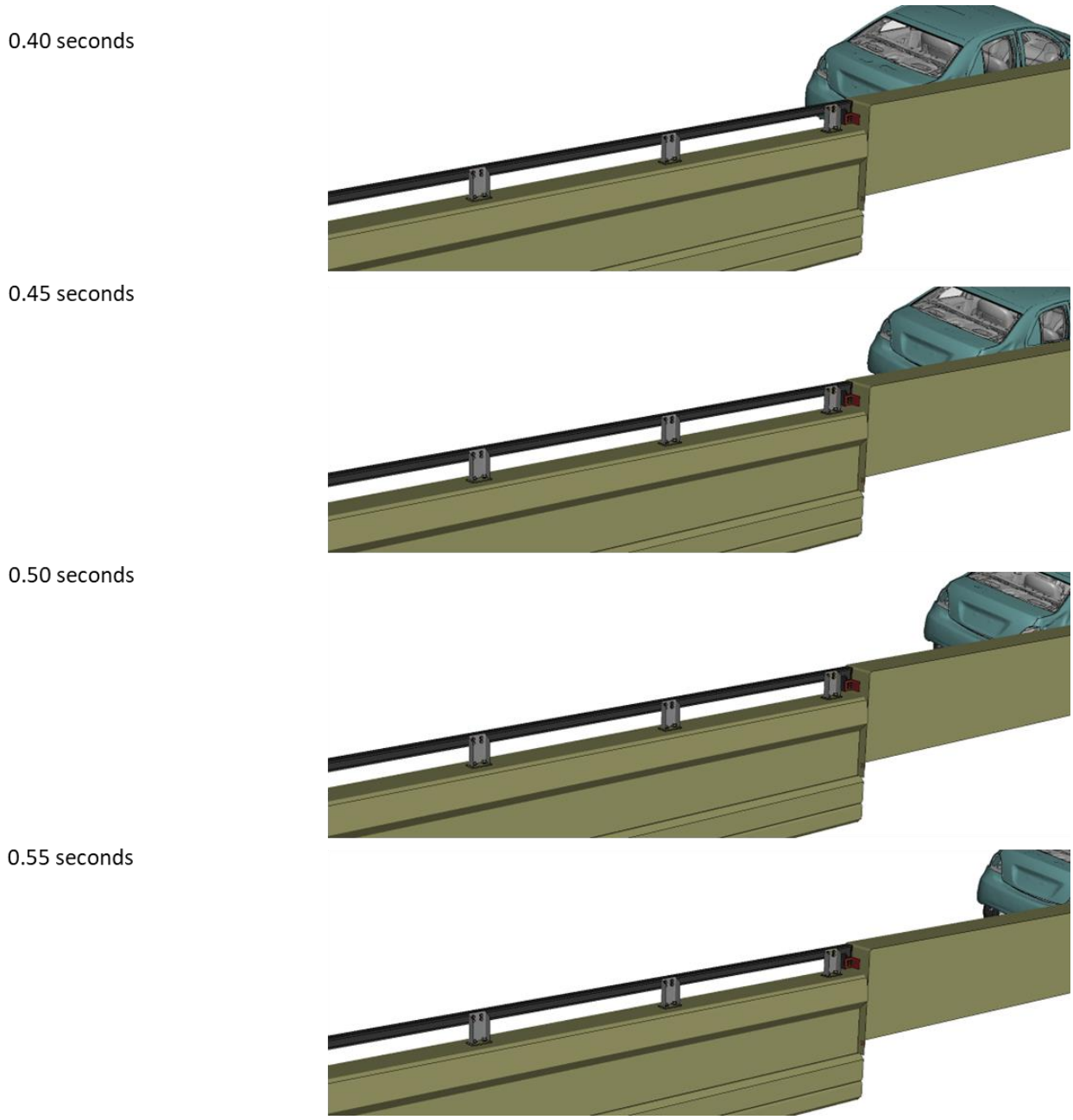

Figure 2 [CONTINUED] Sequential views from analysis of MASH Test 3-10 at 4.6 ft upstream of transition from an isometric viewpoint (KC Model).

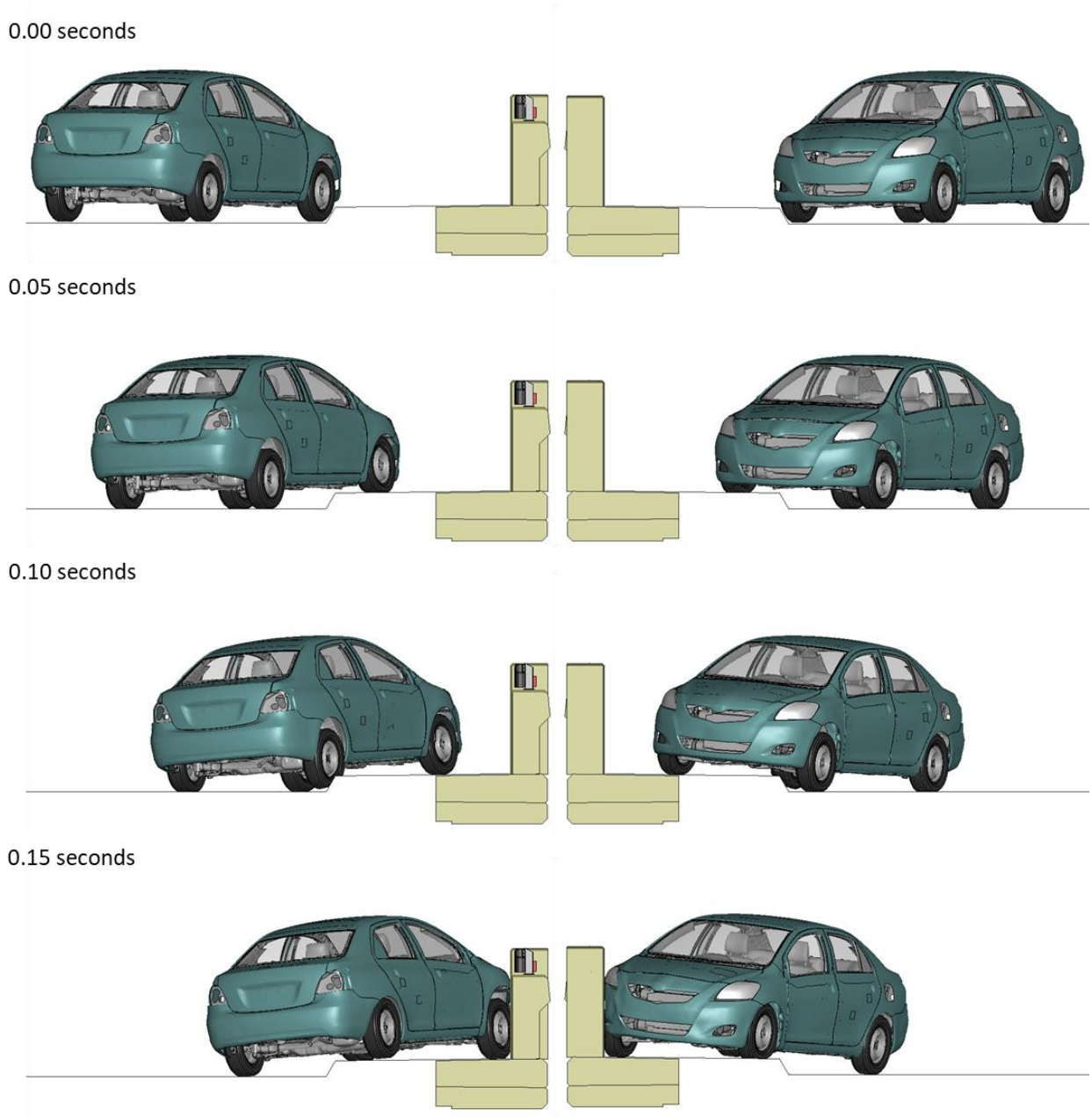

Figure 3. Sequential views from analysis of MASH Test 3-10 at 4.6 ft upstream of transition from a front and back viewpoint (KC Model).

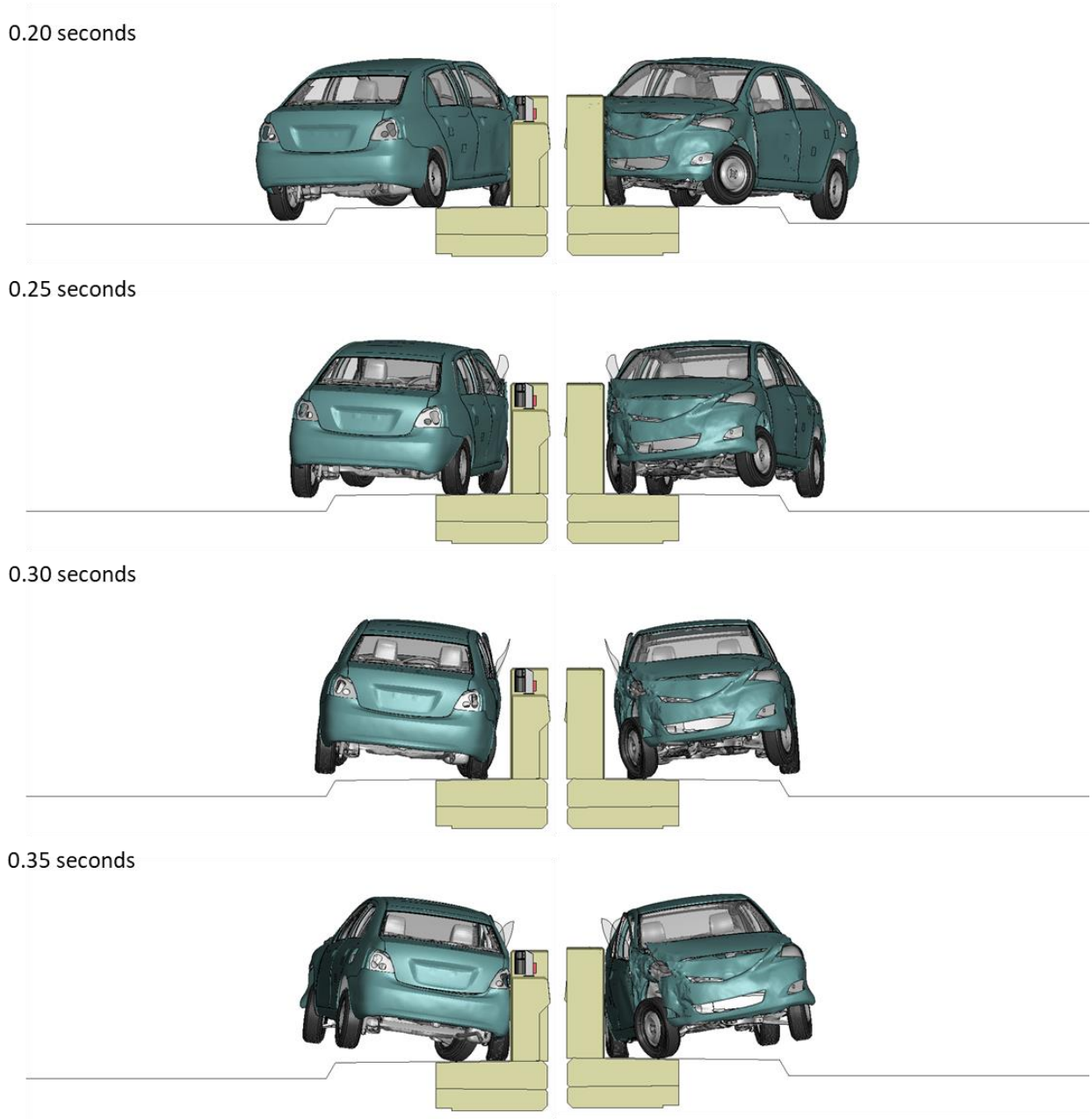

Figure 3 [CONTINUED] Sequential views from analysis of MASH Test 3-10 at 4.6 ft upstream of transition from a front and back viewpoint (KC Model).

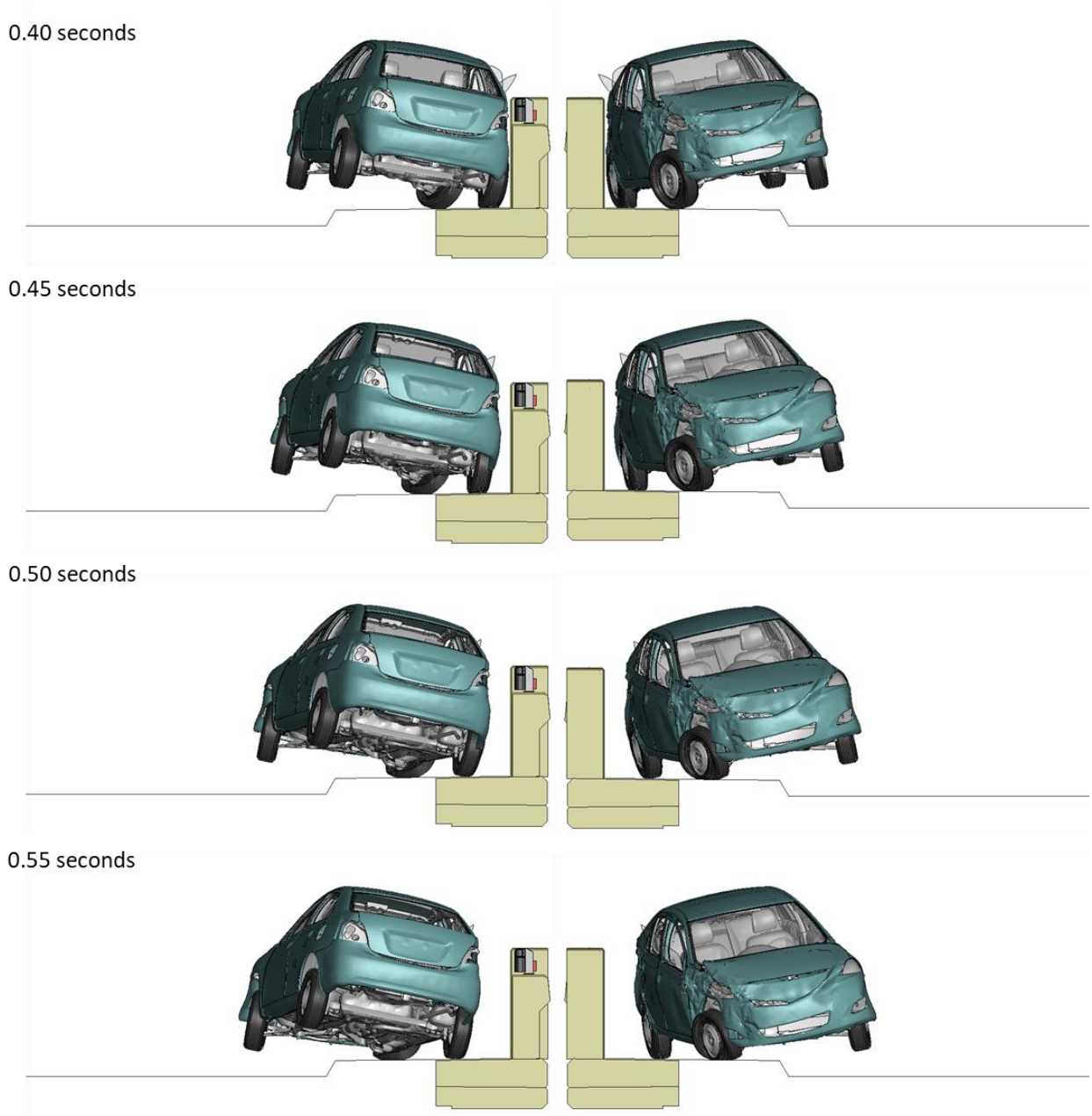

Figure 3 [CONTINUED] Sequential views from analysis of MASH Test 3-10 at 4.6 ft upstream of transition from a front and back viewpoint (KC Model).

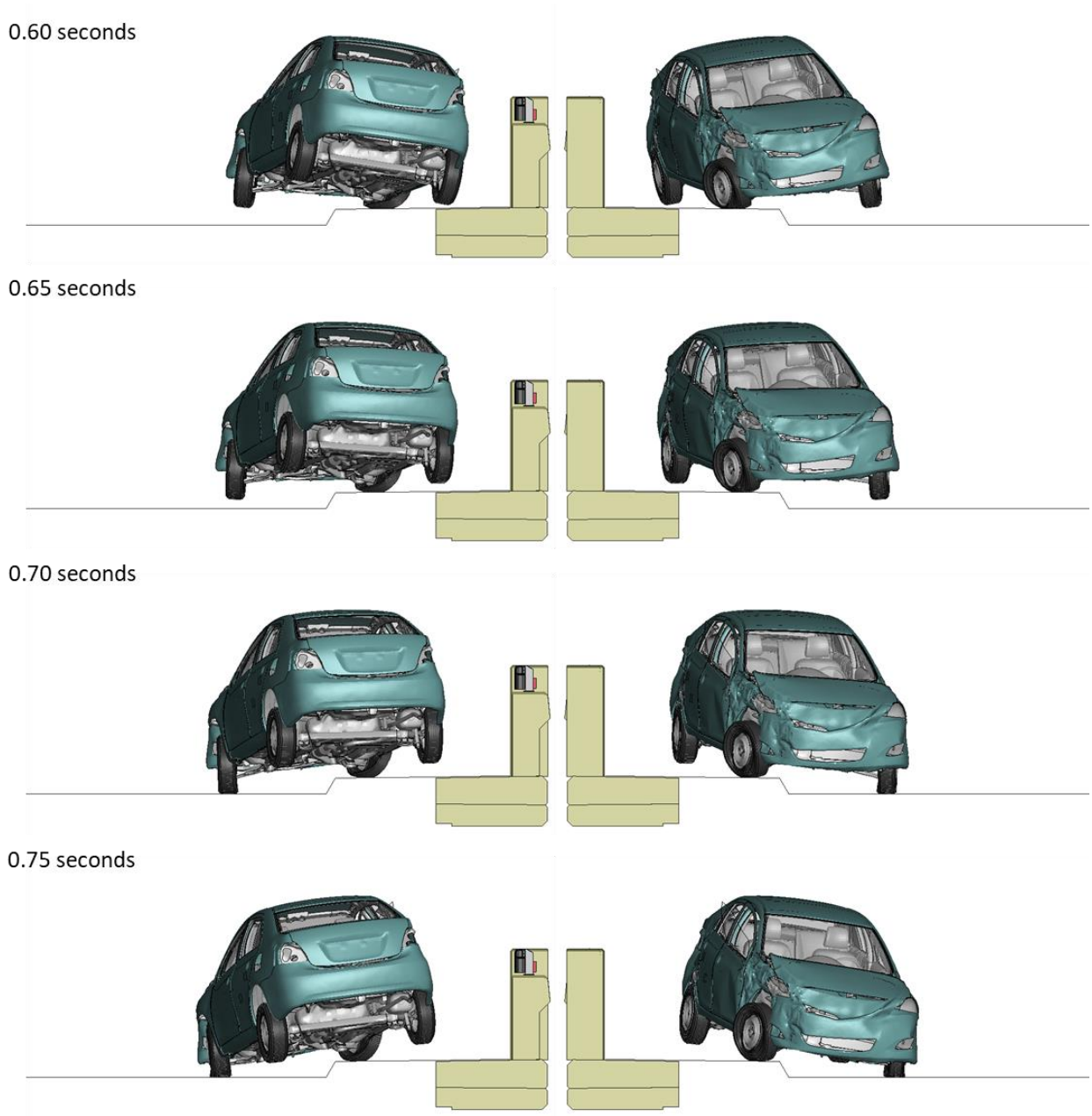

Figure 3 [CONTINUED] Sequential views from analysis of MASH Test 3-10 at 4.6 ft upstream of transition from a front and back viewpoint (KC Model).

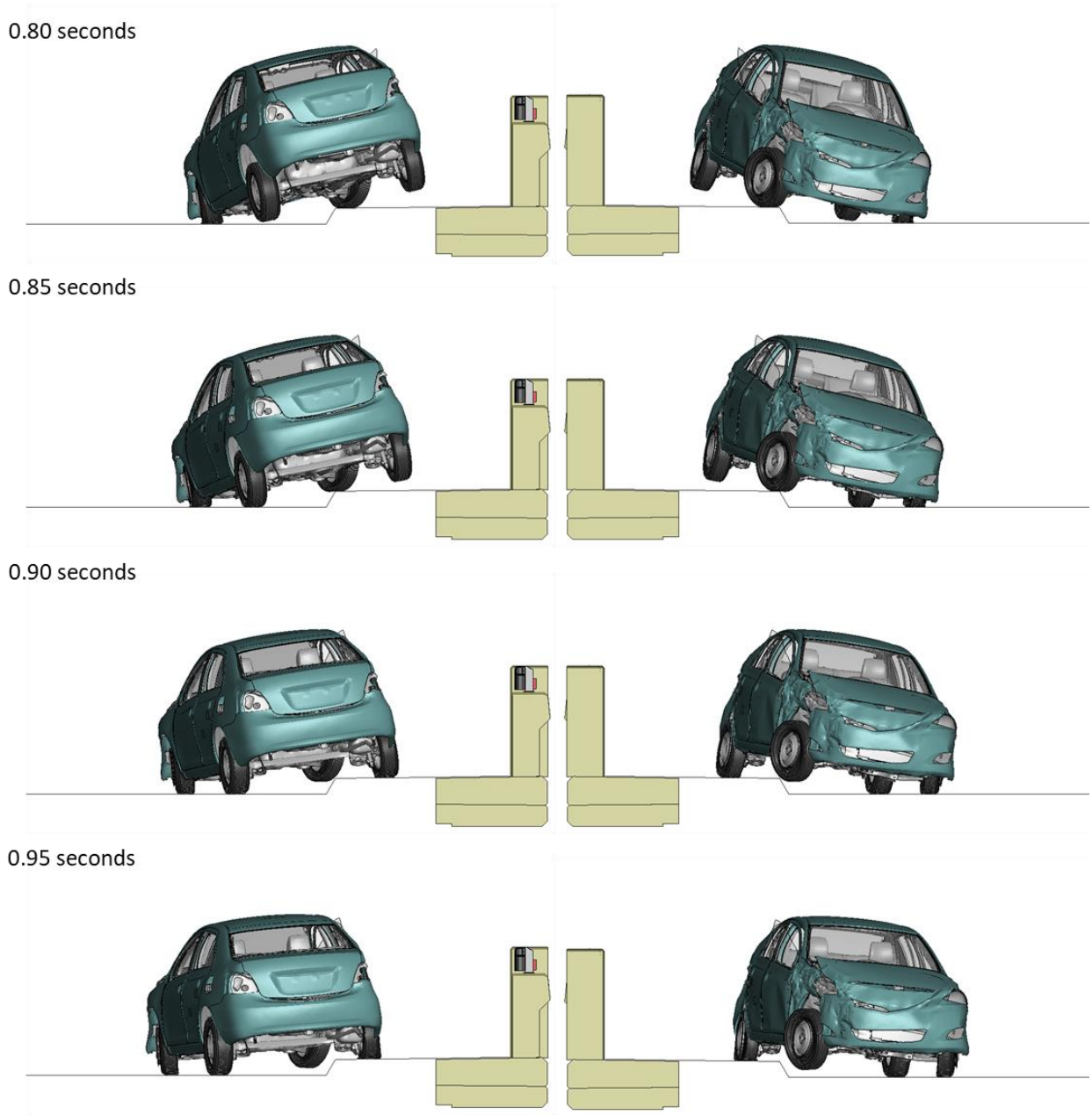

Figure 3 [CONTINUED] Sequential views from analysis of MASH Test 3-10 at 4.6 ft upstream of transition from a front and back viewpoint (KC Model).

Appendix L

Sequential Views for Test 3-11 at 4.26 ft Upstream of Transition (KC Model)

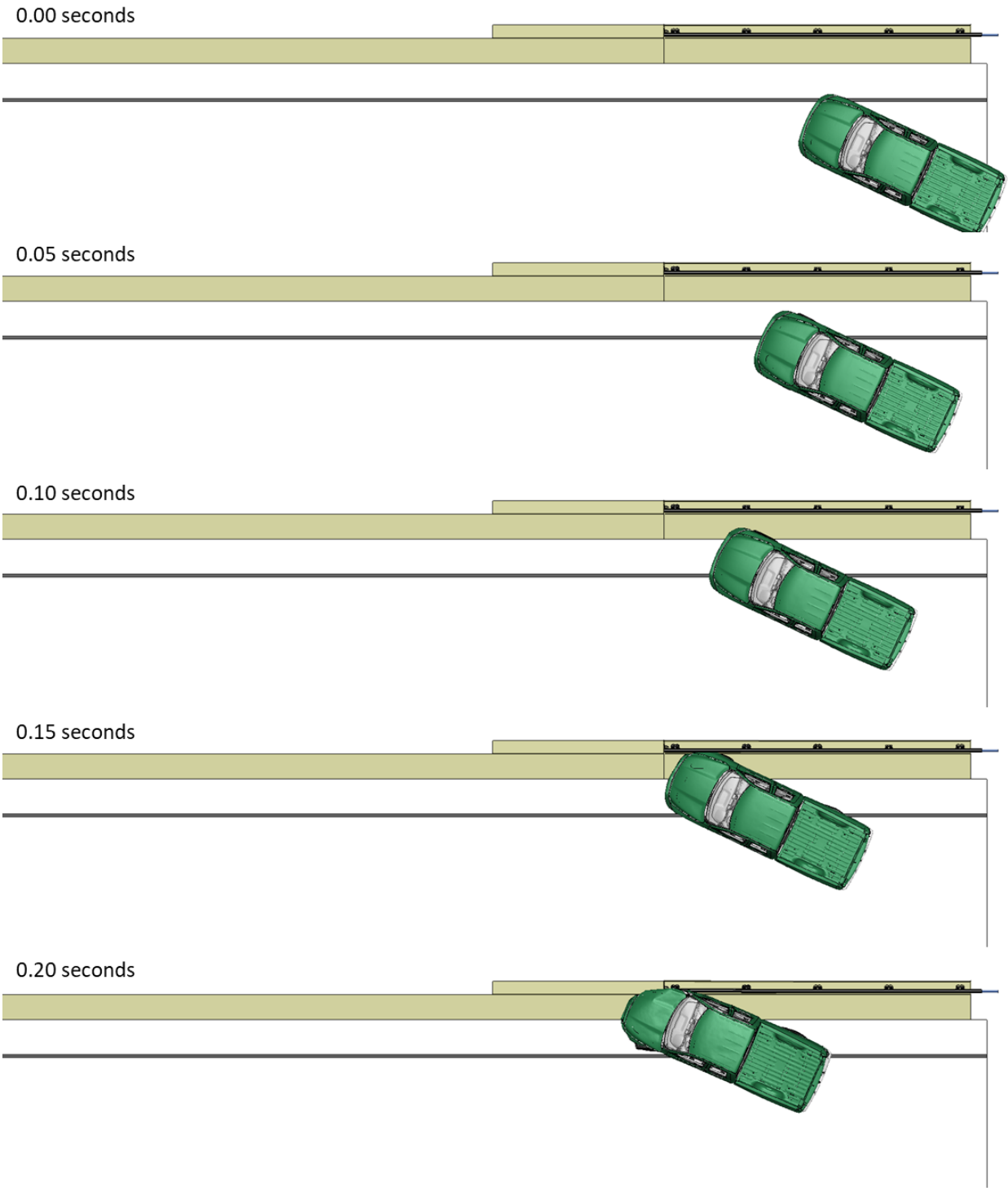

Figure 1. Sequential views from analysis of MASH Test 3-11 at 4.26 ft upstream of transition from an overhead viewpoint (KC Model).

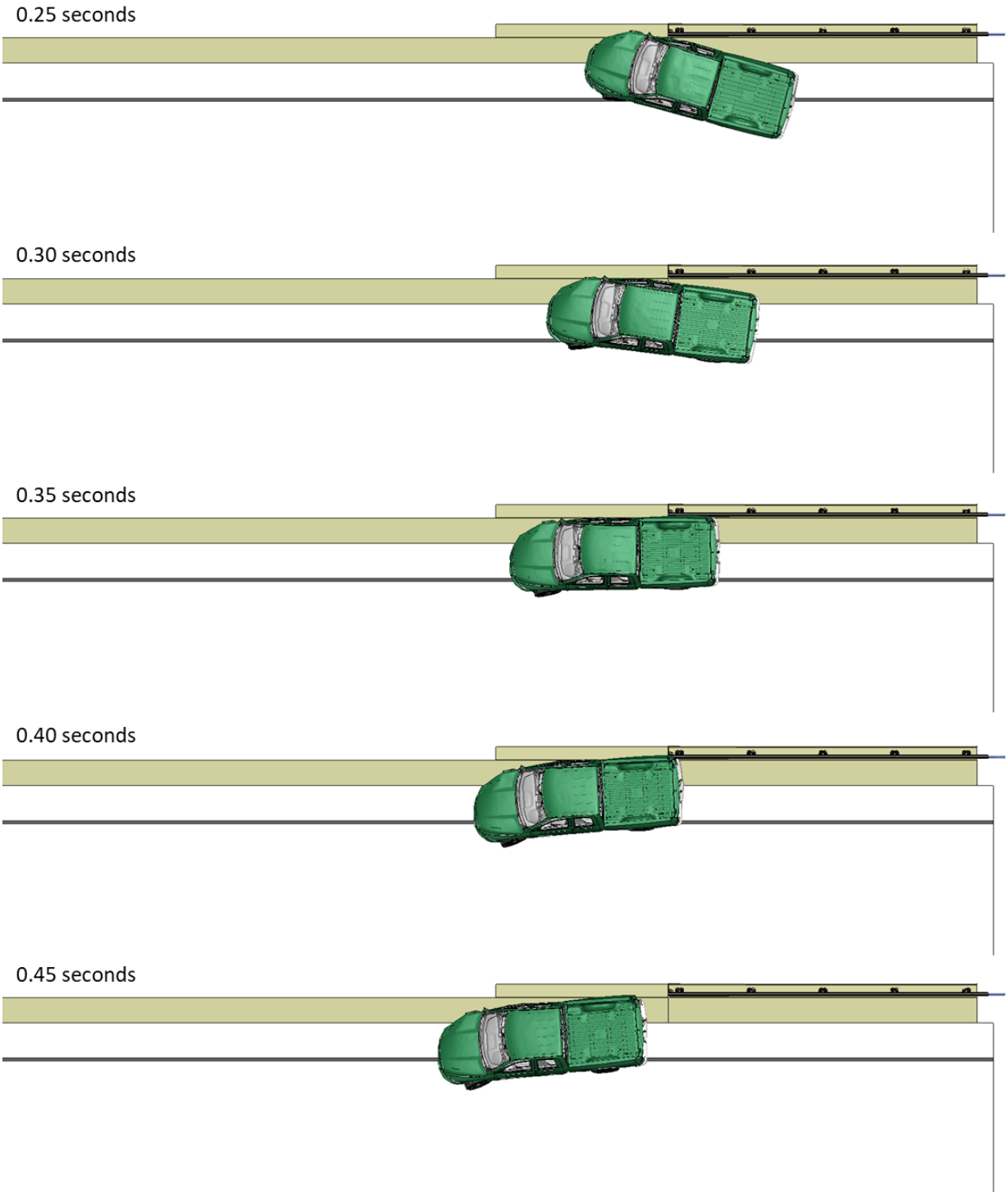

Figure 1 [CONTINUED] Sequential views from analysis of MASH Test 3-11 at 4.26 ft upstream of transition from an overhead viewpoint (KC Model).

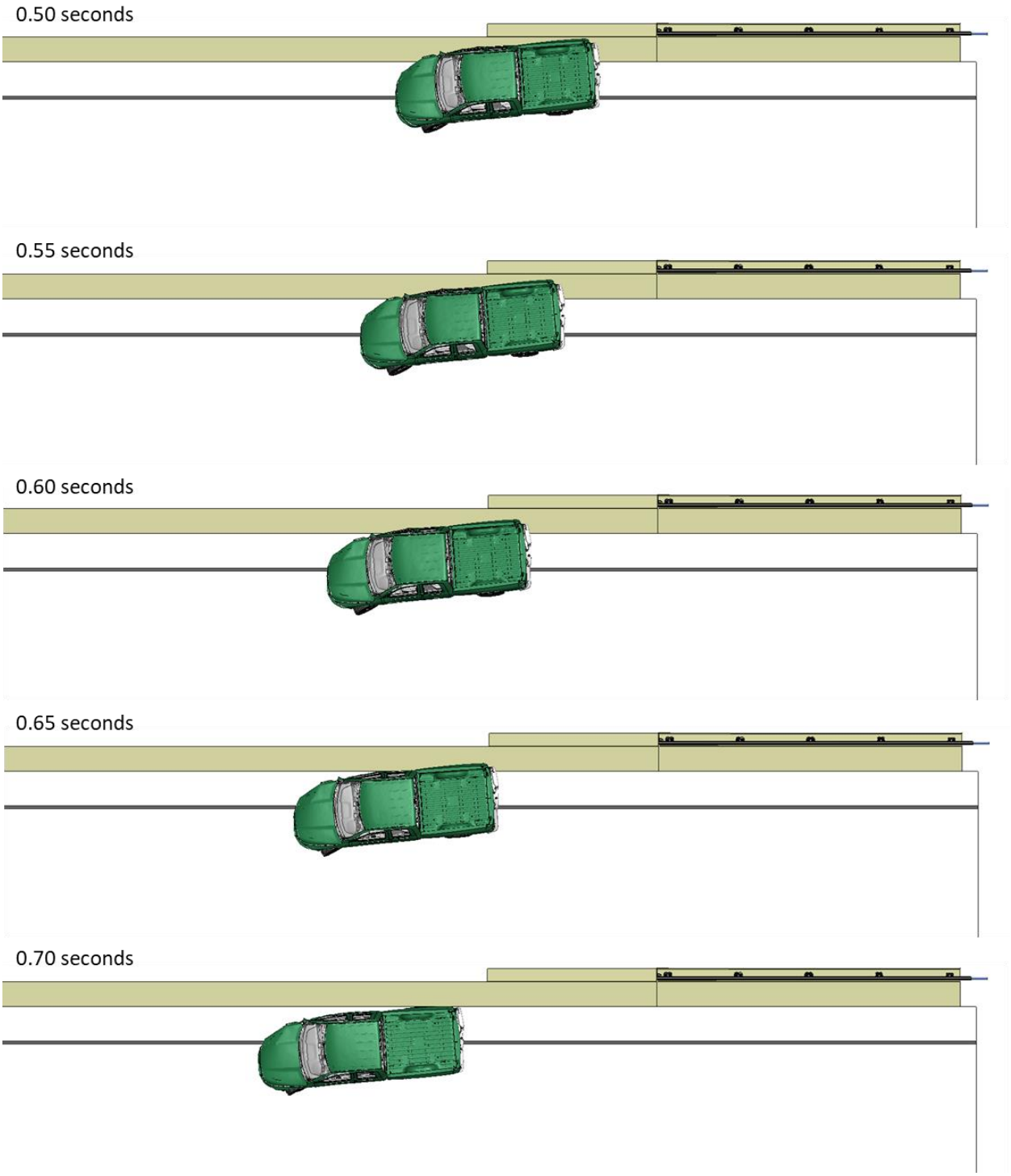

Figure 1 [CONTINUED] Sequential views from analysis of MASH Test 3-11 at 4.26 ft upstream of transition from an overhead viewpoint (KC Model).

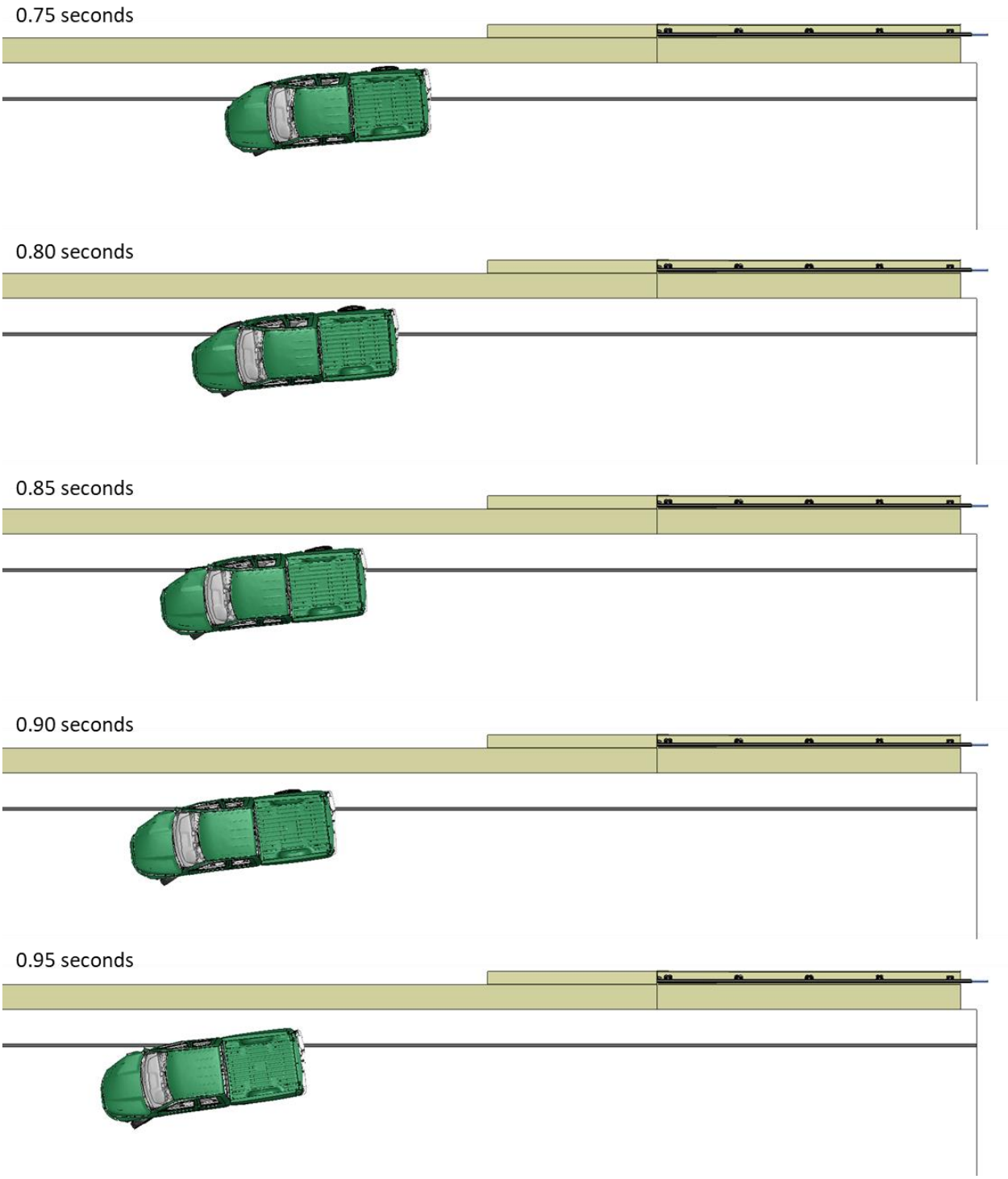

Figure 1 [CONTINUED] Sequential views from analysis of MASH Test 3-11 at 4.26 ft upstream of transition from an overhead viewpoint (KC Model).

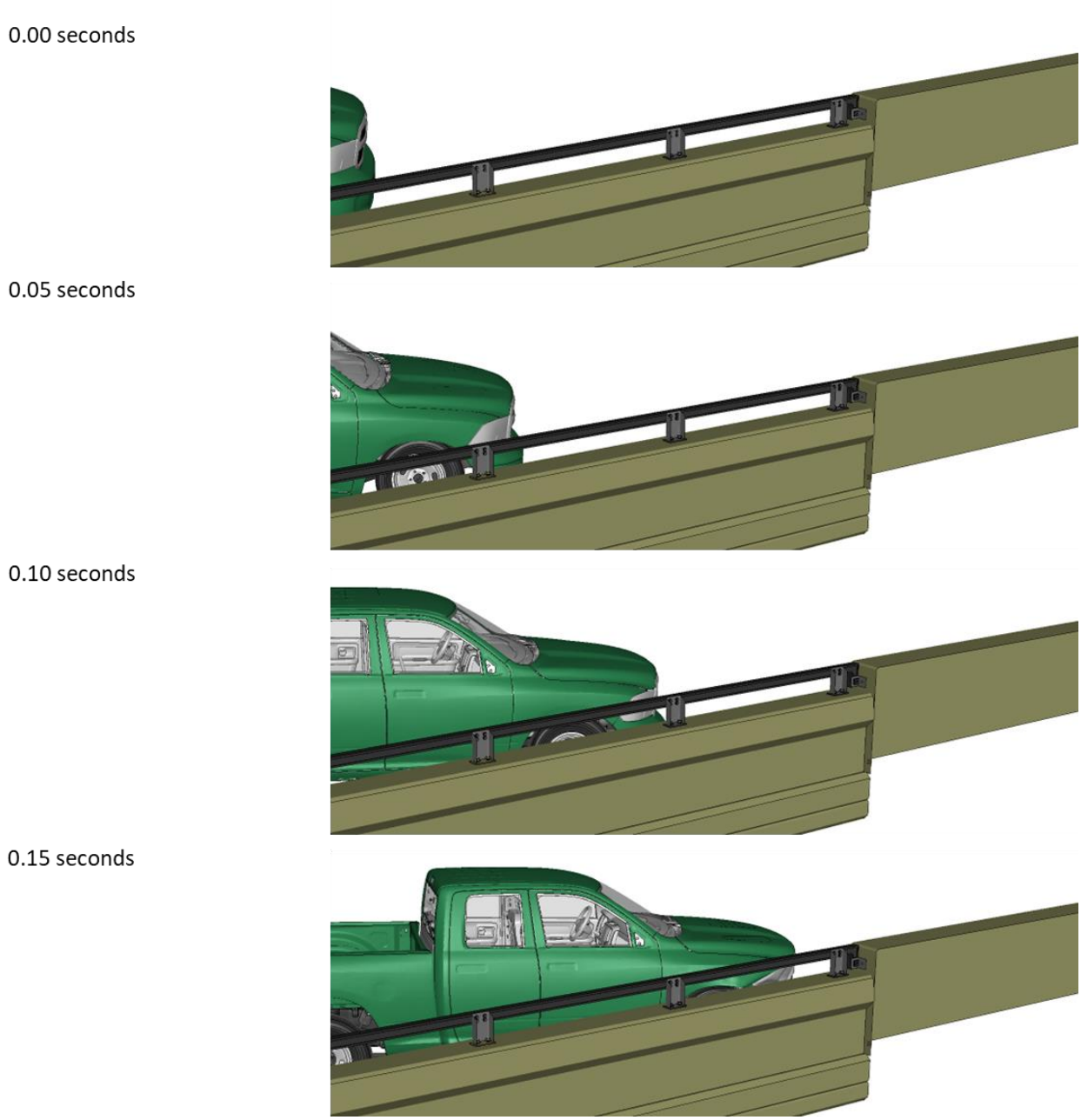

Figure 2. Sequential views from analysis of MASH Test 3-11 at 4.26 ft upstream of transition from an isometric viewpoint (KC Model).

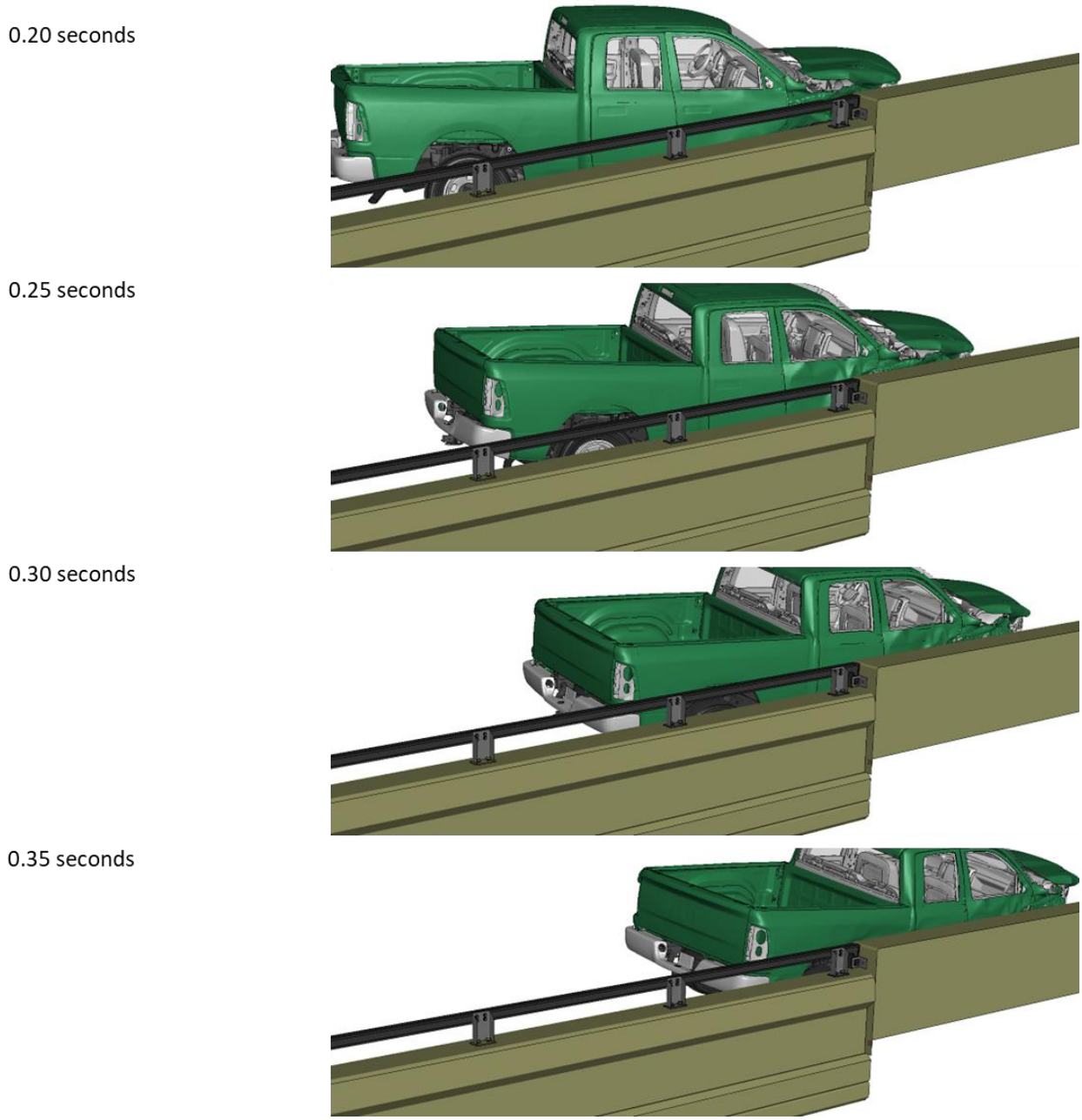

Figure 2 [CONTINUED] Sequential views from analysis of MASH Test 3-11 at 4.26 ft upstream of transition from an isometric viewpoint (KC Model).

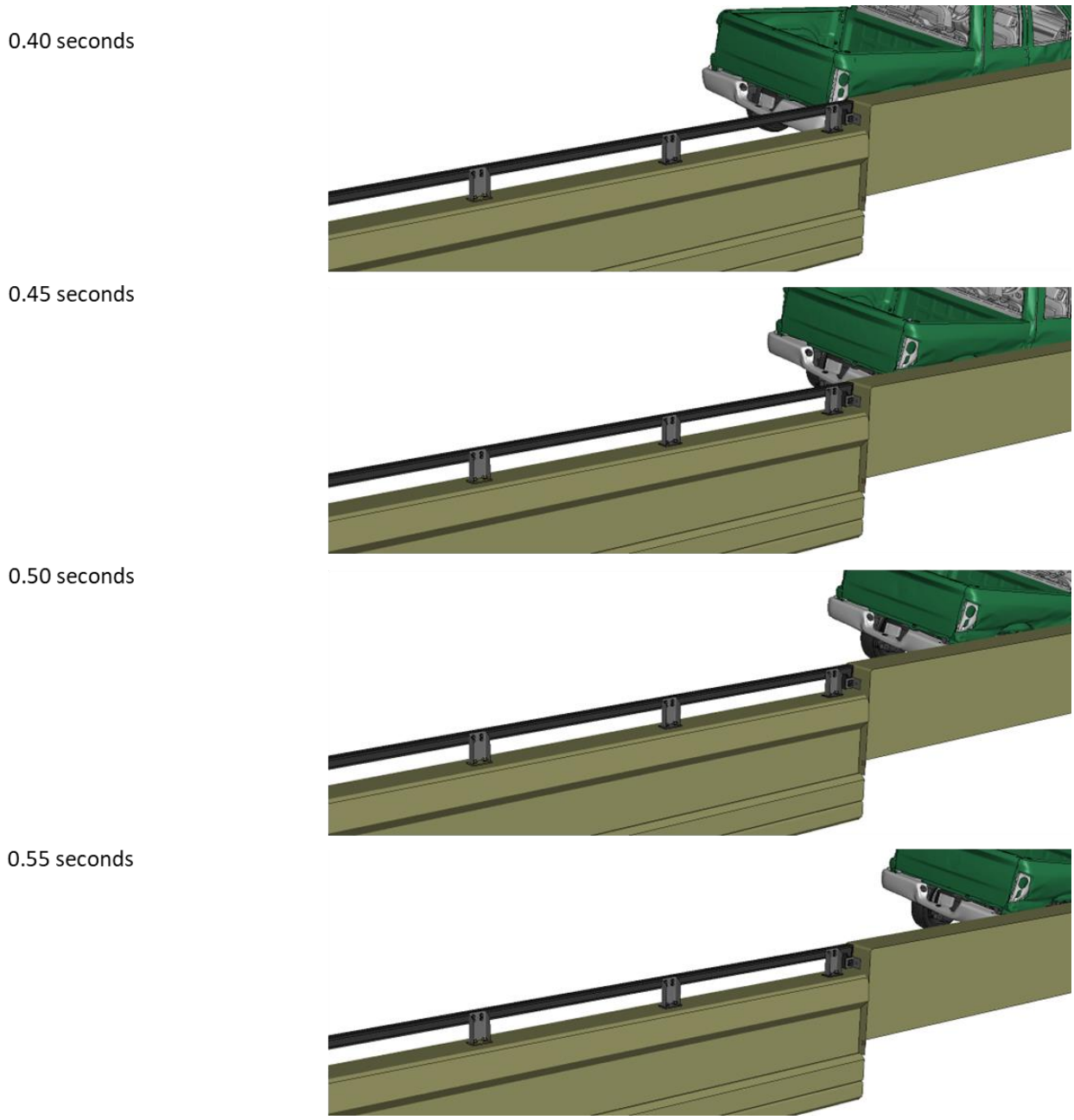

Figure 2 [CONTINUED] Sequential views from analysis of MASH Test 3-11 at 4.26 ft upstream of transition from an isometric viewpoint (KC Model).

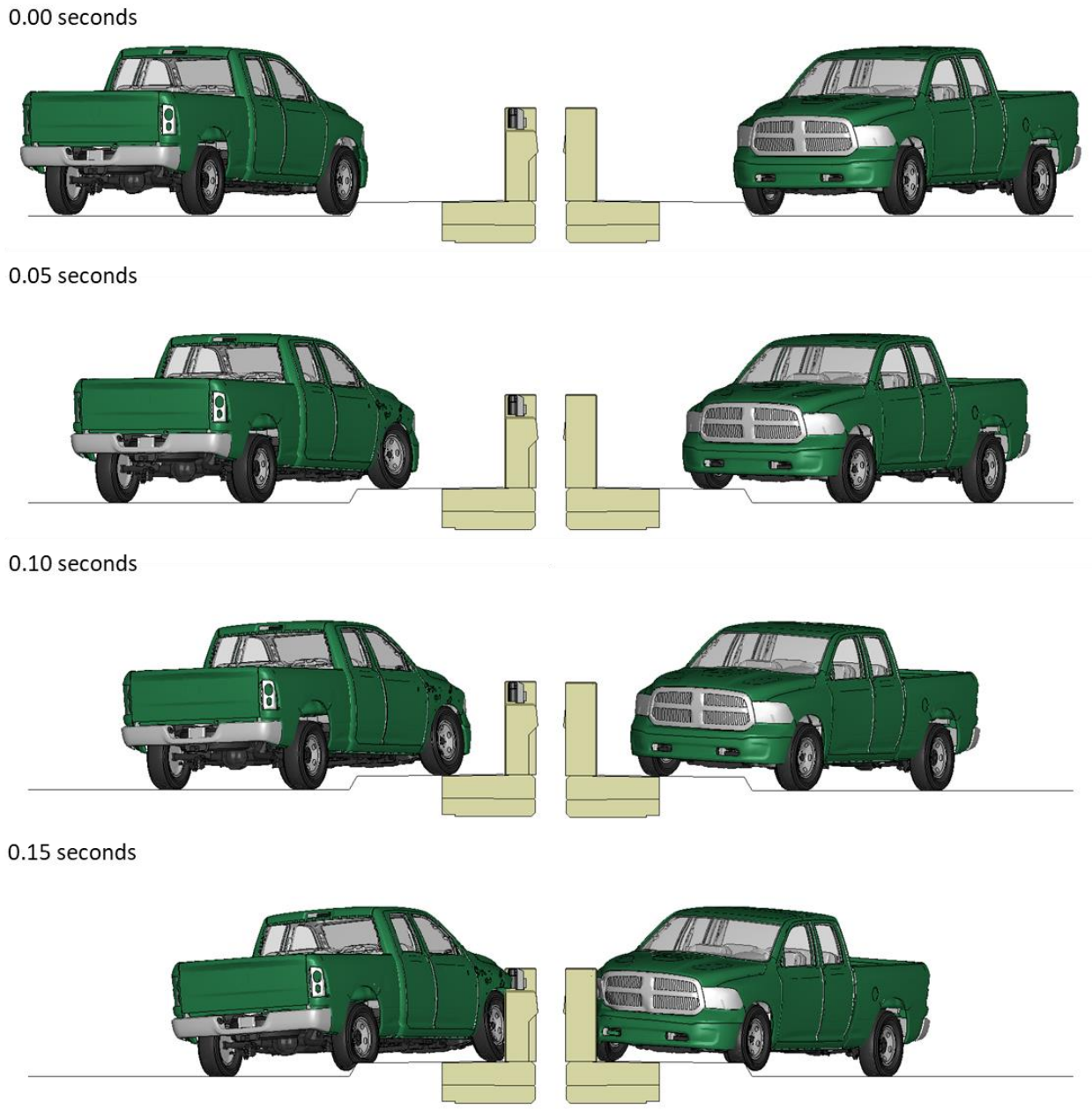

Figure 3. Sequential views from analysis of MASH Test 3-11 at 4.26 ft upstream of transition from a front and back viewpoint (KC Model).

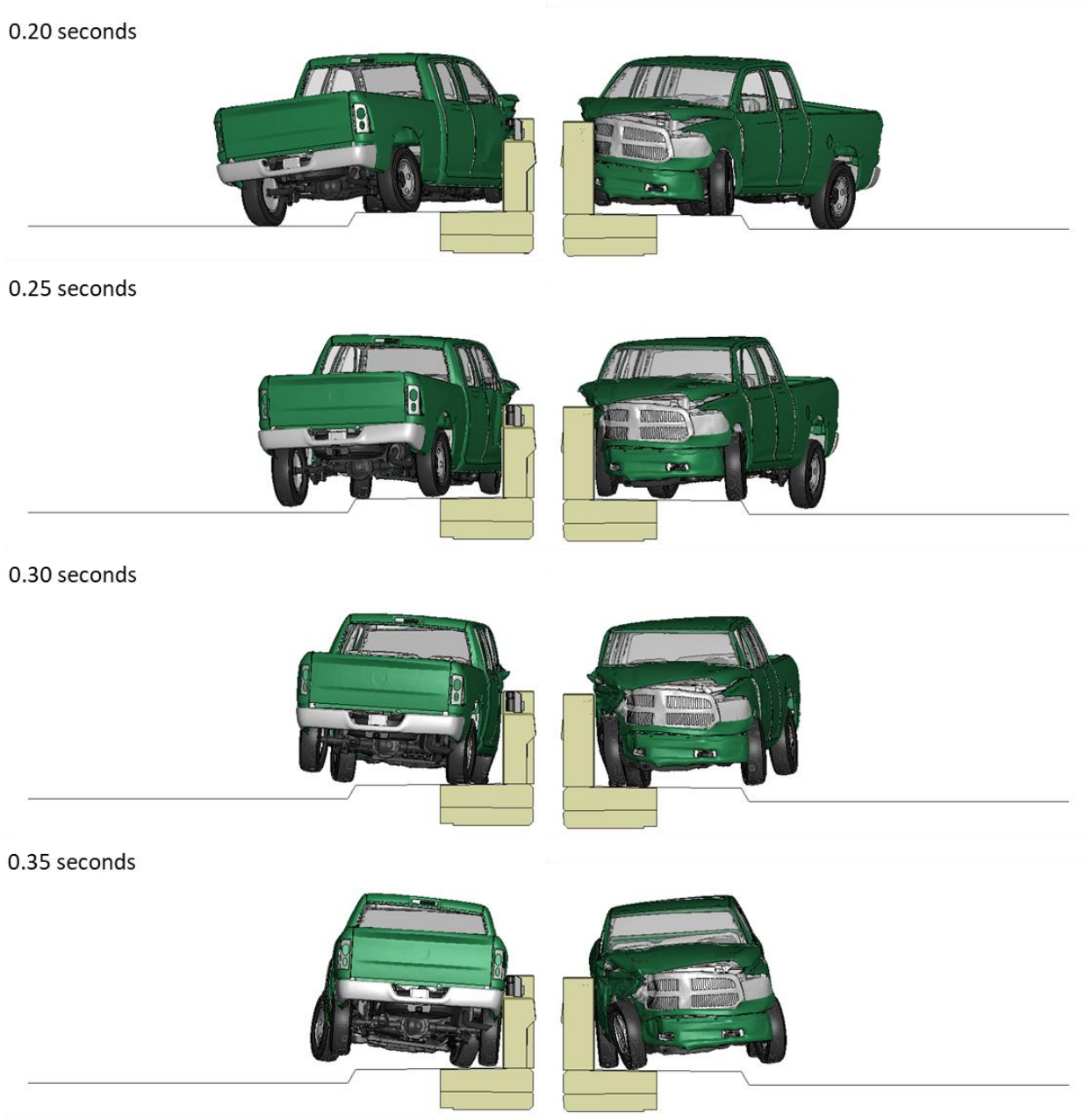

Figure 3 [CONTINUED] Sequential views from analysis of MASH Test 3-11 at 4.26 ft upstream of transition from a front and back viewpoint (KC Model).

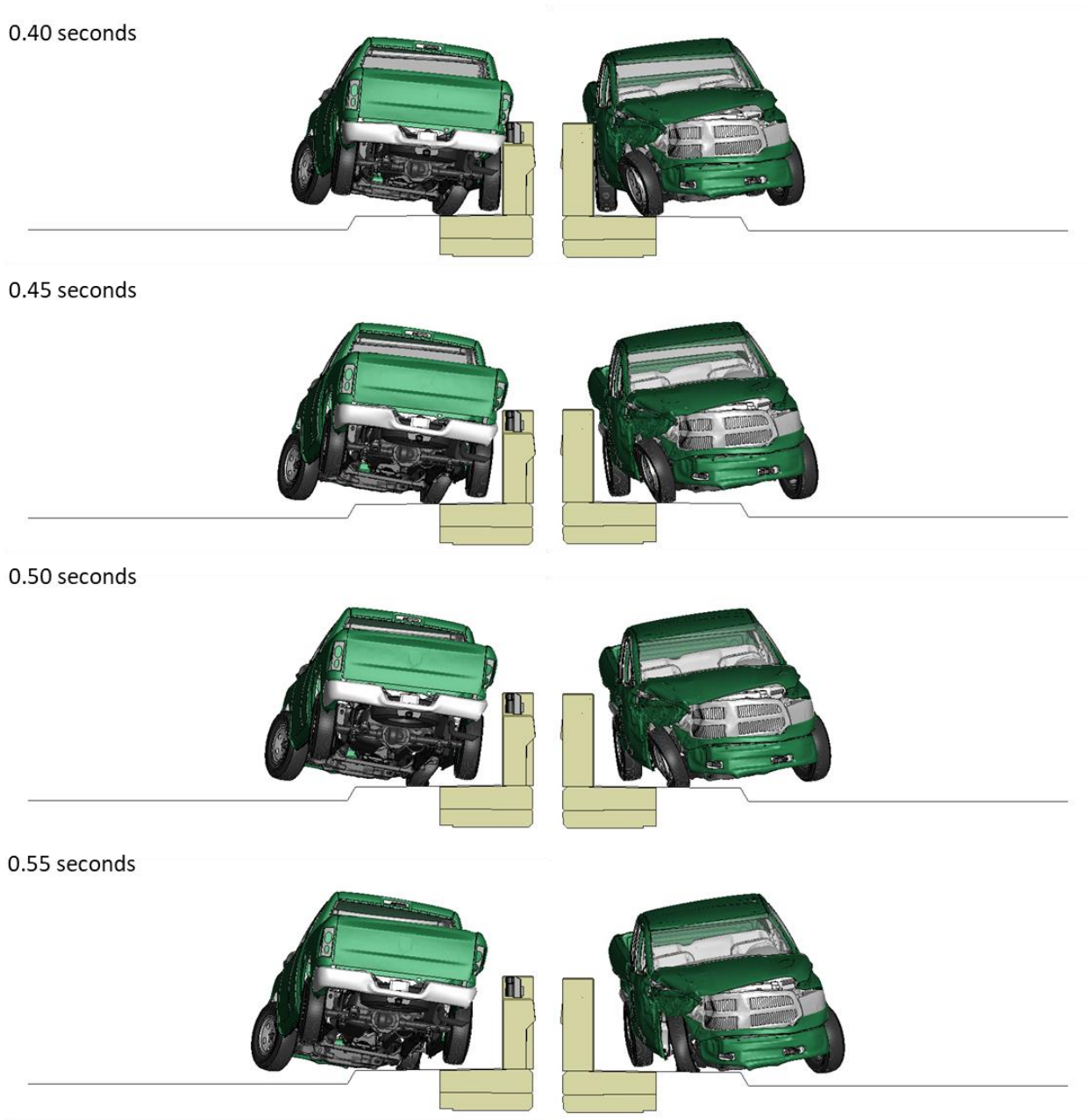

Figure 3 [CONTINUED] Sequential views from analysis of MASH Test 3-11 at 4.26 ft upstream of transition from a front and back viewpoint (KC Model).

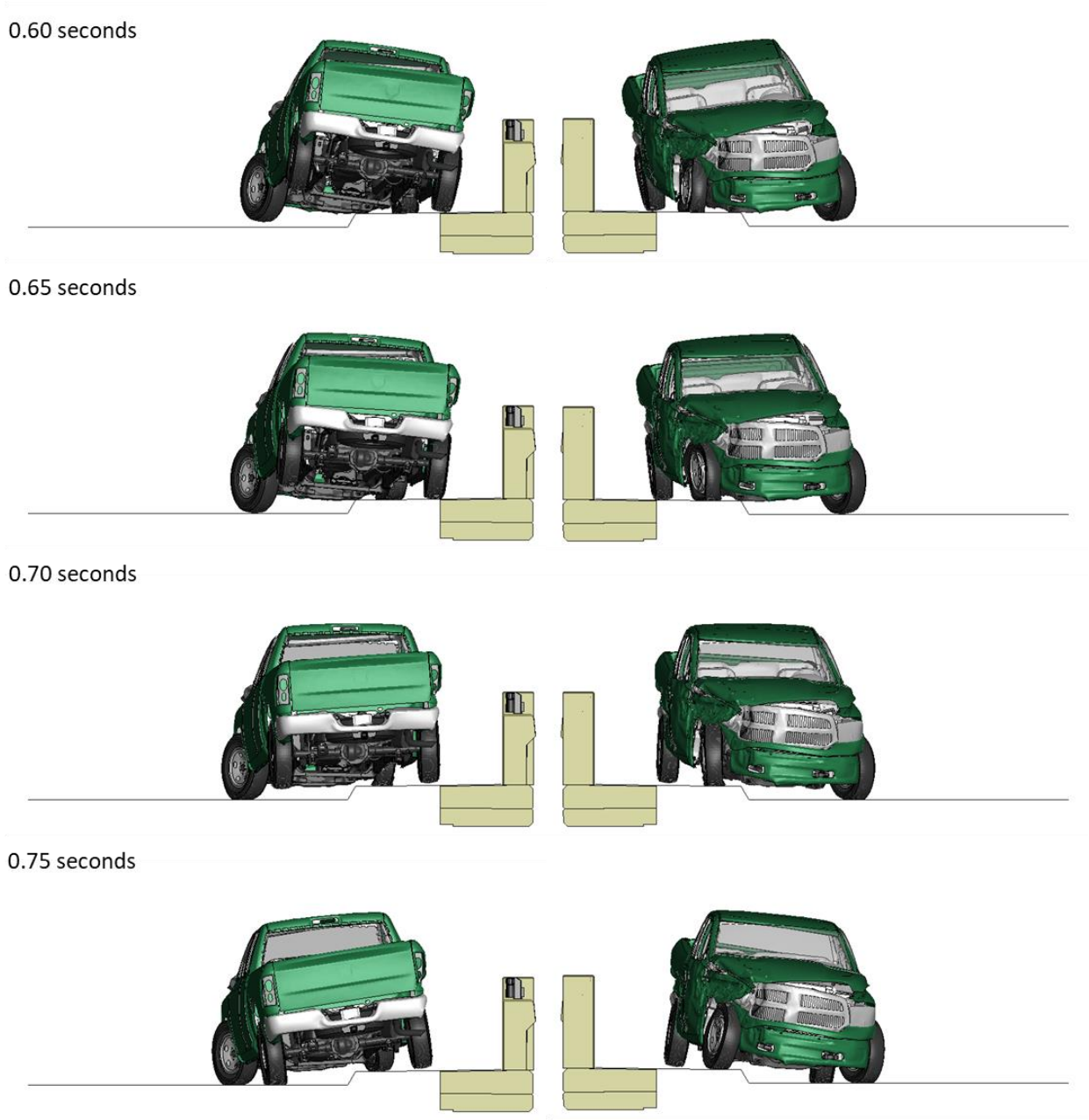

Figure 3 [CONTINUED] Sequential views from analysis of MASH Test 3-11 at 4.26 ft upstream of transition from a front and back viewpoint (KC Model).

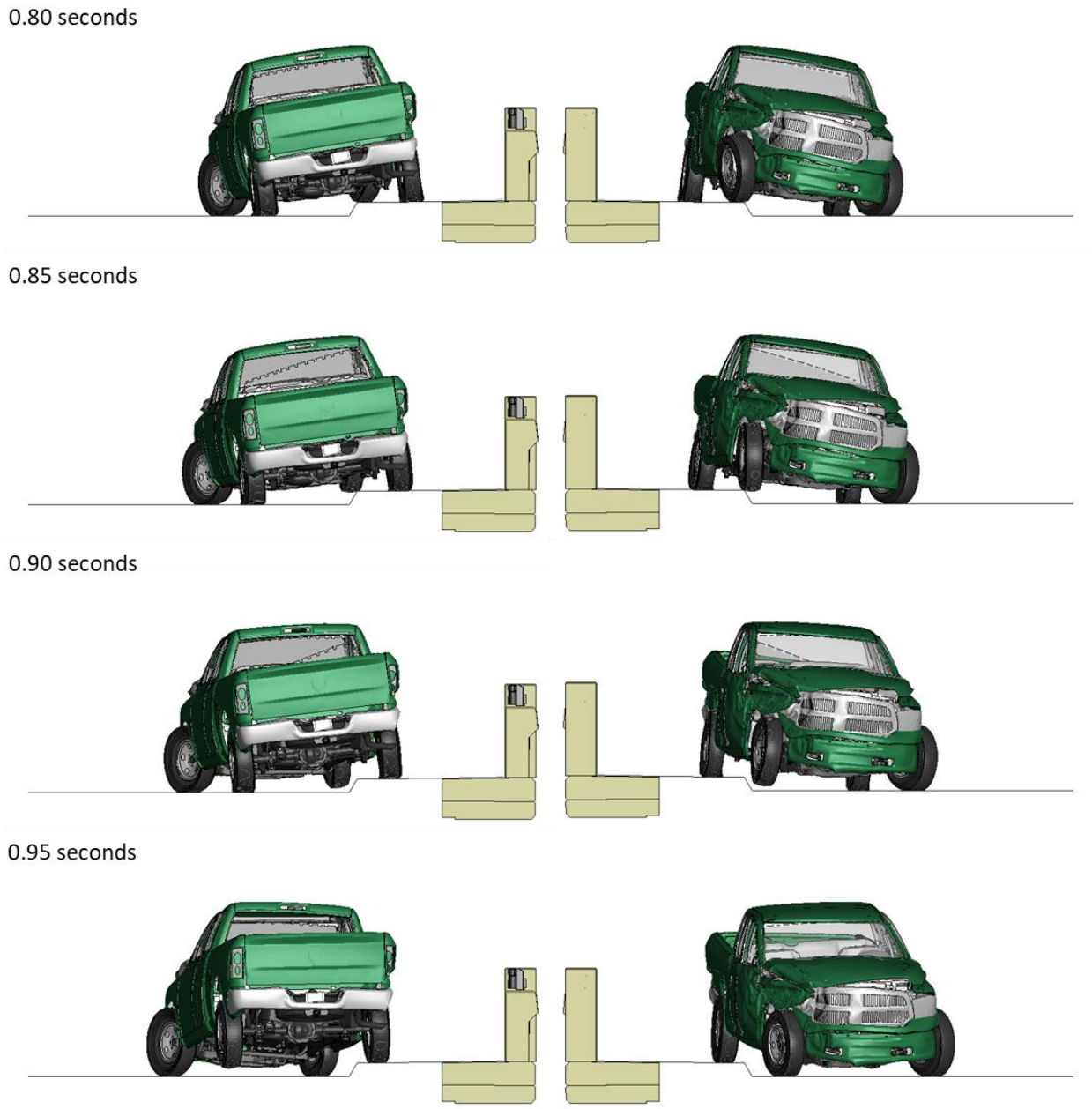

Figure 3 [CONTINUED] Sequential views from analysis of MASH Test 3-11 at 4.26 ft upstream of transition from a front and back viewpoint (KC Model).

Appendix M

Sequential Views for Test 3-11 at 5.26 ft Upstream of Transition (KC Model)

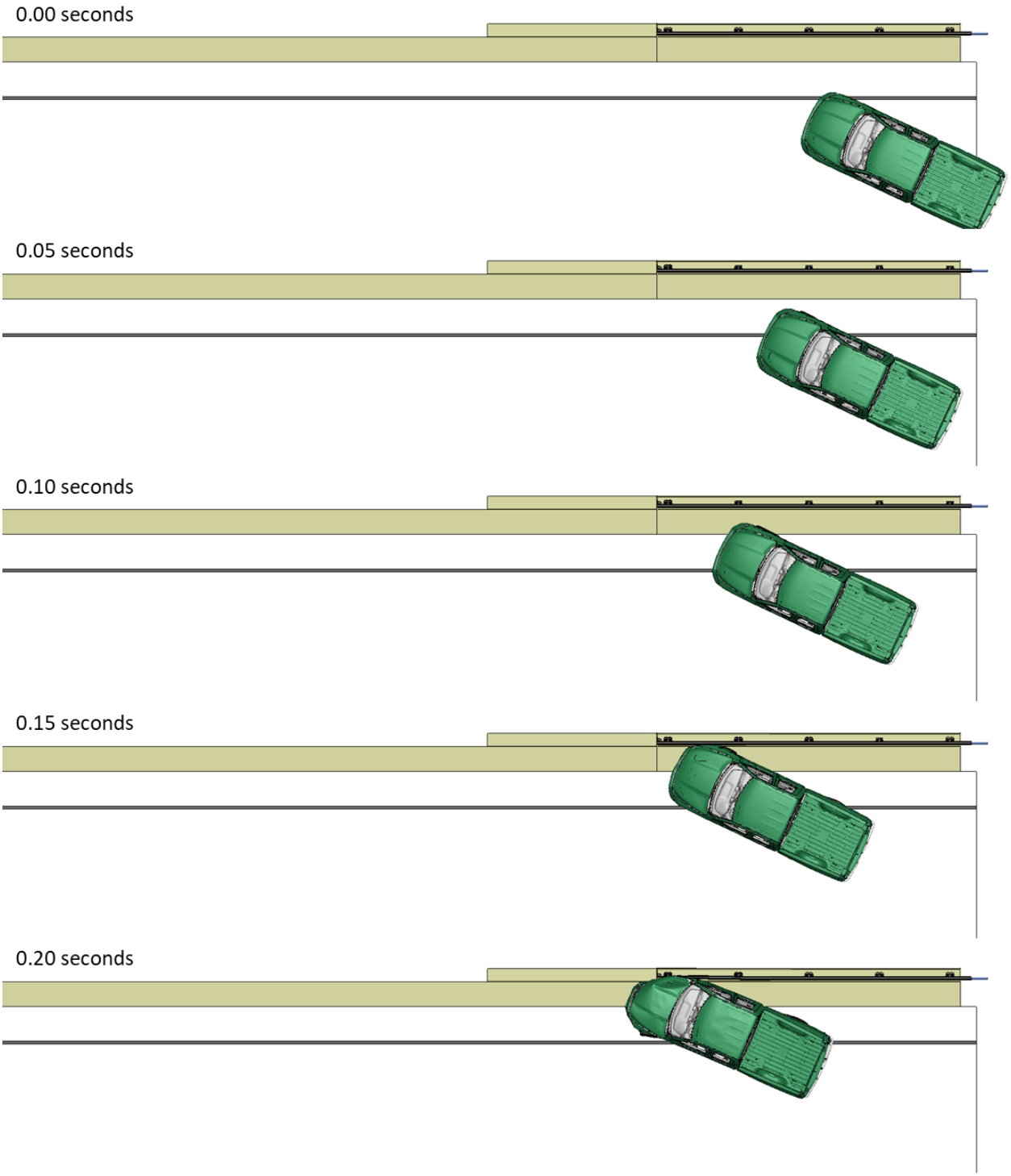

Figure 1. Sequential views from analysis of MASH Test 3-11 at 5.26 ft upstream of transition from an overhead viewpoint (KC Model).

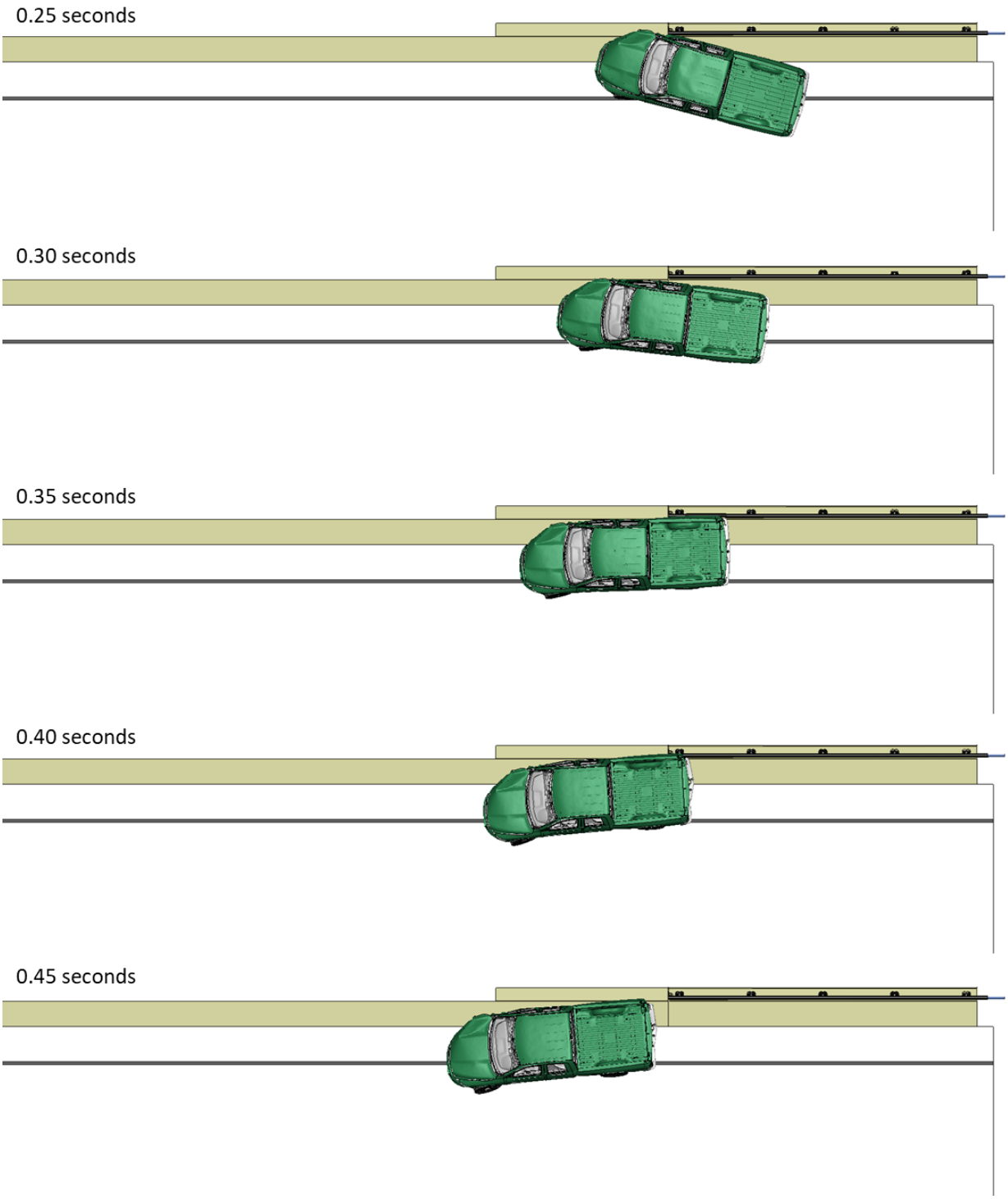

Figure 1 [CONTINUED] Sequential views from analysis of MASH Test 3-11 at 5.26 ft upstream of transition from an overhead viewpoint (KC Model).

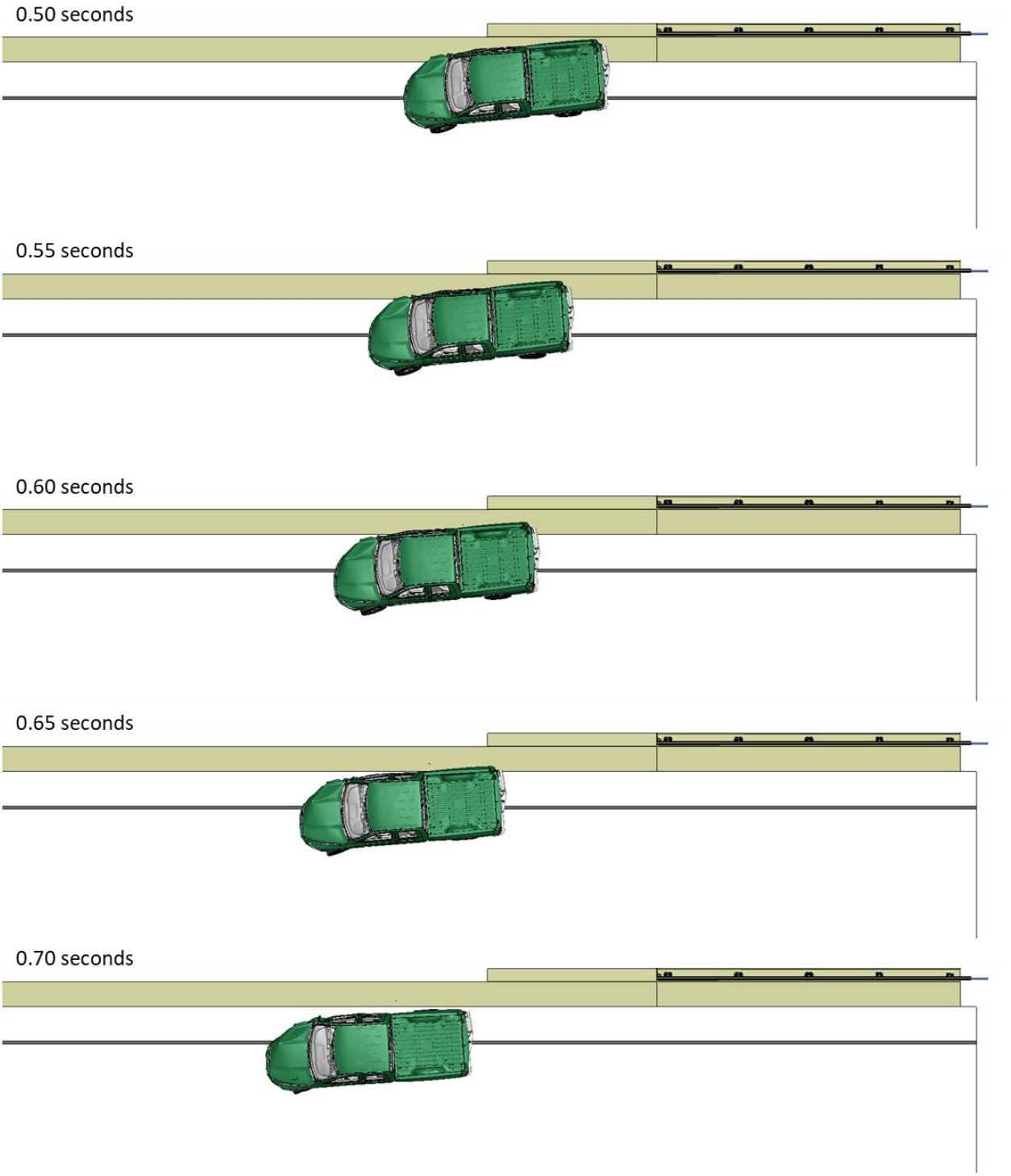

Figure 1 [CONTINUED] Sequential views from analysis of MASH Test 3-11 at 5.26 ft upstream of transition from an overhead viewpoint (KC Model).

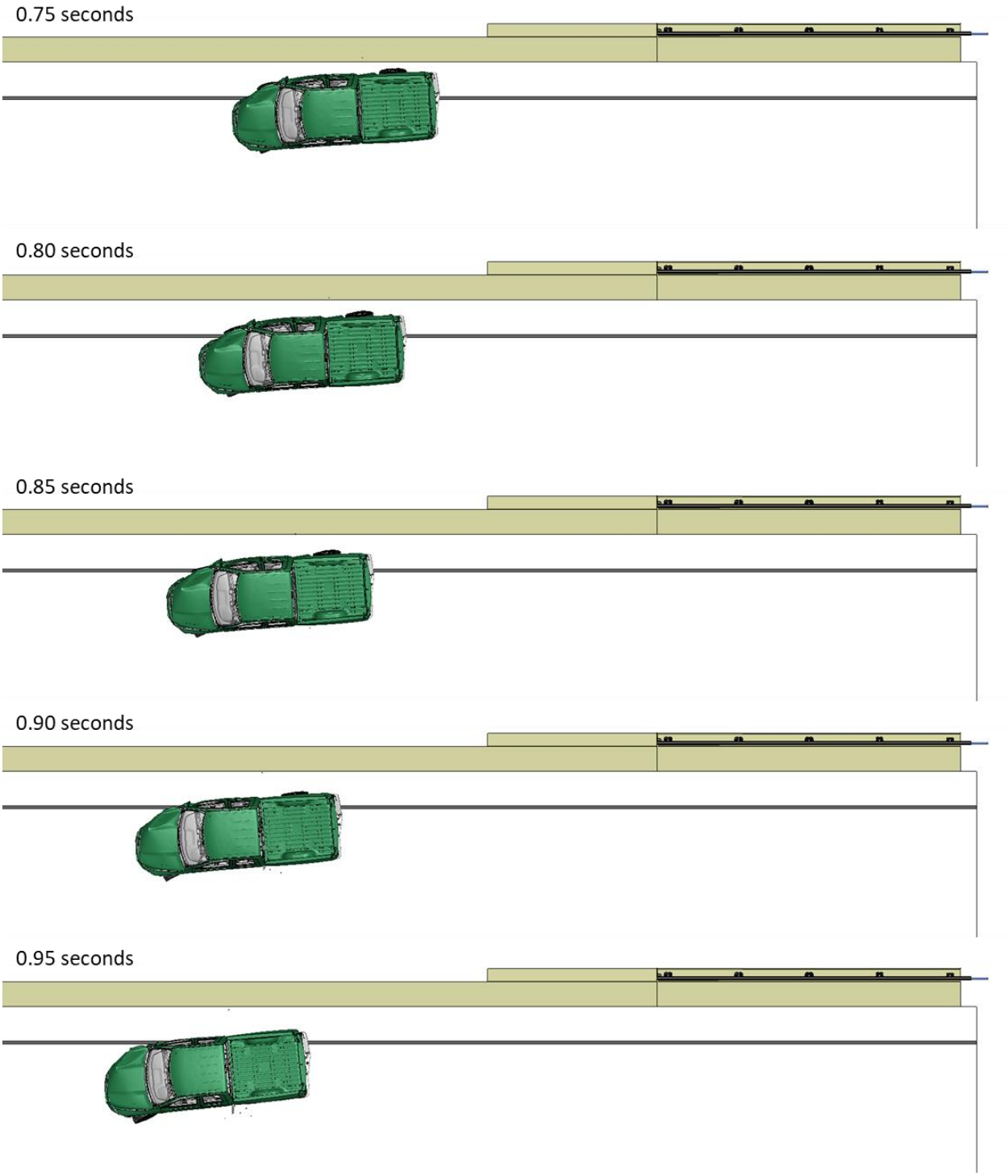

Figure 1 [CONTINUED] Sequential views from analysis of MASH Test 3-11 at 5.26 ft upstream of transition from an overhead viewpoint (KC Model).

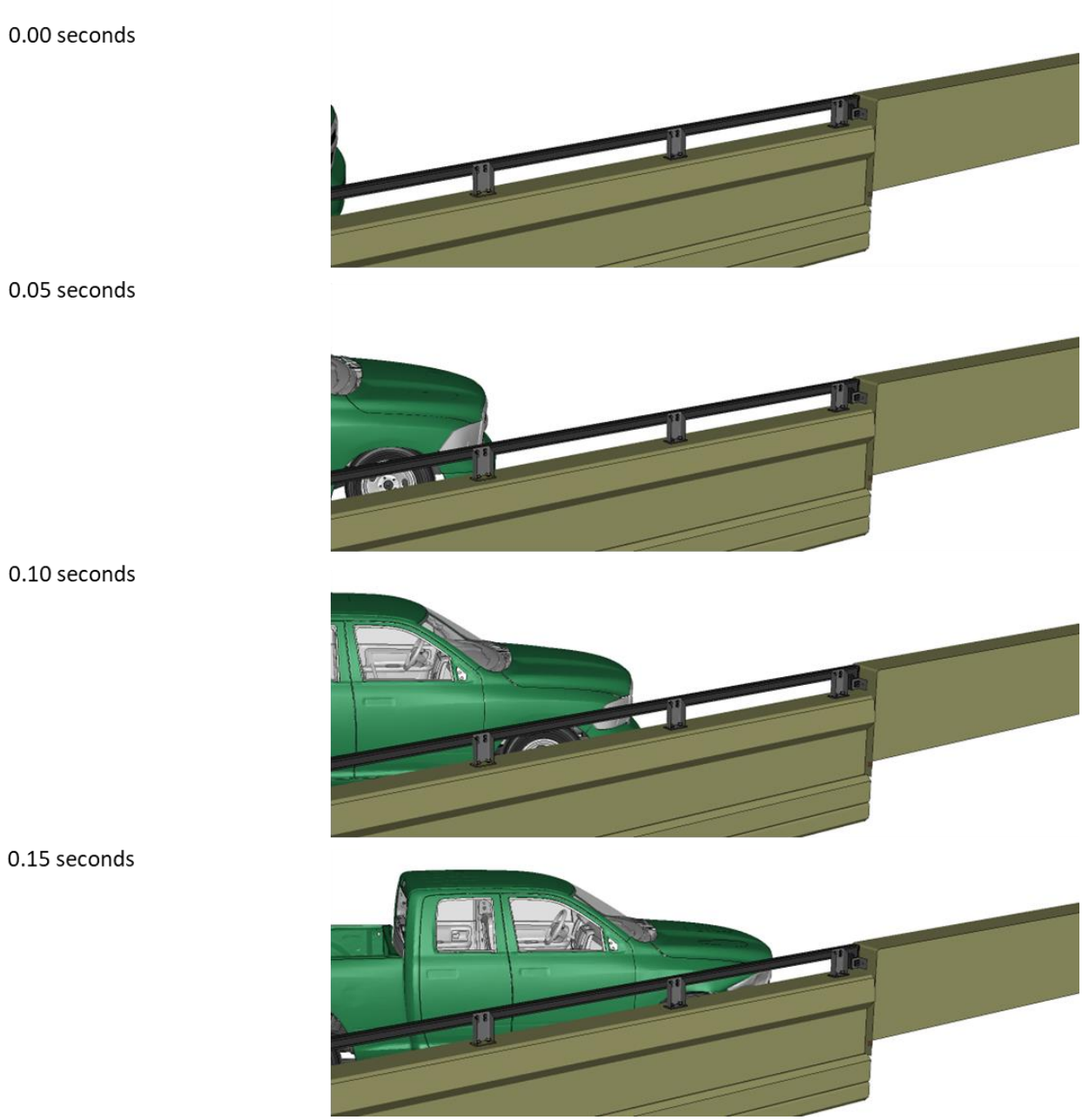

Figure 2. Sequential views from analysis of MASH Test 3-11 at 5.26 ft upstream of transition from an isometric viewpoint (KC Model).

0.20 seconds

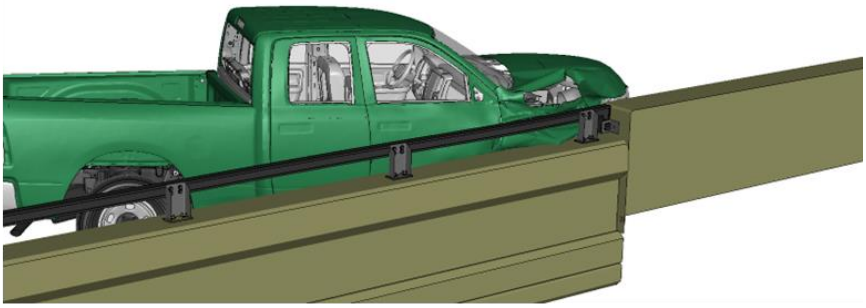

0.25 seconds

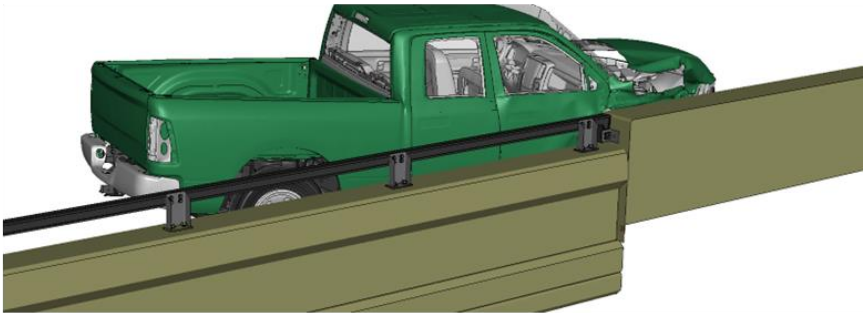

0.30 seconds

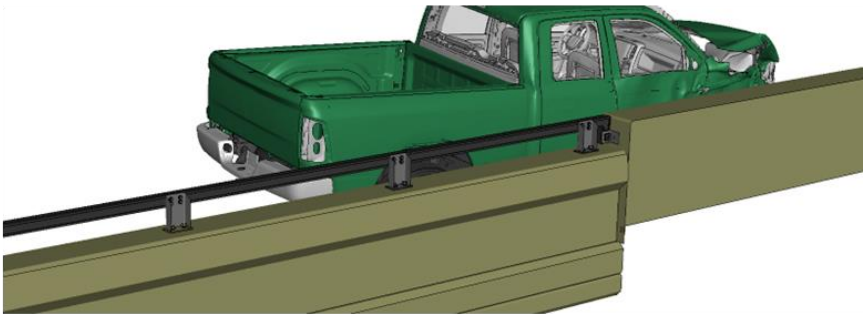

0.35 seconds

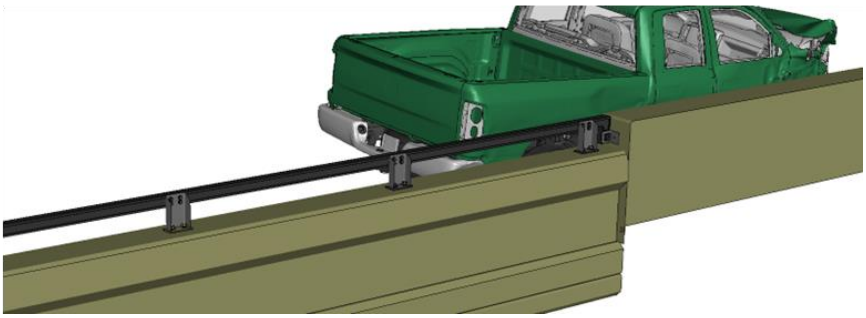

Figure 2 [CONTINUED] Sequential views from analysis of MASH Test 3-11 at 5.26 ft upstream of transition from an isometric viewpoint (KC Model).

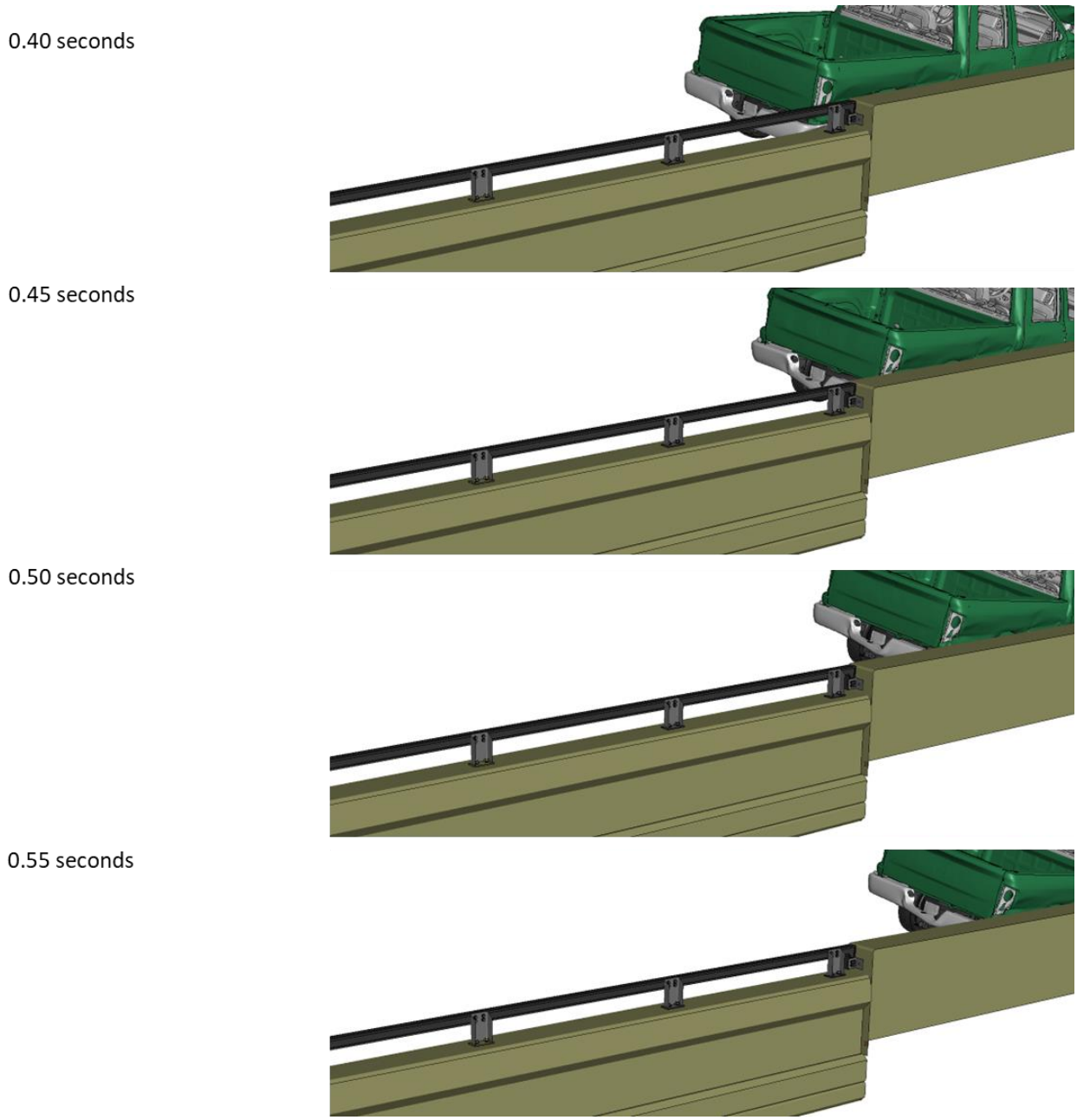

Figure 2 [CONTINUED] Sequential views from analysis of MASH Test 3-11 at 5.26 ft upstream of transition from an isometric viewpoint (KC Model).

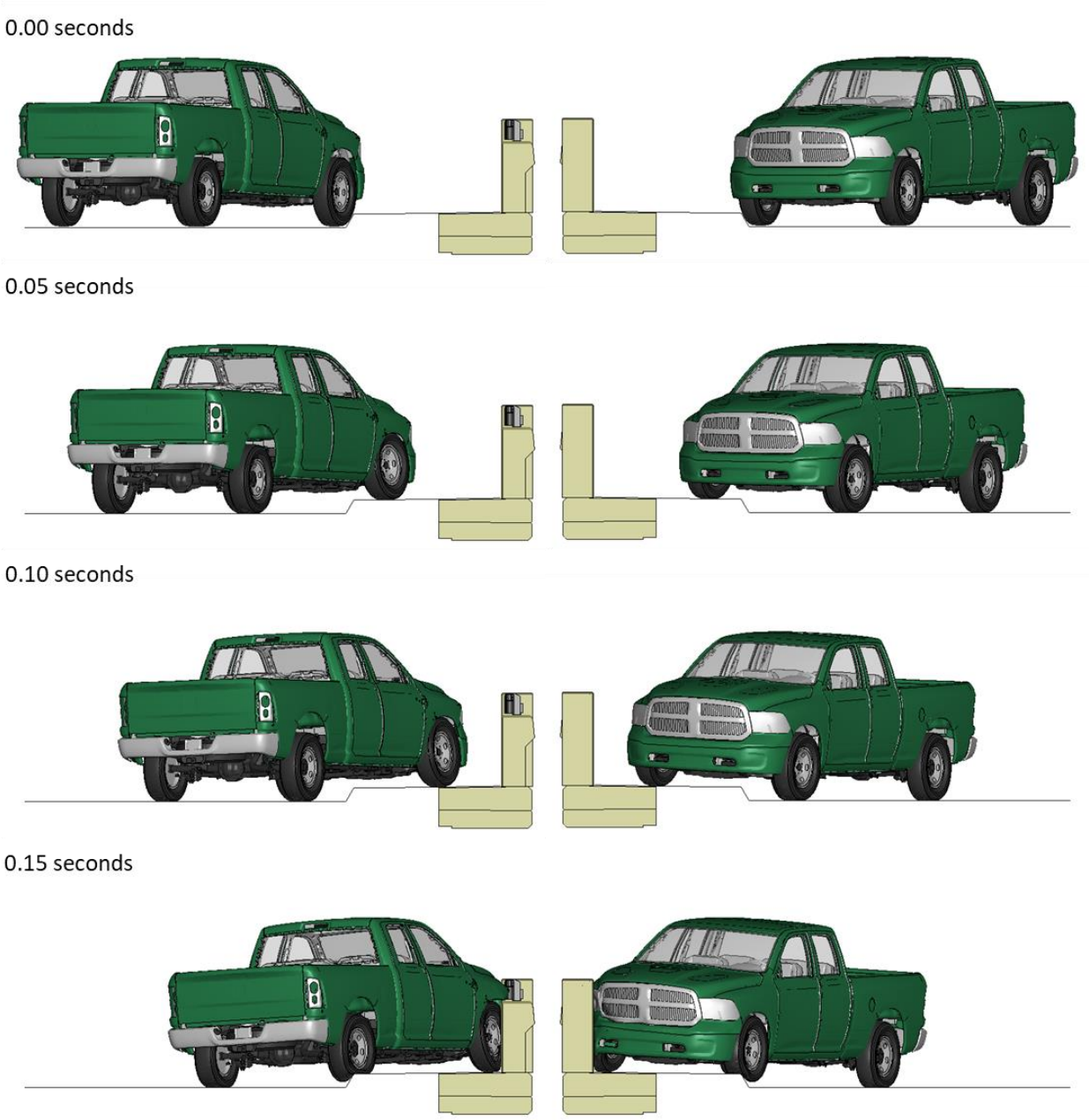

Figure 3. Sequential views from analysis of MASH Test 3-11 at 5.26 ft upstream of transition from a front and back viewpoint (KC Model).

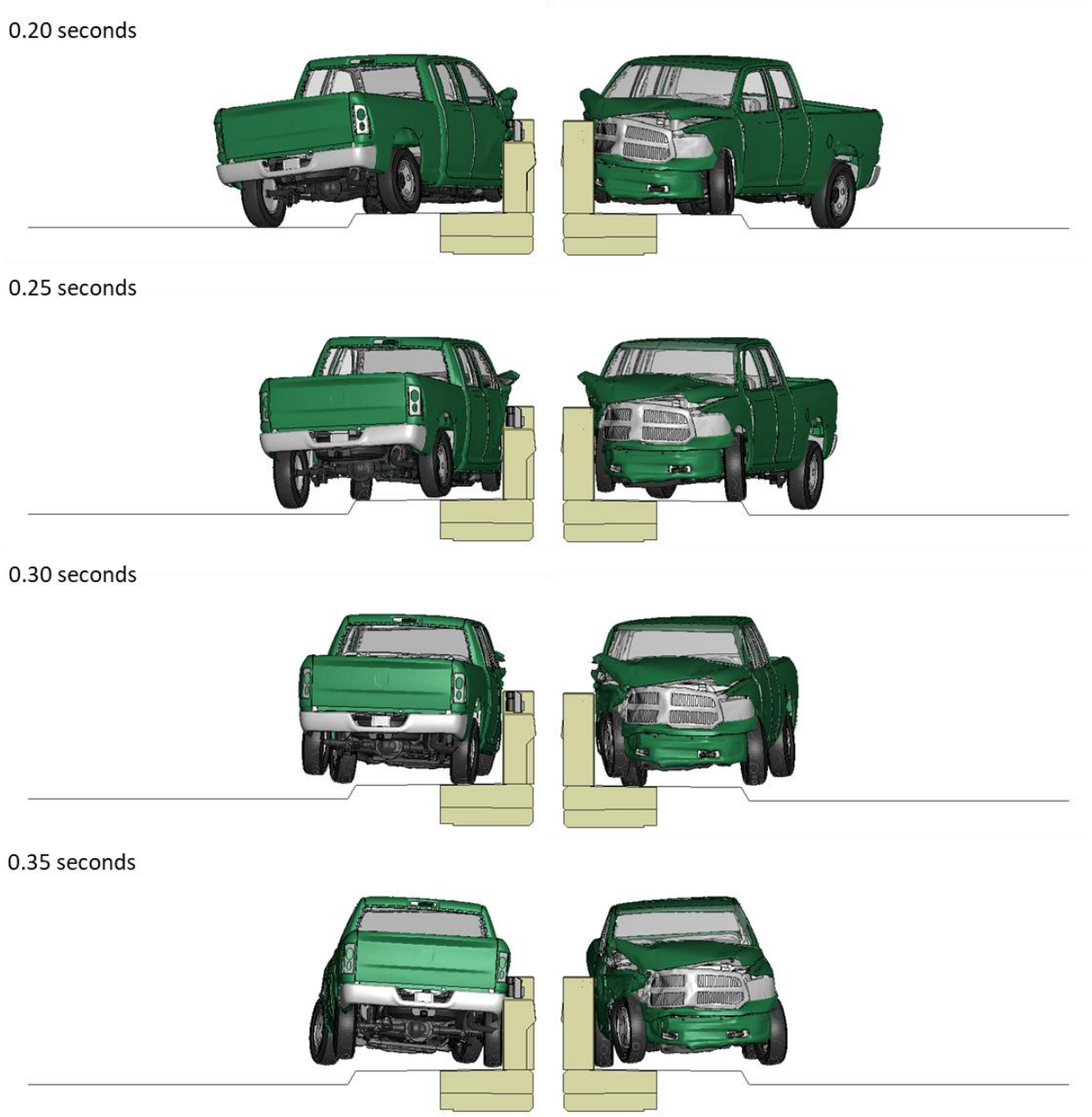

Figure 3 [CONTINUED] Sequential views from analysis of MASH Test 3-11 at 5.26 ft upstream of transition from a front and back viewpoint (KC Model).

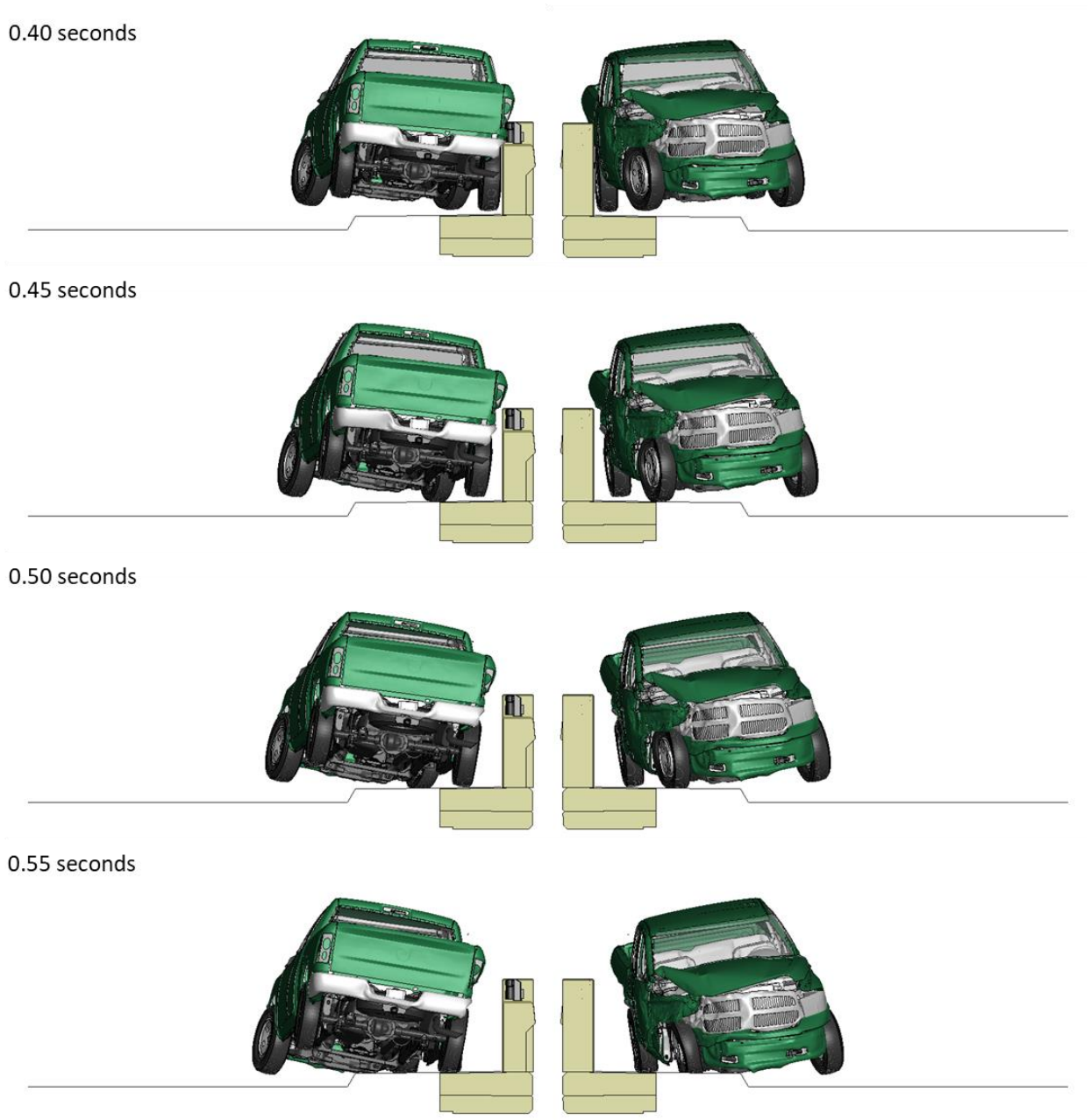

Figure 3 [CONTINUED] Sequential views from analysis of MASH Test 3-11 at 5.26 ft upstream of transition from a front and back viewpoint (KC Model).

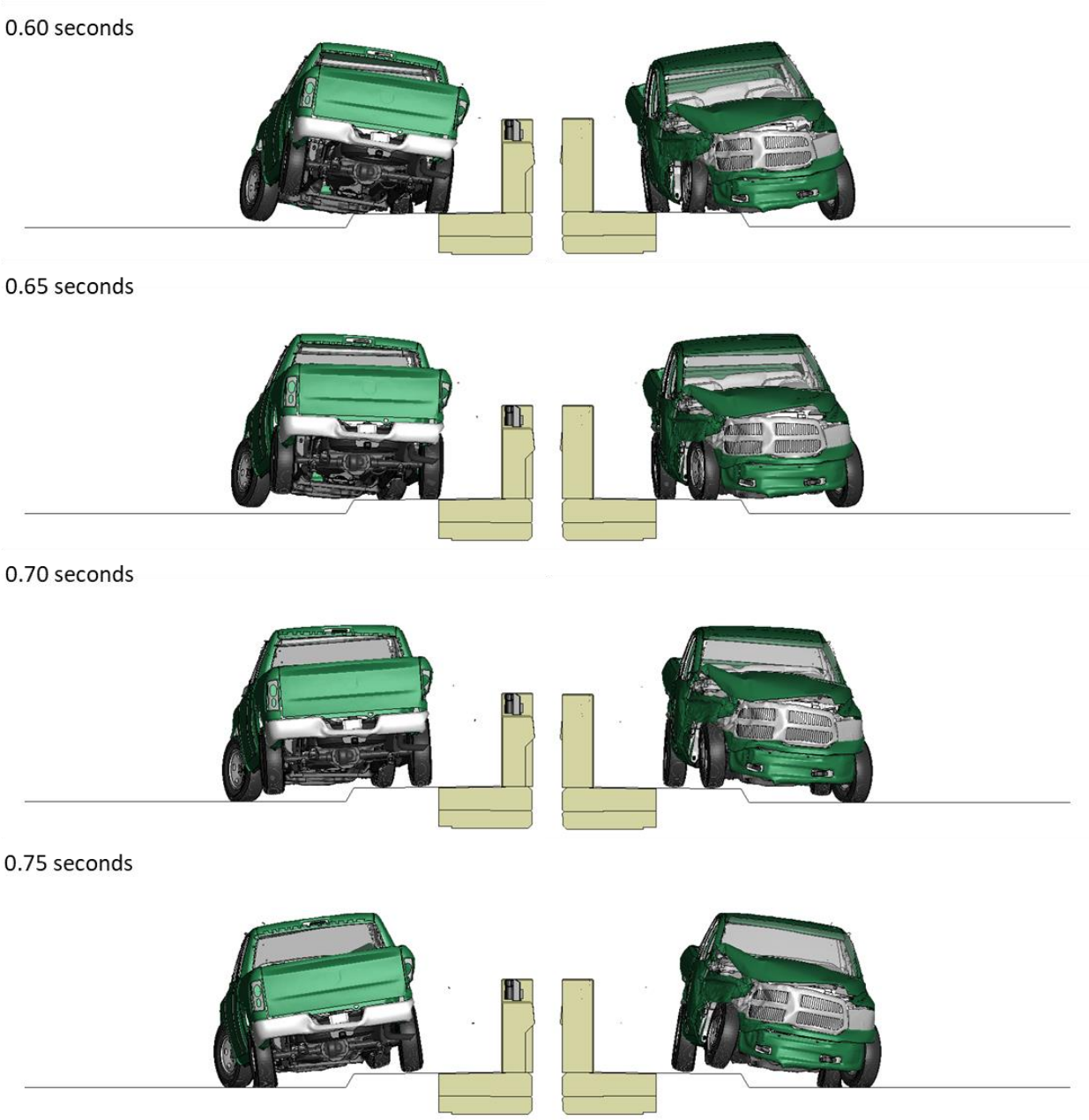

Figure 3 [CONTINUED] Sequential views from analysis of MASH Test 3-11 at 5.26 ft upstream of transition from a front and back viewpoint (KC Model).

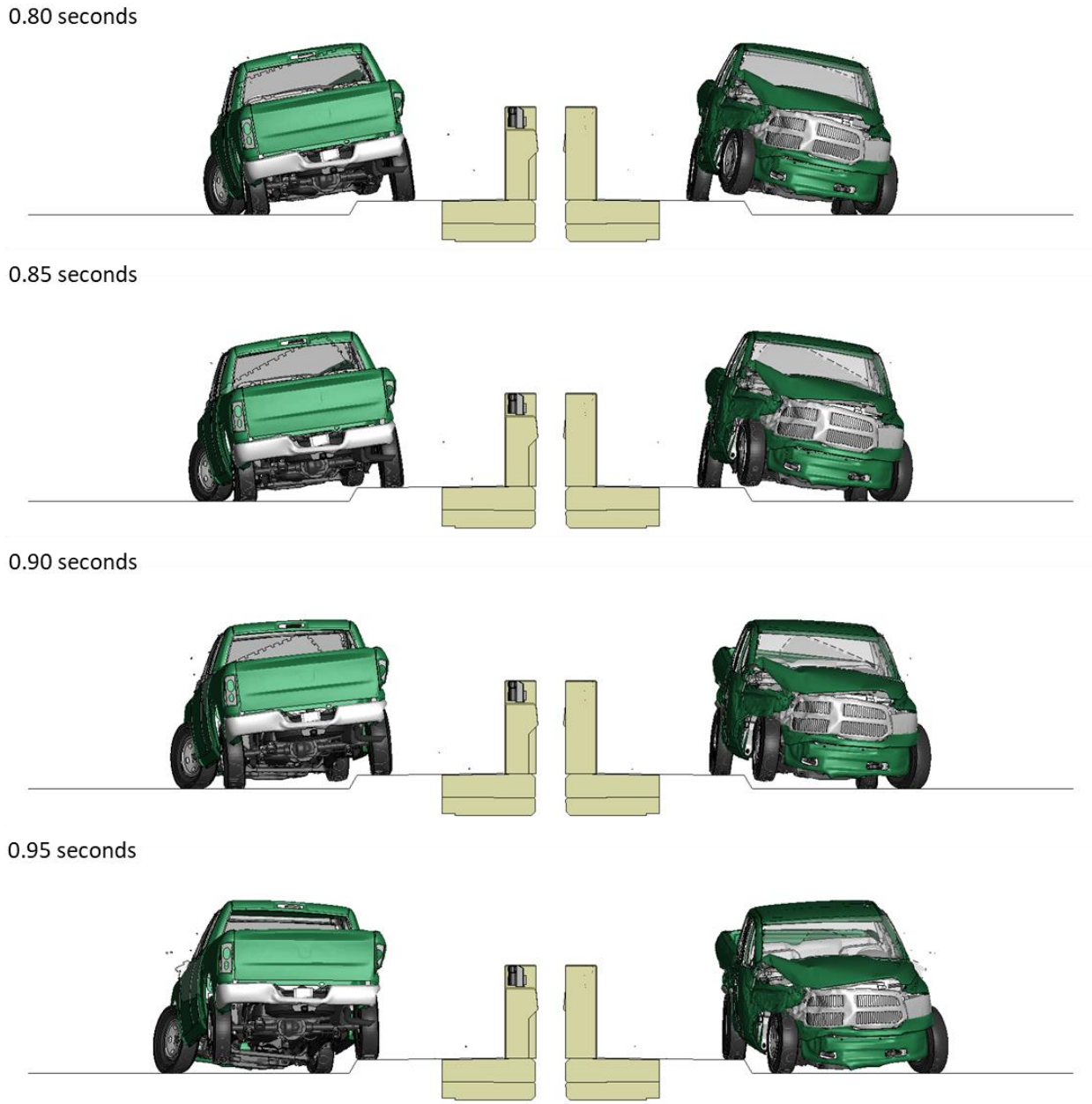

Figure 3 [CONTINUED] Sequential views from analysis of MASH Test 3-11 at 5.26 ft upstream of transition from a front and back viewpoint (KC Model).